

The late Miocene - early Pliocene offshore onshore sedimentary records in the vicinity of Gibraltar



VNIVERSIDAD
D SALAMANCA

Francesca Bulian

TESIS DOCTORAL
SALAMANCA, 2022



Book Cover:

Courtesy of Fulvio Bulian.

Gibraltar Strait sketch modified from Baena Perez et al., 1973. Benthic foraminifer plate from personal collection.



**VNiVERSIDAD
D SALAMANCA**

CAMPUS OF INTERNATIONAL EXCELLENCE

Faculty of Sciences
Geology Department – Area of Paleontology

**The late Miocene – early Pliocene
offshore onshore sedimentary records
in the vicinity of Gibraltar**

Francesca Bulian

Tesis Doctoral

Salamanca, 2022



**VNiVERSIDAD
D SALAMANCA**

CAMPUS OF INTERNATIONAL EXCELLENCE

Facultad de Ciencias
Departamento de Geología – Área de Paleontología

Registros sedimentarios del Mioceno tardío – Plioceno temprano en afloramientos y sondeos marinos próximos a Gibraltar

Memoria de tesis presentada por **Francesca Bulian**
para obtener el grado de Doctora en
Geología por la Universidad de Salamanca con Mención
“Doctor Internacional”

Director de Tesis:

Dr. Francisco Javier Siervo Sánchez

Catedrático del Departamento de Geología, área de Paleontología
Universidad de Salamanca

Salamanca, 2022

Dr. D. **Francisco Javier Sierro Sánchez**, profesor del Área de Paleontología en el Departamento de Geología de la Facultad de Ciencias (Universidad de Salamanca)

Certifica que:

Francesca Bulian ha realizado en el área de Paleontología del departamento de Geología en la Universidad de Salamanca y bajo su supervisión, el trabajo

“Registros sedimentarios del Mioceno tardío - Plioceno temprano en afloramientos y sondeos marinos próximos a Gibraltar”

Y para que conste, firma el presente certificado en Salamanca, enero de 2022.

El director:

Francisco Javier Sierro Sánchez

La doctoranda:

Francesca Bulian



SALTGIANT is a European project funded by the European Union's Horizon 2020 research and innovation programme under the Marie Skłodowska-Curie grant agreement n° 765256.

The cure for anything is salt water - sweat, tears or the sea.

Isak Dinesen

Table of contents

Abstract

Chapter 1. Introduction	1
--------------------------------	---

Chapter 2. Methods	31
---------------------------	----

Chapter 3. Messinian West Alboran Sea record in the proximity of Gibraltar: Early signs of Atlantic-Mediterranean gateway restriction	49
--	----

Chapter 4. Impact of the Mediterranean-Atlantic connectivity and the late Miocene carbon shift of deep-sea communities in the Western Alboran Basin	103
--	-----

Chapter 5. The timing of closure of the last Betic corridor strand inferred from new geochemical and planktic foraminifer data from Montemayor-1 core (Guadalquivir Basin)	159
---	-----

Chapter 6. Reflooding and repopulation of the Mediterranean Sea after the Messinian Salinity Crisis: Benthic foraminifer assemblages and stable isotopes of Spanish basins	199
---	-----

Chapter 7. Conclusions	267
-------------------------------	-----

Appendix

1. List of acronyms	279
---------------------	-----

2. SALTGIANT Research Article: <i>Freshening of the Mediterranean Salt Giant: controversies and certainties around the terminal (Upper Gypsum and Lago-Mare) phases of the Messinian Salinity Crisis</i>	283
--	-----

3. Abstract, Introduction and Conclusions in Spanish	333
--	-----

Acknowledgements	349
-------------------------	-----

Curriculum vitae	355
-------------------------	-----

Abstract

During the late Miocene, tectonic processes led to the closure of the Mediterranean – Atlantic gateways, progressively isolating the Mediterranean Basin from the Global Ocean. This change in gateway configuration modified radically the circulation patterns, water residence time and salinity of the Mediterranean waters leading to the extraordinary paleoenvironmental change known as the Messinian Salinity Crisis (MSC). This event lasted between 5.97 and 5.33 Ma and led to the deposition of huge evaporite accumulations both in the marginal and deep Mediterranean basins. Now, more than 50 years after the Glomar challenger ventured Mediterranean waters, and the evaporites in deep basins were discovered, the debate regarding the conditions and timing of the deposition of the Mediterranean salt giant is still ongoing as many theories regarding the dynamics and chronology of the Gibraltar arc gateway/s closure and reopening are waiting to be validated.

In this optic, the study of cores and outcrops in the proximity of the current Strait of Gibraltar is essential to better understand the evolution of the Mediterranean – Atlantic gateways. In this thesis we perform a detailed planktic and benthic foraminifer, geochemical (XRF and stable isotopes) and sedimentological analyses of Alboran Basin ODP Site 976, DSDP Site 121, industrial boreholes Andaluca-G1, Alboran-A1, land-based sections from southern Spanish basins including Nijar, Sorbas and Malaga and Montemayor-1 core from the Guadalquivir Basin. The obtained results, paired with the interpretation of seismic profiles acquired in the Alboran Basin gave some new insights and results towards the better understanding of the Late Miocene to early Pliocene evolution of the Mediterranean – Atlantic gateways and the effects of the restriction on the Mediterranean environments before and after the MSC. The main outcomes of this thesis are outlined in the next paragraphs, as follows:

- A high-resolution planktonic foraminifer stratigraphy performed on Sites 976 and Montemayor-1 in combination with the analyses of the astronomically driven cyclical changes in the geochemical record enabled the astronomical tuning of the two locations. Having a firm age model allowed to pinpoint the moment when the uplift of the Gibraltar arc gateway/s started affecting the Mediterranean Basin and Betic corridor.
- The first sign of the Mediterranean – Atlantic gateway restriction is visible in the Mediterranean basin from 7.17 Ma, when active tectonism at the Gibraltar arc started uplifting the Betic and Rifian corridors. At ODP Site 976, the uplift is visible from the increase in terrigenous input arriving to the Alboran basin and parallel higher sedimentation rates related with an increased river erosion. On the other hand, the shift from benthic foraminifer open-marine high oxygen fauna to shallow infaunal taxa, tolerant to a wide range of conditions and suboptimal oxygen levels, paired with a significant drop in benthic $\delta^{13}\text{C}$ values suggests that the gateway restriction led to the decrease in bottom water oxygen levels and increase in its residence time much earlier than the onset of the MSC.
- A correlation between data from ODP Site 976 and other Mediterranean records confirmed that the 7.17 Ma gateway restriction, affected at the same time

different locations all over the Mediterranean, inferring a Mediterranean-scale change in thermohaline circulation. From these data we concluded that the West Alboran Basin (WAB) and the East Alboran Basin (EAB) were not separated by a sill at that time but were both part of the Mediterranean realm. Furthermore, it was possible to create a refined Mediterranean circulation model for before and after the 7.17 Ma event.

- The gateway restriction registered in the Mediterranean record since 7.17 Ma, is visible also from the geochemical data of Montemayor-1 core in the Guadalquivir Basin. Because the geochemical data from Montemayor-1 reveals that after 7.15-7.17 Ma, the Guadalquivir Basin was bathed by only one water mass, probably Atlantic, we believe that the connection between the Mediterranean and Atlantic through the Betic corridor was restricted at that time. Consequently, we suggest that the restriction of the last Betic gateway, the Guadalhorce Basin, could have happened at 7.15-7.17 Ma and caused the above-mentioned changes in the Mediterranean paleoenvironment.
- Because the gateway restriction was contemporaneous with the global Late Miocene Carbon Isotope Shift (LMCIS) it was important to discern between global and local effects and compare the Mediterranean and global records. Given the synchronism of the global and local Mediterranean change in the $\delta^{13}\text{C}$ record, a global effect certainly affected the Mediterranean Basin. However, opposite phase relations of the global and local $\delta^{13}\text{C}$ signals with orbital parameters, paired with a higher magnitude change identified in our WAB isotope record suggests that the local imprint overruled the global one. A similar effect can be seen in the Montemayor-1 record, where apart from the changes related to the uplift of the Gibraltar arc, a global signal cannot be overruled.
- Finally, through the development of this thesis it is shown how the dark layer often enriched in organic matter, present at the Miocene – Pliocene boundary in several Mediterranean marginal and deep basins, suggests that the Zanclean reflooding created water column stratification, and reduced bottom water oxygen levels. Such stratification could be the result of a sinking of more saline Atlantic water mass entering into a less saline Mediterranean Basin still under the influence of the Paratethys. The benthic foraminifer repopulation sequence identified at the base of the Pliocene shows similarities with more recent events of repopulation of hostile environments or following low-oxic episodes during sapropel deposition. However, Atlantic values of the benthic $\delta^{13}\text{C}$ registered in the Alboran Basin suggest that bottom water renewal and circulation were efficient during the early Zanclean, preventing the reduction of $\delta^{13}\text{C}$ at the seafloor seen after 7.17 Ma. Furthermore, the slight discrepancies in the benthic foraminifer repopulation sequences of the marginal basins at the Miocene – Pliocene boundary, and the much lighter benthic $\delta^{13}\text{C}$ values in the Malaga Basin can suggest a diachronous reflooding of the shallower marginal basins.

Chapter 1

Introduction

Chapter 1

Introduction

1. The study of marine gateways

*Sumergirse en las cosas es sumergirse en uno mismo.
Todo los demás es quedarse en la superficie.*

Eric Selt

Since the beginning of plate tectonics 2 Ga ago (Stern, 2007), the continental drift has been moving land masses creating and destroying seas, opening, and closing seaways influencing ocean circulation and climate. In the Eocene, the opening of the Drake passage between South America and Antarctica and of the Tasmanian gateway between Antarctica and Australia marked the onset of the circum-Antarctic current which induced a productivity increase and consequent sequestration of atmospheric CO₂, contributing to the global cooling and Antarctic glaciation (Scher and Martin, 2006; Scher et al., 2015). Starting from 4.6 Ma, the emergence of the Isthmus of Panama deeply affected deep ocean circulation and may be the main cause of the establishment of the north Atlantic thermohaline circulation, while in the Pliocene it contributed to the intensification of North Hemisphere glaciation (Haug and Tiedemann, 1998). Therefore, to understand the causal mechanisms behind local and global climate change in many cases is necessary to study how land and water mass distribution was modifying. Bearing this in mind, the here presented PhD thesis aims to investigate the connectivity changes between the Atlantic and the Mediterranean, by analyzing offshore and onshore locations in the proximity of the Strait of Gibraltar.

This Strait has been an item of interest that triggered human curiosity for centuries, as testified by Pliny the Elder who in his *Historia Naturalis* tells the myth about the creation of the Mediterranean Sea (Smith, 2017). The myth describes the Mediterranean as a desert that become connected to the Ocean only after Hercules, with his sword, dug an inlet between Jebel-el-Mina (Africa) and the rock of Gibraltar (Europe) allowing for the ocean water to fill the basin (Figure 1). In the last decades, and after the first DSDP expedition in the Mediterranean (Leg 13; Hsü, 1972), researchers have discovered that the peak restriction of the Mediterranean-Atlantic gateways led to the deposition of km-thick evaporite deposits 5.971 Ma ago, during the extraordinary event known as the Messinian Salinity Crises (Selli, 1964). More recently, Capella et al. (2019) even hypothesized that this event contributed to the late Miocene Global

cooling, because the absence of the Mediterranean Outflow could have modified the north Atlantic thermohaline circulation.

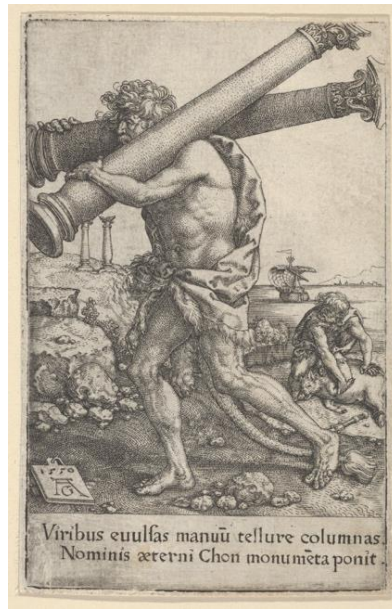


Figure 1: The Pillars of Hercules, from *The Labors of Hercules*, engraving by Heinrich Aldegrever (1550).

In this work we focus, in the first place, on the initial phases of the late Miocene Mediterranean-Atlantic gateways restriction which peak eventually lead to the Messinian Salinity Crisis. Here, apart from establishing a firm timeline and understanding the first effects that the restriction had on the West Alboran Basin (ODP Site 976), we try to understand the relation of this local event with global climate changes. In the second place, the same event is investigated in the Spanish southern margin (Montemayor-1 drill site), present day Guadalquivir Basin, and marine gateway in the late Miocene. Finally, we try to understand the dynamics of the early Pliocene reestablishment of such marine connection and what were the consequences on the marine fauna both in deep (West Alboran Basins) and Marginal basins (Malaga, Sorbas, Nijar basins).

2. Scientific background

2.1 The Mediterranean Sea today

The active Mediterranean thermohaline circulation starts when low saline Atlantic surface waters (Figure 2) enter the Mediterranean and flow northward towards the Gulf of Lions, and eastward across the Sicily Strait reaching the Eastern Mediterranean Basin (EMB). This water becomes progressively saltier

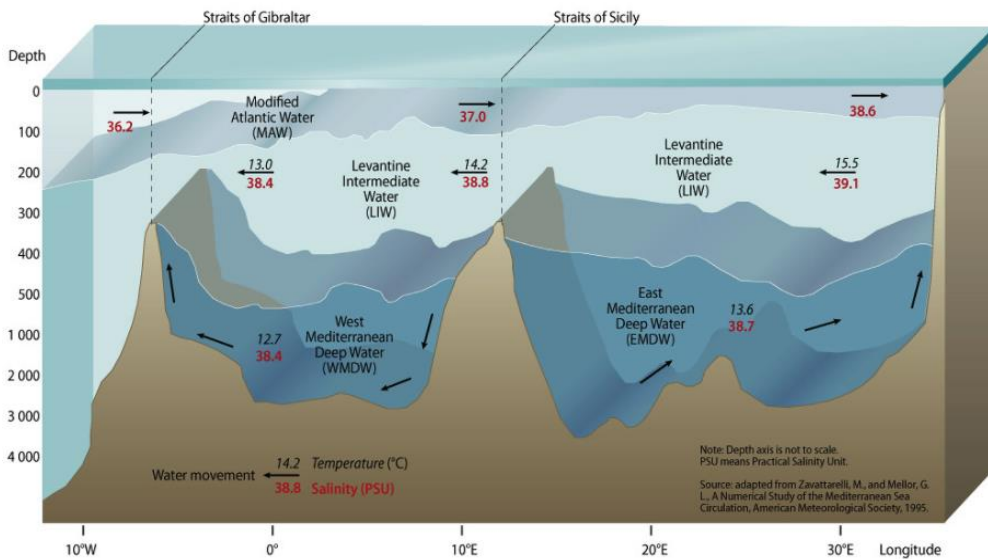


Figure 2: Vertical distribution of the main Mediterranean Sea water masses today (from GRID-Arendal, 2013).

and eventually sinks between 200 and 600 m depth in the northern Levantine basin resulting in the formation of the Levantine Intermediate Water (LIW; Zavattarelli and Mellor, 1995; Buongiorno Nardelli and Salusti, 2000; Pinardi and Masetti, 2000; Pinardi et al., 2019) and finally spreads out in the entire Mediterranean. These saltier (salinity of ~ 38.5 ‰; Rohling et al., 2015) intermediate waters are the main component of the Mediterranean Outflow Water (MOW) to the Atlantic Ocean (Pinardi and Masetti, 2000) establishing a gradient between the Mediterranean and Atlantic. This, in combination with the semi-enclosed basin configuration, where net evaporation exceeds the precipitation, drives an anti-estuarine circulation through the Strait of Gibraltar. At the same time, surface waters of the northern basins like Gulf of Lions and the Adriatic and Aegean Seas (Stommel et al., 1973; Schlitzer et al., 1991; e.g. Lascaratos et al., 1999; Powley et al., 2017), are exposed to cold northerly air

masses that through cooling and evaporation increase the surface water salinities, allowing the water to sink (e.g. Theocharis and Georgopoulos, 1993). Here, the interaction between the LIW and cold surface waters promotes deep water formation (Pinardi and Masetti, 2000) that settles below the depth of the LIW (500 – 2000 m, Figure 2) and consequently below the depth of the Gibraltar and Sicily sills in the Western and Eastern Mediterranean respectively. The renewal of such deep water masses is responsible for an efficient ventilation of the deeper parts of the basin and it can happen through two mechanisms: upward advection where the injection of new deep waters favours the release of the older water, or by upward suction of the deep water over the sill via the Bernoulli aspiration (Stommel et al., 1973). When high freshwater input stratifies the water column, upward advection becomes inexistent and deep water residence time increases promoting the deposition of organic rich sapropel layers (e.g. Rohling et al., 2015).

Due to its configuration and location on a transitional zone, the Mediterranean Basin and its surrounding lands are affected by interactions between mid-latitude and tropical processes (Giorgi and Lionello, 2008). The influence of the North African subtropical high-pressure belt and the central-northern European westerlies make the current Mediterranean summers warm and dry, and the winter mild and wet (e.g. Lolis et al., 2002). While the North Atlantic Oscillation has very little impact on the Mediterranean's climate (Josey et al., 2011), the Mediterranean climate variability is mainly influenced by the Mediterranean Oscillation and the Mediterranean Meridional Circulation. The first is responsible for the enhanced temperature see-saw in winter and spring (Lolis et al., 2002), and the second has a strong impact on the northern Mediterranean precipitation (Martin-Vide and Lopez-Bustins, 2006). The African monsoon influences indirectly the Mediterranean basin climate and circulation through the varying River Nile runoff. In particular, high Nile discharge impact the efficiency of deep-water formation and bottom water ventilation similarly as reported during sapropel formation (Rohling, 1994; Rohling et al., 2015).

2.2 Evolution of the Mediterranean – Atlantic corridors

At present, the Mediterranean is connected to the Atlantic Ocean through the narrow Strait of Gibraltar (only 13 km wide). The latter, in the late Tortonian (11.63 to 7.25 Ma), most probably did not exist, and the Mediterranean – Atlantic water exchange was happening through the Betic (Southern Spain) and Rifian (Northern Morocco) corridors (e.g. Roveri and Manzi, 2006; Flecker et al., 2015; Figure 3).

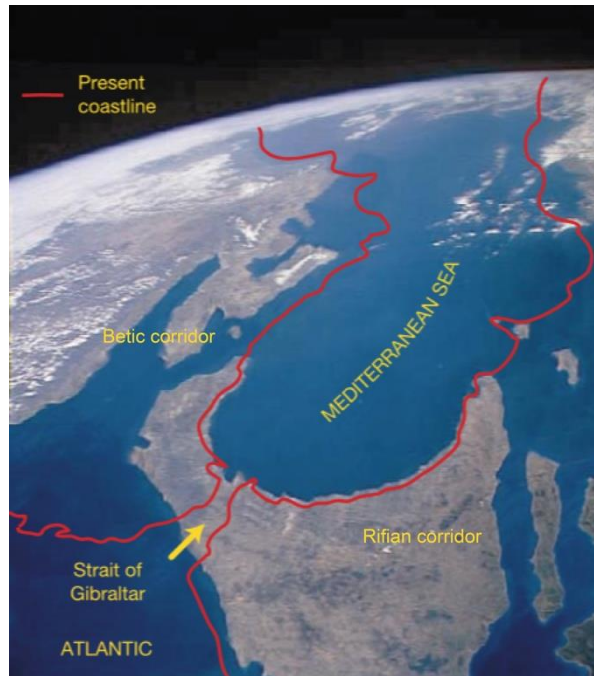


Figure 3: Map illustrating the reconstruction of the late Miocene Atlantic-Mediterranean marine gateways (modified from Duggen et al., 2003). In red the present-day coastline is shown.

The corridors, together with the Alboran Basin, are located on the collision between the African and European plates (Booth-Rea et al., 2007; Do Couto et al., 2016; Spakman et al., 2018). In the Oligocene (30-25 Ma), the plate convergence slowed down starting an E-W trench retreat and slab rollback that resulted in back-arc extension (Rosenbaum et al., 2002; Heit et al., 2017) accompanied by a westward migration of the Alboran domain (Jolivet and Faccenna, 2000; Booth-Rea et al., 2007; Soto et al., 2010; Gómez de la Peña et al., 2020). Around 8 Ma, the African-Iberian subduction zone, initially located east of the Balearic Islands (Spakman and Wortel, 2004; Vergés and Fernández, 2012; Van Hinsbergen et al., 2014), had reached its current position at the Gibraltar Arc (Booth-Rea et al., 2007; Mancilla et al., 2015; Spakman et al., 2018; Capella et al., 2020). Right after the Tortonian-Messinian boundary (7.24 Ma; Hilgen et al., 1995), the westward migration of the Alboran domain had stopped and the slab rollback decelerated (Spakman et al., 2018) initiating a slab tear starting from the eastern margin of the current Spanish southern coast which propagated to the west, reaching the Atlantic (Govers, 2009; Garcia-Castellanos and Villaseñor, 2011; Mancilla et al., 2015).

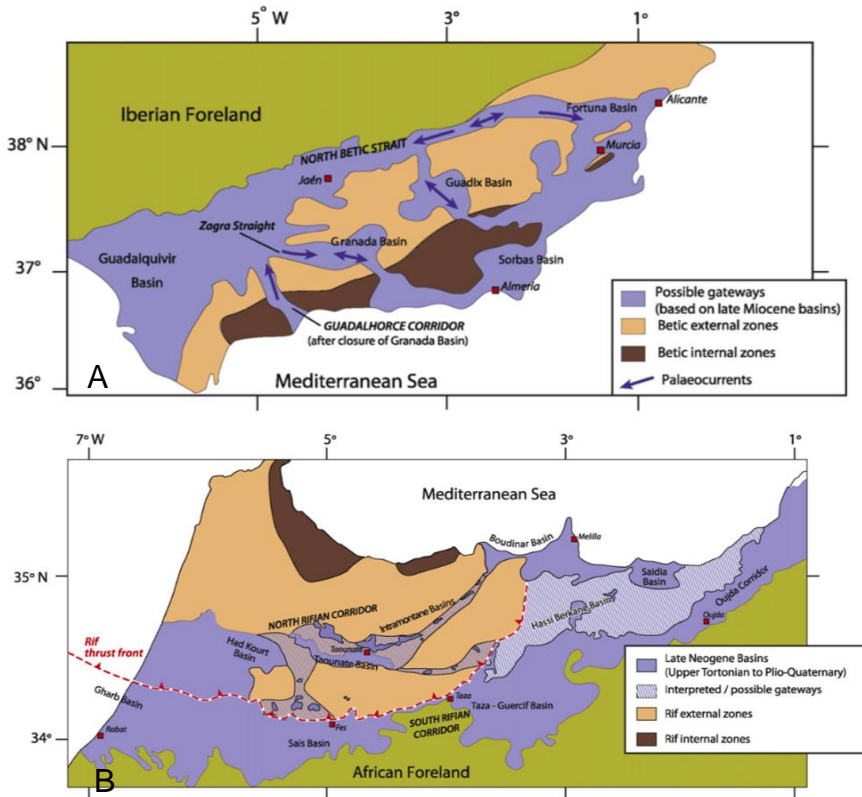


Figure 4: Maps showing the main geological units of the Betic (A) and Rifian (B) corridors (Flecker et al., 2015).

As a consequence, a dynamic topographic movement uplifted the Betics (Garcia-Castellanos and Villaseñor, 2011; Van den Berg et al., 2018; Capella et al., 2020) restricting the Betic corridor (Krijgsman et al., 1999b; Martín et al., 2014; Flecker et al., 2015; Capella et al., 2018). The age of the closure of the last connection through the Betics (Guadalhorce Corridor, Figure 4) is still debated, with ages varying between late Tortonian (~7.6 Ma; Van der Schee et al., 2018) and middle Messinian (6.18 Ma; Martín et al., 2001; Pérez-Asensio et al., 2012; Martín et al., 2014; Pérez-Asensio et al., 2014). A similar uplift occurred on the opposite Alboran coast, where the Rifian corridors were restricted by the progressive crustal thickening produced by the southern indentation of the Moroccan Margin (Fadil et al., 2006) that culminated with the complete closure of its southern strand between 7.1-6.9 Ma, while the northern sectors remained closed since 7.35-7.25 Ma (Tulbure et al., 2017; Capella et al., 2018; Figure 4). In the Mediterranean Sea sedimentological record, the first sign of gateway restriction and isolation from the global ocean have been identified at 7.17 Ma (e.g. Kouwenhoven et al., 1999; Seidenkrantz et al., 2000). From this point onward, deep sea records in the Eastern Mediterranean show a shift from open

marine and oxic to a stressed, suboxic benthic foraminifer fauna (Seidenkrantz et al., 2000; Blanc-Valleron et al., 2002; Kouwenhoven et al., 2003; Kouwenhoven et al., 2006; Di Stefano et al., 2015) while at the same time sapropel deposition becomes much more frequent (Santarelli et al., 1998; Seidenkrantz et al., 2000; Hüsing et al., 2009). A second restriction step is visible from 6.8 Ma both in the Western and Eastern Mediterranean when several proxies imply water-mass stratification and increased bottom water salinity (Kouwenhoven et al., 1999; Sierra et al., 2003; Drinia et al., 2007). The restriction eventually peaked at 5.971 Ma resulting with the extraordinary event known as the Messinian Salinity Crisis (Selli, 1964; Hsü et al., 1973; Selli, 1973). According to most authors (Krijgsman et al., 1999a; Hodell et al., 2001; e.g. Govers, 2009), it was the progressive closure of the Betic and Rifian gateways that led to this environmental crisis. Nonetheless, recent studies suggest that in concomitance with the restriction of these corridors, a proto-Gibraltar Strait was taking over, at least to some extent, the Mediterranean-Atlantic connection as suggested by different authors (Capella et al., 2018; Krijgsman et al., 2018; Capella et al., 2020) which propose that a dynamic subsidence may have affected the Gibraltar Arc during the slab-sinking especially after its steepening at around 8 Ma (Krijgsman et al., 2018).

2.3. Messinian Salinity Crisis and Zanclean reflooding

In 1970, during the first Deep Sea Drilling Project (DSDP) Mediterranean Sea Leg (Leg 13) one of the most exciting scientific discoveries regarding the Mediterranean Sea evolution took place when a basin-wide Messinian evaporitic deposit was discovered buried beneath the deep-sea Pliocene sediments (Figure 5). Since then, a 50 yearlong heated debate started regarding

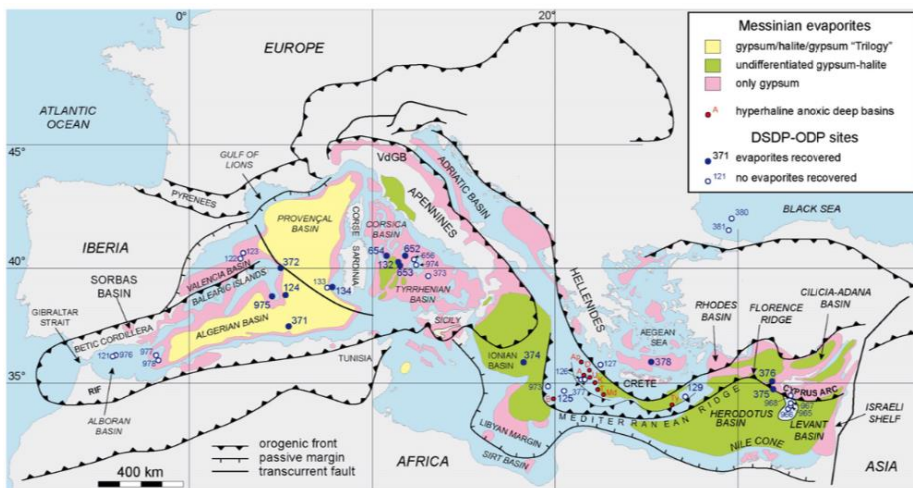


Figure 5: Distribution of Messinian evaporites and location of the DSDP-ODP boreholes which recovered Messinian deposits (Roveri et al., 2014).

the possible conditions, paleoenvironments and timing of these deposits, associated with the Messinian Salinity Crisis (MSC; Selli, 1954; Selli, 1964).

Historically, three different basin configurations (Schmalz, 1991; Nichols, 2009; Figure 6) are considered as possible causes of the MSC, all of them implied some degree of restriction of the Mediterranean-Atlantic connection: (1) a complete dissection model/shallow water to deep basin setting (Hsü et al., 1973; Figure 6A), (2) the tectonic model/shallow water-shallow basin (Nesteroff, 1973; Selli, 1985; Figure 6B) and the (3) deep-basin model/deep water-deep basin Selli (1973; Figure 6C).

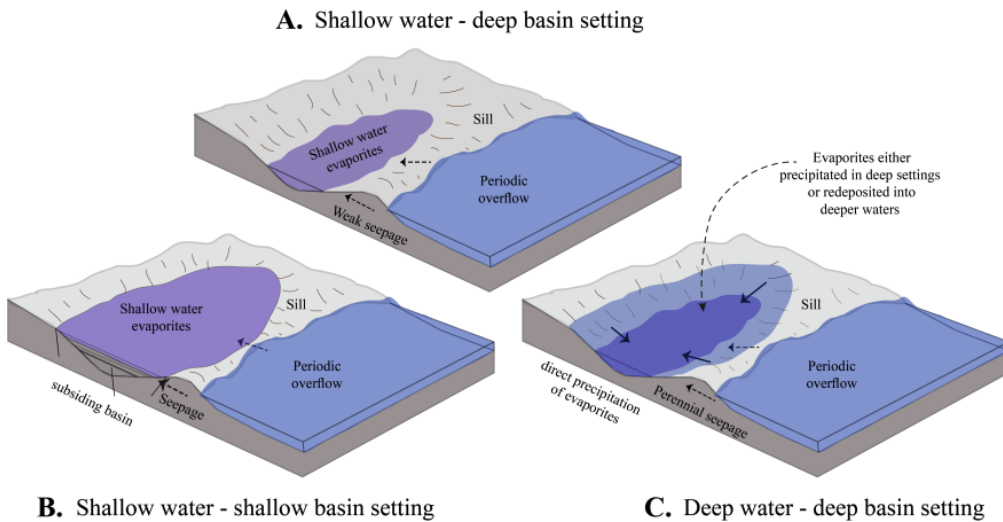


Figure 6: Conceptual models that attempted to explain the depositional mechanism of the Messinian evaporites in the Mediterranean. A) Shallow water – deep basin setting; B) Shallow water – shallow basin setting and C) Deep water – deep basin setting. Diagrams modified after (Nichols, 2009; Ochoa, 2016).

The first stipulated theory, shallow water to deep basin (Hsü et al., 1973), is the one picturing an initially full Mediterranean, repeatedly isolated and evaporated (Schmalz, 1991) until its complete desiccation (Garcia-Castellanos et al., 2009; Cornée et al., 2016), and isolation from the global ocean by a land bridge between Africa and Iberia (García-Alix et al., 2016). In this scenario, the re-establishment of marine conditions is abrupt and fast, lasting only some decades or less (Blanc, 2006; Garcia-Castellanos et al., 2009) and is thought to be caused by the triumph of erosion at the Gibraltar sill by incising the Zanclean channel on the Alboran Sea floor (Estrada et al., 2011). On the other hand, different studies show that marine conditions couldn't return instantaneously and suppose that the connectivity increased gradually (Iaccarino et al., 1999; Pierre et al., 2006) or at least that the faunal response wasn't instantaneous.

An opposite scenario (deep basin model; Selli, 1973), postulates a restricted basin subject to a minimal sea-level lowering (not more than 400 m; Krijgsman and Meijer, 2008) and evaporite deposition in a deep basin environment where surficial inflow of Atlantic waters continued, but outflow was obstructed. In this case, the reflooding is gradual and the Atlantic inflow progressively erodes the sill (Loget et al., 2005), increasing its dimensions and the Mediterranean-Atlantic connectivity.

One last less catastrophic setting, shallow water-shallow basin, describes an intermediate base-level drawdown and the dominance of tectonic vertical movement (Nesteroff, 1973; Selli, 1985) which could lead to different phases of re-connection, or as theorized most recently, different reflooding steps after the initial basin isolation (Clauzon et al., 2005; Estrada et al., 2011; Bache et al., 2012).

In spite of the different proposed scenarios for the MSC, and the realization that up to this moment there are no incontrovertible evidence for supporting unequivocally one of these models, a general consensus has been reached (CIESM, 2008; Roveri et al., 2014) naming the different MSC stages and deposits. In Roveri et al. (2014) we find that the MSC developed in three main stages (Figure 7) differing respectively because of different paleoenvironmental conditions and connectivity with the Atlantic and Paratethys, where the evaporite precipitation is diachronous in marginal (depth range from 0-200 m and 200-1000) and deep basins (water depth >1000 m). During the first stage,

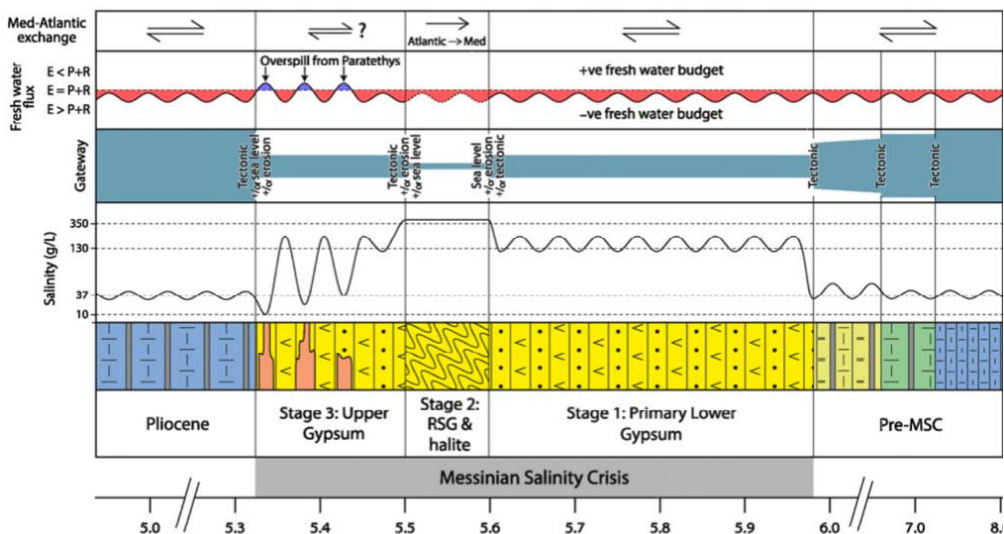


Figure 7: figure showing the main features of the Mediterranean's exchange history in the late Miocene – early Pliocene including lithology, Mediterranean salinity, gateway with the probable drivers (tectonics, erosion, sea level) of changing dimensions and the Mediterranean's fresh water flux where E = evaporation, P = precipitation and R = river discharge (from Flecker et al., 2015).

comprised between 5.97 and 5.6 Ma (Stage 1, Lower Evaporites), evaporite precipitated in the shallow sub basins. The peak of the MSC followed and lasted until 5.55 Ma (Stage 2; Reworked Primary Gypsum and halite), when the deepest basins become the place of evaporite deposition. The third and final phase begins with Upper evaporite accumulation (Stage 3.1 or p-ev1) followed by the deposition of brackish-water sediments that characterize the Lago-Mare facies (Stage 3.2 or p-ev2), formed due to freshwater inputs from the Paratethys (e.g. Roveri et al., 2008; Stoica et al., 2016).

2.4. Relationship between the Miocene - Pliocene global climate and a changing Mediterranean

The Miocene epoch is characterized by numerous changes in climate conditions and environments, often linked with paleogeographic reorganization of land and sea masses.

The Oligo-Miocene closure of the Tethys Ocean and the formation of the proto-Mediterranean (Figure 8) caused a significant reorganization of the oceanic circulation and climate patterns both on local and global scale (Torfstein and Steinberg, 2020). With the closure of the Indian Ocean - Mediterranean Seaway (early-middle Miocene) increased oceanic productivity has been registered in the Levant Basin (Torfstein and Steinberg, 2020) while on a global scale, the Mid-Miocene Climate Optimum (17 - 14.55 Ma) was observed as primary productivity rates increased globally (Zachos et al., 2001; McQuarrie and van Hinsbergen, 2013). During this phase, Antarctic ice volume expansion was minor and characterized by 100 kyr and 400 kyr eccentricity cycles (Baldassini et al., 2021). Afterwards a change from high to low eccentricity and the increase in obliquity variability (Holbourn et al., 2007) led to the Middle Miocene Climatic Transition (14.55 - 13.75 Ma) when the marine environments got warmer and more eutrophic followed by a cold phase (Icehouse Mode; from

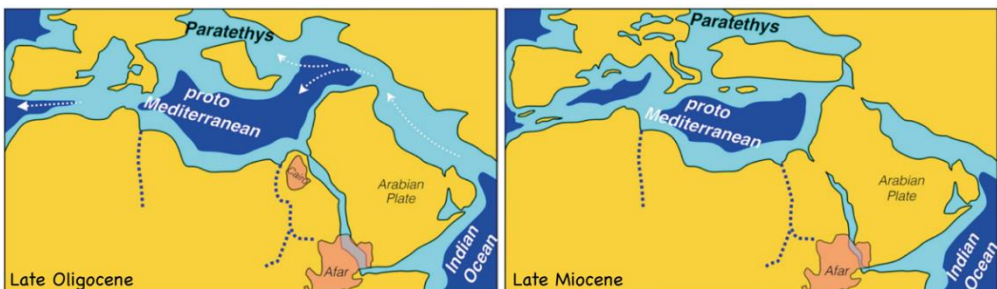


Figure 8: Paleogeographic reconstructions of the proto-Mediterranean basin in the late Oligocene and late Miocene showing the closure of the Indian Ocean - Mediterranean Seaway (modified from Torfstein and Steinberg, 2020).

13.75 Ma) related to the Antarctic ice sheet expansion and associated with a 1.2 Ma obliquity node that followed the low eccentricity phase (Zachos et al., 2001; Holbourn et al., 2007; Baldassini et al., 2021). Nonetheless, one of the most radical changes that affected terrestrial environments and ecosystems is the Late Miocene Carbon Isotope Shift (e.g. Herbert et al., 2016; LMCIS), when between 7.8 and 6.7 Ma (e.g., Hodell et al., 1994; Hodell and Venz-Curtis, 2006; Holbourn et al., 2018), a global decrease in sea surface temperatures of about 6°C has been reconstructed (Tzanova et al., 2015; Herbert et al., 2016) coeval with decreasing $\delta^{13}\text{C}$ values (Hodell et al., 2001; Drury et al., 2018). The LMCIS coincides with one of the most spectacular landscape changes that came from the expansion of C_4 grasslands, that for the bigger part replaced C_3 plant ecosystems (Blondel et al., 2010; Edwards et al., 2010; Pound et al., 2012), while at the same time, the Sahara Desert become established (Schuster, 2006; Zhang et al., 2014). This large-scale shifts in landscape and vegetation coverage lead to major turnovers in terrestrial fauna as well, favoring the proliferation of browsers feeders that fed on grasses and shrubs (Wang et al., 1994; Douady et al., 2003). This vegetation shift may have be one of the causes of the LMCIS, because it may have led to an increase flux of ^{12}C -enriched material into the ocean (Pagani et al., 1999) and it could have altered the ^{12}C fractionation coefficient into marine organic matter driving a permanent excursion of the ocean $\delta^{13}\text{C}_{\text{DIC}}$ (Kump and Arthur, 1999). These changes lead to the aridification of the circum Mediterranean area (e.g. Novello et al., 2015) as well. Because the onset of the LMCIS is contemporaneous with the first signs of Mediterranean-Atlantic gateway at ~7.2 Ma (e.g. Kouwenhoven et al., 1999), some authors (Zhang et al., 2014; Capella et al., 2019) proposed that it was the progressive Mediterranean isolation who preconditioned the global Late Miocene cooling favoring the ocean – atmospheric CO_2 decoupling. Several other studies focused on the possible effect on global climate of the peak Mediterranean -Atlantic restriction during the MSC. Modelling studies by Ivanovic et al. (2014) found that changes in Mediterranean outflow could in fact change the ocean circulation in the North Atlantic and alter surface air temperatures, while Sun and Liu (2006) suggest that the MSC reduced world ocean salinity by 6%, enabling sea-ice formation at higher latitudes. That desiccating the Mediterranean sea would impact sea ice formation in the Northern Hemisphere has been modelled by Murphy et al. (2009) as well.

The Pliocene, on the other hand was characterized by an amelioration of climatic condition as it is dominated by a warm/temperate and more humid climate (Bertini, 1994) at least in the Northern sectors of the Mediterranean area (Fauquette et al., 1999; Bertini and Martinetto, 2011). Accordingly, around 5.3 Ma, the sedimentary record from the Guadalquivir basin (Montemayor-1 well: Jiménez-Moreno et al., 2013), registers maximal values in *Quercus* pollen remains, typical of Mediterranean forest conditions.

3. Rational for this study

3.1. MSC in the proximity of Gibraltar

To validate any of the above mentioned MSC and Zanclean reflooding theories, it is fundamental to understand the Mediterranean-Atlantic connectivity and therefore the evolution of the Gibraltar strait gateway(s), which opening is considered to be the main cause for the re-establishment of open marine conditions after the MSC. In this optic, of particular interest are the areas close to the Gibraltar arch like the Alboran Basin, the Southern Spanish, and Northern Moroccan marginal basins, which sediments could reflect accurately the changes in the Mediterranean environments before, during and after the MSC.

The West Alboran Basin record could contain valuable information regarding changes in the Mediterranean-Atlantic gateway efficiency, sea level changes and circulation during the early Messinian to early Pliocene interval. Because still insufficiently studied, the existing information are on many occasions contradictory and hardly correlatable to what found in the rest of the Mediterranean. For example, even if the Alboran Sea is considered to be a deep basin (>1000 m water depth; Roveri et al., 2014), no evaporites have been found, and the only sediments related to the MSC are a chaotic mass transport deposits (MTD-CU) with gypsum fragments identified in boreholes offshore the Spanish southern coast (Martínez del Olmo and Comas, 2008; del Olmo and Martín, 2016; Lofi, 2018) interpreted as the product of rapid sea level drawdown at the MSC onset (Cameselle and Urgeles, 2016). Why evaporites are absent in the Alboran Basin it is still not completely clear. According to Garcia-Castellanos et al. (2019) the 390 km-long channel identified spreading from gulf of Cadiz to the Algerian basin is the subaqueous expression of the Zanclean re-flooding and breaching of Gibraltar strait. This intense erosion could have transported a big volume of bedrock (500 km³) and sediment (including MSC evaporites) deriving from Gibraltar strait and Alboran Basin (Garcia-Castellanos et al., 2009) eastward, where it could have been deposited. Yet, up to now, such flood deposit have not been identified (Estrada et al., 2011) apart from some possible megabar deposits found in the proximity of the ODP Site 978 (Garcia-Castellanos et al., 2019; Perriñez et al., 2019). Finally, another theory regarding the Mediterranean-Atlantic connectivity is waiting to be better understood. According to García-Alix et al. (2016) and Booth-Rea et al. (2018) the volcanic arch separating the Eastern (EAB) and Western Alboran basin (WAB) could have acted as an alternative gateway to the Gibraltar strait making the WAB part of the Atlantic realm. To disentangle some of these issues and hopefully to obtain some new insights on the Mediterranean - Atlantic connectivity

dynamics during the late Miocene and early Pliocene, in this thesis several West Alboran Basin cores (ODP Site 976, DSDP Site 121, industrial boreholes Andaluca G1 and Alboran A1), Atlantic drill hole (Montemayor-1) and Spanish peri-Mediterranean Basins (Malaga, Nijar and Sorbas basins) outcrops have been studied (Figure 10). Analyzing sediments from the deep basins of both the Atlantic and Mediterranean side gave new insights about the change in Mediterranean-Atlantic connectivity and gateways dynamics before the MSC onset, while the marginal areas were particularly valuable for extracting information regarding the early Pliocene sediment infilling and paleogeographic conditions.

3.2 Saltgiant project

Saltgiant is a project funded by the European Union as part of a Marie Curie European Training Network that started in 2018 aimed to disentangle the formation of one of the largest salt deposits on Earth: The Mediterranean Salt Giant. The project is composed of four working packages (WP, Figure 9) that

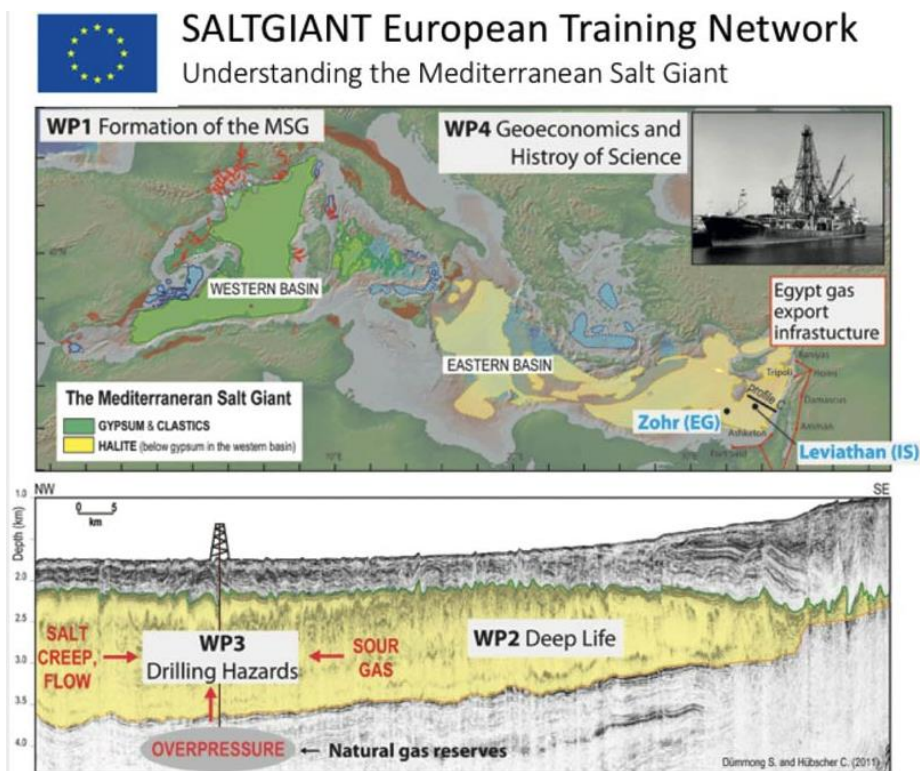


Figure 9: Summary of the Saltgiant project four Work Packages (<https://www.saltgiant-etn.com/research/>).

together form a multidisciplinary network of scientists located in 30 different academic organization around the Mediterranean. The Saltgiant team includes 15 PhD students specialized in different fields from earth science, biology to history and economy that by working together tried to reconstruct into detail the paleogeographic, geochemical and environmental condition necessary to form this km-thick evaporite deposit (WP1) as well as its implications for sub-seafloor microbial life (WP2), risk assessment in the oil industry (WP3), geoeconomics of the Mediterranean region and the history of oceanography (WP4). This doctoral dissertation is part of WP1.

3.3 Research questions and thesis structure

The aims of this PhD are to understand how the Mediterranean - Atlantic connectivity changes affected the Mediterranean environments before and after the MSC and what is the causal mechanism between such paleogeographic variations and global and local climate variability and climate system sensitivity. These goals are summarized through a set of objectives, reported below in form of Research Questions:

1. Which are the evidences of gateway restriction and base level change in the Mediterranean areas most proximal to the Gibraltar arc (West Alboran Basin)?
 - a. When did the first restriction of the Atlantic - Mediterranean gateway happen?
 - b. What were the causes of such restriction?
 - c. Are there any facies related with the MSC that can be found in the Alboran Basin?
 - d. Is it possible to estimate the hiatus produced by the Zanclean reflooding?

These questions have been addressed in Chapter 3 by analyzing into detail the micropaleontological and geochemical content of West Alboran Basin ODP Site 976, DSDP Site 121 and industrial boreholes And-G1 and Alb-A1. In addition, seismic sections available in the same area were used to assess hiatuses and the aspect of the different Messinian facies.

2. How did the first Mediterranean - Atlantic restriction event affect the Mediterranean Marine environments?
 - a. Where was the gateway located?
 - b. Was this event coeval both in the Western and Eastern Mediterranean?
 - c. What was the causal mechanism between the paleogeographic changes in the Mediterranean and global climate changes?

These questions are addressed in Chapter 4 where the changes in the Mediterranean marine environments and circulation patterns are assessed through a study of benthic foraminifer distribution and stable isotope curves from ODP Site 976.

3. Was the isolation of the Mediterranean triggered by a gateway located in the Betic corridor?
 - a. Did the first signs of restriction of the Mediterranean-Atlantic gateway happened because of the definite disconnection of the Guadalhorce corridor?
 - b. If so, when did the Guadalhorce corridor definitely close?
 - c. What were the consequences on the closure of the corridor in the Guadalquivir Basin?

These questions have been addressed in Chapter 5, where the timing of closure of the Guadalhorce corridor is obtained through geochemical data and distribution of planktic foraminifers from the Montemayor-1 core.

4. How did the Zanclean reflooding of the Mediterranean affect marine environments and fauna?
 - a. Which benthic foraminifer species thrived after the re-establishment of an efficient Mediterranean-Atlantic connection?
 - b. What was the sedimentological response to the reflooding in deep and marginal basins?
 - c. Was the reflooding synchronous all over the Mediterranean?
 - d. What was the depth of the deep and marginal basin at the Miocene-Pliocene boundary?

These last set of issues have been tackled in Chapter 6 through the benthic foraminifer and stable isotope analyses of early Pliocene outcrops located in the Sorbas, Nijar and Malaga Basin (southern Spain).

References

- Bache, F., Popescu, S. M., Rabineau, M., Gorini, C., Suc, J. P., Clauzon, G., Olivet, J. L., Rubino, J. L., Melinte-Dobrinescu, M. C., Estrada, F., Londeix, L., Armijo, R., Meyer, B., Jolivet, L., Jouannic, G., Leroux, E., Aslanian, D., Reis, A. T. D., Mocochain, L., Dumurdžanov, N., Zagorchev, I., Lesić, V., Tomić, D., Namik Çağatay, M., Brun, J. P., Sokoutis, D., Csato, I., Uçarkus, G. and Çakir, Z., 2012. A two-step process for the reflooding of the Mediterranean after the Messinian Salinity Crisis. *Basin Research*, 24(2): 125-153.

- Baldassini, N., Foresi, L. M., Lirer, F., Sprovieri, M., Turco, E., Pelosi, N. and Di Stefano, A., 2021. Middle Miocene stepwise climate evolution in the Mediterranean region through high-resolution stable isotopes and calcareous plankton records. *Marine Micropaleontology*, 167: 102030.
- Bertini, A., 1994. Messinian-Zanclean vegetation and climate in north-central Italy. *Historical Biology*, 9(1-2): 3-10.
- Bertini, A. and Martinetto, E., 2011. Reconstruction of vegetation transects for the Messinian–Piacenzian of Italy by means of comparative analysis of pollen, leaf and carpological records. *Palaeogeography, Palaeoclimatology, Palaeoecology*, 304(3-4): 230-246.
- Blanc, P.-L., 2006. Improved modelling of the Messinian Salinity Crisis and conceptual implications. *Palaeogeography, Palaeoclimatology, Palaeoecology*, 238(1-4): 349-372.
- Blanc-Valleron, M.-M., Pierre, C., Caulet, J., Caruso, A., Rouchy, J.-M., Cespuglio, G., Sprovieri, R., Pestrea, S. and Di Stefano, E., 2002. Sedimentary, stable isotope and micropaleontological records of paleoceanographic change in the Messinian Tripoli Formation (Sicily, Italy). *Palaeogeography, Palaeoclimatology, Palaeoecology*, 185(3-4): 255-286.
- Blondel, C., Merceron, G., Andossa, L., Taisso, M. H., Vignaud, P. and Brunet, M., 2010. Dental mesowear analysis of the late Miocene Bovidae from Toros-Menalla (Chad) and early hominid habitats in Central Africa. *Palaeogeography, Palaeoclimatology, Palaeoecology*, 292(1-2): 184-191.
- Booth-Rea, G., Ranero, C. R. and Grevemeyer, I., 2018. The Alboran volcanic-arc modulated the Messinian faunal exchange and salinity crisis. *Scientific reports*, 8(1): 13015.
- Booth-Rea, G., Ranero, C. R., Martínez-Martínez, J. M. and Grevemeyer, I., 2007. Crustal types and Tertiary tectonic evolution of the Alborán sea, western Mediterranean. *Geochemistry, Geophysics, Geosystems*, 8(10).
- Buongiorno Nardelli, B. and Salusti, E., 2000. On dense water formation criteria and their application to the Mediterranean Sea. *Deep Sea Research Part I: Oceanographic Research Papers*, 47(2): 193-221.
- Cameselle, A. L. and Urgeles, R., 2016. Large-scale margin collapse during Messinian early sea-level drawdown: the SW Valencia trough, NW Mediterranean. *Basin Research*, 29: 576-595.
- Capella, W., Barhoun, N., Flecker, R., Hilgen, F., Kouwenhoven, T., Matenco, L., Sierro, F. J., Tulbure, M., Yousfi, M. Z. and Krijgsman, W., 2018. Palaeogeographic evolution of the late Miocene Rifian Corridor (Morocco): reconstructions from surface and subsurface data. *Earth-Science Reviews*, 180: 37-59.
- Capella, W., Flecker, R., Hernández-Molina, F. J., Simon, D., Meijer, P. T., Rogerson, M., Sierro, F. J. and Krijgsman, W., 2019. Mediterranean isolation preconditioning the Earth System for late Miocene climate cooling. *Scientific Reports*, 9(1).

-
- Capella, W., Spakman, W., van Hinsbergen, D. J., Chertova, M. V. and Krijgsman, W., 2020. Mantle resistance against Gibraltar slab dragging as a key cause of the Messinian Salinity Crisis. *Terra Nova*, 32(2): 141-150.
- CIESM, 2008. The Messinian Salinity Crisis from mega-deposits tomicrobiology - A consensus report. N° 33 in CIESM Workshop Monographs[F. Briand, Ed.],168 pages, Monaco.
- Clauzon, G., Suc, J.-P., Popescu, S.-M., Marunteanu, M., Rubino, J.-L., Marinescu, F. and Melinte, M. C., 2005. Influence of Mediterranean sea-level changes on the Dacic Basin (Eastern Paratethys) during the late Neogene: the Mediterranean Lago Mare facies deciphered. *Basin Research*, 17(3): 437-462.
- Cornée, J.-J., Münch, P., Achalhi, M., Merzeraud, G., Azdimousa, A., Quillévéré, F., Melinte-Dobrinescu, M., Chaix, C., Moussa, A. B. and Lofi, J., 2016. The Messinian erosional surface and early Pliocene reflooding in the Alboran Sea: New insights from the Boudinar basin, Morocco. *Sedimentary geology*, 333: 115-129.
- del Olmo, W. M. and Martín, D., 2016. The Messinian record of Spanish onshore and offshore data (Atlantic Ocean and Western Mediterranean Sea). *Petroleum Geoscience*, 22(4): 291-296.
- Di Stefano, A., Baldassini, N. and Alberico, I., 2015. Surface-water conditions in the Mediterranean Basin during earliest Pliocene as revealed by calcareous nannofossil assemblages: Comparison between western and eastern sectors. *Palaeogeography, Palaeoclimatology, Palaeoecology*, 440: 283-296.
- Do Couto, D., Gorini, C., Jolivet, L., Le Bret, N., Augier, R., Gumiaux, C., d'Acremont, E., Ammar, A., Jabour, H. and Auxietre, J.-L., 2016. Tectonic and stratigraphic evolution of the Western Alboran Sea Basin in the last 25 Myrs. *Tectonophysics*, 677: 280-311.
- Douady, C. J., Catzefflis, F., Raman, J., Springer, M. S. and Stanhope, M. J., 2003. The Sahara as a vicariant agent, and the role of Miocene climatic events, in the diversification of the mammalian order Macroscelidea (elephant shrews). *Proceedings of the National Academy of Sciences*, 100(14): 8325-8330.
- Drinia, H., Antonarakou, A., Tsaparas, N. and Kontakiotis, G., 2007. Palaeoenvironmental conditions preceding the Messinian Salinity Crisis: A case study from Gavdos Island. *Geobios*, 40(3): 251-265.
- Drury, A. J., Westerhold, T., Hodell, D. and Röhl, U., 2018. Reinforcing the North Atlantic backbone: revision and extension of the composite splice at ODP Site 982. *Climate of the Past*, 14(3): 321-338.
- Duggen, S., Hoernle, K., Van den Bogaard, P., Rüpke, L. and Morgan, J. P., 2003. Deep roots of the Messinian salinity crisis. *Nature*, 422(6932): 602-606.
- Edwards, E. J., Osborne, C. P., Strömberg, C. A., Smith, S. A. and Consortium, C. G., 2010. The origins of C4 grasslands: integrating evolutionary and ecosystem science. *Science*, 328(5978): 587-591.

- Estrada, F., Ercilla, G., Gorini, C., Alonso, B., Vázquez, J. T., García-Castellanos, D., Juan, C., Maldonado, A., Ammar, A. and Elabbassi, M., 2011. Impact of pulsed Atlantic water inflow into the Alboran Basin at the time of the Zanclean flooding. *Geo-Marine Letters*, 31(5-6), pp.361-376., 31(5-6), pp.361-376.: pp.361-376.
- Fadil, A., Vernant, P., McClusky, S., Reilinger, R., Gomez, F., Ben Sari, D., Mourabit, T., Feigl, K. and Barazangi, M., 2006. Active tectonics of the western Mediterranean: Geodetic evidence for rollback of a delaminated subcontinental lithospheric slab beneath the Rif Mountains, Morocco. *Geology*, 34(7): 529-532.
- Fauquette, S., Suc, J.-P., Guiot, J., Diniz, F., Feddi, N., Zheng, Z., Bessais, E. and Drivaliari, A., 1999. Climate and biomes in the West Mediterranean area during the Pliocene. *Palaeogeography, Palaeoclimatology, Palaeoecology*, 152(1-2): 15-36.
- Flecker, R., Krijgsman, W., Capella, W., De Castro Martins, C., Dmitrieva, E., Mayser, J. P., Marzocchi, A., Modestou, S., Ochoa, D., Simon, D., Tulbure, M., Van Den Berg, B., Van Der Schee, M., De Lange, G., Ellam, R., Govers, R., Gutjahr, M., Hilgen, F., Kouwenhoven, T., Lofi, J., Meijer, P., Sierro, F. J., Bachiri, N., Barhoun, N., Alami, A. C., Chacon, B., Flores, J. A., Gregory, J., Howard, J., Lunt, D., Ochoa, M., Pancost, R., Vincent, S. and Yousfi, M. Z., 2015. Evolution of the Late Miocene Mediterranean–Atlantic gateways and their impact on regional and global environmental change. *Earth-Science Reviews*, 150: 365-392.
- García-Castellanos, D., Estrada, F., Jiménez-Munt, I., Gorini, C., Fernández, M., Vergés, J. and De Vicente, R., 2009. Catastrophic flood of the Mediterranean after the Messinian salinity crisis. *Nature*, 462(7274): 778.
- García-Castellanos, D. and Villaseñor, A., 2011. Messinian salinity crisis regulated by competing tectonics and erosion at the Gibraltar arc. *Nature*, 480(7377): 359.
- García-Castellanos, D., Micallef, A., Estrada, F., Camerlenghi, A., Ercilla, G., Periáñez, R. and Abril, J. M., 2019. The Zanclean megaflood of the Mediterranean—Searching for additional evidence. *Earth-Science Reviews*: 103061.
- García-Alix, A., Minwer-Barakat, R., Martín Suárez, E., Freudenthal, M., Aguirre, J. and Kaya, F., 2016. Updating the Europe–Africa small mammal exchange during the late Messinian. *Journal of Biogeography*, 43(7): 1336-1348.
- Giorgi, F. and Lionello, P., 2008. Climate change projections for the Mediterranean region. *Global and planetary change*, 63(2-3): 90-104.
- Gómez de la Peña, L., Ranero, C. R., Gràcia, E. and Booth-Rea, G., 2020. The evolution of the westernmost Mediterranean basins. *Earth-Science Reviews*: 103445.
- Govers, R., 2009. Choking the Mediterranean to dehydration: the Messinian salinity crisis. *Geology*, 37(2): 167-170.
- GRID-Arendal, 2013. In *State of the Mediterranean Marine and Coastal Environment*.
- Haug, G. H. and Tiedemann, R., 1998. Effect of the formation of the Isthmus of Panama on Atlantic Ocean thermohaline circulation. *Nature*, 393(6686): 673-676.

-
- Heit, B., Mancilla, F. d. L., Yuan, X., Morales, J., Stich, D., Martín, R. and Molina-Aguilera, A., 2017. Tearing of the mantle lithosphere along the intermediate-depth seismicity zone beneath the Gibraltar Arc: The onset of lithospheric delamination. *Geophysical Research Letters*, 44(9): 4027-4035.
- Herbert, T. D., Lawrence, K. T., Tzanova, A., Peterson, L. C., Caballero-Gill, R. and Kelly, C. S., 2016. Late Miocene global cooling and the rise of modern ecosystems. *Nature Geoscience*, 9(11): 843-847.
- Hilgen, F., Krijgsman, W., Langereis, C., Lourens, L., Santarelli, A. and Zachariasse, W., 1995. Extending the astronomical (polarity) time scale into the Miocene. *Earth and Planetary Science Letters*, 136: 495-510.
- Hodell, D. A., Benson, R. H., Kent, D. V., Boersma, A. and Rakic-El Bied, K., 1994. Magnetostratigraphic, biostratigraphic, and stable isotope stratigraphy of an Upper Miocene drill core from the Salé Briqueterie (northwestern Morocco): A high-resolution chronology for the Messinian stage. *Paleoceanography*, 9(6): 835-855.
- Hodell, D. A., Curtis, J. H., Sierro, F. J. and Raymo, M. E., 2001. Correlation of late Miocene to early Pliocene sequences between the Mediterranean and North Atlantic. *Paleoceanography*, 16(2): 164-178.
- Hodell, D. A. and Venz-Curtis, K. A., 2006. Late Neogene history of deepwater ventilation in the Southern Ocean. *Geochemistry, Geophysics, Geosystems*, 7(9).
- Holbourn, A., Kuhnt, W., Schulz, M., Flores, J.-A. and Andersen, N., 2007. Orbitally-paced climate evolution during the middle Miocene "Monterey" carbon-isotope excursion. *Earth and Planetary Science Letters*, 261(3-4): 534-550.
- Holbourn, A. E., Kuhnt, W., Clemens, S. C., Kochhann, K. G., Jöhnck, J., Lübbers, J. and Andersen, N., 2018. Late Miocene climate cooling and intensification of southeast Asian winter monsoon. *Nature communications*, 9(1): 1-13.
- Hsü, K. J., 1972. Origin of saline giants: A critical review after the discovery of the Mediterranean Evaporite. *Earth Science Reviews*, 8(4): 371-396.
- Hsü, K. J., Ryan, W. B. F. and Cita, M. B., 1973. Late miocene desiccation of the mediterranean. *Nature*, 242(5395): 240-244.
- Hüsing, S., Kuiper, K., Link, W., Hilgen, F. J. and Krijgsman, W., 2009. The upper Tortonian-lower Messinian at Monte dei Corvi (Northern Apennines, Italy): completing a Mediterranean reference section for the Tortonian stage. *Earth and Planetary Science Letters*, 282(1-4): 140-157.
- Iaccarino, S. M., Cita, M. B., Gaboardi, S. and Gruppini, G. M., 1999. 15. High-Resolution Biostratigraphy at the Miocene/Pliocene boundary in Holes 974b and 975b, Western Mediterranean1 In *Proceedings of the Ocean Drilling Program: Scientific results Vol. 161*: p. 197.

- Ivanovic, R. F., Valdes, P. J., Flecker, R. and Gutjahr, M., 2014. Modelling global-scale climate impacts of the late Miocene Messinian Salinity Crisis. *Climate of the Past*, 10(2): 607-622.
- Jiménez-Moreno, G., Pérez-Asensio, J. N., Larrasoaña, J. C., Aguirre, J., Civis, J., Rivas-Carballo, M. R., Valle-Hernández, M. F. and González-Delgado, J. A., 2013. Vegetation, sea-level, and climate changes during the Messinian salinity crisis. *Bulletin*, 125(3-4): 432-444.
- Jolivet, L. and Faccenna, C., 2000. Mediterranean extension and the Africa-Eurasia collision. *Tectonics*, 19(6): 1095-1106.
- Josey, S. A., Somot, S. and Tsimplis, M., 2011. Impacts of atmospheric modes of variability on Mediterranean Sea surface heat exchange. *Journal of Geophysical Research: Oceans*, 116(C2).
- Kouwenhoven, T., Seidenkrantz, M.-S. and Van der Zwaan, G., 1999. Deep-water changes: the near-synchronous disappearance of a group of benthic foraminifera from the Late Miocene Mediterranean. *Palaeogeography, Palaeoclimatology, Palaeoecology*, 152(3-4): 259-281.
- Kouwenhoven, T., Morigi, C., Negri, A., Giunta, S., Krijgsman, W. and Rouchy, J.-M., 2006. Paleoenvironmental evolution of the eastern Mediterranean during the Messinian: Constraints from integrated microfossil data of the Pissouri Basin (Cyprus). *Marine Micropaleontology*, 60(1): 17-44.
- Kouwenhoven, T. J., Hilgen, F. J. and Van Der Zwaan, G. J., 2003. Late Tortonian–early Messinian stepwise disruption of the Mediterranean–Atlantic connections: constraints from benthic foraminiferal and geochemical data. *Palaeogeography, Palaeoclimatology, Palaeoecology*, 198(3-4): 303-319.
- Krijgsman, W., Hilgen, F., Raffi, I., Sierro, F. J. and Wilson, D., 1999a. Chronology, causes and progression of the Messinian salinity crisis. *Nature*, 400(6745): 652.
- Krijgsman, W., Langereis, C., Zachariasse, W., Boccaletti, M., Moratti, G., Gelati, R., Iaccarino, S., Papani, G. and Villa, G., 1999b. Late Neogene evolution of the Taza-Guercif Basin (Rifian Corridor, Morocco) and implications for the Messinian salinity crisis. *Marine Geology*, 153(1-4): 147-160.
- Krijgsman, W. and Meijer, P. T., 2008. Depositional environments of the Mediterranean “Lower Evaporites” of the Messinian salinity crisis: Constraints from quantitative analyses. *Marine Geology*, 253(3-4): 73-81.
- Krijgsman, W., Capella, W., Simon, D., Hilgen, F. J., Kouwenhoven, T. J., Meijer, P. T., Sierro, F. J., Tulbure, M. A., van den Berg, B. C. and van der Schee, M., 2018. The Gibraltar corridor: watergate of the messinian salinity crisis. *Marine Geology*, 403: 238-246.
- Kump, L. R. and Arthur, M. A., 1999. Interpreting carbon-isotope excursions: carbonates and organic matter. *Chemical Geology*, 161(1-3): 181-198.

-
- Lascaratos, A., Roether, W., Nittis, K. and Klein, B., 1999. Recent changes in deep water formation and spreading in the eastern Mediterranean Sea: a review. *Progress in Oceanography*, 44(1-3): 5-36.
- Lofi, J., 2018. Seismic atlas of the Messinian salinity crises markers in the Mediterranean sea. *Mem. Soc. géol. fr., n.s.*, 2018, t. 181, and Commission for the Geological Map of the World., 2: 72p.
- Loget, N., Driessche, J. V. D. and Davy, P., 2005. How did the Messinian salinity crisis end? *Terra Nova*, 17(5): 414-419.
- Lolis, C., Bartzokas, A. and Katsoulis, B., 2002. Spatial and temporal 850 hPa air temperature and sea-surface temperature covariances in the Mediterranean region and their connection to atmospheric circulation. *International Journal of Climatology: A Journal of the Royal Meteorological Society*, 22(6): 663-676.
- Mancilla, F. d. L., Booth-Rea, G., Stich, D., Pérez-Peña, J. V., Morales, J., Azañón, J. M., Martín, R. and Giaconia, F., 2015. Slab rupture and delamination under the Betics and Rif constrained from receiver functions. *Tectonophysics*, 663: 225-237.
- Martín, J. M., Braga, J. C. and Betzler, C., 2001. The Messinian Guadalhorce corridor: the last northern, Atlantic–Mediterranean gateway. *Terra Nova*, 13(6): 418-424.
- Martín, J. M., Puga-Bernabéu, A., Aguirre, J. and Braga, J. C., 2014. Miocene Atlantic–Mediterranean seaways in the Betic Cordillera (Southern Spain). *Revista de la sociedad geológica de España*, 27(1): 175-186.
- Martin-Vide, J. and Lopez-Bustins, J. A., 2006. The western Mediterranean oscillation and rainfall in the Iberian Peninsula. *International Journal of Climatology: A Journal of the Royal Meteorological Society*, 26(11): 1455-1475.
- Martínez del Olmo, W. and Comas, M., 2008. Arquitectura sísmica, olistostromas y fallas extensionales en el norte de la cuenca oeste del Mar de Alborán. *Revista de la Sociedad Geológica de España*, 21(3-4): 151-167.
- McQuarrie, N. and van Hinsbergen, D. J., 2013. Retrodeforming the Arabia-Eurasia collision zone: Age of collision versus magnitude of continental subduction. *Geology*, 41(3): 315-318.
- Murphy, L. N., Kirk-Davidoff, D. B., Mahowald, N. and Otto-Bliesner, B. L., 2009. A numerical study of the climate response to lowered Mediterranean Sea level during the Messinian Salinity Crisis. *Palaeogeography, palaeoclimatology, palaeoecology*, 279(1-2): 41-59.
- Nesteroff, W., 1973. Mineralogy, petrography, distribution, and origin of the Messinian Mediterranean evaporites. *Initial reports of the deep sea drilling project*, 13(II): 673-693.
- Nichols, G., 2009. *Sedimentology and stratigraphy*. John Wiley & Sons.

- Novello, A., Lebatard, A.-E., Moussa, A., Barboni, D., Sylvestre, F., Bourlès, D. L., Paillès, C., Buchet, G., Decarreau, A. and Düringer, P., 2015. Diatom, phytolith, and pollen records from a $^{10}\text{Be}/^{9}\text{Be}$ dated lacustrine succession in the Chad basin: Insight on the Miocene–Pliocene paleoenvironmental changes in Central Africa. *Palaeogeography, Palaeoclimatology, Palaeoecology*, 430: 85-103.
- Ochoa, D., 2016. Astrobiochronological Constraints on Margin to deep basin correlations across the Balearic Promontory and the Valencia basin, Universidad de Salamanca.
- Pagani, M., Freeman, K. H. and Arthur, M. A., 1999. Late Miocene atmospheric CO_2 concentrations and the expansion of C4 grasses. *Science*, 285(5429): 876-879.
- Pérez-Asensio, J. N., Aguirre, J., Schmiedl, G. and Civis, J., 2014. Messinian productivity changes in the northeastern Atlantic and their relationship to the closure of the Atlantic–Mediterranean gateway: implications for Neogene palaeoclimate and palaeoceanography. *Journal of the Geological Society*, 171(3): 389-400.
- Pérez-Asensio, J. N., Aguirre, J., Schmiedl, G. and Civis, J., 2012. Impact of restriction of the Atlantic-Mediterranean gateway on the Mediterranean Outflow Water and eastern Atlantic circulation during the Messinian. *Paleoceanography*, 27(3).
- Periáñez, R., Abril, J., Garcia-Castellanos, D., Estrada, F. and Ercilla, G., 2019. An exploratory modelling study on sediment transport during the Zanclean flood of the Mediterranean. *SN Applied Sciences*, 1(4): 364.
- Pierre, C., Caruso, A., Blanc-Valleron, M.-M., Rouchy, J. M. and Orszag-Sperber, F., 2006. Reconstruction of the paleoenvironmental changes around the Miocene–Pliocene boundary along a West–East transect across the Mediterranean. 188-189: 319-340.
- Pinardi, N. and Masetti, E., 2000. Variability of the large scale general circulation of the Mediterranean Sea from observations and modelling: a review. *Palaeogeography, Palaeoclimatology, Palaeoecology*, 158(3-4): 153-173.
- Pinardi, N., Cessi, P., Borile, F. and Wolfe, C. L., 2019. The Mediterranean sea overturning circulation. *Journal of Physical Oceanography*, 49(7): 1699-1721.
- Pound, M. J., Haywood, A. M., Salzmann, U. and Riding, J. B., 2012. Global vegetation dynamics and latitudinal temperature gradients during the Mid to Late Miocene (15.97–5.33 Ma). *Earth-Science Reviews*, 112(1-2): 1-22.
- Powley, H. R., Cappellen, P. and Krom, M. D., 2017. Nutrient cycling in the Mediterranean Sea: the key to understanding how the unique marine ecosystem functions and responds to anthropogenic pressures. *Mediterranean Identities – Environment, Society, Culture*. InTech: 47-77.
- Rohling, E., Marino, G. and Grant, K., 2015. Mediterranean climate and oceanography, and the periodic development of anoxic events (sapropels). *Earth-Science Reviews*, 143: 62-97.
- Rohling, E. J., 1994. Review and new aspects concerning the formation of eastern Mediterranean sapropels. *Marine Geology*, 122(1-2): 1-28.

-
- Rosenbaum, G., Lister, G. S. and Duboz, C., 2002. Reconstruction of the tectonic evolution of the western Mediterranean since the Oligocene. *Journal of the Virtual Explorer*, 8: 107-130.
- Roveri, M. and Manzi, V., 2006. The Messinian salinity crisis: Looking for a new paradigm? *Palaeogeography, Palaeoclimatology, Palaeoecology*, 238(1-4): 386-398.
- Roveri, M., Lugli, S., Manzi, V. and Schreiber, B. C., 2008. The Messinian Sicilian stratigraphy revisited: New insights for the Messinian salinity crisis. *Terra Nova*, 20(6): 483-488.
- Roveri, M., Flecker, R., Krijgsman, W., Lofi, J., Lugli, S., Manzi, V., Sierro, F. J., Bertini, A., Camerlenghi, A. and De Lange, G., 2014. The Messinian Salinity Crisis: past and future of a great challenge for marine sciences. *Marine Geology*, 352: 25-58.
- Santarelli, A., Brinkhuis, H., Hilgen, F., Lourens, L., Versteegh, G. and Visscher, H., 1998. Orbital signatures in a Late Miocene dinoflagellate record from Crete (Greece). *Marine Micropaleontology*, 33(3-4): 273-297.
- Scher, H. D. and Martin, E. E., 2006. Timing and climatic consequences of the opening of Drake Passage. *science*, 312(5772): 428-430.
- Scher, H. D., Whittaker, J. M., Williams, S. E., Latimer, J. C., Kordesch, W. E. and Delaney, M. L., 2015. Onset of Antarctic Circumpolar Current 30 million years ago as Tasmanian Gateway aligned with westerlies. *Nature*, 523(7562): 580-583.
- Schlitzer, R., Roether, W., Oster, H., Junghans, H.-G., Hausmann, M., Johannsen, H. and Michelato, A., 1991. Chlorofluoromethane and oxygen in the Eastern Mediterranean. *Deep Sea Research Part A. Oceanographic Research Papers*, 38(12): 1531-1551.
- Schmalz, R. F., 1991. The Mediterranean salinity crisis: Alternative hypotheses. *Carbonates and evaporites*, 6(2): 121.
- Schuster, M., 2006. The Age of the Sahara Desert. *Science*, 311(5762): 821-821.
- Seidenkrantz, M.-S., Kouwenhoven, T., Jorissen, F., Shackleton, N. and Van der Zwaan, G., 2000. Benthic foraminifera as indicators of changing Mediterranean-Atlantic water exchange in the late Miocene. *Marine geology*, 163(1-4): 387-407.
- Selli, R., 1954. Il Bacino del Metauro. *Giornale di Geologia*, 24: 1-294.
- Selli, R., 1964. The Mayer-Eymar Messinian 1867. Proposal for a neostratotype. *Proc. 21st IGC Copenhagen 1960*, 28: 311-333.
- Selli, R., 1973. An outline of the Italian Messinian. *Messinian events in the Mediterranean*, 7: 150-171.
- Selli, R., 1985. *Tectonic evolution of the Tethyan Sea. (Geological Evolution of the Mediterranean Basin, New York, Springer-Verlag): 571 p. + appendix, index.*

- Sierro, F. J., Flores, J. A., Francés, G., Vazquez, A., Utrilla, R., Zamarréño, I., Erlenkeuser, H. and Barcena, M. A., 2003. Orbitally-controlled oscillations in planktic communities and cyclic changes in western Mediterranean hydrography during the Messinian. *Palaeogeography, Palaeoclimatology, Palaeoecology*, 190: 289-316.
- Smith, R. S., 2017. Myth and Mythography in Pliny's *Geography*, *Naturalis Historia* 3-6'. *Polymnia*.
- Soto, J. I., Fernandez-Ibanez, F., Talukder, A. R. and Martinez-Garcia, P., 2010. Miocene shale tectonics in the northern Alboran Sea (western Mediterranean).
- Spakman, W. and Wortel, R., 2004. A tomographic view on western Mediterranean geodynamics, *The TRANSMED atlas. The Mediterranean region from crust to mantle*. Springer, pp. 31-52.
- Spakman, W., Chertova, M. V., van den Berg, A. and van Hinsbergen, D. J., 2018. Puzzling features of western Mediterranean tectonics explained by slab dragging. *Nature Geoscience*, 11(3): 211.
- Stern, R., 2007. When and how did plate tectonics begin? Theoretical and empirical considerations. *Chinese Science Bulletin*, 52(5): 578-591.
- Stoica, M., Krijgsman, W., Fortuin, A. and Gliozzi, E., 2016. Paratethyan ostracods in the Spanish Lago-Mare: More evidence for interbasinal exchange at high Mediterranean sea level. *Palaeogeography, Palaeoclimatology, Palaeoecology*, 441: 854-870.
- Stommel, H., Bryden, H. and Mangelsdorf, P., 1973. Does some of the Mediterranean outflow come from great depth? *Pure and Applied Geophysics*, 105(1): 879-889.
- Sun, J. and Liu, T., 2006. The age of the Taklimakan Desert. *Science*, 312(5780): 1621-1621.
- Theocharis, A. and Georgopoulos, D., 1993. Dense water formation over the Samothraki and Limnos Plateaux in the north Aegean Sea (eastern Mediterranean Sea). *Continental Shelf Research*, 13(8-9): 919-939.
- Torfstein, A. and Steinberg, J., 2020. The Oligo-Miocene closure of the Tethys Ocean and evolution of the proto-Mediterranean Sea. *Scientific reports*, 10(1): 1-10.
- Tulbure, M., Capella, W., Barhoun, N., Flores, J., Hilgen, F., Krijgsman, W., Kouwenhoven, T., Sierro, F. J. and Yousfi, M. Z., 2017. Age refinement and basin evolution of the North Rifian Corridor (Morocco): No evidence for a marine connection during the Messinian Salinity Crisis. *Palaeogeography, Palaeoclimatology, Palaeoecology*, 485: 416-432.
- Tzanova, A., Herbert, T. D. and Peterson, L., 2015. Cooling Mediterranean Sea surface temperatures during the Late Miocene provide a climate context for evolutionary transitions in Africa and Eurasia. *Earth and Planetary Science Letters*, 419: 71-80.
- Van den Berg, B. C. J., Sierro, F. J., Hilgen, F. J., Flecker, R., Larrasoana, J. C., Krijgsman, W., Flores, J. A. and Mata, M. P., 2018. Imprint of Messinian Salinity Crisis events on the Spanish Atlantic margin. *Newsletters on Stratigraphy*, 51(1): 93-115.

-
- Van der Schee, M., Van den Berg, B. C., Capella, W., Simon, D., Sierro, F. J. and Krijgsman, W., 2018. New age constraints on the western Betic intramontane basins: A late Tortonian closure of the Guadalhorce Corridor? *Terra Nova*, 30(5): 325-332.
- Van Hinsbergen, D. J., Vissers, R. L. and Spakman, W., 2014. Origin and consequences of western Mediterranean subduction, rollback, and slab segmentation. *Tectonics*, 33(4): 393-419.
- Vergés, J. and Fernández, M., 2012. Tethys–Atlantic interaction along the Iberia–Africa plate boundary: The Betic–Rif orogenic system. *Tectonophysics*, 579: 144-172.
- Wang, Y., Cerling, T. E. and MacFadden, B. J., 1994. Fossil horses and carbon isotopes: new evidence for Cenozoic dietary, habitat, and ecosystem changes in North America. *Palaeogeography, Palaeoclimatology, Palaeoecology*, 107(3-4): 269-279.
- Zachos, J., Pagani, M., Sloan, L., Thomas, E. and Billups, K., 2001. Trends, rhythms, and aberrations in global climate 65 Ma to present. *science*, 292(5517): 686-693.
- Zavattarielli, M. and Mellor, G. L., 1995. A numerical study of the Mediterranean Sea circulation. *Journal of Physical Oceanography*, 25(6): 1384-1414.
- Zhang, Z., Ramstein, G., Schuster, M., Li, C., Contoux, C. and Yan, Q., 2014. Aridification of the Sahara desert caused by Tethys Sea shrinkage during the Late Miocene. *Nature*, 513(7518): 401-404.

Chapter 2

Methods

Chapter 2

Methods

1. Overview of the studied sites

The scientific results produced during this PhD thesis rely on a combination of biostratigraphy, cyclostratigraphy, seismic sections, XRF analyses, benthic and planktic foraminifer associations, stable isotope analyses and fieldwork. In this work two deep sea cores and two industrial boreholes from the Alboran Basin, three Southern Spanish outcrops and one Spanish Atlantic margin borehole were studied (Figure 1).

1.1 Alboran Basin



Figure 1: Late Miocene configuration of the Mediterranean-Atlantic gateways showing with the black dots the studied cores and outcrops (modified from Capella, 2017).

1.1.1 Site 121: drilled during the DSDP expedition Leg 13 in the West Alboran Basin structural high, and it was aimed to study the evolution of the Mediterranean Basin. Even though the recovery was poor, 24 cores were taken, and late Miocene sediments were reached. Here we analysed 12 samples from the late Tortonian – early Pliocene interval (from 865 to 625 mbsf).

1.1.2 Site 976 (Hole B): drilled during the ODP Expedition Leg 161 very close to DSDP Site 121 in the same structural high. It reaches the Alboran Basin metamorphic basement, which was the target of the expedition. The drilling recovered late Miocene to Pleistocene sediments for a total of 535.54 meters. In this work we analysed 139 samples from the late Tortonian - early Pliocene interval of the core (from 609 to 564 mbsf).

1.1.3 Exploration well Andalusia-G1: drilled offshore Marbella and penetrated the basin for almost 4 km reaching the Aquitanian. There was no continuous coring,

and the available samples are made by well cuttings. Here we analysed 30 available samples for the late Tortonian - early Pliocene interval.

1.1.4 Exploration well Alboran-A1: drilled offshore Malaga and perforated 2 km of the Alboran Basin sediments, touching the Paleozoic basement. There was no continuous recovery, and 28 cutting samples were analysed from the late Tortonian to early Pliocene.

1.2 Mediterranean southern Spain basins

During several field trips, the Miocene-Pliocene transition from three Spanish southern coast outcrops were sampled. From Malaga Basin (Rio Mendelin section), 33 samples were recovered while from Nijar Basin (Barranco del Negro section) and Sorbas Basin (Zorreras section) 9 and 23 samples were studied, respectively.

1.3 Spanish Atlantic margin

1.3.1 Montemayor-1 borehole: drilled by the Spanish Geological and Mining Institute (IGME-*Instituto Geológico y Minero de España*) is located in the western part of the Guadalquivir basin and with its 260 m it covers a time interval from the late Tortonian to early Pliocene. In this work we analysed 405 samples from the late Tortonian to early Messinian.

2. Geochemical methods

2.1 XRF analyses

X-Ray fluorescence is a rapid, non-destructive analytical capability used in the analysis of marine sediments. Through such method, the changes in minor and major elemental composition of the sedimentological record can be seen. Depending on the dominant element, it is possible to obtain detailed insights of oceanographic and climate processes and to discern fundamental parameters such as calcium carbonate stratigraphy, terrigenous sediment delivery and origin of sedimentary particles (Figure 2; Rothwell, 2015). These analyses permitted to estimate changes in element dominance through time, and to identify trends, patterns, and abrupt changes in the composition of the sedimentological record. The obtained elemental patterns were used for cyclostratigraphy and astronomical tuning of the records.

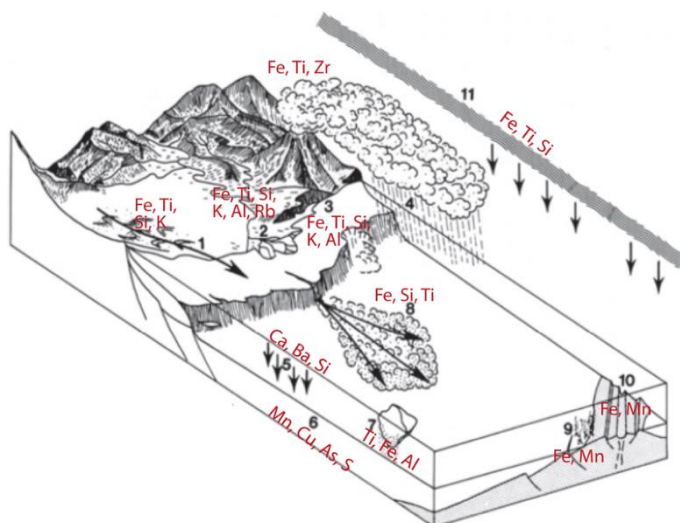


Figure 2: Schematic representation of element pathways to and within the marine environment. 1: aeolian dust input ; 2: Fluvial input; 3: Coastal erosion; 4: Volcanic eruptions; 5: Export productivity; 6: Diagenesis and authigenesis; 7: Ice-rafting; 8: Deep sea sediment transport; 9: Hydrothermal activity; 10: Submarine volcanism and 11: Fall-out from high altitude jet-streams (modified from Rothwell, 2015).

The X-Ray fluorescence datasets used in this work were obtained with two different analytical methods depending on the nature of the available samples. Where an undisturbed continuous coring was available, the split cores were scanned by the X-ray fluorescence (XRF) Avaatech core scanner at MARUM (Research Faculty, Bremen University). The split core surface was cleaned, covered with a 4 μm SPEXCerti Prep Ultralene 1 foil to avoid contamination of the XRF measurements. The here reported data have been acquired by a Canberra X-PIPS Silicon Drift Detector with 150 eV X-ray resolution, the Canberra Digital Spectrum Analyzer DAS 1000, and an Oxford Instruments 50 W XTF5011 X-Ray tube with rhodium (Rh) target material. Maximum scanning resolution was attempted, but due to the bad core preservation and occasional intercalations of perforating mud, the sampling steps were inserted manually ranging between 1 and 7 cm. Two runs were made, one using generator settings of 30 kV, current of 1.0 mA and a sampling time of 15 s, while the second run was performed with 10 kV, 0.2 mA and only 10 s of sampling time.

When only single sediment samples were available, each sample was reduced to a fine powder in an agate mortar, subsequently obtaining tablets of 10 mm in diameter with a manual press with a load of 5 Tm. The tablets were fixed on a glass slide to facilitate their handling. On each tablet, of sufficient thickness to avoid transparency phenomena, 25 random points were measured for 30 s with a Bruker M4 Tornado Spectrometer where the generator settings were set at 50 kV and 150 μA . A representative spectra and semi-quantitative

results of each sample were obtained using the ESPRIT software, set at international standards. This analysis was performed at the General Service of X-ray diffraction at Salamanca University.

2.2 Stable isotope analyses

The oxygen and carbon isotopic composition of fossil foraminifer calcite test has been commonly used in paleoceanography to reconstruct past ocean environmental conditions.

The oxygen isotopic composition of ocean water varies as a function of the evaporation-precipitation balance and reflects changes in ice volume, water temperature and the hydrologic budget. While evaporation extracts preferentially the light oxygen isotope (^{16}O), making the remaining water richer in the heavier ^{18}O isotope, inflow of freshwater normally poor in ^{18}O causes a decrease in the heavy isotope (Pierre, 1999 and references therein). Consequently, warmer temperatures result in lower $\delta^{18}\text{O}$ water values and are usually linked to precession minima due to the higher freshwater discharge from the Nile or other peri Mediterranean regions (Chad, Eonile, Sahabi, Gabes basins; e.g. Griffin, 2002; Tuenter et al., 2003; Rohling and Hilgen, 2007). Because the Mediterranean $\delta^{18}\text{O}$ records usually contain an evident precession component, the $\delta^{18}\text{O}$ record can be used for astronomical tuning (e.g. Hilgen, 1991; Hilgen et al., 1995; Lourens et al., 1996) as has been done in this work.

Ocean $\delta^{13}\text{C}$ composition is controlled by the equilibrium with the atmosphere in the surface and by water renewal at the bottom, and it is always a function of the organic production by photosynthetic organisms that live in the euphotic zone (Laube-Lenfant and Pierre, 1994; Pierre, 1999), the transfer of organic matter to the bottom and deep water renewal. During the photosynthesis, they preferentially extract ^{13}C -depleted CO_2 , enriching the more productive basins with ^{13}C isotope. On the contrary, the degradation of sinking organic matter releases ^{13}C depleted CO_2 leading to a progressive decrease of $\delta^{13}\text{C}$ as we move deeper in the basin. How much the $\delta^{13}\text{C}$ will decrease depends on the quantity of CO_2 added by remineralization, and so, on the water residence time. In this work, we mainly used changes in benthic $\delta^{13}\text{C}$ to estimate variations in bottom water residence time related with the variable Mediterranean-Atlantic water exchange efficiency.

The $\delta^{13}\text{C}$ and $\delta^{18}\text{O}$ analyses were performed both on benthic and planktic foraminifer tests of selected individuals of the same species using a Finnigan MAT 253 mass spectrometer connected to a Kiel IV carbonate preparation device at the Christian-Albrecht University in Kiel (Germany). Sample reaction was induced by individual acid addition (99 % H_3PO_4 at 75 °C) under vacuum. The

evolved carbon dioxide was analysed eight times for each individual sample. As documented by the performance of international [NBS19: +1.95 ‰ VPDB (^{13}C), -2.20 ‰ VPDB (^{18}O); IAEA-603: +2.46 ‰ VPDB (^{13}C), -2.37 ‰ VPDB (^{18}O)] and laboratory-internal carbonate standards [Hela1: +0.91 ‰ VPDB (^{13}C), +2.48 ‰ VPDB (^{18}O); HB1: -12.10 ‰ VPDB (^{13}C), -18.10 ‰ VPDB (^{18}O); SHK: +1.74 ‰ VPDB (^{13}C), -4.85 ‰ VPDB (^{18}O)], analytical precision of stable isotope analysis is better than ± 0.08 ‰ for $\delta^{18}\text{O}$ and better than ± 0.05 ‰ for $\delta^{13}\text{C}$. The obtained values were calibrated relative to Vienna Pee Dee Belemnite (VPDB).

3. Seismic section analyses

In this thesis, several 2D seismic profiles and a 3D seismic cube (Figure 3) acquired in the Alboran Basin by REPSOL exploración S.A., were integrated into the results and correlated to the sediments recovered in ODP Site 976, DSDP Site 121 and drillholes Andalucia-G1 and Alboran-A1. In the first place, such correlation enabled to determine the main late Tortonian-Pliocene facies present in the Alboran Basin. In the second place, it made possible to estimate thicknesses and age intervals represented by single sedimentary packages and provided rough estimates on the age and thicknesses missing where an erosional surface was present.

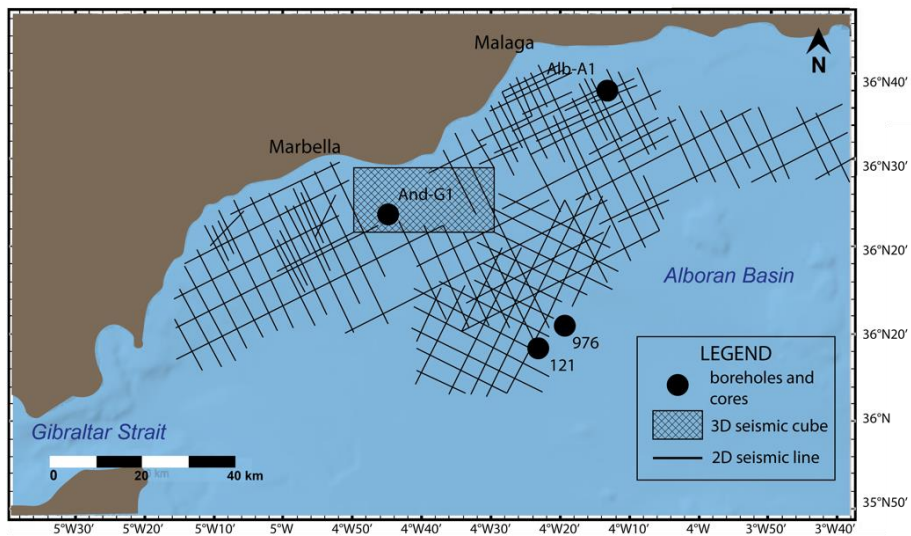


Figure 3: Map showing the available seismic lines used in this work.

4. Micropaleontological analyses

4.1 Benthic and planktic foraminifer assemblages

Foraminifers are marine, free-living, single-celled eukaryotes which secrete an elaborate, solid skeleton (or test) that contains the bulk of the cell and is composed of secreted organic matter, minerals (calcite or aragonite) or agglutinated particles (BouDagher-Fadel, 2012). Based on their life strategy, they can be divided into benthic foraminifers that live attached on plants or the sediment substrate, and planktic foraminifers who float freely in the upper part of the water column.

Benthic foraminifers have all kinds of different shapes and sizes and live on the seafloor or at different depths into the sediment. According to the TROX (Jorissen et al., 1995) and TROX-2 (Van der Zwaan et al., 1999) models, the benthic foraminifer microhabitat depends on the oxygen levels and, if oxygen is present on nutrient availability at the sea floor (Figure 4). In very oligotrophic

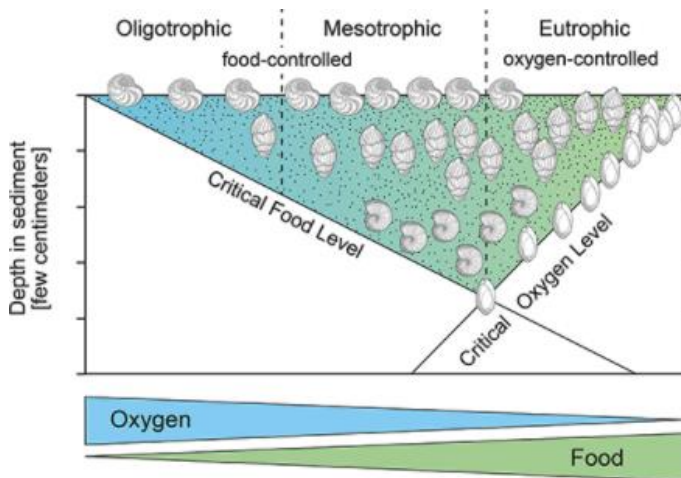


Figure 4: Conceptual model TROX/TROX-2 model of Jorissen et al. (1995) and Van der Zwaan et al. (1999) describing the general dependence of the benthic foraminiferal microhabitat structure on food supply (trophic conditions) and oxygen (www.oxfordre.com).

marine areas oxygen consumption is high and the food particles are consumed at the sediment-water interface, leaving the underlying sediments with very small quantities of organic matter. In such environment, the benthic foraminifer association will be mainly composed by epifaunal species and only by a few shallow infaunal species. In more eutrophic environments, the metabolizable organic matter is no longer restricted to the sediment surface, but reaches deeper sediment layers, enabling the proliferation of deep infaunal taxa. In fully

eutrophic environments the oxygen level determines the penetration depth of the infauna. Here, the degradation of the organic matter in the sediment consumes more oxygen than can be provided creating a food excess in the sediment. If organic flux continues to increase, most of the oxygen will be consumed, and the benthic environment will become shallower. Consequently, studying the benthic foraminifer species distribution and abundances, as well as their microhabitat preferences throughout a sediment record offers valuable information regarding oxygen levels and the amount of nutrients coming to the seafloor. Furthermore, because different benthic foraminifer species inhabit specific depth intervals, water-depth ranges of the dominant species have been commonly used to reconstruct paleodepth variations (Hohenegger, 2005; Pérez-Asensio, 2021). In this work, changes in benthic foraminifer associations have been used as tools to reconstruct changes in the paleoenvironment including past circulation and oxygenation patterns and to estimate possible oscillations in the paleodepth.

Planktic foraminifer inhabit wide latitudinal and temperature zones and their distribution is related mainly to surface water properties like temperature (Figure 5) and salinity (Kucera, 2007). Consequently, the study of planktic

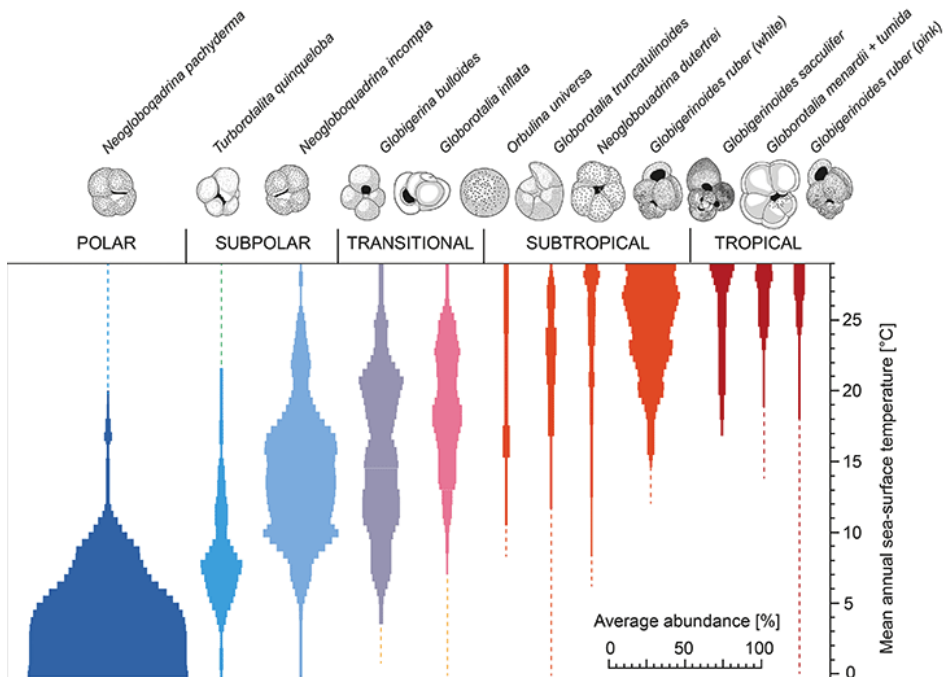


Figure 5: Abundance plots of selected modern planktic foraminiferal species in relation to sea surface temperature (SST). The plots are based on data from surface sediments of the Atlantic Ocean from Kucera et al. (2005) (www.oxfordre.com).

foraminifer assemblages distribution throughout our record enabled us to track changes in environmental conditions.

The variation from a predominately warm to a predominately cold-water species assemblage was used to trace temperature and circulation changes where the cold-water species were associated to an efficient circulation, while water column stratification was implied by the prevalence of warm water species (Sierro et al., 2003). The recognition of cyclical patterns was used for cyclostratigraphy and astronomical tuning.

For the micropaleontological analyses of both benthic and planktic foraminifers, the sediment samples were prepared in the Salamanca University laboratory. All the samples were oven dried, weighted and left to disaggregate overnight in water. Afterwards, the sediment residue was washed over a $>63 \mu\text{m}$ and $>150 \mu\text{m}$ sieve. From the $>150 \mu\text{m}$ fraction at least 200 benthic and 300 planktic foraminifers were counted and classified by species.

4.2 Biostratigraphy

Biostratigraphy is based on the evolution and migration of certain fauna through time, where the appearance, acme or disappearance of a marker species is isochronous and tied to the same age (Gradstein et al., 2012). Consequently, such events have been used to determine the age of the sediments. The late Tortonian-early Pliocene biostratigraphic frame used in this work and applied on the studied locations was based on several planktic foraminifer events derived from the revised planktonic biostratigraphic scale of Lirer et al. (2019). Additionally, two benthic foraminifer bioevent have been also used (Hilgen, 1991; Kouwenhoven et al., 2003). All the bioevents are listed in Table 1.

Table 1: Late-Tortonian-early Pliocene biostratigraphic foraminiferal events in the Mediterranean used in this study Lirer et al. (2019). Only the age of the *S. reticulata* bioevent is taken from Kouwenhoven et al. (2003) and the duration of *U. peregrina-U. pygmaea* event from Hilgen (1991).

Bioevent	Species	Astronomically calibrated age
FO	<i>Globorotalia punctulata</i>	4.52 Ma
FCO	<i>Globorotalia margaritae</i>	5.08 Ma Mediterranean 6.08 Ma Atlantic
Acme interval	<i>Uvigerina peregrina-U. pygmaea</i>	5.226-5.128 Ma/ 5.266-5.079 Ma
Bottom acme	<i>Sphaeroidinelopsis</i> spp.	5.3 Ma
S/D coiling	<i>Neogloboquadrina acostaensis</i>	6.35 Ma
LO	<i>Globorotalia miotumida</i> group	6.52 Ma
Disappearance	<i>Siphonina reticulata</i>	7.167 Ma

Bioevent	Species	Astronomically calibrated age
LO	<i>Globorotalia suturatae</i>	7.17 Ma
FCO	<i>Globorotalia miotumida</i> group	7.24 Ma
LCO	<i>Globorotalia menardii</i> 5 group (dextral)	7.23 Ma
FCO	<i>Globorotalia menardii</i> 5 group (dextral)	7.36 Ma
LCO	<i>Globorotalia menardii</i> 4 group (sinistral)	7.56 Ma

5. Cyclostratigraphy

Long term changes in solar insolation modulate climate and circulation patterns visible in the sedimentological records. The solar radiation reaching the earth's surface at a determinate time and place depends on the shape of the earth's orbit around the sun and of the orientation of the rotational axis. These characteristics are defined by three orbital parameters that include eccentricity, obliquity, and precession, all varying through time with different periodicities, known as Milankovitch's cycles (Figure 6). The eccentricity is characterized by three main periodicities, the 2.3 Ma visible in long geological records, the most prominent at 413 kyr, and 100 kyr obtained as an average of four periods while the obliquity component with larger amplitude is of 41 kyr (Berger, 1977; Strasser et al., 2006). For precession, the dominant periodicities are 23 kyr and 19 kyr, which are commonly found in the geological record.

Because of the peculiar location of the Mediterranean Sea, which is surrounded by continents and only connected to the Atlantic Ocean by a small

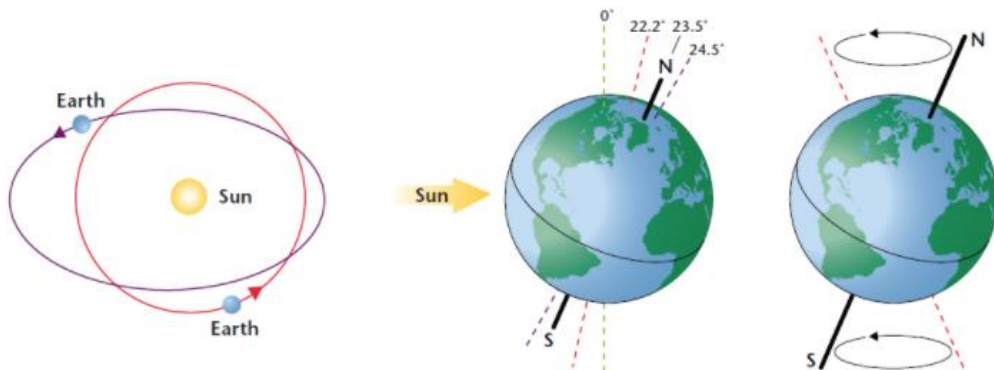


Figure 6: A schematic representation of the three orbital parameters influencing the solar insolation coming to the earth. From left to right: eccentricity, obliquity, and precession (www.theinevitableclimatechange.org).

marine gateway, Mediterranean climate is very sensitive to orbital forcing. Such restricted basin amplifies the astronomically induced changes in the hydrological regime and oceanic circulation (Krijgsman, 2002). Therefore, oscillations of the orbital parameters are recorded in the Mediterranean sedimentary records through changes in physical, biological, and chemical properties of the sediments. During Northern Hemisphere insolation maxima (precession minima), under a hot and more humid climate, the intense precipitation and freshwater discharge to the basin increases the detrital input which dilutes the carbonate content of the sediments that become enriched in terrigenous elements like titanium, zirconium, or rubidium. If the fluvial discharge is strong, during this periods it can create a fresher seawater lid on the surface, hindering water circulation and even inhibit almost completely deep water formation and mixing consequently leading to the deposition of organic rich sapropels (Rossignol-Strick et al., 1982; Rohling, 1994; Rohling et al., 2009; Rohling et al., 2015). On the other hand, during Northern Hemisphere insolation minima (precession maxima), the climate is cold and dry and the freshwater input to the basin reduced. Consequently, the sediments are enriched with carbonates and contain high quantities of calcium and strontium. During this periods, eolic deposits can also be found, usually rich in titanium (De Visser et al., 1989; Larrasoana et al., 2003; Konijnendijk et al., 2014). The recognition of such cyclical changes in the Mediterranean Basin sedimentological record has been used to create an astronomical time scale for the Neogene (Hilgen and Krijgsman, 1999; Hilgen et al., 2015) and significantly facilitated the correlation between different Mediterranean sections (Roveri et al., 2014).

In order to astronomically tune the studied stratigraphic sequences to the astronomical target curve (Laskar et al., 2004) a phase relationship was established between the patterns identified in the stable isotope, XRF or planktic foraminifer record, sedimentary processes and orbital cycles. Phases with heavier $\delta^{18}\text{O}$ values, abundant cold water foraminifer species and high carbonate concentrations were associated to insolation minima, while lighter $\delta^{18}\text{O}$ values, predominant warm water foraminifer species and more abundant detrital elements to insolation maxima. As sonic logs are used in the industry to estimate the porosity and therefore the variation between sand or shale layers, in some cases, sonic log profiles were additionally used to spot the periodicity of the cycles.

References

- Berger, A., 1977. Long-term variations of the earth's orbital elements. *Celestial Mechanics*, 15(1): 53-74.
- BouDagher-Fadel, M. K., 2012. Biostratigraphic and geological significance of planktonic foraminifera, 22. Newnes.
- Capella, W., 2017. Gateway to a vanishing ocean: the tectono-sedimentary evolution of the Rifian Corridor (Morocco) and the Late Miocene isolation of the Mediterranean, University Utrecht.
- De Visser, J., Ebbing, J., Gudjonsson, L., Hilgen, F., Jorissen, F., Verhallen, P. and Zevenboom, D., 1989. The origin of rhythmic bedding in the Pliocene Trubi Formation of Sicily, southern Italy. *Palaeogeography, Palaeoclimatology, Palaeoecology*, 69: 45-66.
- Gradstein, F. M., Ogg, J. G., Schmitz, M. and Ogg, G., 2012. The geologic time scale 2012. elsevier.
- Griffin, D. L., 2002. Aridity and humidity: two aspects of the late Miocene climate of North Africa and the Mediterranean. *Palaeogeography, Palaeoclimatology, Palaeoecology*, 182(1-2): 65-91.
- Hilgen, F., Krijgsman, W., Langereis, C., Lourens, L., Santarelli, A. and Zachariasse, W., 1995. Extending the astronomical (polarity) time scale into the Miocene. *Earth and Planetary Science Letters*, 136: 495-510.
- Hilgen, F. J., 1991. Extension of the astronomically calibrated (polarity) time scale to the Miocene/Pliocene boundary. 107(2): 349-368.
- Hilgen, F. J. and Krijgsman, W., 1999. Cyclostratigraphy and astrochronology of the Tripolo diatomite formation pre-evaporite Messinian, Sicily, Italy. *Terra Nova*, 11(1): 16-22.
- Hilgen, F. J., Hinnov, L. A., Aziz, H. A., Abels, H. A., Batenburg, S., Bosmans, J. H., de Boer, B., Hüsing, S. K., Kuiper, K. F. and Lourens, L. J., 2015. Stratigraphic continuity and fragmentary sedimentation: the success of cyclostratigraphy as part of integrated stratigraphy. *Geological Society, London, Special Publications*, 404(1): 157-197.
- Hohenegger, J., 2005. Estimation of environmental paleogradient values based on presence/absence data: a case study using benthic foraminifera for paleodepth estimation. *Palaeogeography, Palaeoclimatology, Palaeoecology*, 217(1-2): 115-130.
- Jorissen, F. J., de Stigter, H. C. and Widmark, J. G., 1995. A conceptual model explaining benthic foraminiferal microhabitats. *Marine micropaleontology*, 26(1-4): 3-15.
- Konijnendijk, T., Ziegler, M. and Lourens, L., 2014. Chronological constraints on Pleistocene sapropel depositions from high-resolution geochemical records of ODP Sites 967 and 968. *Newsl. Stratigr.*, 47(3): 263-282.

- Kouwenhoven, T. J., Hilgen, F. J. and Van Der Zwaan, G. J., 2003. Late Tortonian–early Messinian stepwise disruption of the Mediterranean–Atlantic connections: constraints from benthic foraminiferal and geochemical data. *Palaeogeography, Palaeoclimatology, Palaeoecology*, 198(3-4): 303-319.
- Krijgsman, W., 2002. The Mediterranean: mare nostrum of earth sciences. *Earth and Planetary Science Letters*, 205(1-2): 1-12.
- Kucera, M., 2007. Planktonic foraminifera as tracers of past oceanic environments. *Developments in marine geology*, Chapter 6: 213-262.
- Larrasoana, J., Roberts, A., Rohling, E., Winkelhofer, M. and Wehausen, R., 2003. Three million years of monsoon variability over the northern Sahara. *Climate Dynamics*, 21(7-8): 689-698.
- Laskar, J., Robutel, P., Joutel, F., Gastineau, M., Correia, A. and Levrard, B., 2004. A long-term numerical solution for the insolation quantities of the Earth. *Astronomy & Astrophysics*, 428(1): 261-285.
- Laube-Lenfant, E. and Pierre, C., 1994. Variability of delta-c-13 of sigma-co2 in ocean waters of the equatorial pacific. *Oceanologica acta*, 17(6): 633-641.
- Lirer, F., Foresi, M., Iaccarino, S., Salvatorini, G., Turco, E., Cosentino, C., Sierro, F. J. and Caruso, A., 2019. Mediterranean Neogene planktonic foraminifer biozonation and biochronology. *Earth-Science Reviews*, 196: 102869.
- Lourens, L. J., Antonarakou, A., Hilgen, F., Van Hoof, A., Vergnaud-Grazzini, C. and Zachariasse, W., 1996. Evaluation of the Plio-Pleistocene astronomical timescale. *Paleoceanography*, 11(4): 391-413.
- Pérez-Asensio, J. N., 2021. Quantitative palaeobathymetric reconstructions based on foraminiferal proxies: a case study from the Neogene of south-west Spain. *Palaeontology*.
- Pierre, C., 1999. The oxygen and carbon isotope distribution in the Mediterranean water masses. *Marine Geology*, 153(1-4): 41-55.
- Rohling, E. and Hilgen, F., 2007. The eastern Mediterranean climate at times of sapropel formation: a review. *Netherlands Journal of Geosciences/Geologie en Mijnbouw(Classic Papers)*.
- Rohling, E., Marino, G. and Grant, K., 2015. Mediterranean climate and oceanography, and the periodic development of anoxic events (sapropels). *Earth-Science Reviews*, 143: 62-97.
- Rohling, E. J., 1994. Review and new aspects concerning the formation of eastern Mediterranean sapropels. *Marine Geology*, 122(1-2): 1-28.
- Rohling, E. J., Abu-Zied, R., Casford, J., Hayes, A. and Hoogakker, B., 2009. The marine environment: present and past. *The physical geography of the Mediterranean*: 33-67.

-
- Rossignol-Strick, M., Nesteroff, W., Olive, P. and Vergnaud-Grazzini, C., 1982. After the deluge: Mediterranean stagnation and sapropel formation. *Nature*, 295(5845): 105-110.
- Rothwell, R. G., 2015. Twenty years of XRF core scanning marine sediments: what do geochemical proxies tell us?, *Micro-XRF Studies of Sediment Cores*. Springer, pp. 25-102.
- Roveri, M., Flecker, R., Krijgsman, W., Lofi, J., Lugli, S., Manzi, V., Sierro, F. J., Bertini, A., Camerlenghi, A. and De Lange, G., 2014. The Messinian Salinity Crisis: past and future of a great challenge for marine sciences. *Marine Geology*, 352: 25-58.
- Sierro, F. J., Flores, J. A., Francés, G., Vazquez, A., Utrilla, R., Zamarreño, I., Erlenkeuser, H. and Barcena, M. A., 2003. Orbitally-controlled oscillations in planktic communities and cyclic changes in western Mediterranean hydrography during the Messinian. *Palaeogeography, Palaeoclimatology, Palaeoecology*, 190: 289-316.
- Strasser, A., Hilgen, F. J. and Heckel, P. H., 2006. Cyclostratigraphy-concepts, definitions, and applications. *Newsletters on Stratigraphy*, 42(2): 75-114.
- Tuenter, E., Weber, S., Hilgen, F. and Lourens, L., 2003. The response of the African summer monsoon to remote and local forcing due to precession and obliquity. *Global and Planetary Change*, 36(4): 219-235.
- Van der Zwaan, G., Duijnste, I., Den Dulk, M., Ernst, S., Jannink, N. and Kouwenhoven, T., 1999. Benthic foraminifers: proxies or problems?: a review of paleocological concepts. *Earth-Science Reviews*, 46(1-4): 213-236.

Chapter 3

Messinian West Alboran Sea
record in the proximity of
Gibraltar: Early signs of Atlantic-
Mediterranean gateway
restriction

Chapter 3

Bulian, F., Sierro, F. J., Ledesma, S., Jiménez-Espejo, F. J. and Bassetti, M. A., 2021. Messinian West Alboran Sea record in the proximity of Gibraltar: Early signs of Atlantic-Mediterranean gateway restriction. *Marine Geology*, 434, p. 106430.

DOI: <https://doi.org/10.1016/j.margeo.2021.106430>

Messinian West Alboran Sea record in the proximity of Gibraltar: Early signs of Atlantic-Mediterranean gateway restriction

Bulian Francesca^{1*}, Sierra Francisco J.¹, Ledesma Santiago²,
Jiménez-Espejo Francisco J.^{3,4}, Bassetti Maria-Angela⁵

¹Dept. de Geología, Univ. de Salamanca, Plaza de los Caídos s/n, 37008, Salamanca, Spain;
e-mail: sierra@usal.es.

²Petroleum Oil & Gas España, Avenida San Luis, 77, 28033, Madrid, Spain;
e-mail: sledesma@naturgy.com

³Instituto Andaluz de Ciencias de la Tierra (CSIC-UGR), Armilla, Spain;
e-mail: fjspejo@ugr.es.

⁴Research Institute for Marine Resources Utilization (Biogeochemistry Program),
JAMSTEC, Yokosuka, Japan; e-mail: fjspejo@ugr.es.

⁵CEFREM-UMR 5110, Université de Perpignan Via Domitia, 52 Avenue Paul Alduy,
66860 Perpignan cedex, France; e-mail: maria-angela.bassetti@univ-perp.fr.

Abstract

Late Miocene sedimentary records in the Gibraltar arch region hold fundamental information on the Atlantic-Mediterranean connectivity before, during and after the Messinian Salinity Crisis (MSC; 5.96-5.33 Ma). In this work we tackle this still unresolved problem through a detailed foraminifer-based biostratigraphy, micro- paleontological and geochemical analyses of four available records (ODP 976B and DSDP 121) and boreholes (Andalucia-G1 and Alboran A1) in the West Alboran Basin (WAB). The combined use of these different analytical techniques together with new seismic stratigraphy enabled us to create a new and revised Upper Tortonian-Lower Pliocene Alboran Sea chronostratigraphic framework and estimate the magnitude of the Zanclean erosion. At Site 976, the dominance of a peculiar cold planktonic foraminifer fauna in the late Tortonian-early Messinian could possibly imply the existence of a proto-Gibraltar Strait, while at ~7.2 Ma, changes towards warmer foraminifer assemblages, increasingly stratified water column and sharp increase in terrestrial input indicate the beginning of the restriction of the Mediterranean from the Atlantic Ocean. Cyclical changes visible both in the elemental composition and foraminifer assemblages from here onward highlight a strong precessional cyclicity, which can be correlated to the first signs of reduced ventilation and sapropel deposition in the Eastern Mediterranean. The integration of seismic profiles and core analyses finally revealed that the Messinian expression in the Alboran basin is limited to two units: one hemipelagic and one chaotic,

*Corresponding author: Francesca Bulian (fra.bulian@usal.es)

most probably connected to the MSC final stages. The Messinian succession in the Alboran basin is topped by an unconformity, most likely related with the Zanclean reflooding, which eroded a sedimentary succession of ~1.67 Ma. An extremely rare phosphate (canaphite) and Mg rich minerals were recognized described and associated to interstitial fluids and diagenetic processes.

1. Introduction

During the last 640 kyr of the Messinian stage (7.245-5.333 Ma; Gradstein et al., 2012), known as the Messinian Salinity Crisis (MSC; Selli, 1964), the Mediterranean went through unparalleled paleogeographic and paleoenvironmental changes (CIESM, 2008; Flecker et al., 2015; Hsü et al., 1977; Roveri et al., 2014), when km-thick evaporite deposits started to accumulate all over the sea floor. These deposits were only the final result of the progressive restriction of the Atlantic-Mediterranean gateways that started already at about 7 Ma, the beginning of the Messinian (Kouwenhoven et al., 2003; Krijgsman et al., 2018; Van den Berg et al., 2018), which produced at least a few hundreds of meters of base level drop (Krijgsman and Meijer, 2008; Roveri et al., 2014) and a final isolation of the basin from the global ocean. The exact chronology, magnitude and nature (tectonic vs. glacio-eustatic; eg. Ohneiser et al., 2015; Sanz de Galdeano and Alfaro, 2004) of the base level change together with the evolution of the gateways and their location is still to be completely understood (Flecker et al., 2015).

Over the last decades a strong effort has been made to investigate on land sections along the Betic and Rifian corridors that connected the Atlantic and Mediterranean during the late Miocene (Benson et al., 1991; Blanc, 2006; Braga et al., 2003; Capella et al., 2018; Corbí et al., 2012; Franseen et al., 1996; García-Veigas et al., 2020; Martín et al., 2001; Soria et al., 1999; Tulbure et al., 2017; Van den Berg et al., 2018; Van Der Laan et al., 2012; Van der Schee et al., 2018; among many others). In contrast, the West Alboran Basin (WAB) which is located at the entrance of the Mediterranean, in the vicinity of the Gibraltar Strait received less attention. Due to its location, the WAB sedimentological succession should contain a record showing the signs of gateway restriction culminating with the deposition of MSC evaporites and topped by Pliocene open marine sediments, corresponding to the Zanclean reflooding. Seismic data revealed that there was no significant in situ evaporite deposition in the Alboran Basin (Bache et al., 2009; Comas et al., 1999; Rouchy and Caruso, 2006), and because of the basin position facing Gibraltar Strait, the re-establishment of marine conditions left a profound impact on its record, leaving an erosional surface (Estrada et al., 2011) and channel (Garcia-Castellanos et al., 2009) as the main traces of the MSC. Apart from this Messinian M reflector (Ryan et al., 1973) other features related with the

MSC are rare and mainly confined to the marginal, shallower sectors like some turbidites and mass-transport deposits identified in a 3D seismic cube offshore Marbella (Martínez del Olmo and Comas, 2008; Martínez del Olmo and Martín, 2016). These deposits, cored by industrial well Andalucía-G1 and Alboran-A1, are mainly composed by benthonic and planktonic foraminifers immersed in a fine clay matrix, with abundant anhydrite minerals and metamorphic rock fragments (Martínez del Olmo and Comas, 2008). Even if never precisely dated, in previous studies they were interpreted as the consequence of sea-level drop during the MSC acme which lead to the erosion and instability of the WAB shelf resulting in sedimentation of mass transport deposits (MTDs) and turbidites into the incised valleys (Martínez del Olmo and Comas, 2008). In this study, we show how such clastic deposits are more likely attributable to base level changes in the MSC final stages, in agreement with the finding of similar coeval units both in the Eastern (Bertoni and Cartwright, 2007; Gvirtzman et al., 2017) and Western Mediterranean (Guerra-Merchán et al., 2010; Soria et al., 2005).

Aside from studying seismic sections and industrial boreholes, others focused on the MSC record sampled by the existing ODP sites, but apart from the initial DSDP/ODP reports (Campillo et al., 1992; Comas et al., 1999; Comas et al., 1996; Serrano et al., 1999), only Popescu et al. (2015) revisits those sites, mainly because of their poor recovery and absence of MSC deposits. To understand the impact of the gateways dynamics, in particular of the Gibraltar Strait and its recently questioned opening time (Krijgsman et al., 2018), we studied the Alboran Sea sedimentary record before and after the salinity crisis. Considering the pre-evaporite Messinian deposits and the early Pliocene sediments from the WAB more into detail, will help us understand when the first tectonic pulses initiated changing the Mediterranean paleogeography, what were the circulation patterns following the gateway evolution and how rapid actually was the re-establishment of open marine conditions at the base of the Zanclean.

In spite of an obvious need for a new drilling expedition in the Alboran basin, targeting areas with a more complete Tortonian-Messinian-Pliocene successions, which are known to exist because of the numerous seismic surveys (Do Couto et al., 2016; Estrada et al., 2011; Soto et al., 2010), is essential to produce a new and more detailed biostratigraphy and chronology of the WAB sites. Most of the identified WAB records have been interpreted from seismic profiles, but because of the limited resolution, only the identification of some seismic units was possible (Do Couto et al., 2016; Jurado and Comas, 1992; Martínez del Olmo and Comas, 2008; Soto et al., 2010), remaining uncertain stage boundaries. In this work we propose a refined planktonic foraminifer-based chronology of the Alboran sites 976 (Hole B; Leg 161), 121 (Leg 13) and two industrial boreholes Andalucía-G1 (And-G1) and Alboran-A1 (Alb-A1) that were included in order

to fill the hiatuses present in the DSDP/ODP sites. Mineralogy and elemental geochemistry of Site 976 have been carried out for generating additional information regarding the paleoenvironments and post depositional diagenetic processes. These re-analysed records give us new important insights regarding the effects (and possible causes) that the profound paleogeographic changes happening since the beginning of the Messinian produced in the WAB.

2. Geological setting

The Alboran Sea is a back arc basin (Horvath and Berckhemer, 1982) that forms a narrow marine embayment of 150 km of width in the westernmost extremity of the Mediterranean Sea (Ryan et al., 1973), just above the area of European and African plate convergence (Gutscher et al., 2002; see Figure 1A).

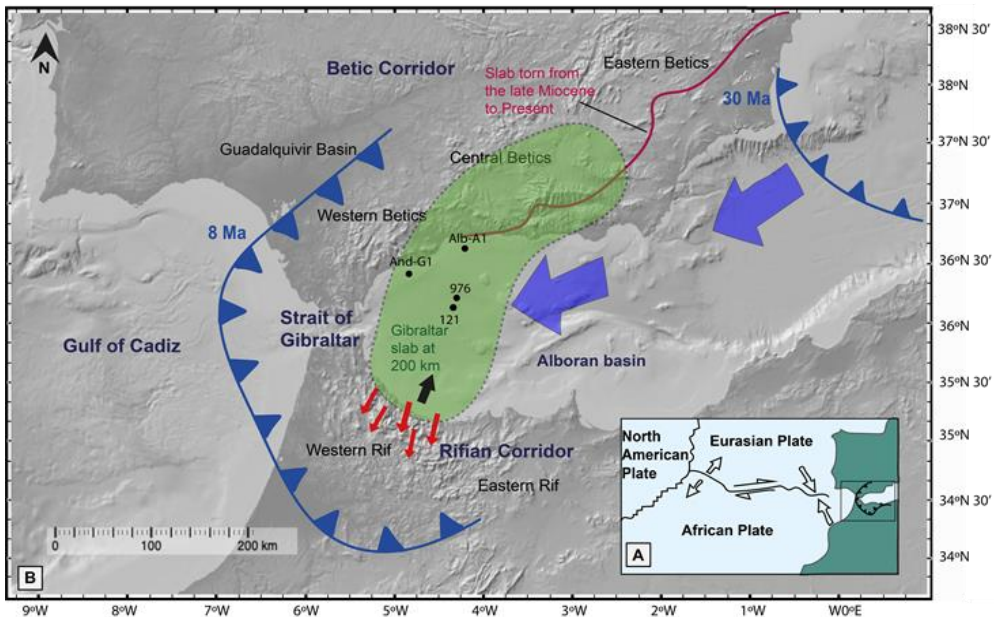


Figure 1: Grayscale topographic map of the Alboran Sea area (<http://www.geomapapp.org/>) showing the main tectonic features of the study area and the studied cores and boreholes (And-G1, 121, 976B and Alb-A1). A) Simplified sketch of African and European Plate collision where the black line with thrust symbols indicates the Gibraltar Arc (modified from Gutscher et al., 2002). B) In blue the present day geometry (since 8 Ma) of the Gibraltar arc trench and its hypothetical position at 30 Ma (Frasca et al., 2016). The green shading is a cartoon representation of the slab while the red arrows show the SSW indentation of the Rif due to NNW slab dragging showed by the black arrow (Capella et al., 2020; Spakman et al., 2018). The red line shows the slab edge tearing from the upper Miocene to the present (Mancilla et al., 2015).

The plate convergence began in the Cretaceous (Dewey et al., 1989) whereas the development towards its current configuration started approximately at ~25-30 Ma during the continental collision between Iberian and African passive margins (Crespo-Blanc and de Lamotte, 2006; Do Couto et al., 2016; Frasca et al., 2016) and subsequent N-S extensional collapse of the Alpine orogen known as Betic-Rif arc (Soto et al., 2010). At this time, the convergence slowed down starting an E-W trench retreat and slab rollback that resulted in back-arc extension (Heit et al., 2017) accompanied with a westward migration of the Alboran domain (Booth-Rea et al., 2007, see Figure 1B). The subduction zone migration lead to a synchronous tholeiitic to calc-alkaline (Duggen et al., 2004) volcanic archipelago development in the EAB (Balanya et al., 2012). Because of the compression of the Alboran domain against the edge of the continent (docking), around 8 Ma the slab rollback decelerated (Spakman et al., 2018) leaving the Gibraltar arc in its current position (Vergés and Fernández, 2012, see Figure 1B) and NNW-directed slab dragging as a residual motion (Capella et al., 2020). Around 8 Ma the regime of the Alboran basin changed and the areas of the Betic and Rifian corridors experienced progressive uplift, taught to be the result of westward moving slab tearing (Garcia-Castellanos and Villaseñor, 2011; Govers, 2009; Mancilla et al., 2015) and coeval indentation of the Moroccan margin (Fadil et al., 2006). After this initial phase, in the early Pliocene northwest-southeast shortening and associated strike-slip faulting began to develop and didn't cease until the Holocene (Soto et al., 2010).

This structural reorganization accompanied by synsedimentary faulting and differential subsidence, lead to the deposition of a thick, Neogene sedimentary infilling (Díaz-Merino et al., 2003), reaching up to 8 km in the main depocenters as the WAB (Iribarren et al., 2009). The Miocene deposition was occasionally perturbed by the development of mud diapirs, associated with mud volcanism which led to the formation of different faults systems and antiforms (Soto et al., 2010) which resulted in the development of the Mud Diapir Province (MDP; López-Rodríguez et al., 2019) in the westernmost sector of the WAB. The latter deformed the sedimentary records, complicating the seismic reflector correlation in some Alboran sectors. In relation to the tectonic regimen of the Alboran basin, it is possible to find syn- and post-rift deposits, where the oldest are of late Burdigalian age (20.44 - 15.95 Ma), and the youngest Quaternary (2.58 Ma - present). The succession is punctuated occasionally by regional unconformities (Do Couto et al., 2016).

The WAB sector studied in this paper is not part of the MDP (López-Rodríguez et al., 2019) and its overall geometry consists of a sedimentary wedge, progressively thickening from the coastal area towards the basement horst at ODP 976 Site. The wedge comprises a Langhian-Holocene sedimentary

succession of which in this paper we studied Upper Tortonian-Lower Pliocene, relevant for the MSC event.

3. Materials and methods

3.1 Planktonic foraminifers and residue analyses

We performed a quantitative study of the planktonic foraminiferal content of a total of 121 samples from ODP Site 976, Leg 161 (36° 12' 18.78" N, 4° 18' 45.78" W; Figure 1A) in the WAB, focusing in particular on the Messinian sediments as well as the latest Tortonian and earliest Pliocene. The cores were sampled at irregular sampling intervals, depending on the sediment availability trying to stay within a density of 10-30 cm when possible. The sediments were dried in the oven and a weighted fraction of each sample was then disaggregated in water and washed over a >63 µm and >150 µm sieve. In this work, the >150 µm fraction has been analyzed. Aliquots containing preferably 300 planktonic foraminifer specimens were identified and counted under a dissection microscope. From this Site, the sand fraction per gram represented by the sum of the >63 µm and >150 µm grain fractions in respect to the total weight of the sample was also calculated.

Additionally, 12 available samples (one for each core section) from the poorly recovered DSDP Site 121, Leg 13 (36° 09.65' N, 04° 22.43' W; Figure 1B), and 50 available samples from industrial boreholes And-G1 (36° 23' 47.62" N, 04° 45' 08.61" W; Figure 1B) and Alb-A1 (36° 36' 3.99" N, 02° 44' 04.02" W; Figure 1B) were analyzed and targeted for qualitative biostratigraphic analyses. Because of the lack of continuous coring in these industrial wells, only some drill cuttings were retrieved making the sample density extremely low and therefore precluding the production of a continuous micropaleontological record. In addition to foraminifers, other particles in the residues were counted (lithic fragments, pyrite, anhydrite particles etc.) to estimate relative proportions.

In order to estimate the plankton response to eventual oceanographic changes, we calculated the abundance of warm, oligotrophic water planktonic foraminifers (WOWPF; mainly *Globigerinoides* spp., *Orbulina universa* and *Globorotalita apertura*) and the abundance of cold eutrophic water planktonic foraminifers (CEWPF; comprising *Globigerina bulloides*, *Globigerinata glutinata* and *Neogloboquadrina* spp.) following Sierro et al. (2003).

3.1.1 Foraminifer biostratigraphy

The proposed planktonic foraminifer biostratigraphy scheme for the late Miocene-early Pliocene of the Alboran Basin was mainly based on bioevents from the recent astronomically calibrated charts compiled by (Lirer et al., 2019). The main planktonic foraminifer bioevents used in this work are reported in Table 1. Additionally, the disappearance of benthic foraminifer species, *Siphonina reticulata* has been used to improve the biostratigraphic interpretation (Kouwenhoven et al., 1999).

Table 1: Late-Miocene-early Pliocene biostratigraphic foraminiferal events in the Mediterranean used in this study are based on the revised planktonic biostratigraphic scale of Lirer et al. (2019). Only the age of the *S. reticulata* bioevent is taken from Kouwenhoven et al. (2003). The numbers are the bio-event abbreviations used in the text and figures.

Bioevent	Species	Astronomically calibrated age	N°
FCO	<i>G. margaritae</i>	5.08 Ma	9
Bottom acme	<i>Sphaeroidinellopsis</i> spp.	5.3 Ma	8
S/D coiling	<i>N. acostaensis</i>	6.35 Ma	7
Disappearance	<i>S. reticulata</i>	7.167 Ma	6
LO	<i>G. suterae</i>	7.17 Ma	5
FCO	<i>G. miotumida</i> group	7.24 Ma	4
LCO	<i>G. menardii</i> 5 group (dextral)	7.23 Ma	3
FCO	<i>G. menardii</i> 5 group (dextral)	7.36 Ma	2
LCO	<i>G. menardii</i> 4 group (sinistral)	7.56 Ma	1

For cutting samples from the industrial boreholes, only last occurrences were considered because of the possible downhole contamination.

3.2 Semi quantitative geochemistry (x-ray fluorescence and mineralogy)

The archive halves of 976B sections (from 61X-7 until 65X-5), were scanned by the X-ray fluorescence (XRF) Avaatech core scanner at MARUM (Research Faculty, Bremen University) in order to determine the concentration of major and trace elements present in the sediment. The split core surface was cleaned, covered with a 4 µm SPEXCerti Prep Ultralene 1 foil to avoid contamination of the XRF measurements. The here reported data have been acquired by a Canberra X-PIPS Silicon Drift Detector with 150 eV X-ray resolution, the Canberra Digital Spectrum Analyzer DAS 1000, and an Oxford Instruments 50W XTF5011 X-Ray tube with rhodium (Rh) target material. Maximum scanning resolution was attempted, but due to the bad core preservation and

occasional intercalations of perforating mud, the sampling steps were inserted manually ranging between 1 and 7 cm. Two runs were made, one using generator settings of 30 kV, current of 1.0 mA and a sampling time of 15 sec, while the second run was performed with 10 kV, 0.2 mA and only 10 sec of sampling time. Some elements were discarded because of their low reliability due to their poor detection. In order to better understand the different factors influencing the geochemical composition of the sediments we performed a principal component analyses (PCA) with the Past version 3.14 software package (Hammer et al., 2008). To achieve normal distribution and minimize the possible bias produced by core surface preparation, changes in lithology and light element signal attenuation (Tjallingii et al., 2007; Weltje and Tjallingii, 2008), prior to performing the PCA the dataset was normalized to the total raw counts of each measure point and then standardized by subtracting the average and dividing by the standard deviation (Davis and Sampson, 1986).

Non-planktonic particles identified in three washed samples of 121 DSDP Site (20R, 19R, 20R) were picked and grinded. Subsequently, X-ray diffractograms were obtained using a Polycrystalline powder diffractometer - Bruker D8 Advance ECO with Cu-K α radiation, automatic slit and LYNXEYE 1D detector. Scans were run from 2 - 64° 2 θ . The obtained diffractograms were interpreted using BRUKER EVA V.10.0.10 software.

3.3 Seismic and downhole logging data

The 2D-3D seismic profile grid available for this study covers practically the whole Northern sector of the WAB (Figure 2). Because of the fragmentary nature of the sedimentological records, these 2D-3D seismic lines and downhole log measurements were used to better correlate the drilling sites and identify eventual discontinuities and hiatuses in the record. Seismic profiles resulted very helpful for mapping the stratigraphic units and build isopach maps. In particular two single (3D crossline and N83_N206_S-83) and one composite 3D-2D seismic line (ALB81-35, ALB81-35B and 3D arbitrary line) acquired at the drill sites locations are highlighted in Figure 2. Aside from some physical properties of the sediments like magnetic susceptibility, the downhole logging tools considered in this study were Gamma ray (natural gamma radiation) and Sonic log (travel time) retrieved from the ODP Log database (<https://www.ldeo.columbia.edu/research/marine-geology-geophysics/odp-log-database>) and industrial drilling reports. To identify the presence of periodicities in the Sonic log velocities time series analyses was performed with Past 3.14 software using the Spectral analyses (simple periodogram).

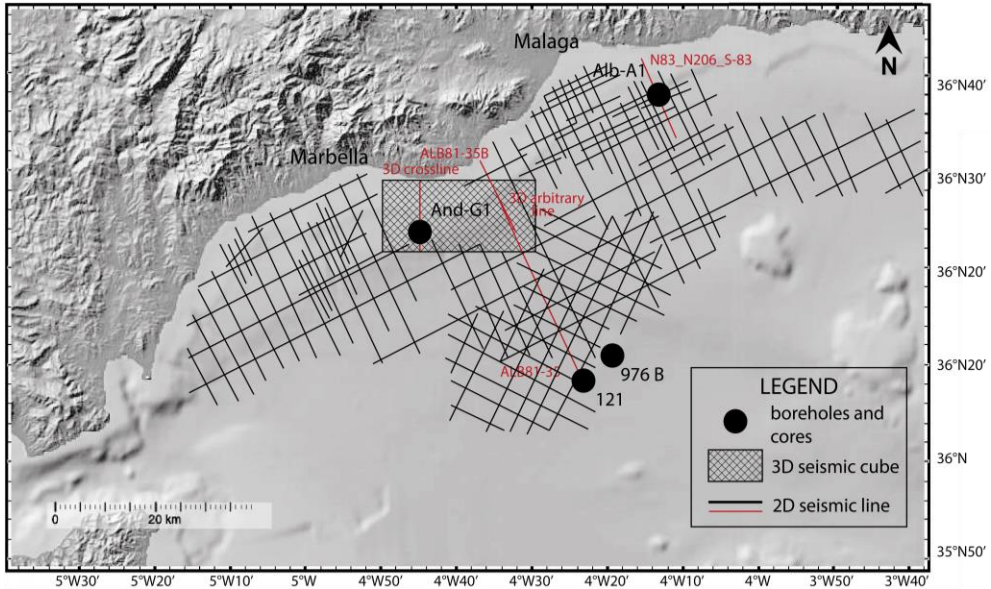


Figure 2: Grayscale topographic map of the Alboran Sea area (<http://www.geomapapp.org/>) showing the studied core and borehole position paired with the 2D-3D seismic grid and studied seismic sections (in red).

4. Late Miocene-early Pliocene seismic units in the WAB

To investigate the pre-evaporite Messinian succession in the WAB we used some seismic profiles (Figure 2) to identify the main sedimentary units and analyzed the micropaleontological, geochemical and mineralogical content of the few boreholes that have been drilled crossing these Late Miocene-Early Pliocene sections. We mainly focused on the analysis of ODP Site 976 with some additional data from DSDP Site 121 and industrial boreholes And-G1 and Alb-A1.

From the composite seismic line in Figure 3 (ALB81-35B, 3D arbitrary line and line ALB81-35B) it is possible to see that sites 976 and 121 are located on a structural high with a visible erosional surface on top (M reflector), highlighting that a big part of the upper Messinian deposits are missing (magenta line in Figure 3). Moving towards the coast, at And-G1 and Alb-A1 wells location, the Messinian sediments, referred in previous studies as Messinian Unit II (Comas et al., 1999), SU 7 (Do Couto et al., 2016) or Unit A6 (Díaz-Merino et al., 2003; Soto et al., 2010), contain two different sub-units (e.g. Figure 3, 4, 5). The lower one is composed by plane-parallel strata, while the upper one displays a more chaotic aspect.



Figure 3: Composite seismic profile (ALB81-35B, 3D arbitrary line and line ALB81-35) showing with a full line, the DSDP Site 121 and with a dashed one the projection of ODP 976 Site and And-G1 industrial well. The colored lines show the top of different geological stages: in yellow: top Tortonian; in black dashed: base of the chaotic deposit; in magenta: top Messinian and M reflector; in green: top Pliocene.

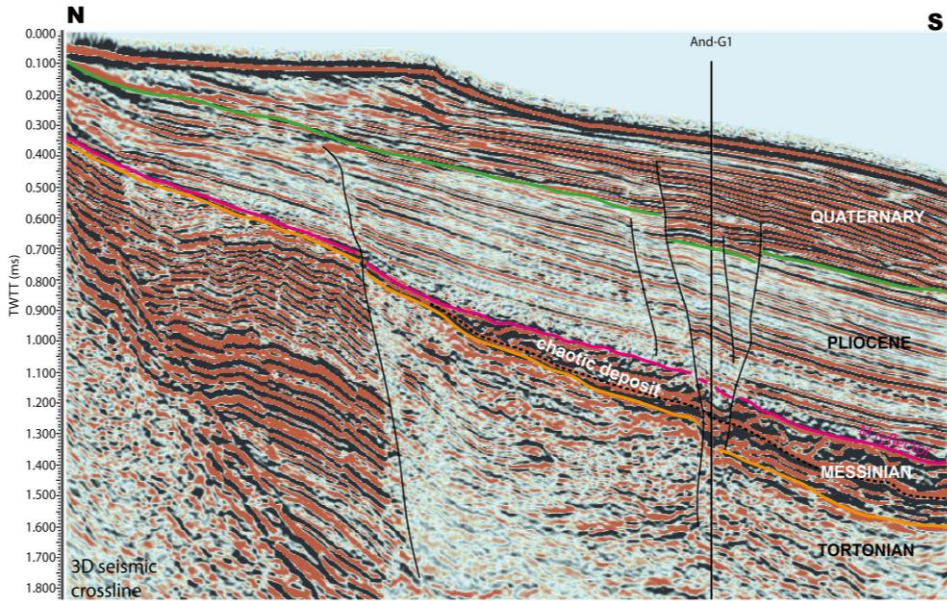


Figure 4: 3D Seismic crossline showing with a full line And-G1 well position. The colored lines show the top of different geological stages: in yellow: top Tortonian; in black dashed: base of the chaotic deposit; in magenta: top Messinian and M reflector; in green: top Pliocene, while the black lines highlight the faults.

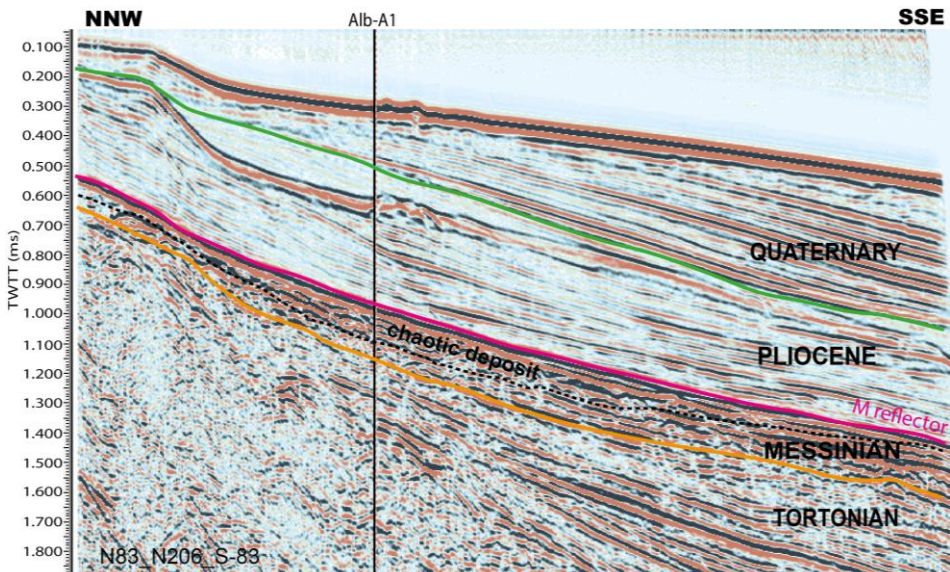


Figure 5: N83_N206_S-83 seismic line with a black full line indicating the position of industrial well Alb-A1. The colored lines show the top of different geological stages: in yellow: top Tortonian; in black dashed: base of the chaotic deposit; in magenta: top Messinian and M reflector; in green: top Pliocene.

The lowermost part of the lower unit was recovered at site 976 and 121 and is characterized by hemipelagic sedimentation as will be described below. In contrast, the chaotic unit is overlying the hemipelagic one only in the northern part of the basin while it was completely eroded towards the south. The chaotic unit is topped by the Pliocene with no apparent unconformity in the North while in the South the reflector truncates the uppermost Messinian deposits, as shown by other authors as well (Comas et al., 1999; Do Couto et al., 2016; Martínez del Olmo and Martín, 2016 and others).

Although we mainly focus on the Messinian hemipelagic unit recorded at Site 976 and 121, we explore the sedimentary characteristics of the chaotic unit (Figure 4 and 5) analyzing sediment cuttings from boreholes And-G1 and Alb-A1. Sediment cuttings analyses and downhole logging data show that this Unit is characterized by lower gamma ray values and higher grain sizes, mainly rich in detrital metamorphic clasts, anhydrite minerals with occasional pyrite (Figures 6 and 7). In the seismic sections, where present, the unit shows higher thicknesses towards the center of the basin, while it pinches out in the proximity of the coast (Figure 3). As the isopach map evidences (Figure 8), this unit extends in a large sector of the Spanish margin, reaching a thickness of up to 240 m in the central parts of the northern WAB to some tens of meters closer to the coast.

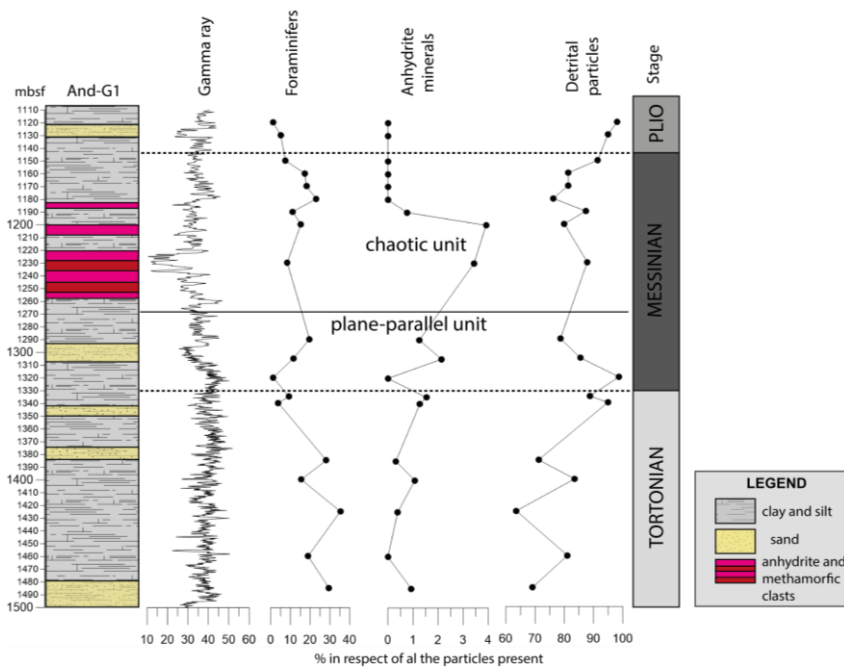


Figure 6: Alboran Basin And-G1 industrial borehole stratigraphic log derived from industrial drilling reports. From left to right the gamma ray, total foraminifers, anhydrite minerals and detrital particles are shown.

Messinian West Alboran Sea record in the proximity of Gibraltar:
Early signs of Atlantic-Mediterranean gateway restriction

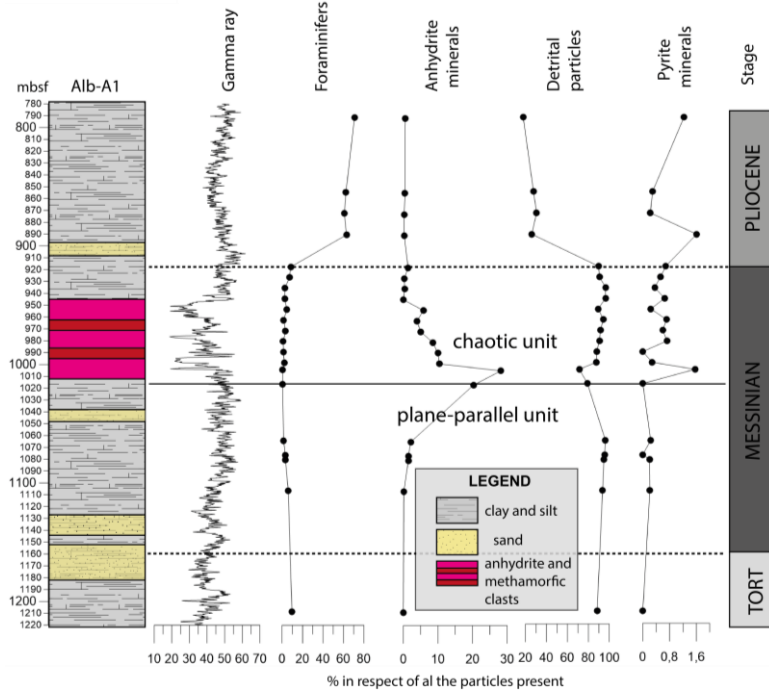


Figure 7: Alboran Basin Alb-A1 industrial borehole stratigraphic log derived from industrial drilling reports. From left to right the gamma ray, total foraminifers, anhydrite minerals, detrital particles and pyrite minerals are shown.

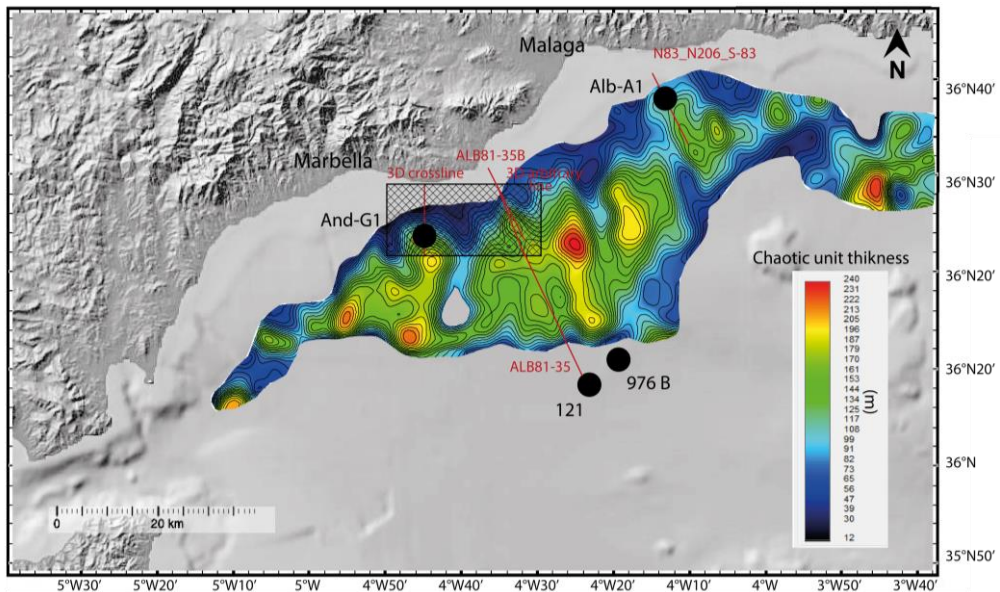


Figure 8: Isopach map showing the thickness of the chaotic unit (top Unit II from Comas et al., 1999). Cold tones indicate low, while warmer tones higher widths.

5. Planktonic and benthonic foraminifer association and biochronology

The biochronology of the four studied cores and boreholes (Figure 9) was based on several planktonic and one benthonic (Figure 10) foraminifer bioevents reported in Table 1.

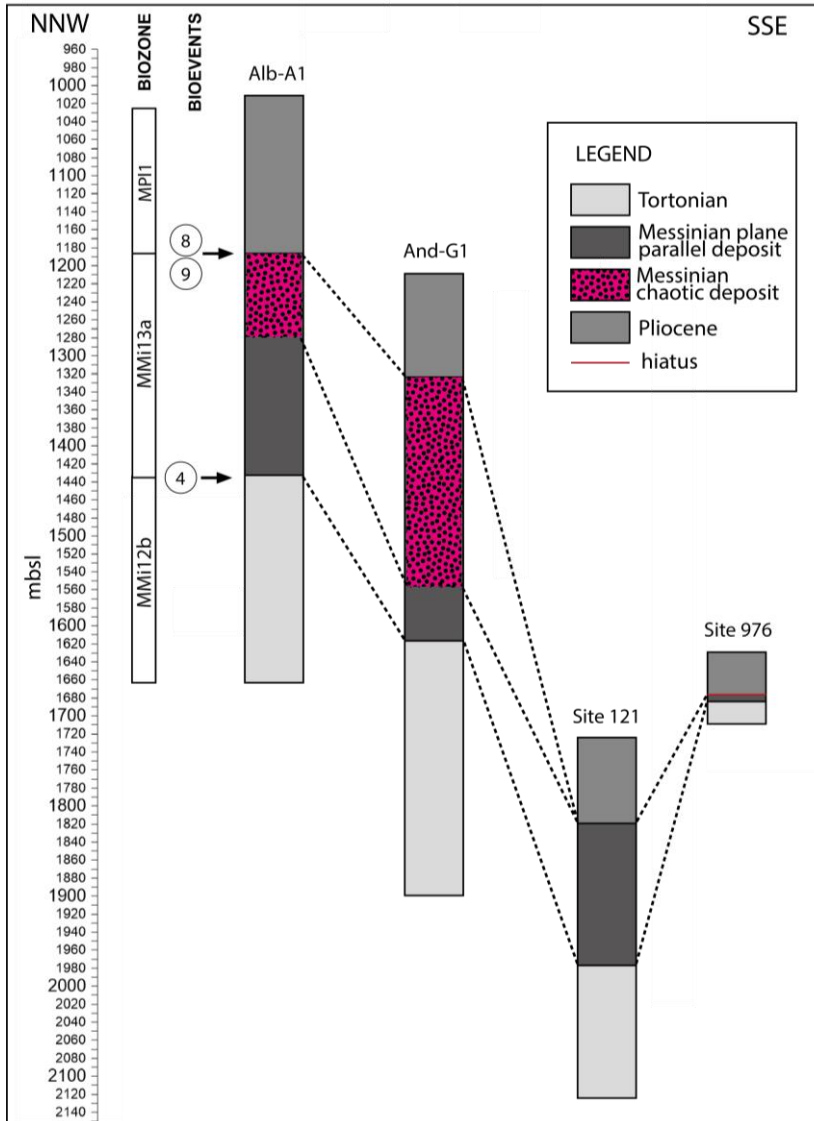


Figure 9: NNW-SSE stratigraphic correlation between the four analysed sites. The main identified biozones (Lirer et al., 2019) include: the *G. menardii* group biozone (MMi12b), the *G. miotumida* group biozone (MMi13a) and the *Sphaeroidinellops* spp. biozone (MPI1). The circled numbers on the left hand-side represent the main stage boundary bioevents (Lirer et al., 2019): 4-FCO of *G. miotumida* (7.24 Ma); 8-bottom acme of *Sphaeroidinellops* spp. (5.3 Ma) and 9-FCO of *G. margaritae* (5.08 Ma) reported in Table 1.

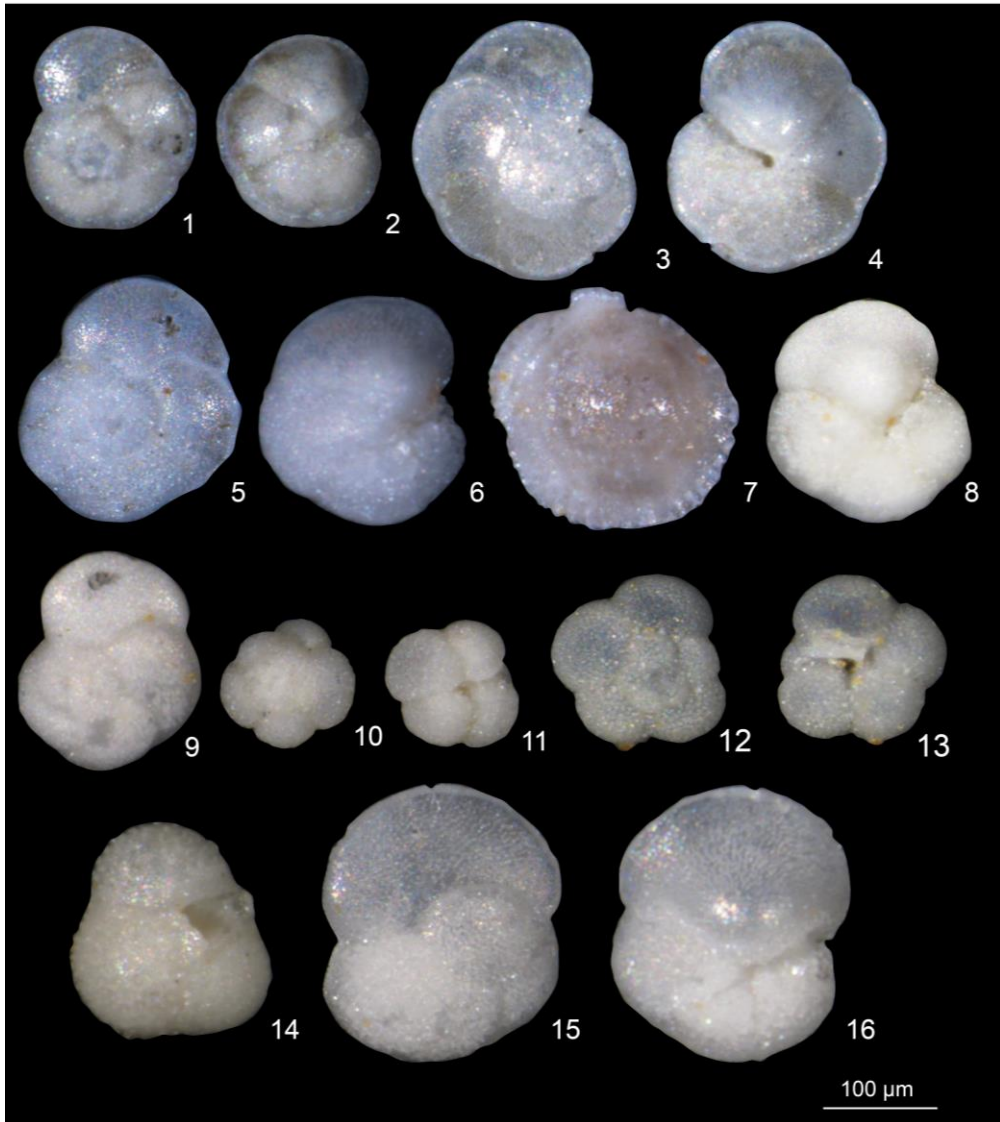


Figure 10: Photographs of planktonic and benthonic biomarker specimens from the studied sites. 1-2: *Globorotalia menardii* 4 on the dorsal (1) and ventral view (2). 3-4: *Globorotalia menardii* 5 on the dorsal (3) and ventral view (4). 5-6: *Globorotalia miotumida* on the dorsal (5) and ventral view (6). 7: *Siphonina reticulata*. 8-9: *Globorotalia scitula* on the dorsal (8) and ventral view (9). 10-13: *Neogloboquadrina acostaensis* sinistral on the dorsal (10) and umbilical view (11); *Neogloboquadrina acostaensis* dextral on the dorsal (12) and umbilical view (13). 14: *Sphaeroidinellopsis* spp. 15-16: *Globorotalia margaritae* on the dorsal (15) and ventral view (16).

5.1 ODP Site 976

The planktonic foraminifer association (Figure 11) of the homogeneous nannofossil-rich claystone and nannofossil sandy claystone (Comas et al., 1996) of Site 976 is mainly composed of *Globigerina bulloides*, *Globorotalita apertura* spp. (*G. apertura* + *G. druryi*) and *neogloboquadrinid* species (*Neogloboquadrina acostaensis* + *Neogloboquadrina atlantica* + *Neogloboquadrina humerosa*). The abundances of planktonic foraminifers are high reaching up to 6000 individuals/gram, while benthonic species are scarcer and reach maximum values of only 80 individuals/gram.

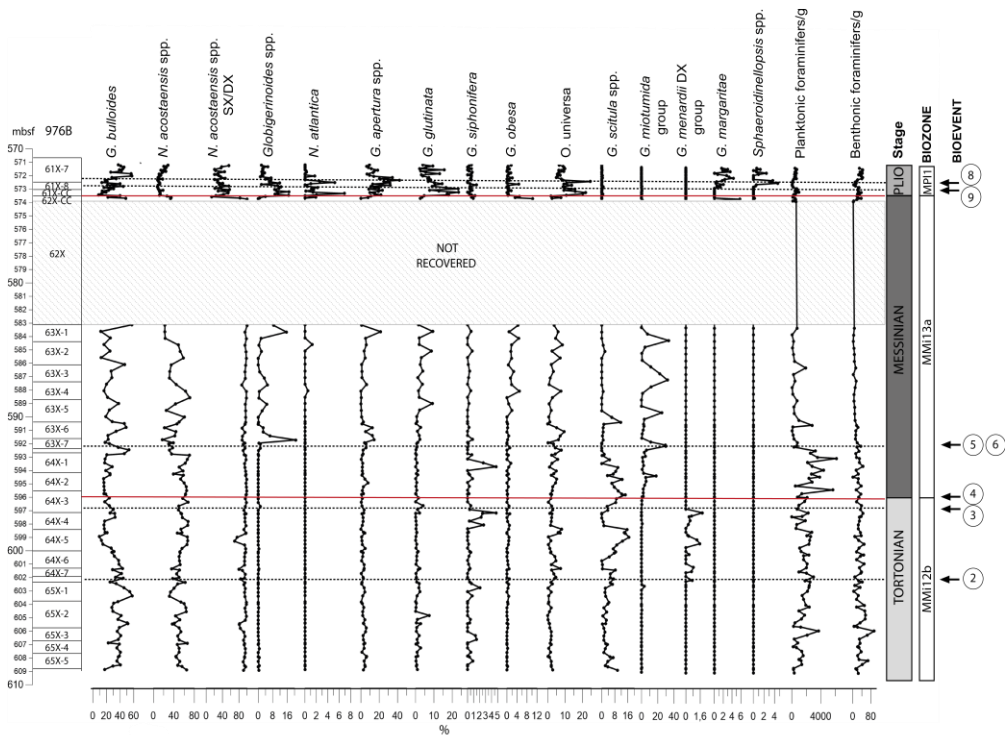


Figure 11: Alboran Basin ODP Site 976. Most abundant planktonic foraminifer species, corresponding biozones and bio-events are shown (Lirer et al., 2019). The main biozones include the *G. menardii* group biozone (MMi12b), the *G. miotumida* group biozone (MMi13a) and the *Sphaeroidinellopsis* spp. biozone (MPT1). The main identified bioevents are reported using number abbreviations: 2-FCO of *G. menardii* 5 group (7.36 Ma); 3-LCO of *G. menardii* 5 group (7.23 Ma); 4-FCO of *G. miotumida* group (7.24 Ma); 5-LO of *G. suterae* (7.17 Ma); 6-Dissaperance of *S. reticulata* (7.167 Ma); 7-5/D coiling change in *N. acostaensis* (6.35 Ma); 8-bottom acme of *Sphaeroidinellopsis* spp. (5.3 Ma) and 9-FCO of *G. margaritae* (5.08 Ma) reported in Table 1. Additionally, the figure shows the planktonic and benthonic foraminifers per gram curves.

The FCO of *G. menardii* 5 group has been located at 601.96 mbsf. This event has been recognized (Sierro, 1985; Sierro et al., 1993) and dated at 7.36 Ma (Hilgen et al., 2000; Lourens et al., 2004) in the Mediterranean and NE Atlantic. The Tortonian-Messinian boundary in the NE Atlantic is characterized by the replacement of the *G. menardii* group (Tjalsma, 1971) by the *G. miotumida* group (Sierro, 1985; Sierro et al., 1993) at an astronomically calibrated age of 7.24 Ma (Hilgen et al., 2000; Lourens et al., 2004). In the Mediterranean the two species do not coexist (Figure 12) and this boundary is associated with the FCO of typical Messinian *G. miotumida* group (Anthonissen and Ogg, 2012; Antonarakou et al., 2004; Sierro, 1985; Sierro et al., 1993). This event was identified at this site at 596 mbsf, in line with the interval defined by the initial ODP reports (Zahn et al., 1999). The sharp decrease of benthonic species *S. reticulata* at 592 mbsf, was correlated to the homonymous event (Figure 12; Section 6 for more details), recorded throughout the Mediterranean basin at 7.167 Ma (Kouwenhoven et al., 1999; Kouwenhoven et al., 2003). This age is further confirmed by the drastic drop in *G. scitula* spp. (Figure 12), mainly composed of *G. suteræ*, which LO has been identified in Gibliscemi section (Sicily, Italy) and astronomically tuned at 7.17 Ma (Hilgen et al., 1995; Lirer et al., 2019). In our record, *neogloboquadrinids* are usually sinistraly-coiled with the exception of the uppermost samples from core 61, above 573.5 mbsf, from where they become dominantly dextral (Figure 11). Based on this we can state that these sediments are certainly younger than 6.35 Ma (Achalhi et al., 2016; Anthonissen and Ogg, 2012; Lourens et al., 2004; Sierro et al., 1993; Sierro et al., 2001). The *Sphaeroidinellopsis* spp. bottom acme has been identified in the Mediterranean at 5.3 Ma (Lourens et al., 2004) and in our record, it can be identified at 572.31 mbsf (Section 5.1.1 for more details). While in the Atlantic the FCO of *G. margaritæ* has been tuned at 6.31 Ma in Ain el Beida section - Atlantic Morocco (Krijgsman et al., 2004), the appearance of this species in the Mediterranean basin has shown a clear delay in respect to the open ocean (Zijderveld et al., 1986). In fact, in the Mediterranean its presence is registered only from 5.08 Ma (Lourens et al., 2004). In Site 976 this event is not clearly visible (Figure 11; Section 5.1.1 for more details).

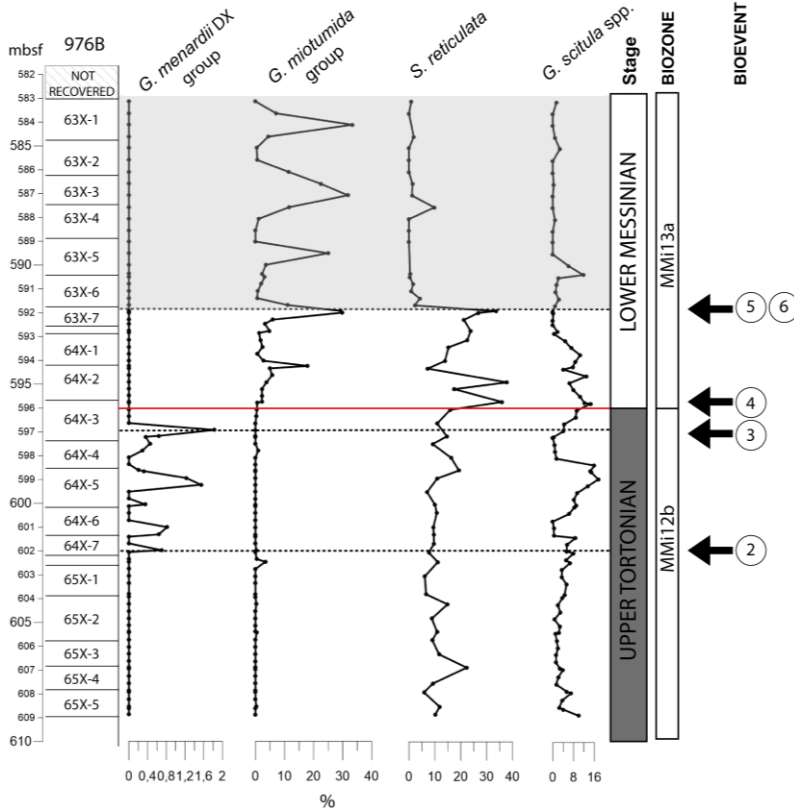


Figure 12: Alboran Basin ODP Site 976. The graph shows the main Tortonian and Messinian planktonic foraminifer biozones from Lirer et al. (2019): *G. menardii* group biozone (MMi12b) and the *G. miotumida* group biozone (MMi13a) while the identified bio-events (Lirer et al., 2019) are marker by number abbreviations: 2-FCO of *G. menardii* 5 group (7.36 Ma); 3-LCO of *G. menardii* 5 group (7.23 Ma); 4-FCO of *G. miotumida* (7.24 Ma); 5-LO of *G. suterae* (7.17 Ma) and 6-Dissaperance of *S. reticulata* (7.167 Ma); reported in Table 1.

5.1.1 Miocene-Pliocene boundary (MPB)

Because of the poor sediment recovery near the MPB of Site 976, the succession of bio events is not easy to interpret (only 3 samples were analyzed from core 62X-CC and their depth position is not certain). Our quantitative distribution of planktonic foraminifer species (Figure 13) shows a pattern that does not fit with the classic biostratigraphic framework for the earliest Pliocene (Cita, 1975; Iaccarino et al., 1999b) which could be related to ecological factors (e.g. Corbí and Soria, 2016; Iaccarino et al., 2007). We clearly identified *Sphaeroidinellopsis* spp. bottom acme at 572 mbsf which is traditionally found at the base of the Pliocene. However, the first occurrence of *G. margaritae* is usually placed in other Mediterranean sections after the bottom acme of *Sphaeroidinellopsis* spp. at around 5.08 Ma, but we found this species regularly

present before the acme, but absent again in the lower most part of core 61, to reappear again in one of the three samples taken in core 62X-CC. We consider that this sample is the result of some technical drilling disturbance in the topmost part of the core catcher because the assemblage is completely different to the other samples. Indeed, If we do not consider this sample, the most abrupt change in the planktonic foraminifer assemblage clearly occurred between core section 61X and 62X. This change is shown by a sudden decrease in relative abundance of *G. bulloides*, *N. acostaensis* spp., *G. miotumida* group and an increase in *O. universa* and *Globigerinoides* spp., etc.. The abundant occurrence of *G. miotumida* group and the dominance of sinistral specimens of *neogloboquadrinids* strongly suggest an early Messinian age for these samples, older than 6.5 Ma, which is the age of the last regular occurrence of *G. miotumida* group in the Sorbas basin (Sierro et al., 2001) and certainly older than 6.35 Ma, when the first change from sinistral to dextral coiling in the *neogloboquadrinids* was registered (Krijgsman et al., 1999; Sierro et al., 2001). Consequently, we place the Messinian-Pliocene boundary between core sections 61X and 62X, although it is not possible to give an exact depth because only a core catcher of 30 cm was recovered in core 62X and its depth position is unknown. This sequence of events suggest that the first sediments overlying the Messinian/Pliocene erosive surface were deposited at the base of the Pliocene and that the first deposits were even older than the bottom acme of *Sphaeroidinellopsis* spp.

Taking a closer look at the foraminifer record, from 573.50 mbsf different changes can be observed. Even though there are no evident variations in the lithology or sediment color (Figure 13), species *O. universa*, *N. atlantica* and *G. glutinata* all show a sharp increase in abundance that continues until 572.60 mbsf. *Orbulina universa* is a warm oligotrophic species currently living in the surface mixed layer, proliferating especially in summer when water is stratified due to the high temperatures and freshwater inputs (Brachert et al., 2015; Sierro et al., 2003). Their peak abundances, in this interval reaching up to 25%, could be connected to the relatively warmer climate recorded after 5.5 Ma in many isotopic and pollen records. The maxima of this warming trend according to Jiménez-Moreno et al. (2013) occurs at the Miocene-Pliocene boundary, as inferred by the highest spreading of *Quercus*. On the other hand, *G. glutinata* and *N. atlantica* are typical cold eutrophic water foraminifers (Sierro et al., 2003). Their appearance could be connected with the first influxes of cold Atlantic waters into the Mediterranean, which would have been faced with sudden and abrupt environmental change. Such environment could have been particularly favorable for the reproduction of ubiquitous and opportunistic species like *G. glutinata*. From 572.3 mbsf, the abundances of the three above mentioned species decrease, which could be indicative of the definite reestablishment of normal marine conditions in the Mediterranean. The latter could have not been

instantaneous but followed the actual Atlantic water ingression with one or more precessional cycles of delay (Di Stefano et al., 2015; Iaccarino et al., 1999a; McKenzie et al., 1990; Pierre et al., 2006).

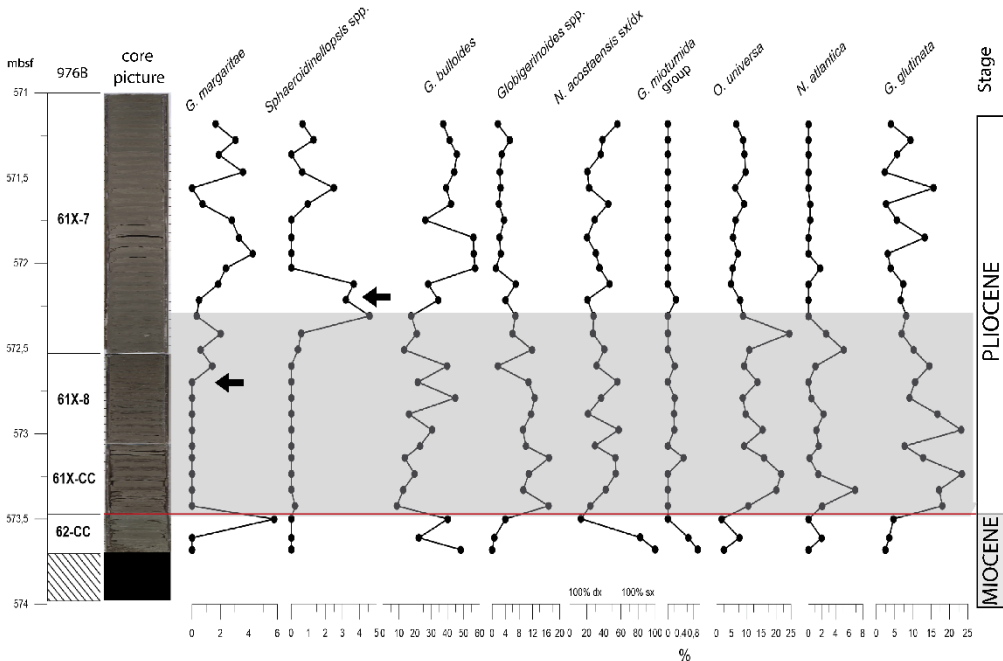


Figure 13: The Miocene-Pliocene boundary in core 976B. Aside from core photographs, some relevant foraminifer species abundances are plotted. Two main bio-events are highlighted by black arrows.

Our results, therefore, indicate the Miocene-Pliocene boundary is not placed between sample 61X-CC (574.13 mbsf) and sample 61X-7, 71-73 cm (572.37 mbsf; Serrano et al., 1999; Zahn et al., 1999) as originally reported in ODP 976 biostratigraphic report (Zahn et al., 1999), but between core 61 and 62, although, we do not see a pronounced change in the sedimentary succession (Figure 13) or a change from brackish environment to open marine conditions (Cita et al., 1978; Pierre et al., 2006) like in many other Mediterranean sites.

Considering the uncertainties associated to depth calculations based on p-wave velocities, we assume that the Messinian-Zanclean boundary located at around 573.50 mbsf coincides with the pronounced erosional surface defined throughout the Alboran basin, probably originated by the Zanclean re-flooding. Our age estimations, however, disagree with the chronostratigraphic framework proposed by Popescu et al. (2015) that moved the Miocene-Pliocene boundary to 585.22 mbsf due to the lowest occurrence of *C. acutus*, highest occurrence of *T. rugosus* at 585.22 mbsf and the lowest occurrence of *C. rugosus*

at 584.02 mbsf, dated respectively at 5.345 Ma, 5.279 Ma and 5.12 Ma (Raffi et al., 2006). This suggests that these nanoplankton events may represent regional occurrences.

5.2 DSDP Site 121

The foraminiferal content of the marls and graded sands that dominate Site 121 (Ryan et al., 1973) is extremely similar to Site 976 and it contains mainly *G. bulloides*, *N. acostaensis*, *G. apertura* and *Globigerinoides* spp. which are usually found in a residue where sand fragments and lithic/detrital particles are abundant. Because of the poor sediment recovery and the low number of samples analysed, age determination was less straightforward and was mainly based on species presence or absence. The last occurrence of *G. menardii* 4 group was placed between 820 and 860 mbsf, this interval must be dated as Late Tortonian (≥ 7.56 Ma), while the Tortonian-Messinian boundary was placed around 820 mbsf, where *G. menardii* 5 group and *G. miotumida* group coexist (Figure 9). The Miocene-Pliocene boundary is difficult to place, as already stated by Ryan et al. (1973) in the DSDP Initial Reports. Nonetheless, the presence of *G. margaritae* and *G. puncticulata* indicate that the sediments at 684 mbsf are already of Pliocene age (between 4.52 and 3.85 Ma) but the exact placement of the FCO events is not possible. These findings suggest that the boundary should be placed between 681 and 689 mbsf.

5.3 Industrial boreholes And-G1 and Alb-A1

The analyzed samples from And-G1 and Alb-A1 are clearly dominated by detrital and lithic particles, while the most abundant planktonic foraminifer species are *G. bulloides*, *N. acostaensis* and *G. apertura*. To identify bio-events in industrial boreholes cuttings it is necessary to keep in mind the possible downhole contamination and therefore it is better to consider last occurrences, while first occurrences are less trustworthy. In the two studied wells, only stage boundaries were identified.

In industrial well And-G1 the Tortonian-Messinian boundary is located at 1330 mbsf, where the last specimens of *G. menardii* 5 group can be identified. Even if foraminifer tests are scarce, the persistent presence of Pliocene species like *G. puncticulata* and *G. margaritae* from 1143 mbsf upward, suggests this sediment is most probably of Pliocene age and at this depth we place Miocene-Pliocene boundary (Figure 9).

A similar configuration and foraminifer content can be found in Alb-A1 borehole. Because of the presence of *G. menardii* 5 group at 1107 and *G. miotumida* group at 1209 mbsf the Tortonian-Messinian boundary was placed somewhere

between these two depths (Figure 9). The Miocene-Pliocene boundary is most probably located between 917 and 891 mbsf, because above this level the *neoglobobadrinids* are dominantly dextral and can be found together with Pliocene foraminifers such as *G. margaritae* and *G. puncticulata*.

6. Early Messinian Atlantic-Mediterranean restriction

6.1 Evidence from the geochemical and micropaleontological record

Immediately after the Tortonian-Messinian boundary (592 mbsf) a remarkable event in the sedimentary and micropaleontologic record was registered at Site 976 (Figure 14). At 7.167 Ma a drastic change in the elemental composition is recorded together with a sharp decrease in benthonic and planktonic foraminifers per gram.

The change in the geochemical record is mainly evident from the PCA, which was performed both on the sediment before (608.96 – 592 mbsf; interval A) and after (592 – 573.5 mbsf; interval B) this event (Figure 14 and 15). In particular, the first principal components (PC1A and PC1B, 71.5% and 45.3% of the total variance) controlled mainly by clay/detrital minerals like Al, Si, K, Ti, Fe, Rb and Zr on the positive, and biogenic elements (Ca and Sr) on the negative side, show an overall increase in values. These changes in the geochemical content strongly suggest that the ratio between the input rate of siliciclastic material and that of biogenic pelagic particles increased at that time. As the sediments mainly consist of nanofossil-rich claystone and nanofossil sandy claystone (Comas et al., 1999), because the sand content decreases upwards (Figure 14), we assume there was an increasing input of detrital clay or silt to the distal regions of the WAB at this time. This enhanced input of fine-grained siliciclastic particles to the basin could be related to uplift along the margins of the WAB. Indeed, from this point onward the sedimentation rate increases dramatically (see section 7.2), supporting an amplification of river erosion and sediment transport to the Alboran Basin. Accordingly, other studies have shown that in the Late Miocene we reach the largest sedimentary contribution in the WAB (Iribarren et al., 2009). This uplift certainly occurred in the Gibraltar Arc that constitutes the borderlands of the WAB. A similar increase in terrigenous versus biogenic input was recorded in the Guadalquivir basin (Van den Berg et al. 2018). This event was also associated to an uplift of the Betic orogen that forms the northern borderland of the WAB and was registered in the axial depocenters of the Guadalquivir basin by the onset of turbidite deposition triggered by the northern movement of the allochthonous unit (Sierra et al., 1995). PC2 (PC2A and PC2B, 13.5% and 26% of the total variance) displays some important changes as well (Figure 14), but only

at 974 mbsf, where the record shows a dominance of S and Br elements linked with more reducing bottom water conditions (Harff et al., 2011) and/or organic matter content (Agnihotri et al., 2008; Ziegler et al., 2008), both possibly inferring to delayed oxygen level change in the western Mediterranean water column. All these evidences support that this tectonic uplift (Garcia-Castellanos and Villaseñor, 2011; Iribarren et al., 2009; Sanz de Galdeano and Alfaro, 2004) was the cause of the first restriction of the Atlantic-Mediterranean water exchange during the Messinian and although an eastern Alboran sill can be excluded, we do not know the exact location of the strait or straits at that time.

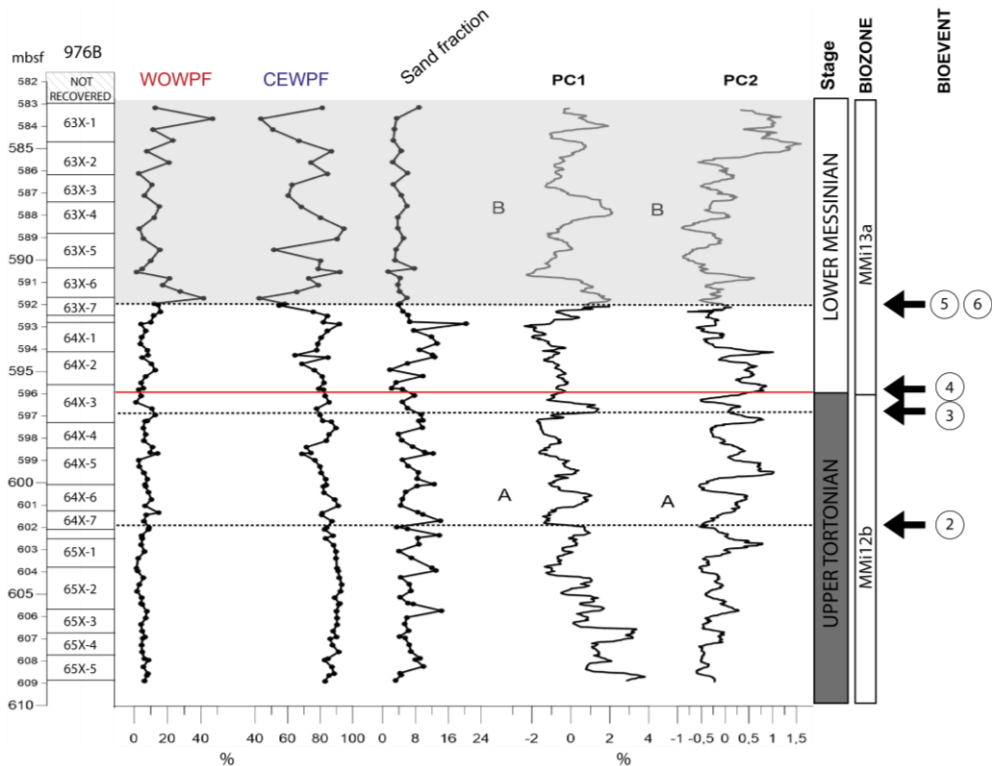


Figure 14: Alboran Basin ODP Site 976. The most visible changes in the micropaleontological and geochemical record registered from 592 mbsf upwards are shown. These include the WOWPF and CEWPF percentages, the sand fraction and the PC1A/B and PC2A/B curves with an 8-point and 16-point moving average respectively. The two identified biozones are the *G. menardii* group biozone (MMi12b) and the *G. miotumida* group biozone (MMi13a) which are reported on the right-hand side and followed by the main bio events indicated with numbers which include: 2-FCO of *G. menardii* 5 group (7.36 Ma); 3-LCO of *G. menardii* 5 group (7.23 Ma); 4-FCO of *G. miotumida* (7.24 Ma); 5-LO of *G. suterae* (7.17 Ma) and 6-Dissappearance of *S. reticulata* (7.167 Ma); all reported following Lirer et al. (2019).

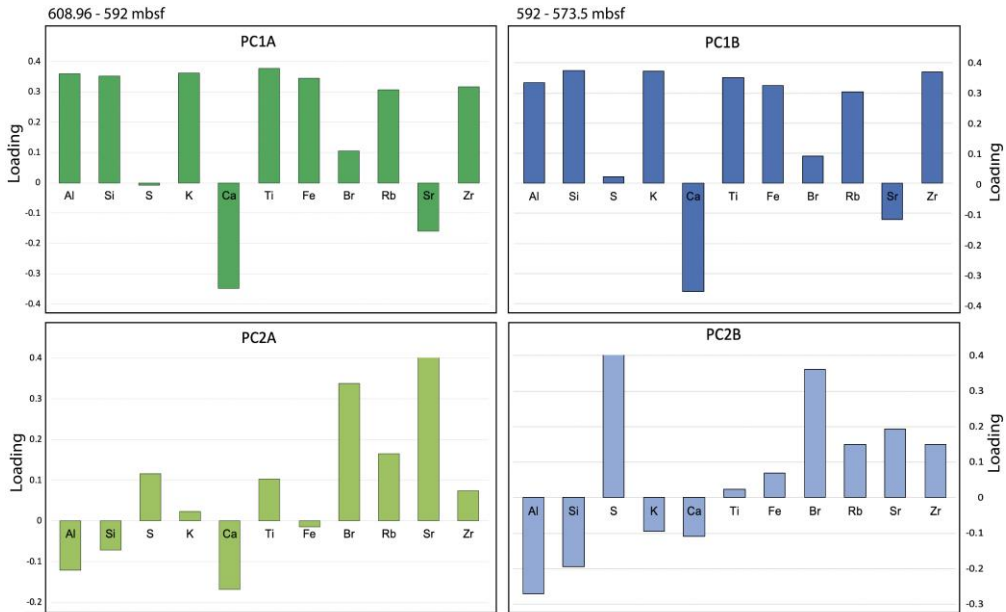


Figure 15: Loadings of the Principal Components of the pre-7.17 Ma sediments (PC1A and PC2A) and post-7.17 Ma sediments (PC1B and PC2B).

This Atlantic-Mediterranean restriction had a profound impact on the Mediterranean ecosystems, which is more visible in the marine meiofauna. At ODP Site 976 the event affected the benthic foraminifer assemblages and was especially recorded by the disappearance of *S. reticulata*. This event has been widely recognized in the eastern Mediterranean at 7.167 Ma (Kouwenhoven et al., 2003; Seidenkrantz et al., 2000).

The strongest restriction impact has been registered in the deep waters of the Eastern and Central Mediterranean, as records from several Italian (Trave section in Di Stefano et al., 2010; Monte Gibliscemi in Kouwenhoven, 2000), Greek (Faneromeni section in Kouwenhoven, 2000; Kouwenhoven and Van der Zwaan, 2006; Metochia section in Seidenkrantz et al., 2000), and Cypriot (Pissouri basin in Kouwenhoven et al., 2006) sites show. These locations register reduced deep marine ventilation and increased nutrient flux to the sea floor as reflected in higher abundance of benthonic low oxygen foraminifer species, indicators of stressed conditions like *Bolivina* spp., *Bulimina aculeata*, *Lenticulina* spp., *Uvigerina peregrina* etc. (Kouwenhoven et al., 2006; Kouwenhoven et al., 1999; Seidenkrantz et al., 2000). Here, the start of the progressive Mediterranean isolation coincides with the beginning of a more regular occurrence (Seidenkrantz et al., 2000) or even the first appearance of sapropel levels (Negri and Villa, 2000; Nijenhuis et al., 1996) which further confirms the increasingly adverse conditions and less oxygenated bottom waters.

At ODP Site 976 the impact of Atlantic-Mediterranean restriction is also visible in the planktonic foraminifer assemblages even though this site is very close to the Atlantic. The planktonic foraminifer assemblages in the late Tortonian and early Messinian up to the 7.167 Ma event, shows low diversity and high abundance of cold-water species such as *G. bulloides* or *N. acostaensis* and the absence of subtropical species such as those of the genus *Globigerinoides* (*G. extremus* + *G. immaturus* + *G. sacculifer*). However, from this point upward the relative abundance of the subtropical species increased (WOWPF, Figure 14). The latter are normally very abundant in the Messinian peripheral basins throughout the Mediterranean, especially at times of precession minima (northern Hemisphere insolation maxima) when the water column is strongly stratified, and warm waters prevailed at the surface. Indeed, the relative abundance of these species usually increases during sapropel formation (Sierro et al., 2003; Sierro et al., 2001 and others) and with the progressive isolation of such basins (Rouchy et al., 1998; Sierro et al., 2003). The almost complete absence of *Globigerinoides* spp. and abundant presence of well diversified planktonic foraminifers in the latest Tortonian of the WAB suggest this was a well ventilated, open deep basin. As the abundance of planktonic foraminifers in the total foraminiferal fauna can be used as an indicator of paleodepth where higher abundances imply higher depths and vice versa (e.g. Van der Zwaan et al., 1990), the high bathymetry is confirmed by the low percentages of benthonic foraminifers.

The high proportion of *G. bulloides* and *neogloboquadrinids* and the complete lack of subtropical species in the Tortonian and earliest Messinian before 7.167 Ma suggest a regime of upwelling with typically high nutrient supply to the surface and strong vertical mixing. This is especially significant because other latest Tortonian-earliest Messinian time equivalent sequences do not show this pronounced dominance of cold-water species (Sierro, 1985; Sierro et al., 2003). In particular, *G. bulloides* is very rich today in the upwelling of Malaga associated to the western gyre formed by the Atlantic surface water after crossing the Gibraltar Strait (Bárcena et al., 2004). Ultimately, all this suggest that Atlantic surface currents could have been flowing to the east along the northern margin of the Alboran Basin during the Tortonian and that due to geostrophic circulation moved southward, forcing the surgency of intermediate cold waters to the surface. Such circulation, even if very similar as today, could have been more intense, promoting the growing of species typical of these nutrient-rich waters and impeding the development of warm water species currently typical of the Mediterranean (Pérez-Folgado et al., 2003). This assumption points to the Gibraltar Strait, or another significant connection close to it, as the possible source of surface water to the Mediterranean at that time. The strong eastward

Atlantic inflow entering the Gibraltar Strait would have generated these anomalous cold conditions in the western Alboran Sea observed until 7.167 Ma.

The shift at 7.167 Ma to planktonic foraminifer assemblages richer in subtropical specimens must be a signal of relative more isolation of the Alboran basin at that time. A more stratified water column at times of summer insolation maxima resulted in higher sea surface temperatures that favored the growth of subtropical species. This restriction was most probably the result of the uplift mentioned above that would have affected both the Betic and Rifian corridors (Fadil et al., 2006; Mancilla et al., 2015; Van den Berg et al., 2018). Anyhow, the beginning of the Mediterranean-Atlantic restriction at 976 Site can also explain why from 7.167 Ma onward, a cyclical behavior of both the geochemical and micropaleontological record becomes obvious. Less water exchange between the Mediterranean and Atlantic would have amplified the impact of the Mediterranean climate changes, making the basin more sensitive to astronomical forcing (Gladstone et al., 2007).

Similar amplification effects are recorded in other western Mediterranean basins such as in the Sorbas basin (Sierro et al., 2003) or in shallower sections from the Central Mediterranean like Monte del Casino section (Kouwenhoven et al., 1999). Analogously as in 976 Site, cyclical sedimentation in the Sorbas basin was accentuated at 7.167 Ma, which was expressed both in the planktonic foraminifer assemblages (warm versus cold species) and the lithological sedimentary cycles. It was at this time when the first indurated layers (opal-rich deposits) occurred in Sorbas concurrently with the onset of diatom-rich sediments in the Tripoli formation in Sicily (Roveri et al., 2014). However, deep water ventilation in Sorbas and at ODP Site 976 remain high after 7.167 Ma in contrast to the Eastern Mediterranean.

The second step in the Atlantic-Mediterranean restriction, which was recorded in Sorbas, just from 6.7 Ma, profoundly reduced deep water ventilation in most Mediterranean basins, resulting in the formation of sapropels in most marginal basins surrounding the Alboran Sea. This is the case of the Sorbas, Nijar and Bajo Segura basins in Spain (Baggley, 2000; Corbí et al., 2020; Fortuin and Krijgsman, 2003; Sierro et al., 1999), where a sharp decrease in the $\delta^{13}\text{C}$ planktonic isotope record and the beginning of sapropel deposition (Upper Abad) testify less oxygenated bottom waters full of organic matter (Sierro et al., 1999; Sierro et al., 2003). Analogously, the Messadit section in the Melilla basin (north Morocco) also shows the onset of sapropel-like deposits and the appearance of low-oxygenated benthic foraminifers (Roger et al., 2000; Van Assen et al., 2006). A similar succession was found in Monte del Casino (Kouwenhoven et al., 1999) that shows a sharp increase of benthic stress adapted species only from this time onward (Kouwenhoven et al., 2003). At ODP Site 976

no evidence of sapropels or low bottom water oxygenation has been recorded, but the sediments accumulated during the time interval were deposited in the peripheral basins were probably eroded during the Messinian or by the Zanclean deluge.

6.2 Amplification of astronomically driven cyclicity in the Western Alboran Basin

The quantitative analysis of planktonic foraminifer species and the elemental geochemical record revealed the occurrence of cyclical changes along the 976 Site record. Even though a hint of cyclical behavior is visible since the Tortonian (A interval; Figure 14), it becomes especially evident from 593-592 mbsf upwards (B interval; Figure 14) and therefore it will be our main focus.

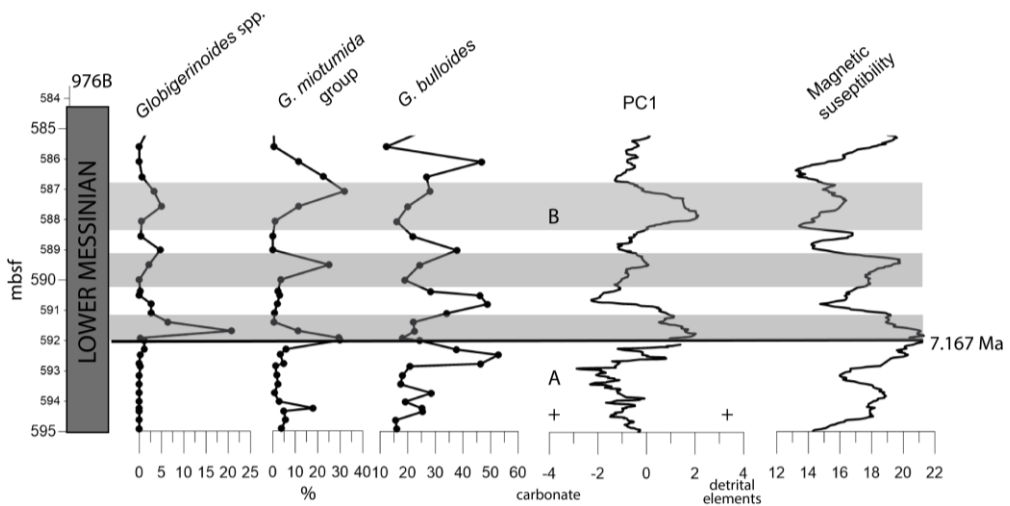


Figure 16: The main cyclical changes after 7.167 Ma are shown. Highlighted in grey are the phases of Northern Hemisphere insolation maxima (precession minima).

Planktonic warm-water species such as *Globigerinoides* spp. and *G. miotumida* group are more abundant at times of PC1B maximum i.e., when the input of siliciclastic elements, such as Si, K, Zr and Ti is the highest (as confirmed by the magnetic susceptibility values; Figure 16). In contrast, *G. bulloides* and cold-water species dominate when the dilution by riverine/detrital input is the lowest (low Si, K, Zr and Ti), and the concentrations of Ca, Sr, and other biogenic elements (S, Br) reach their peaks (Figure 16). PC2 seems to have an overall opposite behavior in respect to PC1 and a juxtaposition is present between organic rich coarser elements and fine ones, poor in organic matter (Figure 14 and 15). This cyclicity is very similar to that seen in the middle upper part of the lower Abad cycles in Sorbas Basin where, peaks of *G. miotumida* group and *Globigerinoides* spp. show an opposite behavior in respect to the *G. bulloides* and

N. acostaensis (Sierro et al., 2003) distribution. The geochemical and micropaleontological study of Ain el Beida (Atlantic Morocco) shows the same behavior as well. There, periods of abundant *Globigerinoides* spp. and high magnetic susceptibility are replaced by phases where Ca and cold water *Neogloboquadrina* spp. dominate the sediments (Van Der Laan et al., 2012). Furthermore, analogous geochemical patterns have been found in Huelva-1 borehole located on the Spanish Atlantic margin, once part of the Betic corridor (Van den Berg et al., 2018). Here, Van den Berg et al. (2018) identified a clear juxtaposition between coarser grained siliciclastic sediments and finer-grained sediments rich in biogenic carbonate.

These are typical of orbitally driven sedimentary cycles. High annual rainfall during Northern Hemisphere summer insolation maxima (precession minima) results in higher freshwater discharge to the Alboran Sea that generates stratification in the water column, warmer sea surface waters and reduced vertical mixing. As a consequence, the relative proportion of warm water species increases. The enhanced river discharge results in higher siliciclastic particles to the Alboran Sea increasing its relative concentrations in the sediments at the expense of the pelagic biogenic carbonate particles, which get diluted. During Northern Hemisphere summer insolation minima, the opposite occurs. Drier and colder phases break water stratification and incentivize the proliferation of cold-water species and the limited river discharges enrich the sediments in biogenic components.

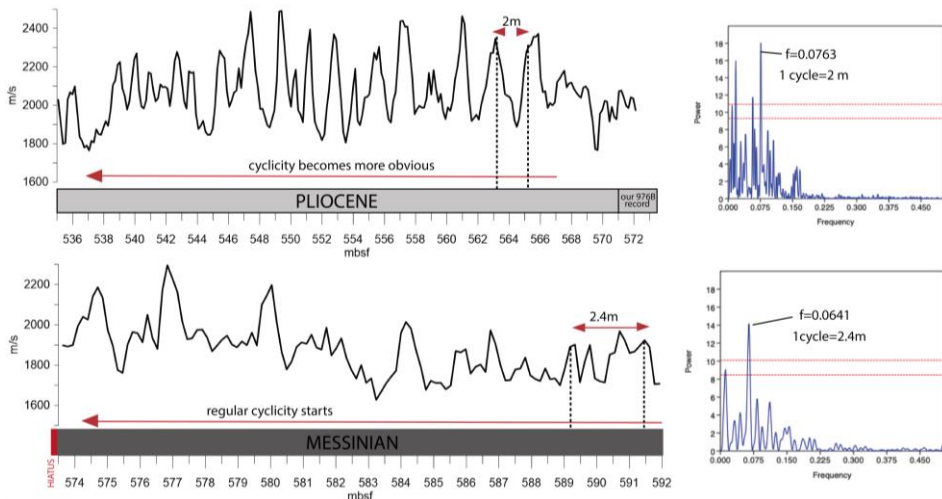


Figure 17: The Sonic log velocities expressed in km/s are shown both for the Messinian record (from 7.167 Ma) and for the Pliocene one (from 5.33 Ma until the Upper Pliocene). On the right, the power spectra from the power spectral analysis shows the frequencies and the respective power values. We indicated the Frequency with the higher value which ultimately served to derive the cyclicities in meters.

The average thickness of each precession cycle as defined by the changes in the planktonic foraminifer assemblages and the geochemical properties during the earliest Messinian is in the order of 2.4 m. This cyclicity is confirmed by the earliest Messinian downhole sonic log velocities (Figure 17) at this Site and a similar sedimentary cyclicity seems to continue in the early Pliocene (ODP Leg 161 Initial reports; Comas et al., 1996). The power spectra analyses performed on earliest Pliocene logs gave a prominent length of 2 m for an average cycle, which is very similar to the average thickness of the precession cycles recognized in the Messinian (Figure 17). Indeed, the interval shown in Figure 13 that correspond to the earliest Pliocene can be tuned to the 405 kyr cycles number 14 and 13 following the nomenclature of Hilgen et al. (2020).

7. Messinian depositional environments and basal Pliocene erosive surface

7.1 Messinian units

The biostratigraphic data of And-G1 and Alb-A1, thought approximate because of problems explained in section 5.3, extrapolated to seismic reflectors (Figure 4 and 5), allow defining the seismic stratigraphy of the northern margin of the basin. We believe that the Tortonian-Messinian boundary in the two sites corresponds to the R2 unconformity at the top of the Tortonian (Soto et al., 2010) which separates the Tortonian Unit III from the Messinian Unit II (Comas et al., 1999). The reflector on top defines the Miocene-Pliocene boundary, followed by a continuous hemipelagic sedimentation containing Pliocene markers. The Messinian record is therefore complete in the industrial wells and includes a younger plane-parallel unit, richer in planktonic foraminifers but still containing abundant detrital particles (Figure 6 and 7), attributed most probably to a turbiditic deposit, correlatable to the hemipelagic nannofossil clays described at deeper locations like Site 976 and Site 121 (Figure 3 and 9).

The latter is topped by a chaotic deposit which interpretation is less straightforward (Figure 3, 4 and 5). It has been interpreted in the past as being a mass transport deposit (MTD) accumulated during the MSC (Estrada et al., 2011; Lofi et al., 2005; Martínez del Olmo and Comas, 2008). The MSC base level lowering could have favored the collapse and erosion of the peripheral margin, in this way creating chaotic mass transport deposits at the base of the slope, similarly to that found in the Gulf of Valencia (Cameselle and Urgeles, 2016; Maillard et al., 2006; Urgeles et al., 2011) or Gulf of Lion (Bache et al., 2009). This could be possibly associated with the Complex Unit or Reworked Lower Gypsum (CU; RLG; Lugli et al., 2013; Roveri et al., 2014) found in concomitance

in both Eastern and Western Mediterranean Basins. Similar deposits have been found at the end of the Messinian base level fall (Bertoni and Cartwright, 2007; Soria et al., 2005) characterized by the transition to a humid climate (Rouchy and Caruso, 2006). In this case, the chaotic WAB deposit would represent the syngenetic product of increased erosion and runoff at the margins resulting with deposition of a clastic deposit made by a combination of fluvio-deltaic, brackish sediments with occasional anhydrite clasts related to the end of Messinian. Similar coeval facies have been reported in the Eastern Mediterranean Levant Basin (Bertoni and Cartwright, 2007; Druckman et al., 1995; Gvirtzman et al., 2017) and in some Western Sectors like the Bajo Segura Basin (Soria et al., 2005) or Malaga Basin (Guerra-Merchán et al., 2010) and have been interpreted as an early Stage 3 'Lago-Mare' deposits (LM). Even if brackish fossils have not been found in And-G1 and Alb-A1 chaotic unit, given its chaotic aspect, clastic composition (Figure 6 and 7) and stratigraphic position right below early Pliocene sediments (Figure 3, 4 and 5), the hypothesis is plausible. The anhydrite minerals together with coarse clasts of metamorphic rocks (phyllites and mica-schists) found in the And-G1 and Alb-A1 chaotic unit (Figure 6 and 7), are very frequent in the Malaguide and Alpujarride complexes along the Spanish coast (Alonso-Chaves et al., 2004; Rodríguez- Fernández et al., 2011). In this area even some Middle and Upper Triassic gypsum deposits have been reported (Escavy et al., 2012). If this is the case, at least a portion of anhydrite fragments and the metamorphic clasts could have been transported during the MSC Stage 3 base level fall as a mass transport deposits to the deeper sectors of the WAB, while some anhydrite fragments could have been formed during Stage 3, like strontium isotope signal confirms for Mavqim Formation in the Levant Basin (Gvirtzman et al., 2017).

7.2. Messinian hiatus and erosive surface

The Messinian-Pliocene transition in the Westernmost Mediterranean is marked by a strong erosional surface that has been traditionally associated to Mediterranean basin refilling after the Messinian Salinity Crisis (Estrada et al., 2011; Garcia-Castellanos et al., 2009), that extends from the Gulf of Cádiz (Atlantic Ocean) to the Algerian Basin (Western Mediterranean). It is attenuated towards the east and some studies indicate a preserved Miocene/Pliocene boundary in Sicilian sections (e.g. Van Couvering et al., 2000). This erosional surface (M reflector) may be seen in the composite seismic line of Figure 3 (magenta line), where the erosion amplitude increases southward towards the structural high near the region where ODP Site 976 and DSDP Site 121 were drilled. The more intense erosion concentrated in the central part of the WAB basin, directly in front of the Camarinal sill, is probably coherent with a higher energy along the Gibraltar corridor hypothesized during the Zanclean flooding

(Garcia-Castellanos et al., 2009). Consequently, from the composite seismic profile (Figure 3) is evident that at Site 976, most of the Messinian is missing. In order to estimate the time span eroded from the sedimentary sequence, we used the cyclicity observed in the earliest Messinian to estimate the age of the youngest Messinian sediments below the Messinian-Pliocene discontinuity at Site 976. Assuming the average thickness of 2.4 m per precession cycle, a thickness of around 18.5 m from the 7.167 Ma to the top of the Messinian at Site 976 (including the non-recovery interval) and an average duration of ~21.7 kyr per precession cycle (Laskar et al., 2004), we obtained an age of ~7 Ma for the top of the Messinian sequence. Doing so, it was possible to estimate the magnitude of the hiatus at around 1.67 Ma (from 7 Ma to 5.33 Ma; see Figure 18). Furthermore, to get a better comprehension of the erosion in the southern distal settings of the WAB, we estimated the thickness in meters of the Messinian seismic units to the north of the Site 976, where these units have been preserved (Figure 3). Calculating the thickness in m of Messinian seismic units would give us a good idea of the actual amount of eroded sediments at the location of Site 976. Using an average Messinian p-wave velocity of 2425 m/s and the TWTT (two-way travel time) thickness for the Messinian sediments of ~375 ms we obtained an estimate of 455 m of thickness for the Messinian sediments. Combining the thickness and the time estimate for the hiatus we calculated an average sedimentation rate of 27 cm/ky for Messinian. Such a high sedimentation rate seems unrealistic for deep marine environments, even at

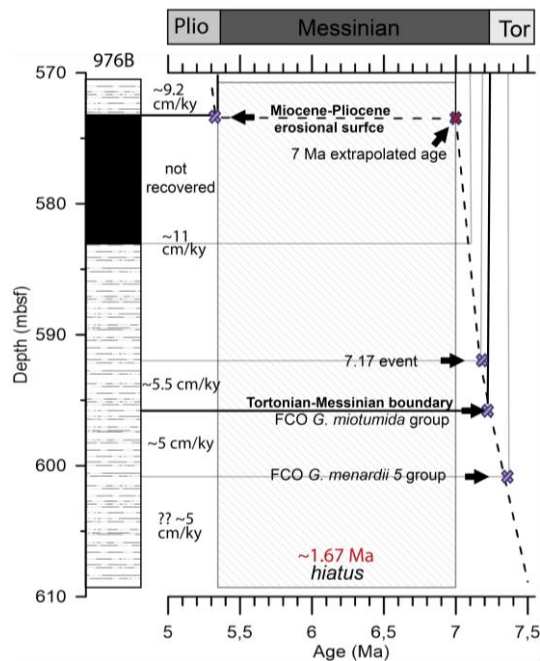


Figure 18: Biochronology and sedimentation rates estimates for Site 976.

times of increased sediment supply but it can be explained if considering the two Messinian units separately (plane parallel and chaotic deposit; see section 7.1). Assuming that the topmost chaotic Messinian unit is a mass transported deposit, it was most probably deposited instantaneously, and its thickness should not be included in sedimentation rate estimates. In this way, the real Messinian thickness to take into account is 273 m deposited in 1.67 Ma, resulting in a realistic sedimentation rate of 16 cm/ky, while the remaining 182 m of the chaotic unit were probably deposited in very short, almost instantaneous geological time.

Even though this erosion and the formation of the Zanclean channel have been usually attributed to the Mediterranean re-flooding after the MSC, similar channels are visible from the seismic records even after the Pliocene (Figure 3, black horizon) making possible an alternative scenario for this erosion. In any case, to confirm or refute this hypothesis further coring is necessary, closer to the Spanish coast, where the Messinian record is better preserved. We hope that the recent IODP proposal *IMMAGE*, will be successful and that new coring will clarify the paleoenvironmental conditions on the Alboran Basin before, during and after the MSC.

8. Post depositional diagenetic processes modifying Messinian sediments

Near the Miocene-Pliocene boundary both in ODP Site 976 (sample 62X, 31-32 cm) and DSDP Site 121 (sample 19R), an indurated greenish sediment mainly composed of dolomite, calcite and quartz have been retrieved (Figure 19). Because of the poor recovery, possibly caused by the same presence of such hard sediments they were not described during the expedition (Comas et al., 1999). Furthermore, in samples 16R, 19R and 20R of Site 121 particular radial spherules, made of a combination of canaphite ($\text{CaNa}_2(\text{P}_2\text{O}_7)_4 \cdot 4(\text{H}_2\text{O})$) and clinochlore ($(\text{Mg,Fe}^{+2})_5\text{Al}(\text{Si}_3\text{Al})\text{O}_{10}(\text{OH})_8$) were identified (Figure 19). Interestingly, X-ray analyses published in the initial IODP report find an anomalous presence of cristobalite (SiO_2) in samples 19R and 20R as well (Ryan et al., 1973).

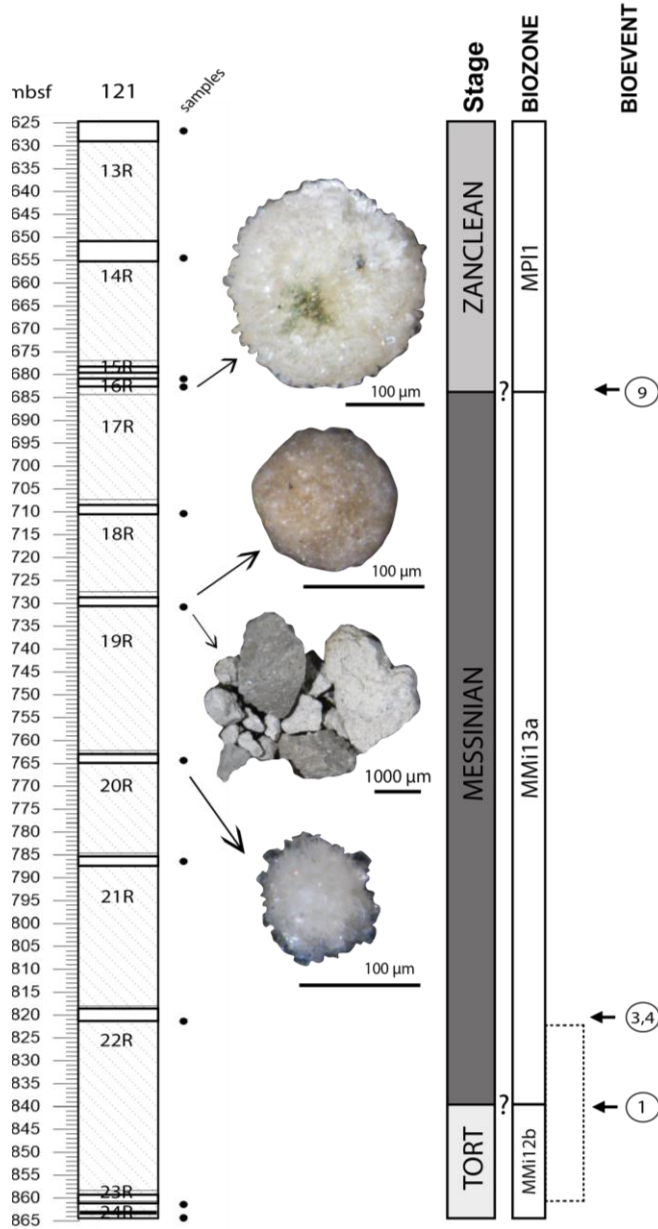


Figure 19: Schematic representation of Alboran basin DSDP site 121 with the analysed samples. The shaded sections show the non-recovered intervals. The photographs of the canaphite-ilmenite-quartz-clinochlore radial spherules and dolomite particles found at the Site are reported at the right from the corresponding samples (20R,19R and 16R). On the right hand-side the identified biozones and bioevents from Lirer et al. (2019) are reported. The biozones include *G. menardii* group biozone (MMi12b) and the *G. miotumida* group biozone (MMi13a) while the main planktonic foraminifer bio-events indicated by the numbers are: 1-LCO of *G. menardii* 4 group (7.56 Ma); 3-LCO of *G. menardii* 5 group (7.23 Ma); 4-FCO of *G. miotumida* (7.24 Ma) and 9-FCO of *G. margaritae* (5.08 Ma) reported in Table 1.

While dolomitized sediments were found in upper Messinian records in other Mediterranean locations like DSDP site 372 and 374 (Leg 42A; Camerlenghi et al., 2019; Hsü et al., 1978) and have been considered as being diagenetically formed by circulation of Mg enriched fluids (Hsü et al., 1978; Martínez-Ruiz et al., 1999), canaphite spherules have never been recorded. Canaphite is a very peculiar and extremely rare orthophosphate in nature and it has been firstly identified in 1985 (Peacor et al., 1985) and defined as a “bathtub mineral”, easily produced synthetically when a rock was put into an evaporating solution rich into dissolved salts (Mayen et al., 2020). In nature its occurrence is restricted to very low temperature environments (e.g., lacustrine evaporites; Queralt et al., 1994) and volcanic rocks diagenesis (Baturin and Derkachev, 2007; both deposited during Miocene) in which solutions are rich only in alkali and alkali earth ions (Rouse et al., 1988). Rarity of canaphite can be linked with the common apatite $\text{Ca}_5(\text{PO}_4)_3(\text{F},\text{Cl},\text{OH})$ crystallization that will sequester all the available phosphorus and will therefore preclude from the formation of canaphite and/or poor preservation because P_2O_7 groups are weak in the presence of Ca-rich fluids and form apatite and other minerals (Goffé et al., 2002). Clinocllore is on the other hand, a much more common clay mineral associated with chlorite; when Mg-rich can be correlated with aeolian and sabkha sediments, while if Fe-rich is typically diagenetic (low temperatures; Huggett, 2015). Nonetheless, in the dolomitic marlstones in the Central Ionian basin (Leg 42A) a similar Mg-phosphate rich evaporate/saline mineral lüneburgite ($\text{Mg}_3\text{B}_2(\text{PO}_4)_2(\text{OH})_6,6\text{H}_2\text{O}$), was found in form of white spherules (1-4 mm), and has been interpreted as a diagenetic product of Mg and B bearing upward migrating brines (Müller, 1978) deriving from deeper sediments containing halite, polyhalite, bischofite, sulfoborite and sylvite (Hsü et al., 1978).

An analogous brine or interstitial fluids (P-Mg-Fe bearing) upward migration process could have been happening in the uppermost Messinian sediments of the Alboran Sea leading to the precipitation of the earlier mentioned minerals in the WAB sediments as well (Figure 20).

Such fluids can have multiple origins. In the first place, considering that both sites are located in a tectonically active region (Comas et al., 1999), on top of a structural high composed of faulted blocks of the Alboran domain metamorphic basement and volcanic rocks (Comas et al., 1999; Maldonado et al., 1992), the phosphate, iron and magnesium ion enrichment in the deep interstitial waters could derive from these basement rocks. Consistently, the basement is composed of a metapelite sequence interlayered with calcite and dolomite marble overlying a banded pelitic migmatitic gneiss, containing large crystals of cordierite, biotite, andalusite and sillimanite (Comas et al., 1999; Comas et al.,

1996). The gneiss could serve as a source of Fe and Mg ions, the latter possibly derived from the metacarbonatic rocks as well.

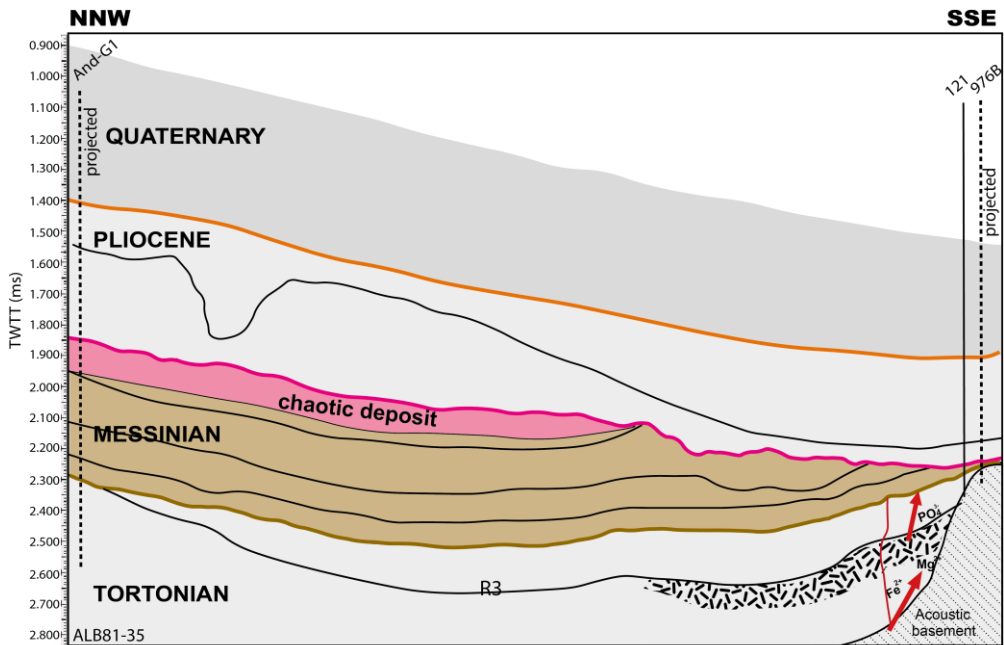


Figure 20: Interpreted seismic profile ALB81-35. In yellow are shown Messinian sediments, progressively more eroded moving towards SSW. In magenta the chaotic Upper Messinian unit is outlined, while the magenta line follows the M reflector. The area with a pattern below R3 unconformity indicates the upper Tortonian volcanoclastic and glauconite unit. Faults are shown in red while the red arrows resemble the possible deep fluid formation and flux path.

On the other hand, the canaphite spherules, enriched in PO_4^{2-} ion, have been retrieved only at Site 121, and therefore the diagenetic fluids could have another source. Phosphate is most commonly found like $\text{Ca}_{10}(\text{PO}_4\text{CO}_3)_6\text{F}_{2-3}$ or carbonate-fluor apatite (Hesse and Schacht, 2011) and is often associated with regions characterized by high organic matter accumulation (Krejci-Graf, 1955) like anoxic basins (Krom and Berner, 1980) or highly productive continental margin (Suess, 1981). Additionally, authigenic apatite can form associated phosphoritic hardgrounds and granular phosphoritic beds during bottom-current winnowing in phases of sea-level fall (Hesse and Schacht, 2011), while in suboxic environments, is frequently accompanied by glauconite formation (Carson and Crowley, 1993; Glenn and Arthur, 1990). On the left flank of Site 976 structural high, a highly reflective late-Tortonian layer package can be found (Figure 3 and 20), the latter traceable all over the Alboran, under the R3 unconformity (Soto et al., 2010; Talukder et al., 2003). Cuttings from industrial well And-G1, revealed that this deposit is composed mainly of high porosity ignimbrite volcanoclastics, rich in quartz and biotite intercalated with occasional

glaucopelagic layers (Repsol drill report). Interstitial fluids and brines contained in such deposits could have incorporated the PO_4^{2-} ion, and while flowing upwards, could have modified diagenetically only the sediments of 121 Site, directly above precipitating canaphite spherules, a similar process to these are canaphites described in the Japan Sea (Baturin and Derkachev, 2007) also associated to Miocene volcanoclastic rocks.

9. Conclusion

Seismic section analyses in the WAB together with borehole sedimentary analyses allowed the characterization of two Messinian units, one composed of plane parallel strata and one chaotic. The first has been related with turbidite deposition near the coast and more hemipelagic deposits in the central parts of the basin. The second, chaotic MTD unit retrieved in drilling cuttings of industrial wells And-G1 and Alb-A1, even if it does not contain in place evaporites, can be related to the MSC final stages triggered by a base-level change.

On the continuously drilled hemipelagic deposits of ODP Site 976 a high-resolution quantitative study of the planktonic foraminifer assemblages led us to propose a biostratigraphic framework for the late Tortonian-early Messinian and earliest Pliocene in the Western Alboran Basin (WAB).

Deep open-marine sedimentation with high percentages of planktonic foraminifers typical of cold, nutrient-rich waters were recorded during the latest Tortonian and earliest Messinian. This particular condition, not encountered at other contemporaneous sites, could suggest that the eastward Atlantic inflow, moving along the southern Spanish coast could promote an eastward circulation similar to that occurring today in the Alboran Basin. The resulting upwelling of cold nutrient rich waters could explain the thriving of such foraminifer species in the Tortonian. Ultimately, these peculiar findings open up the possibility of the existence of a proto-Gibraltar strait as the main source of Atlantic inflow in the Upper Tortonian-Lower Messinian. Nonetheless, this theory remains speculative and need further proof to be completely validated.

Based on our biochronologic record and the astronomically driven cyclical pattern of the planktonic foraminifer assemblages we were able to date the Tortonian-Messinian boundary and the first precession cycles of the Messinian below the major discontinuity observed in many seismic profiles in the WAB. This discontinuity is recorded at Site 976 with a large erosion that removed at least 1.67 Ma and 455 m of the Messinian sedimentary record. The identification of the bottom acme of *Sphaeroidinellopsis* spp. suggests a basal Pliocene age for

the first sediments after the erosion, although there is poor recovery near the boundary.

A high siliciclastic input compared to biogenic carbonate and an increase of the sedimentation rate is observed at 7.167 Ma. We interpreted this event as the result of tectonic uplift in the Gibraltar Arc. This uplift probably caused the major restriction of the Mediterranean-Atlantic gateways at the beginning of the Messinian and represents the first step of restriction prior to the MSC. This event is recorded by reduced deep-water ventilation in the eastern Mediterranean. Nonetheless, our data shows that the impact of this event on the deep marine environments were less pronounced in the Western Mediterranean (WAB) than in the Eastern Mediterranean record. The proximity of the West Alboran Sea to the Atlantic Ocean certainly favored more oxygenated conditions during the earliest Messinian. The reduced Atlantic Mediterranean water exchange after 7.167 Ma amplified the impact of Mediterranean climate variations on its hydrographic conditions and produced evident cyclical changes in the planktonic foraminifer assemblages similar to those recorded in other Mediterranean basins. They were controlled by orbital-driven climate fluctuations with abundant cold-water species during precession maxima and warm water species during precession minima.

The strong tectonic movement is also evident in the intense interstitial fluid activity that led to the alteration of the Messinian sediments and diagenetic deposition of Mg rich minerals and phosphates, including an extremely rare mineral as canaphite.

Acknowledgments

The research leading to these results has received funding from the European Union's Horizon 2020 research and innovation program under the Marie Skłodowska-Curie grant agreement n° 765256 SALTGIANT. All fellow SALTGINAT ESRs and supervisors are thanked for their valuable suggestions and discussions. We would like also to thank Nucleus, in particular the Area of Instrumental Techniques, X-ray Diffraction team of Salamanca University that performed X-ray diffraction analyses on our samples and contributed with significant comments. This research used data and samples collected through ODP Expedition 161 aboard the Joides Resolution. Geochemical data was acquired at the XRF Core Scanner Lab at the MARUM - Center for Marine Environmental Sciences, University of Bremen, Germany. Finally, the authors wish to thank three anonymous reviewers, Adina Paytan, Jesús Miguel Soria and Hugo Corbí for their valuable suggestions and critical comments, which have improved the quality of this paper.

Supplementary data

Bulian, Francesca; Sierro, Francisco J. (2021), "Messinian West Alboran Sea record in the proximity of Gibraltar: early signs of Atlantic-Mediterranean gateway restriction", Mendeley Data, V2, doi: <https://data.mendeley.com/datasets/9mvbg38z3d/2>

References

- Achalhi, M., Münch, P., Cornée, J.-J., Azdimousa, A., Melinte-Dobrinescu, M., Quillévéré, F., Drinia, H., Fauquette, S., Jiménez-Moreno, G., Merzeraud, G., Moussa, A. B., El Kharim, Y., and Feddi, N., 2016, The late Miocene Mediterranean-Atlantic connections through the North Rifian Corridor: New insights from the Boudinar and Arbaa Taourirt basins (northeastern Rif, Morocco): *Palaeogeography, Palaeoclimatology, Palaeoecology*, v. 459, p. 131-152.
- Agnihotri, R., Altabet, M. A., Herbert, T. D., and Tierney, J. E., 2008, Subdecadally resolved paleoceanography of the Peru margin during the last two millennia: *Geochemistry, Geophysics, Geosystems*, v. 9, no. 5.
- Alonso-Chaves, F., Soto, J., Orozco, M., Kilias, A., and Tranos, M., 2004, Tectonic evolution of the Betic Cordillera: an overview: *Bulletin of the Geological Society of Greece*, v. 36, no. 4, p. 1598-1607.
- Anthonissen, D. E., and Ogg, J. G., 2012, Cenozoic and Cretaceous biochronology of planktonic foraminifera and calcareous nannofossils, *The geologic time scale*, Elsevier, p. 1083-1127.
- Antonarakou, A., Drinia, H., and Zachariasse, J., 2004, Cyclostratigraphic determination of the replacement of *Globorotalia menardii* group by *Globorotalia miotumida* group-A significant climatic change signal: *Microbiology*, v. 1, p. 155-175.
- Bache, F., Olivet, J. L., Gorini, C., Rabineau, M., Baztan, J., Aslanian, D., and Suc, J. P., 2009, Messinian erosional and salinity crises: View from the Provence Basin (Gulf of Lions, Western Mediterranean): *Earth and Planetary Science Letters*, v. 286, no. 1-2, p. 139-157.
- Baggley, K. A., 2000, The Late Tortonian- Early Messinian Foraminiferal Record Of The Abad Member (Turre Formation), Sorbas Basin, Almería, South- East Spain: *Palaeontology*, v. 43, no. 6, p. 1069-1112.
- Balanya, J. C., Crespo-Blanc, A., Díaz-Azpiroz, M., Expósito, I., Torcal, F., Pérez-Peña, V., and Booth-Rea, G., 2012, Arc-parallel vs back-arc extension in the Western Gibraltar arc: Is the Gibraltar forearc still active?: *Geologica Acta: an international earth science journal*, v. 10, no. 3, p. 249-263.

- Bárcena, M., Flores, J., Sierro, F., Pérez-Folgado, M., Fabres, J., Calafat, A., and Canals, M., 2004, Planktonic response to main oceanographic changes in the Alboran Sea (Western Mediterranean) as documented in sediment traps and surface sediments: *Marine Micropaleontology*, v. 53, no. 3-4, p. 423-445.
- Baturin, G., and Derkachev, A., 2007, Phosphate inclusions in tuffites from the Krisstofovich Rise (Sea of Japan): *Oceanology*, v. 47, no. 5, p. 730-740.
- Benson, R. H., Rakic- El Bied, K., and Bonaduce, G., 1991, An important current reversal (influx) in the Rifian Corridor (Morocco) at the Tortonian- Messinian boundary: The end of Tethys Ocean: *Paleoceanography*, v. 6, no. 1, p. 165-192.
- Bertoni, C., and Cartwright, J., 2007, Major erosion at the end of the Messinian Salinity Crisis: evidence from the Levant Basin, Eastern Mediterranean: *Basin Research*, v. 19, no. 1, p. 1-18.
- Blanc, P.-L., 2006, Improved modelling of the Messinian Salinity Crisis and conceptual implications: *Palaeogeography, Palaeoclimatology, Palaeoecology*, v. 238, no. 1-4, p. 349-372.
- Booth- Rea, G., Ranero, C. R., Martínez- Martínez, J. M., and Grevemeyer, I., 2007, Crustal types and Tertiary tectonic evolution of the Alborán sea, western Mediterranean: *Geochemistry, Geophysics, Geosystems*, v. 8, no. 10.
- Brachert, T., Bornemann, A., Reuter, M., Galer, S., Grimm, K., and Fassoulas, C., 2015, Upwelling history of the Mediterranean Sea revealed by stunted growth in the planktic foraminifera *Orbulina universa* (early Messinian, Crete, Greece): *International Journal of Earth Sciences*, v. 104, no. 1, p. 263-276.
- Braga, J. C., Martín, J. M., and Quesada, C., 2003, Patterns and average rates of late Neogene-Recent uplift of the Betic Cordillera, SE Spain: *Geomorphology*, v. 50, no. 1-3, p. 3-26.
- Camerlenghi, A., Del Ben, A., Hübscher, C., Forlin, E., Geletti, R., Brancatelli, G., Micallef, A., Saule, M., and Facchin, L., 2019, Seismic markers of the Messinian salinity crisis in the deep Ionian Basin: *Basin Research*.
- Cameselle, A. L., and Urgeles, R., 2016, Large- scale margin collapse during Messinian early sea- level drawdown: the SW Valencia trough, NW Mediterranean: *Basin Research*, v. 29, p. 576-595.
- Campillo, A., Maldonado, A., and Mauffret, A., 1992, Stratigraphic and tectonic evolution of the western Alboran Sea: Late Miocene to Recent: *Geo-Marine Letters*, v. 12, no. 2-3, p. 165-172.
- Capella, W., Barhoun, N., Flecker, R., Hilgen, F., Kouwenhoven, T., Matenco, L., Sierro, F. J., Tulbure, M., Yousfi, M. Z., and Krijgsman, W., 2018, Palaeogeographic evolution of the late Miocene Rifian Corridor (Morocco): reconstructions from surface and subsurface data: *Earth-Science Reviews*, v. 180, p. 37-59.

- Capella, W., Spakman, W., van Hinsbergen, D. J., Chertova, M. V., and Krijgsman, W., 2020, Mantle resistance against Gibraltar slab dragging as a key cause of the Messinian Salinity Crisis: *Terra Nova*, v. 32(2), p. 141-150.
- Carson, G., and Crowley, S., 1993, The glauconite-phosphate association in hardgrounds: examples from the Cenomanian of Devon, southwest England: *Cretaceous Research*, v. 14, no. 1, p. 69-89.
- CIESM, 2008, The Messinian Salinity Crisis from mega-deposits to microbiology - A consensus report: N° 33 in *CIESM Workshop Monographs*[F. Briand, Ed.], 168 pages, Monaco.
- Cita, M. B., 1975, The Miocene/Pliocene boundary: History and definition, in Saito, T. and Burckle, L. H. (eds.): *Late Neogene Epoch Boundaries*: New York, Micropaleontology Press v. Spec. Publ. 1, p. pp. 1-30.
- Cita, M. B., Wright, R. C., Ryan, W. B. F., and Longinelli, A., 1978, Messinian paleoenvironments. In: Hsu, K.J., Montadert, L., et al. (Eds.): *Init. Rep. D.S.D.P.*, v. vol. 42A. US Government Printing Office, Washington, p. 1003-1035.
- Comas, M., Platt, J., Soto, J., and Watts, A., 44. The origin and tectonic history of the Alboran Basin: insights from Leg 161 results, *in Proceedings Proceedings of the Ocean Drilling Program Scientific Results 1999*, Volume 161, p. 555-580.
- Comas, M. C., Zahn, R., Klaus, A., and al., e., 1996, ODP, *Init. Repts.*, 161: College Station, TX (Ocean Drilling Program).
- Corbí, H., Lancis, C., García-García, F., Pina, J.-A., Soria, J. M., Tent-Manclús, J. E., and Viseras, C., 2012, Updating the marine biostratigraphy of the Granada Basin (central Betic Cordillera). Insight for the Late Miocene palaeogeographic evolution of the Atlantic-Mediterranean seaway: *Geobios*, v. 45, no. 3, p. 249-263.
- Corbí, H., and Soria, J. M., 2016, Late Miocene-early Pliocene planktonic foraminifer event-stratigraphy of the Bajo Segura basin: A complete record of the western Mediterranean: *Marine and Petroleum Geology*, v. 77, p. 1010-1027.
- Corbí, H., Soria, J. M., Giannetti, A., and Yébenes, A., 2020, The step-by-step restriction of the Mediterranean (start, amplification, and consolidation phases) preceding the Messinian Salinity Crisis (climax phase) in the Bajo Segura basin: *Geo-Marine Letters*, v. 40(3), p. 1-21.
- Crespo-Blanc, A., and de Lamotte, D. F., 2006, Structural evolution of the external zones derived from the Flysch trough and the South Iberian and Maghrebian paleomargins around the Gibraltar arc: a comparative study: *Bulletin de la Société géologique de France*, v. 177, no. 5, p. 267-282.
- Davis, J. C., and Sampson, R. J., 1986, *Statistics and data analysis in geology*, Wiley New York et al.
- Dewey, J., Helman, M., Knott, S., Turco, E., and Hutton, D., 1989, Kinematics of the western Mediterranean: *Geological Society, London, Special Publications*, v. 45, no. 1, p. 265-283.

- Di Stefano, A., Baldassini, N., and Alberico, I., 2015, Surface-water conditions in the Mediterranean Basin during earliest Pliocene as revealed by calcareous nannofossil assemblages: Comparison between western and eastern sectors: *Palaeogeography, Palaeoclimatology, Palaeoecology*, v. 440, p. 283-296.
- Di Stefano, A., Verducci, M., Lirer, F., Ferraro, L., Iaccarino, S. M., Hüsing, S. K., and Hilgen, F. J., 2010, Paleoenvironmental conditions preceding the Messinian Salinity Crisis in the Central Mediterranean: integrated data from the Upper Miocene Trave section (Italy): *Palaeogeography, Palaeoclimatology, Palaeoecology*, v. 297, no. 1, p. 37-53.
- Díaz-Merino, C., Comas, M., and Martínez del Olmo, W., 2003, Secuencias de depósito neógenas del margen noroeste del Mar de Alborán: Cuenca de Málaga, *Geotemas*, v. 5, p. 61-65.
- Do Couto, D., Gorini, C., Jolivet, L., Le Bret, N., Augier, R., Gumiaux, C., d'Acremont, E., Ammar, A., Jabour, H., and Auxietre, J.-L., 2016, Tectonic and stratigraphic evolution of the Western Alboran Sea Basin in the last 25 Myrs: *Tectonophysics*, v. 677, p. 280-311.
- Druckman, Y., Buchbinder, B., Martinotti, G., Tov, R. S., and Aharon, P., 1995, The buried Afiq Canyon (eastern Mediterranean, Israel): a case study of a Tertiary submarine canyon exposed in Late Messinian times: *Marine Geology*, v. 123, no. 3-4, p. 167-185.
- Duggen, S., Hoernle, K., van den Bogaard, P., and Harris, C., 2004, Magmatic evolution of the Alboran region: The role of subduction in forming the western Mediterranean and causing the Messinian Salinity Crisis: *Earth and Planetary Science Letters*, v. 218, no. 1-2, p. 91-108.
- Escavy, J. I., Herrero, M. J., and Arribas, M. E., 2012, Gypsum resources of Spain: Temporal and spatial distribution: *Ore Geology Reviews*, v. 49, p. 72-84.
- Estrada, F., Ercilla, G., Gorini, C., Alonso, B., Vázquez, J. T., García-Castellanos, D., Juan, C., Maldonado, A., Ammar, A., and Elabbassi, M., 2011, Impact of pulsed Atlantic water inflow into the Alboran Basin at the time of the Zanclean flooding: *Geo-Marine Letters*, 31(5-6), pp.361-376., v. 31(5-6), pp.361-376., p. pp.361-376.
- Fadil, A., Vernant, P., McClusky, S., Reilinger, R., Gomez, F., Ben Sari, D., Mourabit, T., Feigl, K., and Barazangi, M., 2006, Active tectonics of the western Mediterranean: Geodetic evidence for rollback of a delaminated subcontinental lithospheric slab beneath the Rif Mountains, Morocco: *Geology*, v. 34, no. 7, p. 529-532.
- Flecker, R., Krijgsman, W., Capella, W., De Castro Martins, C., Dmitrieva, E., Mayser, J. P., Marzocchi, A., Modestou, S., Ochoa, D., Simon, D., Tulbure, M., Van Den Berg, B., Van Der Schee, M., De Lange, G., Ellam, R., Govers, R., Gutjahr, M., Hilgen, F., Kouwenhoven, T., Lofi, J., Meijer, P., Sierro, F. J., Bachiri, N., Barhoun, N., Alami, A. C., Chacon, B., Flores, J. A., Gregory, J., Howard, J., Lunt, D., Ochoa, M., Pancost, R., Vincent, S., and Yousfi, M. Z., 2015, Evolution of the Late Miocene Mediterranean-Atlantic gateways and their impact on regional and global environmental change: *Earth-Science Reviews*, v. 150, p. 365-392.

- Fortuin, A. R., and Krijgsman, W., 2003, The Messinian of the Nijar Basin (SE Spain): Sedimentation, depositional environments and paleogeographic evolution: *Sedimentary Geology*, v. 160, no. 1-3, p. 213-242.
- Franseen, E. K., Esteban, M., Ward, W. C., and Rouchy, J.-M., 1996, Models for carbonate stratigraphy from Miocene reef complexes of Mediterranean regions: Introduction.
- Frasca, G., Gueydan, F., Brun, J.-P., and Monié, P., 2016, Deformation mechanisms in a continental rift up to mantle exhumation. Field evidence from the western Betics, Spain: *Marine and Petroleum Geology*, v. 76, p. 310-328.
- García-Castellanos, D., Estrada, F., Jiménez-Munt, I., Gorini, C., Fernández, M., Vergés, J., and De Vicente, R., 2009, Catastrophic flood of the Mediterranean after the Messinian salinity crisis: *Nature*, v. 462, no. 7274, p. 778.
- García-Castellanos, D., and Villaseñor, A., 2011, Messinian salinity crisis regulated by competing tectonics and erosion at the Gibraltar arc: *Nature*, v. 480, no. 7377, p. 359.
- García- Veigas, J., Gibert, L., Cendón, D. I., Artiaga, D., Corbí, H., Soria, J. M., Lowenstein, T. K., and Sanz, E., 2020, Late Miocene evaporite geochemistry of Lorca and Fortuna basins (Eastern Betics, SE Spain): Evidence of restriction and continentalization: *Basin Research*, v. 32, no. 5, p. 926-958.
- Gladstone, R., Flecker, R., Valdes, P., Lunt, D., and Markwick, P., 2007, The Mediterranean hydrologic budget from a Late Miocene global climate simulation: *Palaeogeography, Palaeoclimatology, Palaeoecology*, v. 251, no. 2, p. 254-267.
- Glenn, C. R., and Arthur, M. A., 1990, Anatomy and origin of a Cretaceous phosphorite-greensand giant, Egypt: *Sedimentology*, v. 37, no. 1, p. 123-154.
- Goffé, B., Janots, É., Brunet, F., and Poinssot, C., 2002, Déstabilisation du phosphate-diphosphate de thorium (PDT), Th₄ (PO₄)₂P₂O₇, entre 320 et 350° C, porté à 50 MPa en milieu calcique, ou pourquoi le PDT n'a pas d'équivalent naturel: *Comptes Rendus Geoscience*, v. 334, no. 14, p. 1047-1052.
- Govers, R., 2009, Choking the Mediterranean to dehydration: the Messinian salinity crisis: *Geology*, v. 37, no. 2, p. 167-170.
- Gradstein, F. M., Ogg, J. G., Schmitz, M., and Ogg, G., 2012, *The geologic time scale 2012*, elsevier.
- Guerra-Merchán, A., Serrano, F., Garcés, M., Gofas, S., Esu, D., Gliozzi, E., and Grossi, F., 2010, Messinian Lago-Mare deposits near the strait of Gibraltar (Malaga basin, S Spain): *Palaeogeography, Palaeoclimatology, Palaeoecology*, v. 285, no. 3-4, p. 264-276.
- Gutscher, M.-A., Malod, J., Rehault, J.-P., Contrucci, I., Klingelhoefer, F., Mendes-Victor, L., and Spakman, W., 2002, Evidence for active subduction beneath Gibraltar: *Geology*, v. 30, no. 12, p. 1071-1074.
- Gvirtzman, Z., Manzi, V., Calvo, R., Gavrieli, I., Gennari, R., Lugli, S., Reghizzi, M., and Roveri, M., 2017, Intra-Messinian truncation surface in the Levant Basin explained by subaqueous dissolution: *Geology*, v. 45, no. 10, p. 915-918.

- Hammer, Ø., Harper, D., and Ryan, P., 2008, PAST – PALaeontological STatistics, ver. 1.81: Software documentation.
- Harff, J., Endler, R., Emelyanov, E., Kotov, S., Leipe, T., Moros, M., Olea, R., Tomczak, M., and Witkowski, A., 2011, Late Quaternary climate variations reflected in Baltic Sea sediments., *The Baltic Sea Basin*, Springer, Berlin, Heidelberg., p. 99-132.
- Heit, B., Mancilla, F. d. L., Yuan, X., Morales, J., Stich, D., Martín, R., and Molina-Aguilera, A., 2017, Tearing of the mantle lithosphere along the intermediate- depth seismicity zone beneath the Gibraltar Arc: The onset of lithospheric delamination: *Geophysical Research Letters*, v. 44, no. 9, p. 4027-4035.
- Hesse, R., and Schacht, U., 2011, Early diagenesis of deep-sea sediments, *Developments in Sedimentology*, Volume 63, Elsevier, p. 557-713.
- Hilgen, F., Iaccarino, S., Krijgsman, W., Villa, G., Langereis, C., and Zachariasse, W., 2000, The global boundary stratotype section and point (GSSP) of the Messinian Stage (uppermost Miocene): *Episodes*, v. 23, no. 3, p. 172-178.
- Hilgen, F., Krijgsman, W., Langereis, C., Lourens, L., Santarelli, A., and Zachariasse, W., 1995, Extending the astronomical (polarity) time scale into the Miocene: *Earth and Planetary Science Letters*, v. 136, p. 495-510.
- Hilgen, F., Lourens, L., Pälike, H., and Dinarès Turell, J., 2020, Should Unit-Stratotypes and Astrochronozones be formally defined? A dual proposal (including postscriptum): *Newsletters on Stratigraphy*.
- Horvath, F., and Berckhemer, H., 1982, Mediterranean backarc basins: *Alpine-Mediterranean Geodynamics*, v. 7, p. 141-173.
- Hsü, K., Montadert, L., Bernoulli, D., Bizon, G., Cita, M., Erickson, A., Fabricius, F., Garrison, R., Kidd, R., and Mélières, F., 1978, Site 374: Messina abyssal plain: Initial Rep. Deep Sea Drill. Proj, v. 42, p. 175-217.
- Hsü, K. J., Montadert, L., Bernoulli, D., Cita, M. B., Erickson, A., Garrison, R. E., Kidd, R. B., Mélières, F., Müller, C., and Wright, R., 1977, History of the mediterranean salinity crisis: *Nature*, v. 267, no. 5610, p. 399-403.
- Huggett, J. M., 2015, *Clay Minerals*☆, Reference Module in Earth Systems and Environmental Sciences, Elsevier.
- Iaccarino, S., Castradori, D., Cita, M., Di Stefano, E., Gaboardi, S., McKenzie, J., Spezzaferri, S., and Sprovieri, R., 1999a, The Miocene/Pliocene boundary and the significance of the earliest Pliocene flooding in the Mediterranean: *Mem. Soc. Geol. Ital*, v. 54, no. 10, p. 109-131.
- Iaccarino, S., Premoli Silva, I., Biolzi, M., Foresi, L., Lirer, F., Turco, E., and Petrizzo, M., 2007, *Practical manual of Neogene planktonic foraminifera*.

- Iaccarino, S. M., Cita, M. B., Gaboardi, S., and Gruppini, G. M., 1999b, 15. High-Resolution Biostratigraphy at the Miocene/Pliocene boundary in Holes 974b and 975b, Western Mediterranean. In Proceedings of the Ocean Drilling Program: Scientific results v. Vol. 161, p. p. 197.
- Iribarren, L., Vergés, J., and Fernández, M., 2009, Sediment supply from the Betic-Rif orogen to basins through Neogene: Tectonophysics, v. 475, no. 1, p. 68-84.
- Jiménez-Moreno, G., Pérez-Asensio, J. N., Larrasoaña, J. C., Aguirre, J., Civis, J., Rivas-Carballo, M. R., Valle-Hernández, M. F., and González-Delgado, J. A., 2013, Vegetation, sea-level, and climate changes during the Messinian salinity crisis: Bulletin, v. 125, no. 3-4, p. 432-444.
- Jurado, M. J., and Comas, M., 1992, Well log interpretation and seismic character of the Cenozoic sequence in the northern Alboran Sea: Geo-Marine Letters, v. 12, no. 2-3, p. 129-136.
- Kouwenhoven, T., Morigi, C., Negri, A., Giunta, S., Krijgsman, W., and Rouchy, J.-M., 2006, Paleoenvironmental evolution of the eastern Mediterranean during the Messinian: Constraints from integrated microfossil data of the Pissouri Basin (Cyprus): Marine Micropaleontology, v. 60, no. 1, p. 17-44.
- Kouwenhoven, T., Seidenkrantz, M.-S., and Van der Zwaan, G., 1999, Deep-water changes: the near-synchronous disappearance of a group of benthic foraminifera from the Late Miocene Mediterranean: Palaeogeography, Palaeoclimatology, Palaeoecology, v. 152, no. 3-4, p. 259-281.
- Kouwenhoven, T. J., 2000, Survival under stress: benthic foraminiferal patterns and Cenozoic biotic crises, Faculteit Aardwetenschappen.
- Kouwenhoven, T. J., Hilgen, F. J., and Van Der Zwaan, G. J., 2003, Late Tortonian-early Messinian stepwise disruption of the Mediterranean-Atlantic connections: constraints from benthic foraminiferal and geochemical data: Palaeogeography, Palaeoclimatology, Palaeoecology, v. 198, no. 3-4, p. 303-319.
- Kouwenhoven, T. J., and Van der Zwaan, G., 2006, A reconstruction of late Miocene Mediterranean circulation patterns using benthic foraminifera: Palaeogeography, Palaeoclimatology, Palaeoecology, v. 238, no. 1-4, p. 373-385.
- Krejci-Graf, K., 1955, Zur Geochemie der Erdölentstehung, Industrieverl. von Herrenhausen.
- Krijgsman, W., Capella, W., Simon, D., Hilgen, F. J., Kouwenhoven, T. J., Meijer, P. T., Sierro, F. J., Tulbure, M. A., van den Berg, B. C., and van der Schee, M., 2018, The Gibraltar corridor: watergate of the messinian salinity crisis: Marine Geology, v. 403, p. 238-246.
- Krijgsman, W., Gaboardi, S., Hilgen, F., Iaccarino, S., Kaenel, E. d., and Laan, E. v. d., 2004, Revised astrochronology for the Ain el Beida section (Atlantic Morocco): no glacio-eustatic control for the onset of the Messinian Salinity Crisis: Stratigraphy, v. 1, p. 87-101.

- Krijgsman, W., Hilgen, F., Marabini, S., and Vai, G., 1999, New paleomagnetic and cyclostratigraphic age constraints on the Messinian of the Northern Apennines (Vena del Gesso Basin, Italy): *Mem. Soc. Geol. Ital.*, v. 54, no. 2.
- Krijgsman, W., and Meijer, P. T., 2008, Depositional environments of the Mediterranean "Lower Evaporites" of the Messinian salinity crisis: Constraints from quantitative analyses: *Marine Geology*, v. 253, no. 3-4, p. 73-81.
- Krom, M. D., and Berner, R. A., 1980, Adsorption of phosphate in anoxic marine sediments 1: *Limnology and oceanography*, v. 25, no. 5, p. 797-806.
- Laskar, J., Robutel, P., Joutel, F., Gastineau, M., Correia, A., and Levrard, B., 2004, A long-term numerical solution for the insolation quantities of the Earth: *Astronomy & Astrophysics*, v. 428, no. 1, p. 261-285.
- Lirer, F., Foresi, M., Iaccarino, S., Salvatorini, G., Turco, E., Cosentino, C., Sierro, F. J., and Caruso, A., 2019, Mediterranean Neogene planktonic foraminifer biozonation and biochronology: *Earth-Science Reviews*, v. 196, p. 102869.
- Lofi, J., Gorini, C., Berné, S., Clauzon, G., Dos Reis, A. T., Ryan, W. B., and Steckler, M. S., 2005, Erosional processes and paleo-environmental changes in the Western Gulf of Lions (SW France) during the Messinian Salinity Crisis: *Marine Geology*, v. 217, no. 1-2, p. 1-30.
- López-Rodríguez, C., De Lange, G. J., Comas, M., Martínez-Ruiz, F., Nieto, F., Sapart, C. J., and Mogollón, J. M., 2019, Recent, deep-sourced methane/mud discharge at the most active mud volcano in the western Mediterranean: *Marine geology*, v. 408, p. 1-17.
- Lourens, L. J., Hilgen, F., Shackleton, N., Laskar, J., and Wilson, J., 2004, The Neogene Period: In F. M. Gradstein, J. G. Ogg, & A. G. Smith (Eds.), v. A geologic time scale 2004 p. 409-440.
- Lugli, S., Gennari, R., Gvirtzman, Z., Manzi, V., Roveri, M., and Schreiber, B. C., 2013, Evidence of clastic evaporites in the canyons of the Levant basin (Israel): Implications for the Messinian salinity crisis: *Journal of Sedimentary Research*, v. 83, no. 11, p. 942-954.
- Maillard, A., Gorini, C., Mauffret, A., Sage, F., Lofi, J., and Gaullier, V., 2006, Offshore evidence of polyphase erosion in the Valencia Basin (Northwestern Mediterranean): scenario for the Messinian Salinity Crisis: *Sedimentary Geology*, v. 188, p. 69-91.
- Maldonado, A., Campillo, A., Mauffret, A., Alonso, B., Woodside, J., and Campos, J., 1992, Alboran Sea late Cenozoic tectonic and stratigraphic evolution: *Geo-Marine Letters*, v. 12, no. 2-3, p. 179-186.
- Mancilla, F. d. L., Booth-Rea, G., Stich, D., Pérez-Peña, J. V., Morales, J., Azañón, J. M., Martín, R., and Giaconia, F., 2015, Slab rupture and delamination under the Betics and Rif constrained from receiver functions: *Tectonophysics*, v. 663, p. 225-237.

- Martín, J. M., Braga, J. C., and Betzler, C., 2001, The Messinian Guadalhorce corridor: the last northern, Atlantic–Mediterranean gateway: *Terra Nova*, v. 13, no. 6, p. 418-424.
- Martínez del Olmo, W., and Comas, M., 2008, Arquitectura sísmica, olistostromas y fallas extensionales en el norte de la cuenca oeste del Mar de Alborán: *Revista de la Sociedad Geológica de España*, v. 21, no. 3-4, p. 151-167.
- Martínez del Olmo, W., and Martín, D., 2016, The Messinian record of Spanish onshore and offshore data (Atlantic Ocean and Western Mediterranean Sea): *Petroleum Geoscience*, v. 22, no. 4, p. 291-296.
- Martínez-Ruíz, F., Comas, M. C., and Alonso, B., Mineral associations and geochemical indicators in Upper Miocene to Pleistocene sediments in the Alboran Basin, *in* *Proceedings Proc. ODP, Sci. Results 1999, Volume 161*, p. 21-35.
- Mayen, L., Jensen, N. D., Laurencin, D., Marsan, O., Bonhomme, C., Gervais, C., Smith, M. E., Coelho, C., Laurent, G., and Trébosc, J., 2020, A soft-chemistry approach to the synthesis of amorphous calcium ortho/pyrophosphate biomaterials of tunable composition: *Acta biomaterialia*, v. 103, p. 333-345.
- McKenzie, J. A., Sprovieri, R., and Channell, J., 1990, The terminal Messinian flood and earliest Pliocene paleoceanography in the Mediterranean: results from ODP Leg 107, Site 652, Tyrrhenian Sea: *Memorie della Società Geologica Italiana*, v. 44, p. 81-91.
- Müller, J., 1978, Luenbergite $[\text{Mg}_3(\text{PO}_4)_2 \cdot 2\text{B}_2\text{O}_3 \cdot (\text{OH})_4 \cdot 6\text{H}_2\text{O}]$ in upper Miocene Sediments of the eastern Mediterranean Sea.: In: Hsü, K.J, Montadert, L., et al. (Eds.), *Init. Rep. D.S.D.P.*, v. 42A, p. 661-664.
- Negri, A., and Villa, G., 2000, Calcareous nannofossil biostratigraphy, biochronology and paleoecology at the Tortonian/Messinian boundary of the Faneromeni section (Crete): *Palaeogeography, Palaeoclimatology, Palaeoecology*, v. 156, no. 3-4, p. 195-209.
- Nijenhuis, I., Schenau, S., Van der Weijden, C., Hilgen, F., Lourens, L., and Zachariasse, W., 1996, On the origin of upper Miocene sapropelites: a case study from the Faneromeni section, Crete (Greece): *Paleoceanography*, v. 11, no. 5, p. 633-645.
- Ohneiser, C., Florindo, F., Stocchi, P., Roberts, A. P., DeConto, R. M., and Pollard, D., 2015, Antarctic glacio-eustatic contributions to late Miocene Mediterranean desiccation and reflooding: *Nature communications*, v. 6, no. 1, p. 1-10.
- Peacor, D. R., Dunn, P. J., Simmons, W. B., and Wicks, F. J., 1985, Canaphite, a new sodium calcium phosphate from the Paterson area, New Jersey: *Mineralogical Record*, v. 16, p. 467-468.
- Pérez-Folgado, M., Sierro, F. J., Bárcena, M. A., Flores, J. A., Vázquez, A., Utrilla, R., Hilgen, F. J., Krijgsman, W., and Filippelli, G. M., 2003, Western versus eastern Mediterranean paleoceanographic response to astronomical forcing: A high-resolution microplankton study of precession-controlled sedimentary cycles during the Messinian: *Palaeogeography, Palaeoclimatology, Palaeoecology*, v. 190, p. 317-334.

- Pierre, C., Caruso, A., Blanc-Valleron, M.-M., Rouchy, J. M., and Orzsag-Sperber, F., 2006, Reconstruction of the paleoenvironmental changes around the Miocene–Pliocene boundary along a West–East transect across the Mediterranean, v. 188-189, p. 319-340.
- Popescu, S. M., Dalibard, M., Suc, J. P., Barhoun, N., Melinte-Dobrinescu, M. C., Bassetti, M. A., Deaconu, F., Head, M. J., Gorini, C., Do Couto, D., Rubino, J. L., Auxietre, J. L., and Floodpage, J., 2015, Lago Mare episodes around the Messinian-Zanclean boundary in the deep southwestern Mediterranean: Marine and Petroleum Geology, v. 66, p. 55-70.
- Queralt, I., Juliá, R., and F., P., 1994, Canaphite: an uncommon condensed phosphate in lake sediments. : 16th Meeting, Int. Mineral. Assoc., Pisa, Italy, 343 (abs.).
- Raffi, I., Backman, J., Fornaciari, E., Pálike, H., Rio, D., Lourens, L., and Hilgen, F., 2006, A review of calcareous nannofossil astrobiochronology encompassing the past 25 million years: Quaternary Science Reviews, v. 25, no. 23-24, p. 3113-3137.
- Rodríguez- Fernández, J., Azor, A., and Miguel Azañón, J., 2011, The Betic intramontane basins (SE Spain): stratigraphy, subsidence, and tectonic history: Tectonics of sedimentary basins: Recent advances, p. 461-479.
- Roger, S., Münch, P., Cornée, J., Saint Martin, J., Féraud, G., Pestrea, S., Conesa, G., and Moussa, A. B., 2000, $^{40}\text{Ar}/^{39}\text{Ar}$ dating of the pre-evaporitic Messinian marine sequences of the Melilla basin (Morocco): a proposal for some biosedimentary events as isochrons around the Alboran Sea: Earth and Planetary Science Letters, v. 179, no. 1, p. 101-113.
- Rouchy, J., Taberner, C., Blanc-Valleron, M.-M., Sprovieri, R., Russell, M., Pierre, C., Di Stefano, E., Pueyo, J., Caruso, A., and Dinares-Turell, J., 1998, Sedimentary and diagenetic markers of the restriction in a marine basin: the Lorca Basin (SE Spain) during the Messinian: Sedimentary Geology, v. 121, no. 1-2, p. 23-55.
- Rouchy, J. M., and Caruso, A., 2006, The Messinian salinity crisis in the Mediterranean basin: A reassessment of the data and an integrated scenario: Sedimentary Geology, v. 188-189, p. 35-67.
- Rouse, R. C., Peacor, D. R., and Freed, R. L., 1988, Pyrophosphate groups in the structure of canaphite $\text{CaNa}_2\text{Pt}_2\text{O}_7 \cdot 4\text{H}_2\text{O}$: The first occurrence of a condensed phosphate as a mineral: American Mineralogist, v. 73, p. 168-171.
- Roveri, M., Flecker, R., Krijgsman, W., Lofi, J., Lugli, S., Manzi, V., Sierro, F. J., Bertini, A., Camerlenghi, A., and De Lange, G., 2014, The Messinian Salinity Crisis: past and future of a great challenge for marine sciences: Marine Geology, v. 352, p. 25-58.
- Ryan, W., Hsu, K., Cita, M., Dumitrica, P., Lort, J., Maync, W., Nesterhoff, W., Pautot, G., Stradner, H., and Wezel, L., 1973, Western Alboran Basin-Site 121: Initial Reports of the Deep Sea Drilling Project, v. 13, p. 43-49.
- Sanz de Galdeano, C., and Alfaro, P., 2004, Tectonic significance of the present relief of the Betic Cordillera: Geomorphology, v. 63, no. 3-4, p. 175-190.

- Seidenkrantz, M.-S., Kouwenhoven, T., Jorissen, F., Shackleton, N., and Van der Zwaan, G., 2000, Benthic foraminifera as indicators of changing Mediterranean–Atlantic water exchange in the late Miocene: *Marine geology*, v. 163, no. 1-4, p. 387-407.
- Selli, R., 1964, The Mayer-Eymar Messinian 1867. Proposal for a neostratotype. : *Proc. 21st IGC Copenhagen 1960*, v. 28, p. 311-333.
- Serrano, F., González-Donoso, J. M., and Linares, D., 14. biostratigraphy and paleoceanography of the Pliocene at sites 975 (Menorca rise) and 976 (Alboran sea) from a quantitative analysis of the planktonic foraminiferal assemblages, *in* *Proceedings of the Ocean Drilling Program. Scientific results 1999*, Volume 161, Ocean Drilling Program, p. 185-195.
- Sierro, F., González Delgado, J., Dabrio, C., Flores, J., and Civis, J., 1995, Late Neogene depositional sequences in the foreland basin of Guadalquivir (SW Spain): *WORLD AND REGIONAL GEOLOGY*, v. 1, no. 6, p. 339-345.
- Sierro, F. J., 1985, The replacement of the “*Globorotalia menardii*” group by the *Globorotalia miotumida* group: An aid to recognizing the Tortonian-Messinian boundary in the Mediterranean and adjacent Atlantic: *Marine Micropaleontology*, v. 9, no. 6, p. 525-535.
- Sierro, F. J., Flores, J., Zamarreno, I., Vázquez, A., Utrilla, R., Francés, G., Hilgen, F., and Krijgsman, W., 1999, Messinian pre-evaporite sapropels and precession-induced oscillations in western Mediterranean climate: *Marine Geology*, v. 153, no. 1-4, p. 137-146.
- Sierro, F. J., Flores, J. A., Civis, J., González Delgado, J. A., and Francés, G., 1993, Late Miocene globorotaliid event-stratigraphy and biogeography in the NE-Atlantic and Mediterranean: *Marine Micropaleontology*, v. 21, no. 1-3, p. 143-167.
- Sierro, F. J., Flores, J. A., Francés, G., Vazquez, A., Utrilla, R., Zamarreño, I., Erlenkeuser, H., and Barcena, M. A., 2003, Orbitally-controlled oscillations in planktic communities and cyclic changes in western Mediterranean hydrography during the Messinian: *Palaeogeography, Palaeoclimatology, Palaeoecology*, v. 190, p. 289-316.
- Sierro, F. J., Hilgen, F. J., Krijgsman, W., and Flores, J. A., 2001, The Abad composite (SE Spain): a Messinian reference section for the Mediterranean and the APTS, v. 168, no. 1-2, p. 141-169.
- Soria, J., Caracuel, J., Yébenes, A., Fernández, J., and Viseras, C., 2005, The stratigraphic record of the Messinian salinity crisis in the northern margin of the Bajo Segura Basin (SE Spain): *Sedimentary Geology*, v. 179, no. 3-4, p. 225-247.
- Soria, J., Fernández, J., and Viseras, C., 1999, Late Miocene stratigraphy and palaeogeographic evolution of the intramontane Guadix Basin (Central Betic Cordillera, Spain): implications for an Atlantic–Mediterranean connection: *Palaeogeography, Palaeoclimatology, Palaeoecology*, v. 151, no. 4, p. 255-266.
- Soto, J. I., Fernandez-Ibanez, F., Talukder, A. R., and Martinez-Garcia, P., 2010, Miocene shale tectonics in the northern Alboran Sea (western Mediterranean).

- Spakman, W., Chertova, M. V., van den Berg, A., and van Hinsbergen, D. J., 2018, Puzzling features of western Mediterranean tectonics explained by slab dragging: *Nature Geoscience*, v. 11, no. 3, p. 211.
- Suess, E., 1981, Phosphate regeneration from sediments of the Peru continental margin by dissolution of fish debris: *Geochimica et Cosmochimica Acta*, v. 45, no. 4, p. 577-588.
- Talukder, A., Comas, M., and Soto, J., 2003, Pliocene to Recent mud diapirism and related mud volcanoes in the Alboran Sea (Western Mediterranean): Geological Society, London, Special Publications, v. 216, no. 1, p. 443-459.
- Tjallingii, R., Röhl, U., Kölling, M., and Bickert, T., 2007, Influence of the water content on X- ray fluorescence core- scanning measurements in soft marine sediments: *Geochemistry, Geophysics, Geosystems*, v. 8, no. 2.
- Tjalsma, R. C., 1971, Stratigraphy and foraminifera of the Neogene of the eastern Guadalquivir Basin (southern Spain): Utrecht University.
- Tulbure, M., Capella, W., Barhoun, N., Flores, J., Hilgen, F., Krijgsman, W., Kouwenhoven, T., Sierro, F. J., and Yousfi, M. Z., 2017, Age refinement and basin evolution of the North Rifian Corridor (Morocco): No evidence for a marine connection during the Messinian Salinity Crisis: *Palaeogeography, Palaeoclimatology, Palaeoecology*, v. 485, p. 416-432.
- Urgeles, R., Camerlenghi, A., Garcia- Castellanos, D., De Mol, B., Garcés, M., Vergés, J., Haslam, I., and Hardman, M., 2011, New constraints on the Messinian sealevel drawdown from 3D seismic data of the Ebro Margin, western Mediterranean: *Basin Research*, v. 23, no. 2, p. 123-145.
- Van Assen, E., Kuiper, K., Barhoun, N., Krijgsman, W., and Sierro, F., 2006, Messinian astrochronology of the Melilla Basin: stepwise restriction of the Mediterranean-Atlantic connection through Morocco: *Palaeogeography, Palaeoclimatology, Palaeoecology*, v. 238, no. 1-4, p. 15-31.
- Van Couvering, J. A., Castradori, D., Cita, M. B., Hilgen, F. J., and Rio, D., 2000, The base of the Zanclean Stage and of the Pliocene Series: *Episodes*, v. 23, no. 3, p. 179-187.
- Van den Berg, B. C. J., Sierro, F. J., Hilgen, F. J., Flecker, R., Larrasoaña, J. C., Krijgsman, W., Flores, J. A., and Mata, M. P., 2018, Imprint of Messinian Salinity Crisis events on the Spanish Atlantic margin: *Newsletters on Stratigraphy*, v. 51, no. 1, p. 93-115.
- Van Der Laan, E., Hilgen, F. J., Lourens, L. J., De Kaenel, E., Gaboardi, S., and Iaccarino, S., 2012, Astronomical forcing of Northwest African climate and glacial history during the late Messinian (6.5-5.5Ma): *Palaeogeography, Palaeoclimatology, Palaeoecology*, v. 313-314, p. 107-126.
- Van der Schee, M., Van den Berg, B. C., Capella, W., Simon, D., Sierro, F. J., and Krijgsman, W., 2018, New age constraints on the western Betic intramontane basins: A late Tortonian closure of the Guadalhorce Corridor?: *Terra Nova*, v. 30, no. 5, p. 325-332.

- Van der Zwaan, G., Jorissen, F., and De Stigter, H., 1990, The depth dependency of planktonic/benthic foraminiferal ratios: constraints and applications: *Marine Geology*, v. 95, no. 1, p. 1-16.
- Vergés, J., and Fernández, M., 2012, Tethys–Atlantic interaction along the Iberia–Africa plate boundary: The Betic–Rif orogenic system: *Tectonophysics*, v. 579, p. 144-172.
- Weltje, G. J., and Tjallingii, R., 2008, Calibration of XRF core scanners for quantitative geochemical logging of sediment cores: Theory and application: *Earth and Planetary Science Letters*, v. 274, no. 3-4, p. 423-438.
- Zahn, R., Comas, M. C., and Klaus, A., 1999, *Proc. ODP, Sci. Results, 161*: College Station, TX (Ocean Drilling Program).
- Ziegler, M., Jilbert, T., de Lange, G. J., Lourens, L. J., and Reichart, G. J., 2008, Bromine counts from XRF scanning as an estimate of the marine organic carbon content of sediment cores: *Geochemistry, Geophysics, Geosystems*, v. 9, no. 5.
- Zijderveld, J. D., Zachariasse, J. W., Verhallen, P. J., and Hilgen, F. J., 1986, The age of the Miocene-Pliocene boundary: *Newsletters on Stratigraphy*, p. 169-181.

Chapter 4

Impact of the Mediterranean-Atlantic
connectivity and the late Miocene
carbon shift on deep-sea
communities in the
Western Alboran Basin

Chapter 4

Bulian, F., Kouwenhoven, T. J., Jiménez-Espejo, F. J., Krijgsman, W., Andersen N. and Sierro, F. J., (in press). Impact of the Mediterranean-Atlantic connectivity and the late Miocene carbon shift on deep-sea communities in the Western Alboran Basin, *Palaeogeography, Palaeoclimatology, Palaeoecology*.

Impact of the Mediterranean-Atlantic connectivity and the late Miocene carbon shift on deep-sea communities in the Western Alboran Basin

Francesca Bulian^{1*}, Tanja J. Kouwenhoven², Francisco J. Jiménez-Espejo,^{3,4}
Wout Krijgsman⁵, Nils Andersen⁶, Francisco J. Sierro¹

¹ Dept. de Geología, Univ. de Salamanca, Plaza de los Caídos s/n, 37008, Salamanca, Spain; sierro@usal.es.

² Department of Earth Sciences, Utrecht University, Princetonlaan 8a, 3584 CB, Utrecht, The Netherlands; T.J.Kouwenhoven@uu.nl.

³ Instituto Andaluz de Ciencias de la Tierra (CSIC-UGR), Armilla, Spain; fjjspejo@ugr.es.

⁴ Research Institute for Marine Resources Utilization (Biogeochemistry Program), JAMSTEC, Yokosuka, Japan.

⁵ Paleomagnetic Laboratory Fort Hoofddijk, Utrecht University, Budapestlaan 17, 3584 CD, Utrecht, The Netherlands; W.Krijgsman@uu.nl.

⁶ Leibniz-Laboratory for Radiometric Dating and Isotope Research, Christian-Albrechts-Universität Kiel, Max-Eyth-Str.11-13, 24118 Kiel, Germany; nandersen@leibniz.uni-kiel.de.

Abstract

Integration of foraminiferal and geochemical data (stable isotope and elemental composition) from West Alboran Basin (WAB) ODP Site 976 allowed evaluation of the effects of the initial Mediterranean – Atlantic restriction event preceding the Messinian Salinity Crisis (MSC) in a context of late Miocene cooling and diminishing water – mass exchange close to Gibraltar Strait.

At 7.17 Ma a prominent shift in benthic foraminifer abundances from dominantly oxic taxa to species tolerating oxygen deficiency, paired with a drop in $\delta^{13}\text{C}$ values, suggest that the restriction of the Mediterranean-Atlantic gateways profoundly affected the WAB deep waters. From 7.17 Ma onward, deep-water stagnation increased the bottom water residence time and led to oxygen depletion. Similar changes, already identified in other Mediterranean basins imply that the first signs of Mediterranean-Atlantic restriction significantly predated the onset of the MSC also in the WAB, an area sometimes considered more under the influence of the Atlantic. Simultaneously, a marked amplitude increase of several element-log ratios reveals a clear cyclical pattern related with precession. Together with new $\delta^{18}\text{O}$ data, the identification of cyclical

*Corresponding author: Francesca Bulian (fra.bulian@usal.es)

patterns allowed improving the age model of Site 976 and consequently enabled an accurate correlation with other Mediterranean, mostly land-based sections. Comparing the records, we were able to correlate the event at a basinal scale and to refine thermohaline circulation models of the Mediterranean after 7.17 Ma.

Because this Mediterranean-scale change was contemporaneous with the global Late Miocene Carbon Isotope Shift (LMCIS) it was important to discern between global and local effects. Given the synchronicity of the global and local Mediterranean change in the $\delta^{13}\text{C}$ record, a global effect certainly affected the Mediterranean Basin. However, opposite phase relations of the global and local $\delta^{13}\text{C}$ signals with orbital parameters, paired with a higher magnitude change identified in our WAB isotope record suggests that the local imprint overruled the global one.

1. Introduction

The late Miocene was characterized by major changes in global ecosystems and climate. Between $\sim 7.8 - 6.7$ Ma a cooling of around 6°C was reported (Tzanova et al., 2015; Herbert et al., 2016; Holbourn et al., 2018) contemporaneous with the Late Miocene Carbon Isotope Shift (LMCIS) characterized by a global shift in the $\delta^{13}\text{C}$ of oceanic dissolved inorganic carbon ($\delta^{13}\text{C}_{\text{DIC}}$) (Hodell et al., 1994; Hodell et al., 2001; Hodell and Venz- Curtis, 2006). On land, large-scale aridification and expansion of C_4 grasslands (Blondel et al., 2010; Edwards et al., 2010; Pound et al., 2012) led, amongst others, to the establishment of the Sahara desert (Hodell et al., 1994; Schuster, 2006; Sepulchre et al., 2006; Zhang et al., 2014; Herbert et al., 2016). During this period, the Mediterranean area was affected by an important paleogeographic reorganization. The Mediterranean Sea was connected to the Atlantic Ocean through the Rifian Corridor in Northern Morocco and the Betic Corridor in Southern Spain (e.g. Martín et al., 2014; Flecker et al., 2015; Achalhi et al., 2016), hosting a marine exchange significantly larger than in the present Strait of Gibraltar. However, during the Tortonian, a dynamic tectonic movement uplifted the Gibraltar Arc (Garcia-Castellanos and Villaseñor, 2011; Van den Berg et al., 2018; Capella et al., 2020) and consequently, the Betic and Rifian corridors started losing their efficiency (Krijgsman et al., 1999; Martín et al., 2014; Flecker et al., 2015; Capella et al., 2018) and progressively closed. The age of closure of the last connection through the Betic gateway (Guadalhorce Corridor) is still debated, with ages varying between late Tortonian (~ 7.6 Ma; Guerra-Merchán et al., 2010; Corbí et al., 2012; Van der Schee et al., 2018) and middle Messinian (6.18 Ma; Martín et al., 2001). For the Rifian corridor there is more agreement on the timing and most probably the southern strand closed between 7.1 - 6.9 Ma while the northern sectors around 7.35 - 7.25 Ma (Tulbure et al., 2017; Capella et al., 2018). The effects of the gateway restriction become visible

in Mediterranean sediments immediately after the Tortonian – Messinian boundary, around 7.17 Ma (Seidenkrantz et al., 2000 and references therein; Blanc-Valleron et al., 2002; Kouwenhoven et al., 2003). From this time onward Mediterranean land-based sections register a shift towards benthic foraminiferal faunas indicating reduced oxygen levels (e.g., dominated by bolivinids, buliminids and uvigerinids). A parallel drop in benthic and planktic $\delta^{13}\text{C}$ (Kouwenhoven et al., 1999; Seidenkrantz et al., 2000; Kouwenhoven et al., 2003; Kontakiotis et al., 2019) testifies a profound change in Mediterranean circulation. Concurrently, the sensitivity of the basin to climatically induced changes increased, and precession-controlled fluctuations in the freshwater budget became visible in geochemical and micropaleontological records (Sierro et al., 2003), resulting in more regular sapropel deposition in the Eastern Mediterranean (Santarelli et al., 1998; Seidenkrantz et al., 2000; Hüsing et al., 2009).

Throughout the Messinian, the connections between the Mediterranean and Atlantic eventually became heavily restricted (Simon and Meijer, 2015), culminating at ~5.97 Ma (Manzi et al., 2013), with the Messinian Salinity Crisis (MSC) and widespread evaporite deposition (Hsü et al., 1973; Manzi et al., 2008; Roveri et al., 2014a). Because the closure of the Betic and Rifian gateways predates the MSC, an additional connection was necessary to regulate water inflow from the Atlantic to provide the necessary ions and trigger the MSC. Concordantly, recent studies (Capella et al., 2018; Krijgsman et al., 2018; Capella et al., 2020) suggest that a proto – Gibraltar Strait could have acted as the Mediterranean-Atlantic sill before and/or during the MSC.

In this study, we analyse the late Tortonian (7.5 Ma) – early Messinian (7 Ma) benthic foraminifer assemblages and geochemical data (both stable isotope and XRF data) from a 26 m long interval of Ocean Drilling Project (ODP) Site 976 located in the West Alboran Basin (WAB). Because the circulation of this area is strongly related with water exchange at Gibraltar Strait we aim to get a more detailed comprehension of the effects of gateway restriction at locations close to the Atlantic connections. Benthic foraminifers are great indicators of environmental conditions and, paired with $\delta^{18}\text{O}$ and $\delta^{13}\text{C}$ stable isotope records and geochemical element data, allow the reconstruction of paleoenvironments and deep – water hydrographic changes affecting the WAB before and after the 7.17 Ma restriction event initially identified at this site by Bulian et al. (2021) at 592 mbsf. The benthic $\delta^{18}\text{O}$ record allows elaborating a more accurate chronology for the late Tortonian – early Messinian at Site 976 and the benthic $\delta^{13}\text{C}$ isotopic record reveals how global and local changes affected the Mediterranean Basin. Finally, comparison between the WAB and Western and Eastern Mediterranean records allowed a Mediterranean scale perspective of the circulation changes after 7.17 Ma.

2. Study area: oceanographic setting and circulation of the modern Mediterranean

The Alboran Basin is a transitional area between the semi-enclosed Mediterranean Sea and the Atlantic Ocean that can be divided into a western (WAB) and an eastern (EAB) basin. Its circulation is very intense and strongly related with water exchange at Gibraltar Strait where the inflow of low-salinity Atlantic waters (surface water) and outflow of high salinity Mediterranean waters occur (Figure 1). Such configuration results in two anti-cyclonic gyres: the Western and Eastern Alboran Gyres (Masqué et al., 2003 and references therein). The low saline Atlantic surface waters (salinity of 36.1 – 36.2 ‰; Rohling et al., 2015 and references therein) entering the Mediterranean flow northward towards the Gulf of Lions and eastward across the Sicily Strait reaching the Eastern Mediterranean Basin (EMB). Along this trajectory, the water becomes salty and eventually sinks in the northern Levantine basin resulting in the formation of the Levantine intermediate water (LIW; Zavatarelli and Mellor, 1995; Buongiorno Nardelli and Salusti, 2000; Pinardi and Masetti, 2000; Pinardi et al., 2019). The LIW settles between 200 and 600 m (Pinardi and Masetti, 2000) and spreads out in the entire Mediterranean. In the northern basins like the Gulf of Lions and the Adriatic and Aegean Seas (Stommel et al., 1973; Schlitzer et al., 1991; e.g. Lascaratos et al., 1999; Powley et al., 2017), surface waters are exposed to cold northerly air masses producing a strong surface buoyancy loss through

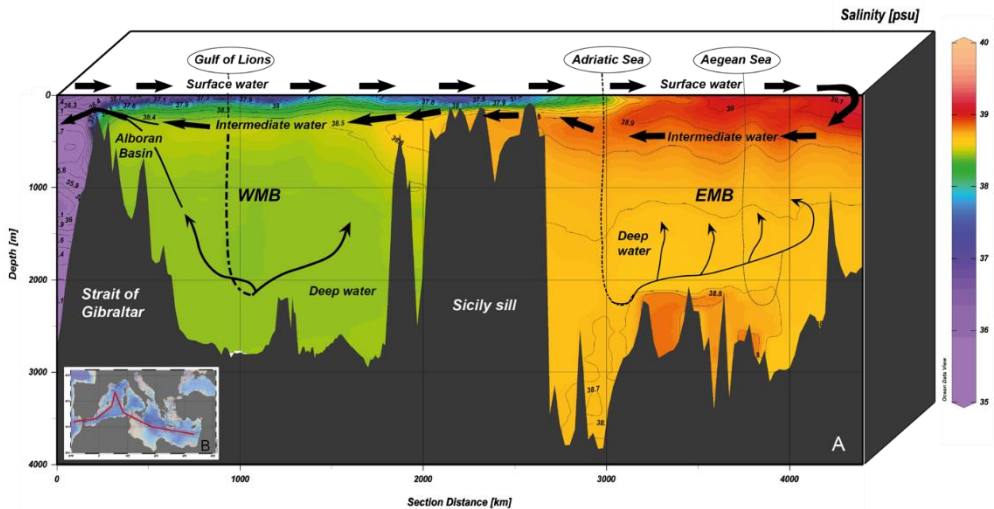


Figure 1: (A) West to East Mediterranean Sea salinity profile produced using Ocean Data View (Schlitzer, 2015) and the general circulation of the Mediterranean Sea (arrows). Alongside to the colour coding, isohalines have been contoured to better show salinity changes. (B) The map displays the 4500 km long transect (red line) of which data (MEDARGroup, 2002) is assimilated into the profile.

cooling and evaporation, allowing the water to sink (e.g. Theocharis and Georgopoulos, 1993). Here, the interaction between the LIW and cold surface waters promotes deep water formation (Pinardi and Masetti, 2000) which is responsible for ventilation at the sea floor. These saltier (salinity of ~ 38.5 ‰; Rohling et al., 2015) intermediate waters are the main component of the Mediterranean Outflow Water (MOW) to the Atlantic Ocean (Pinardi and Masetti, 2000) and are the cause of the salinity gradient between the Mediterranean and Atlantic. This gradient triggers an anti-estuarine circulation active at least since the closure of the connection with the Indian Ocean (Karami et al., 2011).

Bottom water oxygenation in the Alboran Basin depends on the rate of deep water renewal, which is driven, in turn, by deep-water formation in the Gulf of Lions and the rate of Bernoulli aspiration exporting deep water to the Atlantic through the MOW (Stommel et al., 1973). Deep water formation depends on the Mediterranean hydrologic budget and heat exchange with the atmosphere, since the intensity of the African monsoon and Mediterranean rainfall has a strong impact on the net freshwater loss (e.g. Rohling et al., 2009; Marzocchi et al., 2015). During the last 13.5 Ma (Rohling et al., 2015 and references therein; Simon et al., 2017), the enhanced freshwater runoff (Rohling and De Rijk, 1999; Larrasoana et al., 2003; Bianchi et al., 2006; Osborne et al., 2010; Hennekam et al., 2014) associated with stronger African monsoons during times of northern hemisphere summer insolation maxima led to greater surface productivity, water-mass stratification (Rossignol-Strick, 1985; Bosmans et al., 2015) and episodes of deep-water oxygen starvation, leading to deposition of anoxic layers (sapropels) in the EMB and organic rich layers (ORL) in the Western Mediterranean Basin (WMB; e.g. Rogerson et al., 2008; Emeis and Weissert, 2009; Rohling et al., 2015). This geographic variation is related to the different efficiency of deep - water renewal (Rohling et al., 2015). Bernoulli aspiration over a sill is dependent on the outflow velocity and density gradient below the depth of the sill (Stommel et al., 1973; Rogerson et al., 2008; Rogerson et al., 2012). Currently, because the outflow velocity at the Sicily sill is low and density stratification below the sill is high, deep water renewal of the EMB is less efficient (Rohling et al., 2015) than in the west. In the WMB, higher velocities and reduced stratification in combination with the vertical advection with the LIW, permits the flushing of deep - water masses over the Gibraltar Strait preventing sapropel formation.

3. Material and methods

3.1 ODP Site 976 (single Hole B)

New benthic foraminifer and geochemical data are derived from ODP Site 976 (Leg 161; 36° 12' 18.78" N, 4° 18' 45.78" W; 1108.0 m water depth), in the northern sector of the WAB (Figure 2), ~100 km to the east of the Gibraltar Strait. The studied sediments (609 – 583 mbsf) are mainly composed of homogeneous nannofossil-rich claystone and nannofossil (sandy) claystone (Comas et al., 1996). The sediment does not show color changes, but a precessionally dominated cyclicity, especially from 592 mbsf upwards (7.17 Ma), has been highlighted from X-ray fluorescence measurements and planktic foraminifer associations (Bulian et al., 2021). The analysed core sections cover the time interval from the late Tortonian (7.5 Ma) to the early Messinian (7 Ma), followed by a non-recovery interval that extends until the base of the Zanclean (~5.33 Ma). The stage boundaries are defined using planktonic foraminifer bioevents from Bulian et al. (2021).

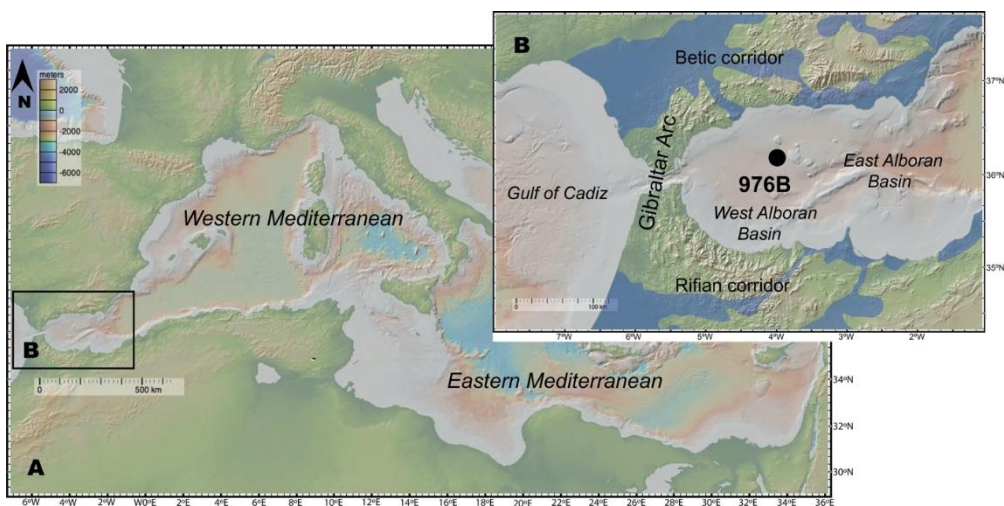


Figure 2: (A) Topographic map of the Mediterranean Sea area and (B) topographic map of the Alboran Basin showing the location of ODP Site 976 used in this study (<http://www.geomapapp.org/>) and in blue the location of the former Betic and Rifian corridors during the late Tortonian modified after Capella et al. (2020).

3.2 Sample preparation

With an average sampling step of 0.3 m (~4 kyr) 93 samples were prepared for micropaleontological and geochemical analyses. The samples were dry weighed, disintegrated in water and washed over a set of 150 μm and 63 μm sieves. Studies have shown that when dealing with paleoenvironmental

reconstructions there is not a significant difference between the results obtained upon analyzing the >125 µm and >150 µm sample fractions (Weinkauff and Milker, 2018), hence, in this study the >150 µm washed residues used for planktic foraminifer analyses (Bulian et al., 2021) were selected for benthic foraminifer counts. From the same fraction, both planktic and benthic foraminifers were picked for stable isotope analyses.

3.3 Benthic foraminifer analyses

Benthic foraminifers were analysed in 59 out of the 93 samples prepared. The sampling resolution varied between 0.3 and 0.6 m resulting in an age resolution of approximately 5 to 10 kyr. Aliquots, preferably containing 150–300 benthic foraminifer specimens, were obtained using a micro splitter. The specimens were hand-picked under a dissection microscope, identified and counted. Entire samples were used when the number of foraminifers was small and samples containing less than 50 specimens were not included in the dataset. The counts were transferred to relative frequencies.

Diversity of the benthic foraminiferal assemblages has been estimated with the Shannon index, which corrects for different sample sizes, and is expressed by the formula $H = -K \sum_{i=1}^n pi \log(pi)$ (Murray, 1991; Spellerberg and Fedor, 2003), where pi is the proportion of the i^{th} species and K a positive constant that takes into account the unit of measure (Shannon, 1948).

The percentage of planktic foraminifers in the foraminiferal fauna (%P) is expressed as $P/(P+B)*100$. The %P values obtained this way can be used as a first indicator of paleodepth or increasing distance to shore, where greater values indicate higher depths and vice versa (Gibson, 1989; Van der Zwaan et al., 1990). The %P is sensitive to disturbance of the deep-water environment such as hypoxia, organic flux and preferential dissolution of planktic foraminifers (Sen Gupta and Machain-Castillo, 1993b; Jorissen et al., 1995; Loubère, 1996; Kucera, 2007; Nguyen et al., 2011), factors affecting the reliability of %P. To avoid the effect of hypoxia, Van der Zwaan et al. (1999) and Van Hinsbergen et al. (2005) suggest excluding infaunal foraminifer species (i.e. species living in the sediment). In this study, the %P values have been estimated with and without infaunal species (i.e. *Globobulimina* spp., *Chilostomella* spp. and all species of the genus *Uvigerina*, *Bulimina* and *Bolivina*) and both paleodepth estimates have been compared with literature data on depth limits of benthic foraminifers (e.g. Pérez-Asensio et al., 2012 and references therein).

Benthic foraminiferal accumulation rates (BFARs) were used as a paleoproductivity proxy because fluctuations were found to indicate changes in surface productivity and nutrient fluxes (Herguera, 1992; Herguera, 2000).

BFARs were calculated from the product of the number of benthic foraminifers per gram of dry sediment (BF/g), the sedimentation rate (cm/kyr) estimated in Bulian et al. (2021) and dry bulk density (g/cm³) interpolated from shipboard physical properties data in ODP Initial Reports for Site 976 (Comas et al., 1996).

Because infaunal foraminifers become more abundant under low-oxygen conditions and/or high organic matter fluxes while epifaunal species (i.e. living at or on top the sediment-water interface) are less tolerant to low-oxygen levels (e.g. Corliss and Chen, 1988; Jorissen et al., 1995; Gooday, 2003), the epifaunal/infaunal ratio (E/I) can highlight changes in bottom-water oxygenation. This ratio is expressed as $E/(E+I)$ where E is the sum of the relative abundances of epifaunal and I of infaunal benthic foraminifers.

Since the sediments were deposited at bathyal depth (Section 5.2), the sum of displaced shallow-water benthic foraminifer species including *Elphidium* spp., *Rosalina* spp., discorbids and *C. lobatulus* (Supplement 1) was used as an indicator of downslope transport. Usually, a higher number of displaced individuals is linked with intense currents (Fentimen et al., 2020 and references therein) that can efficiently transport these shallow water, sometimes epiphytic species (Langer, 1993) to deeper parts of the basin.

In order to gain insight in the variations of the benthic species assemblages through time, a Principal Components Analyses (PCA) was performed using Past 4.02 software (Hammer et al., 2001). The most abundant ($\geq 3\%$) 24 variables were introduced into the analysis, consisting of species, genera and higher order categories. Single and fragmentary occurrences and ill-defined rest groups were removed from the data. To identify species groups presenting similar trends and hence occurring in similar environments, a hierarchical cluster analyses (Pearson correlation: Past 4.02 software; Hammer et al., 2001) was performed including the same 24 variables. When species from a genus were scarcely present, but a genus as a whole considered indicative of analogous environmental conditions, their sum was utilized. *Cancris* spp. contains the species *C. oblongus* and *C. auriculus*, *Bolivina dilatata* is the sum of *B. dilatata* and *B. spathulata*, while in *Pullenia quinqueloba* group, both forms with four and five chambers were included. Because unilocular and uniserial hyaline foraminifers were very diverse but each taxon occurred in low abundances, they were taken together in the unilocular + uniserial group which comprises unilocular taxa, including *Lagena* and *Procerolagena* spp., *Nodosaria* spp., and *Pseudonodosaria* spp.

3.4 Geochemical analyses

3.4.1 Stable isotopes

From the washed residues of all 93 samples prepared, between 10 and 20 specimens of the planktic foraminifer *Globigerina bulloides* were picked and cleaned ultrasonically for oxygen and carbon stable isotope analyses. Even after the cleaning, some specimens were still cemented by calcite and therefore 34 samples were discarded (21 from the intervals 599.80-600.39 mbsf; 596.06-598.07 mbsf; 592.84-594.33 mbsf and 13 irregularly distributed from 601 mbsf downward). Of the benthic foraminiferal content, 2 to 10 specimens of *Cibicidoides kullenbergi* were picked and analyzed for oxygen and carbon isotopes. The analyses were performed with a Finnigan MAT 253 mass spectrometer connected to a Kiel IV carbonate preparation device at the Christian-Albrechts University in Kiel (Germany). Sample reaction was induced by individual acid addition (99% H₃PO₄ at 75 °C) under vacuum. The evolved carbon dioxide was analysed eight times for each individual sample. As documented by the performance of international [NBS19: +1.95 ‰ VPDB (¹³C), -2.20 ‰ VPDB (¹⁸O); IAEA-603: +2.46 ‰ VPDB (¹³C), -2.37 ‰ VPDB (¹⁸O)] and laboratory-internal carbonate standards [Hela1: +0.91 ‰ VPDB (¹³C), +2.48 ‰ VPDB (¹⁸O); HB1: -12.10 ‰ VPDB (¹³C), -18.10 ‰ VPDB (¹⁸O); SHK: +1.74 ‰ VPDB (¹³C), -4.85 ‰ VPDB (¹⁸O)], analytical precision of stable isotope analysis is better than ±0.08 ‰ for δ¹⁸O and better than ±0.05 ‰ for δ¹³C. The obtained values were calibrated relative to Vienna Pee Dee Belemnite (VPDB).

The gradient between the benthic and planktic δ¹³C (Δδ¹³C) was calculated. Doing so, it is important to consider that a foraminifer shell reflects the δ¹³C composition of the dissolved inorganic carbon of the seawater where it calcifies, but usually not in isotopic equilibrium with seawater (Hillaire-Marcel and Ravelo, 2007). Therefore, it is necessary to correct the δ¹³C values for the deviation from equilibrium caused by the vital effect before discussing absolute values. In the case of *Globigerina bulloides*, we compared ODP Site 976 data with values measured for the present-day water column and core tops (modern sediment samples) of the Alboran Sea region. Core top δ¹³C data of *G. bulloides* from ODP Site 977 in EAB yield an average value of -0.75 ‰ (Pérez-Folgado et al., 2004), and core top studies from WAB core HER-GC-UB-6 show values of about -0.5 ‰ (Pérez-Asensio et al., 2020), whereas present-day surface waters from the Alboran Basin show values of around 1.4 ‰. The total negative disequilibrium of the δ¹³C reported in *G. bulloides* tests amounts to ~2‰ (in agreement with laboratory studies; Spero and Lea, 1996), the difference between -0.6 ‰ as the δ¹³C core-top average and 1.4 ‰ from the surface waters. The planktic isotope values were therefore adjusted by adding 2‰ (δ¹³C planktic

corrected). The $\delta^{13}\text{C}$ measurements obtained on *C. kullenbergi* do not need any corrections, because this species precipitates in isotopic equilibrium with bottom water (Wefer and Berger, 1991; Hodell et al., 2001; Hillaire-Marcel and Ravelo, 2007).

3.4.2 Major elements

For the elemental analyses, the archive half of the core was scanned with an XRF Avaatech core scanner at MARUM (Research Faculty, Bremen University, Germany). The data reported here have been acquired by a Canberra X-PIPS Silicon Drift Detector with 150 eV X-ray resolution, the Canberra Digital Spectrum Analyzer DAS 1000, and an Oxford Instruments 50W XTF5011 X-Ray tube with rhodium (Rh) target material. Due to the bad core preservation and occasional intercalations of perforating mud, the sampling steps were inserted manually ranging between 1 and 7 cm (0.2-1 kyr). To detect both light and heavy elements, two runs were performed, the first using generator settings of 30 kV, current of 1.0 mA and a sampling time of 15 sec, while the second run was performed with 10 kV, 0.2 mA and 10 sec sampling time. Because the obtained data are not quantitative, but are expressed in counts, element-log ratios are preferred for the data interpretation (Weltje and Tjallingii, 2008; Rothwell, 2015). Considering the conservative behaviour and terrigenous origin of aluminum (Calvert and Pedersen, 2007; Martinez-Ruiz et al., 2015), Al - normalization was used following other geochemical studies of high detrital input areas like the WMB and EMB (e.g. Jimenez-Espejo et al., 2007; Rodrigo-Gámiz et al., 2014; Martinez-Ruiz et al., 2015). In this study the following element - log Al - normalized ratios have been used: titanium/aluminum (Ti/Al), potassium/aluminum (K/Al), rubidium/aluminum (Rb/Al) alongside with the titanium/calcium (Ti/Ca) and sulphur/titanium (S/Ti) element - log ratios (Bahr et al., 2005; Hoang et al., 2010; Harff et al., 2011). The Principal Component Analyses performed on this dataset was published in Bulian et al. (2021), while the element - log normalized ratios are shown in this study.

3.5 Spectral analyses

Spectral analysis was performed on the benthic $\delta^{18}\text{O}$ and $\delta^{13}\text{C}$ record and element log ratios in order to identify the nature and significance of the periodic changes present. The spectral analysis was carried out in depth and time domain using PAST software (Hammer et al., 2001) on evenly resampled datasets. Frequency peaks over 95% confidence were considered significant.

4. Results

4.1 Distribution of benthic foraminifer assemblages

The data set contains 76 taxa (Supp. 1). The distribution of the benthic foraminifer species with abundances $\geq 3\%$ is shown in Figure 3.

4.1.1 608.9 to 592 mbsf

The lowermost 17 m of the studied interval covers the upper Tortonian and lower Messinian (Figure 3) and includes the Tortonian/Messinian boundary at 596 mbsf (first common occurrence (FCO) of the planktic species *Globorotalia miotumida* group; Bulian et al., 2021). The benthic foraminifer assemblages are well preserved and moderately diversified. The record is dominated by *Siphonina reticulata* (up to 60%), with *Pullenia bulloides* and *Cibicidoides kullenbergi* both reaching 30% of the total abundance (Figure 3). Accessory species (5 – 10%) are *Cibicidoides italicus*, *C. robertsonianus*, *Cibicides lobatulus*, *C. ungerianus*, *Melonis pompilioides*, *M. barleeanus* and *Karreriella bradyi*. *Anomalinoidea helcinus* is found only in the topmost 2 m of this interval.

4.1.2 592 to 583.12 mbsf

Above 592 mbsf several benthic species disappear (e.g. *C. italicus*, *S. reticulata* and *C. kullenbergi*), while others increase (e.g. *M. soldanii*, *M. pompilioides*, *Oridorsalis umbonatus*, *B. dilatata*; Figure 3). A sharp peak in the abundance of *M. soldanii* (30%) is followed with a slight delay by *M. pompilioides* (up to 30%) and high frequencies ($\geq 40\%$) of *O. umbonatus*. Other taxa showing a clear increase in abundance are *Sigmoilopsis schlumbergeri*, *Fissurina* spp., *Pullenia quinqueloba*, *B. dilatata* and *K. bradyi*, the latter reaching 20% abundance. A gradual increasing upward trend can be identified in *Gyroidina soldanii* and *M. barleeanus*. *Cibicidoides bradyi* and *C. robertsonianus* show an initial increase in frequency, not exceeding 6%, before disappearing completely above 588 mbsf.

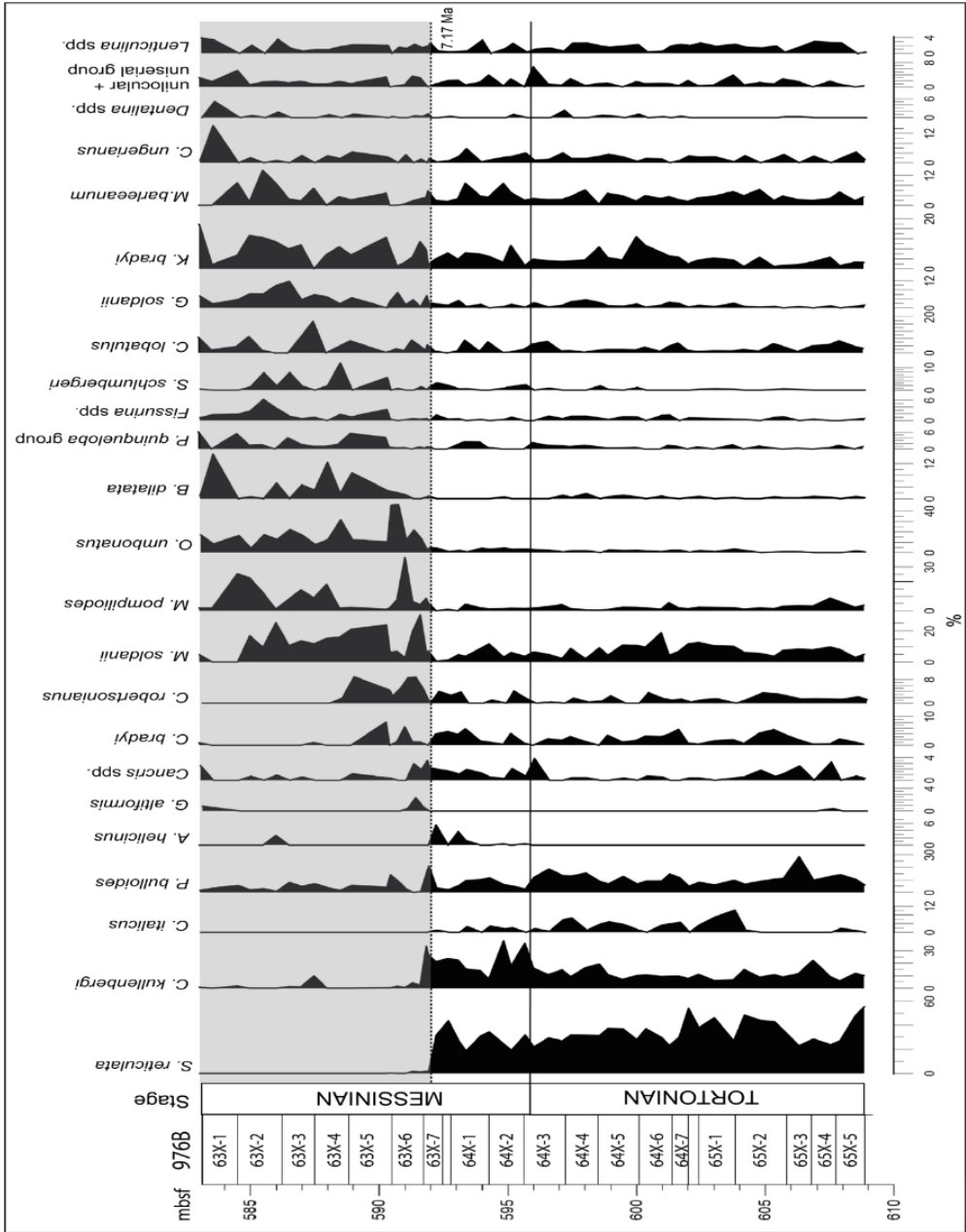


Figure 3: Relative abundances of the benthic foraminifer species $\geq 3\%$ selected for the statistical analyses against depth and stages of Site 976. The continuous black line highlights the Tortonian – Messinian boundary while the dashed line and the grey band highlight the 7.17 Ma restriction event.

4.2 Paleocological and statistical parameters of the benthic foraminifer assemblage

The paleocological and statistical parameters used in this study are shown in Figure 4 and can be found in Supp. 2. The %P curves both with and without the infaunal benthic species, show an analogous behaviour (Figure 4 a) and remain fairly constant until 592 mbsf when two episodes with lowered %P are registered (at 591 and 587.5 mbsf), the youngest corresponding with the highest (20%) peak of displaced foraminifers. The sum of displaced benthic foraminifers (Figure 4 b) fluctuates between 2% and 14% with a 20% peak at 587 mbsf. The Shannon diversity index (Figure 4 c) shows a slight upward increasing trend, with

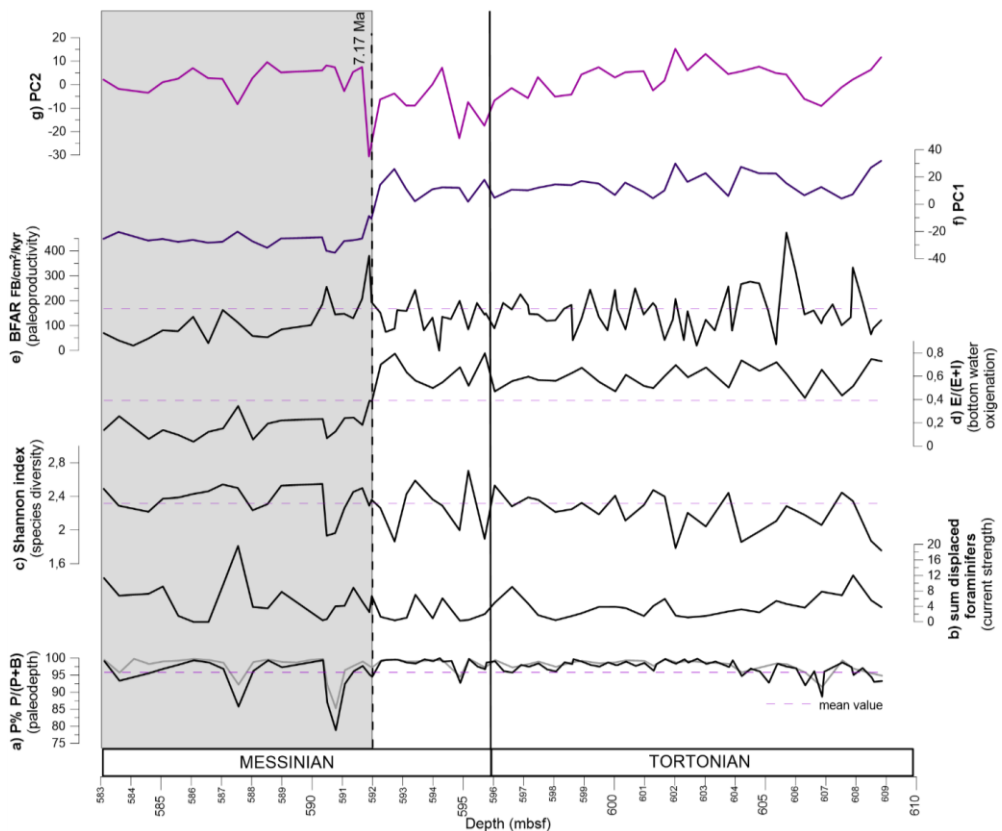


Figure 4: The obtained paleocological and statistical parameters for Site 976: a) The percentage of planktic foraminifers estimated with benthic infaunal species (in black) and without them (in grey; P%); b) Sum of displaced benthic foraminifers; c) Shannon index; d) Epifaunal/Infaunal ratio (E/(E+I)); e) Benthic foraminifers accumulation rate (BFAR); f) First Principal Component (PC1); g) Second Principal Component (PC2); Both Principal components reflect the change in benthic foraminifer assemblage before and after the 7.17 ma event. The grey rectangle highlights these changes. The full black line highlights the Tortonian – Messinian boundary while the dashed one the 7.17 Ma restriction event.

large shifts in values from the base to 590 mbsf when it remains constant towards the top of the studied core section. Simultaneous with the shift in the benthic foraminifer assemblage, the E/(E/I) ratio (Figure 4 d) displays a radical drop in values above 592 mbsf which persists until the top of the record. The BFAR values show relatively large variations around the mean of ~200 benthic foraminifera/cm²/kyr throughout most of the Tortonian (Figure 4 e). Towards the Tortonian-Messinian boundary values increase and at 592 mbsf, they gradually start to decrease, and stabilize around lower values (~100).

4.3 Statistical analysis of the benthic foraminifer assemblages

The Principal Components Analyses (PCA; Supp. 2) yields two statistically significant components, PC1 and PC2, together explaining 63.6% of the variance within the dataset (48.12% on PC1 and 15.15% on PC2). The third and further axes explain less than 10% of the variance and are not considered. The loadings, i.e. the contribution of each individual variable on a component (axis), are given in Table 1. The two most positive loadings for PC1 are *S. reticulata* and *C. kullenbergi* while the negative ones are *M. pompilioides*, *M. barleeanum* and *O. umbonatus* (Table 1).

Table 1: PCA loadings for the species imported into statistical analyses of Site 976.

Species	PC1	PC2
<i>A. helycinus</i>	0.00274	-0.01662
<i>B. dilatata</i>	-0.06129	0.02499
<i>C. brady</i>	0.02432	0.01051
<i>C. italicus</i>	0.03768	0.02794
<i>C. kullenbergi</i>	0.25215	-0.78923
<i>C. lobatulus</i>	-0.03673	-0.01403
<i>C. robertsonianus</i>	-0.01829	0.04527
<i>C. ungerianus</i>	0.00169	-0.00621
<i>Cancris</i> spp.	-0.00025	-0.03941
<i>Dentalina</i> spp.	-0.00842	-0.00779
<i>Fissurina</i> spp.	-0.01879	0.01915
<i>G. altiformis</i>	-0.00272	-0.01768
<i>G. soldanii</i>	-0.07641	-0.00928
<i>K. bradyi</i>	-0.08663	0.06684
<i>Lenticulina</i> spp.	-0.00498	-0.00129
<i>M. barleeanum</i>	-0.00119	-0.04937
<i>M. pompilioides</i>	-0.17122	-0.06904
<i>M. soldanii</i>	-0.13135	0.28641
<i>Nodosaria</i> spp.	-0.01254	0.02003
<i>O. umbonatus</i>	-0.38708	0.26736
<i>P. bulloides</i>	0.07948	-0.17932
<i>P. quinqueloba</i>	-0.03085	0.00787
<i>S. reticulata</i>	0.84227	0.41526
<i>S. schlumbergeri</i>	-0.04373	0.02013

The positive loadings for PC2 are *S. reticulata* and *O. umbonatus* together with *M. soldanii*, and the most negative loadings on PC2 are of *C. kullenbergi* and *P. bulloides*. From PC1 and PC2 (Figure 4) two major faunal assemblages can be identified. The first one is associated with upper Tortonian-lowermost Messinian samples (until 592 mbsf) and is characterized by species loading positively on PC1 such as *S. reticulata* and *C. italicus*, and species loading negatively *C. kullenbergi* and *P. bulloides*. The second assemblage characterizes the Messinian deposits from 592 mbsf upwards and is dominated by *O. umbonatus* and *M. soldanii* loading positively and *M. pompilioides* loading negatively on PC2.

The dendrogram (Figure 5; Supp. 2) highlights the clear partition between the pre- and post- 592 mbsf assemblages as well as the changes in species distribution reflected in Cluster 2. Above 592 mbsf, a first increase in Cluster 2A (*C. bradyi*, *C. robertsonianus* and *A. helycinus*) is visible related with the establishment of clear cyclical juxtaposition between Clusters 2D (*C. lobatulus* and *M. pompilioides*) and 2C (unilocular+uniserial group, *P. quinqueloba* group, *Cancris* spp., *M. barleeanum*, *M. soldanii*, *S. schlumbergeri*, *Fissurina* spp., *K. bradyi*, *G. soldanii* and *O. umbonatus*). Cluster 2B (*Lenticulina* spp., *B. dilatata*, *Dentalina* spp. and *C. ungerianus*) is present throughout the record, with a peak at the topmost part of the studied interval.

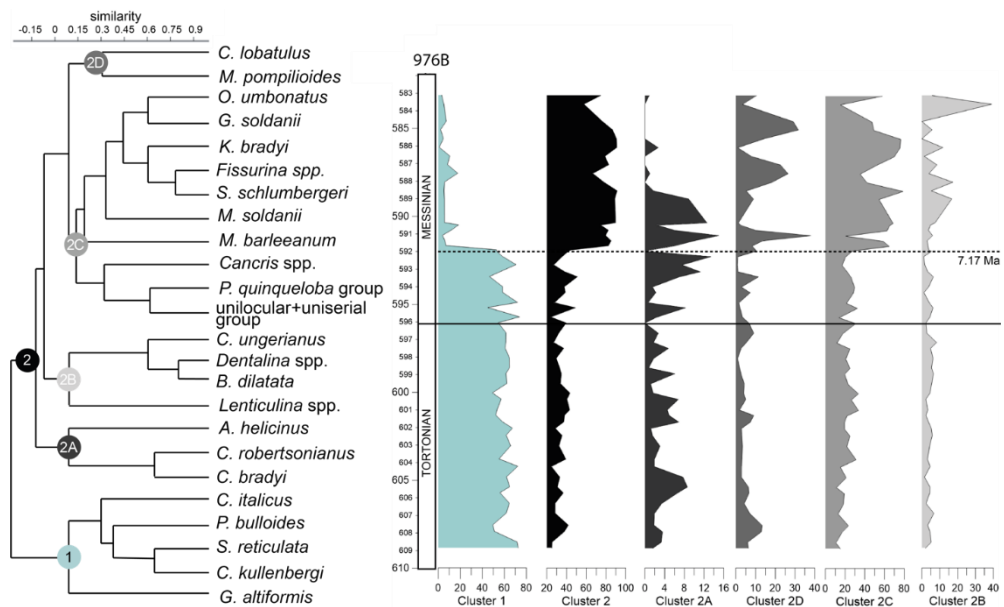


Figure 5: Dendrograms resulting from hierarchical clustering that divided the benthic faunas into two main clusters (Cluster 1 and 2) and four sub clusters (Cluster 2A, 2B, 2C and 2D). All the cluster have been plotted against depth on the right-hand side. The continuous black line highlights the Tortonian - Messinian boundary while the dashed one the 7.17 Ma restriction event.

4.4 Oxygen and carbon isotope records

Throughout the Tortonian and the lowermost Messinian, both $\delta^{18}\text{O}$ curves display a general trend towards heavier values, which is more accentuated in the benthic $\delta^{18}\text{O}$ record (Figure 6 d, e; Supp. 3). Both records show a decrease between 592 and 588 mbsf. The planktic $\delta^{13}\text{C}$ record (Figure 6 a) displays a general stable trend fluctuating around the mean value of $\sim 0\text{‰}$ ($\sim 2\text{‰}$ when corrected) throughout the Tortonian and Messinian. The benthic $\delta^{13}\text{C}$ values vary between $+1$ and -1.8‰ showing a significant negative excursion of $\sim 1\text{‰}$ starting at 592 mbsf, and a mean value around -1‰ persists until the top of the record. The sharp negative benthic $\delta^{13}\text{C}$ drop, in comparison with the stable planktic $\delta^{13}\text{C}$ is evident in the $\Delta\delta^{13}\text{C}$ gradient curve (Figure 6 c), which increases from 1.5‰ below 592 mbsf to 2.8‰ above this depth. The benthic and planktic $\delta^{13}\text{C}$ records are in phase as well as the $\delta^{18}\text{O}$ curves and show a general cyclical behaviour throughout the entire section. The same phase relationship between all four datasets is also visible.

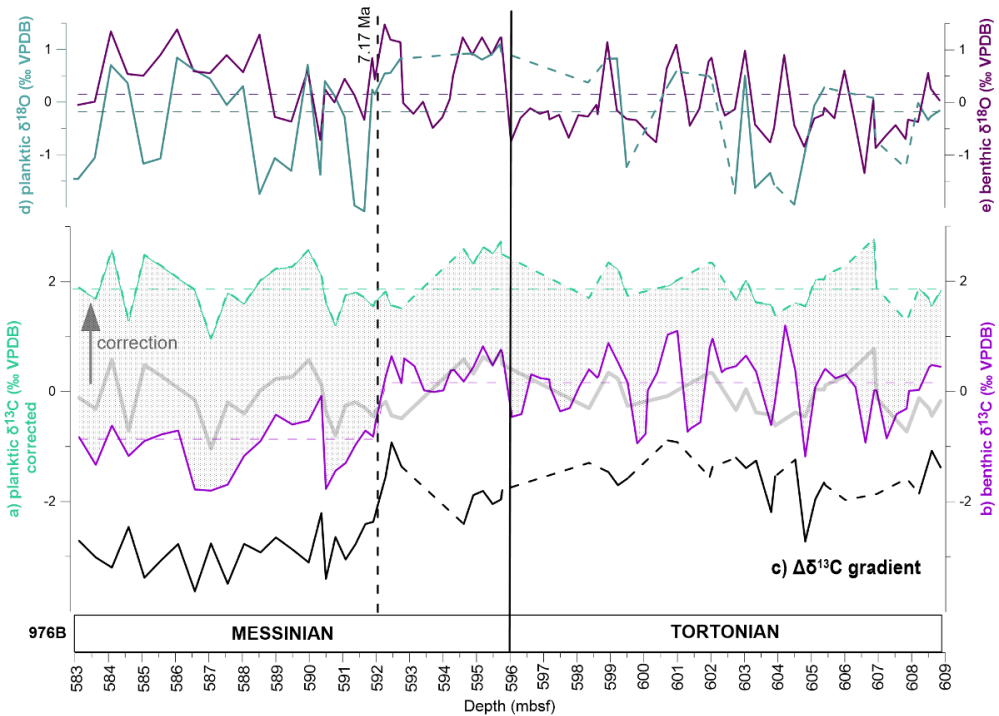


Figure 6: Upper Tortonian and lower Messinian stable isotope curves from ODP Site 976: a) corrected planktic (*G. bulloides*) $\delta^{13}\text{C}$ curve (original curve in grey); b) benthic (*C. kullenbergi*) $\delta^{13}\text{C}$ curve; c) benthic - planktic $\Delta\delta^{13}\text{C}$ carbon gradient; d) planktic (*G. bulloides*) $\delta^{18}\text{O}$ isotopic record; e) benthic (*C. kullenbergi*) $\delta^{18}\text{O}$ isotopic record. The dashed lines indicate the mean value while the planktic record discontinuous lines shows intervals where planktic data could not be measured due to intense calcification. The black line shows the Tortonian - Messinian boundary while the dashed one highlights the 7.17 Ma restriction event.

4.5 Semiquantitative elemental geochemistry

All the semiquantitative elemental data and the normalized element - log ratios used in this research can be found in Supp. 4. The Zr/Al ratio (Figure 7 a) oscillates around a mean of -0.1 throughout the uppermost Tortonian and lower Messinian. At 592 mbsf the values sharply increase and so do the oscillation amplitudes. The Zr/Al, Ti/Al and Rb/Al (Figure 7 a, b, c) curves show overall a similar trend, with a sharp increase at 592 mbsf. The Ti/Ca ratio (Figure 7 d) decreases from the bottom up to 593 mbsf when the values and amplitudes increase and stay high throughout the rest of the record. The S/Ti ratio (Figure 7 e) shows a generally oscillating and upward increasing trend in three steps, with increasingly higher values especially above 592 mbsf and the largest peak in the uppermost part of the Messinian record, just below the non-recovery interval. An analogous phase relationship can be seen in the Zr/Al, Ti/Al, Rb/Al and Ti/Ca ratios.

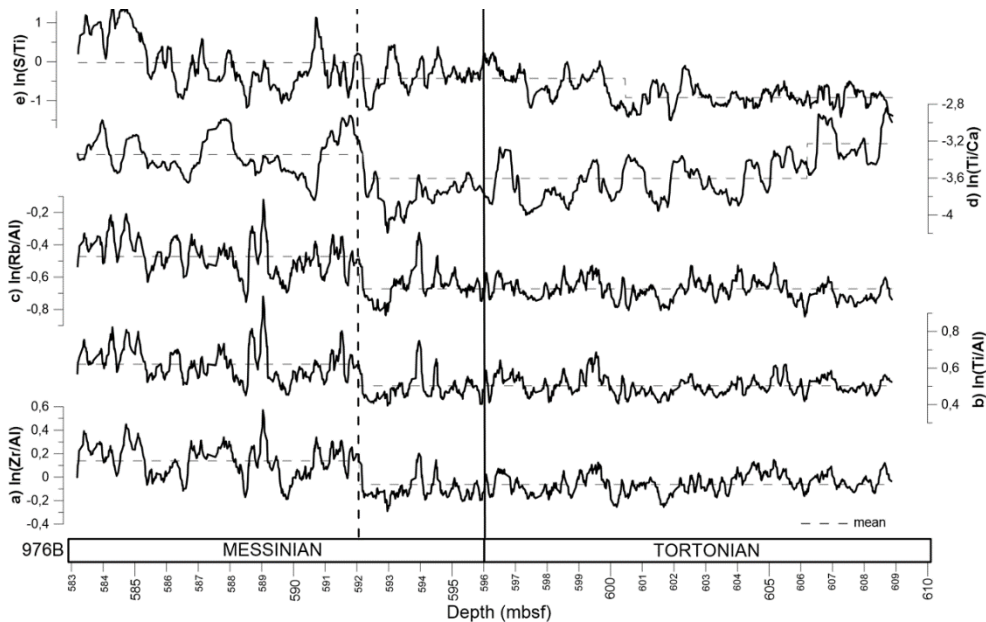


Figure 7: Proxies derived from geochemical data of ODP Site 976: a) $\ln(\text{Zr}/\text{Al})$ ratio; b) $\ln(\text{Ti}/\text{Al})$ ratio; c) $\ln(\text{Rb}/\text{Al})$ ratio; d) $\ln(\text{Ti}/\text{Ca})$ ratio and e) $\ln(\text{S}/\text{Ti})$ ratio. The black line shows the Tortonian - Messinian boundary while the dashed one highlights the 7.17 Ma restriction event.

5. Discussion

5.1 Improved age model

5.1.1 Mechanisms driving the sedimentary cyclicity before and after the 7.17 Ma restriction event

The cyclical patterns of the sedimentological and micropaleontological record, especially in the interval 592-583.12 mbsf, have been discussed in Bulian et al. (2021). The sedimentological record of the interval before 592 mbsf (7.17 Ma) did not show a clear cyclicity and therefore a precise cycle to cycle tuning was not possible using the foraminifer assemblages. However, the cyclical changes in planktic oxygen isotopes in the Mediterranean mainly reflect freshwater budget oscillations and sea surface temperatures as warmer temperatures and humid climates result in lighter oxygen isotope ratios (Lourens et al., 1996; Rohling and Cooke, 1999; Lisiecki and Raymo, 2005), while benthic carbon isotopes reflect changes in organic carbon remineralization that are, in turn, driven by variations in deep water ventilation and organic carbon flux to the seafloor (Laube-Lenfant and Pierre, 1994; Pierre, 1999). Hence, the new stable isotope records can be used to elaborate a more accurate age model of the entire record. Concordantly, the cyclical pattern in the newly acquired stable isotope data is evident both before and after 592 mbsf and it has been confirmed by spectral analyses which yielded cycles of 6.6 m and 1.4 m for the lower interval (592 – 609 mbsf) and of 3.3 m and 2 m for the upper interval (583 – 592; Figure 8).

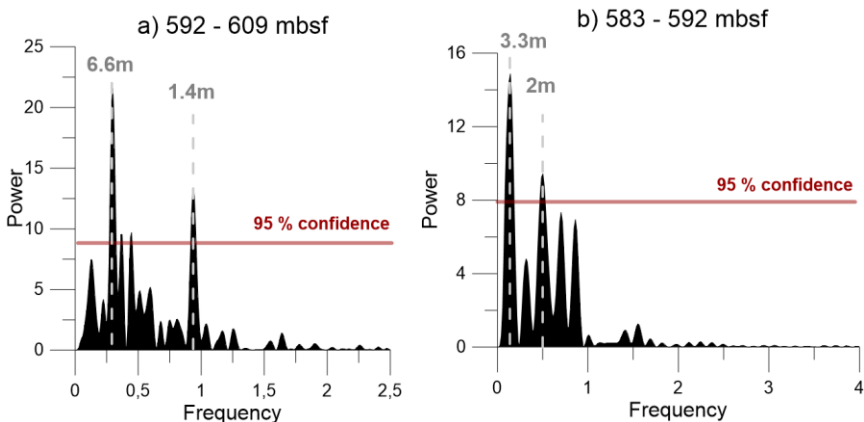


Figure 8: Power spectrum of the benthic $\delta^{18}\text{O}$ record of Site 976 before and after the restriction event at 592 mbsf with the main cyclicities expressed in meters. The 95% confidence interval is indicated by the red line.

Below 592 mbsf the geochemical cycles visible in the $\delta^{18}\text{O}$ and $\delta^{13}\text{C}$ record covary (Figure 9). In the 592 – 609 mbsf interval, maxima of planktic and benthic $\delta^{18}\text{O}$ were linked to summer insolation minima assuming they are correlated with lower rates of Nile discharge and decreasing annual rainfall, causing increasing surface salinities and lower surface temperatures (Bosmans et al., 2015; Rohling et al., 2015 and references therein). The resulting enhanced surface densities favour vertical mixing and deep – water formation enabling a good Rb, Zr, Si) to the basin. Here, however, an opposite behaviour is observed. Higher detrital element supply (higher Ti/Ca, Rb/ Al, Ti/ Al and Zr/ Al ratios, e.g. Figure 9) are associated with high planktic and benthic $\delta^{18}\text{O}$ and high benthic ventilation that should result in high benthic $\delta^{13}\text{C}$ values associated with insolation minima. During these times, the lower rainfall in the Alboran watersheds should also

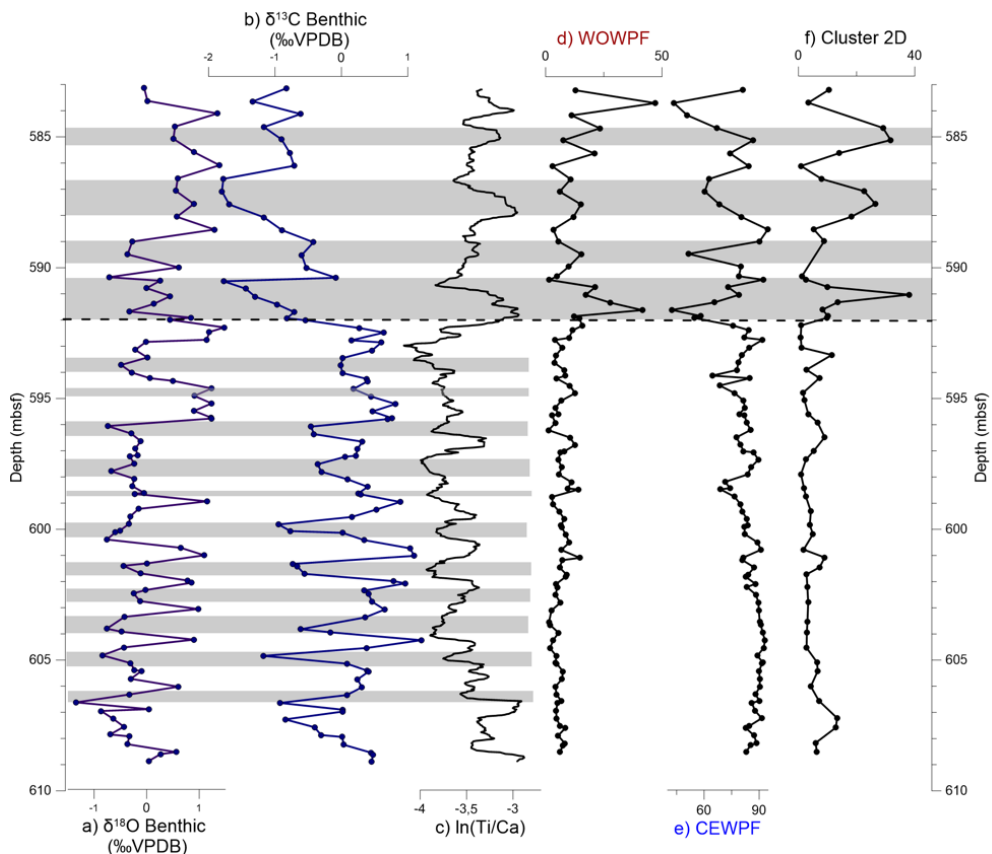


Figure 9: Precessionally driven cyclicity evident in the ODP Site 976 record shown in depth domain. From left to right: a) benthic $\delta^{13}\text{C}$ curve; b) benthic $\delta^{18}\text{O}$ curve (benthic curves are used because the record is more continuous); c) $\ln(\text{Ti}/\text{Ca})$ ratio; d) the sum of warm oligotrophic water planktic foraminifer species (WOWPF; Bulian et al., 2021); e) the sum of cold eutrophic water planktic foraminifer species (CEWPF; Bulian et al., 2021); f) distribution of benthic Cluster 2D. The shaded rectangles highlight the cycles before and after the restriction event.

result in lower river supply of detrital elements (e.g. Ti, $\delta^{13}\text{C}$, suggesting an unexpected higher detrital input at times of insolation minima. If river supply as the source of clastic particles is ruled out, terrigenous particles must necessarily derive from wind-blown dust from north Africa (e.g. Calvert and Pedersen, 2007; Martinez-Ruiz et al., 2015). Analogous phase relations were found in the Trubi formation in Sicily (beige layers signal of Trubi formation; De Visser et al., 1989) and in EMB Site 967 (Leg 160; Larrasoaña et al., 2003 and references therein; Konijnendijk et al., 2014), where most of the detrital input occurs during insolation minima. The clastic particles were not supplied by rivers, but by wind-transported dust from North Africa, strongly diluting the carbonate content of the sediments.

By contrast, above 592 mbsf higher detrital element supply (high Ti/Ca, Zr/Al, Ti/Al or Rb/Al) covaries with lighter planktic and benthic $\delta^{18}\text{O}$ and $\delta^{13}\text{C}$ (Figure 9). Here, higher values of these ratios are linked to insolation maxima when humid conditions dominate the Mediterranean and high annual precipitation and enhanced riverine discharge (Rohling et al., 2015 and references therein) promote water column stratification and the proliferation of warm oligotrophic water planktic foraminifer species (WOWPF) together with an enrichment in detrital elements (Ti, Zr, Rb; Figure 9). Contemporaneously, low salinity surface water prevents deep water formation and ventilation of the bottom resulting in increased bottom water residence time, evidenced by lighter benthic $\delta^{13}\text{C}$ values. Above 592 mbsf, during insolation minima cold eutrophic water planktic species (CEWPF; Figure 9) co-occur with sediments enriched in biogenic elements (Ca and Sr; Bulian et al., 2021) and light $\delta^{18}\text{O}$ and $\delta^{13}\text{C}$ values. These cycles can be interpreted as dilution cycles where fluvial detrital input replaced eolian dust as the main diluting factor. Cyclical behaviour can also be seen in at least the first three insolation maxima in the benthic foraminifer record. The increase of Cluster 2D, dominated by allochthonous *C. lobatulus*, together with *M. pompilioides* (Figure 9), known to proliferate when levels of terrestrial refractory organic matter are high (Poli et al., 2012 and references therein), can be explained by the increased terrigenous/fluvial input coming to the basin. Similar orbitally-driven climatic alternations were described in the Sorbas (Vázquez et al., 2000; Sierro et al., 2003), Gavdos Basins (Seidenkrantz et al., 2000; Pérez-Folgado et al., 2003) and the Balearic promontory (Frigola et al., 2008), while Greek, and Italian sections (Seidenkrantz et al., 2000; Krijgsman et al., 2002; Hüsing et al., 2009; Di Stefano et al., 2010) show an alternation between normal marine and sapropel sedimentation (Section 5.4). In addition, a similar climate signature and cyclicity has been observed in Atlantic locations proximal to the Mediterranean like SW Spain and NW Morocco (Van Der Laan et al., 2012; Van den Berg et al., 2015).

5.1.2 Astronomical tuning of the geochemical record

First order calibration of the benthic and planktic $\delta^{18}\text{O}$ curves of Site 976 was achieved using foraminifer bioevents and stage boundaries from Bulian et al. (2021). Reliable bioevents include the FCO of planktic *Globorotalia menardii* 5 group at 601.96 mbsf, the FCO of *G. miotumida* group at 594.9 mbsf and the disappearance of *Globorotalia suterae* at 592 mbsf (Bulian et al., 2021) (Figure 10). The *Globorotalia suterae* event has been astronomically calibrated at 7.17 Ma (Lirer et al., 2019). The *G. menardii* 5 group event has been calibrated at 7.36 Ma and the *G. miotumida* group event at 7.24 Ma (Lirer et al., 2019) and have been recorded respectively in cycle 11 and 16 of the Faneromeni section in Crete (grey marls, Figure 10) (Krijgsman et al., 1994; Hilgen et al., 1995; Santarelli et al., 1998) and cycle 9 and 15 of Oued Akrech section in Morocco (reddish layers) (Hilgen et al., 2000). In the two sections, these cycles have been correlated with Northern Hemisphere summer insolation maxima phases (Krijgsman et al., 1994; Hilgen et al., 1995; Santarelli et al., 1998). In the Faneromeni section, the insolation maxima peak between cycle 17 and 18 does not materialize while in the Oued Akrech section it is represented by cycle 17 (Figure 10). Considering that the cyclicity at 976 Site is also driven by precession (1.4 and 2 m cycles while the 3.3 and 6.6 m cycle are related to other orbital parameters), we used the cycles identified in the two sections as an aid for astronomical tuning. For the lower part of the record (592-609 mbsf), the insolation maxima peaks corresponding to the grey layers in Faneromeni section (cycles F7 to F18) and reddish intervals in Oued Akrech section (cycles OA5 to OA18) were related with $\delta^{18}\text{O}$, $\delta^{13}\text{C}$ and Ti/Ca minima. In the upper part of the core (583-592 mbsf) insolation maxima phases derived from $\delta^{18}\text{O}$, $\delta^{13}\text{C}$ and CEWPF minima and Ti/Ca, WOWPF and benthic Cluster 2D maxima and were related with cycles F18 - F23 of Faneromeni section and Cycles OA18 - OA21 in Oued Akrech section (Figure 10). The evident change in sedimentation rates visible after the tuning are probably the cause of the different phase relationship before and after the 7.17 Ma event (Figure 10).

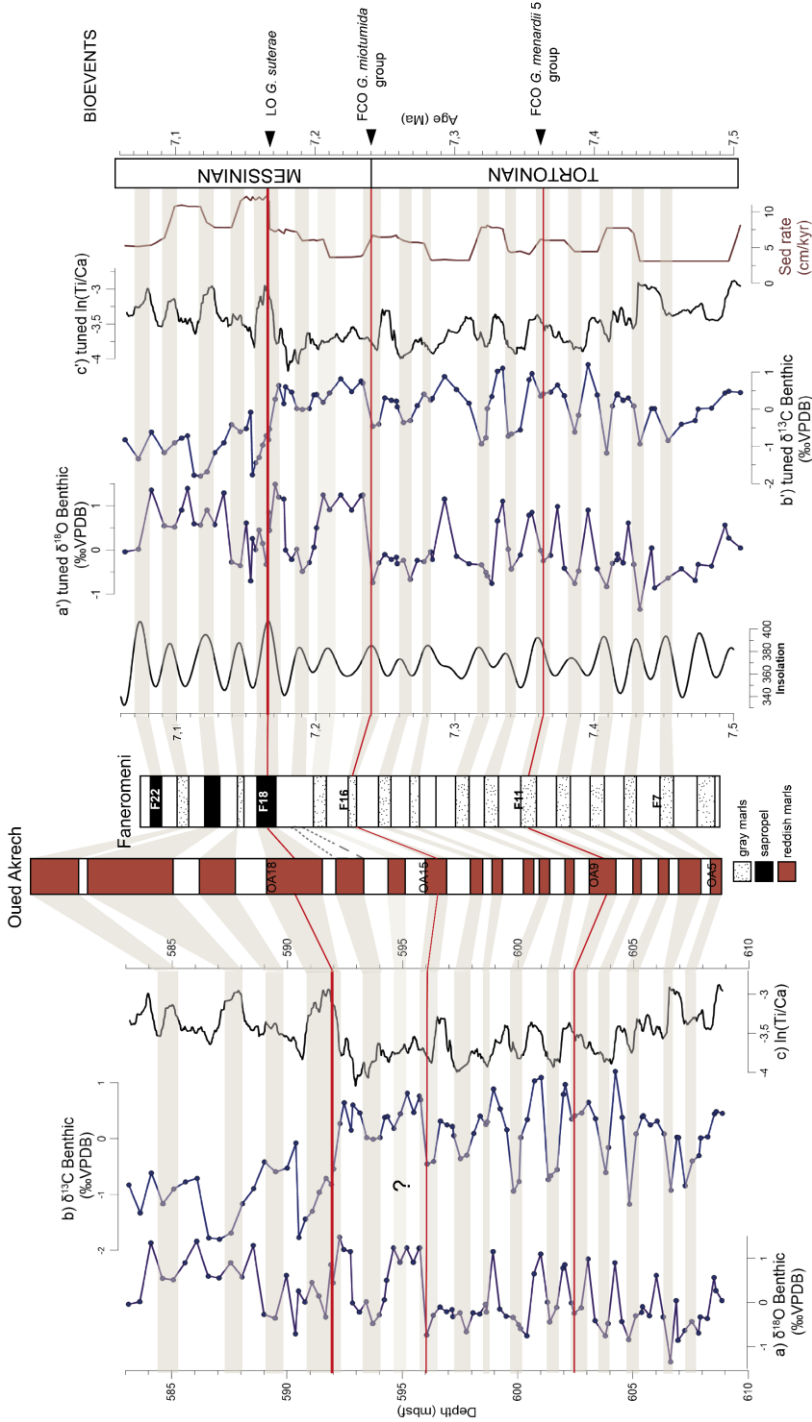


Figure 10: Age model of ODP Site 976 based on tuning to the insolation curve of the benthic $\delta^{18}\text{O}$ and $\delta^{13}\text{C}$ curve and $\ln(\text{Ti}/\text{Ca})$ ratio. On the left, the records are displayed in depth domain (a, b, c) while on the right in time domain paired with the obtained sedimentation rate (a', b', c'). In the Middle, the correlation with the cycles from Oued Akrech (Hilgen et al., 2000) and Faneromeni sections (Krijgsman et al., 1994; Hilgen et al., 1995; Santarelli et al., 1998) is shown. The black arrows show the main foraminifer bioevents (Bulian et al., 2021) highlighted by the red lines

5.2 Paleo-water depth reconstruction

Based on a mean %P between 95 and 100% (Figure 4), the calculated paleodepth using the transfer function in Van der Zwaan et al. (1990) and Van Hinsbergen et al. (2005) would be ~1000 – 1200m. This is in fact the maximum paleodepth that can be resolved with this method, so extra constraint is needed. Many benthic foraminifers occupy a considerable depth range, but some species or species groups can give an indication of paleo-water depth. Amongst the most abundant benthic foraminifer species recorded in the late Tortonian-early Messinian part of the record (608.9 – 592 mbsf) are *S. reticulata* and *C. kullenbergi*, together with *C. italicus* and *C. robertsonianus*, considered epifaunal species occurring at middle bathyal water depths (Wright, 1978; Sgarrella and Moncharmont Zei, 1993; Schönfeld, 1997; Violanti et al., 2011; Pérez-Asensio et al., 2012). The third most common taxon, *P. bulloides*, has been reported from neritic to abyssal water depths (200-4000 m; Pelum et al., 1976; Pflum et al., 1976; Bornmalm, 1997) but is usually considered a deep-water taxon (e.g. Mackensen et al., 1985; Van Marle, 1988; Mackensen et al., 1993). Mesobathyal depths have not been uniformly defined and environmental parameters are more instrumental than water depth (e.g., Jorissen et al., 2007). In addition, the bathyal range is more condensed in the Mediterranean than in the open ocean (Bandy & Chierici, 1966). Here, water depths between ~500 and ~2000 m are considered mesobathyal (differing from for instance Wright, 1978, who considers epibathyal and mesobathyal, and Schönfeld, 1997, who considers upper- and lower bathyal depths). Considering the abundances of *C. kullenbergi* and *S. reticulata* and the near absence of *Cibicides wuellerstorfi*, which has an upper depth limit of ~1200 m (Bandy and Chierici, 1966; Wright, 1978), the estimated depth range is approximately 1000 – 1500 m for Site 976. *Elphidium* and *Rosalina* spp., discorbids and *C. lobatulus* are present in abundances between 5% and 10% (Figure 3; Appendix 1) with two maxima of 15% and 20% around 589 m. When found in deep environments, these shallow-water, sometimes epiphytic taxa (Jorissen, 1987; Langer, 1993) are considered displaced (e.g. Murray, 2006) and cannot be used in the paleodepth reconstruction.

After 7.17 Ma high abundances of *O. umbonatus*, *M. pompilioides*, *M. soldanii* and *K. bradyi* indicate that a mesobathyal environment persists after the 7.17 Ma event (Bandy and Chierici, 1966; Wright, 1978 and references therein; Mackensen et al., 1993; Sen Gupta and Machain-Castillo, 1993a; Loubère, 1996; Bornmalm, 1997; Pérez- Asensio et al., 2012; Kaminski et al., 2013).

5.3 Deterioration of deep-water circulation at 7.17 Ma

5.3.1 Environmental changes and aging of deep-water masses

One of the most abundant species in the upper Tortonian-lowermost Messinian (before 7.17 Ma) record is *S. reticulata*, which has been associated with oxic conditions (Gebhardt, 1999; Kouwenhoven et al., 2003), however has also been reported from hypoxic bottom waters (Katz and Thunell, 1984; Denne and Sen Gupta, 1991; Sgarrella and Moncharmont Zei, 1993; Barra et al., 1998). The species is associated with high abundances of *Cibicidoides* species and *P. bulloides*. *Cibicidoides* species are generally considered epifaunal and associated with oligotrophic, well oxygenated waters (e.g. Lutze and Coulbourn, 1984; Corliss and Chen, 1988; Corliss, 1991; Kaiho and Lamolda, 1999). *Cibicidoides kullenbergi* has also been found encrusted on top of substrates (Lutze and Thiel, 1989; Koho et al., 2008) and in high abundances (50%) in a mesotrophic canyon environment (Koho et al., 2008), suggesting it has opportunistic characteristics and can turn to a filter feeding life mode. *Pullenia bulloides* has been associated with areas of elevated productivity (Mackensen et al., 1985; Mackensen et al., 1993). These species (Cluster 1; Figure 3 and 5) are generally present during the Tortonian and earliest Messinian in other Mediterranean sites (Seidenkrantz et al., 2000; Kouwenhoven et al., 2003; Kouwenhoven et al., 2006; Iaccarino et al., 2008; Di Stefano et al., 2010). Gradual increase of the Shannon diversity between 608.9-592 mbsf reflects the entry of several species in the benthic foraminiferal record (Figure 3; Supp. 1). The BFAR values vary around a mean of ~150 specimens/cm²/kyr and stay stable through the lowermost Messinian (Figure 4), suggesting a constant, moderate productivity. The benthic $\delta^{13}\text{C}$ values remain high with short term negative excursions (Figure 6) pointing to an efficiently ventilated water column. A sill efficiently connecting the Mediterranean and Atlantic permitted a significant inflow-outflow, and allowed the Bernoulli aspiration to maintain effective deep water flushing of the seafloor as confirmed by several modeling studies (Alhammoud et al., 2010; Topper and Meijer, 2015). However, the high amplitude oscillations in the benthic $\delta^{13}\text{C}$ records suggest that even if deep water renewal was overall effective and prevented sea - floor anoxia in the WMB (values similar as open Atlantic ones; section 7.3), there was a strong precessionally driven variability (around 1 ‰) suggesting weakened deep water formation during northern hemisphere summer insolation maxima. The $\delta^{13}\text{C}$ negative excursions could have been additionally reinforced by deep water admixture with a proto - LIW $\delta^{13}\text{C}$ carrying an EMB $\delta^{13}\text{C}$ signal (Section 5.4).

The change in the benthic assemblages after 7.17 Ma can be correlated with a similar shift in benthic foraminiferal assemblages occurring at other Mediterranean locations (Seidenkrantz et al., 2000; Kouwenhoven et al., 2003;

Kouwenhoven et al., 2006) during deposition of the sapropel astronomically dated by Hilgen et al. (1995) at 7.167 Ma (Section 5.4). The higher abundances of shallow infaunal taxa, tolerating a wide range of conditions and suboptimal oxygen levels (Koho et al., 2008; Kaminski et al., 2013; Cluster 2, Figure 5) suggests a decrease in bottom-water oxygen levels. According to the TROX model (Trophic-Oxygen: Jorissen et al., 1995), environmental factors predominantly determining species composition of benthic foraminifer assemblages are organic flux and oxygenation of the sea floor; where oxygen levels are more instrumental in establishing the presence or absence of species, whereas quantity and quality (fresh vs degraded) of organic flux structure the communities and determine the relative abundances (Van der Zwaan et al., 1999; Jorissen et al., 2007). This implies that a decrease in bottom-water oxygen and an increase or change of composition of organic flux occurred at the same time, leading to disappearance or decreasing abundances of sensitive species and increasing abundances of more tolerant species. In the WAB, deep infaunal taxa were not dominant at this stage (e.g. *Globobulimina*, *Chilostomella* spp., *B. aculeata*, *B. dilatata*; Jorissen et al., 2007 and references therein) and anoxic conditions were not reached. Assumptions regarding paleo productivity based on BFAR were not possible for this interval, because the BFAR values lose reliability under reduced oxygen levels (Naidu and Malmgren, 1995). However, a decrease in oxygen levels is also suggested by the rise in S/Ti values. As S can be bound to organic matter (e.g. Lückge et al., 2002), higher S contents in the sediments suggest a higher organic carbon content. Oxidation of organic matter consumes oxygen, therefore a S enrichment suggests an efficient organic matter preservation associated with lowered oxygen levels in the bottom waters (Harff et al., 2011). Further changes in the circulation can be deduced from the $\delta^{13}\text{C}$ record of benthic and planktic foraminifers. The sharp drop in the benthic $\delta^{13}\text{C}$ record from 0‰ to -1 ‰ (Figure 6) and the sharp increase in the $\Delta\delta^{13}\text{C}$ to an average value of -2.8 ‰ imply a prominent increase in residence time of bottom waters in the WAB (Laube-Lenfant and Pierre, 1994).

Coeval with the shift from oxygenated to hypoxic benthic environments, the drop in benthic $\delta^{13}\text{C}$ was recorded in other Mediterranean basins suggesting that the 7.17 Ma event had a significant impact on the Mediterranean thermohaline circulation (Section 5.4.2). A shallower strait would mean higher vertical density gradient below the sill depth resulting in a weaker Bernoulli aspiration, inhibiting deep water outflow to the Atlantic. Consequently, deep-water renewal could only be achieved if deep-water formation rates were high enough to result in advection into intermediate water masses. However, in the WAB deep-water formation was not intense enough to incorporate the deeper waters into the MOW, resulting in bottom water aging and oxygen depletion. Surface waters, on the contrary, were less affected (stable planktic $\delta^{13}\text{C}$; Figure

6) possibly because of the proximity of Site 976 to the Mediterranean-Atlantic gateways where the influence of surface-water inflow carrying the high Atlantic $\delta^{13}\text{C}$ signature was stronger. Likewise, while the planktic $\delta^{18}\text{O}$ trend is stable, the benthic $\delta^{18}\text{O}$ record shows an increasing upward trend suggesting progressively higher bottom water salinities.

5.3.2 Location of the late Tortonian-early Messinian Mediterranean-Atlantic gateway

The Mediterranean scale change in bottom water ventilation excludes the possibility that the WAB was a satellite basin of the Atlantic Ocean and confirms that it was part of the Mediterranean Basin contrary to what was proposed recently. Booth-Rea et al. (2018) suggested that the main gateway restricting the connection between the Mediterranean and the Atlantic during the MSC was located along a volcanic archipelago in the EAB extending southward from the Cabo de Gata region in Southern Spain to the African continent. According to the authors, the emersion of this archipelago would have isolated the WAB from the rest of the Mediterranean and acted as a barrier separating the WAB and the EAB making the WAB an open marine refuge connected with the Atlantic Ocean. This hypothesis was supported by the absence of obvious signs of restriction before 6.8 Ma in previously studied WMB sections like the lower Abad member in the Sorbas basin, where sapropels were only deposited after 6.8 Ma (Sierro et al., 2003). Our new evidence from ODP Site 976 shows that the 7.17 Ma gateway shoaling affected the WAB, confirming that the restriction occurred in the west rather than in the east of the WAB as suggested by Booth-Rea et al. (2018). Hence, we consider that the 7.17 Ma event was triggered by the restriction of the previously defined Gibraltar Arc gateways (see Introduction).

5.4 A Mediterranean scale change in thermohaline circulation: comparison between the Western and Eastern Mediterranean Basins

With the aim of reconstructing the Mediterranean deep and intermediate circulation before and after the 7.17 Ma gateway restriction event, the Site 976 record has been compared with geochemical, sedimentological and micropaleontological data collected in other Mediterranean sections (Figure 11 a) including intermediate (300-600 m depth) and deep-water signals (>800 m depth). The depth reconstructions based on foraminifer assemblages and %P values reported in literature (Ryan, 1976; Kouwenhoven et al., 1999; e.g. Baggley, 2000; Roger et al., 2000; Fortuin and Krijgsman, 2003; Kouwenhoven et al., 2003; Krijgsman et al., 2006; Hüsing et al., 2009; Di Stefano et al., 2010; Corbí et al., 2020), helped define the intermediate (Sorbas, Bajo Segura, Nijar, Murcia, Melilla, Pissouri Basins and Trave, Monte dei Corvi and Faneromeni sections)

and deep basins (Alboran Basin, Balearic promontory, Monte del Casino, Monte Gibliscemi and Metochia sections).

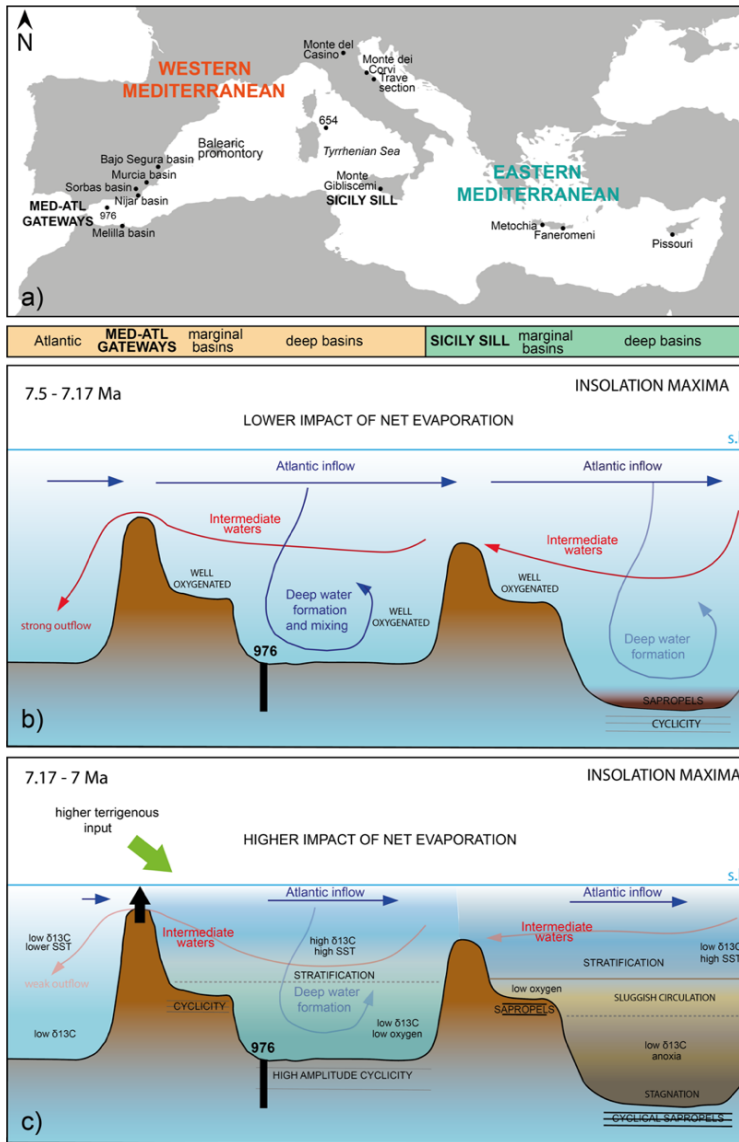


Figure 11: a) Generalized map of the Mediterranean Sea showing the basins, sections and ODP Sites mentioned in this section. Cartoon showing the Mediterranean thermohaline circulation: b) before (from present circulation studies like Pinardi and Masetti, 2000) and c) after the 7.17 Ma event. circulation patterns adapted from (Alhammoud et al., 2010) and (Topper and Meijer, 2015).

5.4.1 Mediterranean thermohaline circulation until 7.17 Ma

Based on the foraminiferal record, before 7.17 Ma the Western Mediterranean Basin (WMB) was an open marine environment with a well ventilated water column as no sapropels or organic rich layers have been recorded neither in the intermediate basins like Sorbas (Sierro et al., 2003), Nijar (Fortuin and Krijgsman, 2003), Murcia (Krijgsman et al., 2006), Bajo Segura (Corbí et al., 2020) nor in deeper basins such as the Balearic promontory (Ochoa et al., 2015), the Tyrrhenian Sea (Kastens et al., 1988; Glacon et al., 1990) and Alboran Basin. In contrast, sapropels were formed in the Eastern Mediterranean Basin (EMB) during the most prominent insolation maxima. Bottom water anoxia was recorded in deep water sections like Metochia in Greece (Seidenkrantz et al., 2000), the Italian Monte Gibliscemi (Sprovieri et al., 1996; Sprovieri et al., 1999; Blanc-Valleron et al., 2002; Kouwenhoven et al., 2003) and Monte del Casino sections (Krijgsman et al., 1997; Kouwenhoven et al., 2003), and marginal locations like Italian Monte dei Corvi (Hüsing et al., 2009) section. Comparison of the benthic $\delta^{13}\text{C}$ from Site 976 (this study) with the Metochia section in the EMB and the Atlantic $\delta^{13}\text{C}$ records (Figure 12), shows that both the EMB and WMB were well ventilated at times of insolation minima, showing high $\delta^{13}\text{C}$ values comparable to those recorded at the Atlantic side of the Rifian corridor (e.g. Sale Briqueterie). Still, at times of insolation maxima, a weaker deep water Mediterranean thermohaline circulation probably occurred in both basins. During these times a strong benthic $\delta^{13}\text{C}$ depletion was recorded in the WAB (Figure 12), where values well below the Atlantic ones were found indicating that deep Mediterranean waters immediately to the east of the late Miocene Straits (Betic and Rifian corridors, proto-Gibraltar strait?) were considerably older than the coeval Atlantic water mass. Nonetheless, probably because this area benefited of a local deep - water source like the Gulf of Lions, bottom water anoxia was prevented and lower $\delta^{13}\text{C}$ values could reflect the LIW signal from the east. However, these events of anoxia were not registered in the benthic $\delta^{13}\text{C}$ record (see the Metochia record in Figure 12) because isotope analyses were only carried out in the non - sapropelic samples. Even though the Mediterranean-Atlantic connection was wide open, the presence of sapropels in the EMB suggests a less efficient deep/intermediate water circulation than in the WMB. This discrepancy can be explained by the weaker Bernoulli aspiration at the Sicily sill (Rohling et al., 2015) that would block the incorporation of part of the deep water in the outflow to the WMB, preventing an efficient ventilation of the bottom (Figure 11 b).

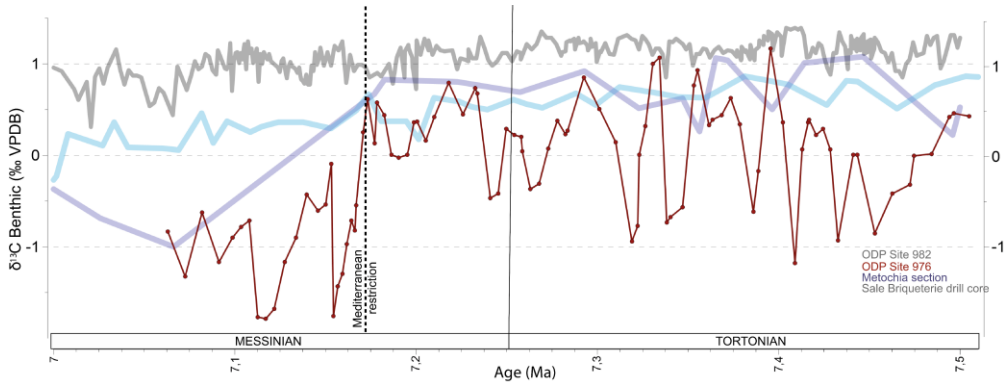


Figure 12: Comparison between benthic $\delta^{13}\text{C}$ records of Site 976 in red (this study), Atlantic Ocean ODP Site 982 (Drury et al., 2018) in grey, Metochia section (Seidenkrantz et al., 2000) in purple, and Atlantic drill site Sale Briqueterie (Hodell et al., 1994) in light blue. In order to compare the absolute values of the curves, the isotope records that were measured on different benthic foraminifer species than Site 976 were corrected according to their offset with respect to *C. kullenbergi* reported in literature. Metochia and Sale Briqueterie records were obtained from *P. ariminensis*. The correction of the offset with respect to *C. kullenbergi* was obtained using the correction factors from Van der Laan et al. (2006), where isotope analyses performed on samples from the Loulja section (Morocco) both on *C. pachyderma* and *P. ariminensis* showed an interspecific offset of 0.627‰ for $\delta^{13}\text{C}$ measurements. The isotopic record of Site 982 ODP, measured on *C. wuellerstorfi* or *C. mundulus* did not need any correction because no offset has been found between the two species (Hodell et al., 2001; Holbourn et al., 2007; Holbourn et al., 2018). The continuous black line highlights the Tortonian - Messinian boundary while the dashed one the 7.17 Ma restriction event.

5.4.2 Mediterranean thermohaline circulation after 7.17 Ma

With a shallowing of 120 m at the Strait of Gibraltar (Myers et al., 1998; Rohling et al., 2015) assumed for the last glacial maximum, salinities above 40 psu have been modelled for the Mediterranean. Similarly at 7.17 Ma, the reduced water exchange with the Atlantic led not only to a longer bottom water residence time but possibly to higher bottom water salinities (e.g. Meijer, 2006). With a shallower strait, the Bernoulli aspiration depth would reduce, producing progressively saltier and higher density deep waters increasing the density contrast between what was left of the Atlantic inflow and Mediterranean deep - water masses, favouring water - mass stratification (as shown by models, e.g. Meijer, 2006), a less efficient deep water circulation and consequently increased bottom water residence time (e.g. Sierro et al., 2003). Under this regime and at smaller time scales, precession forced cyclical changes in the hydrological budget would, during periods of enhanced freshwater discharge, further enhance stratification leaving a stronger impact on the Mediterranean circulation (Simon et al., 2017).

At Site 976, deterioration of the deep circulation at 7.17 Ma is visible from the sharp drop in benthic $\delta^{13}\text{C}$ and the shift towards more hypoxic benthic foraminifer associations, while water column stratification is indicated by the first appearance of the warm water planktonic foraminifer genus *Globigerinoides* (Bulian et al., 2021) and by the sharp $\Delta\delta^{13}\text{C}$ gradient. From 7.17 Ma onward, similar changes have been recorded at several WMB shallow marginal basins. In the Bajo Segura (Corbí et al., 2020) and Murcia (Krijgsman et al., 2006) basins an increase of benthic stress taxa has been reported, suggesting a moderate reduction in deep – water ventilation while the beginning of cyclical deposition of diatomite rich layers in the Nijar (Fortuin and Krijgsman, 2003) and Sorbas (Sierro et al., 2003) basins suggest higher sensitivity towards precessionally induced climate variability (Figure 11 c). Yet, the deep WMB water never reached anoxia as sapropels do not occur in the marginal basins until the second restriction step at 6.8-6.7 Ma, when the first sapropels are identified at the base of the Upper Abad member (Sierro et al., 2001; Sierro et al., 2003) in the Sorbas and Nijar basins. The WAB surface waters, in addition, were not affected by the restriction (e.g. Sorbas Basin-Sierro et al., 2003 and this study), suggesting the presence of an Atlantic inflow with the typical high planktic $\delta^{13}\text{C}$ of the open ocean. One exception in the WMB is the Tyrrhenian basin as the sedimentological record of ODP Site 654 shows, starting around 7.2 Ma, deposition of dolomitic dark shales characterized by extremely rare or absent foraminifers (Glacon et al., 1990) suggesting the installation of an anoxic bottom environment. However, Roveri et al. (2014b) and Borsetti et al. (1990) suggest that these sediments are actually much younger and that hiatus explains this anomaly. In the EMB on the other hand, oxygen depleted conditions are visible from the onset of euxinic shale and sapropel deposition in the marginal Monte dei Corvi (Hüsing et al., 2009) and Faneromeni sections (Santarelli et al., 1998), together with more frequent sapropels in deep locations like Metochia and Monte del Casino sections (Kouwenhoven et al., 1999; Seidenkrantz et al., 2000). In the EMB, the abrupt $\delta^{13}\text{C}$ decrease in benthic (Figure 12) and planktic records (e.g. Metochia section: Seidenkrantz et al., 2000; Monte Gibliscemi: Sprovieri et al., 1996; Monte del Casino: Kouwenhoven et al., 2003 and Faneromeni section: Kontakiotis et al., 2019) suggest that significant increase in residence time affected both deep and intermediate water cells. At the same time, a trend towards heavier values of both planktic and benthic $\delta^{18}\text{O}$ curves from Metochia and Monte del Casino sections possibly indicate higher bottom water salinities (Kouwenhoven et al., 2003). Planktic species indicating stressful conditions (*Turborotalita quinqueloba*, *Globigerinita glutinata*, *Globigerinella obesa*, *Orbulina universa*) (Seidenkrantz et al., 2000; Kouwenhoven et al., 2006; Di Stefano et al., 2010) together with benthic species implying limited oxygen levels and increased salinities become more abundant in the marginal basins, while deep basins show low diversity benthic foraminifer assemblages, often dominated by

bolivinids (e.g. Seidenkrantz et al., 2000). The proliferation of this benthic species can be attributed to increased salinities and reduced oxygen levels, changes conformable with a gateway restriction scenario.

From 7.17 Ma onward, the restriction of the Mediterranean-Atlantic gateway/s and reduction of water exchange between the two basins, paired with the negative Mediterranean freshwater budget resulted in a change in the thermohaline circulation that impacted to different extents the WAB and EMB. Higher density contrast between WMB deep - water masses and inflowing Atlantic surface waters resulted in increasing vertical density gradients leading to water column stratification. Here, close to the gateway, surface waters were able to preserve the Atlantic isotopic signal while deep waters show clear signs of aging and decreasing oxygen levels. These effects are linked with aspiration depth reduction (i.e., Bernoulli aspiration) at the Gibraltar gateway/s which limited water outflow and with less deep - water formation in the Gulf of Lions related to presence of dense Levantine intermediate water from the East, which could not mix with the much fresher Atlantic water given the too high density contrast. More pronounced effects have been recorded in the EMB. It is likely that the presence of the Sicily sill with even lower aspiration depth hindered, for the larger part, the escape of deep waters from the EMB towards the WMB, resulting in aged, anoxic, and stagnant bottom waters with sapropel deposition during insolation maxima. Longer water residence time has been registered in EMB surface waters as well. Here, far from the Atlantic Ocean, surface waters could reflect the deep-water signal. In particular, the different configuration of the WMB and EMB and consequent non identical reaction to circulation changes have been noticed also in the Plio-Quaternary Mediterranean records, where during insolation maxima sapropels form only in the EMB, while in the WMB bottom waters never reach anoxia but only enrichment in organic matter that allows the development of ORLs (e.g. Murat, 1999; Rogerson et al., 2008). This suggests that from 7.17 Ma onward, the configuration of the Mediterranean Basin was very similar to the recent one. Nonetheless, to better understand the Mediterranean-Atlantic connectivity and circulation prior to this event late Miocene continuous records from other deep WMB are needed.

5.5 Correlation of the Mediterranean restriction and LMCIS

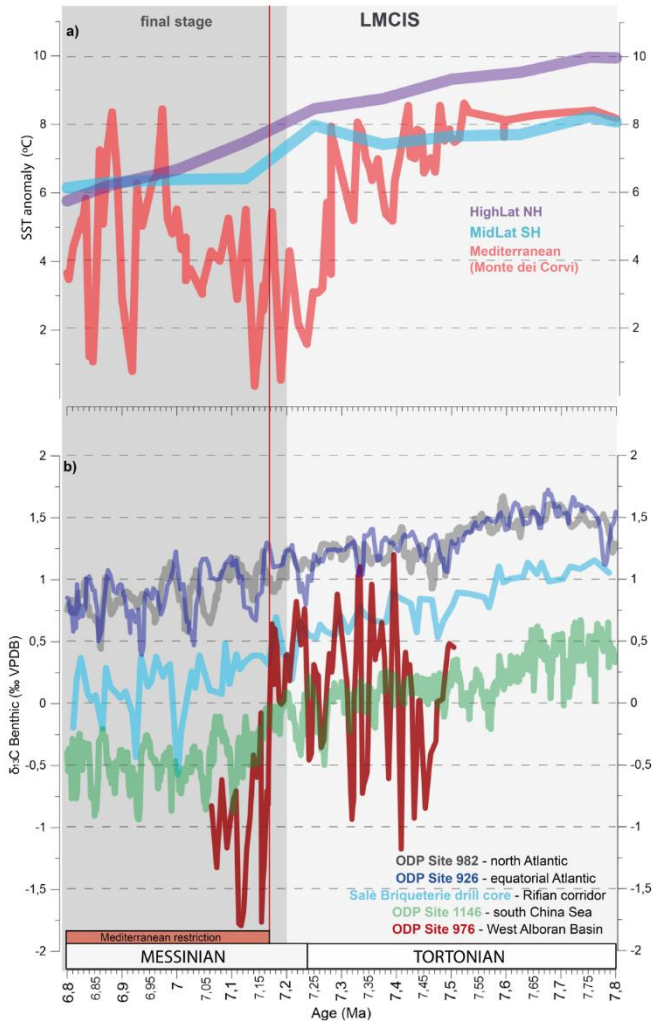


Figure 13. a) Sea surface temperatures (SST) for Northern Hemisphere high-latitudes, Southern Hemisphere mid-latitudes (Herbert et al., 2016) and Mediterranean Sea (Monte dei Corvi section, Italy; Tzanova et al., 2015); b) Comparison between benthic $\delta^{13}\text{C}$ records of ODP Site 976 in red (this study), Atlantic ODP Site 982 in grey (Drury et al., 2018), Equatorial Atlantic ODP Site 926 in dark blue (Drury et al., 2017), Salé Briqueterie drill core - Rifian corridor in light blue (Hodell et al., 1994), and South China Sea ODP 1146 Site in green (Holbourn et al., 2018; Holbourn et al., 2021). In order to compare the absolute values of the curves, the isotope records that were measured on other benthic foraminifera species than for Site 976 were corrected according to their offset with respect to *C. kullenbergi* reported in literature. The Salé Briqueterie record was obtained from *P. ariminensis* and to correct its offset the correction factors were taken from Van der Laan et al. (2006, Loulja section, Morocco), where $\delta^{13}\text{C}$ analyses performed both on *C. pachyderma* (should yield equivalent values as *C. kullenbergi*; Riveiros et al., 2010) and *P. ariminensis* showed an interspecific offset of 0.627‰. When the isotopic record was obtained measuring *C. wuellerstorfi* or *C. mundulus* (ODP sites 982, 1146 and 926) no correction has been applied because no offset has been found between the three species (Hodell et al., 2001; Holbourn et al., 2007; Holbourn et al., 2018). Light grey shading marks the LMCIS while the dark grey shading its final stages.

During the Late Miocene cooling (7.5 – 5.5 Ma) a global decrease in sea surface temperatures (SST) of about 6°C (compared to the mean present day SST) has been reconstructed (Herbert et al., 2016) contemporaneously with a global decrease in $\delta^{13}\text{C}$ oceanic values (Figure 13 a and b) related with the LMCIS (7.8 – 6.7 Ma; Hodell et al., 1994; Hodell et al., 2001; Hodell and Venz- Curtis, 2006). During this period of time of 1.1 Ma, the amplitude of the $\delta^{13}\text{C}$ decrease reached 0.75 ‰ in the Atlantic and 1‰ in the Pacific ocean which is visible for example in Atlantic ODP sites 982 (Hodell et al., 2001; Drury et al., 2018), 926 (Drury et al., 2017), the Salé Briqueterie core (Hodell et al., 1994) and China Sea ODP Site 1146 (Holbourn et al., 2018; Holbourn et al., 2021). In this work we will focus only on the final stage of the LMCIS (7.2 Ma – 6.8 Ma) part of which is recorded at Site 976 (Figure 13 b). Over the final 0.4 Ma of the LMCIS, in the Atlantic sites the $\delta^{13}\text{C}$ dropped with 0.30-0.35 ‰, while in the South China Sea a more pronounced drop of ~0.75 ‰, (Holbourn et al., 2018) has been registered. At Site 976, the amplitude of the $\delta^{13}\text{C}$ drop (~1 ‰), which occurred at exactly 7.17 Ma coinciding with the major restriction event, is even higher (Figure 13 b) and is clearly more abrupt when compared with the more gradual change observed in the open Ocean. However, at Site 1146, the most significant decrease in benthic $\delta^{13}\text{C}$ the LMCIS occurred between 7.2 and 7 Ma (Holbourn et al., 2018) making it almost coeval with the 7.17 Ma event (Figure 13 b). A detailed comparison between the two benthic $\delta^{13}\text{C}$ records, however, reveals different responses of the two systems (Figure 14). The benthic $\delta^{13}\text{C}$ from ODP Site 1146 follows a global pattern of lower benthic $\delta^{13}\text{C}$ at glacial periods with larger ice volume (higher benthic $\delta^{18}\text{O}$) during obliquity minima probably due to a greater CO_2 storage in the deep ocean (Holbourn et al., 2018). By contrast, the Mediterranean benthic $\delta^{13}\text{C}$ cyclicity is controlled by northern hemisphere summer insolation and lower benthic $\delta^{13}\text{C}$ values are recorded during insolation maxima. This implies that, while open ocean stable isotope signals are dominated by obliquity, the Mediterranean Sea record is modulated by precession. According to our age model (Figure 10), the two pronounced drops in $\delta^{13}\text{C}$ recorded at Site 976 after 7.17 Ma (590.5 and 587 mbsf) show higher amplitudes because they occurred during a period of interference between obliquity and precession (when the two curves are in phase), when changes in freshwater budget are amplified. The latter can be correlated to the first and second prominent sapropels (Figure 14: black layers at 34.5 and 37 m) in the Faneromeni section in the EMB (cycles F18-F22; Krijgsman et al., 1994; Hilgen et al., 1995; Santarelli et al., 1998), while smaller changes in the $\delta^{13}\text{C}$ record are linked to low amplitude peaks in summer insolation during obliquity minima resulting in the deposition of gray marls instead of sapropels (35.5 and 38 m; Santarelli et al., 1998). In a highly restricted basin with elevated bottom – water salinities like the Mediterranean, the increase in precipitation that characterizes summer insolation maxima would result in high amounts of low-density freshwaters, promoting strong water stratification.

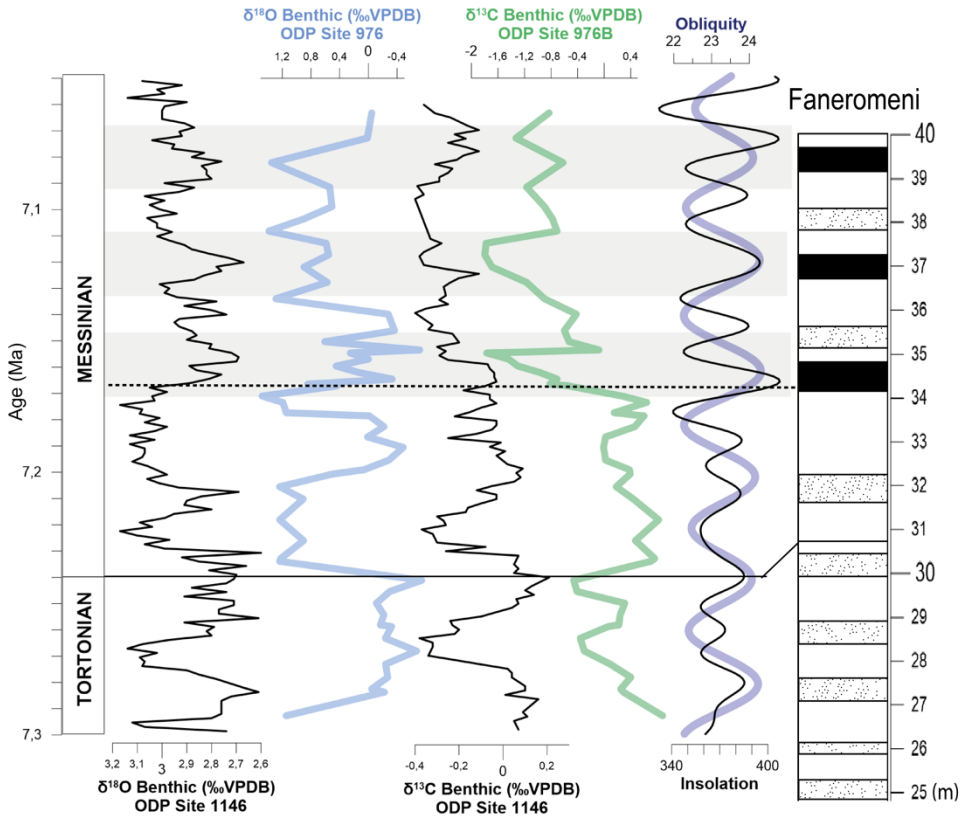


Figure 14: The benthic $\delta^{18}\text{O}$ and $\delta^{13}\text{C}$ curves from China Sea ODP 1146 Site (Holbourn et al., 2018; Holbourn et al., 2021) and WAB ODP 976 Site are shown followed by the obliquity curve by Laskar et al. (2004). The grey shadings highlight obliquity maxima phases and correlate them with sapropel deposition in Faneromeni section (Krijgsman et al., 1994; Hilgen et al., 1995; Santarelli et al., 1998). The continuous black line highlights the Tortonian – Messinian boundary while the dashed one the 7.17 Ma restriction event.

Under these circumstances deep – water formation would not be possible and therefore deep – water renewal would be blocked resulting in an increased residence time of deep water with subsequent lowering of the $\delta^{13}\text{C}$. The lower CO_2 levels (Zhang et al., 2013; Tanner et al., 2020) that characterize the LMCIS have also been linked to a global increase in ice volume (Drury et al., 2016; Herbert et al., 2016). In a context of tectonic uplift that progressively reduced the section of the Mediterranean – Atlantic straits, a sea level drop associated with ice volume expansion during the LMCIS could have further reduced the water exchange with the Atlantic and amplified the drop in benthic $\delta^{13}\text{C}$. This could explain why the South China Sea continued to reflect a global signal while the stronger isolation of the Mediterranean from the Global Ocean made it more sensitive to local hydrological budget changes.

The global cooling during the LMCIS (Herbert et al., 2016) seems to be recorded in the Mediterranean Monte dei Corvi section where the SST underwent a sudden drop (Figure 13 a) of $\sim 6^{\circ}\text{C}$ dated at 7.25 Ma (Tzanova et al., 2015). Apart from an overall SST decrease, SST values are lower at times of vertical mixing during insolation minima and higher at times of strong stratification of the water column during sapropel formation (Tzanova et al. 2015). The lowest temperatures in Monte del Corvi occur during an interval in the earliest Messinian without sapropel formation (Tzanova et al., 2015) suggesting vertical mixing was permanent during this time. Cooling in northern Europe and the influence of northern winter winds, similar to the Bora winds today (Boldrin et al., 2009 and references therein), may have lowered the SST and favoured mixing of the water column during this period. Winter mixing would have increased nutrient content at the surface stimulating phytoplankton productivity and alkenone production. Contrary to the Adriatic, the WAB registers vertical mixing before 7.17 Ma and more stratification after this event probably due to the southern position of the Alboran Basin, far from the influence of the northern cool winds. Indeed, today the southern margin of the Mediterranean is more prone to water stratification favouring the growth of warmer-water planktonic foraminifer species (Azibeiro et al., in prep) where the stratification is only broken in the northern coast of the Alboran Sea due to the upwelling cells associated with the anticyclonic gyres. This explains the continuous dominance of cold-water species before 7.17 Ma in the Alboran Basin when a more intense exchange resulted in higher upwelling intensities. The lower Atlantic Mediterranean exchange after 7.17 Ma reduced the upward advection of cold water, favouring stratification that reduced the proportion of cold - water species and increased the warm oligotrophic, especially at times of insolation maxima. This argues in favour of water stratification and the subsequent surface warming as the main cause of the higher proportion of warm water species in the WAB, implying that the restriction of the Mediterranean-Atlantic gateways was the main force influencing Mediterranean circulation after 7.17 Ma, while the cooling visible in Monte dei Corvi section can be a localized event.

6. Conclusions

The integrated upper Tortonian-lower Messinian micropaleontological and geochemical data of ODP Site 976 in the West Alboran Basin (WAB) presented in this study improved the age control based on cyclostratigraphy. Using as tie points planktic foraminifer bio events in combination with new stable isotope and elemental records allowed the creation of a new improved age model. This enabled a more detailed correlation with other Mediterranean records and

confirmed that the gateway restriction starting from 7.17 Ma changed the WAB marine environments at the same time it affected different locations all over the basin, suggesting a Mediterranean-scale change in thermohaline circulation. From these data follows that the WAB and EAB were not separated by a sill, which would render the WAB a satellite basin of the Atlantic, but that the WAB was part of the Mediterranean realm.

Until 7.17 Ma, the WAB represented a deep-water well-ventilated environment, indicating efficient water exchange through the Gibraltar gateway/s. Starting from 7.17 Ma, the intense uplift of the Gibraltar Arc caused the progressive closure of the Betic and Rifian corridors and a diminished connection with the Global Ocean. This paleogeographic reorganization impacted the deeper part of the WAB as reflected by the benthic foraminiferal fauna, which became dominated by shallow infaunal taxa, tolerant to a wide range of conditions and suboptimal oxygen levels. These observations, paired with a significant drop in benthic $\delta^{13}\text{C}$ values suggests that the progressive Mediterranean-Atlantic gateway restriction led to the decrease in bottom water oxygen levels and increase in its residence time.

The correlation between Site 976 and previously published data, enabled to refine models of the Mediterranean circulation before and after 7.17 Ma. The restriction of the gateways resulted in stratification of the WMB water column and showed that while the bottom waters were depleted in oxygen, the intermediate waters were better ventilated. This evaluation also confirmed that, because of the presence of the Sicily sill, the impact of stratification was much higher in the EMB where it led to sapropel deposition, absent in the WMB.

The paleoenvironmental change at 7.17 Ma coincided with the LMCIS (7.6 to 6.8/7 Ma), a global event characterised by cooling and a shift to lighter $\delta^{13}\text{C}$. In particular, the correlation of the isotope data of Site 976 with those of ODP Site 1146 in the South China Sea showed that both basins register a larger and more instantaneous $\delta^{13}\text{C}$ shift. However, the phase relations of the isotope record with astronomical parameters (precession, obliquity) are different. Site 1146 reflects global phase relations connected to glacial stages, whereas the phase relations in the WAB depend on hydrological budget changes suggesting a much stronger local effect in the Mediterranean. Considering that the LMCIS has been related to ice volume expansion, the gateway restriction effects on the Mediterranean could have been further amplified by a relative sea level drop.

Acknowledgments

The authors appreciate the work of Jose Ignacio Martin Cruz in sample processing and preparation. Furthermore, all fellow ESRs and supervisors from the SALTGIANT project are thanked for their valuable suggestions and discussions. Two anonymous reviewers are gratefully acknowledged for critical reading and detailed comments which were very helpful to improve the original manuscript. This research used data and samples collected through ODP Expedition 161 aboard the Joides Resolution. Geochemical data was acquired at the XRF Core Scanner Lab at the MARUM – Center for Marine Environmental Sciences, University of Bremen, Germany. This research has received funding from the European Union’s Horizon 2020 research and innovation program under the Marie Skłodowska-Curie grant agreement n° 765256 SALTGIANT.

Data statement

All data used in this study are available in the public repository Mendeley Data as: Bulian, Francesca; Sierro, Francisco J.; Kouwenhoven, Tanja J.; Andersen, Nils (2021), “Geochemical and micro-paleontological analyses from ODP Site 976B (Leg 161) in the West Alboran Basin”, Mendeley Data, V3, doi: <https://data.mendeley.com/datasets/ggpmmxr8k3/3>

References

- Achalhi, M., Münch, P., Cornée, J.-J., Azdimousa, A., Melinte-Dobrinescu, M., Quillévéré, F., Drinia, H., Fauquette, S., Jiménez-Moreno, G., Merzeraud, G., Moussa, A. B., El Kharim, Y. and Feddi, N., 2016. The late Miocene Mediterranean-Atlantic connections through the North Rifian Corridor: New insights from the Boudinar and Arbaa Taourirt basins (northeastern Rif, Morocco). *Palaeogeography, Palaeoclimatology, Palaeoecology*, 459: 131-152.
- Alhammoud, B., Meijer, P. T. and Dijkstra, H. A., 2010. Sensitivity of Mediterranean thermohaline circulation to gateway depth: A model investigation. *Paleoceanography*, 25(2).
- Baggley, K. A., 2000. The Late Tortonian- Early Messinian Foraminiferal Record Of The Abad Member (Turre Formation), Sorbas Basin, Almería, South- East Spain. *Palaeontology*, 43(6): 1069-1112.
- Bahr, A., Lamy, F., Arz, H., Kuhlmann, H. and Wefer, G., 2005. Late glacial to Holocene climate and sedimentation history in the NW Black Sea. *Marine Geology*, 214(4): 309-322.

- Bandy, O. L. and Chierici, M. A., 1966. Depth-temperature evaluation of selected California and Mediterranean bathyal foraminifera. *Marine Geology*, 4(4): 259-271.
- Barra, D., Bonaduce, G. and Sgarrella, E., 1998. Paleoenvironmental bottom water conditions in the early Zanclean of the Capo Rossello area (Agrigento, Sicily). *BOLLETTINO-SOCIETA PALEONTOLOGICA ITALIANA*, 37: 61-88.
- Bianchi, D., Zavatarelli, M., Pinardi, N., Capozzi, R., Capotondi, L., Corselli, C. and Masina, S., 2006. Simulations of ecosystem response during the sapropel S1 deposition event. *Palaeogeography, Palaeoclimatology, Palaeoecology*, 235(1-3): 265-287.
- Blanc-Valleron, M.-M., Pierre, C., Caulet, J., Caruso, A., Rouchy, J.-M., Cespuglio, G., Sprovieri, R., Pestrea, S. and Di Stefano, E., 2002. Sedimentary, stable isotope and micropaleontological records of paleoceanographic change in the Messinian Tripoli Formation (Sicily, Italy). *Palaeogeography, Palaeoclimatology, Palaeoecology*, 185(3-4): 255-286.
- Blondel, C., Merceron, G., Andossa, L., Taisso, M. H., Vignaud, P. and Brunet, M., 2010. Dental mesowear analysis of the late Miocene Bovidae from Toros-Menalla (Chad) and early hominid habitats in Central Africa. *Palaeogeography, Palaeoclimatology, Palaeoecology*, 292(1-2): 184-191.
- Boldrin, A., Carniel, S., Giani, M., Marini, M., Aubry, F. B., Campanelli, A., Grilli, F. and Russo, A., 2009. Effects of bora wind on physical and biogeochemical properties of stratified waters in the northern Adriatic. *Journal of Geophysical Research: Oceans*, 114(C8).
- Booth-Rea, G., Ranero, C. R. and Grevemeyer, I., 2018. The Alboran volcanic-arc modulated the Messinian faunal exchange and salinity crisis. *Scientific reports*, 8(1): 13015.
- Bornmalm, L., 1997. Taxonomy and paleoecology of late Neogene benthic foraminifera from the Caribbean Sea and eastern equatorial Pacific Ocean. *Fossils and Strata* No. 41 pp. 1-96.
- Borsetti, A., Curzi, P., Landuzzi, V., Mutti, M., Lucchi, F. R., Sartori, R., Tomadin, L. and Zuffa, G., 1990. Messinian and pre-Messinian sediments from ODP Leg 107 sites 652 and 654 in the Tyrrhenian Sea: sedimentologic and petrographic study and possible comparisons with Italian sequences. *Proceedings of the ODP, Scientific Results*, 107: 169-186.
- Bosmans, J., Drijfhout, S., Tuenter, E., Hilgen, F., Lourens, L. J. and Rohling, E., 2015. Precession and obliquity forcing of the freshwater budget over the Mediterranean. *Quaternary Science Reviews*, 123: 16-30.
- Bulian, F., Sierro, F. J., Ledesma, S., Jiménez-Espejo, F. J. and Bassetti, M.-A., 2021. Messinian West Alboran Sea record in the proximity of Gibraltar: Early signs of Atlantic-Mediterranean gateway restriction. *Marine Geology*: 106430.

- Buongiorno Nardelli, B. and Salusti, E., 2000. On dense water formation criteria and their application to the Mediterranean Sea. *Deep Sea Research Part I: Oceanographic Research Papers*, 47(2): 193-221.
- Calvert, S. and Pedersen, T., 2007. Chapter fourteen elemental proxies for palaeoclimatic and palaeoceanographic variability in marine sediments: interpretation and application. *Developments in Marine Geology*, 1: 567-644.
- Capella, W., Barhoun, N., Flecker, R., Hilgen, F., Kouwenhoven, T., Matenco, L., Sierro, F. J., Tulbure, M., Yousfi, M. Z. and Krijgsman, W., 2018. Palaeogeographic evolution of the late Miocene Rifian Corridor (Morocco): reconstructions from surface and subsurface data. *Earth-Science Reviews*, 180: 37-59.
- Capella, W., Spakman, W., van Hinsbergen, D. J., Chertova, M. V. and Krijgsman, W., 2020. Mantle resistance against Gibraltar slab dragging as a key cause of the Messinian Salinity Crisis. *Terra Nova*, 32(2): 141-150.
- Comas, M. C., Zahn, R., Klaus, A. and al., e., 1996. ODP, Init. Repts., 161: College Station, TX (Ocean Drilling Program).
- Corbí, H., Lancis, C., García-García, F., Pina, J.-A., Soria, J. M., Tent-Manclús, J. E. and Viseras, C., 2012. Updating the marine biostratigraphy of the Granada Basin (central Betic Cordillera). Insight for the Late Miocene palaeogeographic evolution of the Atlantic-Mediterranean seaway. *Geobios*, 45(3): 249-263.
- Corbí, H., Soria, J. M., Giannetti, A. and Yébenes, A., 2020. The step-by-step restriction of the Mediterranean (start, amplification, and consolidation phases) preceding the Messinian Salinity Crisis (climax phase) in the Bajo Segura basin. *Geo-Marine Letters*, 40(3): 1-21.
- Corliss, B. H. and Chen, C., 1988. Morphotype patterns of Norwegian Sea deep-sea benthic foraminifera and ecological implications. *Geology*, 16(8): 716-719.
- Corliss, B. H., 1991. Morphology and microhabitat preferences of benthic foraminifera from the northwest Atlantic Ocean. *Marine Micropaleontology*, 17(3-4): 195-236.
- De Visser, J., Ebbing, J., Gudjonsson, L., Hilgen, F., Jorissen, F., Verhallen, P. and Zevenboom, D., 1989. The origin of rhythmic bedding in the Pliocene Trubi Formation of Sicily, southern Italy. *Palaeogeography, Palaeoclimatology, Palaeoecology*, 69: 45-66.
- Denne, R. A. and Sen Gupta, B. K., 1991. Association of bathyal foraminifera with water masses in the northwestern Gulf of Mexico. *Marine Micropaleontology*, 17(3-4): 173-193.
- Di Stefano, A., Verducci, M., Lirer, F., Ferraro, L., Iaccarino, S. M., Hüsing, S. K. and Hilgen, F. J., 2010. Palaeoenvironmental conditions preceding the Messinian Salinity Crisis in the Central Mediterranean: integrated data from the Upper Miocene Trave section (Italy). *Palaeogeography, Palaeoclimatology, Palaeoecology*, 297(1): 37-53.

- Drury, A. J., John, C. M. and Shevenell, A. E., 2016. Evaluating climatic response to external radiative forcing during the late Miocene to early Pliocene: New perspectives from eastern equatorial Pacific (IODP U1338) and North Atlantic (ODP 982) locations. *Paleoceanography*, 31(1): 167-184.
- Drury, A. J., Westerhold, T., Frederichs, T., Tian, J., Wilkens, R., Channell, J. E., Evans, H., John, C. M., Lyle, M. and Röhl, U., 2017. Late Miocene climate and time scale reconciliation: Accurate orbital calibration from a deep-sea perspective. *Earth and Planetary Science Letters*, 475: 254-266.
- Drury, A. J., Westerhold, T., Hodell, D. and Röhl, U., 2018. Reinforcing the North Atlantic backbone: revision and extension of the composite splice at ODP Site 982. *Climate of the Past*, 14(3): 321-338.
- Edwards, E. J., Osborne, C. P., Strömberg, C. A., Smith, S. A. and Consortium, C. G., 2010. The origins of C4 grasslands: integrating evolutionary and ecosystem science. *Science*, 328(5978): 587-591.
- Emeis, K. and Weissert, H., 2009. Tethyan-Mediterranean organic carbon-rich sediments from Mesozoic black shales to sapropels. *Sedimentology*, 56(1): 247-266.
- Fentimen, R., Lim, A., Rüggeberg, A., Wheeler, A. J., Van Rooij, D. and Foubert, A., 2020. Impact of bottom water currents on benthic foraminiferal assemblages in a cold-water coral environment: The Moira Mounds (NE Atlantic). *Marine Micropaleontology*, 154: 101799.
- Flecker, R., Krijgsman, W., Capella, W., De Castro Martins, C., Dmitrieva, E., Mayser, J. P., Marzocchi, A., Modestou, S., Ochoa, D., Simon, D., Tulbure, M., Van Den Berg, B., Van Der Schee, M., De Lange, G., Ellam, R., Govers, R., Gutjahr, M., Hilgen, F., Kouwenhoven, T., Lofi, J., Meijer, P., Sierro, F. J., Bachiri, N., Barhoun, N., Alami, A. C., Chacon, B., Flores, J. A., Gregory, J., Howard, J., Lunt, D., Ochoa, M., Pancost, R., Vincent, S. and Yousfi, M. Z., 2015. Evolution of the Late Miocene Mediterranean-Atlantic gateways and their impact on regional and global environmental change. *Earth-Science Reviews*, 150: 365-392.
- Fortuin, A. R. and Krijgsman, W., 2003. The Messinian of the Nijar Basin (SE Spain): Sedimentation, depositional environments and paleogeographic evolution. *Sedimentary Geology*, 160(1-3): 213-242.
- Frigola, J., Moreno, A., Cacho, I., Canals, M., Sierro, F., Flores, J. and Grimalt, J., 2008. Evidence of abrupt changes in Western Mediterranean Deep Water circulation during the last 50 kyr: A high-resolution marine record from the Balearic Sea. *Quaternary International*, 181(1): 88-104.
- Garcia-Castellanos, D. and Villaseñor, A., 2011. Messinian salinity crisis regulated by competing tectonics and erosion at the Gibraltar arc. *Nature*, 480(7377): 359.
- Gebhardt, H., 1999. Middle to Upper Miocene benthonic foraminiferal palaeoecology of the Tap Marls (Alicante Province, SE Spain) and its palaeoceanographic implications. *Palaeogeography, Palaeoclimatology, Palaeoecology*, 145(1-3): 141-156.

- Gibson, T. G., 1989. Planktonic benthonic foraminiferal ratios: modern patterns and Tertiary applicability. *Marine Micropaleontology*, 15(1-2): 29-52.
- Glacon, G., Grazzini, C. V., Iaccarino, S., Rehault, J.-P., Randrianasolo, A., Sierro, J. F., Weaver, P., Channell, J., Torii, M. and Hawthorne, T., 1990. Planktonic foraminiferal events and stable isotope records in the upper Miocene, Site 654. In Kastens, K. A., Mascle, J., et al., Proc. ODP, Sci. Results, 107: College Station, TX (Ocean Drilling Program), 415–427. doi:10.2973/odp.proc.sr.107.157.1990.
- Gooday, A. J., 2003. Benthic foraminifera (Protista) as tools in deep-water palaeoceanography: environmental influences on faunal characteristics. *Advances in Marine Biology*, 46: 1-90.
- Guerra-Merchán, A., Serrano, F., Garcés, M., Gofas, S., Esu, D., Gliozzi, E. and Grossi, F., 2010. Messinian Lago-Mare deposits near the strait of Gibraltar (Malaga basin, S Spain). *Palaeogeography, Palaeoclimatology, Palaeoecology*, 285(3-4): 264-276.
- Hammer, Ø., Harper, D. A. and Ryan, P. D., 2001. PAST: Paleontological statistics software package for education and data analysis. *Palaeontologia Electronica*, 4(1): 9.
- Harff, J., Endler, R., Emelyanov, E., Kotov, S., Leipe, T., Moros, M., Olea, R., Tomczak, M. and Witkowski, A., 2011. Late Quaternary climate variations reflected in Baltic Sea sediments., *The Baltic Sea Basin*. Springer, Berlin, Heidelberg., pp. 99-132.
- Hennekam, R., Jilbert, T., Schnetger, B. and de Lange, G. J., 2014. Solar forcing of Nile discharge and sapropel S1 formation in the early to middle Holocene eastern Mediterranean. *Paleoceanography*, 29(5): 343-356.
- Herbert, T. D., Lawrence, K. T., Tzanova, A., Peterson, L. C., Caballero-Gill, R. and Kelly, C. S., 2016. Late Miocene global cooling and the rise of modern ecosystems. *Nature Geoscience*, 9(11): 843-847.
- Herguera, J., 2000. Last glacial paleoproductivity patterns in the eastern equatorial Pacific: benthic foraminifera records. *Marine Micropaleontology*, 40(3): 259-275.
- Herguera, J. C., 1992. Deep-sea benthic foraminifera and biogenic opal: glacial to postglacial productivity changes in the western equatorial Pacific. *Marine Micropaleontology*, 19(1-2): 79-98.
- Hilgen, F., Krijgsman, W., Langereis, C., Lourens, L., Santarelli, A. and Zachariasse, W., 1995. Extending the astronomical (polarity) time scale into the Miocene. *Earth and Planetary Science Letters*, 136: 495-510.
- Hilgen, F., Bissoli, L., Iaccarino, S., Krijgsman, W., Meijer, R., Negri, A. and Villa, G., 2000. Integrated stratigraphy and astrochronology of the Messinian GSSP at Oued Akrech (Atlantic Morocco). *Earth and Planetary Science Letters*, 182(3-4): 237-251.
- Hillaire-Marcel, C. and Ravelo, A., 2007. The use of Oxygen and Carbon isotopes of Foraminifera in Paleoceanography. Burlington: Elsevier Science. In: Hillaire-Marcel, C. & De Vernal, A. (eds.) *Developments in Marine Geology: Proxies in Late Cenozoic Paleoceanography*.

- Hoang, V. L., Clift, P. D., Schwab, A. M., Huuse, M., Nguyen, D. A. and Zhen, S., 2010. Large-scale erosional response of SE Asia to monsoon evolution reconstructed from sedimentary records of the Song Hong-Yinggehai and Qiongdongnan basins, South China Sea. *Geological Society, London, Special Publications*, 342(1): 219-244.
- Hodell, D. A., Benson, R. H., Kent, D. V., Boersma, A. and Rakic- El Bied, K., 1994. Magnetostratigraphic, biostratigraphic, and stable isotope stratigraphy of an Upper Miocene drill core from the Salé Briqueterie (northwestern Morocco): A high-resolution chronology for the Messinian stage. *Paleoceanography*, 9(6): 835-855.
- Hodell, D. A., Curtis, J. H., Sierro, F. J. and Raymo, M. E., 2001. Correlation of late Miocene to early Pliocene sequences between the Mediterranean and North Atlantic. *Paleoceanography*, 16(2): 164-178.
- Hodell, D. A. and Venz- Curtis, K. A., 2006. Late Neogene history of deepwater ventilation in the Southern Ocean. *Geochemistry, Geophysics, Geosystems*, 7(9).
- Holbourn, A., Kuhnt, W., Schulz, M., Flores, J.-A. and Andersen, N., 2007. Orbitally-paced climate evolution during the middle Miocene "Monterey" carbon-isotope excursion. *Earth and Planetary Science Letters*, 261(3-4): 534-550.
- Holbourn, A., Kuhnt, W., Clemens, S. C. and Heslop, D., 2021. A ~ 12 Myr Miocene Record of East Asian Monsoon variability from the South China Sea. *Paleoceanography and Paleoclimatology*, 36(7): e2021PA004267.
- Holbourn, A. E., Kuhnt, W., Clemens, S. C., Kochhann, K. G., Jöhnck, J., Lübbers, J. and Andersen, N., 2018. Late Miocene climate cooling and intensification of southeast Asian winter monsoon. *Nature communications*, 9(1): 1-13.
- Hsü, K. J., Ryan, W. B. F. and Cita, M. B., 1973. Late miocene desiccation of the mediterranean. *Nature*, 242(5395): 240-244.
- Hüsing, S., Kuiper, K., Link, W., Hilgen, F. J. and Krijgsman, W., 2009. The upper Tortonian-lower Messinian at Monte dei Corvi (Northern Apennines, Italy): completing a Mediterranean reference section for the Tortonian stage. *Earth and Planetary Science Letters*, 282(1-4): 140-157.
- Iaccarino, S. M., Bertini, A., Di Stefano, A., Ferraro, L., Gennari, R., Grossi, F., Lirer, F., Manzi, V., Menichetti, E., Ricci Lucchi, M. and Taviani, M., 2008. The Trave section (Monte dei Corvi, Ancona, Central Italy): an integrated paleontological study of the Messinian deposits. *Stratigraphy*, 5(3-4): pp.281-306.
- Jimenez-Espejo, F. J., Martinez-Ruiz, F., Sakamoto, T., Iijima, K., Gallego-Torres, D. and Harada, N., 2007. Paleoenvironmental changes in the western Mediterranean since the last glacial maximum: high resolution multiproxy record from the Algero-Balearic basin. *Palaeogeography, Palaeoclimatology, Palaeoecology*, 246(2-4): 292-306.
- Jorissen, F., Fontanier, C. and Thomas, E., 2007. Paleoclimatological Proxies Based on Deep-Sea Benthic Foraminiferal Assemblage Characteristics, 1(07), doi: 10.1016/S1572-5480(07): 01012-3.

- Jorissen, F. J., 1987. The distribution of benthic foraminifera in the Adriatic Sea. *Marine Micropaleontology*, 12: 21-48.
- Jorissen, F. J., de Stigter, H. C. and Widmark, J. G., 1995. A conceptual model explaining benthic foraminiferal microhabitats. *Marine micropaleontology*, 26(1-4): 3-15.
- Kaiho, K. and Lamolda, M. A., 1999. Catastrophic extinction of planktonic foraminifera at the Cretaceous-Tertiary boundary evidenced by stable isotopes and foraminiferal abundance at Caravaca, Spain. *Geology*, 27(4): 355-358.
- Kaminski, M. A., Kender, S., Ciurej, A., Balç, R. and Setoyama, E., 2013. Pliocene agglutinated benthic foraminifera from Site U1341 in the Bering Sea (IODP Expedition 323). *Geological Quarterly*, 57(2): 335-342.
- Karami, M., De Leeuw, A., Krijgsman, W., Meijer, P. T. and Wortel, M., 2011. The role of gateways in the evolution of temperature and salinity of semi-enclosed basins: An oceanic box model for the Miocene Mediterranean Sea and Paratethys. *Global and Planetary Change*, 79(1-2): 73-88.
- Kastens, K., Mascle, J., Auroux, C., Bonatti, E., Broglia, C., Channell, J., Curzi, P., Emeis, K.-C., Glaçon, G. and Hasegawa, S., 1988. ODP Leg 107 in the Tyrrhenian Sea: Insights into passive margin and back-arc basin evolution. *Geological Society of America Bulletin*, 100(7): 1140-1156.
- Katz, M. E. and Thunell, R. C., 1984. Benthic foraminiferal biofacies associated with Middle Miocene to Early Pliocene oxygen-deficient conditions in the eastern Mediterranean. *The Journal of Foraminiferal Research*, 14(3): 187-202.
- Koho, K., García, R. d., De Stigter, H., Epping, E., Koning, E., Kouwenhoven, T. and Van der Zwaan, G., 2008. Sedimentary labile organic carbon and pore water redox control on species distribution of benthic foraminifera: A case study from Lisbon-Setúbal Canyon (southern Portugal). *Progress in Oceanography*, 79(1): 55-82.
- Konijnendijk, T., Ziegler, M. and Lourens, L., 2014. Chronological constraints on Pleistocene sapropel depositions from high-resolution geochemical records of ODP Sites 967 and 968. *Newsl. Stratigr.*, 47(3): 263-282.
- Kontakiotis, G., Besiou, E., Antonarakou, A., Zarkogiannis, S., Kostis, A., Mortyn, P., Moissette, P., Cornée, J.-J., Schulbert, C. and Drinia, H., 2019. Decoding sea surface and paleoclimate conditions in the eastern Mediterranean over the Tortonian-Messinian Transition. *Palaeogeography, Palaeoclimatology, Palaeoecology*, 534: 109312.
- Kouwenhoven, T., Seidenkrantz, M.-S. and Van der Zwaan, G., 1999. Deep-water changes: the near-synchronous disappearance of a group of benthic foraminifera from the Late Miocene Mediterranean. *Palaeogeography, Palaeoclimatology, Palaeoecology*, 152(3-4): 259-281.
- Kouwenhoven, T., Morigi, C., Negri, A., Giunta, S., Krijgsman, W. and Rouchy, J.-M., 2006. Paleoenvironmental evolution of the eastern Mediterranean during the Messinian: Constraints from integrated microfossil data of the Pissouri Basin (Cyprus). *Marine Micropaleontology*, 60(1): 17-44.

- Kouwenhoven, T. J., Hilgen, F. J. and Van Der Zwaan, G. J., 2003. Late Tortonian–early Messinian stepwise disruption of the Mediterranean–Atlantic connections: constraints from benthic foraminiferal and geochemical data. *Palaeogeography, Palaeoclimatology, Palaeoecology*, 198(3-4): 303-319.
- Krijgsman, W., Hilgen, F., Langereis, C. and Zachariasse, W., 1994. The age of the Tortonian/Messinian boundary. *Earth and Planetary Science Letters*, 121: 533-547.
- Krijgsman, W., Hilgen, F., Negri, A., Wijbrans, J. and Zachariasse, W., 1997. The Monte del Casino section (northern Apennines, Italy): a potential Tortonian/Messinian boundary stratotype? *Palaeogeography, Palaeoclimatology, Palaeoecology*, 133(1-2): 27-47.
- Krijgsman, W., Langereis, C., Zachariasse, W., Boccaletti, M., Moratti, G., Gelati, R., Iaccarino, S., Papani, G. and Villa, G., 1999. Late Neogene evolution of the Taza-Guercif Basin (Rifian Corridor, Morocco) and implications for the Messinian salinity crisis. *Marine Geology*, 153(1-4): 147-160.
- Krijgsman, W., Blanc-Valleron, M.-M., Flecker, R., Hilgen, F., Kouwenhoven, T., Merle, D., Orszag-Sperber, F. and Rouchy, J.-M., 2002. The onset of the Messinian salinity crisis in the Eastern Mediterranean (Pissouri Basin, Cyprus). *Earth and Planetary Science Letters*, 194(3-4): 299-310.
- Krijgsman, W., Leewis, M. E., Garcés, M., Kouwenhoven, T. J., Kuiper, K. F. and Sierro, F. J., 2006. Tectonic control for evaporite formation in the Eastern Betics (Tortonian; Spain). *Sedimentary Geology*, 188: 155-170.
- Krijgsman, W., Capella, W., Simon, D., Hilgen, F. J., Kouwenhoven, T. J., Meijer, P. T., Sierro, F. J., Tulbure, M. A., van den Berg, B. C. and van der Schee, M., 2018. The Gibraltar corridor: watergate of the messinian salinity crisis. *Marine Geology*, 403: 238-246.
- Kucera, M., 2007. Planktonic foraminifera as tracers of past oceanic environments. *Developments in marine geology*, Chapter 6: 213-262.
- Langer, M. R., 1993. Epiphytic foraminifera. *Marine Micropaleontology*, 20(3-4): 235-265.
- Larrasoana, J., Roberts, A., Rohling, E., Winklhofer, M. and Wehausen, R., 2003. Three million years of monsoon variability over the northern Sahara. *Climate Dynamics*, 21(7-8): 689-698.
- Lascaratos, A., Roether, W., Nittis, K. and Klein, B., 1999. Recent changes in deep water formation and spreading in the eastern Mediterranean Sea: a review. *Progress in Oceanography*, 44(1-3): 5-36.
- Laskar, J., Robutel, P., Joutel, F., Gastineau, M., Correia, A. and Levrard, B., 2004. A long-term numerical solution for the insolation quantities of the Earth. *Astronomy & Astrophysics*, 428(1): 261-285.
- Laube-Lenfant, E. and Pierre, C., 1994. Variability of delta-c-13 of sigma-co2 in ocean waters of the equatorial pacific. *Oceanologica acta*, 17(6): 633-641.

- Lirer, F., Foresi, M., Iaccarino, S., Salvatorini, G., Turco, E., Cosentino, C., Sierro, F. J. and Caruso, A., 2019. Mediterranean Neogene planktonic foraminifer biozonation and biochronology. *Earth-Science Reviews*, 196: 102869.
- Lisiecki, L. E. and Raymo, M. E., 2005. A Pliocene- Pleistocene stack of 57 globally distributed benthic $\delta^{18}\text{O}$ records. *Paleoceanography*, 20(1): 1-17.
- Loubère, P., 1996. The surface ocean productivity and bottom water oxygen signals in deep water benthic foraminiferal assemblages. *Marine Micropaleontology*, 28(3-4): 247-261.
- Lourens, L. J., Antonarakou, A., Hilgen, F., Van Hoof, A., Vergnaud- Grazzini, C. and Zachariasse, W., 1996. Evaluation of the Plio- Pleistocene astronomical timescale. *Paleoceanography*, 11(4): 391-413.
- Lückge, A., Horsfield, B., Littke, R. and Scheeder, G., 2002. Organic matter preservation and sulfur uptake in sediments from the continental margin off Pakistan. *Organic Geochemistry*, 33(4): 477-488.
- Lutze, G. and Coulbourn, W., 1984. Recent benthic foraminifera from the continental margin of northwest Africa: community structure and distribution. *Marine Micropaleontology*, 8(5): 361-401.
- Lutze, G. and Thiel, H., 1989. Epibenthic foraminifera from elevated microhabitats; *Cibicidoides wuellerstorfi* and *Planulina ariminensis*. *The Journal of Foraminiferal Research*, 19(2): 153-158.
- Mackensen, A., Sejrup, H. and Jansen, E., 1985. The distribution of living benthic foraminifera on the continental slope and rise off southwest Norway. *Marine Micropaleontology*, 9(4): 275-306.
- Mackensen, A., Fu, D., Grobe, H. and Schmiedl, G., 1993. Benthic foraminiferal assemblages from the eastern South Atlantic Polar Front region between 35 and 57 S: distribution, ecology and fossilization potential. *Marine Micropaleontology*, 22(1-2): 33-69.
- Manzi, V., Iaccarino, S. M., Lugli, S. and Roveri, M., 2008. Messinian salinity crisis revisited-II: New views of a vanished ocean. *Stratigraphy*, 5(3-4): 225-226.
- Manzi, V., Gennari, R., Hilgen, F., Krijgsman, W., Lugli, S., Roveri, M. and Sierro, F. J., 2013. Age refinement of the Messinian salinity crisis onset in the Mediterranean. *Terra Nova*, 25(4): 315-322.
- Martín, J. M., Braga, J. C. and Betzler, C., 2001. The Messinian Guadalhorce corridor: the last northern, Atlantic-Mediterranean gateway. *Terra Nova*, 13(6): 418-424.
- Martín, J. M., Puga-Bernabéu, A., Aguirre, J. and Braga, J. C., 2014. Miocene Atlantic-Mediterranean seaways in the Betic Cordillera (Southern Spain). *Revista de la sociedad geológica de España*, 27(1): 175-186.

- Martinez-Ruiz, F., Kastner, M., Gallego-Torres, D., Rodrigo-Gámiz, M., Nieto-Moreno, V. and Ortega-Huertas, M., 2015. Paleoclimate and paleoceanography over the past 20,000 yr in the Mediterranean Sea Basins as indicated by sediment elemental proxies. *Quaternary Science Reviews*, 107: 25-46.
- Marzocchi, A., Lunt, D., Flecker, R., Bradshaw, C., Farnsworth, A. and Hilgen, F., 2015. Orbital control on late Miocene climate and the North African monsoon: insight from an ensemble of sub-precessional simulations. *Climate of the Past*, 11(10): 1271-1295.
- Masqué, P., Fabres, J., Canals, M., Sanchez-Cabeza, J., Sanchez-Vidal, A., Cacho, I., Calafat, A. and Bruach, J., 2003. Accumulation rates of major constituents of hemipelagic sediments in the deep Alboran Sea: a centennial perspective of sedimentary dynamics. *Marine Geology*, 193(3-4): 207-233.
- MEDARGroup, 2002. Medatlas 2002: Mediterranean and Black Sea Database of Temperature, Salinity and Biochemical Parameters – Climatological Atlas. IFREMER, Brest, France.
- Meijer, P. T., 2006. A box model of the blocked-outflow scenario for the Messinian Salinity Crisis. *Earth and Planetary Science Letters*, 248(1-2): 486-494.
- Murat, A., 1999. 41. Pliocene- Pleistocene occurrence of sapropels in the Western Mediterranean Sea and their relation to Eastern Mediterranean Sapropels, *Proceedings of the Ocean Drilling Program, Scientific Results*, pp. 519-527.
- Murray, J., 1991. *Ecology and palaeoecology of benthic foraminifera*: Longman Scientific and Technical. Harlow, Essex, UK.
- Murray, J. W., 2006. *Ecology and applications of benthic foraminifera*. Cambridge University Press.
- Myers, P. G., Haines, K. and Rohling, E. J., 1998. Modeling the paleocirculation of the Mediterranean: The Last Glacial Maximum and the Holocene with emphasis on the formation of sapropel S 1. *Paleoceanography*, 13(6): 586-606.
- Naidu, P. D. and Malmgren, B. A., 1995. Do benthic foraminifer records represent a productivity index in oxygen minimum zone areas? An evaluation from the Oman Margin, Arabian Sea. *Marine Micropaleontology*, 26(1-4): 49-55.
- Nguyen, T. M. P., Petrizzo, M. R., Stassen, P. and Speijer, R. P., 2011. Dissolution susceptibility of Paleocene-Eocene planktic foraminifera: Implications for palaeoceanographic reconstructions. *Marine Micropaleontology*, 81(1-2): 1-21.
- Ochoa, D., Sierro, F. J., Lofi, J., Maillard, A., Flores, J.-A. and Suárez, M., 2015. Synchronous onset of the Messinian evaporite precipitation: First Mediterranean offshore evidence. *Earth and Planetary Science Letters*, 427: 112-124.
- Osborne, A. H., Marino, G., Vance, D. and Rohling, E., 2010. Eastern Mediterranean surface water Nd during Eemian sapropel S5: monitoring northerly (mid-latitude) versus southerly (sub-tropical) freshwater contributions. *Quaternary Science Reviews*, 29(19-20): 2473-2483.

- Pelum, C., Frerichs, W. and Sliter, W., 1976. Gulf of Mexico deep-water foraminifers In: William V. Slitter (Ed.). *Cushman Found. Form. Res. Spec.*, 14: 1-124.
- Pérez-Asensio, J. N., Aguirre, J., Schmiedl, G. and Civis, J., 2012. Messinian paleoenvironmental evolution in the lower Guadalquivir Basin (SW Spain) based on benthic foraminifera. *Palaeogeography, Palaeoclimatology, Palaeoecology*, 326: 135-151.
- Pérez-Asensio, J. N., Frigola, J., Pena, L. D., Sierro, F. J., Reguera, M. I., Rodríguez-Tovar, F. J., Dorador, J., Asioli, A., Kuhlmann, J. and Huhn, K., 2020. Changes in western Mediterranean thermohaline circulation in association with a deglacial Organic Rich Layer formation in the Alboran Sea. *Quaternary Science Reviews*, 228: 106075.
- Pérez-Folgado, M., Sierro, F. J., Bárcena, M. A., Flores, J. A., Vázquez, A., Utrilla, R., Hilgen, F. J., Krijgsman, W. and Filippelli, G. M., 2003. Western versus eastern Mediterranean paleoceanographic response to astronomical forcing: A high-resolution microplankton study of precession-controlled sedimentary cycles during the Messinian. *Palaeogeography, Palaeoclimatology, Palaeoecology*, 190: 317-334.
- Pérez-Folgado, M., Sierro, F. J., Flores, J. A., Grimalt, J. O. and Zahn, R., 2004. Paleoclimatic variations in foraminifer assemblages from the Alboran Sea (Western Mediterranean) during the last 150 ka in ODP Site 977. *Marine Geology*, 212(1-4): 113-131.
- Pérez-Asensio, J. N., Aguirre, J., Schmiedl, G. and Civis, J., 2012. Impact of restriction of the Atlantic- Mediterranean gateway on the Mediterranean Outflow Water and eastern Atlantic circulation during the Messinian. *Paleoceanography*, 27(3).
- Pflum, C. E., Frerichs, W. E. and Sliter, W. V., 1976. Gulf of Mexico Deep-water Foraminifers, 14. Cushman Foundation for Foraminiferal Research.
- Pierre, C., 1999. The oxygen and carbon isotope distribution in the Mediterranean water masses. *Marine Geology*, 153(1-4): 41-55.
- Pinardi, N. and Masetti, E., 2000. Variability of the large scale general circulation of the Mediterranean Sea from observations and modelling: a review. *Palaeogeography, Palaeoclimatology, Palaeoecology*, 158(3-4): 153-173.
- Pinardi, N., Cessi, P., Borile, F. and Wolfe, C. L., 2019. The Mediterranean sea overturning circulation. *Journal of Physical Oceanography*, 49(7): 1699-1721.
- Poli, M. S., Meyers, P. A., Thunell, R. C. and Capodivacca, M., 2012. Glacial- interglacial variations in sediment organic carbon accumulation and benthic foraminiferal assemblages on the Bermuda Rise (ODP Site 1063) during MIS 13 to 10. *Paleoceanography*, 27(3).
- Pound, M. J., Haywood, A. M., Salzmann, U. and Riding, J. B., 2012. Global vegetation dynamics and latitudinal temperature gradients during the Mid to Late Miocene (15.97-5.33 Ma). *Earth-Science Reviews*, 112(1-2): 1-22.

- Powley, H. R., Cappellen, P. and Krom, M. D., 2017. Nutrient cycling in the Mediterranean Sea: the key to understanding how the unique marine ecosystem functions and responds to anthropogenic pressures. *Mediterranean Identities – Environment, Society, Culture*. InTech: 47-77.
- Riveiros, N. V., Waelbroeck, C., Skinner, L., Roche, D. M., Duplessy, J.-C. and Michel, E., 2010. Response of South Atlantic deep waters to deglacial warming during Terminations V and I. *Earth and Planetary Science Letters*, 298(3-4): 323-333.
- Rodrigo-Gámiz, M., Martínez-Ruiz, F., Rodríguez-Tovar, F. J., Jiménez-Espejo, F. J. and Pardo-Igúzquiza, E., 2014. Millennial-to centennial-scale climate periodicities and forcing mechanisms in the westernmost Mediterranean for the past 20,000 yr. *Quaternary Research*, 81(1): 78-93.
- Roger, S., Münch, P., Cornée, J., Saint Martin, J., Féraud, G., Pestrea, S., Conesa, G. and Moussa, A. B., 2000. $^{40}\text{Ar}/^{39}\text{Ar}$ dating of the pre-evaporitic Messinian marine sequences of the Melilla basin (Morocco): a proposal for some biosedimentary events as isochrons around the Alboran Sea. *Earth and Planetary Science Letters*, 179(1): 101-113.
- Rogerson, M., Cacho, I., Jimenez- Espejo, F., Reguera, M., Sierro, F. J., Martinez- Ruiz, F., Frigola, J. and Canals, M., 2008. A dynamic explanation for the origin of the western Mediterranean organic- rich layers. *Geochemistry, Geophysics, Geosystems*, 9(7).
- Rogerson, M., Bigg, G. R., Rohling, E. and Ramirez, J., 2012. Vertical density gradient in the eastern North Atlantic during the last 30,000 years. *Climate dynamics*, 39(3-4): 589-598.
- Rohling, E., Marino, G. and Grant, K., 2015. Mediterranean climate and oceanography, and the periodic development of anoxic events (sapropels). *Earth-Science Reviews*, 143: 62-97.
- Rohling, E. J. and Cooke, S., 1999. Stable oxygen and carbon isotopes in foraminiferal carbonate shells, *Modern Foraminifera*. Springer, pp. 239-258.
- Rohling, E. J. and De Rijk, S., 1999. Holocene Climate Optimum and Last Glacial Maximum in the Mediterranean: the marine oxygen isotope record. *Marine Geology*, 153(1-4): 57-75.
- Rohling, E. J., Abu-Zied, R., Casford, J., Hayes, A. and Hoogakker, B., 2009. The marine environment: present and past. *The physical geography of the Mediterranean*: 33-67.
- Rossignol-Strick, M., 1985. Mediterranean Quaternary sapropels, an immediate response of the African monsoon to variation of insolation. *Palaeogeography, Palaeoclimatology, Palaeoecology*, 49(3-4): 237-263.
- Rothwell, R. G., 2015. Twenty years of XRF core scanning marine sediments: what do geochemical proxies tell us?, *Micro-XRF Studies of Sediment Cores*. Springer, pp. 25-102.

- Roveri, M., Flecker, R., Krijgsman, W., Lofi, J., Lugli, S., Manzi, V., Sierro, F. J., Bertini, A., Camerlenghi, A. and De Lange, G., 2014a. The Messinian Salinity Crisis: past and future of a great challenge for marine sciences. *Marine Geology*, 352: 25-58.
- Roveri, M., Lugli, S., Manzi, V., Gennari, R. and Schreiber, B. C., 2014b. High-resolution strontium isotope stratigraphy of the messinian deep mediterranean basins: Implications for marginal to central basins correlation. *Marine Geology*, 349: 113-125.
- Ryan, W. B., 1976. Quantitative evaluation of the depth of the western Mediterranean before, during and after the Late Miocene salinity crisis. *Sedimentology*, 23(6): 791-813.
- Santarelli, A., Brinkhuis, H., Hilgen, F., Lourens, L., Versteegh, G. and Visscher, H., 1998. Orbital signatures in a Late Miocene dinoflagellate record from Crete (Greece). *Marine Micropaleontology*, 33(3-4): 273-297.
- Schlitzer, R., Roether, W., Oster, H., Junghans, H.-G., Hausmann, M., Johannsen, H. and Michelato, A., 1991. Chlorofluoromethane and oxygen in the Eastern Mediterranean. *Deep Sea Research Part A. Oceanographic Research Papers*, 38(12): 1531-1551.
- Schlitzer, R., 2015. Data analysis and visualization with Ocean Data View. *CMOS Bulletin SCMO*, 43(1): 9-13.
- Schönfeld, J., 1997. The impact of the Mediterranean Outflow Water (MOW) on benthic foraminiferal assemblages and surface sediments at the southern Portuguese continental margin. *Marine Micropaleontology*, 29(3-4): 211-236.
- Schuster, M., 2006. The Age of the Sahara Desert. *Science*, 311(5762): 821-821.
- Seidenkrantz, M.-S., Kouwenhoven, T., Jorissen, F., Shackleton, N. and Van der Zwaan, G., 2000. Benthic foraminifera as indicators of changing Mediterranean-Atlantic water exchange in the late Miocene. *Marine geology*, 163(1-4): 387-407.
- Sen Gupta, B. K. and Machain-Castillo, M. L., 1993a. Benthic foraminifera in oxygen-poor habitats. *20(3-4)*: 183-201.
- Sen Gupta, B. K. and Machain-Castillo, M. L., 1993b. Benthic foraminifera in oxygen-poor habitats. *Marine Micropaleontology*, 20(3-4): 183-201.
- Sepulchre, P., Ramstein, G., Fluteau, F., Schuster, M., Tiercelin, J.-J. and Brunet, M., 2006. Tectonic uplift and Eastern Africa aridification. *Science*, 313(5792): 1419-1423.
- Sgarrella, F. and Moncharmont Zei, M., 1993. Benthic foraminifera of the Gulf of Naples (Italy): systematics and autoecology. *Bollettino della Società Paleontologica Italiana*(2).
- Shannon, C. E., 1948. A mathematical theory of communication. *Bell system technical journal*, 27(3): 379-423.

- Sierro, F. J., Hilgen, F. J., Krijgsman, W. and Flores, J. A., 2001. The Abad composite (SE Spain): a Messinian reference section for the Mediterranean and the APTS. 168(1-2): 141-169.
- Sierro, F. J., Flores, J. A., Francés, G., Vazquez, A., Utrilla, R., Zamarréño, I., Erlenkeuser, H. and Barcena, M. A., 2003. Orbitally-controlled oscillations in planktic communities and cyclic changes in western Mediterranean hydrography during the Messinian. *Palaeogeography, Palaeoclimatology, Palaeoecology*, 190: 289-316.
- Simon, D., Marzocchi, A., Flecker, R., Lunt, D. J., Hilgen, F. J. and Meijer, P. T., 2017. Quantifying the Mediterranean freshwater budget throughout the late Miocene: New implications for sapropel formation and the Messinian Salinity Crisis. *Earth and Planetary Science Letters*, 472: 25-37.
- Spellerberg, I. F. and Fedor, P. J., 2003. A tribute to Claude Shannon (1916-2001) and a plea for more rigorous use of species richness, species diversity and the 'Shannon-Wiener' Index. *Global ecology and biogeography*, 12(3): 177-179.
- Spero, H. J. and Lea, D. W., 1996. Experimental determination of stable isotope variability in *Globigerina bulloides*: implications for paleoceanographic reconstructions. *Marine Micropaleontology*, 28(3-4): 231-246.
- Sprovieri, M., Bellanca, A., Neri, R., Mazzola, S., Bonanno, A., Patti, B. and Sorgente, R., 1999. Astronomical calibration of late Miocene stratigraphic events and analysis of precessionally driven paleoceanographic changes in the Mediterranean basin. *Memorie della Società Geologica Italiana*, 54: 7-24.
- Sprovieri, R., Di Stefano, E., Caruso, A. and Bonomo, S., 1996. High resolution stratigraphy in the Messinian Tripoli Formation in Sicily. *Paleopelagos*, 6: 415-435.
- Stommel, H., Bryden, H. and Mangelsdorf, P., 1973. Does some of the Mediterranean outflow come from great depth? *Pure and Applied Geophysics*, 105(1): 879-889.
- Tanner, T., Hernández- Almeida, I., Drury, A. J., Guitián, J. and Stoll, H., 2020. Decreasing atmospheric CO₂ during the late Miocene Cooling. *Paleoceanography and Paleoclimatology*: e2020PA003925.
- Theocharis, A. and Georgopoulos, D., 1993. Dense water formation over the Samothraki and Limnos Plateaux in the north Aegean Sea (eastern Mediterranean Sea). *Continental Shelf Research*, 13(8-9): 919-939.
- Topper, R. and Meijer, P. T., 2015. Changes in Mediterranean circulation and water characteristics due to restriction of the Atlantic connection: a high-resolution ocean model. *Climate of the Past*, 11(2): 233-251.
- Tulbure, M., Capella, W., Barhoun, N., Flores, J., Hilgen, F., Krijgsman, W., Kouwenhoven, T., Sierro, F. J. and Yousfi, M. Z., 2017. Age refinement and basin evolution of the North Rifian Corridor (Morocco): No evidence for a marine connection during the Messinian Salinity Crisis. *Palaeogeography, Palaeoclimatology, Palaeoecology*, 485: 416-432.

- Tzanova, A., Herbert, T. D. and Peterson, L., 2015. Cooling Mediterranean Sea surface temperatures during the Late Miocene provide a climate context for evolutionary transitions in Africa and Eurasia. *Earth and Planetary Science Letters*, 419: 71-80.
- Van den Berg, B. C. J., Sierro, F. J., Hilgen, F. J., Flecker, R., Larrasoaña, J. C., Krijgsman, W., Flores, J. A., Mata, M. P., Bellido Martín, E., Civis, J. and González-Delgado, J. A., 2015. Astronomical tuning for the upper Messinian Spanish Atlantic margin: Disentangling basin evolution, climate cyclicity and MOW. 135: 89-103.
- Van den Berg, B. C. J., Sierro, F. J., Hilgen, F. J., Flecker, R., Larrasoaña, J. C., Krijgsman, W., Flores, J. A. and Mata, M. P., 2018. Imprint of Messinian Salinity Crisis events on the Spanish Atlantic margin. *Newsletters on Stratigraphy*, 51(1): 93-115.
- Van der Laan, E., Snel, E., De Kaenel, E., Hilgen, F. and Krijgsman, W., 2006. No major deglaciation across the Miocene- Pliocene boundary: integrated stratigraphy and astronomical tuning of the Loulja sections (Bou Regreg area, NW Morocco). *Paleoceanography*, 21(3).
- Van Der Laan, E., Hilgen, F. J., Lourens, L. J., De Kaenel, E., Gaboardi, S. and Iaccarino, S., 2012. Astronomical forcing of Northwest African climate and glacial history during the late Messinian (6.5-5.5Ma). *Palaeogeography, Palaeoclimatology, Palaeoecology*, 313-314: 107-126.
- Van der Schee, M., Van den Berg, B. C., Capella, W., Simon, D., Sierro, F. J. and Krijgsman, W., 2018. New age constraints on the western Betic intramontane basins: A late Tortonian closure of the Guadalhorce Corridor? *Terra Nova*, 30(5): 325-332.
- Van der Zwaan, G., Jorissen, F. and De Stigter, H., 1990. The depth dependency of planktonic/benthic foraminiferal ratios: constraints and applications. *Marine Geology*, 95(1): 1-16.
- Van der Zwaan, G., Duijnste, I., Den Dulk, M., Ernst, S., Jannink, N. and Kouwenhoven, T., 1999. Benthic foraminifers: proxies or problems?: a review of paleocological concepts. *Earth-Science Reviews*, 46(1-4): 213-236.
- Van Hinsbergen, D. J. J., Kouwenhoven, T. J. and Van Der Zwaan, G. J., 2005. Paleobathymetry in the backstripping procedure: Correction for oxygenation effects on depth estimates. 221(3-4): 245-265.
- Van Marle, L., 1988. Bathymetric distribution of benthic foraminifera on the Australian-Irian Jaya continental margin, eastern Indonesia. *Marine Micropaleontology*, 13(2): 97-152.
- Vázquez, A., Utrilla, R., Zamarrero, I., Sierro, F., Flores, J., Francés, G. and Barcena, M., 2000. Precession-related sapropelites of the Messinian Sorbas Basin (South Spain): paleoenvironmental significance. *Palaeogeography, Palaeoclimatology, Palaeoecology*, 158(3-4): 353-370.
- Violanti, D., Dela Pierre, F., Trenkwald, S., Lozar, F., Clari, P., Irace, A. and D'Atri, A., 2011. Biostratigraphic and paleoenvironmental analyses of the Messinian/Zanclean boundary and Zanclean succession in the Moncucco quarry (Piedmont, northwestern Italy). *Bulletin de la Société géologique de France*, 182(2): 149-162.

- Wefer, G. and Berger, W. H., 1991. Isotope paleontology: growth and composition of extant calcareous species. *Marine Geology*, 100(1-4): 207-248.
- Weinkauf, M. F. and Milker, Y., 2018. The effect of size fraction in analyses of benthic foraminiferal assemblages: a case study comparing assemblages from the > 125 and > 150 μm size fractions. *Frontiers in Earth Science*, 6: 37.
- Weltje, G. J. and Tjallingii, R., 2008. Calibration of XRF core scanners for quantitative geochemical logging of sediment cores: Theory and application. *Earth and Planetary Science Letters*, 274(3-4): 423-438.
- Wright, R., 1978. 41. Neogene paleobathymetry of the Mediterranean based on benthic foraminifers from DSDP Leg 42a. *Initial Reports DSDP*, 42: 837-847.
- Zavatarielli, M. and Mellor, G. L., 1995. A numerical study of the Mediterranean Sea circulation. *Journal of Physical Oceanography*, 25(6): 1384-1414.
- Zhang, Y. G., Pagani, M., Liu, Z., Bohaty, S. M. and DeConto, R., 2013. A 40-million-year history of atmospheric CO₂. *Philosophical Transactions of the Royal Society A: Mathematical, Physical and Engineering Sciences*, 371(2001): 20130096.
- Zhang, Z., Ramstein, G., Schuster, M., Li, C., Contoux, C. and Yan, Q., 2014. Aridification of the Sahara desert caused by Tethys Sea shrinkage during the Late Miocene. *Nature*, 513(7518): 401-404.

Chapter 5

The timing of closure of the last
Betic corridor strand inferred from
new geochemical and planktic
foraminifer data from
Montemayor-1 core
(Guadalquivir Basin)

Chapter 5

The timing of closure of the last Betic corridor strand
inferred from new geochemical and planktic
foraminifer data from Montemayor-1 core
(Guadalquivir Basin)

In collaboration with
Francisco J. Sierro and Nils Andersen

The timing of closure of the last Betic corridor strand inferred from new geochemical and planktic foraminifer data from Montemayor-1 core (Guadalquivir Basin)

In collaboration with Francisco J. Sierro¹ and Nils Andersen²

¹ Dept. de Geología, Univ. de Salamanca, Plaza de los Caídos s/n, 37008, Salamanca, Spain, e-mail: sierro@usal.es

² Leibniz-Laboratory for Radiometric Dating and Isotope Research, Christian-Albrechts-Universität Kiel, Max-Eyth-Str. 11-13, 24118 Kiel, Germany, e-mail: nandersen@leibniz.uni-kiel.de

Abstract

In this work we present a new high resolution geochemical (XRF and stable isotope) and micropaleontological record of the Tortonian –Messinian interval of the Montemayor-1 core located in the Guadalquivir Basin. This new data enabled the high-resolution tuning of the lower interval of the core (6.37 Ma – 8 Ma) and consequently to precisely date environmental changes happening at that time in the Guadalquivir Basin and relate them to Mediterranean and global events. At 7.15 – 7.17 Ma, in concomitance with a shallowing of the basin the bottom water residence time, temperature and salinity increased. These changes have been associated with a reduction of the Mediterranean Outflow Water reaching The Guadalquivir Basin as a consequence of the restriction of the last strand of the Betic corridor connecting the Mediterranean and the Atlantic, the Guadalhorce. This hypothesis is in line with the analogous changes observed in several Mediterranean Sea locations, where from 7.17 Ma a reduced Mediterranean – Atlantic connection is visible. Furthermore, the change in phase relationship between the Northern Hemisphere summer insolation minima peaks and the biogenic carbonate, now in opposite phase, already reported by some authors in the upper part of the record (5.33 Ma – 5.77 Ma) have been confirmed by the newly acquired data. The planktic foraminifer and isotope data shown in this work supports the previously proposed mechanism and confirm that the colder and arid climate present during Northern Hemisphere insolation minima could have a negative effect on the vegetation cover resulting in more erosion and terrigenous input, diluting the biogenic content.

1. Introduction

Today, the intercontinental Mediterranean Sea is connected to the Atlantic Ocean through the Gibraltar Strait. This configuration has been present at least since the beginning of the Pliocene (e.g., Hsü et al., 1973; Blanc, 2002; Garcia-Castellanos et al., 2009; Roveri et al., 2014), when the Camarinal sill was breached

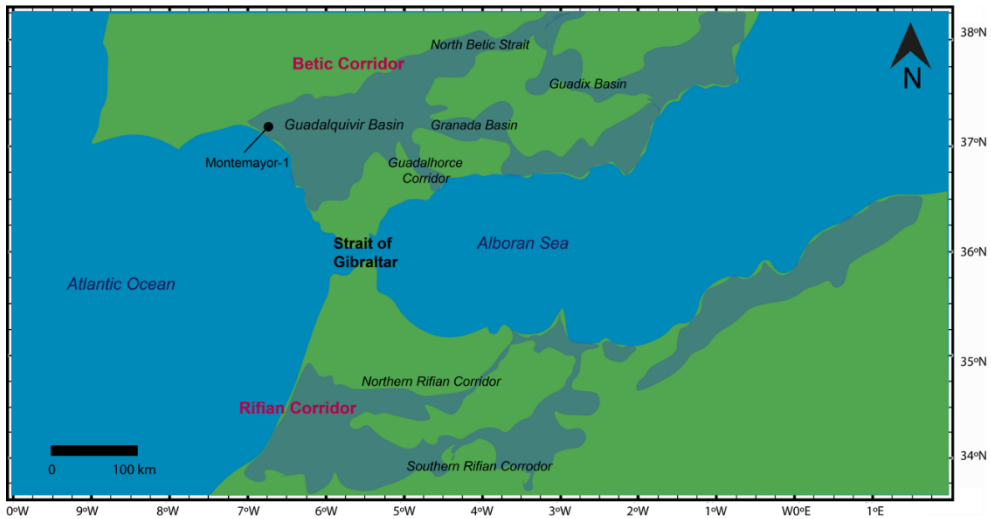


Figure 1: Schematic map of the Alboran Sea area showing the location of the Montemayor-1 core. The blue shading represents the area formerly occupied by the Betic and Rifian corridors (Capella et al., 2020).

and an efficient Mediterranean – Atlantic connection was established ending the dramatic event known as the Messinian Salinity Crises (MSC; Hsü et al., 1973; Selli, 1973; Krijgsman et al., 1999). During the 700 kyr that lasted this event (5.967 – 5.332 Ma), a reduced or completely absent connection between the Atlantic Ocean and Mediterranean Sea led to the deposition of more than a kilometer thick succession of evaporites (e.g., CIESM, 2008 and references therein).

The progressive closure of the Mediterranean – Atlantic gateway that led to the MSC started already in the Tortonian, with the restriction of the Betic and Rifian corridors (Figure 1), acting as marine gateways since the Miocene (e.g., Popov et al., 2004; Bialik et al., 2019). During the last decades extensive field work in Southern Spain and Northern Morocco outcrops has been done trying to pinpoint the exact timing of the closure of the Betic and Rifian gateway strands which resulted as being a difficult task considering the intense uplift and erosion that affected the Gibraltar Arc area (e.g., Fadil et al., 2006; Garcia-Castellanos and Villaseñor, 2011; Mancilla et al., 2015). Regarding the Rifian corridor, most probably the southern strand closed between 7.1 – 6.9 Ma while the northern sectors around 7.35 – 7.25 Ma (Krijgsman and Langereis, 2000; Tulbure et al., 2017; Capella et al., 2018). The Betic corridor had different strands that closed at different times. The North Betic strait closed first, at ~ 7.6 Ma, restriction in the Granada Basin is thought to start with the beginning of evaporite deposition in this basin between 7.37 and 7.24 Ma (Corbí et al., 2012) while the Guadix Basin was initially thought to have restricted at 7.8 Ma (Betzler et al., 2006), timing eventually disputed because of the presence of an

unconformity (Hüsing et al., 2010). Finally, the last Betic connection was through the Guadalorce Corridor (GC), which permitted the connection between the Atlantic and the Mediterranean through the Guadalquivir Basin (GB).

Numerous studies have been carried out on the GC outcrops, but given the continuity of the record, most of the paleoenvironmental studies were carried on the Montemayor-1 and Huelva-1 cores, drilled in the westernmost sector of the GB (Figure 1). In particular, paleomagnetism (Larrasoña et al., 2008; Larrasoña et al., 2014), benthic foraminifers associations (Pérez-Asensio et al., 2013; Pérez-Asensio et al., 2014), XRF data (Van den Berg et al., 2015; Van den Berg et al., 2018), stable isotope (Pérez-Asensio et al., 2012) and pollen records (Jiménez-Moreno et al., 2013) have been all acquired on Montemayor-1 core. These studies showed that the continuous shallowing upward sequence of the GB was marked by glacio-eustatic fluctuations and changes in vegetation linked to climate glacial-interglacial variability (Jiménez-Moreno et al., 2013) that changed the regional surface water productivity (Pérez-Asensio et al., 2014) as well as by astronomically induced cycles characterized by an alternation of different elemental compositions (Van den Berg et al., 2015). Stable isotope studies on the other hand, were able to pin point the progressive diminishment in the strength of the MOW especially between 6.35 and 6.18 Ma (Pérez-Asensio et al., 2012) which resulted with a drastic sedimentation rates increase (Larrasoña et al., 2008; Larrasoña et al., 2014) and intensification of the upwelling (high abundances of benthic foraminifer *Uvigerina peregrina* s.l.) (Pérez-Asensio et al., 2014). Consequently, several authors suggested that the closure of the GB occurred only at 6.18 Ma (Martín et al., 2001; Pérez-Folgado et al., 2004; Pérez-Asensio et al., 2012; Pérez-Asensio et al., 2012).

The chronology of the Montemayor-1 core was obtained from a combination of planktic foraminifer bio-events, magnetostratigraphy (Larrasoña et al., 2008) and elemental geochemistry cyclostratigraphy data (Van den Berg et al., 2015). Cycle to cycle astronomically tuned record of the core covers only the late Messinian (6.37-5.33 Ma), as does the geochemical dataset which prevents to investigate whether the first signs of restriction of the Gibraltar gateway/s visible in the Mediterranean Basin since 7.17 Ma (Kouwenhoven et al., 1999; Kouwenhoven, 2000; Seidenkrantz et al., 2000; Kouwenhoven et al., 2003; Bulian et al., 2021), were related with changes in the GB. Consequently, in this study we principally focused on the late Tortonian-early Messinian interval in the Montemayor-1 core improving significantly the astronomical tuning of the lower core interval (236-257.3 mcd) and producing a new high resolution geochemical (stable isotope and XRF geochemistry) and planktic foraminifer dataset. These new data enabled to pinpoint the definite closure of the last Betic corridor strand, the GB, and to correlate its closure to Mediterranean and Global events.

2. Geological setting and core stratigraphy

The Guadalquivir basin (GB) is a WSW to the ENE elongated triangular basin located in the south of the Iberian Peninsula that formed during the Late Serravallian-Early Tortonian (Figure 2a). Towards the west it opens to the Atlantic Ocean, to the north is limited by the Iberian Massif while to the south it is bounded by the Betic Cordillera (Figure 2a) constituting its foreland (Sierro et al., 1996; González-Delgado et al., 2004).

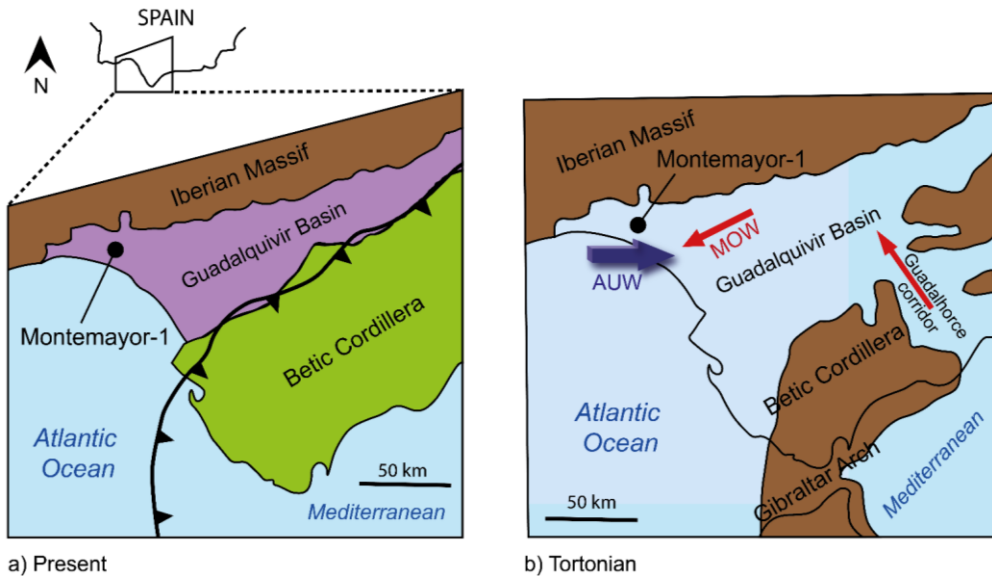


Figure 2: a) Geological map of the Guadalquivir basin with the location of Montemayor-1 borehole. b) paleogeographic reconstruction of the Guadalquivir area during the Tortonian (based on Martín et al., 2009; Larrasoña et al., 2014) showing the flow direction and location of the Mediterranean Outflow Water and Atlantic Upwelled Water (after Pérez-Asensio et al., 2012).

During the early-middle Miocene the NW-directed convergence between the Eurasian and African plates caused the stacking of the Betic external tectonic units leading to the downward flexural subsidence of the Iberian basement and subsequent infilling of the basin (Sierro et al., 1996; Berástegui et al., 1998; Ledesma, 2000; Garcia-Castellanos et al., 2002) which mainly witnessed continuous marine to continental sedimentation (Aguirre, 1992; Sierro et al., 1996; Martín et al., 2009; Salvany et al., 2011; González-Delgado et al., 2004). In the Tortonian-early Messinian, following the uplift of the Betic cordillera, the GB became a large embayment and represented the Atlantic side of the Betic corridor which (Figure 1b), together with the Rifian passages in Morocco, enabled the connection between the Mediterranean Basin and Atlantic Ocean (Benson et al., 1991; Martín et al., 2001). Here, warm and salty Mediterranean Outflow Waters (MOW) leaving the Mediterranean encountered fresh and cool Atlantic Upwelled Waters (AUW; Figure 1b) forming a two-layered water

column (Martín et al., 2001; Pérez- Asensio et al., 2012). The GB shows a continuous sedimentary fill composed of a lower marine sequence (late Tortonian – early Pliocene) and an upper continental sequence (Aguirre, 1992; Sierra et al., 1996; Salvany et al., 2011; González-Delgado et al., 2004). The lower part of the marine sequence shows huge sedimentary structures suggesting that Mediterranean waters were flowing out into the Atlantic at current velocities estimated at 1-1.5 m/s (Martín et al., 2001).

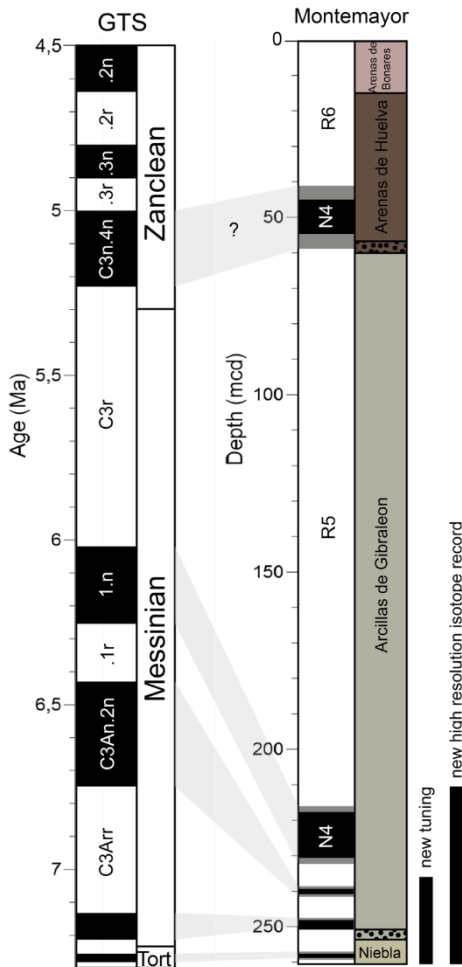


Figure 3: On the left the Tortonian - Zanclean magnetostratigraphic chrons from Lourens et al. (2004). In the Middle the magnetostratigraphic results for Montemayor-1 core (Larrasoña et al., 2008; Larrasoña et al., 2014) and on the right the lithological column showing the different formations present in Montemayor-1 core (Niebla Formation, Arcillas de Gibraleón Formation, Arenas de Huelva Formation and Arenas de Bonares Formation).

The persistent uplift of the Betic Cordillera progressively closed the Guadix corridor and Granada Basin (Braga et al., 2003; Martín et al., 2009), and finally the GC, considered as the last Betic Mediterranean-Atlantic connection (Martín et al., 2001). The definite closure of the GC is still debated and the ages vary between late Tortonian (7.6 Ma; Van der Schee et al., 2018a) and middle Messinian (6.18 Ma; Martín et al., 2001; Pérez-Asensio et al., 2012; Martín et al., 2014; Pérez-Asensio et al., 2014).

The Montemayor-1 core (37°16'N, 6°49'W; 52 m elevation) was drilled in the northwestern margin of the GB (Figure 2), a tectonically inactive area where the sedimentary sequence reaches its maximum thickness. The base of the core is characterized by 1.5 m of Paleozoic-Mesozoic substrate composed of reddish clays (Figure 3). The basement is overlaid by the four lowermost lithostratigraphic

units that characterize the GB sedimentary infill (Sierra et al., 1996; González-Delgado et al., 2004). The lowermost unit, 5 m thick, corresponds to the cemented carbonate-siliciclastic coastal deposits of the Niebla Formation (Tortonian) which are followed by deep marine greenish-blue clays of Arcillas de Gibraleón Formation (late Tortonian-Messinian) that with their 198 m cover the largest part of the Montemayor-1 core. At the base of the of Arcillas de Gibraleón a 3 m thick glauconitic layer can be identified. At 60 m the Messinian clay, which is topped by another glauconite layer, separates these deposits from the shallow marine sands and silts of the Arenas de Huelva Formation (early Pliocene), 42 m thick.

A discontinuity at 18 m is overlain by 14.5 m of brownish transitional sands of Arenas de Bonares Formation (late Pliocene-Pleistocene) and 3.5 m of recent soil marking the end of the Montemayor-1 core (Larrasoña et al., 2008; Larrasoña et al., 2014).

3. Materials and methods

3.1 Stable isotope analyses

In order to improve the resolution of the pre-existing stable isotope dataset (Pérez-Asensio et al., 2012; interval 210-240 m) and to complete the record until the base of the core (236-257.3 m), foraminifer shells from 405 samples of Montemayor-1 core were analyzed for stable isotope content ($\delta^{13}\text{C}$ and $\delta^{18}\text{O}$). When possible, a sampling step of 10 cm was applied in order to get a high-resolution dataset. The analyses were performed on ultrasonically cleaned 5-10 individuals of benthic foraminifer species *Cibicoides pachyderma* and 10-20 specimens of planktic foraminifer *Globigerina bulloides* from the >150 μm size fraction.

The analyses were performed with a Finnigan MAT 253 mass spectrometer connected to a Kiel IV carbonate preparation device at the Christian-Albrechts University in Kiel (Germany). Sample reaction was induced by individual acid addition (99% H_3PO_4 at 75 °C) under vacuum. The evolved carbon dioxide was analysed eight times for each individual sample. As documented by the performance of international [NBS19: +1.95 ‰ VPDB (^{13}C), -2.20 ‰ VPDB (^{18}O); IAEA-603: +2.46 ‰ VPDB (^{13}C), -2.37 ‰ VPDB (^{18}O)] and laboratory-internal carbonate standards [Hela1: +0.91 ‰ VPDB (^{13}C), +2.48 ‰ VPDB (^{18}O); HB1: -12.10 ‰ VPDB (^{13}C), -18.10 ‰ VPDB (^{18}O); SHK: +1.74 ‰ VPDB (^{13}C), -4.85 ‰ VPDB (^{18}O)], analytical precision of stable isotope analysis is better than ± 0.08 ‰ for $\delta^{18}\text{O}$ and better than ± 0.05 ‰ for $\delta^{13}\text{C}$. The obtained values were calibrated relative to Vienna Pee Dee Belemnite (VPDB).

3.2 XRF analyses

Because cyclical changes in the sediment chemical composition were recognized in the Montemayor-1 core from 60 m to 237 m (Van den Berg et al., 2015; Van den Berg et al., 2018) and were used for astronomical tuning, we performed XRF analyses on the missing 237-253.7 m interval to have a complete geochemical dataset and be able to tune efficiently the entire record. A total of 162 samples were taken (every 10 cm) and each one was reduced to fine powder in an agate mortar, subsequently obtaining tablets of 10 mm in diameter with a manual press with a load of 5 Tm. The tablets were fixed on a glass slide to facilitate their handling. On each tablet, of sufficient thickness to avoid transparency phenomena, 25 random points were measured for 30 s with a Bruker M4 Tornado Spectrometer where the generator settings were set at 50 kV and 150 μ A. A representative spectra and semi-quantitative results of each sample were obtained using the ESPRIT software, set at international standards. This analysis was performed at the General Service of X-ray diffraction at Salamanca University (Nucleus).

The results obtained for the major elements were expressed in wt% (weight%) of the oxide while the light elements in ppm (parts per million) of the element. To make the dataset comparable to the published geochemical record, the wt% of each oxide was transformed into the wt% of the element itself. To do so every oxide wt% was multiplied by its atomic weight and then divided by the atomic weight of the major element (Ragland, 1989). Furthermore, the values of the light elements that were expressed in ppm were transformed in wt%. Additionally, to obtain some information regarding the origin of the sediments, grainsize and oxygenation at the bottom the ratios Zr/Al, Si/K and Mg/Fe were used.

3.2.1 Statistics

To produce a statistically robust dataset and perform a Principal Component Analyses (PCA) more corrections were necessary. Because lighter elements emit a smaller signal, their emission is prone to attenuation which makes lighter elements emitted signal to scatter (Tjallingii et al., 2007; Weltje and Tjallingii, 2008). In order to account for such differences and achieve a normal distribution, the dataset was additionally normalized to the total wt% of each measure point and standardized by subtracting the average and dividing by the standard deviation (Davis and Sampson, 1986). This normalisation allowed the direct comparison between major and trace elements and for each element to be represented in the PCA. Finally, to enable a direct comparison between the new data here presented and the PCA previously obtained by Van den Berg et al.

(2015), the same elements were included in the analyses (Fe, Al, Ca, Ti, Zr, Si, K, Rb and Sr).

3.3 Planktic foraminifer analyses

A quantitative study of the planktic foraminiferal content was performed on 236 samples from Montemayor-1 core covering the interval 198.5 – 257 mcd. The core was sampled with an increasing upward sampling step from 0.2 m at the base to 1 m at the top of the studied interval based on the increasing sedimentation rate (Van den Berg et al., 2015; Van den Berg et al., 2018). Each sample was dried in the oven, disaggregated in water overnight and subsequently washed over a >150 μm and >63 μm sieve. From the >150 μm fraction at least 300 planktic foraminifer specimens were classified into species and counted under a microscope.

Following Sierró et al. (2003), the abundance of warm, oligotrophic water planktic foraminifers (WOWPF) was calculated and expressed as the sum of *Globigerinoides* spp., *Orbulina universa* and *Globoturborotalita apertura*. In this way it was possible to estimate possible responses of the planktic fauna to changes in the oceanographic setting of the basin.

3.4 Spectral analyses

To establish the nature and significance of the periodic changes in the stable isotope, elemental and planktic foraminifer dataset of Montemayor-1 core older record (257 – 210 mcd), a spectral analysis was performed. The analysis was carried out using Past software (Hammer et al., 2001) with the Redfit procedure which allows to assess datasets with uneven sampling step. The spectral peaks higher than the 95% confidence interval were considered significant (Monte Carlo method).

4. Results

4.1 Stable isotope record

The stable isotope data from 257 to 210 mcd of core Montemayor-1 is shown in Figure 4. The planktic $\delta^{18}\text{O}$ curve (Figure 4 a) shows a stable trend with values

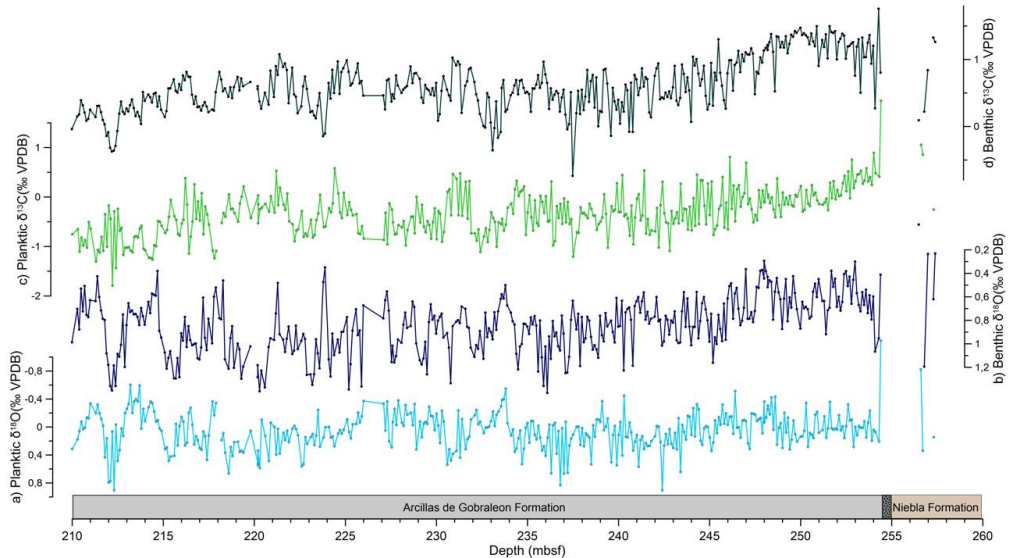


Figure 4: Montemayor-1 core stable isotope data measured from benthic and planktic foraminifer shells. a) Planktic $\delta^{18}\text{O}$ record (*G. bulloides*); b) Benthic $\delta^{18}\text{O}$ record (*C. pachyderma*); c) Planktic $\delta^{13}\text{C}$ record (*G. bulloides*) and d) Benthic $\delta^{13}\text{C}$ record (*C. pachyderma*). On the bottom, the lithological column is shown.

around 0.1 and -0.1 ‰ until 234 m of depth when they drop until minimum values of ~ -0.4 ‰. At the depth of 225 m, the planktic $\delta^{18}\text{O}$ curve rises again towards higher values and stays around ~ 0.2 ‰ for the next 10 m when values decrease again reaching a minimum of ~ -0.6 ‰. The general trend of the benthic $\delta^{18}\text{O}$ curve (Figure 4 b) displays a similar pattern as the planktic one, with analogous minima and maxima. Nonetheless, a change towards heavier values is visible at 245 m depth, where from ~ 0.6 ‰ there is an increase until ~ 0.8 ‰ that persists until the end of the record. In both the planktic and benthic $\delta^{13}\text{C}$ curves (Figure 4 c and d) there is a visible decreasing upward trend. In the planktic record the latter is more gradual and from values of ~ 0.5 ‰ at the bottom, values of ~ -1 ‰ are reached at the top of the section. The benthic record shows a more abrupt shift that can be pinpointed at 248 mcd where from ~ 1.5 ‰ the curve reaches ~ 0.5 ‰. This value persists until 216 mcd, when the curve almost reaches 0 ‰.

4.2 Principal Component Analyses and geochemical record

The PCA was performed to make the data matrix visualization easier and to highlight the relationship between the single elements. The first three statistically significant Principal components account for 81% of the total variance with the PC1 and PC2 describing respectively the 66.1% and 15.06%.

The two most important negative loadings for PC1 are Ca and Sr (Figure 5 a), while the positive loading comprises several elements including Al, Si, K, Ti, Fe, Rb and Zr. For PC2 (Figure 5 b) the negative loading is represented mostly by Zr, and to a lesser extent by Si and Fe, while on the positive side Al, Rb and Sr are dominant.

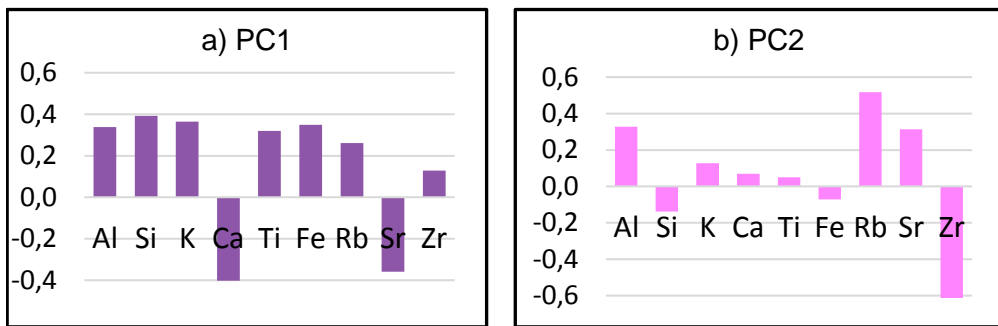


Figure 5: Loadings of the Principal component performed on the geochemical record of Montemayor-1 core: a) PC1 and b) PC2.

The PC1 scores curve (Figure 6 a) shows a sudden decrease upward at 253 mcd from where an increasing upward tendency starts until the end of the record. On the contrary, the PC2 record (Figure 5 b) starts with an increasing upward tendency that stabilises at the same depth and persists steadily until 240 mcd, when values diminish once again.

The V and Cr wt%, and the Si/K record show a prominent change at 248 mcd (Figure 6 c, d, f). Here both the V wt% and the Si/K curves significantly drop, while the Cr wt% sharply rises simultaneously with an increase in the oscillation amplitudes. The Mn/Fe record is relatively stable in the first part of the record, while it progressively increases from 247 mcd until 238, when values descend again (Figure 6 e). Finally, after a sharp drop in values registered at 252 mcd, the Zr/Al record keeps a stable trend until the end of the record.

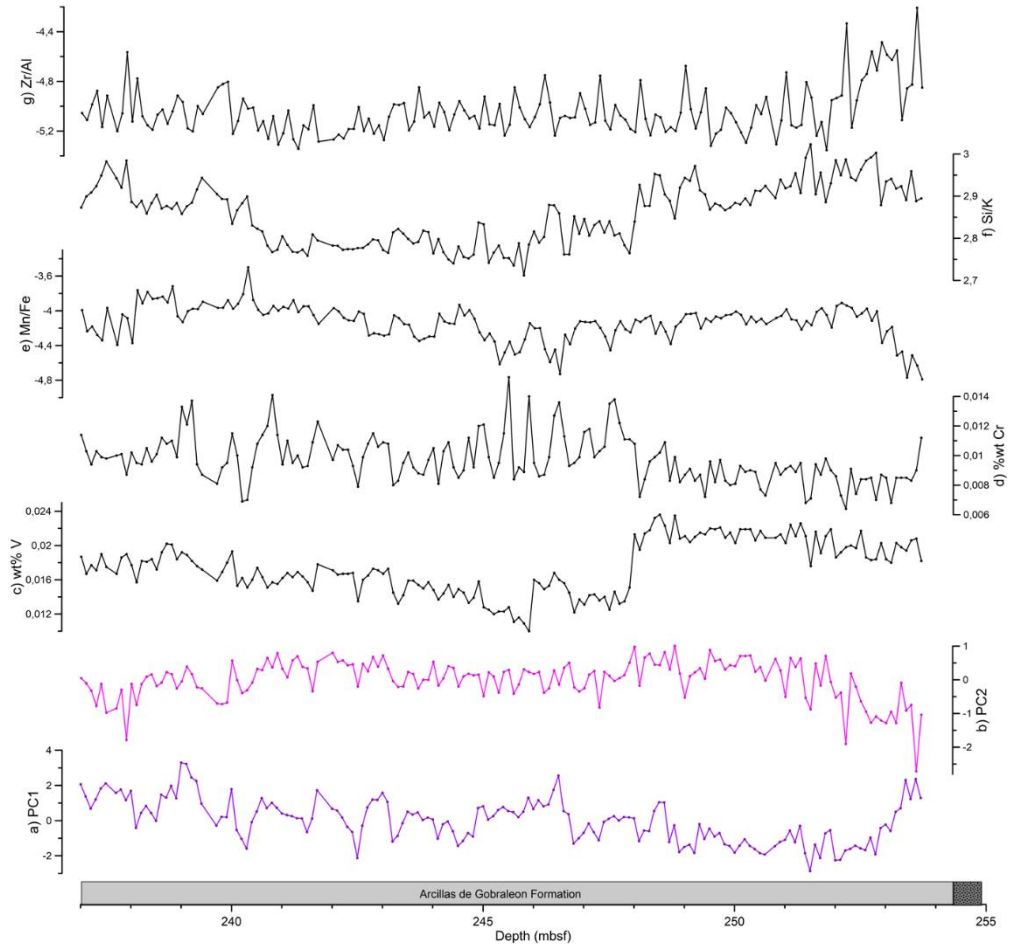


Figure 6: Montemayor-1 core geochemical records in depth domain: a) PC1 scores; b) PC2 scores; c) wt% V; d) wt% Cr; e) Mn/Fe ratio; f) Si/K ratio and e) Zr/Al ratio. The black vertical line highlights the sharp change occurring in several records at 248 mcd.

4.3 Planktic foraminifer distribution

While within the siliciclastic coastal deposits of the Niebla Formation only one sample contained planktic foraminifers, the following Arcillas de Gibrleon Formation holds a very abundant and diverse planktic foraminifer association (Figure 7). The latter is mainly composed of *Globigerina bulloides*, *Globoturborotalita apertura* spp. (*G. apertura* + *G. druryi* + *G. nepenthes*), *Orbulina univversa*, *Globigerinoides* spp. (*G. extremus* + *G. immaturus* + *G. quadrilobatus* + *G. trilobus* + *G. sacculifer*), *Neogloboquadrina acostaensis* and to a lesser extent by *Globobigerinita glutinata*. From the base of the section until 248 mcd, the sum of the WOWPF stays stable at ~30%, when it sharply increases until ~50% where it stays until the end of the record.

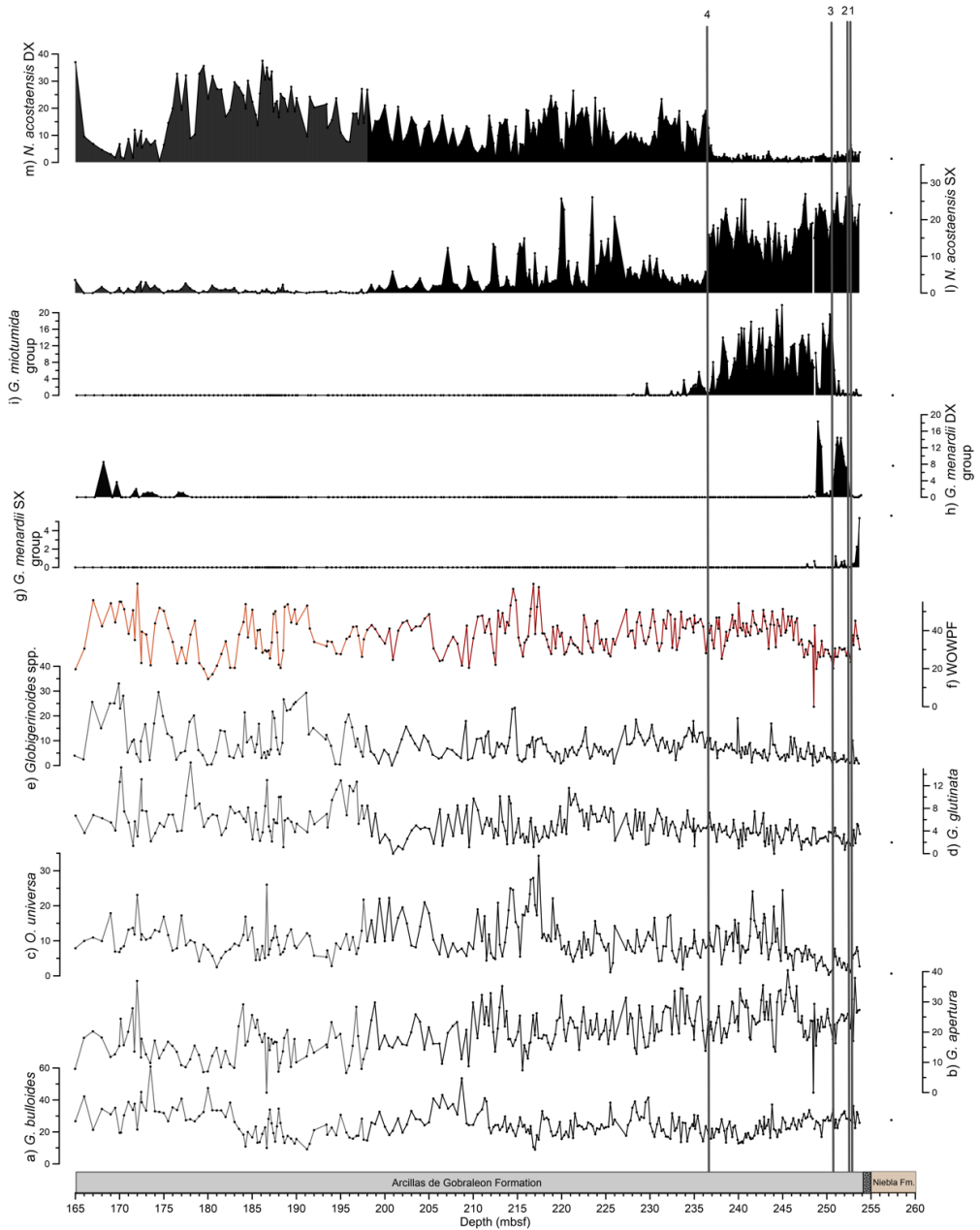


Figure 7: Planktic foraminifer distribution in Montemayor-1 core: a-e) most abundant species; f) the sum of WOWPF and g-m) the main biostratigraphic markers where the vertical lines and numbers denote the events of (Siero et al., 2003). The interval 165-198 mcd highlighted in grey and light red derive from the master thesis of Joana Ferreira and Sandra Rocha (Ferreira, 2016; Rocha, 2017).

5. Age model

5.1 Biostratigraphic and magnetostratigraphic pointers

To create a solid age model several pointers were used including top and bottom ages of chrons defined through magnetic measurements (Larrasoña et al., 2008; Larrasoña et al., 2014) and planktic foraminifer bioevents (Figure 6; Table 1). Regarding the magnetostratigraphic pointers, only the ones justified by abundant measurement points and in line with our new biostratigraphic tie points were employed, in this case only Chron C3An.2n (Lourens, 2004). The base of this chron has been identified at 241.1 mcd while its top at 247 mcd (Larrasoña et al., 2008) dated respectively at 6.73 Ma and 6.43 Ma (Lourens, 2004). The two older chrons (C3Br.1n and C3Bn) employed by Larrasoña et al. (2008) for the first tuning of Montemayor-1 core were here excluded from the age model because of the low resolution of the paleomagnetic measurements in this interval and their discrepancy with the new planktic foraminifer biostratigraphic events identified in this work i.e. events 1 and 2 (Sierro et al., 1993). The planktic foraminifer biostratigraphic scheme used is based on recent astronomically calibrated charts compiled by Lirer et al. (2019) while the numbering of each bioevent is taken from Sierro et al. (1993; Table 1).

Table 1: Planktic foraminifer bio events and magnetostratigraphic pointers used for the tuning of the Montemayor-1 core. The biostratigraphic scheme used relies on Lirer et al. (2019), while the magnetostratigraphy derives from Larrasoña et al. (2008).

Event	Astronomically calibrated age (Ma)	Depth (mcd)	Nº
Top C3An.2n	6.73 Ma	241.1 m	
S/D coiling <i>N. acostaensis</i>	6.35 Ma	236.5 m	4
Base C3An.2n	6.43 Ma	237.1 m	
FCO <i>G. miotumida</i> group	7.24 Ma	250.4 m	3
LCO <i>G. menardii</i> 5 group (dextral)	7.24 Ma	250.4 m	3
FCO <i>G. menardii</i> 5 group (dextral)	7.36 Ma	252.4 m	2
LCO <i>G. menardii</i> 4 group (sinistral)	7.51 Ma	252.9 m	1

In Montemayor-1 core the Last Common Occurrence (LCO) of *G. menardii* 4 group has been located at 252.9 mcd. The event has been recognized in the NE Atlantic and Mediterranean by Sierro (1985) and Sierro et al. (1993) and it has been astronomically calibrated at 7.51 Ma (Hilgen et al., 2000a; Hilgen et al., 2000b; Lourens et al., 2004). The next bioevent found is the First Common Occurrence (FCO) of *G. menardii* group 5 (Sierro, 1985; Sierro et al., 1993) recognized at 252.4 mcd and dated at 7.36 Ma (Hilgen et al., 2000a; Hilgen et al.,

2000b; Lourens et al., 2004). In the NE Atlantic, the Tortonian – Messinian boundary (7.24 Ma; Hilgen et al., 2000a; Hilgen et al., 2000b; Lourens et al., 2004) is characterized by the replacement of the *G. menardii* 5 group by the *G. miotumida* group (Tjalsma, 1971; Sierro, 1985; Sierro et al., 1993). In Montemayor-1 core, this replacement happens at 250.4 mcd but it is not definitive, at 250 mcd *G. menardii* 5 groups reappears again with high values and lasts for one more meter until 251 mcd (Figure 6). Finally, at 236.5 mcd, the *N. acostaensis* coiling change from sinistral to dextral can be identified clearly (Figure 6). The latter has been recognized from NE Atlantic cores (Sierro, 1985; Sierro et al., 1993) and Mediterranean outcrops (Sierro et al., 2001; Hüsing et al., 2009) where it has been astronomically tuned at 6.35 Ma (Sierro et al., 1993; Sierro et al., 2001; Lourens et al., 2004; Anthonissen and Ogg, 2012; Achalhi et al., 2016). All the pointers used for the tuning of the lower part of the Montemayor-1 core (236-257.3 mcd) proposed in this work are reported in Table 1.

5.2 Astronomical tuning

Previous studies performed on the Montemayor-1 core (Van den Berg et al., 2015) and other boreholes in the GB like Huelva (Van den Berg et al., 2018) and Casanieves (Ledesma, 2000) show how the late Messinian-early Pliocene sedimentation is mainly controlled by a climatic cyclicity related to astronomical forcing. Consequently, we can assume that such climate influence was controlling the deposition of the late Tortonian – early Messinian sediments of Montemayor-1 core enabling the astronomical tuning of the lowest part of the section (236-257.3 mcd). To see whether this assumption was true, and to prove if a cyclical pattern could be identified, we compared the spectral analyses obtained on the records that usually reflect well precessional cyclicity like the planktic $\delta^{18}\text{O}$ dataset, the geochemical PC1 and the distribution of WOWPF. Previous studies (Ledesma, 2000; Van den Berg et al., 2015; Van den Berg et al., 2018) prove that the sedimentation in the GB contains a clear precessional cyclicity that can be identified in the geochemical record, where northern hemisphere summer insolation maxima and minima are marked in turn by high abundances of terrigenous elements and low contents of biogenic particles and vice versa. During insolation maxima the warm-water foraminifers proliferate, and $\delta^{18}\text{O}$ values are lighter because of the warmer surface waters and the continental ice melting (Rohling and Cooke, 1999).

The spectral analyses from the three records yielded similar cyclicities (1.25 – 1.31 m) but because the sedimentation rate is very low, the sampling step was not dense enough to see precessional cycles while the eccentricity was well visible. Consequently, the new part of the Montemayor-1 record was tuned combining the planktic and magnetostratigraphic pointers (Table 1, Figure 8)

with the tuning to the eccentricity curve (Laskar et al., 2004) which modulates the effect of precession. This astronomical tuning was confirmed by the PC1 performed on the XRF geochemical record of the neighbour curve Huelva-1, where the same eccentricity cycles are visible (Van den Berg et al., 2018).

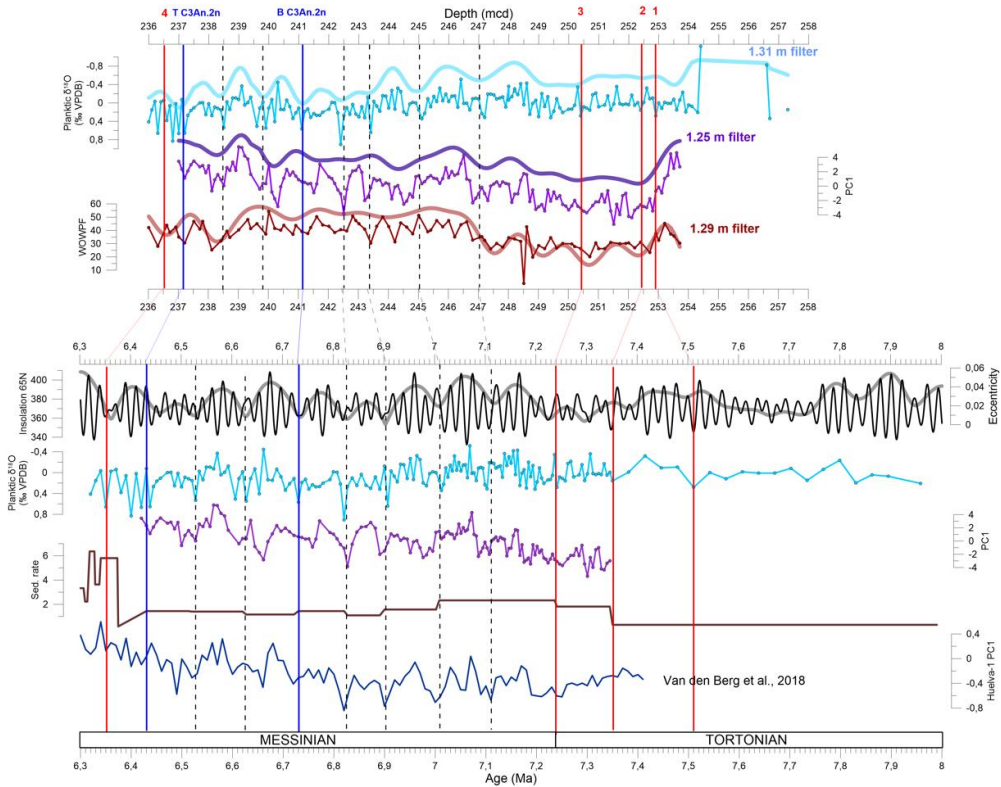


Figure 8: Above, the planktic foraminifer $\delta^{18}\text{O}$ dataset, the PC1 and the WOWPF distribution in Montemayor-1 core unfiltered and filtered data in depth domain. Below, the same records in time domain obtained by using biostratigraphic (red lines) and magnetostratigraphic (blue lines) tie points and a cyclostratigraphic tuning to the eccentricity curve (Laskar et al., 2004). In addition the sedimentation rate is shown as well as the PC1 from the neighbor site Huelva-1 which shows analogous cyclicity (Van den Berg et al., 2018).

6. Discussion

6.1 Mechanisms driving sediment cyclicity and sedimentation rates

After integrating our new data with the already available elemental composition (Van den Berg et al., 2018), stable isotope (Pérez-Asensio et al., 2012) and planktic foraminifer counts (Ferreira, 2016; Rocha, 2017) datasets, we obtain

a complete record for the Montemayor-1 core, from late Tortonian to the base of the Pliocene (Figure 9). Here, three different units can be identified based on changes in sedimentation rate and phase relationship between different parameters: the new interval (6.37 Ma – 8 Ma), the middle interval (5.77 Ma- 6.37 Ma) and the upper interval (5.33 Ma – 5.77 Ma). A possible connection between these changes in the GB with the MSC events in the adjacent Mediterranean basin and global and local climate changes have been discussed.

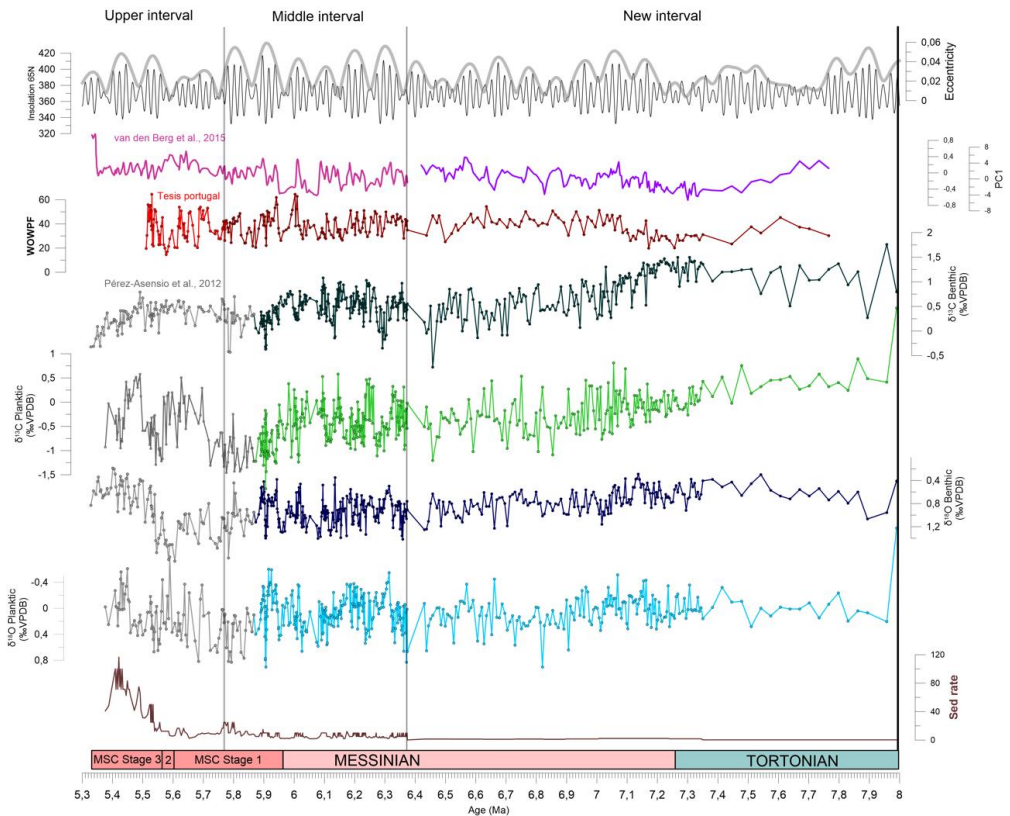


Figure 9: The Montemayor-1 8 – 5.33 Ma record in time domain including: the estimated sedimentation rate, the planktic and benthic $\delta^{18}\text{O}$ record, the planktic and benthic $\delta^{13}\text{C}$, the WOWPF, the PC1 resulting from the XRF geochemical record and the insolation and eccentricity curves used for the tuning (Laskar et al., 2004). The stable isotope record from 5.87 to 5.33 Ma derive from Pérez-Asensio et al. (2012), the WOWPF between 5.77 Ma and 5.51 Ma has been obtained with data from (Ferreira, 2016; Rocha, 2017) and the PC1 in the interval 6.35 to 5.33 Ma from (Van den Berg et al., 2015).

6.1.1 Improvement of the tuning and cyclicity of the lower interval (6.37 Ma – 8 Ma)

This interval is characterized by very low sedimentation rate of 0.3 cm/kyr until 7.35 Ma, where it slightly increases to values between 2.3 and 1.4 cm/kyr

(Figure 9). The geochemical cycles are visible only after the increase in sedimentation rate and while the astronomical solution cannot be resolved on a precessional scale, the higher amplitude precession signal that corresponds to eccentricity maxima are clearly visible and were used for the tuning of this interval (Figure 8). In this way the resolution and precision of the age model, based on 12 tie-points was significantly improved in respect to the one proposed by (Larrasoña et al., 2008) that considered only two bioevents and three magnetic chrons. The poor paleomagnetic resolution for this interval did not allow to accurately date these magnetic reversals (see section 5.1). The cyclicity in this interval is forced by cyclical changes in rainfall with more terrigenous elements present at time of eccentricity maxima (high amplitude precession) when the carbonate supply to the GB is low and vice versa. The eccentricity maxima peaks concordantly can be related to higher values of WOWPF, lighter $\delta^{18}\text{O}$ and heavier $\delta^{13}\text{O}$ values, implying warmer water temperatures and good water column ventilation respectively (Figures 8 and 9).

6.1.2 Cyclicity in the middle interval (5.77 Ma- 6.37 Ma)

The rise in sedimentation rate that oscillates between 6.3 cm/kyr and 22 cm/kyr (Figure 8), enables to clearly identify geochemical and micropaleontological cycles modulated by precession as already visible in the PC1 from (Van den Berg et al., 2015). The PC1 showed in fact how biogenic carbonate concentrated at times of Northern Hemisphere insolation minima, while the increase in rainfall during Northern Hemisphere Insolation maxima enhanced the terrigenous supply to the basin. These cycles are evident from our new isotope and planktic foraminifer data as Northern Hemisphere Insolation maxima shows the same phase relationship with higher abundances of WOWPF, lighter $\delta^{18}\text{O}$ and heavier $\delta^{13}\text{C}$ values. Analogous cyclical patterns have been registered in Messinian sediments from the Mediterranean Basin (e.g., Sierra et al., 2003: Sorbas Basin; Bulian et al., 2021; Alboran Basin) and Atlantic margins (e.g., Van Der Laan et al., 2012: Ain el Beida-Atlantic Morocco; Hodell et al., 2013: Iberian margin).

6.1.3 Cyclicity and increased sedimentation rate in the upper interval (5.33 Ma – 5.77 Ma)

As already pointed out by Van den Berg et al. (2015) in the upper interval of Montemayor-1 core (5.33 Ma – 5.77 Ma), a change in phase relationships is recognizable in the PC1 geochemical dataset, in respect to the cyclicity observed in the rest of the core (5.77 – 8 Ma). Here, even if sedimentary cycles seem to be driven by regular alternations in the rate of terrigenous supply to the basin, Northern Hemisphere insolation maxima are related with enrichment in biogenic carbonate, while insolation minima are linked to increases in

terrigenous supply. Additionally, this upper interval shows, in particular between 5.55 and 5.33, a remarkable increase in sedimentation rate where values up to 89 cm/kyr are reached (Figure 9), which reflected in the higher thicknesses of the cycles as well.

Van den Berg et al. (2015) interpreted the change in cyclicity as being a consequence of the site's increased proximity to the coast and of the changes in erosion rates. Coarser particles were able to reach the new shallower site location changing the composition of detrital fraction from mainly clay to silt. When the coarse-grained terrigenous input from the shelf was high, the biogenic carbonate and clay fraction would be diluted, while during low input, the biogenic carbonate would increase. Furthermore, changes in erosion rates led by changes

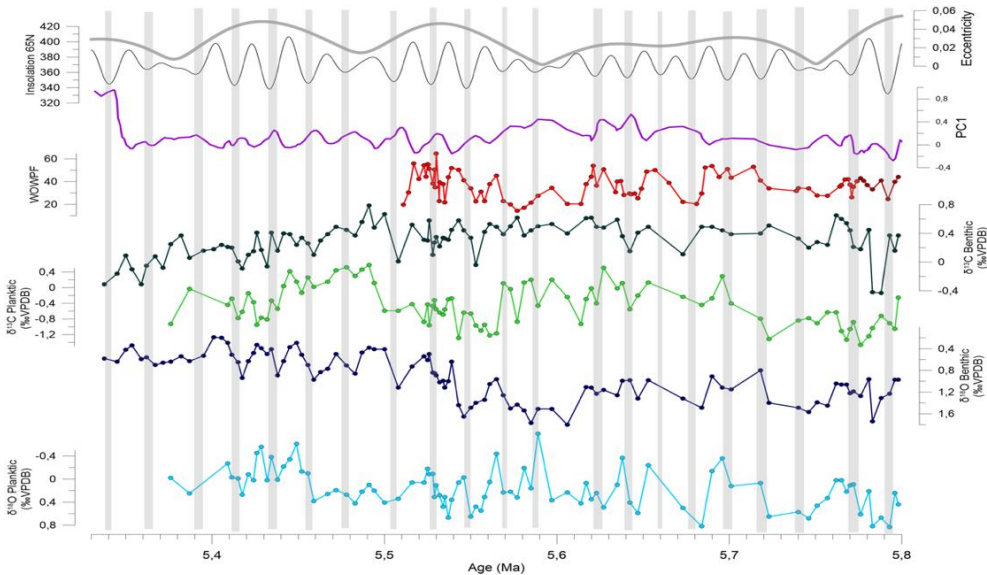


Figure 10: The Montemayor-1 upper interval records in time domain. The stable isotope record derive from Pérez-Asensio et al. (2012), the WOWPF has been obtained with data from (Ferreira, 2016; Rocha, 2017) and the PC1 from Van den Berg et al. (2018).

in local climate could justify the different phase relationship between high terrigenous input and insolation that we see in this part of the record. The colder and arid climate present during Northern Hemisphere insolation minima could have a negative effect on the vegetation cover resulting in more erosion and terrigenous input to the basin at the expense of the biogenic carbonate which would be diluted. On the contrary, even if riverine discharge was higher during Northern Hemisphere summer insolation maxima, the sediment concentration was lower and consisting primarily of clays. Concordantly, for this time interval, palynological studies (Jiménez-Moreno et al., 2013) show the same cyclicity between wet and dry periods. This depositional model, mainly influenced by

the site location and local climate has been confirmed by the new planktic foraminifer records. A high abundance of WOWPF during isolation maxima confirms the biogenic origin of the carbonates excluding the possibility of higher detrital carbonate input during insolation maxima (Figure 10).

Contemporaneous with the cyclicity pattern change, from 5.77 Ma Jiménez-Moreno et al. (2013) observes an abrupt drop of the dinocyst/pollen ratio. The latter, because the pollen coming from the continent decreases with the distance to the shore, has been used as eustatic oscillation proxy, where lower values can be related to a relative sea level drop at Montemayor-1 site. The latter has been also suggested by the abrupt decrease in abundance of benthic foraminifer species *Uvigerina peregrina* which does not tolerate high terrestrial organic matter input (Pérez-Asensio et al., 2014). This shallowing is in line with the change in the granulometry of the terrigenous supply coming to the GB inferred from the geochemical dataset (Van den Berg et al., 2015) and with a progressive infilling of the basin happening from east to west (Sierro et al., 1996; Iribarren et al., 2009).

The shallowing becomes even more significant at 5.55 Ma, when sedimentation rates of 90 cm/ky are reached. These sediment accumulation rates are more than 10 times higher than the ones reconstructed for the late Miocene Atlantic Margin (Iribarren et al., 2009; 6cm/kyr) and are similar to those reported for Holocene contourite deposits in the Gulf of Cadiz (80-120 cm/kyr; de Castro et al., 2021) and therefore are probably the result of a significant regional reorganization or global climate rather than just local climate and sediment supply changes. In fact, these changes could be linked with Stage 2 (5.6 - 5.55 Ma) and Stage 3 (5.55 Ma - 5.33 Ma) of the MSC (Roveri et al., 2014). The onset of Stage 2 marked the acme of the MSC with halite and clastic gypsum deposits accumulating in the Mediterranean basins as a consequence of sea level drawdown (which magnitude is still largely debated, e.g., Ryan, 1976: 1700 m; Krijgsman and Meijer, 2008: 400 m; Roveri et al., 2008a: 200 m; Urgeles et al., 2011: 800 - 1300 m; Micallef et al., 2018: 1300 - 2400 m) inferred by the formation of the Messinian erosional surface (e.g., CIESM, 2008; Roveri et al., 2014 and references therein). The onset of Stage 3 began with glacial stage 12 (TG12) during which a significant sea level drop could have restricted even more the Atlantic inflow to the Mediterranean (Meijer and Krijgsman, 2005; Hilgen et al., 2007; Marzocchi et al., 2016). As it is most likely that the major sea level drawdown was for the bigger part induced by tectonic uplift of the Betic and Gibraltar region and only subordinately by only climate changes (Roveri and Manzi, 2006; Roveri et al., 2008b; Omodeo Salé et al., 2012; Pérez-Asensio et al., 2013), Van den Berg et al. (2018) suggests that the increase in sedimentation rates is a consequence of the enhanced erosion due to the intense tectonic activity in the area. This could be a plausible mechanism since sedimentation rate increase due to uplift of this region has been recorded since 7.17 Ma in Alboran Basin,

when the first signs of Mediterranean – Atlantic gateway became visible in the sedimentary record (Bulian et al., 2021).

6.2 Correlation with global and Mediterranean events

6.2.1 Changes in the surface and deep-water masses

The new astronomical tuning for the lower part of the Montemayor-1 core allows a detailed correlation of the isotope records with astronomically tuned available isotope datasets. Here we focus on benthic $\delta^{18}\text{O}$ records (Figure 11) from Salé Briqueterie borehole (Hodell et al., 1994), Gibrleon outcrop (located in the GB; Hilgen, unpublished), Huelva-1 core (located in the GB; Sierro, unpublished), Atlantic Sites 982 of ODP Leg 162 (Hodell et al., 2001; Drury et al., 2018), 1085 from ODP Leg 175 (Vidal et al., 2002) and Alboran Basin Site 976 from ODP Leg 161 (Bulian et al., in press).

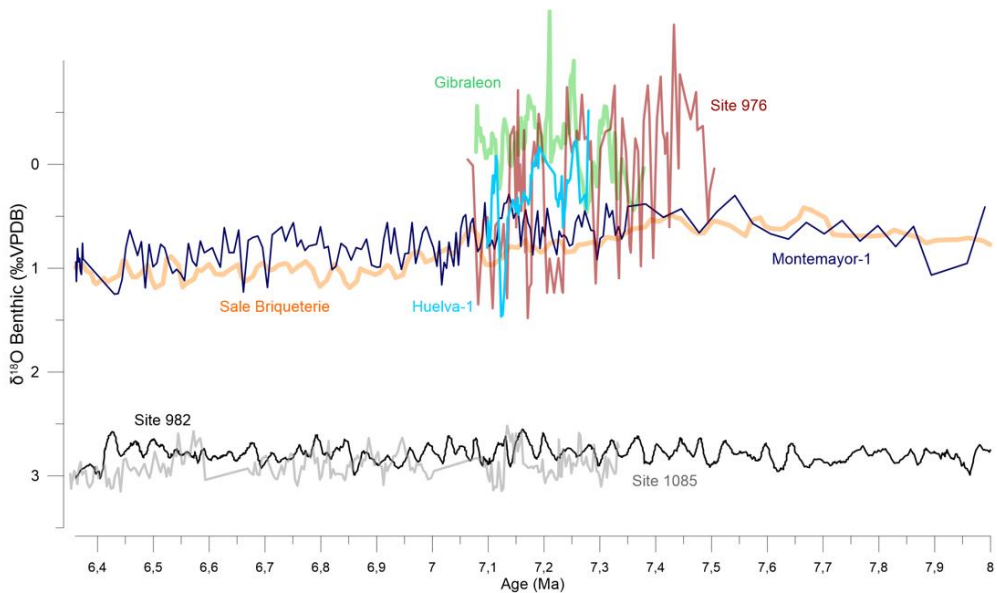


Figure 11: Comparison between benthic $\delta^{18}\text{O}$ records of Montemayor-1 borehole in blue (this study), North Atlantic ODP Site 982 in black (Hodell et al., 2001; Drury et al., 2018), South Atlantic Site 1085 (Vidal et al., 2002) in grey, Salé Briqueterie drill core in orange (Hodell et al., 1994), Alboran Basin Site 976 (Bulian et al., in press), Gibrleon quarry in green (Hilgen, unpublished data) and Huelva-1 core in light blue (Sierro, unpublished). To compare the absolute values of the curves, the isotope records that were measured on other benthic foraminifer species than for Montemayor-1 were corrected according to their offset with respect to *C. pachyderma* reported in literature. The Sale Briqueterie, Gibrleon and Huelva-1 records were obtained from *P. ariminensis* and to correct its offset the correction factors were taken from Van der Laan et al. (2006, Loulja section, Morocco), where $\delta^{18}\text{O}$ analyses performed both on *C. pachyderma* and *P. ariminensis* showed an interspecific offset of 0.065‰. When the isotopic record was obtained measuring *C. wuellerstorfi* or *C. mundulus* (ODP sites 982) no correction has been applied because no offset has been found between these species and *C. pachyderma* (Hodell et al., 2001; Holbourn et al., 2007; Holbourn et al., 2018).

In the lower interval of Montemayor-1 core, the benthic and planktic $\delta^{18}\text{O}$ record shows a very similar trend but are not in phase (Figure 4) until 7.14 – 7.15 Ma. This opposite relationship can suggest the presence of two water masses, one Atlantic and one Mediterranean implying an Atlantic – Mediterranean connection through the GB. After 7.14 – 7.15 Ma the two records start having the same phase relationship (Figure 4) and follows the benthic Atlantic $\delta^{18}\text{O}$ trend (Figure 11) as well which can suggest the presence of the same water mass in the entire water column, probably of Atlantic origin. This could mean that around 7.15-7.14 Ma the Mediterranean Outflow Water (MOW) through the GB was reduced, and that the only water mass bathing the Montemayor-1 site was Atlantic. Nonetheless, higher in the record, this relationship is not so straightforward in some places, which may be related with the data resolution in this part of the section in comparison to the middle and top parts, where this relationship is clearly visible (Pérez- Asensio et al., 2012; Van den Berg et al., 2015).

Not only the phase relationship but also the values of the $\delta^{18}\text{O}$ change at 7.14 – 7.15 Ma. At this time the constant benthic $\delta^{18}\text{O}$ Montemayor-1 record starts showing increasingly heavier values up core, which is also visible from the Sale Briqueterie data and Huelva-1 core and has been reported from several other Moroccan sections (Hodell et al., 1989). The initial constant oxygen values paired with Mediterranean like numbers from Huelva-1 core can confirm a steady MOW flux (current values for the MOW range between 0.4 and 1.6 ‰, Sierro et al., 2020) while the progressively heavier $\delta^{18}\text{O}$ benthic values can be related with a cooler, more Atlantic water mass that replaced the Mediterranean water. Alternatively, the change in benthic $\delta^{18}\text{O}$ values can be related with increased ice volume and/or increased salinity and density of the water mass. Similarly, the oxygen isotopes from Site 976 displays an increasing upward tendency as well, but the values oscillated with much higher amplitudes caused by the increased sensitivity of a restricting basin (Bulian et al., 2021). While a rise in salinity could be expected in the progressively restricting Mediterranean Basin, in Montemayor-1 Site a global change in temperature might also be present. The latter could be caused by the Late Miocene Global cooling, when SST decreases of around 6°C was derived (Tzanova et al., 2015; Herbert et al., 2016; Holbourn et al., 2018) from organic U^{K}_{37} proxy. This trend is not visible in the Atlantic sites 982 and 1085 nor in Gibraleon quarry. The Atlantic Sites 982 and 1085 show much heavier but stable values, which suggests that the global cooling was not induced by sea level change but other forcing. Some authors hypothesized that the cessation of the MOW could be the cause of the cooling because this would have altered the thermohaline circulation of the North Atlantic (e.g., Pérez-Asensio et al., 2012; Pérez-Asensio et al., 2013; Capella et al., 2019). The Gibraleon benthic $\delta^{18}\text{O}$ data yields much lighter values and after an initial increasing

upward trend from 7.4 to 7.3 Ma, where values coincide with Mediterranean ones it stabilizes around lighter values. This could have been the result of the presence of a Mediterranean water mass with values similar as in the Alboran Basin, while at the deeper sites such as Montemayor-1 the water signal would have been Atlantic. This could be similar to what we have today in the Gulf of Cadiz where the MOW is present between 500 and 1500 m, while above and below Atlantic water can be found. Alternatively, because of the lower depth of Gibraleon, the water column temperature might have been higher than in the deeper Montemayor-1 core explaining the much lighter benthic $\delta^{18}\text{O}$ measurements. Considering that the most probably after 7.15 - 7.17 Ma the MOW was much weaker or not present at all, the second hypothesis is more likely (see following Section 6.2.2).

6.2.2 *First signs of Guadalquivir Corridor isolation*

At 7.18 Ma, Van den Berg et al. (2018) finds in the geochemical records of Huelva-1 borehole located in the GB basin an increase in cycle amplitude. The authors relate this change with an enhanced reaction to climate forcing due to the restriction of the Betic corridor. The restriction, most likely caused by the uplift of the Gibraltar arch area (Sanz de Galdeano and Alfaro, 2004; Iribarren et al., 2009; Garcia-Castellanos and Villaseñor, 2011), is evident, almost contemporaneously (7.167 Ma) from several Mediterranean records (e.g., Kouwenhoven et al., 1999; Seidenkrantz et al., 2000; Kouwenhoven et al., 2003; Kouwenhoven and Van der Zwaan, 2006; Di Stefano et al., 2010; Bulian et al., 2021) where it manifests as a reduction in bottom water ventilation.

In the new geochemical and micropaleontological dataset of Montemayor-1 core here presented, a sharp change is registered in several records around the same time (7.17 - 7.15 Ma; Figure 12). From 7.17 Ma, the PC1 values rise which can be related with an increase in terrigenous versus biogenic input to the basin possibly connected with the increased river erosion due to the intense tectonic activity. Concordantly, at 7.2 Ma Sierro et al. (1990), Sierro et al. (1996) and Ledesma (2000) report the emplacement of the last olistostrome in GB and the shallowing of the area which got progressively filled with sediments. Analogous changes in input have been found at Alboran Basin Site 976 (Bulian et al., 2021) and have been interpreted as a consequence of the uplift as well. Curiously, while the overall terrigenous input increases at Montemayor-1 site, the Si/K ratio decreases which can be due to either a decrease in siliciclastic accumulation, or to reduced bottom water currents (de Castro et al., 2021) and accumulation of finer sediments rich in K (Lopez et al., 2006). A reduced bottom current and finer grain sizes are in line with the cessation of the MOW through one of the last Betic branches, the Guadalorce (Van der Schee et al., 2018b) or the

Granada corridors which were restricting since the latest Tortonian and could therefore represent the definite closure of the connection between the Mediterranean and Atlantic through the Betics. This has been implied by the change towards heavier benthic $\delta^{18}\text{O}$ values as well (see previous section). A recent study performed on Site U1389, located in the main descending core of the MOW in the Gulf of Cadiz shows how beds with no sand are linked with periods of weak MOW and lighter benthic $\delta^{13}\text{C}$ values that correspond with phases of sapropel deposition in the Mediterranean Basin (Sierra et al., 2020). Similarly, contemporaneously with the decrease in Si/K ratio, at Montemayor-1 site benthic and planktic $\delta^{13}\text{C}$ values start decreasing (Figure 11), while in the Mediterranean reduced bottom water oxygen levels are implied by the change in benthic fauna at a basin scale (e.g., Kouwenhoven et al., 1999; Seidenkrantz et al., 2000; Kouwenhoven et al., 2003; Kouwenhoven and Van der Zwaan, 2006; Di Stefano et al., 2010; Bulian et al., 2021) and by the more common sapropel deposition in the eastern sectors of the basin (Nijenhuis et al., 1996; Negri and Villa, 2000; Seidenkrantz et al., 2000).

The benthic $\delta^{13}\text{C}$ signal at Montemayor-1 can be influenced by a variety of processes, including global changes in carbon budget, residence time of bottom water masses and efficiency of organic matter degradation by microbial action (Mackensen and Schmiedl, 2019 and references therein). Raddatz et al. (2011) studying the benthic $\delta^{13}\text{C}$ signal in the Pleistocene Gulf of Cadiz relates heavier values with an efficient MOW and therefore low residence time, while lighter values could be caused by the presence of the nutrient-rich $\delta^{13}\text{C}$ -depleted Southern Component Water (SCW) which was found to replace the MOW at intermediate depth during glacial periods. This explains why lighter benthic $\delta^{13}\text{C}$ values are registered after 7.16 Ma in Montemayor-1 site as well and why the isotope signal could possibly include both a global and local component. The low $\delta^{13}\text{C}$ values may imply local changes and an increased bottom water residence and reduced ventilation related to the cessation of the MOW. Reduced ventilation can be implied by the higher Cr%wt, which usually accumulates in marine sediments under suboxic conditions (Calvert and Pedersen, 2007). Nonetheless, other proxies of reduced oxygen content, %wt V (Hübner et al., 2003; Calvert and Pedersen, 2007) and Mn/Fe (Spofforth et al., 2008), tells the opposite, and with its lower values would suggest higher oxygen levels. One possible explanation for this discrepancy could lay in the very low concentration of the V and Cr, which could have made the measurements unreliable. Furthermore, apart from the local signal a global one could be superimposed in the Montemayor-1 $\delta^{13}\text{C}$ record. Between 7.5 and 5.5 Ma, the Late Miocene Carbon Isotope Shift (LMCIS) took place at a global scale resulting in a decrease of approximately 1 ‰ of the global $\delta^{13}\text{C}$ of oceanic dissolved inorganic carbon ($\delta^{13}\text{C}_{\text{DIC}}$) (Hodell et al., 1994; Hodell et al., 2001; Hodell and Venz- Curtis, 2006).

From 7.15 Ma, the GB witnessed another marked change, an increase in the % of WOWPF. The proliferation of warmer species may suggest higher surface water temperatures and water column stratification which we would not expect if considering the dominance of colder Atlantic water mass or of an Atlantic Upwelled Water (Pérez-Asensio et al., 2014) in the GB. Consequently, considering the concomitant shallowing of the basin and the reduction of the bottom water ventilation, we can assume that the heavier benthic $\delta^{18}\text{O}$ values are not related with a global scale cooling but rather with a local cooling associated to a change in the source of bottom waters due to reduced advection of the warmer Mediterranean water and its replacement by colder Atlantic intermediate water as the basin became more and more isolated from the Mediterranean.

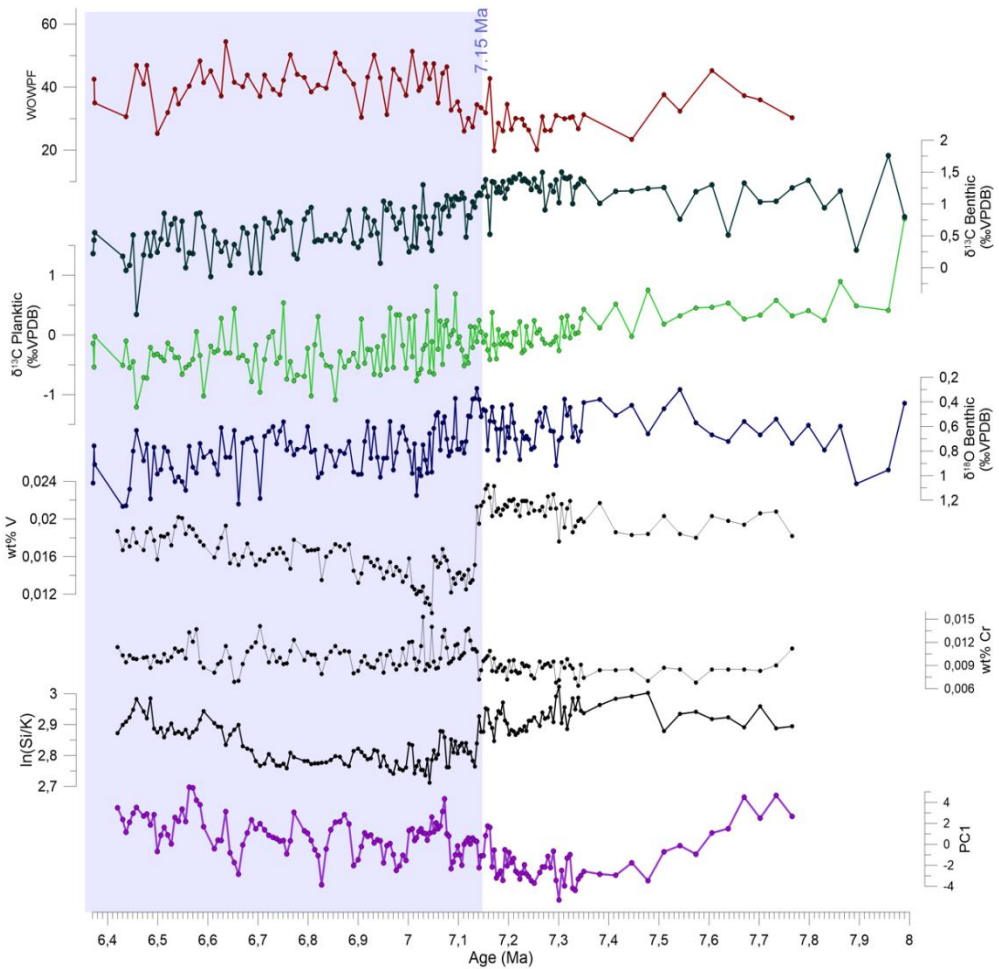


Figure 12: The Montemayor-1 lower interval where changes can be identified from 7.15-7.16 Ma.

Thus, the uplift of the Gibraltar arch registered from 7.15 – 7.17 Ma probably led to the disconnection between the GB and the Mediterranean resulting in a progressive shallowing and warming of the basin, its rapid infilling by fine terrigenous material, and reduction of the MOW advection to the GB. On the other hand, the lower $\delta^{13}\text{C}$ values could have been both related with the disconnection from the Mediterranean and the global LMCIS. This new evidence discard previous theories which, based on low resolution isotope data considered that the Betic corridor disconnection happened only at 6.18 Ma (Martín et al., 2001; Martín et al., 2009; Pérez- Asensio et al., 2012), and supports theories considering a late Tortonian – early Messinian closure of the connection (e.g., Ledesma, 2000; Flecker et al., 2015; Van der Schee et al., 2018a).

7. Conclusions

The newly acquired stable isotope and elemental data from the lower interval of Montemayor-1 core (236-257.3 mcd = 6.37 Ma – 8 Ma) enabled a high-resolution astronomical tuning. Low sedimentation rates that characterize this interval did not allow the recognition of a precessional cyclicity, but revealed eccentricity cycles modulated by precession, which, together with the new planktic foraminifer bioevents, were used for the astronomical tuning.

The complete elemental and stable isotope Montemayor-1 record from the late Tortonian (8 Ma) to the base on the Pliocene (5.3 Ma), made possible the identification of three different intervals (low, middle and upper), characterized by distinct sedimentation rates and terrigenous-carbonate phase relationships. The lower and middle interval sedimentation rates were relatively low (5 – 20 cm/kyr), and display a common precession forced cyclical change with increased terrigenous input during Northern Hemisphere Summer Insolation maxima and increased biogenic carbonate rich material during Northern Hemisphere Summer insolation minima. In contrast, the upper interval, as already pointed out by Van den Berg et al. (2015), shows very high sedimentation rates (20 – 90 cm/kyr) and an opposite phase relationship. In this work, the new planktic foraminifer data confirms the previously proposed mechanism, considering that the shallowing of the GB allowed for coarser sediment to reach Montemayor-1 site while the colder and arid climate present during Northern Hemisphere insolation minima had a negative effect on the vegetation cover resulting in more erosion and terrigenous input in the basin at the expense of the biogenic carbonate.

Based on the new age model, the events of increase terrigenous input, bottom water residence time, temperature, salinity and the shallowing registered in the GB from 7.15 – 7.17 Ma are contemporaneous with changes

reported from numerous Mediterranean locations (e.g., Kouwenhoven et al., 1999; Seidenkrantz et al., 2000; Kouwenhoven et al., 2003; Kouwenhoven and Van der Zwaan, 2006; Di Stefano et al., 2010; Bulian et al., 2021). Here, from 7.17 Ma increased bottom water residence time and decreased bottom oxygenation have been inferred from stable isotope and micropaleontological data. Therefore, the 7.15 – 7.17 event in Montemayor-1 core may be associated with the reduction of the MOW as a consequence of the restriction of the last Betic corridor, the GC.

Nonetheless, because this event is contemporaneous with the LMICS and the late Miocene global cooling, we cannot exclude that part of the signal contained in the geochemical and micropaleontological data reflects these global events, even if probably only for the minor part.

Acknowledgments

The authors appreciate the work of Jose Ignacio Martin Cruz in sample processing and preparation. Furthermore, all fellow ESRs and supervisors from the SALTGIANT project are thanked for their valuable suggestions and discussions. We would also like to thank Nucleus, in particular the Area of Instrumental Techniques, X-ray Diffraction team of Salamanca University that performed the X-ray geochemical analyses on our samples. This research leading to these results has received funding from the European Union's Horizon 2020 research and innovation program under the Marie Skłodowska-Curie grant agreement n° 765256 SALTGIANT.

References

- Achalhi, M., Münch, P., Cornée, J.-J., Azdimoussa, A., Melinte-Dobrinescu, M., Quillévéré, F., Drinia, H., Fauquette, S., Jiménez-Moreno, G., Merzeraud, G., Moussa, A. B., El Kharim, Y. and Feddi, N., 2016. The late Miocene Mediterranean-Atlantic connections through the North Rifian Corridor: New insights from the Boudinar and Arbaa Taourirt basins (northeastern Rif, Morocco). *Palaeogeography, Palaeoclimatology, Palaeoecology*, 459: 131-152.
- Aguirre, J., 1992. Evolución de las asociaciones fósiles del Plioceno medio de Cabo de Roche (Cadiz). *Revista española de paleontología*(3): 3-10.
- Anthonissen, D. E. and Ogg, J. G., 2012. Cenozoic and Cretaceous biochronology of planktonic foraminifera and calcareous nannofossils, *The geologic time scale*. Elsevier, pp. 1083-1127.

- Benson, R. H., Rakic- El Bied, K. and Bonaduce, G., 1991. An important current reversal (influx) in the Rifian Corridor (Morocco) at the Tortonian- Messinian boundary: The end of Tethys Ocean. *Paleoceanography*, 6(1): 165-192.
- Berástegui, X., Banks, C., Puig, C., Taberner, C., Waltham, D. and Fernández, M., 1998. Lateral diapiric emplacement of Triassic evaporites at the southern margin of the Guadalquivir Basin, Spain. *Geological Society, London, Special Publications*, 134(1): 49-68.
- Betzler, C., Braga, J. C., Martín, J. M., Sanchez-Almazo, I. M. and Lindhorst, S., 2006. Closure of a seaway: stratigraphic record and facies (Guadix basin, Southern Spain). *International Journal of Earth Sciences*, 95(5): 903-910.
- Bialik, O. M., Frank, M., Betzler, C., Zammit, R. and Waldmann, N. D., 2019. Two-step closure of the Miocene Indian Ocean Gateway to the Mediterranean. *Scientific reports*, 9(1): 1-10.
- Blanc, P.-L., 2002. The opening of the Plio-Quaternary Gibraltar Strait: assessing the size of a cataclysm. *Geodinamica acta*, 15(5-6): 303-317.
- Braga, J. C., Martín, J. M. and Quesada, C., 2003. Patterns and average rates of late Neogene-Recent uplift of the Betic Cordillera, SE Spain. *Geomorphology*, 50(1-3): 3-26.
- Bulian, F., Sierro, F. J., Ledesma, S., Jiménez-Espejo, F. J. and Bassetti, M.-A., 2021. Messinian West Alboran Sea record in the proximity of Gibraltar: Early signs of Atlantic-Mediterranean gateway restriction. *Marine Geology*: 106430.
- Calvert, S. and Pedersen, T., 2007. Chapter fourteen elemental proxies for palaeoclimatic and palaeoceanographic variability in marine sediments: interpretation and application. *Developments in Marine Geology*, 1: 567-644.
- Capella, W., Barhoun, N., Flecker, R., Hilgen, F., Kouwenhoven, T., Matenco, L., Sierro, F. J., Tulbure, M., Yousfi, M. Z. and Krijgsman, W., 2018. Palaeogeographic evolution of the late Miocene Rifian Corridor (Morocco): reconstructions from surface and subsurface data. *Earth-Science Reviews*, 180: 37-59.
- Capella, W., Flecker, R., Hernández-Molina, F. J., Simon, D., Meijer, P. T., Rogerson, M., Sierro, F. J. and Krijgsman, W., 2019. Mediterranean isolation preconditioning the Earth System for late Miocene climate cooling. *Scientific Reports*, 9(1).
- Capella, W., Spakman, W., van Hinsbergen, D. J., Chertova, M. V. and Krijgsman, W., 2020. Mantle resistance against Gibraltar slab dragging as a key cause of the Messinian Salinity Crisis. *Terra Nova*, 32(2): 141-150.
- CIESM, 2008. The Messinian salinity crisis from mega-deposits to microbiology. In: Briand, F. (Ed.), A consensus report, in 33ème CIESM Workshop Monographs, 33. CIESM, 16, bd de Suisse, MC-98000, Monaco: pp. 1-168.

- Corbí, H., Lancis, C., García-García, F., Pina, J.-A., Soria, J. M., Tent-Manclús, J. E. and Viseras, C., 2012. Updating the marine biostratigraphy of the Granada Basin (central Betic Cordillera). Insight for the Late Miocene palaeogeographic evolution of the Atlantic-Mediterranean seaway. *Geobios*, 45(3): 249-263.
- Davis, J. C. and Sampson, R. J., 1986. *Statistics and data analysis in geology*, 646. Wiley New York et al.
- de Castro, S., Hernández- Molina, F. J., de Weger, W., Jiménez- Espejo, F. J., Rodríguez- Tovar, F. J., Mena, A., Llave, E. and Sierro, F. J., 2021. Contourite characterization and its discrimination from other deep- water deposits in the Gulf of Cadiz contourite depositional system. *Sedimentology*, 68(3): 987-1027.
- Di Stefano, A., Verducci, M., Lirer, F., Ferraro, L., Iaccarino, S. M., Hüsing, S. K. and Hilgen, F. J., 2010. Paleoenvironmental conditions preceding the Messinian Salinity Crisis in the Central Mediterranean: integrated data from the Upper Miocene Trave section (Italy). *Palaeogeography, Palaeoclimatology, Palaeoecology*, 297(1): 37-53.
- Drury, A. J., Westerhold, T., Hodell, D. and Röhl, U., 2018. Reinforcing the North Atlantic backbone: revision and extension of the composite splice at ODP Site 982. *Climate of the Past*, 14(3): 321-338.
- Fadil, A., Vernant, P., McClusky, S., Reilinger, R., Gomez, F., Ben Sari, D., Mourabit, T., Feigl, K. and Barazangi, M., 2006. Active tectonics of the western Mediterranean: Geodetic evidence for rollback of a delaminated subcontinental lithospheric slab beneath the Rif Mountains, Morocco. *Geology*, 34(7): 529-532.
- Ferreira, J. N. A. G., 2016. Foraminíferos de Montemayor-1 (Huelva, Espanha) e inferência das mudanças climáticas de há 5, 6 a 5, 5 Ma.
- Flecker, R., Krijgsman, W., Capella, W., De Castro Martins, C., Dmitrieva, E., Mayser, J. P., Marzocchi, A., Modestou, S., Ochoa, D., Simon, D., Tulbure, M., Van Den Berg, B., Van Der Schee, M., De Lange, G., Ellam, R., Govers, R., Gutjahr, M., Hilgen, F., Kouwenhoven, T., Lofi, J., Meijer, P., Sierro, F. J., Bachiri, N., Barhoun, N., Alami, A. C., Chacon, B., Flores, J. A., Gregory, J., Howard, J., Lunt, D., Ochoa, M., Pancost, R., Vincent, S. and Yousfi, M. Z., 2015. Evolution of the Late Miocene Mediterranean-Atlantic gateways and their impact on regional and global environmental change. *Earth-Science Reviews*, 150: 365-392.
- García-Castellanos, D., Estrada, F., Jiménez-Munt, I., Gorini, C., Fernández, M., Vergés, J. and De Vicente, R., 2009. Catastrophic flood of the Mediterranean after the Messinian salinity crisis. *Nature*, 462(7274): 778.
- García-Castellanos, D. and Villaseñor, A., 2011. Messinian salinity crisis regulated by competing tectonics and erosion at the Gibraltar arc. *Nature*, 480(7377): 359.
- García- Castellanos, D., Fernandez, M. and Torné, M., 2002. Modeling the evolution of the Guadalquivir foreland basin (southern Spain). *Tectonics*, 21(3): 9-1-9-17.
- González-Delgado, J. A., Civis, J., Dabrio, C. J., Goy, J. L., Ledesma, S. and Pais, J., 2004. Cuenca del Guadalquivir. in *Geología de España*, ed. J. A. Vera (Madrid: SGE-IGME): 543-550.

- Hammer, Ø., Harper, D. A. and Ryan, P. D., 2001. PAST: Paleontological statistics software package for education and data analysis. *Palaeontologia Electronica*, 4(1): 9.
- Herbert, T. D., Lawrence, K. T., Tzanova, A., Peterson, L. C., Caballero-Gill, R. and Kelly, C. S., 2016. Late Miocene global cooling and the rise of modern ecosystems. *Nature Geoscience*, 9(11): 843-847.
- Hilgen, F., Bissoli, L., Iaccarino, S., Krijgsman, W., Meijer, R., Negri, A. and Villa, G., 2000a. Integrated stratigraphy and astrochronology of the Messinian GSSP at Oued Akrech (Atlantic Morocco). *Earth and Planetary Science Letters*, 182(3-4): 237-251.
- Hilgen, F., Iaccarino, S., Krijgsman, W., Villa, G., Langereis, C. and Zachariasse, W., 2000b. The global boundary stratotype section and point (GSSP) of the Messinian Stage (uppermost Miocene). *Episodes*, 23(3): 172-178.
- Hilgen, F., Kuiper, K., Krijgsman, W., Snel, E. and van der Laan, E., 2007. Astronomical tuning as the basis for high resolution chronostratigraphy: the intricate history of the Messinian Salinity Crisis. *Stratigraphy*, 4(2-3): 231-238.
- Hodell, D., Crowhurst, S., Skinner, L., Tzedakis, P. C., Margari, V., Channell, J. E., Kamenov, G., Maclachlan, S. and Rothwell, G., 2013. Response of Iberian Margin sediments to orbital and suborbital forcing over the past 420 ka. *Paleoceanography*, 28(1): 185-199.
- Hodell, D. A., Benson, R. H., Kennett, J. P. and Rakic- El Bied, K., 1989. Stable isotope stratigraphy of latest Miocene sequences in northwest Morocco: the Bou Regreg section. *Paleoceanography*, 4(4): 467-482.
- Hodell, D. A., Benson, R. H., Kent, D. V., Boersma, A. and Rakic- El Bied, K., 1994. Magnetostratigraphic, biostratigraphic, and stable isotope stratigraphy of an Upper Miocene drill core from the Salé Briqueterie (northwestern Morocco): A high-resolution chronology for the Messinian stage. *Paleoceanography*, 9(6): 835-855.
- Hodell, D. A., Curtis, J. H., Sierro, F. J. and Raymo, M. E., 2001. Correlation of late Miocene to early Pliocene sequences between the Mediterranean and North Atlantic. *Paleoceanography*, 16(2): 164-178.
- Hodell, D. A. and Venz- Curtis, K. A., 2006. Late Neogene history of deepwater ventilation in the Southern Ocean. *Geochemistry, Geophysics, Geosystems*, 7(9).
- Holbourn, A., Kuhnt, W., Schulz, M., Flores, J.-A. and Andersen, N., 2007. Orbitally-paced climate evolution during the middle Miocene "Monterey" carbon-isotope excursion. *Earth and Planetary Science Letters*, 261(3-4): 534-550.
- Holbourn, A. E., Kuhnt, W., Clemens, S. C., Kochhann, K. G., Jöhnck, J., Lübbers, J. and Andersen, N., 2018. Late Miocene climate cooling and intensification of southeast Asian winter monsoon. *Nature communications*, 9(1): 1-13.
- Hsü, K. J., Ryan, W. B. F. and Cita, M. B., 1973. Late miocene desiccation of the mediterranean. *Nature*, 242(5395): 240-244.

- Hübner, A., De Lange, G., Dittmer, J. and Halbach, P., 2003. Geochemistry of an exotic sediment layer above sapropel S-1: mud expulsion from the Urania Basin, eastern Mediterranean? *Marine geology*, 197(1-4): 49-61.
- Hüsing, S., Kuiper, K., Link, W., Hilgen, F. J. and Krijgsman, W., 2009. The upper Tortonian–lower Messinian at Monte dei Corvi (Northern Apennines, Italy): completing a Mediterranean reference section for the Tortonian stage. *Earth and Planetary Science Letters*, 282(1-4): 140-157.
- Hüsing, S., Oms, O., Agustí, J., Garcés, M., Kouwenhoven, T., Krijgsman, W. and Zachariasse, W.-J., 2010. On the late Miocene closure of the Mediterranean–Atlantic gateway through the Guadix basin (southern Spain). *Palaeogeography, Palaeoclimatology, Palaeoecology*, 291(3-4): 167-179.
- Iribarren, L., Vergés, J. and Fernández, M., 2009. Sediment supply from the Betic–Rif orogen to basins through Neogene. *Tectonophysics*, 475(1): 68-84.
- Jiménez-Moreno, G., Pérez-Asensio, J. N., Larrasoaña, J. C., Aguirre, J., Civis, J., Rivas-Carballo, M. R., Valle-Hernández, M. F. and González-Delgado, J. A., 2013. Vegetation, sea-level, and climate changes during the Messinian salinity crisis. *Bulletin*, 125(3-4): 432-444.
- Kouwenhoven, T., Seidenkrantz, M.-S. and Van der Zwaan, G., 1999. Deep-water changes: the near-synchronous disappearance of a group of benthic foraminifera from the Late Miocene Mediterranean. *Palaeogeography, Palaeoclimatology, Palaeoecology*, 152(3-4): 259-281.
- Kouwenhoven, T. J., 2000. Survival under stress: benthic foraminiferal patterns and Cenozoic biotic crises. *Faculteit Aardwetenschappen*.
- Kouwenhoven, T. J., Hilgen, F. J. and Van Der Zwaan, G. J., 2003. Late Tortonian–early Messinian stepwise disruption of the Mediterranean–Atlantic connections: constraints from benthic foraminiferal and geochemical data. *Palaeogeography, Palaeoclimatology, Palaeoecology*, 198(3-4): 303-319.
- Kouwenhoven, T. V. and Van der Zwaan, G., 2006. A reconstruction of late Miocene Mediterranean circulation patterns using benthic foraminifera. *Palaeogeography, Palaeoclimatology, Palaeoecology*, 238(1-4): 373-385.
- Krijgsman, W., Langereis, C., Zachariasse, W., Boccaletti, M., Moratti, G., Gelati, R., Iaccarino, S., Papani, G. and Villa, G., 1999. Late Neogene evolution of the Taza–Guercif Basin (Rifian Corridor, Morocco) and implications for the Messinian salinity crisis. *Marine Geology*, 153(1-4): 147-160.
- Krijgsman, W. and Langereis, C., 2000. Magnetostratigraphy of the Zobzit and Koudiat Zarga sections (Taza–Guercif basin, Morocco): implications for the evolution of the Rifian Corridor. *Marine and Petroleum Geology*, 17(3): 359-371.
- Krijgsman, W. and Meijer, P. T., 2008. Depositional environments of the Mediterranean “Lower Evaporites” of the Messinian salinity crisis: Constraints from quantitative analyses. *Marine Geology*, 253(3-4): 73-81.

- Larrasoana, J., González-Delgado, J., Civis, J., Sierro, F., Alonso-Gavilán, G. and Pais, J., 2008. Magnetobiostratigraphic dating and environmental magnetism of Late Neogene marine sediments recovered at the Huelva-1 and Montemayor-1 boreholes (lower Guadalquivir basin, Spain). *Geo-Temas*, 10: 1175-1178.
- Larrasoana, J. C., Liu, Q., Hu, P., Roberts, A. P., Mata, P., Civis, J., Sierro, F. J. and Pérez-Asensio, J. N., 2014. Paleomagnetic and paleoenvironmental implications of magnetofossil occurrences in late Miocene marine sediments from the Guadalquivir Basin, SW Spain. *Frontiers in microbiology*, 5: 71.
- Laskar, J., Robutel, P., Joutel, F., Gastineau, M., Correia, A. and Levrard, B., 2004. A long-term numerical solution for the insolation quantities of the Earth. *Astronomy & Astrophysics*, 428(1): 261-285.
- Ledesma, S., 2000. Astrobiocronología y estratigrafía de alta resolución del Neógeno de la Cuenca del Guadalquivir-Golfo de Cádiz. PhD thesis, Universidad de Salamanca, 464.
- Lirer, F., Foresi, M., Iaccarino, S., Salvatorini, G., Turco, E., Cosentino, C., Sierro, F. J. and Caruso, A., 2019. Mediterranean Neogene planktonic foraminifer biozonation and biochronology. *Earth-Science Reviews*, 196: 102869.
- Lopez, P., Navarro, E., Marce, R., Ordoñez, J., Caputo, L. and Armengol, J., 2006. Elemental ratios in sediments as indicators of ecological processes in Spanish reservoirs. *limnetica*, 25(1-2): 499-512.
- Lourens, L., 2004. 21 The Neogene Period. *A geologic time scale 2004*: 409-440.
- Lourens, L. J., Hilgen, F., Shackleton, N., Laskar, J. and Wilson, J., 2004. The Neogene Period. In F. M. Gradstein, J. G. Ogg, & A. G. Smith (Eds.), *A geologic time scale 2004*: 409-440.
- Mackensen, A. and Schmiedl, G., 2019. Stable carbon isotopes in paleoceanography: atmosphere, oceans, and sediments. *Earth-Science Reviews*, 197: 102893.
- Mancilla, F. d. L., Booth-Rea, G., Stich, D., Pérez-Peña, J. V., Morales, J., Azañón, J. M., Martín, R. and Giaconia, F., 2015. Slab rupture and delamination under the Betics and Rif constrained from receiver functions. *Tectonophysics*, 663: 225-237.
- Martín, J. M., Braga, J. C. and Betzler, C., 2001. The Messinian Guadalhorce corridor: the last northern, Atlantic-Mediterranean gateway. *Terra Nova*, 13(6): 418-424.
- Martín, J. M., Braga, J. C., Aguirre, J. and Puga-Bernabéu, Á., 2009. History and evolution of the North-Betic Strait (Prebetic Zone, Betic Cordillera): a narrow, early Tortonian, tidal-dominated, Atlantic-Mediterranean marine passage. *Sedimentary Geology*, 216(3-4): 80-90.
- Martín, J. M., Puga-Bernabéu, A., Aguirre, J. and Braga, J. C., 2014. Miocene Atlantic-Mediterranean seaways in the Betic Cordillera (Southern Spain). *Revista de la sociedad geológica de España*, 27(1): 175-186.

- Marzocchi, A., Flecker, R., Van Baak, C. G., Lunt, D. J. and Krijgsman, W., 2016. Mediterranean outflow pump: An alternative mechanism for the Lago-mare and the end of the Messinian Salinity Crisis. *Geology*, 44(7): 523-526.
- Meijer, P. T. and Krijgsman, W., 2005. A quantitative analysis of the desiccation and re-filling of the Mediterranean during the Messinian Salinity Crisis. *Earth and Planetary Science Letters*, 240(2): 510-520.
- Micallef, A., Camerlenghi, A., Garcia-Castellanos, D., Otero, D. C., Gutscher, M.-A., Barreca, G., Spatola, D., Facchin, L., Geletti, R. and Krastel, S., 2018. Evidence of the Zanclean megaflood in the eastern Mediterranean Basin. *Scientific reports*, 8(1): 1078.
- Negri, A. and Villa, G., 2000. Calcareous nannofossil biostratigraphy, biochronology and paleoecology at the Tortonian/Messinian boundary of the Faneromeni section (Crete). *Palaeogeography, Palaeoclimatology, Palaeoecology*, 156(3-4): 195-209.
- Nijenhuis, I., Schenau, S., Van der Weijden, C., Hilgen, F., Lourens, L. and Zachariasse, W., 1996. On the origin of upper Miocene sapropelites: a case study from the Faneromeni section, Crete (Greece). *Paleoceanography*, 11(5): 633-645.
- Omodeo Salé, S., Gennari, R., Lugli, S., Manzi, V. and Roveri, M., 2012. Tectonic and climatic control on the Late Messinian sedimentary evolution of the Nijar Basin (Betic Cordillera, Southern Spain). *Basin Research*, 24(3): 314-337.
- Pérez-Asensio, J. N., Aguirre, J., Schmiedl, G. and Civis, J., 2012. Messinian paleoenvironmental evolution in the lower Guadalquivir Basin (SW Spain) based on benthic foraminifera. *Palaeogeography, Palaeoclimatology, Palaeoecology*, 326: 135-151.
- Pérez-Asensio, J. N., Aguirre, J., Jiménez-Moreno, G., Schmiedl, G. and Civis, J., 2013. Glacioeustatic control on the origin and cessation of the Messinian salinity crisis. *Global and Planetary Change*, 111: 1-8.
- Pérez-Asensio, J. N., Aguirre, J., Schmiedl, G. and Civis, J., 2014. Messinian productivity changes in the northeastern Atlantic and their relationship to the closure of the Atlantic-Mediterranean gateway: implications for Neogene palaeoclimate and palaeoceanography. *Journal of the Geological Society*, 171(3): 389-400.
- Pérez-Folgado, M., Sierro, F. J., Flores, J. A., Grimalt, J. O. and Zahn, R., 2004. Paleoclimatic variations in foraminifer assemblages from the Alboran Sea (Western Mediterranean) during the last 150 ka in ODP Site 977. *Marine Geology*, 212(1-4): 113-131.
- Pérez-Asensio, J. N., Aguirre, J., Schmiedl, G. and Civis, J., 2012. Impact of restriction of the Atlantic-Mediterranean gateway on the Mediterranean Outflow Water and eastern Atlantic circulation during the Messinian. *Paleoceanography*, 27(3).
- Popov, S. V., Rögl, F., Rozanov, A. Y., Steininger, F. F., Shcherba, I. G. and Kovac, M., 2004. Lithological-paleogeographic maps of Paratethys-10 maps late Eocene to pliocene.

- Raddatz, J., Rüggeberg, A., Margreth, S., Dullo, W.-C. and Expedition, I., 2011. Paleoenvironmental reconstruction of Challenger Mound initiation in the Porcupine Seabight, NE Atlantic. *Marine Geology*, 282(1-2): 79-90.
- Ragland, P. C., 1989. Basic analytical petrology.
- Rocha, S. C. d. S., 2017. Foraminíferos planctónicos de Montemayor-1 e relação com as variações orbitais, entre 5,77 e 5,61 Ma.
- Rohling, E. J. and Cooke, S., 1999. Stable oxygen and carbon isotopes in foraminiferal carbonate shells, *Modern Foraminifera*. Springer, pp. 239-258.
- Roveri, M. and Manzi, V., 2006. The Messinian salinity crisis: Looking for a new paradigm? *Palaeogeography, Palaeoclimatology, Palaeoecology*, 238(1-4): 386-398.
- Roveri, M., Bertini, A., Cosentino, D., Di Stefano, A., Gennari, R., Gliozzi, E., Grossi, F., Iaccarino, S. M., Lugli, S., Manzi, V. and Taviani, M., 2008a. A high-resolution stratigraphic framework for the latest Messinian events in the Mediterranean area. *Stratigraphy*, 5(3-4): 323-342.
- Roveri, M., Lugli, S., Manzi, V. and Schreiber, B. C., 2008b. The Messinian Sicilian stratigraphy revisited: New insights for the Messinian salinity crisis. *Terra Nova*, 20(6): 483-488.
- Roveri, M., Flecker, R., Krijgsman, W., Lofi, J., Lugli, S., Manzi, V., Sierro, F. J., Bertini, A., Camerlenghi, A. and De Lange, G., 2014. The Messinian Salinity Crisis: past and future of a great challenge for marine sciences. *Marine Geology*, 352: 25-58.
- Ryan, W. B., 1976. Quantitative evaluation of the depth of the western Mediterranean before, during and after the Late Miocene salinity crisis. *Sedimentology*, 23(6): 791-813.
- Salvany, J. M., Larrasoana, J. C., Mediavilla, C. and Rebollo, A., 2011. Chronology and tectono-sedimentary evolution of the Upper Pliocene to Quaternary deposits of the lower Guadalquivir foreland basin, SW Spain. *Sedimentary Geology*, 241(1-4): 22-39.
- Sanz de Galdeano, C. and Alfaro, P., 2004. Tectonic significance of the present relief of the Betic Cordillera. *Geomorphology*, 63(3-4): 175-190.
- Seidenkrantz, M.-S., Kouwenhoven, T., Jorissen, F., Shackleton, N. and Van der Zwaan, G., 2000. Benthic foraminifera as indicators of changing Mediterranean-Atlantic water exchange in the late Miocene. *Marine geology*, 163(1-4): 387-407.
- Selli, R., 1973. An outline of the Italian Messinian. *Messinian events in the Mediterranean*, 7: 150-171.
- Sierro, F., Delgado, J. G., Dabrio, C. and Flores, J., 1990. The Neogene of the Guadalquivir Basin (SW Spain).

- Sierro, F. J., 1985. The replacement of the “Globorotalia menardii” group by the Globorotalia miotumida group: An aid to recognizing the Tortonian-Messinian boundary in the Mediterranean and adjacent Atlantic. *Marine Micropaleontology*, 9(6): 525-535.
- Sierro, F. J., Flores, J. A., Civis, J., González Delgado, J. A. and Francés, G., 1993. Late Miocene globorotaliid event-stratigraphy and biogeography in the NE-Atlantic and Mediterranean. *Marine Micropaleontology*, 21(1-3): 143-167.
- Sierro, F. J., González-Delgado, A., Dabrio, C. J., Flores, A. and Civis, J., 1996. Late Neogene depositional sequences in the foreland basin of Guadalquivir (SW Spain). in *Tertiary Basins of Spain*, eds P. F. Friend and C. J. Dabrio (Cambridge: Cambridge University Press): 339-345.
- Sierro, F. J., Hilgen, F. J., Krijgsman, W. and Flores, J. A., 2001. The Abad composite (SE Spain): a Messinian reference section for the Mediterranean and the APTS. 168(1-2): 141-169.
- Sierro, F. J., Flores, J. A., Francés, G., Vazquez, A., Utrilla, R., Zamarreño, I., Erlenkeuser, H. and Barcena, M. A., 2003. Orbitally-controlled oscillations in planktic communities and cyclic changes in western Mediterranean hydrography during the Messinian. *Palaeogeography, Palaeoclimatology, Palaeoecology*, 190: 289-316.
- Sierro, F. J., Hodell, D. A., Andersen, N., Azibeiro, L. A., Jimenez- Espejo, F. J., Bahr, A., Flores, J. A., Ausin, B., Rogerson, M. and Lozano- Luz, R., 2020. Mediterranean overflow over the last 250 kyr: freshwater forcing from the tropics to the ice sheets. *Paleoceanography and Paleoclimatology*, 35(9): e2020PA003931.
- Spofforth, D. J., Pälike, H. and Green, D., 2008. Paleogene record of elemental concentrations in sediments from the Arctic Ocean obtained by XRF analyses. *Paleoceanography*, 23(1).
- Tjallingii, R., Röhl, U., Kölling, M. and Bickert, T., 2007. Influence of the water content on X- ray fluorescence core- scanning measurements in soft marine sediments. *Geochemistry, Geophysics, Geosystems*, 8(2).
- Tjalsma, R. C., 1971. Stratigraphy and foraminifera of the Neogene of the eastern Guadalquivir Basin (southern Spain), Utrecht University.
- Tulbure, M., Capella, W., Barhoun, N., Flores, J., Hilgen, F., Krijgsman, W., Kouwenhoven, T., Sierro, F. J. and Yousfi, M. Z., 2017. Age refinement and basin evolution of the North Rifian Corridor (Morocco): No evidence for a marine connection during the Messinian Salinity Crisis. *Palaeogeography, Palaeoclimatology, Palaeoecology*, 485: 416-432.
- Tzanova, A., Herbert, T. D. and Peterson, L., 2015. Cooling Mediterranean Sea surface temperatures during the Late Miocene provide a climate context for evolutionary transitions in Africa and Eurasia. *Earth and Planetary Science Letters*, 419: 71-80.

- Urgeles, R., Camerlenghi, A., Garcia- Castellanos, D., De Mol, B., Garcés, M., Vergés, J., Haslam, I. and Hardman, M., 2011. New constraints on the Messinian sealevel drawdown from 3D seismic data of the Ebro Margin, western Mediterranean. *Basin Research*, 23(2): 123-145.
- Van den Berg, B. C. J., Sierro, F. J., Hilgen, F. J., Flecker, R., Larrasoña, J. C., Krijgsman, W., Flores, J. A., Mata, M. P., Bellido Martín, E., Civis, J. and González-Delgado, J. A., 2015. Astronomical tuning for the upper Messinian Spanish Atlantic margin: Disentangling basin evolution, climate cyclicity and MOW. 135: 89-103.
- Van den Berg, B. C. J., Sierro, F. J., Hilgen, F. J., Flecker, R., Larrasoña, J. C., Krijgsman, W., Flores, J. A. and Mata, M. P., 2018. Imprint of Messinian Salinity Crisis events on the Spanish Atlantic margin. *Newsletters on Stratigraphy*, 51(1): 93-115.
- Van Der Laan, E., Hilgen, F. J., Lourens, L. J., De Kaenel, E., Gaborardi, S. and Iaccarino, S., 2012. Astronomical forcing of Northwest African climate and glacial history during the late Messinian (6.5–5.5Ma). *Palaeogeography, Palaeoclimatology, Palaeoecology*, 313-314: 107-126.
- Van der Schee, M., Van den Berg, B. C., Capella, W., Simon, D., Sierro, F. J. and Krijgsman, W., 2018a. New age constraints on the western Betic intramontane basins: A late Tortonian closure of the Guadalhorce Corridor? *Terra Nova*, 30(5): 325-332.
- Van der Schee, M., Van den Berg, B. C. J., Capella, W., Simon, D., Sierro, F. J. and Krijgsman, W., 2018b. New age constraints on the western Betic intramontane basins: A late Tortonian closure of the Guadalhorce Corridor? *Terra Nova*, 30(5): 325-332.
- Vidal, L., Bickert, T., Wefer, G. and Röhl, U., 2002. Late Miocene stable isotope stratigraphy of SE Atlantic ODP Site 1085: Relation to Messinian events. *Marine Geology*, 180(1-4): 71-85.
- Weltje, G. J. and Tjallingii, R., 2008. Calibration of XRF core scanners for quantitative geochemical logging of sediment cores: Theory and application. *Earth and Planetary Science Letters*, 274(3-4): 423-438.

Chapter 6

Reflooding and repopulation of
the Mediterranean Sea after the
Messinian Salinity Crisis: Benthic
foraminifer assemblages and
stable isotopes of Spanish basins

Chapter 6

Reflooding and repopulation of the Mediterranean Sea
after the Messinian Salinity Crisis: Benthic foraminifer
assemblages and stable isotopes of Spanish basins

Bulian F., Kouwenhoven T. J., Andersen N.,
Krijgsman W., Sierro F. J.

To be submitted to *Palaeography*,
Palaeoclimatology, *Palaeoecology*

Reflooding and repopulation of the Mediterranean Sea after the Messinian Salinity Crisis: Benthic foraminifer assemblages and stable isotopes of Spanish basins

Bulian F.^{1*}, Kouwenhoven T. J.², Andersen N.³, Krijgsman W.⁴, Sierro F. J.¹

¹ Dept. de Geología, Univ. de Salamanca, Plaza de los Caídos s/n, 37008,
Salamanca, Spain, e.mail: sierro@usal.es.

² Faculty of Earth Sciences, Utrecht University, The Netherlands.
e-mail: T.J.Kouwenhoven@uu.nl.

³ Leibniz-Laboratory for Radiometric Dating and Isotope Research,
Christian-Albrechts-Universität Kiel, Max-Eyth-Str.11-13, 24118 Kiel,
Germany, e-mail: nandersen@leibniz.uni-kiel.de.

⁴ Palaeomagnetic Laboratory Fort Hoofddijk, Utrecht University, Budapestlaan 17,
3584 CD, Utrecht, The Netherlands, e-mail: W.Krijgsman@uu.nl.

Abstract

Sedimentological, benthic foraminifer and stable isotope analyses performed on early Pliocene sediments from Alboran Basin ODP Site 976 and southern Spanish land-based sections in the Malaga, Nijar and Sorbas Basins enabled the reconstruction of the Mediterranean environmental conditions immediately after the Messinian Salinity Crisis. The presence at the Miocene – Pliocene boundary of a dark layer often enriched in organic matter, suggests that the Zanclean reflooding has created water column stratification, and reduced bottom water oxygen levels. Considering that such layer was found at deep and marginal locations further from the Gibraltar gateway/s, a Mediterranean scale water-mass stratification can be assumed. This scenario could be the result of sinking saline Atlantic waters inflowing into a less saline Mediterranean Basin still under the influence of the Paratethys. Similar environmental conditions have been suggested by the benthic foraminifer repopulation sequence identified which shows similarities with Recent assemblages repopulating hostile environments or recovery from low-oxic episodes during sapropel deposition. Nonetheless, Atlantic values of the benthic $\delta^{13}\text{C}$ registered in the Alboran basin suggest that bottom water renewal rates were quite high during the early Zanclean, preventing the reduction of $\delta^{13}\text{C}$ at the seafloor seen in the Messinian. These observations, paired with the gradual deepening of the basins suggests that the Zanclean reflooding led to a progressive shift from stressed and instable environments towards benthic associations typical of an efficient circulation and bottom water ventilation. Finally, considering some differences in the benthic foraminifer associations present after the Miocene – Pliocene boundary of the marginal basins, and the discrepancy between the bottom-water isotope values in

*Corresponding author: fra.bulian@usal.es

the Malaga Basin and the deep basin values, a diachronous reflooding of the shallower Mediterranean marginal basins seems a plausible scenario.

1. Introduction

Since the 1970's there is an ongoing debate regarding the end of the Messinian Salinity Crisis (MSC) and the exact dynamics of restoration of marine conditions. Through time three main reflooding scenarios were proposed: (1) an instantaneous inundation of an (almost) desiccated Mediterranean at 5.33 Ma, corresponding to the base of the Zanclean (Hsü, 1972; Blanc, 2002; Loget and Van Den Driessche, 2006; Garcia-Castellanos et al., 2009; García-Alix et al., 2016); (2) high Mediterranean water level during the latest Messinian with rapid restoration of the Atlantic-Mediterranean connection characterised by a minor sea-level rise across the Messinian-Zanclean transition (Loget et al., 2005; Pierre et al., 2006; Roveri and Manzi, 2006; Cornée et al., 2016; Marzocchi et al., 2016; Andreetto et al., 2021b) and (3) a two stage reflooding with the major reflooding taking place at 5.46 Ma, in the Messinian (Estrada et al., 2011; Bache et al., 2012; Pérez-Asensio et al., 2013; Bache et al., 2015). The three models differ not only in the dynamics of the reflooding itself, but also in the timing and base level fluctuations. To test and validate the most probable scenario it is necessary to better understand the palaeoenvironmental conditions present after the MSC and therefore to analyse the late Messinian - early Zanclean sedimentary record at locations close to the Mediterranean - Atlantic gateway.

In this work, we studied three onshore outcrops from Neogene basins in southern Spain which contain well preserved late Miocene-early Pliocene sedimentary successions: the Rio Mendelin section in the Malaga Basin, the Barranco del Negro section in the Nijar Basin and the Zorreras section in the Sorbas Basin. In addition, we analysed the early Zanclean sediments retrieved at ODP Site 976, in the West Alboran Basin, located in front of the Gibraltar gateway. During the late Miocene, these basins were part of the Mediterranean realm and consequently their sediments could have registered the first influx of Atlantic waters as well as the water levels and palaeoenvironmental conditions present at that time in the western Mediterranean. We performed a detailed benthic foraminifer and stable isotope analyses of these four sites to better understand the environmental changes that occurred in the Mediterranean after the MSC as well as the dynamics of the reflooding itself.

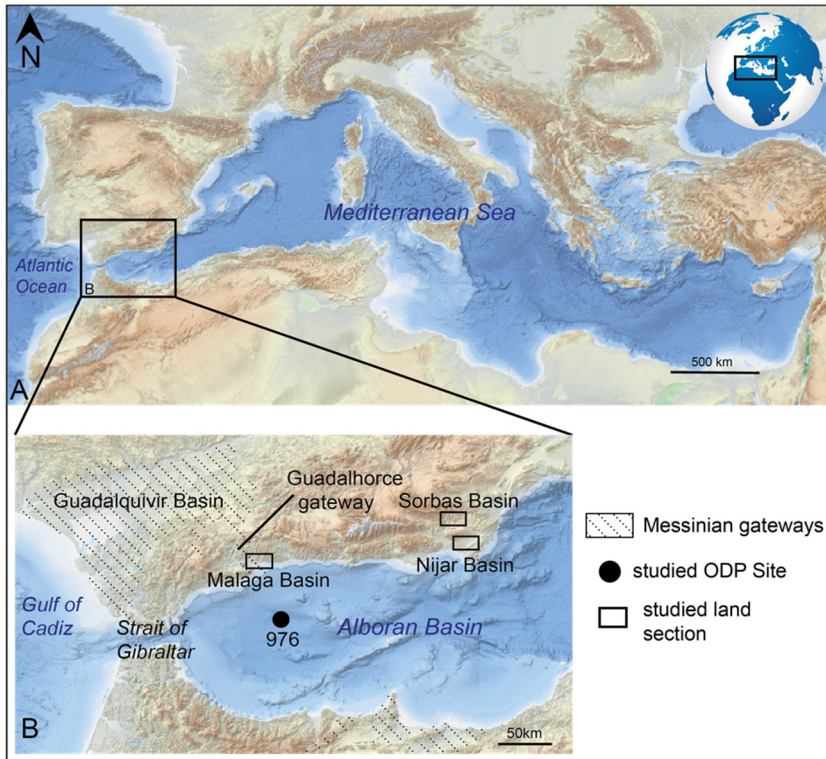


Figure 1: A) Bathymetric map of the Mediterranean region (from <https://portal.emodnet-bathymetry.eu/>) where the rectangle shows the studied area. B) Bathymetric map of the Alboran Basin. The black dot and rectangles indicate the studied ODP Site and onshore sections respectively. The dotted areas show the extension of the Messinian gateways (after Martín et al., 2014).

2. Geological setting

2.1 Neogene Basins of the Betic Cordillera

The Malaga Basin (Figure 1) is an intermontane E-W oriented basin located in the westernmost sector of the Betic Cordillera (Sanz De Galdeano and Vera, 1992). The basin is drained by the Guadalhorce River and bounded to the north by the Malaga Mountains, to the south by the Mijas Sierra and to the east by the Alboran Basin (Mediterranean Sea, Figure 1). Its post-orogenic infilling is composed of upper Tortonian to Quaternary sediments (e.g. Guerra-Merchán et al., 2008). The section analysed in this study (Rio Mendelín section; $36^{\circ}45'2.53''\text{N}$; $4^{\circ}25'57.26''\text{W}$) comprises late Messinian deposits related to the final stage of the MSC (Lago-Mare unit) and the lower Zanclean. The Lago-Mare (LM) unit is composed of two fining-upward sequences each constituted by a conglomeratic

lower member (alluvial fan environment) and a pelitic upper member (subaqueous environment), the two separated by an unconformity, a locally ferruginous hard erosive surface that laterally passes to a concordant contact (Guerra-Merchán et al., 2008; Guerra-Merchán et al., 2010). The Río Mendelín section is located in an ancient fluvial valley, incised during the latest Tortonian or during the MSC acme sea level drop, which, based on the Paratethyan affinity of its faunal content, was progressively refilled during the dilution phase at the end of the Messinian (Guerra-Merchán et al., 2010; Do Couto et al., 2014). The Pliocene sediments, deposited with an erosional contact at the margins and a gradual conformable contact in the centre of the basin on top of the LM unit (Figure 2), represent the re-establishment of normal marine conditions in the



Figure 2: Field photograph of the Miocene-Pliocene boundary in the Malaga Basin (Rio Mendelin section).

Malaga Basin. In this study, we analysed 23.5 m of the Rio Mendelin section, including 2 uppermost metres of the LM sequence followed, with a transitional contact, by early Pliocene sediments composed of 25 cm of yellow silty sediments, 25 cm of grey clays overlain by 20.5 metres of yellowish clays (Figure 5 A). The Nijar and Sorbas basins are intermontane basins developed above the metamorphic nappes of the southern Betics (Figure 1; Sanz De Galdeano and Vera, 1992). The sedimentary infilling of the basins occurred during the late Miocene (Tortonian and Messinian), Pliocene and Quaternary (Dabrio et al., 1981; Serrano, 1990; Omodeo Salé et al., 2012). During the Miocene, until the end of MSC Stage 1, the two basins were connected to the Mediterranean, which entered the Nijar Basin from the south and the Sorbas Basin through NW-SE trending corridors north of Nijar (Fortuin and Krijgsman, 2003).

In this work, the upper Messinian-lower Zanclean sediments from the Nijar and Sorbas basins have been studied. In the Sorbas Basin, lower Pliocene sediments (Gochar Fm) lie on top of the Zorreras member which mainly consists of palaeosols, fluvio-deltaic reddish silts and sandstones, grey-coloured sandstones and conglomerates intercalated by up to 4 whitish, massive carbonate beds (Manzi and Roveri, 2009; Aufgebauer and McCann, 2011; Roveri et al., 2018; Roveri et al., 2019b) containing euryhaline ostracod specimens of Paratethyan affinity like *Cyprideis* sp. (e.g., Aufgebauer and McCann, 2011). The Zorreras member has been considered as the equivalent of the LM facies (Rouchy and Caruso, 2006). The marine early Pliocene sands (Figure 3) show a

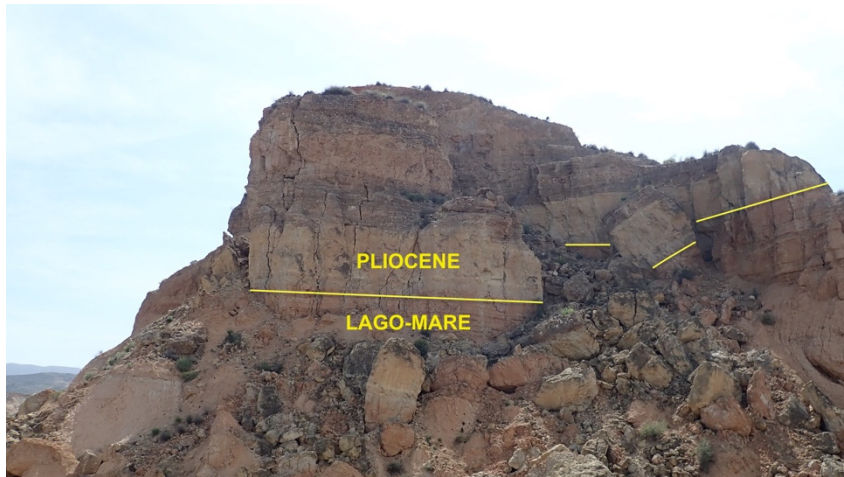


Figure 3: Field photograph of the Miocene-Pliocene boundary in the Sorbas Basin (Zorreras section).

few metres above the boundary a fossiliferous horizon rich in bivalves (Figure 5 B) that can be traced throughout the basin (Mather and Stokes, 2001; Roveri et al., 2019b). Here, we analysed the uppermost 2 m of the Zorreras section ($37^{\circ} 6' 9.87''$ N; $2^{\circ} 6' 46.78''$ W) composed of 5 cm of reddish LM deposits, 30 cm of grey deposits containing carbonate nodules and 60 cm of Zanclean massive sands including the intercalated bivalve horizon (Figure 5 B).

In the Nijar Basin (Figure 1), the upper Messinian is composed of alternations of marly LM facies and conglomerate alluvial beds (Omodeo Salé et al., 2012) of the Feos Formation, which are overlain by the lowermost Zanclean with an unconformity in the marginal parts of the basin and a conformable contact at the centre (Fortuin and Krijgsman, 2003; Aguirre and Sánchez-Almazo, 2004; Roveri et al., 2019a). This study focuses on the Barranco del Negro section (Figure 5 C; $37^{\circ} 0' 35.02''$ N; $1^{\circ} 58' 23.02''$ W; Figure 4) in the northeastern



Figure 4: Field photograph of the Miocene-Pliocene boundary in the Nijar Basin (Barranco del Negro section).

part of the Nijar Basin. Here, the Miocene - Pliocene boundary (MPB) can be clearly identified, with a sharp contact over uppermost Messinian sediments, a 5 cm-thick black and 5 cm-thick grey layer topped by lower Zanclean massive yellow marine sands, characterised at the base by a 1 cm-thick layer with bivalve shell fragments (Figure 5 C).

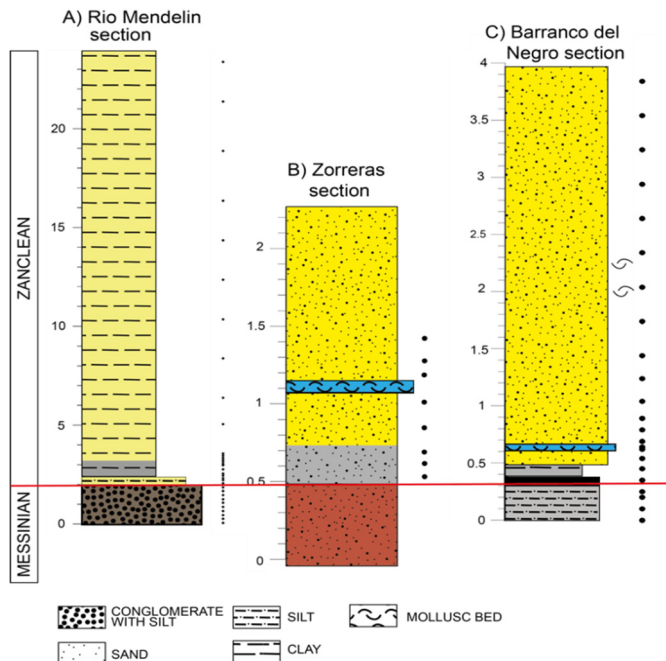


Figure 5: Stratigraphic logs of the three sections studied in Southern Spain. A) Rio Mendelin section; B) Zorreras section, C) Barranco del Negro section. The black dots represent the analysed samples.

2.2 Alboran Basin

The Alboran Basin is a transitional area between the semi-enclosed Mediterranean Sea and the Atlantic Ocean (Figure 1) characterised by very intense circulation that is strongly related with water exchange at the Gibraltar Strait where the relatively low salinity Atlantic waters encounter high salinity Mediterranean water masses.

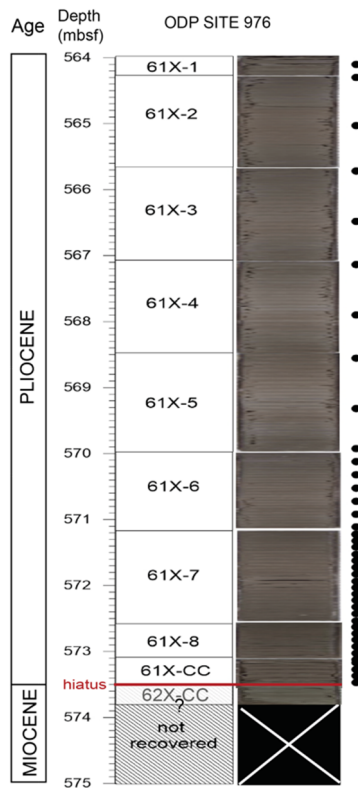


Figure 6: Early Pliocene core sections from ODP Site 976 with corresponding core photographs. The black dots represent the analysed samples.

ODP Site 976 ($36^{\circ} 12' 18.78''$ N, $4^{\circ} 18' 45.78''$ W) is located in the northern sector of the West Alboran Basin (WAB; Western Mediterranean), ~100 km to the east of the Gibraltar Strait on top of a continental crustal horst that formed during early- to mid-Miocene rifting (Comas et al., 1996). The marine lower Pliocene sediments recovered at this site are mainly composed of homogeneous nannofossil-rich claystone and sandy claystone (Comas et al., 1996) with no visible changes in colour. We analysed 32 samples from the lower Pliocene of core 61. From the underlying core 62, only section 62X-CC was recovered and only three samples were collected. Because of their uncertain stratigraphic position, these have been excluded from interpretation (Bulian et al., 2021). Consequently, the actual contact between Miocene and Pliocene sediments was not recovered. With the aid of seismic interpretation and regional biostratigraphy, the MPB has been placed at the base of core 61 (Bulian et al., 2021), corresponding with a visible erosional surface. This erosion has been associated with the Zanclean reflooding, when after the breaching of the Gibraltar Strait, the Atlantic water would have abruptly entered

the Mediterranean (Garcia-Castellanos et al., 2009; Estrada et al., 2011) and produced a marked incision (Esteras et al., 2000; Blanc, 2002). Alternatively, if a modest drawdown is considered a hyperpycnal submarine cascading erosion (Roveri et al., 2014b) could be the creation mechanism. The time slice represented by the hiatus has been estimated at 1.67 Ma (Bulian et al., 2021) and includes the majority of the middle-upper Messinian sediments.

3. Methodology

3.1 Micropalaeontological analyses

For this study, a total of 95 samples (33 from Rio Mendelin section, 32 from ODP Site 976, 21 from the Barranco del Negro section, 9 from the Zorreras section) taken with variable sampling steps (10 cm-2 m) were selected for micropalaeontological analyses. The samples were oven dried at 40°C and washed over 63 µm and 150 µm sieves. For faunal analysis, aliquots of the 150 µm fraction of on average 150-200 benthic foraminifers and 200-300 planktic foraminifers were counted. The counts were then transferred to relative frequencies. Samples yielding less than 50 benthic foraminifer specimens were not included in the interpretation. The benthic foraminifer content of the Zorreras section has been studied in a semi-quantitative way based on the presence or absence of species considering that very few specimens were found. Similarly, in the three land-based sections the presence of ostracods was recorded, and only the LM marker species (*Cyprideis* sp.) was identified from the assemblage.

The diversity of the benthic foraminiferal assemblages has been estimated through the Shannon index (H, Murray, 1991; Spellerberg and Fedor, 2003), expressed by the formula:

$$H = -K \sum_{i=1}^n pi \log(pi)$$

where pi is the proportion of the i^{th} species and K a positive constant.

As previously done for the Messinian sediments of the deep-sea core (Site 976; Bulian et al., in press), the sum of displaced shallow-water benthic foraminifer species, *Elphidium* spp., *Rosalina* spp., discorbids and *Cibicides lobatulus* was calculated. Because a relatively high number of displaced specimens indicates downslope transport (Fentimen et al., 2020 and references therein) this sum has been used as an indicator of bottom water currents in the basin.

Statistical analyses

To identify the distributional patterns of species assemblages occurring in similar environments, a hierarchical cluster analyses (Pearson correlation: Past 4.02 software; Hammer et al., 2001; Hammer et al., 2008) was performed on the most abundant ($\geq 3\%$) variables of each data set except from the Zorreras and Barranco del Negro sections. Single and fragmentary occurrences were removed whereas single species from the same genus, when considered indicative of

analogous environmental conditions, were grouped together. *Nodosaria* spp. comprises unilocular spp., *Nodosaria* spp., *Pseudonodosaria* spp., *Lagena* spp. and *Procerolagena* spp., *Cancriis* spp. contains the species *C. oblongus* and *C. auriculus*, *Uvigerina peregrina* includes both *Uvigerina peregrina* and *U. pygmaea*, while *Bulimina striata* is the sum of *B. striata* and *B. striata mexicana*. In *Pullenia quinqueloba*, both forms with four and five chambers were included.

3.2 Palaeo – water depth estimates

Initial palaeo-water depth estimates were performed using the $(P/(P+B))*100$ ratio (%P; Gibson, 1989; Van der Zwaan et al., 1990), which, even though this reflects general sea-level trends, has many disadvantages related to sensitivity to changing oxygen levels, food availability and preferential dissolution of the planktic fauna (e.g., Sen Gupta and Machain-Castillo, 1993; Jorissen et al., 1995; Kucera, 2007). To improve palaeodepth reliability, we excluded from the ratio the infaunal foraminifer species that are not directly dependent on the flux of organic matter to the sea floor, which forms the basis for the regression function (Van der Zwaan et al., 1999; Van Hinsbergen et al., 2005). However, this approach still does not account for planktic foraminifer dissolution. Therefore, to obtain an independent quantification of the palaeobathymetry we estimated the palaeo-water depth using one of the several equations (e.g. Hohenegger, 2005; Hohenegger et al., 2008; Avnaim-Katav et al., 2016; Milker et al., 2017) based exclusively on the benthic foraminifer fauna. In this work we apply the transfer function proposed by Hohenegger (2005) considering that this is reliable in deeper environments and has been evaluated previously by Baldi and Hohenegger (2008) in the Vienna Basin and by Pérez-Asensio et al. (2012) in the Guadalquivir basin. The equation, here used as modified by Hohenegger et al. (2008) and Baldi and Hohenegger (2008) includes the relative abundances of each species and their depth ranges (Table 1):

$$Paleodepth (m) = \sum_{j=1}^k [(l_j * n_j) / d_j] / \sum_{j=1}^k (n_j / d_j)$$

where n_j is the relative abundance of the n^{th} species, l_j the mean species depth, and d_j the dispersion. As suggested by Hohenegger (2005), to calculate the mean species depth for shallower marginal basins (e.g., Rio Mendelin section) we used the geometric means, while for deeper basins (ODP Site 976), in order to avoid underestimation the arithmetic mean. In addition, to avoid over- or underestimating palaeodepths, the depth markers comprised in the calculation are all autochthonous species and reported in Table 1.

Table 1: The bathymetric ranges, mean species depth and standard deviation of the benthic foraminifer species used for palaeo – water depth reconstruction. The species used for Rio Mendelin section are underlined, while the ones employed for ODP Site 976 have an asterisk. Depth ranges are based on previously published work of: 1 Wright (1979), 2 Wright (1978), 3 Lutze and Coulbourn (1984), 4 Pflum et al. (1976), 5 Lutze and Wefer (1980), 6 Haake (1982), 7 Barbieri and Panieri (2004), 8 Van Hinsbergen et al. (2005), 9 Violanti et al. (2011), 10 Corbí (2010), 11 Van Morkhoven et al. (1986), 12 De Stigter et al. (1998), 13 Baggley (2000), 14 Gebhardt (1993), 15 Berggren and Haq (1976), 16 Pérez-Asensio et al. (2012), 17 Poag and Tresslar (1981), 18 De Stigter et al. (1998), 19 Bandy and Chierici (1966), 20 De Rijk et al. (2000), 21 De Rijk et al. (1999); 22 Sen Gupta and Machain-Castillo (1993), 23 Murray (2006), 24 Bizon and Bizon (1984), 25 Mendes et al. (2012), 26 Ohga and Kitazato (1997), 27 Milker and Schmiedl (2012), 28 Alve (2003), 29 Austin and Evans (2000), 30 Schmiedl et al. (1997), 31 Suokhrie et al. (2021), 32 Russo et al. (2007) and 33 (Hayward, 2004)

Species	min depth	max depth	SD
<i>Amphycorina</i> spp.*	9	2860	1425.5
<i>Anomalinooides helacinus</i> *	600	2000	700.0
<u><i>Asterigerina planorbis</i></u>	200	400	1000.0
<u><i>Bolivina dilatata</i></u>	15	3000	1492.5
<u><i>Bolivina spathulata</i></u>	30	3547	1758.5
<u><i>Bulimina aculeata</i></u> *	5	4000	1997.5
<u><i>Bulimina elongata</i></u>	16	200	92.0
<u><i>Bulimina mexicana</i></u>	100	2000	950.0
<u><i>Bulimina striata</i></u> *	100	800	350.0
<i>Cancris oblongus</i> *	30	500	60.0
<i>Chilostomella</i> spp.*	700	1900	600.0
<i>Cibicides brady</i> *	200	3000	1400.0
<u><i>Cibicidoides pseudoungerianus/ungarianus</i></u> *	50	4000	1975.0
<u><i>Cibicidoides kullenbergi</i></u> *	1000	4000	500.0
<u><i>Cibicidoides lobatulus</i></u>	20	1300	640.0
<u><i>Cibicidoides pachyderma</i></u> *	30	4000	1985.0
<u><i>Cibicides dutemplei</i></u> *	100	600	250.0
<i>Dentalina</i> spp.*	30	1200	585.0
<u><i>Fursenkoina acuta</i></u>	0	600	300.0
<i>Globobulimina</i> spp.*	1000	1500	250.0
<u><i>Globobulimina turgida</i></u>	30	150	60.0
<i>Globocassidulina subglobosa</i> *	50	4000	1975.0
<i>Gyroidina altiformis</i> *	30	600	285.0
<u><i>Gyroidina soldanii</i></u> *	100	5000	2450.0
<i>Karriella bradyi</i> *	100	3000	1450.0
<u><i>Lenticulina</i> spp.</u> *	600	1500	450.0
<i>Martinotiella communis</i> *	200	3000	1400.0
<i>Melonis barleeanus</i> *	13	3974	1980.5
<i>Melonis pompilioides</i> *	100	3000	1450.0
<i>Melonis soldanii</i> *	90	1000	455.0
<i>Nodosaria</i> spp.*	30	1700	235.0

Species	min depth	max depth	SD
<i>Nonion fabum</i>	0	200	100.0
<i>Oridorsalis stellatus</i>	250	1500	625.0
<i>Oridorsalis umbonatus</i> *	65	4000	1967.5
<i>Planulina ariminensis</i> *	70	1300	615.0
<i>Pullenia bulloides</i>	60	4000	1970.0
<i>Pullenia quinqueloba</i> *	50	2000	975.0
<i>Signoilopsis schlumbergeri</i> *	57	1500	721.5
<i>Sphaeroidina bulloides</i> *	100	2000	950.0
<i>Stainforthia fusiformis</i>	0	2200	1080.0
<i>Textularia calva</i>	0	2000	1000.0
<i>Trifarina bradyi</i>	0	600	300.0
<i>Uvigerina peregrina</i> *	100	4400	2150.0
<i>Uvigerina rutila</i> *	200	1000	1400.0

3.3 Estimation of bottom-water oxygen levels

The benthic foraminifer distribution in the sediment depends on the organic flux and oxygenation at the sea floor (Jorissen et al., 1995; Van der Zwaan et al., 1999). Consequently these processes represent some of the most sensitive indicators of dissolved oxygen (Kaiho, 1994) as species with deep infaunal (> 3 cm below the sediment-water interface; BSWI) and intermediate infaunal (>0.7 cm BSWI) microhabitat preferences thrive when oxygen levels are reduced, while epifaunal ones (0-0.7 cm BSWI) prefer better oxygenated bottom waters (e.g. Corliss and Chen, 1988; Jorissen et al., 1995; Schmiedl et al., 2000; Gooday, 2003).

These microhabitat preferences, paired with morphological characteristics (size, wall thickness, shape) can be used to outline three groups of benthic foraminifer indicators (Table 2) defining respectively oxic (>1.5 ml/l O₂), suboxic (0.3 - 1.5 ml/l O₂) and dysoxic (0.1 - 0.3 ml/l O₂) environments (Kaiho, 1991; Kaiho, 1994; Kaiho, 1999). Additionally, within the dysoxic indicators three different groups (A, B, C) have been defined (Kaiho, 1994) where group C includes species that have intermediate characteristics between suboxic and dysoxic markers. Using these indicators, it is possible to calculate the Benthic Foraminifera Oxygen Index (BFOI; Kaiho, 1991; Kaiho, 1994; Kaiho, 1999) obtaining five different conditions of dissolved oxygen: anoxic (-55), dysoxic (-50 - -40), suboxic (-40 - 0), low oxic (0-50), high oxic (50 - 100). The index proved to accurately reproduce measured dissolved oxygen values in the Marmara Sea and therefore can probably be used to evaluate bottom oxygen levels in the rest of the Mediterranean as well (Kaminski, 2012). Nonetheless, the interpretation of the BFOI is prone to bias when very low-diversity assemblages are studied and consequently, this estimate has not been applied on samples with a Shannon index ≤ 1 (Kaiho, 1994). Moreover, studies on recent benthic foraminifers suggest

that quantitative reconstruction of oxygen levels higher than 1 ml/l is probably not possible (Jorissen et al., 2007 and references therein).

The BFOI has been calculated following the formula (Kaiho, 1994) :

$$\text{BFOI} = \left(\frac{O}{(O + D)} \right) * 100$$

where O and D (with O>0) are the numbers of oxic and dysoxic indicator specimens, respectively.

When O=0 and I>0, the equation:

$$\text{BFOI} = \left(\left(\frac{I}{(I + D)} \right) - 1 \right) * 100$$

is used instead, where I is the sum of suboxic indicators. The suboxic indicators included in group C are excluded (Kaiho, 1994) from the formula.

Table 2: Microhabitat preference of benthic foraminifera from Rio Mendelin section and ODP Site 976 (0-0.7 cm BSWI), infauna (>0.7 cm BSWI) and deep infauna (> 3 cm BSWI).

Oxic	Suboxic (Groups A and B)	Dysoxic
<i>Cibicides brady</i>	<i>Amphycorina</i>	<i>Bolivina dilatata</i>
<i>Cibicidoides dutempli</i>	<i>Anomalinoidea helicinus</i>	<i>Bolivina reticulata</i>
<i>Cibicidoides kullenbergi</i>	<i>Asterigerina planorbis</i> .	<i>Bolivina seminuda</i>
<i>Cibicidoides lobatulus</i>	<i>Bulimina elongata</i>	<i>Bolivina spathulata</i>
<i>Cibicidoides pachyderma</i>	<i>Bulimina striata</i>	<i>Chilostomella</i> spp.
<i>Cibicidoides pseudoungarianus</i>	<i>Cancris oblongus</i>	<i>Fursenkoina acuta</i>
<i>Cibicidoides ungerianus</i>	<i>Dentalina</i> spp.	<i>Globobulimina</i> spp.
<i>Sphaeroidina bulloides</i>	<i>Epistominella trinacria</i>	<i>Globobulimina turgida</i>
	<i>Globocassidulina subglobosa</i>	
	<i>Gyroidina altiformis</i>	
	<i>Gyroidina soldanii</i>	
	<i>Karreriella bradyi</i>	
	<i>Lenticulina</i> spp.	
	<i>Martinotiella communis</i>	
	<i>Melonis barleeanus</i>	
	<i>Melonis pompilioides</i>	
	<i>Melonis soldanii</i>	
	<i>Nodosaria</i> spp.	
	<i>Nonion fabum</i>	
	<i>Oridorsalis stellatus</i>	
	<i>Oridorsalis umbonatus</i>	
	<i>Planulina ariminensis</i>	
	<i>Pullenia bulloides</i>	
	<i>Pullenia quinqueloba</i>	
	<i>Sigmoilopsis schlumbergeri</i>	
	<i>Textularia calva</i>	

Oxic	Suboxic (Groups A and B)	Dysoxic
	<i>Trifarina bradyi</i>	
	<i>Uvigerina peregrina</i>	
	<i>Uvigerina rutila</i>	

3.4 Stable isotope measurements

Epifaunal taxa such as *Cibicides* spp. and *Cibicidoides* spp. were found to secrete calcite close to equilibrium with the ambient sea water, displaying minor vital and minimal ontogenetic effects (Theodor et al., 2016a; Theodor et al., 2016b; Jöhnck et al., 2021 and references therein), and therefore 2 to 10 specimens of *Cibicidoides pachyderma* were picked from ODP Site 976 samples for stable isotope analyses. The analysis was only possible until 571.18 m because extreme calcification of specimens from the younger part of the studied sequence at ODP Site 976 persisted even after ultrasonic cleaning. For the Rio Mendelin section, other species were chosen given the absence of *C. pachyderma*. For the more basal samples *Cibicidoides dutemplei* was picked, while starting from 1 m and going upwards, *Cibicidoides ungerianus* was chosen. The species *Epistominella trinacria* was picked in the first two samples because the lowermost level is monospecific and the next level nearly so (88.6%). More than one species was picked where possible, to obtain intraspecific correction factors. All measurements were transformed to *C. ungerianus*. This species has been reported to yield comparable values as *C. pachyderma* (Kaboth et al., 2017). Based on two paired measurements the *E. trinacria* values were corrected by adopting a value equal to the average offset from the *C. dutemplei* values (-0.21 for $\delta^{13}\text{C}$ and 1.46 for $\delta^{18}\text{O}$ values). The *C. dutemplei* record and the corrected *E. trinacria* data points were then all adjusted using the average offset found in six paired measurements between *C. dutemplei* and *C. ungerianus* (0.33 for $\delta^{13}\text{C}$ and -0.03 for $\delta^{18}\text{O}$ values). Samples from the Barranco del Negro section were not picked for stable isotope analyses because part of the foraminifers are not in situ.

The stable isotope analyses were performed with a Finnigan MAT 253 mass spectrometer connected to a Kiel IV carbonate preparation device at the Christian-Albrechts University in Kiel (Germany). Sample reaction was induced by individual acid addition (99% H_3PO_4 at 75 °C) under vacuum. The evolved carbon dioxide was analysed eight times for each individual sample. As documented by the performance of international [NBS19: +1.95 ‰ VPDB (^{13}C), -2.20 ‰ VPDB (^{18}O); IAEA-603: +2.46 ‰ VPDB (^{13}C), -2.37 ‰ VPDB (^{18}O)] and laboratory-internal carbonate standards [Hela1: +0.91 ‰ VPDB (^{13}C), +2.48 ‰ VPDB (^{18}O); HB1: -12.10 ‰ VPDB (^{13}C), -18.10 ‰ VPDB (^{18}O); SHK: +1.74 ‰ VPDB (^{13}C), -4.85 ‰ VPDB (^{18}O)], analytical precision of stable isotope analysis is better than ± 0.08 ‰ for $\delta^{18}\text{O}$ and better than ± 0.05 ‰ for $\delta^{13}\text{C}$. The obtained values were calibrated relative to Vienna Pee Dee Belemnite (VPDB).

4. Results

4.1 Malaga Basin: Rio Mendelin section

4.1.1 Micropalaeontology and stable isotopes

The first 2 metres of the analysed section (LM deposits) are barren of planktic and benthic foraminifers and contain high abundances of ostracods, mainly *Cyprideis* sp. (LM unit, Figure 7). Only at the base of the Pliocene, benthic

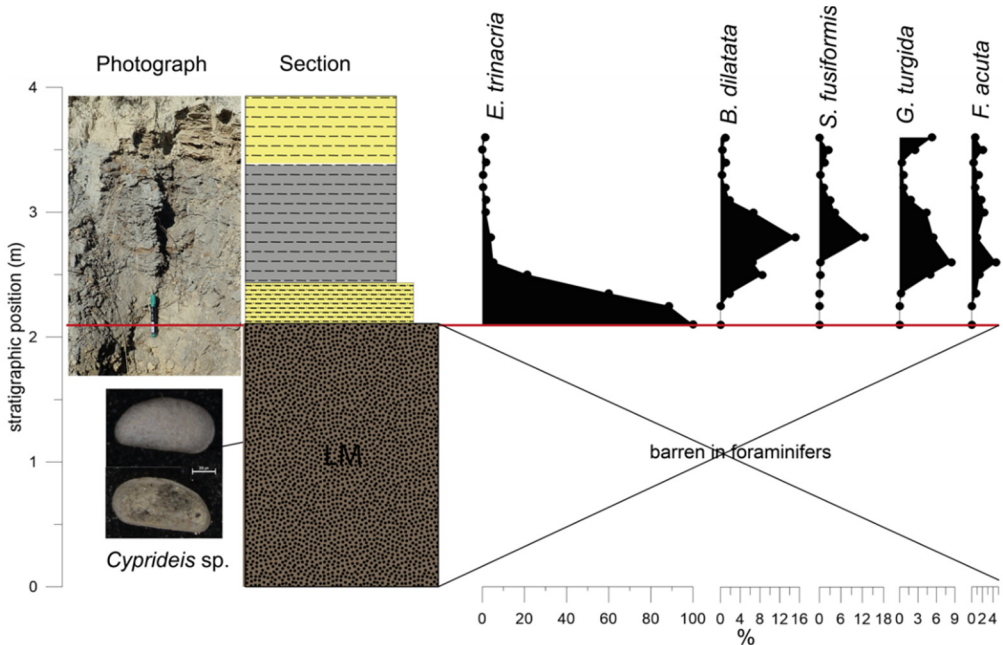


Figure 7: Base of the Rio Mendelin section. From left to right the photo of the Miocene-Pliocene boundary, the stratigraphic section and the first benthic foraminifer species that repopulate early Pliocene environments. In addition, a photo of the predominant late Messinian ostracod species *Cyprideis* sp. is shown.

foraminifers appear and are present throughout the analysed section. Considering this distribution, and the good preservation of the specimens which do not show any signs of prolonged transport or alteration, the foraminifers can be considered in-situ. Optical microscope pictures of the benthic foraminifer species are shown in Plates 1 and 2.

The first benthic foraminifer species to appear is *Epistominella trinacria* which characterises only the first 60 cm of the section after the barren interval (Figure 8). The species disappears almost completely at the base of the grey layer when other species start to appear such as *Fursenkoina acuta*, *Globobulimina*

turgida, *Bolivina dilatata* and *Stainforthia fusiformis* (Figure 7) which are limited to this interval. At the same level, several other species appear and stay present throughout the entire record (Figure 8). The most abundant amongst them is

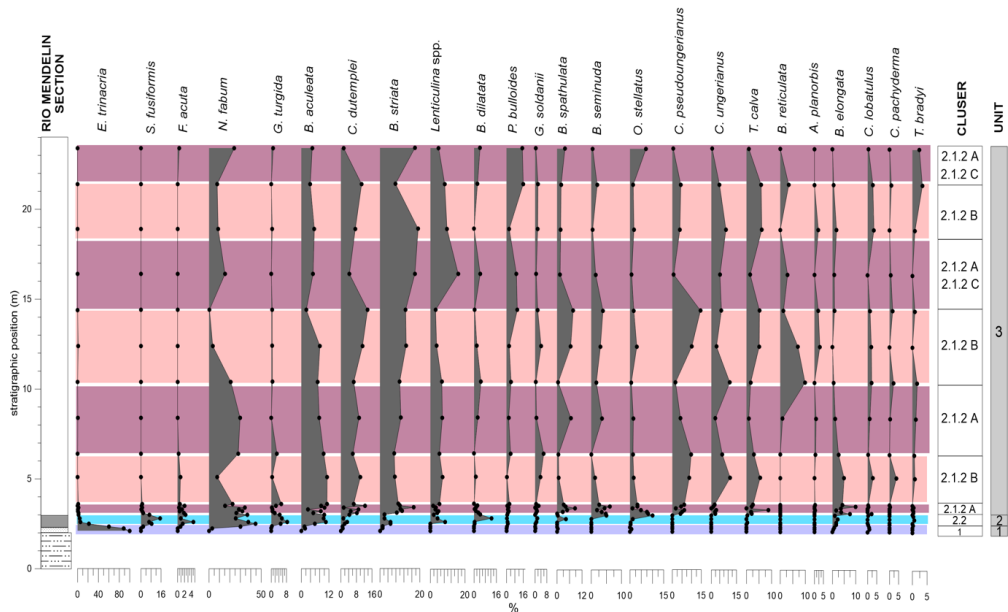


Figure 8: Variations in relative abundances of major benthic foraminiferal taxa. Colour bands correspond to foraminiferal assemblages characterizing the sample clustering in Figure 9.

Nonion fabum (~ 50 %), followed by *Bulimina striata* (~20 %), *C. dutemplei* (~15 %), *C. ungerianus* (~15 %), *Cibicoides pseudoungerianus* (~15 %) *Bulimina aculeata* (~12 %) and *Lenticulina* spp. (~10-20 %).

Cluster analysis performed on the most significant benthic foraminifer species (>3 %) aided recognition of distributional patterns and two main clusters: Cluster 1 and Cluster 2 (Figure 9 A and B). Cluster 2 is composed of two subclusters, Cluster 2.1 and 2.2, the first composed of a total of four subclusters (Figure 9). These clusters group different benthic foraminifer species based on their stratigraphic position enabling the distinction of three different units: Unit 1, Unit 2 and Unit 3 (Figure 8). Cluster 1, defining Unit 1, dominates from 2 – 2.5 m in the section and is represented by only one species, *E. trinacria*. The following 0.5 m (2.5 – 3 m) composing Unit 2 are dominated by *F. acuta*, *G. turgida*, *B. dilatata* and *S. fusiformis* forming Cluster 2.2. Overlapping with Cluster 2.2 but continuing until ~4 m, is Cluster 2.1.2 A, which eight benthic foraminifer species. Among these, higher abundances are represented by *N. fabum* reaching ~50%, *B. striata* reaching ~25% and *Lenticulina* spp. up to ~20% of the total

abundance. The remaining species of Cluster 2.1.2 A range between ~5 and 12% (Figure 8 and 9). At ~4 m, Cluster 2.1.2 B becomes dominant (Figure 9 B) with eight benthic foraminifer species where *C. dutemplei*, *C. pseudoungerianus* and *C. ungerianus* dominate the assemblage reaching values of ~15 – 16% of the total abundance (Figure 8 and 9). Apart from *T. calva* that reaches ~10%, the remaining species are subordinate and, in many cases, do not reach 5% of abundance (Figure 8 and 9). The final Cluster, 2.1.2 C, is composed of *Pullenia bulloides* and *Trifarina bradyi* showing an overall increasing upward trend (Figure 8). Both species reach maximum values around the top of the analysed section (~16 and 5% respectively) and display a general trend in phase with Cluster 2.1.2 A and Cluster 2.2 (Figure 8 and 9). This last unit, Unit 3 (3 – 23.5 m), is characterised by a regular interchange (every 3-4 m until the top of the section) of the most abundant Clusters 2.1.2 A (+Cluster 2.1.2 C and Cluster 2.2) and 2.1.2 B, marking a clear cyclical juxtaposition between the two assemblages.

The benthic foraminifer diversity rises throughout the record (H index from 0 to \geq ~2.9; Figure 9 B) and so does the %P that increases from 0 % to ~40 % at the base of the section to remain stable at ~40 – 50 %. The record also shows a

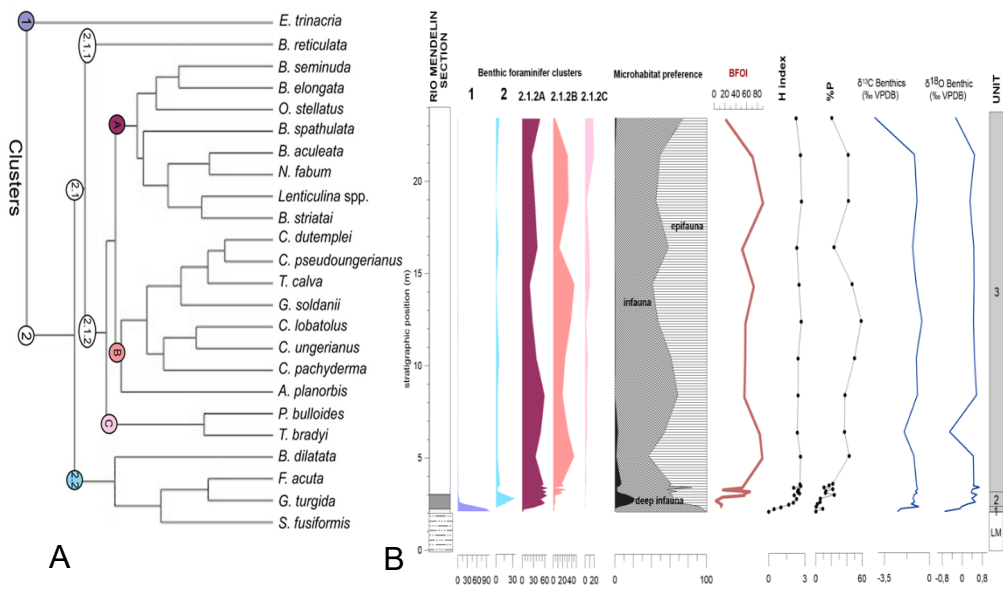


Figure 9: A) Dendrogram resulting from the hierarchical clustering in the Rio Mendelin section which divided the benthic foraminifer species in two main species clusters (Cluster 1 and Cluster 2) and two subclusters (Clusters 2.1 and 2.2). Cluster 2.1 separates in turn in two subordinate cluster branches, Cluster 2.1.1 and Cluster 2.1.2. The clusters have been highlighted with specific colors. B) from left to right: Clusters 1, 2.2, 2.1.2 A and 2.1.2 C plotted against stratigraphic position; Microhabitat distribution of the most abundant benthic foraminifer species; The BFOI estimation (Kaiho, 1994); Shannon diversity index; % of planktic foraminifers; Benthic $\delta^{13}\text{C}$ and $\delta^{18}\text{O}$ isotopic record (*C. ungerianus*).

change in the benthic foraminifer microhabitat preferences visible as an interchange between dominantly infaunal or epifaunal taxa that mimics the juxtaposition between Clusters 2.1.2 A (+Cluster 2.1.2 C and Cluster 2.2) and 2.1.2 B. Deep infauna is present only in the grey layer of Unit 2 reaching a maximum of ~20%. Since the three low-diversity samples at the base were excluded from the estimate, the BFOI is lowest in the grey layer (~3 - 12 %; Figure 9 B), and after 4 m increases and oscillates between 60 and 90 %, showing the highest values (~85 - 90 %) in correspondence with intervals where epifaunal species dominate (Figure 9 B).

From 3 m upward, planktic foraminifers become increasingly abundant and are characterised by an assemblage dominated by *Globigerinoides* spp., *Globoturborotalita apertura* and *Globigerina bulloides* (Figure 10). Less dominant species include *Globigerinata glutinata*, *Orbulina universa* and *Neogloboquadrina acostaensis* (Figure 10), and at 7.4 m a few *Globorotalia margaritae* are identified.

The benthic stable isotope record of Rio Mendelin section is shown in Figure 9 B. After the first two samples that show values of ~-2 ‰, the benthic $\delta^{13}\text{C}$ remains stable at ~-1 ‰ with only two oscillations towards lighter values at 7 and 23.5 m. The benthic $\delta^{18}\text{O}$ trend is very similar. The lowermost samples show an increasing upward trend that from ± 0.7 ‰ shifts to ± 0.6 ‰ at 3 m in the section and stays stable throughout the record apart from two negative excursions at the same stratigraphic position as in the $\delta^{13}\text{C}$ curve.

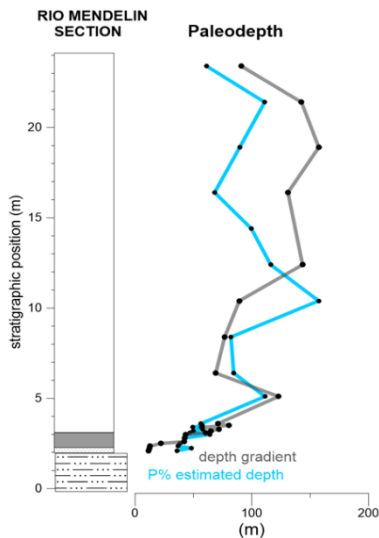


Figure 10: Calculated palaeodepths for the Rio Mendelin section. The grey line is the palaeodepth estimated by gradient analysis (Hohenegger, 2005; Hohenegger et al., 2008). The blue line is the palaeodepth estimated by using the %P (Van der Zwaan et al., 1990).

4.1.2 Palaeo-water depth reconstruction

Since the benthic foraminifers are considered indigenous, palaeodepth has been calculated for the Rio Mendelin section. A first approximation of the palaeodepth can be derived from the $\%P = 100 \cdot P / (P+B)$ (%P; Van der Zwaan et al., 1990; Figure 9 B). Applying the regression in the e-power formula (equation 7 on p. 13), the palaeodepth varied from a minimum of < 50 m at the base of the section ($\%P \sim 0 - 10$ %) to a maximum depth of ~150 m ($\%P \sim 40$ %) at 10 m. The mean palaeodepth oscillates around 100 m. The palaeodepth reconstruction based on the transfer function of (Hohenegger, 2005; Hohenegger et al., 2008) corresponds with the %P until 7 m in the section. From here upwards, the difference between the reconstructions amounts to some 50 - 80 m.



Plate 1: Optical microscope photos of the most abundant (>3%) benthic foraminifer species of Rio Mendelin section. **1** *Textularia calva*; **2** *Bolivina seminuda*; **3** *Bolivina spathulata*; **4** *Bolivina dilatata*; **5** *Bolivina reticulata*; **6** *Stainforthia fusiformis*; **7 a, b** *Trifarina bradyi*; **8 a, b** *Fursenkoina acuta*; **9** *Bulimina striata* var. *mexicana*; **10 a, b** *Bulimina striata*; **11** *Bulimina elongata*; **12** *Bulimina aculeata*; **6**; **13** *Globobulimina turgida*; **14** *Nonion fabum*; **15 a, b** *Asterigerina planorbis*: **a** spiral view, **b** umbilical view; **16** *Lenticulina* sp.. Scale bar = 100 μm.

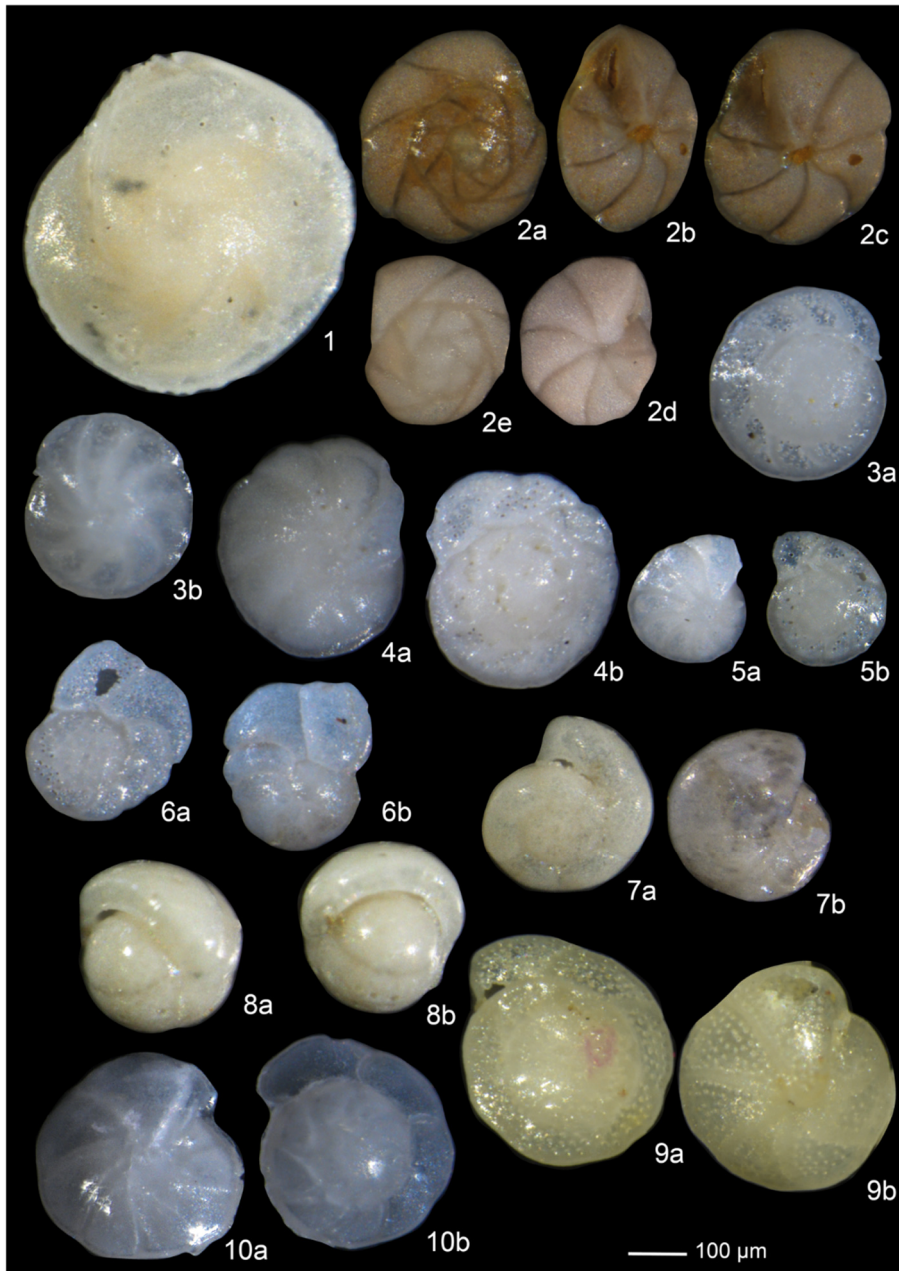


Plate 2: Optical microscope photos of the most abundant (>3%) benthic foraminifer species of Rio Mendelin section. **1** *Lenticulina* sp.; **2** c.f. *Epistominella trinacria*: **a, d** spiral view, **b** apertural view, **c, e** umbilical view; **3** *Cibicoides pachyderma*: **a** spiral view, **b** umbilical view; **4** *Cibicoides ungerianus*: **a** spiral view, **b** umbilical view; **5** *Cibicoides pseudoungerianus*: **a** spiral view, **b** umbilical view; **6** *Cibicides lobatulus*: **a** spiral view, **b** umbilical view; **7** *Gyroidina soldanii*: **a** spiral view, **b** umbilical view; **8** *Pullenia bulloides*: **a** lateral view, **b** apertural view; **9** *Cibicides dutemplei*: **a** spiral view, **b** umbilical view; **10** *Oridorsalis stellatus*: **a** spiral view, **b** umbilical view. Scale bar = 100 μ m.

4.2 Nijar Basin: Barranco del Negro section

Benthic and planktic foraminifers are present in the entire studied Barranco del Negro section. Carbonate has secreted on the planktic specimens, but the benthic species are well preserved (Plate 3 and 4). Although they are scarce, until 2 m in the section we have identified brackish disarticulated ostracods, mainly *Cyprideis* sp. In addition, brackish gasteropoda are present until the calcarenite deposition (0.5 m in Figure 11; Plate 3). A bivalve-rich horizon is identified at 0.64 m, and bivalve shells are also found at 2 and 2.3 m in the section, without being concentrated in a horizon (Figure 5 C). At the top (3.5 m), burrows are observed probably from the genus *Thalassinoides*.

The most abundant benthic foraminifer species present in Barranco del Negro record (Figure 11) are *C. lobatulus* (~15 – 30 %), *Bolivina. spathulata* (~15 – 30 %) and *Elphidium* spp. (~10 – 15 %), with the subordinate occurrence of *C. ungerianus* (~10 %), *Cibicidoides kullenbergi* (~10 %) and *Planulina ariminensis* (~10 %). The first 0.5 m of the section are dominated by *B. spathulata* (~15 %), *Rectouvigerina cylindrica*, *P. ariminensis*, *Uvigerina rutila* and *C. lobatulus*, all reaching ~10 % of abundance. After 0.5 m, *Valvulineria* spp. (~20 %), *Chilostomella* spp. (~15 %), and *Globobulimina* spp. (~5 %) sharply increase but remain present only for 1 m in the section (0.5 – 1.5 m), while *M. soldanii* (~5 %) and *Cassidulina* spp. (~5 %), which show a parallel appearance, can be found with high values for 2 m in the section (0.5 – 2.5 m). The interval between 1 and 2 m is characterised by high abundances of *E. trinacria* (~15 – 25 %) and *B. spathulata* (~15 %), and from 2 m until the top of the section *Spiroplectinella deperdita* (~15 – 20 %), *Cibicides refulgens* (~10 %), *P. bulloides* (~5 – 10 %), *Lenticulina* spp. (~8 %), and *Sphaeroidina bulloides* (~7 %) dominate the record.

The Shannon diversity index of the Barranco del Negro section shows a relatively stable trend throughout the record with an average value of 2.6. The %P shows an upward decreasing trend with the highest average values at the base of the section (~95 %) and lower average values at the top (~75 %; Figure 11).

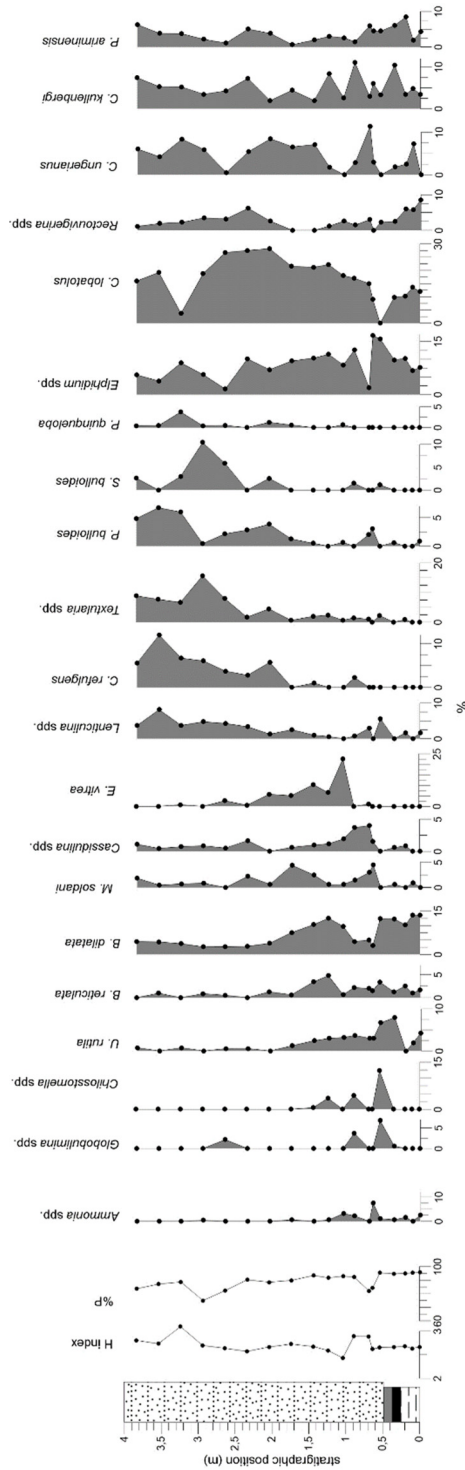


Figure 11: The Barranco del Negro section where from left to right: the Shannon diversity index, the % of planktic foraminifers, benthic foraminifer por gram and the variations in relative abundances of most abundant benthic foraminifer taxa are shown.

The dominant planktic foraminifer species present in the Barranco del Negro record are *G. bulloides*, *Globigerinoides* spp. and *N. acostaensis*, with the subordinate presence of *O. universa* and *Globorotalia miotumida*. The uppermost two samples contain some specimens of *G. margaritae*. The presence in almost every sample of typical Messinian species like *G. miotumida* and *N. acostaensis* sx (Table 3; Sierro et al., 1993) suggests that the planktic foraminifers might be reworked. Reworking of the planktic foraminifers is further suggested by the presence of brackish ostracod and gastropod species together with marine fauna at the base of the section. The concomitant presence of lower neritic to bathyal benthic foraminifer species and shallow water taxa (see Section 5.2) indicates that reworking also involved benthic species.

Table 3: Stratigraphic position of some of the samples from Barranco del Negro section where the shells/gram, ostracods/gram, percentages of Messinian species like *G. miotumida* and *N. acostaensis* sx were counted.

Position	Shells/gram	Ostracods/gram	% <i>G. miotumida</i>	% <i>N. acostaensis</i> sx
3.84	3.29	3.29	0.71	1.22
2.94	0.00	0.00	1.45	4.17
2.04	14.74	6.98	0.48	0.72
1.44	1.25	1.25	0.42	0.72
1.04	1.18	1.42	0.92	8.76
0.69	49.81	3.94	0.00	2.33
0.54	23.39	3.37	0.00	1.48
0.35	21.60	0.22	1.03	4.94
0.20	2.70	0.19	0.51	5.58

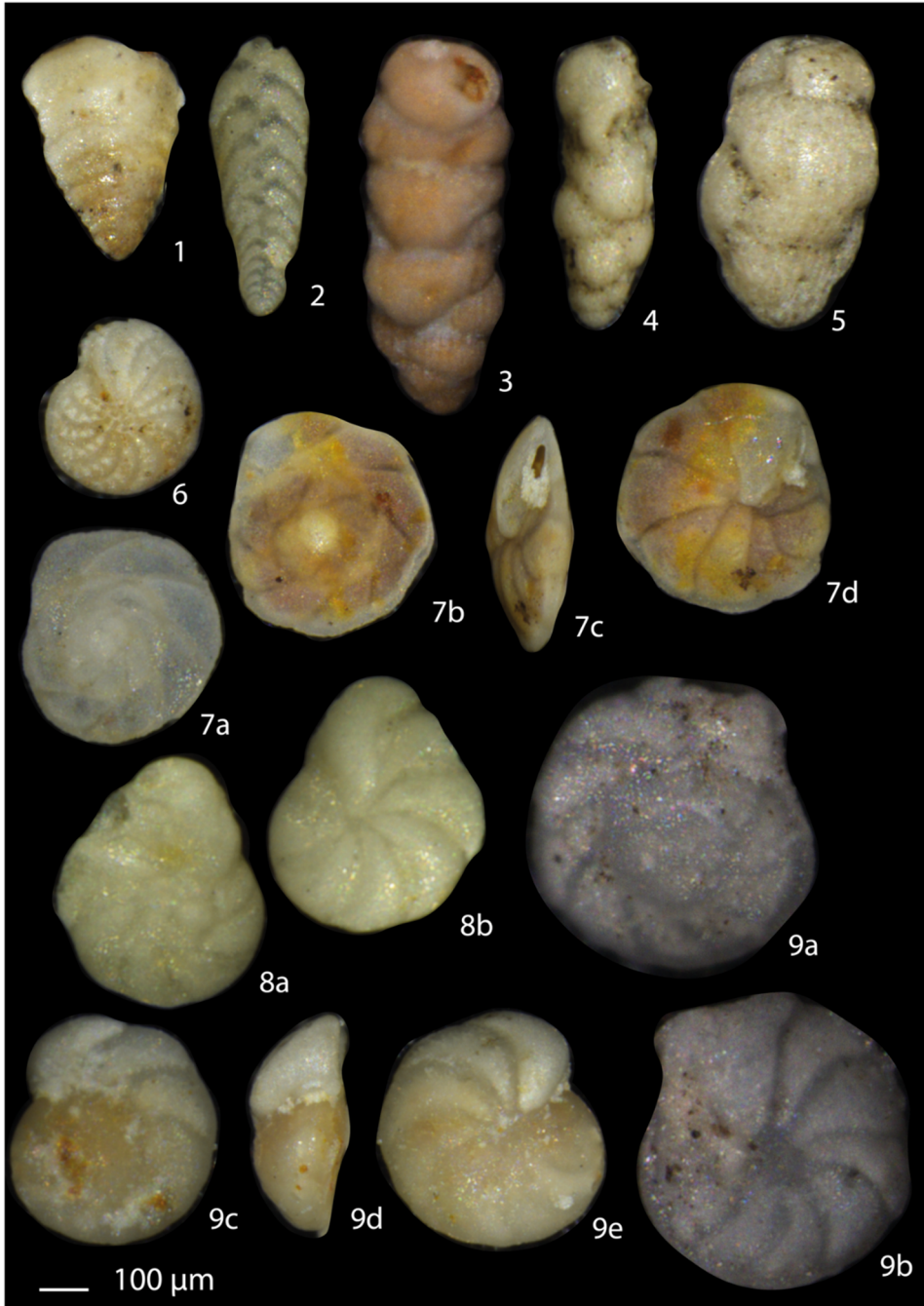


Plate 3: Optical microscope photos of the most abundant (>3%) benthic foraminifer species of Barranco del Negro section. **1** *Spiroplectinella deperdita*; **2** *Bolivina spathulata*; **3, 4** *Rectouvoigerina cylindrica*; **5** *Uvoigerina rutila*; **6** *Elphidium* sp.; **7** *Epistominella trinacria*: **a, b** spiral view, **c** apertural view, **d** umbilical view; **8** *Valoulineria* sp.: **a** spiral view, **b** umbilical view; *Cibicides ungerianus*: **a, c** spiral view, **d** apertural view, **b, e** umbilical view. Scale bar = 100 μm.

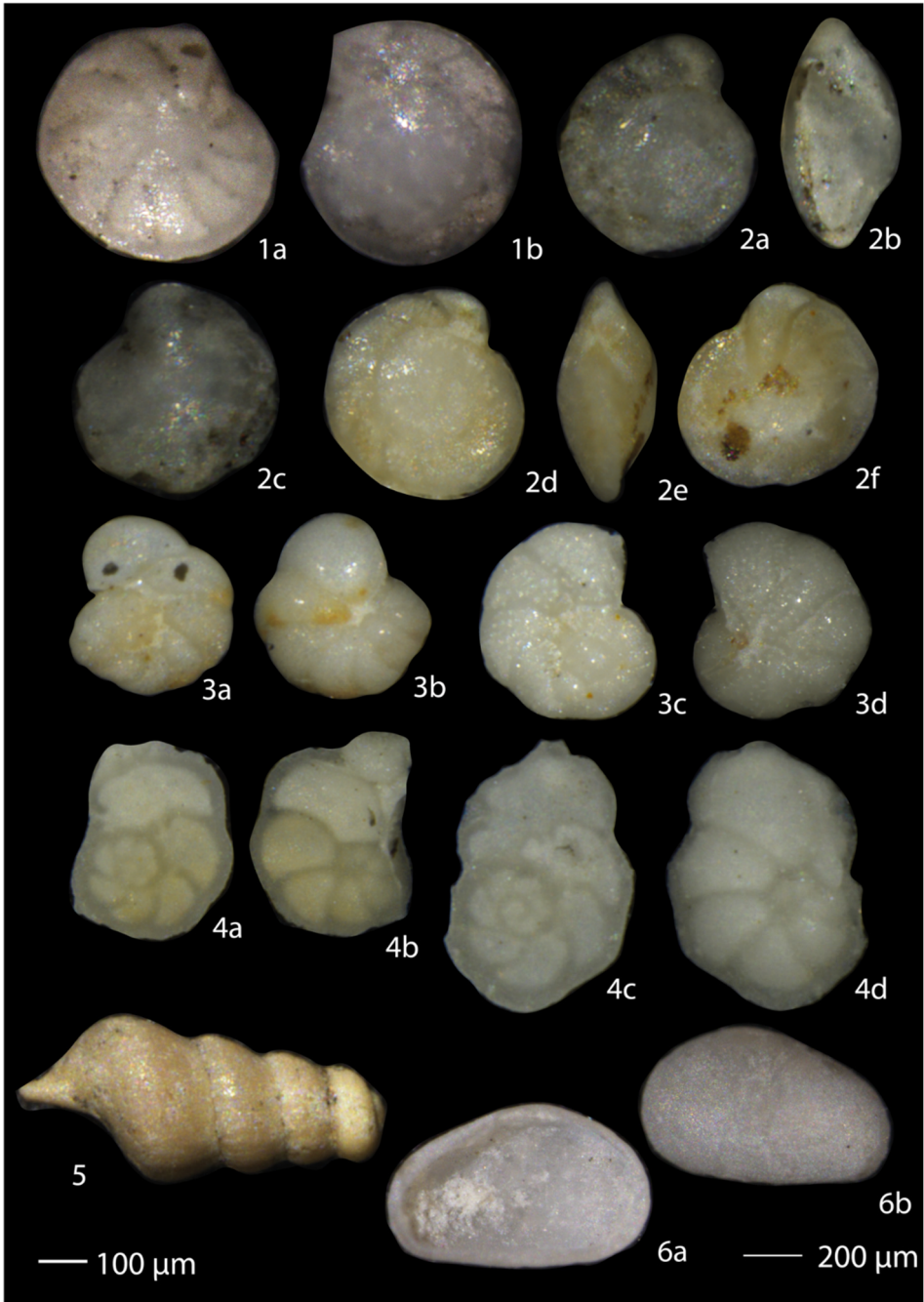


Plate 4: Optical microscope photos of the most abundant (>3%) benthic foraminifer species and one gastropod and ostracod species of Brranco del Negro section. **1** *Cibicoides pseudoungerianus*: **a** spiral view, **b** umbilical view; **2** *Cibicoides kullenbergi*: **a**, **d** spiral view, **b**, **e** apertural view, **c**, **f** umbilical view; *Cibicides lobatulus*: **a**, **c** spiral view, **d**, **e** umbilical view; *Cibicides refulgens*: **a**, **c** spiral view, **d**, **e** umbilical view; **5** gastropod; **6** *Cyprideis* sp.. Scale bar = 100 µm, 200 µm for the ostracod.

4.3 Sorbas basin: Zorreras section

In the Zorreras section foraminifers are very scarce but well preserved, even though their surface is sometimes covered by minerals. The first benthic foraminifers appear at the base of the grey layer, rich in calcareous nodules. From that level upward very scarce specimens of *N. fabum* and even fewer *Elphidium* spp. are present in the analysed samples, until the top of the section, right on top of the transgressive bivalve lag (Figure 5 B). Planktic foraminifers are absent.

4.4 Alboran Basin: ODP Site 976

4.4.1 *Micropalaeontological content and stable isotopes*

In the lower Pliocene sediments of ODP Site 976 benthic and planktic foraminifers show well preserved tests, even though they are sometimes overgrown with calcite. We consider the foraminifers as being in situ and suitable for palaeoenvironmental analyses. Ostracods were not found at this site. Optical microscope photos of the benthic foraminifera species are shown in Plates 5 and 6.

The base of the studied core is characterised by a significant peak abundance of *Bulimina aculeata* (~30 %), which disappears at 573 mbsf, and by *Melonis barleeanus* (~25 %), *Lenticulina* spp. (~18 %), *S.bulloides* (~12 %), *Nodosaria* spp. (~10 %) and *M. soldanii* (~12 %) remaining present throughout the record. From 572.4 mbsf, the abundances of *Globocassidulina subglobosa* (~20 – 40 %), *Uvigerina peregrina* (~30 %), *Bulimina striata* (~12 %) increase. At 569 mbsf, coinciding with a sharp decrease of *U. peregrina*, the percentage of reworked species rises to ~10 % (Figure 12).

The dendrogram divides the benthic assemblages in two main clusters (Cluster 1 and Cluster 2) and of three subclusters (Cluster 2.2.2, Cluster 2.2.1 and Cluster 2.1). The clusters allow the identification of four stratigraphic units (Unit 1, Unit 2, Unit3, Unit 4) characterised by the benthic foraminifer assemblages in the dendrogram. The two species of Cluster 1 dominate the first 0.5 m of the studied interval and represent Unit 1 (573.5-573.1 mbsf). In this Unit, *B. aculeata* reaches 30%, *C. dutemplei* only reaches 4% and both can also be found in the overlying Unit 2, before disappearing almost completely in Unit 3. Less abundant in Unit 1 are the species forming Cluster 2.2.2 which dominate Unit 2 (Figure 13 B). Cluster 2.2.2 extends from 573.1 until 572.5 mbsf and contains 19 benthic species (Figure 13 A). Most abundant are *M. barleeanus* and *Lenticulina* spp., with maximum relative abundances of 30 % and 20 % respectively (Figure 12), followed by *M. soldanii* reaching 10 % and *Nodosaria* spp. and *Globobulimina*

spp. which both have a maximum abundance of 8 %. The remaining species characterising Unit 2 do not surpass 6 % of abundance.

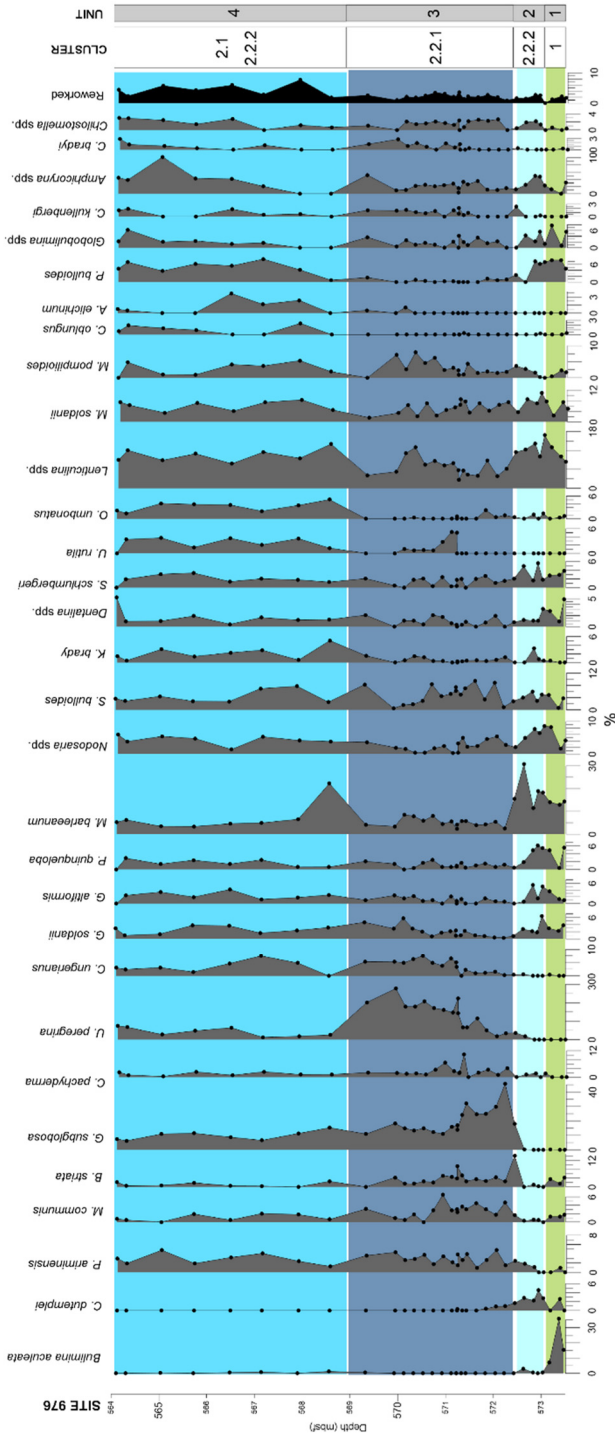


Figure 12: ODP Site 976: Variations in relative abundances of major benthic foraminiferal taxa. Color bands correspond to foraminiferal assemblages associated with the clusters of the dendrogram (Figure 13) and Units 1-4.

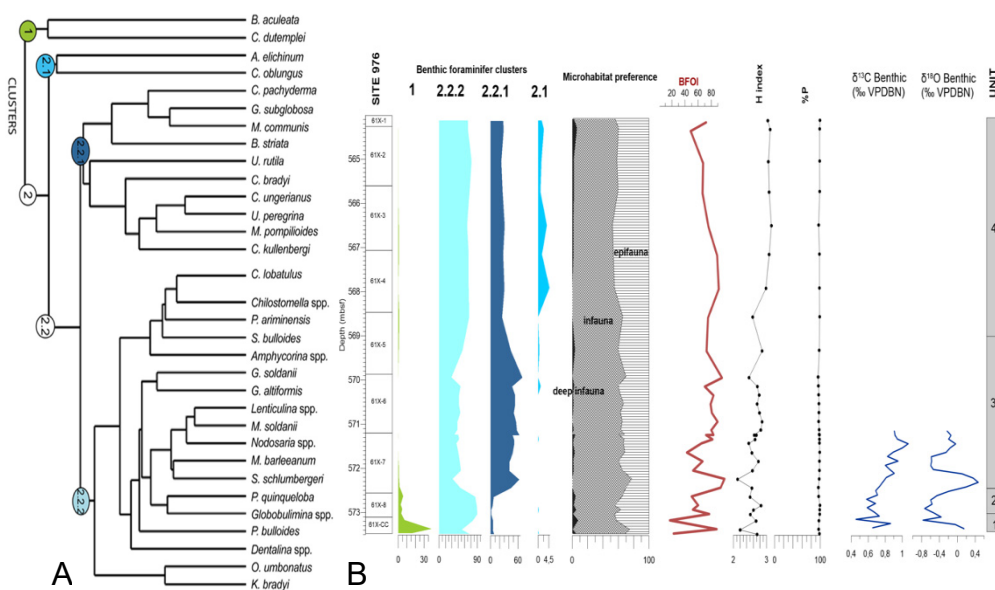


Figure 13: ODP Site 976: A) Dendrogram resulting from the hierarchical clustering that divided the benthic foraminifer species in two main species clusters (Cluster 1, Cluster 2) and two subclusters (Clusters 2.1 and 2.2). Cluster 2.2 in turn branches into two subordinate branches as well (Cluster 2.2.1 and 2.2.2). The used clusters have been highlighted with specific colors. B) From left to right: Clusters 1, 2.1, 2.2.1 and 2.2.2 plotted against stratigraphic position; Microhabitat distribution of the most abundant benthic foraminifer species; The BFOI estimation (Kaiho, 1994); Shannon diversity index; % of planktic foraminifers; Benthic $\delta^{13}\text{C}$ and $\delta^{18}\text{O}$ isotopic record (*C. pachyderma*).

Unit 3 (572.5-569 mbsf) not only shows a change in benthic foraminifer association but also a sharp increase in BFOI reaching a value of 85, remaining relatively stable until the top of the record. The dominant species of Unit 3 are comprised in Cluster 2.2.1 (Figure 13 A). Among the dominating species of Unit 3 are *G. subglobosa* (~45 %), *U. peregrina* (~30 %), *C. pachyderma* (~25 %) and *C. ungerianus* (~20 %), whereas the remaining species of Cluster 2.2.1 vary in abundance between 6 and 12 % (Figure 12). Finally, the topmost Unit 4 with 6 m thickness is the thickest interval from 569 mbsf until the top of the record (Figure 13 B). This Unit is composed of the association of Cluster 2.2.2 together with the taxa in Cluster 2.1. Cluster 2.1 includes only two species, *Anomalinoidea helicinus* and *Cancris oblongus* (Figure 13 A), the first being the most abundant reaching 10% abundance (Figure 11). The other dominant species of Unit 4 are mostly part of Cluster 2.2.2 (Figure 13 B) and include *Lenticulina* spp. (~16 %), *Amphycorina* spp. (~10 %), *M. soldanii* (~10 %) and *S. bulloides* (~8 %). Additionally, Unit 4 contains significant abundances of *G. subglobosa* (~15 %) and *C. ungerianus* (~20 %) from Cluster 2.2.1 as well as the higher percentages of displaced benthic foraminifers (~10%).

The record is characterised by increasing diversity of benthic foraminifers (H index increasing upward; Figure 13 B). Planktic foraminifers are very abundant throughout the record (~95 %).

Although the microhabitat preferences do not show major changes over the studied interval and infaunal species prevail with a stable 65 %, the BFOI shows significant oscillations. Especially until 571.5 mbsf, the values vary from ~20 to a maximum of ~85 and stabilise at ~80 % in Unit 3 (Figure 13 B).

At 572.5 mbsf, the Pliocene markers *G. margaritae* and *Sphaeroidinellopsis* spp. appear, while the dominant planktic foraminifer species are *G. bulloides*, *G. apertura* and *N. acostaensis*. Less dominant species include *Globorotalia scitula*, *Globigerinoides* spp., *Neogloboquadrina atlantica*, *G. glutinata* and *O. universa*.

The benthic stable isotope record of Site 976 covers only the first ~3 m of the Pliocene sequence (Figure 13 B). The benthic $\delta^{13}\text{C}$ curve displays a continuous increasing upward trend, from a minimum of ~0.4 ‰ to maximum values of ~1 ‰ towards the top of the studied interval. The benthic $\delta^{18}\text{O}$ record oscillates between ~-0.8 and -0.2 ‰ and shows a positive peak at 572.8 mbsf, when it reaches values of ~0.6 ‰.

4.4.2 Palaeo-water depth reconstruction

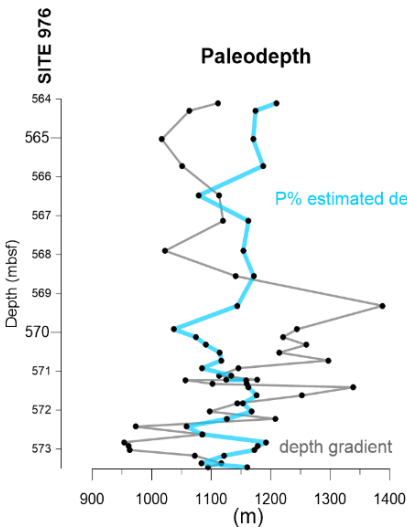


Figure 14: Calculated palaeodepths for ODP Site 976. The grey line is the palaeodepth estimated by gradient analysis (Hohenegger, 2005; Hohenegger et al., 2008). The blue line is the palaeodepth estimated by using the %P (Van der Zwaan et al., 1990).

the rest of the record varies between 0 and 200 m.

Because the benthic foraminifers are considered in situ, palaeodepth has been calculated for ODP Site 976. A first approximation of the palaeodepth can be derived from the $\%P = 100 \cdot P / (P + B)$ (%P; Van der Zwaan et al., 1990; Figure 13 B). Applying the regression in the e-power formula (equation 7 on p. 13), the palaeodepth was relatively stable and varied between a minimum of ~1000 m ($\%P \sim 98\%$) and a maximum depth of ~1200 m. The palaeodepth reconstruction based on the transfer function (Figure 14) of (Hohenegger, 2005; Hohenegger et al., 2008) yields lower values in 1/3 of the section, apart from the interval from 571 and 569 mbsf. The depth variability is also higher and values vary between 950 and 1400 m. The difference between the reconstructions amounts to a maximum of 250 m in this interval, while throughout



Plate 5: Optical microscope photos of some of the most abundant (>3%) benthic foraminifer species identified at Site 976. **1** *Sigmoilopsis schlumbergeri*; **2** *Martinotiella communis*; **3** *Karreriella bradyi*; **4a-b** *Lagena* spp.; **5** *Pseudonodosaria* spp.; **6** *Amphicoryna* spp.; **7** *Dentalina* spp.; **8** *Bulimina striata*; **9** *Bulimina aculeata* **10** *Uvigerina peregrina*; **11a-b** *Globobulimina* spp.; **12a-b** *Uvigerina rutila*; **13** *Globocassidulina subglobosa*; **14** *Sphaeroidina bulloides*; **15** *Anomalinooides elichinum*; **16** *Lenticulina* spp.; Scale bar = 100 μm .

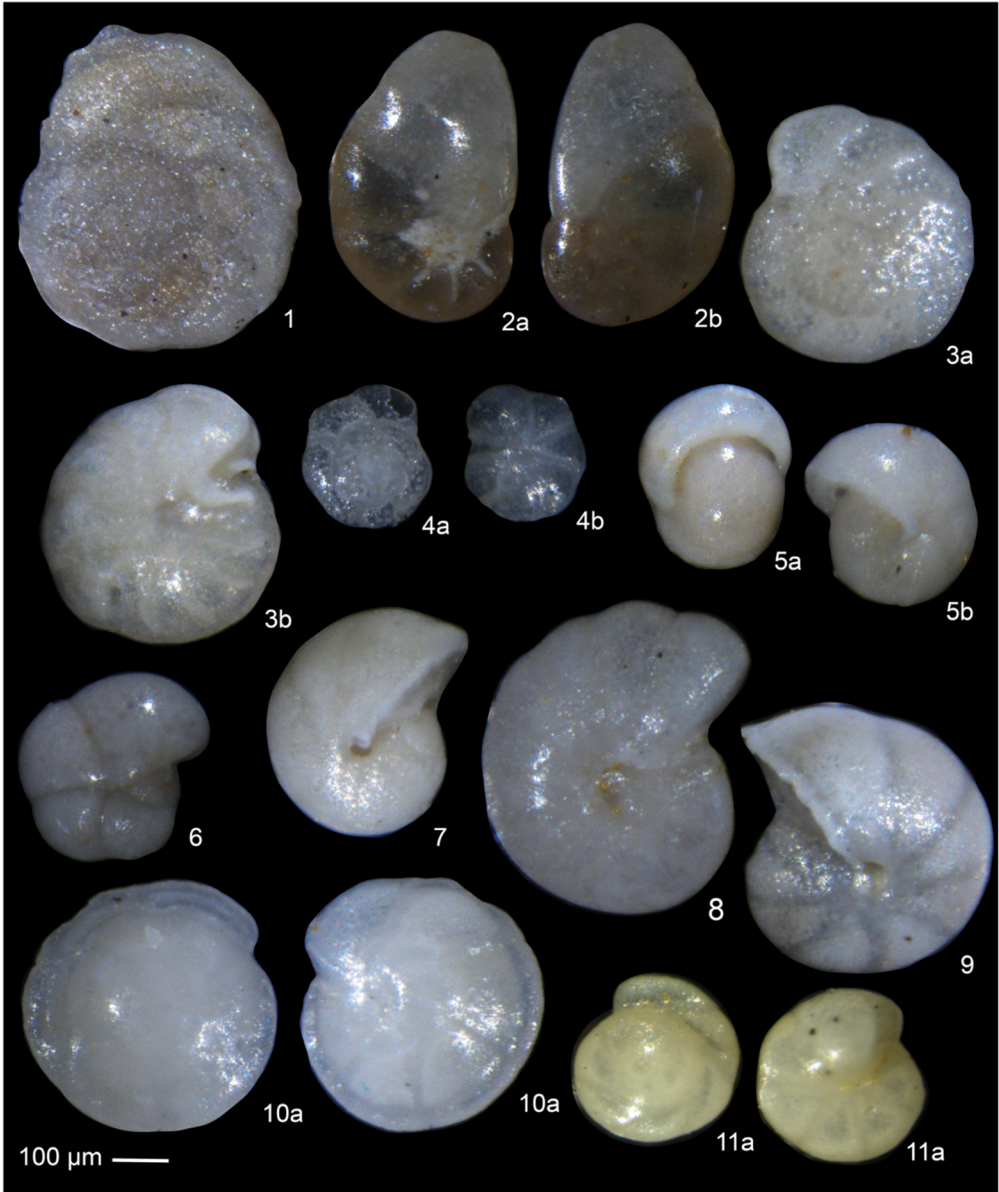


Plate 6: Optical microscope photos of some of the most abundant (>3%) benthic foraminifer species identified at Site 976. **1** *Planulina ariminensis*; **2** *Cancris oblongis*: **a** spinal view, **b** umbilical view; **3** *Cibicidoides ungerianus*: **a** spinal view, **b** umbilical view; **4** *Cibicides bradyi*: **a** spinal view, **b** umbilical view; **5** *Pullenia bulloides*: **a** apertural view, **b** lateral view; **6** *Pullenia quinqueloba*; **7** *Melonis soldanii*; **8** *Melonis barleanus*; **9** *Melonis pompilioides*; **10** *Oridorsalis umbonatus*; **11** *Gyroidina altiformis*: **a** spinal view, **b** umbilical view Scale bar = 100 μm.

5. Discussion

5.1 Distinctive black/grey layers at the Miocene-Pliocene boundary

The nature of the MPB in the Mediterranean is expressed in several ways including conformable contacts above continental facies (Sorbas Basin, e.g., Roveri et al., 2018), shallow (Nijar Basin: Bassetti et al., 2006, this work; Malaga Basin: Guerra-Merchán et al., 2008, this work) and deep LM deposits (Eraclea Miono: e.g., Brolsma, 1978; Sites 975 and 974: Iaccarino and Bossio, 1999; Iaccarino et al., 1999a) or with an erosional surface both in deep and shallow basins (e.g., Chelif Basin: Rouchy et al., 2007; Vera Basin: Caruso et al., 2020; Alboran Basin: Bulian et al., 2021), marked at some locations by the intercalation of conglomerates, breccias or small clasts (Site 975: Iaccarino et al., 1999b; East Alboran Basin: Garcia-Castellanos et al., 2019; Levant Basin: Madof et al., 2019).

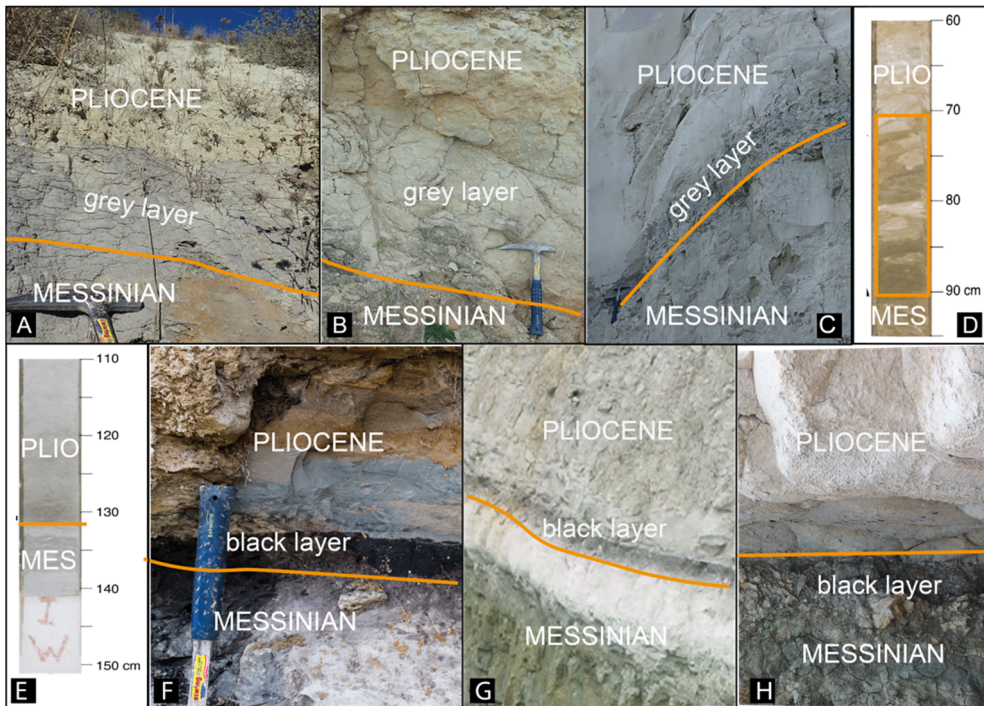


Figure 15: Photographs of the Miocene-Pliocene boundary from some of the mentioned locations. A) Rio Mendelin section; B) Sorbas Basin; C) Eraclea Minoa section D) ODP Site 974 (Iaccarino et al., 1999b); E) ODP Site 975 (Iaccarino et al., 1999b); F) Barranco del Negro section; G) Moncucco quarry in Piedmont Basin (Trenkwalder et al., 2008) and H) Zakynthos island in Greece (courtesy of K. Agiadi).

In several land sections and offshore sites (in Italy, Crete, Cyprus, Ionian Islands, Spain, Algeria), the boundary is recognized through marked changes in lithology, carbonate content or stable isotopes of carbonates (Iaccarino et al., 1999b; Pierre et al., 2006; Rouchy et al., 2007). A particularly striking lithology identified at the MPB in the Piedmont Basin (Figure 15 G; Trenkwalder et al., 2008; Dela Pierre et al., 2016), Northern Apennines (Botteghino, Buttafuoco and Montepetra sections; Gennari et al., 2008; Grossi et al., 2008), Northern Italy (Riforgiato et al., 2011), Cyprus (Rouchy et al., 2001; Manzi et al., 2016) and DSDP Site 376 (Cita et al., 1978), and Zakynthos (Figure 15 H; personal communication by K. Agiadi) is a cm/dm-thick black layer deposited conformably above the LM deposits. This black layer is usually rich in organic matter (Gennari et al., 2008: T.O.C < 5 %; Trenkwalder et al., 2008; Manzi et al., 2016) and scarce in planktic and benthic foraminifers which are usually typical Pliocene species or reworked Miocene to Eocene species or in some cases both (Cita and Zocchi, 1978; Gennari et al., 2008; Manzi et al., 2016), while at some locations microfossils are absent (e.g. Moncuoco quarry: Trenkwalder et al., 2008). The palaeoenvironmental significance of such dark layer remains still largely unknown, even if it has been interpreted as a result of rapid change in water salinity (e.g. Gennari et al., 2008). In the Barranco del Negro section of the Nijar Basin, the MPB is also marked by a distinct black layer (Figure 15 F) that contains small gastropods, some ostracods from the genus *Cyprideis* and abundant planktic and benthic foraminifers, probably reworked (see section 5.2). In other sections in the Nijar basin like Los Ranchos (Pérez-Asensio et al., 2021) or Barranco de los Castellanos (Aguirre and Sánchez-Almazo, 2004) such layer is absent, while in the Los Feos section the MPB is represented by a grey layer containing reworked foraminifers (Bassetti et al., 2006; Bulian, unpublished data).

A similar but less intense lithological change is registered with the deposition of a grey clay layer in the Rio Mendelin section (75 cm thick), conformably above shallow water late Messinian sediments. In the Sorbas Basin, a grey layer containing carbonate nodules was deposited at the base of the Pliocene, overlying reddish continental late Messinian deposits (Figure 15 B). A grey layer has been also identified at the MPB in Eraclea Minoa where it tops the Arenazzolo formation (Figure 14 C; Brolsma, 1978; Pierre et al., 2006; Bulian, unpublished data). In deeper locations like ODP sites 975 (South Balearic Basin) and 974 (Tyrrhenian Basin; Iaccarino and Bossio, 1999; Iaccarino et al., 1999a; Figure 15 D, E), the grey layer is deposited at the MPB and suggesting a potential organic matter accumulation and reduced oxygen levels possibly caused by water column stratification, while the small clasts found in the Balearic Basin have been interpreted as the result of the first ingress of Atlantic waters into the Mediterranean Basin (Iaccarino and Bossio, 1999).

To understand better the depositional mechanisms of the dark layer and to assess whether water column stratification was present during the early Zanclean, it is fundamental to consider the palaeoenvironment present in the Mediterranean before the reestablishment of an efficient Mediterranean – Atlantic connection (i.e., LM phase). As suggested by the presence of a Paratethyan brackish fauna (ostracods, molluscs and dinocyst) in most upper Messinian sediments (e.g., Iaccarino et al., 1999b; Fortuin and Krijgsman, 2003; Orszag-Sperber, 2006; Rouchy and Caruso, 2006; Roveri et al., 2008; Guerra-Merchán et al., 2014; Stoica et al., 2016), the Mediterranean was most probably invaded by Paratethyan waters that created a brackish water layer (up to 250 m of thickness) on the Mediterranean surface (Marzocchi et al., 2016). Considering the most accepted deep basin MSC model (CIESM, 2008; Roveri et al., 2014a), the inflow of Paratethyan waters would lower the salinity of the Mediterranean marginal basins. At the MPB, with the increase of the Atlantic inflow, the marginal basins, filled with brackish water, would be invaded by more saline Atlantic waters which sank creating a stratified water column. This stratification could favour bottom water oxygen depletion and organic matter accumulation and explain the deposition of organic rich layers. These black layers thus represent the first reaction of the system to the reflooding, before the mixing of the two water masses and establishment of normal marine conditions. Similarly, in the Black Sea region, marine flooding events from the Mediterranean, characterised by the presence of foraminifers and calcareous nannofossils (Krijgsman et al., 2010; Radionova et al., 2012) first create anoxic conditions as exemplified by a conspicuous dark layer barren of Paratethyan ostracods (Stoica et al., 2016). Such events have been identified in the late-Langhian (Sant et al., 2019), Pontian (Stoica et al., 2016) and even Pleistocene (Ross, 1978; Schrader, 1978) Black Sea sediments. In the Mediterranean the MPB layer assumes two different aspects, and sometimes it materializes as a blacker layer and other times it displays only a grey shade. Consequently, it appears that the conditions at the time of the Atlantic incursion in the Mediterranean were different depending on the location and depth at the time of the reflooding. A strong water-mass stratification could lead to oxygen depleted environments and the accumulation of organic matter with the formation of a black layer. This could occur in basins located below the oxic/anoxic interface, while in basins located in the upper, more ventilated, part of the water column the bottom water properties were less affected. In the Sorbas Basin, where the latest Messinian environment was continental, the grey layer materialises as a palaeosol-like horizon and shows a gradual transition to a shallow marine environment.

The mechanism described for the deposition of the dark layers in the marginal basins is compatible with a LM scenario where the Paratethys water lid over the Mediterranean freshens the margins of the basin. Nonetheless, such

scenario for the deepest basins would mean a stratified water column and bottom water oxygen depletion already in the latest Messinian, like it happens during sapropel deposition, when a freshwater lid prevents the oxygenation of deep waters (e.g. Rohling et al., 2015 and references therein). In Stage 2 of the MSC, when the majority of salt was deposited, its dissolution in deep water layers would have caused stratification (e.g., Krijgsman et al., 2018), but during Stage 3 when evaporite precipitation ceased, this was probably not the case unless deep water is in contact with salt bodies (e.g., De Lange et al., 1990). From shallow and deep late Messinian Mediterranean sites any evidence of anoxia or reduced oxygen levels is missing and considering that the dark interval has been identified at the MPB of deep basins as well, the late Messinian palaeoenvironmental scenario must be revised. To explain a dark, sometimes organic-rich layer and the occurrence of stress taxa at the MPB all over the Mediterranean we suggest that the early Pliocene water column was stratified to some extent both in the margins and in the deeper basins. Such stratification could only form if Paratethyan brackish waters and/or fresh riverine inflow would have decreased the total salinity of the basin (not excluding a discrete vertical density gradient) allowing the Atlantic saltier waters to enter the basin, sink, and initially develop a stratified water column.

At Site 976, the dark layer has not been found. We consider this absence related to the vicinity to the Gibraltar gateway and the presence of an important erosional surface (see Section 2.2; Bulian et al., 2021).

5.2 Benthic foraminifer repopulation sequence

Repopulation of the benthic environment by foraminifers after the MSC has been reported from sites across the Mediterranean and at different water depths (e.g., Sicily: Brolsma, 1978; Sgarrella et al., 1997, 1999; Barra, 1998; Piemonte: Violanti et al., 2009, 2011; central Italy: Riforgiato et al., 2011; Tyrrhenian Sea: Sprovieri and Hasegawa, 1990; Iaccarino et al., 1999; Cyprus: Rouchy et al., 2001; Spain: Nijar Basin: Van de Poel, 1991, Pérez-Asensio et al., 2021; Vera Basin: Caruso et al., 2020). Uppermost Messinian LM deposits were either barren or containing brackish to fresh/continental faunas, including reworked biota. Early Pliocene repopulation by benthic foraminifers shows similarities with recent recovery from biologically and chemically hostile environments, and with repopulation following low-oxic or azoic episodes during sapropel deposition. In Recent environments repopulation is reported after short-lived events on geological time scales (e.g. hurricanes, ash falls or shelf anoxia: (e.g., Alve, 1999; Kuhnt et al., 2005; Platon et al., 2005; and references therein). Recovery from short-lived events is not directly comparable to fossil settings, since the temporal resolution of fossil samples is at least a century (Rohling et al., 1997). Repopulation after sapropel deposition differs between sites, depending on

depth, hydrographic regime, and local environmental conditions, and repopulation sequences within the same basinal setting also differ between sapropels. Although different taxa may be involved in each repopulation sequence, Jorissen (1991 and references therein) discerns some general patterns when morphogroups are considered rather than abundances of individual species. The author defines four morphogroups, of which three apply to repopulation sequences (for references Jorissen, *op. cit.*, Table 1): group A. deep infauna tolerating extreme hypoxia in relatively stable environments (e.g., *Chilostomella* and *Globobulimina* spp.); group B. intermediate infauna, less tolerant to extreme hypoxia (elongated bi- and triserial taxa, e.g., bolivinids, buliminids, *Cassidulinoides* spp.); group C. so-called 'phytodetritus species', commonly small, biconvex and trochospiral taxa tolerating oxic to hypoxic, unstable environments and reproducing fast after seasonal input of fresh phytodetritus (e.g., small *Epistominella*, *Eponides* and *Gyroidina* spp.). Depending on local environmental conditions, either group A or group C will precede group B in a repopulation event. Benthic faunas containing among others *Epistominella* spp. were found in early Zanclean sections and cores throughout the Mediterranean (e.g., Sgarrella et al., 1997 (Sicily); Iaccarino et al., 1999b (Tyrrhenian Sea); Rouchy et al., 2001 (Cyprus); Aguirre et al., 2006 (Nijar Basin, Spain); Cipollari et al., 2013 (Adana Basin, Turkey); Caruso et al., 2020 (Vera Basin, Spain)) and are often considered benthic markers for the earliest Zanclean reflooding of the Mediterranean.

5.2.1 Marginal basins

Rio Mendelin section (Malaga Basin)

In the Rio Mendelin section, the benthic foraminifer assemblage of Unit 1 at the base of the section is poorly diversified and the sample immediately above the LM contains a monospecific assemblage composed of *Epistominella trinacria* (Figure 8). This species was described in Pliocene sapropels by Verhallen (1991) without further details; its occurrence is explained by analogy with other *Epistominella* species (mentioned in Group C cf. Jorissen, 1999). In recent environments *Epistominella* species have been found associated with seasonal deposition of fresh phytodetritus in oxic as well as sub-oxic (but not anoxic) environments (*E. exigua*: Gooday, 1988; Gooday, 1993; *E. vitrea*: Gooday and Hughes, 2002; Platon et al., 2005; Langezaal et al., 2006). Smart et al. (1994) proposed the use of *E. exigua* as a proxy for pulsed supply of organic matter to a generally oligotrophic sea floor. In the fossil record, *Epistominella* species have been found just below, and in repopulation sequences above sapropels and after the MSC in the lower Pliocene (see above). Occurrence of epistominellids suggests that these earliest Pliocene environments were oxic to sub-oxic, and

prone to seasonal variations. In Unit 1, planktic foraminifers are barely present (Figure 9).

The abundance of *E. trinacria* declines rapidly after the lowermost, monospecific sample and the abundance of *Nonion fabum* increases to nearly 50% at the top of Unit 1. *Nonion* spp. are versatile species, related to high food availability and organic carbon content, phytodetritus and typically low oxygen conditions, although they can be found living under oxic conditions as well (Fontanier et al., 2002; Diz et al., 2004; Mendes et al., 2004; Mojtahid et al., 2006). Subordinate species increasing in abundance in Unit 1 are *Stainforthia fusiformis*, *Fursenkoina acuta* and *Globobulimina turgida* (Group A cf. Jorissen, 1999; Cluster 2.2). These taxa suggest a transition from an unstable, relatively oxic environment characterised by *E. trinacria* towards a more stable, more differentiated but also more hypoxic environment towards Unit 2, the grey layer (Jorissen, 1999). Together with these species tolerating severe hypoxia, *Bulimina aculeata*, *B. elongata*, and *Bolivina dilatata* appear, elongated bi- and triserial taxa less resistant to hypoxia (Jorissen, *op. cit.*, Group B). Towards the top of Unit 2, *B. seminuda* and *Oridorsalis stellatus* increase in abundance (cluster 2.1.2A, Figure 9), suggesting a renewed, or continued, repopulation in more oxic and less stable conditions toward the yellowish strata of Unit 3. At the same time, planktic foraminifers become more abundant and keep increasing towards the top of the section (Figure 9). This repopulation sequence is comparable to the one identified after Quaternary sapropel layers (S1, S5, S6) at different Mediterranean sites (Jorissen, 1999). The base of Unit 3 reflects a more stable normal marine assemblage under relatively oxic conditions: the diversity (H) increases to 3 and the BFOI, which is minimal in the grey layer supporting rather strong hypoxia, increases to 80% in Unit 3 (Figure 9) and the hypoxia-tolerant species of cluster 2 decrease in abundance or disappear.

The Cluster 2.1.2 A assemblage prevails in the record until 4 m (Figure 8 and 9), when Cluster 2.1.2 B composed of *C. dutemplei*, *C. pseudoungerianus*, *C. ungerianus* and *Textularia calva* becomes dominant. Even though *Textularia* spp. are tolerant to food-enriched and oxygen-deficient conditions (Naehler et al., 2012), the predominant genus *Cibicides/Cibicidoides*, epifaunal to shallow infaunal and with low tolerance to oxygen deficiency (van der Zwaan, 1982; Jorissen et al., 2007), suggests relatively well oxygenated waters and moderate productivity for this interval (until 6.4 m). Such conditions are confirmed by the highest corresponding oxygen index, which reaches values close to high oxic environments (BFOI = ~90%; Figure 9), slightly higher than the ones of Cluster 2.1.2 A. Beginning in Unit 3, the benthic foraminifer assemblages show a clear alternation between Cluster 2.1.2 A and Cluster 2.1.2 B (Figure 9), hence between a predominantly infaunal assemblage (buliminids, bolivinids, *N. fabum*, *Lenticulina* spp.) linked to high productivity and reduced oxygen content at the

seafloor, and an epifaunal one, characterised by *Cibicides/Cibicidoides* species and indicating more oxic conditions. Despite the lack of time control, we suggest these cycles are most probably the result of an alternation between phases characterised by lower versus higher nutrient input and riverine discharge to the basin associated to changes in the freshwater budget (see Section 5.4). The benthic and planktic $\delta^{18}\text{O}$ (Figure 9) in fact show the heaviest values in concomitance of Cluster 2.1.2 B peaks, suggesting a possible astronomical control over the cyclicity.

In summary, the instantaneous appearance of a monospecific benthic foraminiferal fauna consisting of the 'phytodetritus species' *Epistominella* marks the start of benthic repopulation following the incursion of marine waters and an unstable palaeoenvironment characterised by high seasonality and relatively high oxygen levels. The grey clays (Unit 2) reflect stable, quiet conditions under rather severe hypoxia, more likely water stratification related to further sea-level rise than influx of large amounts of organic matter. Apparently, when sea level rose further circulation and ventilation ameliorated, eventually supporting a diverse open marine benthic foraminiferal assemblage. Analogous early Pliocene conditions have been suggested by the repopulation sequence found at the Cava Serredi section (Central Italy; Riforgiato et al., 2011), where lowermost Zanclean sediments are dominated by phytodetritus feeders and shallow infaunal group species (*Epistominella*, *Bolivina*, *Bulimina*), while after a few metres shallow infauna group dominates.

Barranco del Negro section (Nijar Basin)

The calcarenites above the black and grey layer suggest a nearshore, dynamic environment (see section 5.3.1), but the reconstruction of palaeoenvironments and the repopulation by benthic foraminifers are complicated by the presence of reworked planktic foraminifers throughout the section (Section 4.2; Table 3). Foraminifers are found in continental deposits below, and in the black-grey layer. We assume these levels are barren and the few foraminifers encountered reworked. The number of benthic foraminifers per gram of sediment (BF/g; Figure 11), which is very low in the black and grey layer, rises steadily suggesting that the number of reworked and displaced foraminifers is relatively low, and more indigenous benthic foraminifers start occurring above the black-grey layer. In the first sample above the grey level *Chilostomella* and *Globobulimina* species appear which, if in situ, may be part of a repopulation sequence in an initially stable, hypoxic-anoxic environment (Group A of Jorissen, 1999).

The benthic foraminifer species expected to thrive in a deltaic or shoreface, dynamic palaeoenvironment is *Cibicides lobatulus* (Hald and Korsun, 1997).

Cibicides lobatulus is absent in the sample with *Chilostomella* and *Globobulimina* spp. and the abundance then rises to nearly 30%, suggesting that at least part could be in situ. Not expected to thrive in shallow, dynamic shoreface environments are *C. kullenbergi*, *P. ariminensis*, *U. rutila*, and probably also *C. pseudoungerianus*, *C. ungerianus* and *S. bulloides*; this would imply that together with the Miocene planktic foraminifers, these lower neritic to bathyal benthic foraminifers are reworked throughout the section.

Assuming that other species (e.g., *Spiroplectinella deperdita*, *Elphidium* spp., *Pullenia bulloides*, *P. quinqueloba*, *Lenticulina* spp., *Cassidulina* spp.?) may at least be partially in situ, the benthic foraminifer assemblages are in agreement with shallow, high-energy environments. Several opportunistic taxa feeding on fresh phytodetritus indicate episodes of intermittent, seasonal supply of organic matter. Among these are *Valvulineria* spp. including *V. bradyana* (Amorosi et al., 2013; Goineau et al., 2015 and references therein), with a maximum abundance of 20% at ± 1 m. A maximum abundance of 30% *Epistominella trinacria* occurs at ± 1.5 m and is here not associated with repopulation. Apart from *Cibicides refulgens* and *C. lobatulus*, living attached to hard substrates, the taxa here assumed to be in situ are shallow infaunal and indicate a generally more oligo- to mesotrophic, hypoxic environment towards the top of the sampled section (e.g., Jorissen, 1987; Kaiho, 1999; Murray, 2006).

Zorreras section (Sorbas Basin)

In the Zorreras section, where the upper Messinian is continental, the lowermost Pliocene sediments consist of clastic sands. Planktic foraminifers are absent, benthic foraminifers are scarce and low-diverse and no clear repopulation sequence is found. The first species to appear in the grey layer is monospecific *Nonion fabum*, included in the shallow infauna group, which is in the Rio Mendelin section the dominant species immediately following the level with monospecific *Epistominella trinacria*. Here, the presence of numerous calcareous nodules together with *N. fabum* known to tolerate shallow inner shelf environments end eutrophic conditions (Fontanier et al., 2002; Murray, 2006; Duchemin et al., 2008), suggest that the palaeoenvironment was not permanently under water. Intermittent water inputs could have entered the basin through a geological barrier at the Mediterranean connection. While *Nonion fabum* dominates the entire section, at 1.1 and 1.2 m above the base of the Pliocene some *Elphidium* spp. and rare *C. lobatulus* appear. This suggests a gradual ingression of marine waters and a nearshore marine environment which was permanently established after the strong transgressive pulse that deposited a 5-cm thick bivalve-rich horizon.

5.2.2 Deep basin

ODP Site 976 (Alboran Basin)

The lowermost Pliocene Unit 1 at Site 976 may not be the very basal Pliocene because there is an interval of non-recovery in core 62, right below the first Pliocene sediments (Figure 6). A relatively diverse planktic assemblage is present from the base of the studied interval, with *Globorotalia margaritae* and *Sphaeroidinellopsis* spp. appearing at 572.6 m and 572.3 m respectively (Bulian et al., 2021). A benthic repopulation sequence comparable to the Rio Mendelin section is not developed at Site 976. Phytodetritus species (small biconvex taxa: epistominellids, *G. subglobosa*, small *Gyroidina* spp.) and deep infaunal taxa (e.g., *Chilostomella* and *Globobulimina* spp.; Jorissen, 1999) each amount to not more than 5%. Unit 1 is characterised by a single peak of *B. aculeata* (> 35%) and *C. dutemplei* (6%) together forming Cluster 1 (Figure 12). *Bulimina aculeata* is one of the more opportunistic taxa in the Mediterranean (De Rijk et al., 2000), feeding on detritus (Altenbach et al., 1999) and tolerating suboxic environments (Gebhardt, 1999). *Cibicides dutemplei* is generally assumed to tolerate little oxygen deficiency; however, *Cibicides* spp. have been found in oxygen-deficient environments as well and may be more sensitive to fresh (undegraded) food particles than to hypoxia (Jorissen et al., 2007). Barra et al. (1998) found that *C. dutemplei* tolerates oxygen depletion and elevated productivity. Unit 1 further contains a moderately diverse benthic assemblage ($H = 2.8$) consisting of most species in Cluster 2.2.2. Considering the abundance peak of *B. aculeata* co-occurring with stress tolerant species present in Unit 1 such as *M. barleeanum*, *M. soldanii* (Caralp, 1989; Koho et al., 2008), and *Lenticulina* spp. (Sen Gupta and Machain-Castillo, 1993; Kaiho, 1994) the basal Pliocene bottom-water environment of Site 976 was probably characterised by relatively high organic carbon supply and reduced oxygen levels, in agreement with the BFOI values (as low as ~20). Similar conditions are present throughout Unit 2, until 572.5 mbsf. Where Unit 1 is defined by the peak occurrence of *B. aculeata*, benthic foraminifer distribution in Unit 2 is still dominated by infaunal, sub-oxic taxa, represented by Cluster 2.2.2. (Figure 13).

The appearance of the benthic foraminifer association of Unit 3 (Figure 12 and 13) testifies a change in environmental conditions. The abundances of taxa in Units 1 and 2 decline (e.g., *C. dutemplei*, *M. barleeanus*, *Gyroidina*, *Globobulimina*, *Lenticulina* and *Pullenia* spp.). Taxa increasing in abundance include *G. subglobosa* (up to 40%) and later *U. peregrina* (Cluster 2.2.1). Although shallow infaunal taxa are still dominating the assemblage and the diversity (H-index) does not increase, the BFOI rises from a mean of 40 to a mean of 80 (Figure 13).

Dominance of *G. subglobosa* in the benthic foraminifer association (in both size fractions 150 μm and 63 μm) has been found in the oxygen minimum zone (OMZ) of the Sulu Sea under low oxygen conditions and high fluxes of organic matter (e.g., Miao and Thunell, 1993), but also in the generally oxic and oligotrophic environments of the Porcupine Abyssal Plain where the spring bloom delivers pulsed supply of fresh organic matter (Gooday, 1993). It has been found in moderately dysaerobic environments characterised by efficient preservation of organic matter (Loubère et al., 1988) as well as in early Pliocene recolonization successions (Barra et al., 1998). In the south Atlantic this species occurs on sandy substrate in strong bottom currents (Mackensen et al., 1985; Mackensen et al., 1993). Together with increasing abundance of *Planulina ariminensis* which is an epifaunal to elevated species, this can be related to an intensification of deep basin circulation activity during the final stage of Mediterranean infilling. *Uvigerina peregrina* is a shallow infaunal species associated with upwelling currents and labile organic material (Fontanier et al., 2002; Koho et al., 2008; Schmiedl et al., 2010). In addition, the *U. peregrina* interval identified in three other deep sites is referred to as the *U. pygmea-U. peregrina* event (Sgarrella et al., 1997; Barra et al., 1998; Iaccarino et al., 1999b) and has been used to confirm the early Pliocene age of the sediments.

Other species associated with this assemblage include *S. bulloides* and *B. striata* indicating an elevated organic carbon content (Sen Gupta and Machain-Castillo, 1993). *Cibicidoides pachyderma* and *P. ariminensis* can indicate well-oxygenated conditions (Schmiedl et al., 2000; Schmiedl et al., 2003), but they also tolerate oxygen deficiency and sustained organic matter fluxes (Bernhard and Gupta, 1999). The benthic foraminifer assemblage indicates a change in environmental conditions toward better circulation and installation of an upwelling regime. The change towards higher and more stable BFOI (~80-95) suggest a progressive increase in oxygen levels.

From 569 mbsf, the Cluster 2.2.2 association returns (Figure 13), with a maximum abundance of *M. barleeanus* (25%) at the base and with additional presence of *C. oblongus* and *A. helycinus* (Cluster 2.1). *Anomalinoidea helycinus* indicates increased productivity and/or preservation of organic matter (Barra et al., 1998) while *C. oblongus* can also be related to high organic flux and lower oxygen (Murray, 2006).

Despite differences, repopulation of the early Pliocene bottom-water environments at deep Mediterranean sites has elements in common. The earliest Pliocene is characterised by the presence of phytodetritus feeders at Site 975 and Eraclea Minoa (e.g., *Eponides pusillus* and *Epistominella exigua*) and contains shallow infaunal species at Sites 976 and 975 (e.g., *Bulimina* spp. and *Bolivina* spp.). All sites are characterised in the early Zanclean by reduced oxygen

conditions and high organic flux. After this first interval, all sites are characterised by a gradual amelioration of circulation that from sluggish changes into more oxygenated and in Eraclea Minoa to fully open marine conditions.

5.3 Early Pliocene palaeodepth reconstructions

5.3.1 *This study*

Rio Mendelin section (Malaga Basin)

According to the palaeodepth reconstruction based on Hohenegger (2005) and Van der Zwaan et al. (1990) and in agreement with the distribution of the benthic foraminifers, the first metre of Pliocene sediments of the Rio Mendelin section in the Malaga Basin shows an inner neritic environment (20-100 m) that has deepened to outer neritic depths (100-200 m) towards the top of the sampled record. The deepening-upward sequence is consistent with the transgressive nature of the earliest Pliocene sediments found in the hinterland of the Alboran Basin, filling the previously excavated canyons, such as the Guadalhorce (e.g. Schoorl and Veldkamp, 2003). Analogous shallow marine environments have been found in several other southern Spanish marginal basins like Bajo Segura (Soria et al., 2005; García-García et al., 2011; Corbí and Soria, 2016), Sorbas (Roveri et al., 2018; this study), Vera (Fortuin et al., 1995; Caruso et al., 2020) and Nijar (Bassetti et al., 2006; Pérez-Asensio et al., 2021; this study).

Barranco del Negro section (Nijar Basin)

The palaeodepth reconstruction of the Barranco del Negro section is primarily based on sedimentology, macrofauna (bivalves) and the ichnofossil *Thalassinoides*, since it cannot be not a priori known which benthic foraminifers are reworked or displaced. Above the black-and-grey layer, the sediments are dominantly composed of bioclastic sandstones, lacking structure except some planar bedding. These sediments have been interpreted as deltaic (Aguirre, 1998) or shoreface deposits (Omodeo Salé et al., 2012; Donovan et al., 2021), overlying the black-and-grey layer in a ravinement (transgressive) surface. This limits the depositional depth to shelf, in the case of lower shoreface probably not deeper than ~15-50 m, the precise depth depending on particular hydrographic settings (e.g., Anthony and Aagaard, 2020). *Thalassinoides* burrows and bivalve macrofauna including oysters usually occur in relatively shallow-water environments (Droser and Bottjer, 1987; Gingras et al., 2008; Roveri et al., 2018; Sharafi et al., 2021), although in more recent geological times they are also found at bathyal depths (Uchman and Demircan, 1999; Van Rooij et al., 2010). The

shells in the bivalve bed at 0.64 m are mostly broken, indicating high-energy environments, but bivalves are better preserved higher in the section, and together with the *Thalassinoides* burrows at 3 m indicate somewhat quieter environments, suggesting that a slight deepening may have occurred. In the top of the section a few *G. margaritae* are found, indicating deposition of the section during (MP11-) MP12.

In the nearby Los Ranchos section Perez-Asensio et al. (2021) reconstruct a palaeodepth of 274 m (upper slope) immediately after the MPB. A black-to-grey layer is absent; Pliocene silts and sands are deposited on top of a marly interval attributed to the LM. Reworking is only reported from these marls. The authors find shallowing-upward after the lowermost 4 m of Pliocene sediments and consider benthic foraminifers indicating upper slope environments in these basal 4 m to be indigenous (e.g., *Planulina ariminensis*). Comparing the two sections, the Pliocene silts and sands at Los Ranchos may have been deposited in a more distal environment than the inner-middle neritic calcarenites of the Barranco del Negro section reported here; however, if both sequences are deposited shortly after the MPB we infer that at the Los Ranchos section no initial deepening after the MPB is recorded.

Zorreras section (Sorbas Basin)

Considering the micropalaeontological content, the Sorbas Basin was characterised by a continental environment during the latest Messinian stage. The first Pliocene sediments to deposit are grey sands rich in carbonate nodules suggesting a very shallow, at times exposed environment. The Sorbas Basin foraminifer data are only qualitative; however, because of the absence of planktic foraminifers and the presence of shallow water taxa like *Nonion fabum* and *Elphidium* spp. (Hayward et al., 2001; Murray, 2006; Milker, 2010; Tulbure et al., 2017) the early Pliocene palaeodepth must have been less than 100 m.

Site 976

The palaeo-water depth reconstruction performed on the benthic foraminifer record of ODP Site 976 suggests that in the early Pliocene the East Alboran Basin was a lower bathyal environment (>1000 m). Analogous depths have been reported for the early Messinian at the same site (Bulian et al., in press). Similar early Pliocene palaeodepths have been reconstructed for the Tyrrhenian Basin and South Balearic Basin (Iaccarino and Bossio, 1999; Iaccarino et al., 1999a) as well as basins in Sicily (Sgarrella et al., 1997; Barra et al., 1998; Sgarrella et al., 1999).

5.3.2 Comparison with other locations

In general, depth reconstructions for earliest Zanclean DSDP and ODP Sites have been in the order of upper- to mesobathyal depths (1000 m and more). DSDP Leg 42A, Site 371 (South Balearic Basin) was estimated to be 1200-1400 m deep from the earliest Pliocene (Wright, 1978). For Leg 107, Sites 652-654 (Tyrrhenian Basin) and Leg 161, Site 974 (Tyrrhenian Sea) and 975 (Balearic Basin), the depth of MP11 was also estimated to be bathyal (McKenzie et al., 1990; Sprovieri and Hasegawa, 1990; Iaccarino et al., 1999a). Based on planktic foraminifer biostratigraphy, the MP11 in Site 975 (Iaccarino et al., 1999) is complete. This would imply that the Pliocene refill of this - and other - deep basins happened instantaneously on a geological time scale, or alternatively, the basins were not dry at that time, for which scenario recently new arguments have been given (e.g., Marzocchi et al., 2016; Stoica et al., 2016).

It is not always clear whether LM sediments are preserved in these deep basins but in most marginal basins, studied in land-based sections and several cores, the Zanclean sediments are found overlying continental and/or brackish LM facies (Fortuin et al., 2000; Guerra-Merchán et al., 2010; Caruso et al., 2020; Andreetto et al., 2021a and references therein; Andreetto et al., 2021b). At deeper marginal basins with age control based on planktic foraminifers shows that where the MPB is continuous and the MP11 zone is complete, for instance at Eraclea Minoa (Brotsma, 1978; Sgarrella et al., 1997) instantaneous refill to bathyal depth must have occurred immediately after the MSC. Similarly, abrupt early Zanclean refill to bathyal depth is reported at sections in Piemonte (Violanti et al., 2009; Trenkwalder et al., 2008). At Cava Serredi (Tuscany: Riforgiato et al., 2011) the MPB seems to be continuous, but planktic foraminifers of MP11 and MP12 (*Sphaeroidinellopsis* spp.; *G. margaritae*) are not reported. Here the refill seems to be gradual, an initial circa-littoral palaeodepth is reported, deepening to outer neritic after 30 cm and to upper bathyal at ~7 m; however, the actual base of the Zanclean may be missing at this location. This would imply that a (rapid) deepening of at least 500 m occurred at the base of the Zanclean.

For shallower marginal basins, where age control is sub-optimal or even absent, the picture is less clear and erosional surfaces are often reported to be associated with the MPB. Despite the erosional surface in the Cuevas del Almanzora section in the Vera Basin, the MP11 zone is reported to be complete. Caruso et al. (2020) reconstruct a water depth of >250 m immediately after the MPB, which implies that the erosional surface removed part of the LM deposits. This may be related to base level variations during the latest Messinian, as was suggested by Gargani and Rigollet (2007), Stoica et al., (2016) and Andreetto et al. (2021b). At the Los Ranchos section however, a palaeodepth of 274 m immediately after the MPB (Perez-Asensio et al., 2021) is more likely caused by absence of the

basal Pliocene since only *G. margaritae* and no *Sphaeroidinellopsis* spp. are found, and no benthic repopulation sequence is reported. However, at Rio Mendelin, where we do find a benthic repopulation sequence (see section 5.2.1), the refill appears to have occurred later, only one sample quite large *G. margaritae* are found. This suggests that Zanclean refill in the shallower marginal basins may be diachronous, a possible explanation being the interplay between (local) tectonics and flexural response of the marginal basins to (un-) loading (Govers et al., 2009).

5.4 Efficiency of the early Pliocene Mediterranean – Atlantic connections

In order to better understand Mediterranean-Atlantic connectivity changes at the onset of the Pliocene as well as salinity and temperature differences between the Mediterranean and Atlantic, the newly acquired early Pliocene benthic $\delta^{13}\text{C}$ and $\delta^{18}\text{O}$ isotopic records from Site 976 and the Rio Mendelin section have been compared with the Atlantic ODP Site 982 (Drury et al., 2018) and IODP Site U1387 (Hernández-Molina et al., 2013; Van Der Schee et al., 2016; Figure 16 and 17). Site U1387 is located in the gulf of Cadiz, on the Atlantic side of the Strait of Gibraltar at 559 m water depth (Hernández-Molina et al., 2013), which is bathed today by the Mediterranean Outflow Water MOW. This water mass is composed mainly by Levantine Intermediate Water and a small component of the West Mediterranean Deep Water averaging 13°C and 38.4 psu (Bryden and Stommel, 1984; Bryden et al., 1994; Hernandez-Molina et al., 2014). Site 982 is located in the north Atlantic at a water depth of 1135.3 m (Jansen et al., 1996) and bathed currently by the cold ($3\text{--}8^\circ\text{C}$) and less saline (34.95–35.2 ‰) North Atlantic Deep Water (NADW; Ochoa and Bray, 1991; Venz et al., 1999; Hernández-Molina et al., 2016).

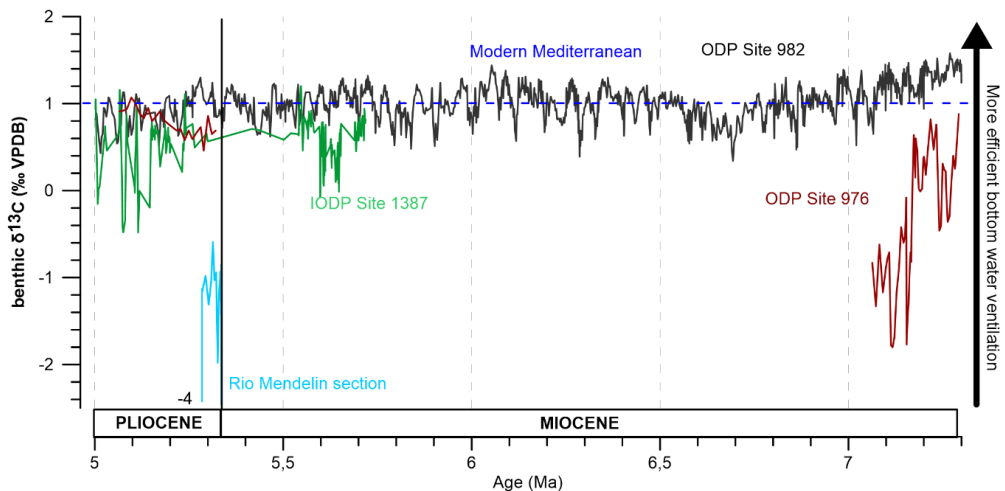


Figure 16: Comparison between benthic $\delta^{13}\text{C}$ records of Site 976 and the Rio Mendelin section (this study) with Atlantic Ocean ODP Site 982 (Drury et al., 2018) and IODP Site 1387 (Van Der Schee et al., 2016). The dashed line shows modern Mediterranean benthic $\delta^{18}\text{O}$ value (Pérez-Asensio et al., 2020).

The early Pliocene benthic $\delta^{13}\text{C}$ values at Site 976 are initially analogous to the ones registered at the Gulf of Cadiz (Figure 16; Site 1387) and become increasingly heavier up core when they reach the Atlantic curve (Site 982), which reflects the well ventilated high $\delta^{13}\text{C}$ of the NADW. In contrast, the more depleted Messinian $\delta^{13}\text{C}$ values from Site 976 (average value around -1) reflect the longer bottom-water residence time of Mediterranean caused by the reduced Mediterranean - Atlantic exchange (Bulian et al., in press). In the Pliocene, with the reestablishment of an efficient Mediterranean - Atlantic water exchange, Site 976 benthic $\delta^{13}\text{C}$ rise to Atlantic values. Nonetheless, benthic species present at the base of the Pliocene suggest both reduced oxygen levels and high organic carbon content which is not visible from the benthic $\delta^{13}\text{C}$. This discrepancy can be explained by assuming that the high bottom water renewal rate and DIC (Dissolved Inorganic Carbon) characterised by high $\delta^{13}\text{C}$ was not large enough to dramatically reduce the $\delta^{13}\text{C}$ at the seafloor, even if high remineralisation rates were present. Early Pliocene benthic $\delta^{13}\text{C}$ values from the marginal Rio Mendelin section are generally significantly lower than Atlantic and Mediterranean values showing a $\sim 2\%$ offset. This suggests that while the Mediterranean was efficiently connected with the Atlantic, this marginal basin could have still been isolated from the Mediterranean. This is not necessarily true for all the marginal basins if we consider that because of the local tectonics and basin configuration the reflooding was locally a diachronous process (see section 5.3.2).

The $\delta^{18}\text{O}$ values for the early Pliocene in the marginal Rio Mendelin section and deep ODP Site 976 are very similar and most probably reflect a comparable

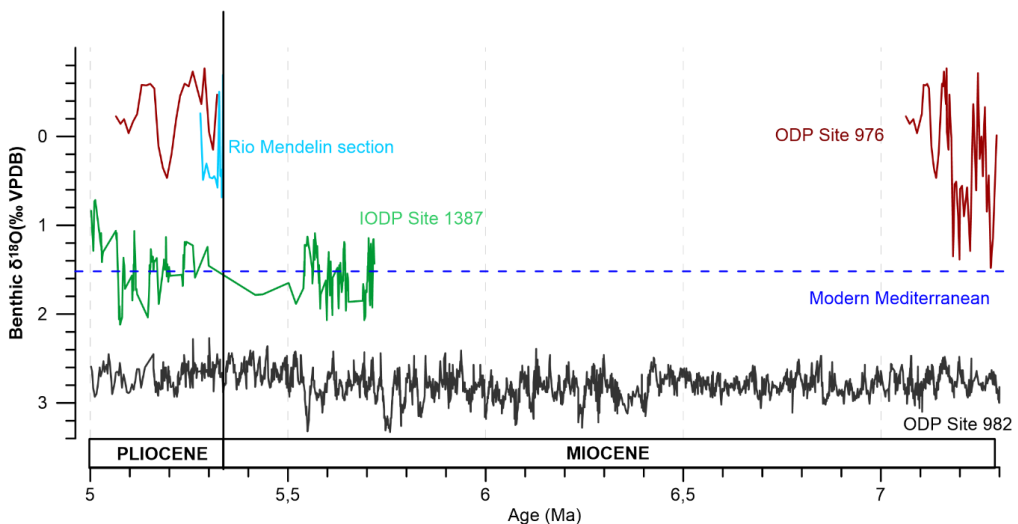


Figure 17: Comparison between benthic $\delta^{18}\text{O}$ records of Site 976 and Rio Mendelin section (this study) with Atlantic Ocean ODP Site 982 (Drury et al., 2018) and IODP Site 1387 (Van Der Schee et al., 2016). The dashed line shows modern Mediterranean benthic $\delta^{18}\text{O}$ value (Pérez-Asensio et al., 2020) corrected in respect to the Lisiecki and Raymo (2005) global curve.

temperature and salinity (Figure 17). The almost 2 ‰ offset that the Mediterranean data show with respect to the Gulf of Cadiz record can be interpreted in different ways. As the MOW is composed by a mixture of LIW (deriving mostly from the Eastern Mediterranean) and the WMDW (West Mediterranean Deep Water) higher salinity in the eastern Mediterranean during the early Pliocene could have resulted in heavier $\delta^{18}\text{O}$ values of the MOW registered in the Gulf of Cadiz when compared with the oxygen isotope values from Alboran Sea deep waters. An alternative interpretation could be related with the much colder temperatures normally registered in intermediate water of the North Atlantic that are only warmed in the vicinity of Gibraltar because of the influence of the MOW. This suggests that at the depth of Site U1387 the thermal influence of the MOW was low during the early Pliocene which could be explained by the MOW moving at shallower depths than today. Another scenario that could justify such offset between the benthic $\delta^{18}\text{O}$ in the Alboran Sea and the Gulf of Cadiz is that Mediterranean seawater salinity and $\delta^{18}\text{O}$ were lower than today. Lower salinities agree with the latest Messinian scenario previously discussed, where the Mediterranean water would contain a strong Paratethyan signal partly maintained through the early Pliocene as well. If this was the case, the hydrological regime of the Mediterranean in the early Pliocene would have been less negative than the present one, eventually achieved as more Atlantic water was able to enter the basin. Even more extreme is the offset between the Mediterranean benthic $\delta^{18}\text{O}$ and Atlantic Site 982 records. A 3 ‰ difference is probably present because of the extreme temperature and salinity differences between a semi enclosed warm and saline Mediterranean and the colder less saline open ocean.

Conclusions

The studied late Messinian - early Pliocene sections in the Spanish basins register the benthic foraminifer repopulation sequence and sedimentological changes linked with the reestablishment of normal marine conditions after the MSC and give important information about the water level across the MPB.

In the marginal sections, the earliest Pliocene sediments show as a dark layer, usually grey or black, which possibly deposited because of the ingression of Atlantic waters into the basin. This layer, identified in deep and marginal basins all over the Mediterranean, and often enriched in organic matter, could imply water column stratification, and reduced bottom water oxygen levels. Such conditions could develop in a scenario where the Atlantic inflow reaching the Mediterranean was more saline than the Mediterranean waters still under the influence of the Paratethys, causing them to sink and stratify the water

column. Lower salinity of sMediterranean water are indicated by light benthic $\delta^{18}\text{O}$ values, much lighter than the ones found in the early Pliocene Gulf of Cadiz. The early Pliocene of Site 976 located in the Alboran Basin does not show a dark layer, probably because of its proximity with the Strait of Gibraltar and strong erosion produced by the inflowing Atlantic waters that could have eroded the basal Pliocene layers.

The analyses performed on benthic foraminifer associations enabled a more detailed reconstruction of the early Pliocene Mediterranean environments. With the early Pliocene sea-level rise normal marine conditions were re-established in the Mediterranean as can be deduced from the planktic and benthic foraminifer assemblages characterising the early Pliocene. The benthic foraminifer repopulation identified in the studied basins is comparable with other Mediterranean sections and shows similarities with Recent recovery from hostile environments and repopulation following low-oxic episodes during sapropel deposition. With some exceptions, due to an inner neritic and intermittently continental setting in the Sorbas Basin and the erosional surface at the MPB of site 976, the general repopulation trend shows a shift from stressed and unstable environments to benthic associations indicating an amelioration of the circulation and bottom water ventilation. The first benthic faunas that appear are in line with reduced bottom water oxygen levels and stratified water column in agreement with the deposition of the dark layers at the MPB.

By studying the benthic foraminifer associations, a palaeodepth estimate was also possible. In the marginal Spanish basins, the estimated palaeobathymetry for the early Pliocene was similar ranging between 50 and 150 m. In the Malaga Basin, the earliest Pliocene palaeodepth does not exceed 50 m, and eventually reaches values of 150 m. In the Sorbas and Nijar Basins, the presence of macrofossils and fossil traces suggests high energy shallow environments just after the MPB, while towards the top of the sections deeper, less high-energy environments were probably established. These observations imply a progressive deepening of the Mediterranean margins as the Mediterranean – Atlantic connectivity was becoming more efficient. In addition, a comparison with palaeodepths and repopulation sequences at other Mediterranean sites suggests that in the shallow marginal basins the reflooding may have been diachronous due to the effects of local tectonics and flexural responses to loading and unloading. At Site 976, the early Pliocene is characterised by a bathyal environment (> 1000 m), which is within the range we find today.

Although the water column may have been stratified and organic matter accumulating, the high $\delta^{13}\text{C}$ levels from Site 976 testify that bottom water renewal in the deep basins was immediately efficient after the reflooding and

that an efficient basin-scale circulation was re-established. The values are in fact almost 2‰ higher than the ones registered in concomitance with the first gateway restriction at 7.17 Ma. Due to diachronous refill shallow marginal basins (e.g. the Malaga Basin) may have needed more time to reach an efficient bottom water circulation.

Acknowledgments

The authors appreciate the work of Jose Ignacio Martin Cruz in sample processing and preparation. Robert Speijer is thanked for his input when classifying benthic foraminifer species while Federico Andretto for his advice regarding ostracod identification. We also appreciate the useful information regarding the location of outcrops provided by Frits Hilgen while all fellow ESRs and supervisors from the SALTGIANT project are thanked for their valuable suggestions and discussions. A part of the samples used in this research were collected through ODP Expedition 161 aboard the Joides Resolution. This research has received funding from the European Union's Horizon 2020 research and innovation program under the Marie Skłodowska-Curie grant agreement n° 765256 SALTGIANT.

References

- Aguirre, J., 1998. El Plioceno del SE de la Península Ibérica (provincia de Almería). Síntesis estratigráfica, sedimentaria, bioestratigráfica y paleogeográfica. *Revista de la Sociedad Geológica de España*, 11(3): 297-316.
- Aguirre, J. and Sánchez-Almazo, I. M., 2004. The Messinian post-evaporitic deposits of the Gafares area (Almería-Níjar basin, SE Spain). A new view of the "Lago-Mare" facies. *Sedimentary Geology*, 168(1-2): 71-95.
- Aguirre, J., Pérez-Muñoz, A. and Sanchez-Almazo, I., 2006. Benthic foraminifer assemblages in the lower Pliocene deposits of the Almeria-Níjar Basin (SE Spain). *Revista española de micropaleontología*, 38(2): 411-428.
- Altenbach, A. V., Pflaumann, U., Schiebel, R., Thies, A., Timm, S. and Trauth, M., 1999. Scaling percentages and distributional patterns of benthic foraminifera with flux rates of organic carbon. *The Journal of Foraminiferal Research*, 29(3): 173-185.
- Alve, E., 1999. Colonization of new habitats by benthic foraminifera: a review. *Earth-Science Reviews*, 46(1-4): 167-185.
- Alve, E., 2003. A common opportunistic foraminiferal species as an indicator of rapidly changing conditions in a range of environments. *Estuarine, Coastal and Shelf Science*, 57(3): 501-514.

- Amorosi, A., Rossi, V. and Vella, C., 2013. Stepwise post-glacial transgression in the Rhône Delta area as revealed by high-resolution core data. *Palaeogeography, Palaeoclimatology, Palaeoecology*, 374: 314-326.
- Andreetto, F., Aloisi, G., Raad, F., Heida, H., Flecker, R., Agiadi, K., Lofi, J., Blondel, S., Bulian, F. and Camerlenghi, A., 2021a. Freshening of the Mediterranean Salt Giant: controversies and certainties around the terminal (Upper Gypsum and Lago-Mare) phases of the Messinian Salinity Crisis. *Earth-Science Reviews*: 103577.
- Andreetto, F., Matsubara, K., Beets, C., Fortuin, A., Flecker, R. and Krijgsman, W., 2021b. High Mediterranean water-level during the Lago-Mare phase of the Messinian Salinity Crisis: insights from the Sr isotope records of Spanish marginal basins (SE Spain). *Palaeogeography, Palaeoclimatology, Palaeoecology*, 562: 110139.
- Anthony, E. J. and Aagaard, T., 2020. The lower shoreface: Morphodynamics and sediment connectivity with the upper shoreface and beach. *Earth-Science Reviews*: 103334.
- Aufgebauer, A. and McCann, T., 2011. Messinian to Pliocene transition in the deep part of the Sorbas Basin, SE Spain – A new description of the depositional environment during the Messinian Salinity Crisis. (With 8 figures and 1 table). *Neues Jahrbuch für Geologie und Palaontologie-Abhandlungen*, 259(2): 177.
- Austin, W. and Evans, J., 2000. NE Atlantic benthic foraminifera: modern distribution patterns and palaeoecological significance. *Journal of the Geological Society*, 157(3): 679-691.
- Avnaim-Katav, S., Milker, Y., Schmiedl, G., Sivan, D., Hyams-Kaphzan, O., Sandler, A. and Almogi-Labin, A., 2016. Impact of eustatic and tectonic processes on the southeastern Mediterranean shelf during the last one million years: Quantitative reconstructions using a foraminiferal transfer function. *Marine Geology*, 376: 26-38.
- Bache, F., Popescu, S. M., Rabineau, M., Gorini, C., Suc, J. P., Clauzon, G., Olivet, J. L., Rubino, J. L., Melinte-Dobrinescu, M. C., Estrada, F., Londeix, L., Armijo, R., Meyer, B., Jolivet, L., Jouannic, G., Leroux, E., Aslanian, D., Reis, A. T. D., Mocochain, L., Dumurdžanov, N., Zagorchev, I., Lesić, V., Tomić, D., Namik Çağatay, M., Brun, J. P., Sokoutis, D., Csato, I., Uçarkus, G. and Çakir, Z., 2012. A two-step process for the reflooding of the Mediterranean after the Messinian Salinity Crisis. *Basin Research*, 24(2): 125-153.
- Bache, F., Gargani, J., Suc, J. P., Gorini, C., Rabineau, M., Popescu, S. M., Leroux, E., Couto, D. D., Jouannic, G., Rubino, J. L., Olivet, J. L., Clauzon, G., Dos Reis, A. T. and Aslanian, D., 2015. Messinian evaporite deposition during sea level rise in the Gulf of Lions (Western Mediterranean). *Marine and Petroleum Geology*, 66: 262-277.
- Baggley, K. A., 2000. The Late Tortonian-Early Messinian Foraminiferal Record Of The Abad Member (Turre Formation), Sorbas Basin, Almería, South-East Spain. *Palaeontology*, 43(6): 1069-1112.

- Baldi, K. and Hohenegger, J., 2008. Paleoecology of benthic foraminifera of the Baden-Sooss section (Badenian, Middle Miocene, Vienna Basin, Austria). *Geologica Carpathica*, 59(5): 411-424.
- Bandy, O. L. and Chierici, M. A., 1966. Depth-temperature evaluation of selected California and Mediterranean bathyal foraminifera. *Marine Geology*, 4(4): 259-271.
- Barbieri, R. and Panieri, G., 2004. How are benthic foraminiferal faunas influenced by cold seeps? Evidence from the Miocene of Italy. *Palaeogeography, Palaeoclimatology, Palaeoecology*, 204(257): 275.
- Barra, D., Bonaduce, G. and Sgarrella, E., 1998. Paleoenvironmental bottom water conditions in the early Zanclean of the Capo Rossello area (Agrigento, Sicily). *Bollettino-societa paleontologica Italiana*, 37: 61-88.
- Bassetti, M. A., Miculan, P. and Sierro, F. J., 2006. Evolution of depositional environments after the end of Messinian Salinity Crisis in Nijar basin (SE Betic Cordillera). *Sedimentary Geology*, 188: 279-295.
- Berggren, W. and Haq, B. U., 1976. The Andalusian stage (Late Miocene): biostratigraphy, biochronology and paleoecology. *Palaeogeography, Palaeoclimatology, Palaeoecology*, 20(1-2): 67-129.
- Bernhard, J. M. and Gupta, B. K. S., 1999. Foraminifera of oxygen-depleted environments, Modern foraminifera. Springer, pp. 201-216.
- Bizon, G. and Bizon, J., 1984. Distribution des foraminifères sur le plateau continental au large du Rhône. *Ecologie des microorganismes en Méditerranée occidentale 'ECOMED'*. Association Française des Techniciens du Pétrole, Paris: 84-94.
- Blanc, P.-L., 2002. The opening of the Plio-Quaternary Gibraltar Strait: assessing the size of a cataclysm. *Geodinamica acta*, 15(5-6): 303-317.
- Brolsma, M. J., 1978. Quantitative foraminiferal analysis and environmental interpretation of the Pliocene and topmost Miocene on the south coast of Sicily, Utrecht University.
- Bryden, H. and Stommel, H., 1984. Limiting processes that determine basic features of the circulation in the Mediterranean-Sea. *Oceanologica Acta*, 7(3): 289-296.
- Bryden, H. L., Candela, J. and Kinder, T. H., 1994. Exchange through the Strait of Gibraltar. *Progress in Oceanography*, 33(3): 201-248.
- Bulian, F., Sierro, F. J., Ledesma, S., Jiménez-Espejo, F. J. and Bassetti, M.-A., 2021. Messinian West Alboran Sea record in the proximity of Gibraltar: Early signs of Atlantic-Mediterranean gateway restriction. *Marine Geology*: 106430.
- Caralp, M. H., 1989. Size and morphology of the benthic foraminifer *Melonis barleeanum*; relationships with marine organic matter. *The Journal of Foraminiferal Research*, 19(3): 235-245.

- Caruso, A., Blanc-Valleron, M.-M., Da Prato, S., Pierre, C. and Rouchy, J. M., 2020. The late Messinian "Lago-Mare" event and the Zanclean Reflooding in the Mediterranean Sea: New insights from the Cuevas del Almanzora section (Vera Basin, South-Eastern Spain). *Earth-Science Reviews*, 200: 102993.
- CIESM, 2008. The Messinian salinity crisis from mega-deposits to microbiology. In: Briand, F. (Ed.), *A consensus report, in 33ème CIESM Workshop Monographs*, 33. CIESM, 16, bd de Suisse, MC-98000, Monaco: pp. 1-168.
- Cipollari, P., Cosentino, D., Radeff, G., Schildgen, T. F., Faranda, C., Grossi, F., Gliozzi, E., Smedile, A., Gennari, R. and Darbaş, G., 2013. Easternmost Mediterranean evidence of the Zanclean flooding event and subsequent surface uplift: Adana Basin, southern Turkey. *Geological Society, London, Special Publications*, 372(1): 473-494.
- Cita, M. and Zocchi, M., 1978. Distribution patterns of benthic foraminifera on floor of Mediterranean Sea. *Oceanologica Acta*, 1(4): 445-462.
- Cita, M. B., Wright, R. C., Ryan, W. B. F. and Longinelli, A., 1978. Messinian paleoenvironments. In: Hsü, K.J., Montadert, L., et al. (Eds.). *Init. Rep. D.S.D.P.*, vol. 42A. US Government Printing Office, Washington: 1003-1035.
- Comas, M. C., Zahn, R., Klaus, A. and al., e., 1996. ODP, *Init. Repts.*, 161: College Station, TX (Ocean Drilling Program).
- Corbí, H., 2010. Los foraminíferos de la cuenca neógena del Bajo Segura (sureste de España): bioestratigrafía y cambios paleoambientales en relación con la Crisis de Salinidad del Mediterráneo.
- Corbí, H. and Soria, J. M., 2016. Late Miocene-early Pliocene planktonic foraminifer event-stratigraphy of the Bajo Segura basin: A complete record of the western Mediterranean. *Marine and Petroleum Geology*, 77: 1010-1027.
- Corliss, B. H. and Chen, C., 1988. Morphotype patterns of Norwegian Sea deep-sea benthic foraminifera and ecological implications. *Geology*, 16(8): 716-719.
- Cornée, J.-J., Münch, P., Achalhi, M., Merzeraud, G., Azdimousa, A., Quillévéré, F., Melinte-Dobrinescu, M., Chaix, C., Moussa, A. B. and Lofi, J., 2016. The Messinian erosional surface and early Pliocene reflooding in the Alboran Sea: New insights from the Boudinar basin, Morocco. *Sedimentary geology*, 333: 115-129.
- Dabrio, C. J., Esteban, M. and Martin, J. M., 1981. The coral reef of Nijar, Messinian (uppermost Miocene), Almeria Province, SE Spain. *Journal of Sedimentary Research*, 51(2): 521-539.
- De Lange, G., Middelburg, J., Van der Weijden, C., Catalano, G., Luther Iii, G., Hydes, D., Woittiez, J. and Klinkhammer, G., 1990. Composition of anoxic hypersaline brines in the Tyro and Bannock Basins, eastern Mediterranean. *Marine Chemistry*, 31(1-3): 63-88.
- De Rijk, S., Troelstra, S. and Rohling, E., 1999. Benthic foraminiferal distribution in the Mediterranean Sea. *The Journal of Foraminiferal Research*, 29(2): 93-103.

- De Rijk, S., Jorissen, F., Rohling, E. and Troelstra, S., 2000. Organic flux control on bathymetric zonation of Mediterranean benthic foraminifera. *Marine Micropaleontology*, 40(3): 151-166.
- De Stigter, H., Jorissen, F. and Van der Zwaan, G., 1998. Bathymetric distribution and microhabitat partitioning of live (Rose Bengal stained) benthic foraminifera along a shelf to bathyal transect in the southern Adriatic Sea. *The Journal of Foraminiferal Research*, 28(1): 40-65.
- Dela Pierre, F., Natalicchio, M., Lozar, F., Bonetto, S. M. R., Carnevale, G., Cavagna, S., Colombero, S., Sabino, M. and Violanti, D., 2016. The Northernmost record of the Messinian salinity crisis (Piedmont Basin, NW Italy).
- Diz, P., Francés, G., Costas, S., Souto, C. and Alejo, I., 2004. Distribution of benthic foraminifera in coarse sediments, Ría de Vigo, NW Iberian margin. *The Journal of Foraminiferal Research*, 34(4): 258-275.
- Do Couto, D., Popescu, S.-M., Suc, J.-P., Melinte-Dobrinescu, M. C., Barhoun, N., Gorini, C., Jolivet, L., Poort, J., Jouannic, G. and Auxietre, J.-L., 2014. Lago Mare and the Messinian salinity crisis: evidence from the Alboran Sea (S. Spain). *Marine and Petroleum Geology*, 52: 57-76.
- Donovan, S. K., Jones, S. J., King, A. R. and Harper, D. A., 2021. Pliocene trace fossils from oyster substrates in the Nijar Basin, Betic Cordillera, southern Spain. *Proceedings of the Geologists' Association*.
- Droser, M. L. and Bottjer, D. J., 1987. Development of ichnofabric indices for strata deposited in high-energy nearshore terrigenous clastic environments.
- Drury, A. J., Westerhold, T., Hodell, D. and Röhl, U., 2018. Reinforcing the North Atlantic backbone: revision and extension of the composite splice at ODP Site 982. *Climate of the Past*, 14(3): 321-338.
- Duchemin, G., Jorissen, F. J., Le Loc'h, F., Andrieux-Loyer, F., Hily, C. and Thouzeau, G., 2008. Seasonal variability of living benthic foraminifera from the outer continental shelf of the Bay of Biscay. *Journal of Sea Research*, 59(4): 297-319.
- Esteras, M., Izquierdo, J., Sandoval, N. and Mamad, A., 2000. Evolución morfológica y estratigráfica pliocuaternaria del umbral de Camarinal (Estrecho de Gibraltar) basada en sondeos marinos. *Rev. Soc. Geol. España*, 13(3-4): 539-550.
- Estrada, F., Ercilla, G., Gorini, C., Alonso, B., Vázquez, J. T., García-Castellanos, D., Juan, C., Maldonado, A., Ammar, A. and Elabbassi, M., 2011. Impact of pulsed Atlantic water inflow into the Alboran Basin at the time of the Zanclean flooding. *Geo-Marine Letters*, 31(5-6), pp.361-376., 31(5-6), pp.361-376.: pp.361-376.
- Fentimen, R., Lim, A., Rüggeberg, A., Wheeler, A. J., Van Rooij, D. and Foubert, A., 2020. Impact of bottom water currents on benthic foraminiferal assemblages in a cold-water coral environment: The Moira Mounds (NE Atlantic). *Marine Micropaleontology*, 154: 101799.

- Fontanier, C., Jorissen, F., Licari, L., Alexandre, A., Anschutz, P. and Carbonel, P., 2002. Live benthic foraminiferal faunas from the Bay of Biscay: faunal density, composition, and microhabitats. *Deep Sea Research Part I: Oceanographic Research Papers*, 49(4): 751-785.
- Fortuin, A., Kelling, J. and Roep, T. B., 1995. The enigmatic Messinian-Pliocene section of Cuevas del Almanzora (Vera Basin, SE Spain) revisited—erosional features and strontium isotope ages. *Sedimentary Geology*, 97(3-4): 177-201.
- Fortuin, A., Krijgsman, W., Hilgen, F. and Sierro, F., 2000. Late Miocene Mediterranean desiccation: topography and significance of the Salinity Crisis' erosion surface on-land in southeast Spain: Comment. *Sedimentary Geology*, 133: 167-174.
- Fortuin, A. R. and Krijgsman, W., 2003. The Messinian of the Nijar Basin (SE Spain): Sedimentation, depositional environments and paleogeographic evolution. *Sedimentary Geology*, 160(1-3): 213-242.
- García-Castellanos, D., Estrada, F., Jiménez-Munt, I., Gorini, C., Fernández, M., Vergés, J. and De Vicente, R., 2009. Catastrophic flood of the Mediterranean after the Messinian salinity crisis. *Nature*, 462(7274): 778.
- García-Castellanos, D., Micallef, A., Estrada, F., Camerlenghi, A., Ercilla, G., Periáñez, R. and Abril, J. M., 2019. The Zanclean megaflood of the Mediterranean—Searching for additional evidence. *Earth-Science Reviews*: 103061.
- García-García, F., Corbí, H., Soria, J. and Viseras, C., 2011. Architecture analysis of a river flood-dominated delta during an overall sea-level rise (early Pliocene, SE Spain). *Sedimentary Geology*, 237(1-2): 102-113.
- García-Alix, A., Minwer-Barakat, R., Martín Suárez, E., Freudenthal, M., Aguirre, J. and Kaya, F., 2016. Updating the Europe–Africa small mammal exchange during the late Messinian. *Journal of Biogeography*, 43(7): 1336-1348.
- Gargani, J. and Rigollet, C., 2007. Mediterranean Sea level variations during the Messinian salinity crisis. *Geophysical Research Letters*, 34(10).
- Gebhardt, H., 1993. Neogene foraminifera from the Eastern Rabat area (Morocco): stratigraphy, palaeobathymetry and palaeoecology. *Journal of African Earth Sciences (and the Middle East)*, 16(4): 445-464.
- Gebhardt, H., 1999. Middle to Upper Miocene benthonic foraminiferal palaeoecology of the Tap Marls (Alicante Province, SE Spain) and its palaeoceanographic implications. *Palaeogeography, Palaeoclimatology, Palaeoecology*, 145(1-3): 141-156.
- Gennari, R., Iaccarino, S. M., Di Stefano, A., Sturiale, G., Cipollari, P., Manzi, V., Roveri, M. and Cosentino, D., 2008. The Messinian -Zanclean boundary in the Northern Apennine. *Stratigraphy*, 5(3-4): 307-322.
- Gibson, T. G., 1989. Planktonic benthonic foraminiferal ratios: modern patterns and Tertiary applicability. *Marine Micropaleontology*, 15(1-2): 29-52.

- Gingras, M. K., Dashtgard, S. E., MacEachern, J. A. and Pemberton, S. G., 2008. Biology of shallow marine ichnology: a modern perspective. *Aquatic Biology*, 2(3): 255-268.
- Goineau, A., Fontanier, C., Mojtahid, M., Fanget, A.-S., Bassetti, M.-A., Berné, S. and Jorissen, F., 2015. Live-dead comparison of benthic foraminiferal faunas from the Rhône prodelta (Gulf of Lions, NW Mediterranean): Development of a proxy for palaeoenvironmental reconstructions. *Marine Micropaleontology*, 119: 17-33.
- Gooday, A. J., 1988. A response by benthic foraminifera to the deposition of phytodetritus in the deep sea. *Nature*, 332(6159): 70-73.
- Gooday, A. J., 1993. Deep-sea benthic foraminiferal species which exploit phytodetritus: characteristic features and controls on distribution. *Marine Micropaleontology*, 22(3): 187-205.
- Gooday, A. J. and Hughes, J. A., 2002. Foraminifera associated with phytodetritus deposits at a bathyal site in the northern Rockall Trough (NE Atlantic): seasonal contrasts and a comparison of stained and dead assemblages. *Marine Micropaleontology*, 46(1-2): 83-110.
- Gooday, A. J., 2003. Benthic foraminifera (Protista) as tools in deep-water palaeoceanography: environmental influences on faunal characteristics. *Advances in Marine Biology*, 46: 1-90.
- Grossi, F., Cosentino, D. and Gliozzi, E., 2008. Late Messinian Lago-Mare ostracods and palaeoenvironments of the central and eastern Mediterranean Basin. *Bollettino della Società Paleontologica Italiana*, 47(2): 131-146.
- Guerra-Merchán, A., Serrano, F., Garcés, M., Gofas, S., López Garrido, A., El Kadiri, K. and Hlila, R., 2008. Caracterización de la sedimentación Lago Mare (Messiniense terminal) y de la transgresión del comienzo del Plioceno en la cuenca de Málaga (Cordillera Bética). *Geogaceta*, 44: 207-210.
- Guerra-Merchán, A., Serrano, F., Garcés, M., Gofas, S., Esu, D., Gliozzi, E. and Grossi, F., 2010. Messinian Lago-Mare deposits near the strait of Gibraltar (Malaga basin, S Spain). *Palaeogeography, Palaeoclimatology, Palaeoecology*, 285(3-4): 264-276.
- Guerra-Merchán, A., Serrano, F., Hlila, R., El Kadiri, K., de Galdeano, C. S. and Garcés, M., 2014. Tectono-sedimentary evolution of the peripheral basins of the Alboran Sea in the arc of Gibraltar during the latest Messinian-Pliocene. *Journal of Geodynamics*, 77: 158-170.
- Haake, F. W., 1982. Occurrences of living and dead salt marsh foraminifera in the interior of northern Germany.
- Hald, M. and Korsun, S., 1997. Distribution of modern benthic foraminifera from fjords of Svalbard, European Arctic. *The Journal of Foraminiferal Research*, 27(2): 101-122.
- Hammer, Ø., Harper, D. A. and Ryan, P. D., 2001. PAST: Paleontological statistics software package for education and data analysis. *Palaeontologia Electronica*, 4(1): 9.
- Hammer, Ø., Harper, D. and Ryan, P., 2008. PAST – PALaeontological STatistics, ver. 1.81. Software documentation.

- Hayward, B. W., Carter, R., Grenfell, H. R. and Hayward, J. J., 2001. Depth distribution of Recent deep-sea benthic foraminifera east of New Zealand, and their potential for improving paleobathymetric assessments of Neogene microfaunas. *New Zealand Journal of Geology and Geophysics*, 44(4): 555-587.
- Hayward, B. W., 2004. Foraminifera-based estimates of paleobathymetry using Modern Analogue Technique, and the subsidence history of the early Miocene Waitemata Basin. *New Zealand Journal of Geology and Geophysics*, 47(4): 749-767.
- Hernández-Molina, F., Stow, D., Alvarez-Zarikian, C. and Expedition, I., 2013. IODP Expedition 339 in the Gulf of Cadiz and off West Iberia: decoding the environmental significance of the Mediterranean outflow water and its global influence. *Scientific Drilling*, 16: 1-11.
- Hernández-Molina, F., Sierro, F., Llave, E., Roque, C., Stow, D., Williams, T., Lofi, J., Van der Schee, M., Arnáiz, A. and Ledesma, S., 2016. Evolution of the gulf of Cadiz margin and southwest Portugal contourite depositional system: Tectonic, sedimentary and paleoceanographic implications from IODP expedition 339. *Marine Geology*, 377: 7-39.
- Hernandez-Molina, F. J., Stow, D. A. V., Alvarez-Zarikian, C. A., Acton, G., Bahr, A., Balestra, B., Ducassou, E., Flood, R., Flores, J. A., Furota, S., Grunert, P., Hodell, D., Jimenez-Espejo, F., Kim, J. K., Krissek, L., Kuroda, J., Li, B., Llave, E., Lofi, J., Lourens, L., Miller, M., Nanayama, F., Nishida, N., Richter, C., Roque, C., Pereira, H., Sanchez Goni, M. F., Sierro, F. J., Singh, A. D., Sloss, C., Takashimizu, Y., Tzanova, A., Voelker, A., Williams, T. and Xuan, C., 2014. Onset of Mediterranean outflow into the North Atlantic. 344(6189): 1244-1250.
- Hohenegger, J., 2005. Estimation of environmental paleogradient values based on presence/absence data: a case study using benthic foraminifera for paleodepth estimation. *Palaeogeography, Palaeoclimatology, Palaeoecology*, 217(1-2): 115-130.
- Hohenegger, J., Andersen, N., Baldi, K., Coric, S., Pervesler, P., Rupp, C. and Wagreich, M., 2008. Paleoenvironment of the Early Badenian (Middle Miocene) in the southern Vienna Basin (Austria)-multivariate analysis of the Baden-Soos section. *Geologica Carpathica*, 59(5): 461-488.
- Hsü, K. J., 1972. Origin of saline giants: A critical review after the discovery of the Mediterranean Evaporite. *Earth Science Reviews*, 8(4): 371-396.
- Iaccarino, S. and Bossio, A., 1999. Paleoenvironment of uppermost Messinian sequences in the western Mediterranean (Sites 974, 975, and 978). In *Proceedings of the Ocean Drilling Program, Scientific Results Vol. 161*: pp. 529-541.
- Iaccarino, S., Castradori, D., Cita, M., Di Stefano, E., Gaboardi, S., McKenzie, J., Spezzaferri, S. and Sprovieri, R., 1999a. The Miocene/Pliocene boundary and the significance of the earliest Pliocene flooding in the Mediterranean. *Mem. Soc. Geol. Ital.*, 54(10): 109-131.

-
- Iaccarino, S. M., Cita, M. B., Gaborardi, S. and Gruppini, G. M., 1999b. 15. High-Resolution Biostratigraphy at the Miocene/Pliocene boundary in Holes 974b and 975b, Western Mediterranean¹ In Proceedings of the Ocean Drilling Program: Scientific results Vol. 161: p. 197.
- Jansen, E., Raymo, M. E. and Blum, P., 1996. 1. Leg 162: new frontiers on past climates, Proceedings ODP, Initial Reports, pp. 5-20.
- Jöhnck, J., Holbourn, A., Kuhnt, W. and Andersen, N., 2021. Oxygen isotope offsets in deep-water benthic foraminifera. *Journal of Foraminiferal Research*, 51(3): 225-244.
- Jorissen, F., Fontanier, C. and Thomas, E., 2007. Paleooceanographical Proxies Based on Deep-Sea Benthic Foraminiferal Assemblage Characteristics, 1 (07), doi: 10.1016/S1572-5480(07): 01012-3.
- Jorissen, F. J., 1987. The distribution of benthic foraminifera in the Adriatic Sea. *Marine Micropaleontology*, 12: 21-48.
- Jorissen, F. J., de Stigter, H. C. and Widmark, J. G., 1995. A conceptual model explaining benthic foraminiferal microhabitats. *Marine micropaleontology*, 26(1-4): 3-15.
- Jorissen, F. J., 1999. Benthic foraminiferal successions across Late Quaternary Mediterranean sapropels. *Marine Geology*, 153(1-4): 91-101.
- Kaboth, S., de Boer, B., Bahr, A., Zeeden, C. and Lourens, L. J., 2017. Mediterranean Outflow Water dynamics during the past~ 570 kyr: Regional and global implications. *Paleoceanography*, 32(6): 634-647.
- Kaiho, K., 1991. Global changes of Paleogene aerobic/anaerobic benthic foraminifera and deep-sea circulation. *Palaeogeography, Palaeoclimatology, Palaeoecology*, 83(1-3): 65-85.
- Kaiho, K., 1994. Benthic foraminiferal dissolved-oxygen index and dissolved-oxygen levels in the modern ocean. *Geology*, 22(8): 719-722.
- Kaiho, K., 1999. Effect of organic carbon flux and dissolved oxygen on the benthic foraminiferal oxygen index (BFOI). *Marine micropaleontology*, 37(1): 67-76.
- Kaminski, M. A., 2012. Calibration of the benthic foraminiferal oxygen index in the Marmara Sea. *Geological Quarterly*, 56(4): 757-764, doi: 10.7306/gq.1061.
- Koho, K., García, R. d., De Stigter, H., Epping, E., Koning, E., Kouwenhoven, T. and Van der Zwaan, G., 2008. Sedimentary labile organic carbon and pore water redox control on species distribution of benthic foraminifera: A case study from Lisbon-Setúbal Canyon (southern Portugal). *Progress in Oceanography*, 79(1): 55-82.
- Krijgsman, W., Stoica, M., Vasiliev, I. and Popov, V. V., 2010. Rise and fall of the Paratethys Sea during the Messinian Salinity Crisis. 290(1-2): 183-191.
- Krijgsman, W., Capella, W., Simon, D., Hilgen, F. J., Kouwenhoven, T. J., Meijer, P. T., Sierro, F. J., Tulbure, M. A., van den Berg, B. C. and van der Schee, M., 2018. The Gibraltar corridor: watergate of the messinian salinity crisis. *Marine Geology*, 403: 238-246.

- Kucera, M., 2007. Planktonic foraminifera as tracers of past oceanic environments. *Developments in marine geology*, Chapter 6: 213-262.
- Kuhnt, W., Luderer, F., Nederbragt, S., Thurow, J. and Wagner, T., 2005. Orbital-scale record of the late Cenomanian–Turonian oceanic anoxic event (OAE-2) in the Tarfaya Basin (Morocco). *International Journal of Earth Sciences*, 94(1): 147-159.
- Langezaal, A., Jorissen, F., Braun, B., Chaillou, G., Fontanier, C., Anschutz, P. and Van der Zwaan, G., 2006. The influence of seasonal processes on geochemical profiles and foraminiferal assemblages on the outer shelf of the Bay of Biscay. *Continental Shelf Research*, 26(15): 1730-1755.
- Lisiecki, L. E. and Raymo, M. E., 2005. A Pliocene-Pleistocene stack of 57 globally distributed benthic $\delta^{18}\text{O}$ records. *Paleoceanography*, 20(1): 1-17.
- Loget, N., Driessche, J. V. D. and Davy, P., 2005. How did the Messinian salinity crisis end? *Terra Nova*, 17(5): 414-419.
- Loget, N. and Van Den Driessche, J., 2006. On the origin of the Strait of Gibraltar. *Sedimentary Geology*, 188: 341-356.
- Loubère, P., Banonis, G. and Jakiel, R., 1988. *Globocassidulina subglobosa* (Brady); environmental control of species abundance and specimen test size. *The Journal of Foraminiferal Research*, 18(1): 6-15.
- Lutze, G. and Coulbourn, W., 1984. Recent benthic foraminifera from the continental margin of northwest Africa: community structure and distribution. *Marine Micropaleontology*, 8(5): 361-401.
- Lutze, G. F. and Wefer, G., 1980. Habitat and asexual reproduction of *Cyclorbicula compressa* (Orbigny), Soritidae. *The Journal of Foraminiferal Research*, 10(4): 251-260.
- Mackensen, A., Sejrup, H. and Jansen, E., 1985. The distribution of living benthic foraminifera on the continental slope and rise off southwest Norway. *Marine Micropaleontology*, 9(4): 275-306.
- Mackensen, A., Fu, D., Grobe, H. and Schmiedl, G., 1993. Benthic foraminiferal assemblages from the eastern South Atlantic Polar Front region between 35 and 57 S: distribution, ecology and fossilization potential. *Marine Micropaleontology*, 22(1-2): 33-69.
- Madof, A. S., Bertoni, C. and Lofi, J., 2019. Discovery of vast fluvial deposits provides evidence for drawdown during the late Miocene Messinian salinity crisis. *Geology*, 47(2): 171-174.
- Manzi, V. and Roveri, M., 2009. The Terminal Carbonate Complex: the record of sea-level changes during the Messinian salinity crisis. *GeoActa*, 8: 63-77.
- Manzi, V., Lugli, S., Roveri, M., Dela Pierre, F., Gennari, R., Lozar, F., Natalicchio, M., Schreiber, B. C., Taviani, M. and Turco, E., 2016. The Messinian salinity crisis in Cyprus: A further step towards a new stratigraphic framework for Eastern Mediterranean. *Basin Research*, 28(2): 207-236.

-
- Martín, J. M., Puga-Bernabéu, A., Aguirre, J. and Braga, J. C., 2014. Miocene Atlantic-Mediterranean seaways in the Betic Cordillera (Southern Spain). *Revista de la sociedad geológica de España*, 27(1): 175-186.
- Marzocchi, A., Flecker, R., Van Baak, C. G., Lunt, D. J. and Krijgsman, W., 2016. Mediterranean outflow pump: An alternative mechanism for the Lago-mare and the end of the Messinian Salinity Crisis. *Geology*, 44(7): 523-526.
- Mather, A. E. and Stokes, M., 2001. Marine to continental transition. A Field Guide to the Neogene Sedimentary Basins of the Almería Province, SE Spain: 186-224.
- McKenzie, J. A., Sprovieri, R. and Channell, J., 1990. The terminal Messinian flood and earliest Pliocene paleoceanography in the Mediterranean: results from ODP Leg 107, Site 652, Tyrrhenian Sea. *Memorie della Società Geologica Italiana*, 44: 81-91.
- Mendes, I., Gonzalez, R., Dias, J., Lobo, F. and Martins, V., 2004. Factors influencing recent benthic foraminifera distribution on the Guadiana shelf (Southwestern Iberia). *Marine Micropaleontology*, 51(1-2): 171-192.
- Mendes, I., Dias, J. A., Schönfeld, J. and Ferreira, Ó., 2012. Distribution of living benthic foraminifera on the northern Gulf of Cadiz continental shelf. *The Journal of Foraminiferal Research*, 42(1): 18-38.
- Miao, Q. and Thunell, R. C., 1993. Recent deep-sea benthic foraminiferal distributions in the South China and Sulu Seas. *Marine Micropaleontology*, 22(1-2): 1-32.
- Milker, Y., 2010. Western Mediterranean shelf foraminifera: Recent distribution, Holocene sea-level reconstructions, and paleoceanographic implications.
- Milker, Y. and Schmiedl, G., 2012. A taxonomic guide to modern benthic shelf foraminifera of the western Mediterranean Sea. *Palaeontologia electronica*, 15(2): 1-134.
- Milker, Y., Weinkauf, M. F., Titschack, J., Freiwald, A., Krüger, S., Jorissen, F. J. and Schmiedl, G., 2017. Testing the applicability of a benthic foraminiferal-based transfer function for the reconstruction of paleowater depth changes in Rhodes (Greece) during the early Pleistocene. *PloS one*, 12(11): e0188447.
- Mojtahid, M., Jorissen, F., Durrieu, J., Galgani, F., Howa, H., Redois, F. and Camps, R., 2006. Benthic foraminifera as bio-indicators of drill cutting disposal in tropical east Atlantic outer shelf environments. *Marine Micropaleontology*, 61(1-3): 58-75.
- Murray, J., 1991. *Ecology and palaeoecology of benthic foraminifera*: Longman Scientific and Technical. Harlow, Essex, UK.
- Murray, J. W., 2006. *Ecology and applications of benthic foraminifera*. Cambridge University Press.
- Naeher, S., Geraga, M., Papatheodorou, G., Ferentinos, G., Kaberi, H. and Schubert, C. J., 2012. Environmental variations in a semi-enclosed embayment (Amvrakikos Gulf, Greece)-reconstructions based on benthic foraminifera abundance and lipid biomarker pattern. *Biogeosciences*, 9(12): 5081-5094.

- Ochoa, J. and Bray, N., 1991. Water mass exchange in the Gulf of Cadiz. Deep Sea Research Part A. Oceanographic Research Papers, 38: S465-S503.
- Ohga, T. and Kitazato, H., 1997. Seasonal changes in bathyal foraminiferal populations in response to the flux of organic matter (Sagami Bay, Japan). *Terra Nova*, 9(1): 33-37.
- Omodeo Salé, S., Gennari, R., Lugli, S., Manzi, V. and Roveri, M., 2012. Tectonic and climatic control on the Late Messinian sedimentary evolution of the Nijar Basin (Betic Cordillera, Southern Spain). *Basin Research*, 24(3): 314-337.
- Orszag-Sperber, F., 2006. Changing perspectives in the concept of “Lago-Mare” in Mediterranean Late Miocene evolution. *Sedimentary Geology*, 188: 259-277.
- Pérez-Asensio, J. N., Aguirre, J., Schmiedl, G. and Civis, J., 2012. Messinian paleoenvironmental evolution in the lower Guadalquivir Basin (SW Spain) based on benthic foraminifera. *Palaeogeography, Palaeoclimatology, Palaeoecology*, 326: 135-151.
- Pérez-Asensio, J. N., Aguirre, J., Jiménez-Moreno, G., Schmiedl, G. and Civis, J., 2013. Glacioeustatic control on the origin and cessation of the Messinian salinity crisis. *Global and Planetary Change*, 111: 1-8.
- Pérez-Asensio, J. N., Frigola, J., Pena, L. D., Sierro, F. J., Reguera, M. I., Rodríguez-Tovar, F. J., Dorador, J., Asioli, A., Kuhlmann, J. and Huhn, K., 2020. Changes in western Mediterranean thermohaline circulation in association with a deglacial Organic Rich Layer formation in the Alboran Sea. *Quaternary Science Reviews*, 228: 106075.
- Pérez-Asensio, J. N., Rodríguez-Tovar, F. J., Łaska, W. and Uchman, A., 2021. Palaeoenvironmental changes after the Messinian Salinity Crisis in the Mediterranean Almería-Níjar Basin (SE Spain) recorded by benthic foraminifera. *Palaeogeography, Palaeoclimatology, Palaeoecology*: 110536.
- Pflum, C. E., Frerichs, W. E. and Sliter, W. V., 1976. Gulf of Mexico Deep-water Foraminifers, 14. Cushman Foundation for Foraminiferal Research.
- Pierre, C., Caruso, A., Blanc-Valleron, M.-M., Rouchy, J. M. and Orszag-Sperber, F., 2006. Reconstruction of the paleoenvironmental changes around the Miocene–Pliocene boundary along a West–East transect across the Mediterranean. 188-189: 319-340.
- Platon, E., Gupta, B. K. S., Rabalais, N. N. and Turner, R. E., 2005. Effect of seasonal hypoxia on the benthic foraminiferal community of the Louisiana inner continental shelf: The 20th century record. *Marine Micropaleontology*, 54(3-4): 263-283.
- Poag, C. W. and Tresslar, R. C., 1981. Living foraminifers of West Flower Garden Bank, northernmost coral reef in the Gulf of Mexico. *Micropaleontology*, 27(1): 31-62.
- Radionova, E. P., Golovina, L. A., Filippova, N. Y., Trubikhin, V. M., Popov, S. V., Goncharova, I. A., Vernigorova, Y. V. and Pinchuk, T. N., 2012. Middle-Upper Miocene stratigraphy of the Taman Peninsula, Eastern Paratethys. *Central European Journal of Geosciences*, 4(1): 188-204.

- Riforgiato, F., Foresi, L. M., Di Stefano, A., Aldinucci, M., Pelosi, N., Mazzei, R., Salvatorini, G. and Sandrelli, F., 2011. The Miocene/Pliocene boundary in the Mediterranean area: New insights from a high-resolution micropalaeontological and cyclostratigraphical study (Cava Serredi section, Central Italy). *305(1-4)*: 310-328.
- Rohling, E., Jorissen, F. and De Stigter, H., 1997. 200 year interruption of Holocene sapropel formation in the Adriatic Sea. *Journal of Micropalaeontology*, *16(2)*: 97-108.
- Rohling, E., Marino, G. and Grant, K., 2015. Mediterranean climate and oceanography, and the periodic development of anoxic events (sapropels). *Earth-Science Reviews*, *143*: 62-97.
- Ross, D. A., 1978. Summary of results of Black Sea drilling.
- Rouchy, J., Orszag-Sperber, F., Blanc-Valleron, M.-M., Pierre, C., Rivière, M., Combourieu-Nebout, N. and Panayides, I., 2001. Paleoenvironmental changes at the Messinian-Pliocene boundary in the eastern Mediterranean (southern Cyprus basins): significance of the Messinian Lago-Mare. *Sedimentary Geology*, *145(1-2)*: 93-117.
- Rouchy, J. M. and Caruso, A., 2006. The Messinian salinity crisis in the Mediterranean basin: A reassessment of the data and an integrated scenario. *Sedimentary Geology*, *188-189*: 35-67.
- Rouchy, J. M., Caruso, A., Pierre, C., Blanc-Valleron, M.-M. and Bassetti, M. A., 2007. The end of the Messinian salinity crisis: evidences from the Chelif Basin (Algeria). *Palaeogeography, Palaeoclimatology, Palaeoecology*, *254(3-4)*: 386-417.
- Roveri, M. and Manzi, V., 2006. The Messinian salinity crisis: Looking for a new paradigm? *Palaeogeography, Palaeoclimatology, Palaeoecology*, *238(1-4)*: 386-398.
- Roveri, M., Lugli, S., Manzi, V. and Schreiber, B. C., 2008. The Messinian Sicilian stratigraphy revisited: New insights for the Messinian salinity crisis. *Terra Nova*, *20(6)*: 483-488.
- Roveri, M., Flecker, R., Krijgsman, W., Lofi, J., Lugli, S., Manzi, V., Sierro, F. J., Bertini, A., Camerlenghi, A. and De Lange, G., 2014a. The Messinian Salinity Crisis: past and future of a great challenge for marine sciences. *Marine Geology*, *352*: 25-58.
- Roveri, M., Manzi, V., Bergamasco, A., Falcieri, F. M., Gennari, R., Lugli, S. and Schreiber, B. C., 2014b. Dense shelf water cascading and messinian canyons: A new scenario for the mediterranean salinity crisis. *American Journal of Science*, *314(3)*: 751-784.
- Roveri, M., Gennari, R., Persico, D., Rossi, F. P., Lugli, S., Manzi, V., Reghizzi, M. and Taviani, M., 2018. A new chronostratigraphic and palaeoenvironmental framework for the end of the Messinian salinity crisis in the Sorbas Basin (Betic Cordillera, southern Spain). *Geological Journal*.

- Roveri, M., Gennari, R., Ligi, M., Lugli, S., Manzi, V. and Reghizzi, M., 2019a. The synthetic seismic expression of the Messinian salinity crisis from onshore records: Implications for shallow-to deep-water correlations. *Basin Research*, 31(6): 1121-1152.
- Roveri, M., Gennari, R., Persico, D., Rossi, F. P., Lugli, S., Manzi, V., Reghizzi, M. and Taviani, M., 2019b. A new chronostratigraphic and palaeoenvironmental framework for the end of the Messinian salinity crisis in the Sorbas Basin (Betic Cordillera, southern Spain). *Geological Journal*, 54(3): 1617-1637.
- Russo, B., Curcio, E. and Iaccarino, S., 2007. Paleocology and paleoceanography of a Langhian succession (Tremeti Islands, southern Adriatic Sea, Italy) based on benthic foraminifera. *Bollettino della Società Paleontologica Italiana*, 46: 107-124.
- Sant, K., Palcu, D., Turco, E., Di Stefano, A., Baldassini, N., Kouwenhoven, T., Kuiper, K. and Krijgsman, W., 2019. The mid-Langhian flooding in the eastern Central Paratethys: integrated stratigraphic data from the Transylvanian Basin and SE Carpathian Foredeep. *International Journal of Earth Sciences*, 108(7): 2209-2232.
- Sanz De Galdeano, C. and Vera, J. A., 1992. Stratigraphic record and palaeogeographical context of the Neogene basins in the Betic Cordillera, Spain. *Basin Research*, 4(1): 21-36.
- Schmiedl, G., Mackensen, A. and Müller, P., 1997. Recent benthic foraminifera from the eastern South Atlantic Ocean: dependence on food supply and water masses. *Marine Micropaleontology*, 32(3-4): 249-287.
- Schmiedl, G., De Bovée, F., Buscail, R., Charriere, B., Hemleben, C., Medernach, L. and Picon, P., 2000. Trophic control of benthic foraminiferal abundance and microhabitat in the bathyal Gulf of Lions, western Mediterranean Sea. *Marine Micropaleontology*, 40(3): 167-188.
- Schmiedl, G., Mitschele, A., Beck, S., Emeis, K.-C., Hemleben, C., Schulz, H., Sperling, M. and Weldeab, S., 2003. Benthic foraminiferal record of ecosystem variability in the eastern Mediterranean Sea during times of sapropel S5 and S6 deposition. *Palaeogeography, Palaeoclimatology, Palaeoecology*, 190: 139-164.
- Schmiedl, G., Kuhnt, T., Ehrmann, W., Emeis, K.-C., Hamann, Y., Kotthoff, U., Dulski, P. and Pross, J., 2010. Climatic forcing of eastern Mediterranean deep-water formation and benthic ecosystems during the past 22 000 years. *Quaternary Science Reviews*, 29(23-24): 3006-3020.
- Schoorl, J. and Veldkamp, A., 2003. Late Cenozoic landscape development and its tectonic implications for the Guadalhorce valley near Alora (Southern Spain). *Geomorphology*, 50(1-3): 43-57.
- Schrader, H.-J., 1978. Quaternary through Neogene History of the Black Sea, Deduced from the Paleocology of Diatoms, Silicoflagellates, Ebridians, and Chrysomonads.
- Sen Gupta, B. K. and Machain-Castillo, M. L., 1993. Benthic foraminifera in oxygen-poor habitats. 20(3-4): 183-201.

- Serrano, F., 1990. El Mioceno mediq en el; rea de Níjar (Almeria, Espana). *Rev. Soc. Geo. España*, 3: 1-2.
- Sgarrella, F., Sprovieri, R., Di stefano, E. and Caruso, A., 1997. Paleooceanographic conditions at the base of the Pliocene in the Southern Mediterranean Basin. *Rivista Italiana di Paleontologia e Stratigrafia*, 103(2).
- Sgarrella, F., Sprovieri, R., Di Stefano, E., Caruso, A., Sprovieri, M. and Bonaduce, G., 1999. The Capo Rossello bore-hole (Agrigento, Sicily) cyclostratigraphic and paleooceanographic reconstructions from quantitative analyses of the Zanclean foraminiferal assemblages. *Rivista Italiana di Paleontologia e Stratigrafia*, 105(2).
- Sharafi, M., Rodríguez-Tovar, F. J., Janočko, J., Bayet-Goll, A., Mohammadi, M. and Khanehbad, M., 2021. Environmental significance of trace fossil assemblages in a tide-wave-dominated shallow-marine carbonate system (Lower Cretaceous), northern Neo-Tethys margin, Kopet-Dagh Basin, Iran. *International Journal of Earth Sciences*: 1-24.
- Sierro, F. J., Flores, J. A., Civis, J., González Delgado, J. A. and Francés, G., 1993. Late Miocene globorotaliid event-stratigraphy and biogeography in the NE-Atlantic and Mediterranean. *Marine Micropaleontology*, 21(1-3): 143-167.
- Smart, C. W., King, S. C., Gooday, A. J., Murray, J. W. and Thomas, E., 1994. A benthic foraminiferal proxy of pulsed organic matter paleofluxes. 23(2): 89-99.
- Soria, J., Caracuel, J., Yébenes, A., Fernández, J. and Viseras, C., 2005. The stratigraphic record of the Messinian salinity crisis in the northern margin of the Bajo Segura Basin (SE Spain). *Sedimentary Geology*, 179(3-4): 225-247.
- Spellerberg, I. F. and Fedor, P. J., 2003. A tribute to Claude Shannon (1916–2001) and a plea for more rigorous use of species richness, species diversity and the ‘Shannon-Wiener’ Index. *Global ecology and biogeography*, 12(3): 177-179.
- Sprovieri, R. and Hasegawa, S., 1990. Plio-Pleistocene benthic foraminifer stratigraphic distribution in the deep-sea record of the Tyrrhenian Sea (ODP Leg 107), Proceedings of the Ocean Drilling Program, Scientific Results. Ocean Drilling Program College Station, TX, pp. 429-459.
- Stoica, M., Krijgsman, W., Fortuin, A. and Gliozzi, E., 2016. Paratethyan ostracods in the Spanish Lago-Mare: More evidence for interbasinal exchange at high Mediterranean sea level. *Palaeogeography, Palaeoclimatology, Palaeoecology*, 441: 854-870.
- Suokhrie, T., Saraswat, R. and Nigam, R., 2021. Multiple Ecological Parameters Affect Living Benthic Foraminifera in the River-Influenced West-Central Bay of Bengal. *Frontiers in Marine Science*, 8: 467.
- Theodor, M., Schmiedl, G., Jorissen, F. and Mackensen, A., 2016a. Stable carbon isotope gradients in benthic foraminifera as proxy for organic carbon fluxes in the Mediterranean Sea. *Biogeosciences*, 13(23): 6385-6404.

- Theodor, M., Schmiedl, G. and Mackensen, A., 2016b. Stable isotope composition of deep-sea benthic foraminifera under contrasting trophic conditions in the western Mediterranean Sea. *Marine Micropaleontology*, 124: 16-28.
- Trenkwalder, S., Violanti, D., d'Atri, A., Lozar, F., Dela Pierre, F. and Irace, A., 2008. The Miocene/Pliocene boundary and the Early Pliocene micropalaeontological record: new data from the Tertiary Piedmont Basin (Moncucco Quarry, Torino Hill, Northwestern Italy). *Bollettino della Società Paleontologica Italiana*, 47 (2): 87-103.
- Tulbure, M., Capella, W., Barhoun, N., Flores, J., Hilgen, F., Krijgsman, W., Kouwenhoven, T., Sierro, F. J. and Yousfi, M. Z., 2017. Age refinement and basin evolution of the North Rifian Corridor (Morocco): No evidence for a marine connection during the Messinian Salinity Crisis. *Palaeogeography, Palaeoclimatology, Palaeoecology*, 485: 416-432.
- Uchman, A. and Demircan, H., 1999. Trace fossils of Miocene deep-sea fan fringe deposits from the Cingöz Formation, southern Turkey, *Annales Societatis Geologorum Poloniae*, pp. 125-135.
- Van Der Schee, M., Sierro, F. J., Jiménez-Espejo, F. J., Hernández-Molina, F. J., Flecker, R., Flores, J. A., Acton, G., Gutjahr, M., Grunert, P., García-Gallardo, Á. and Andersen, N., 2016. Evidence of early bottom water current flow after the Messinian Salinity Crisis in the Gulf of Cadiz. 380: 315-329.
- Van der Zwaan, G., Jorissen, F. and De Stigter, H., 1990. The depth dependency of planktonic/benthic foraminiferal ratios: constraints and applications. *Marine Geology*, 95(1): 1-16.
- Van der Zwaan, G., Duijnste, I., Den Dulk, M., Ernst, S., Jannink, N. and Kouwenhoven, T., 1999. Benthic foraminifers: proxies or problems?: a review of paleocological concepts. *Earth-Science Reviews*, 46(1-4): 213-236.
- van der Zwaan, G. J., 1982. *Paleoecology of late Miocene Mediterranean foraminifera*, Utrecht University.
- Van Hinsbergen, D. J. J., Kouwenhoven, T. J. and Van Der Zwaan, G. J., 2005. Paleobathymetry in the backstripping procedure: Correction for oxygenation effects on depth estimates. 221(3-4): 245-265.
- Van Morkhoven, F. M., Berggren, W. A. and Edwards, A. S., 1986. Cenozoic cosmopolitan deep-water benthic foraminifera. *Bulletin des centres de Recherches exploration-production elf-aquitaine*(11).
- Van Rooij, D., De Mol, L., Le Guilloux, E., Wisshak, M., Huvenne, V., Moeremans, R. and Henriët, J.-P., 2010. Environmental setting of deep-water oysters in the Bay of Biscay. *Deep Sea Research Part I: Oceanographic Research Papers*, 57(12): 1561-1572.
- Venz, K. A., Hodell, D. A., Stanton, C. and Warnke, D. A., 1999. A 1.0 Myr record of Glacial North Atlantic Intermediate Water variability from ODP site 982 in the northeast Atlantic. *Paleoceanography*, 14(1): 42-52.

- Verhallen, P. J., 1991. Late Pliocene to Early Pleistocene Mediterranean mud-dwelling foraminifera: influence of a changing environment on community structure and evolution, Utrecht University.
- Violanti, D., Dela Pierre, F., Trenkwalder, S., Lozar, F., Clari, P., Irace, A. and D'Atri, A., 2011. Biostratigraphic and palaeoenvironmental analyses of the Messinian/Zanclean boundary and Zanclean succession in the Moncucco quarry (Piedmont, northwestern Italy). *Bulletin de la Société géologique de France*, 182(2): 149-162.
- Wright, R., 1978. 41. Neogene paleobathymetry of the Mediterranean based on benthic foraminifers from DSDP Leg 42a. *Initial Reports DSDP*, 42: 837-847.
- Wright, R., 1979. Benthic foraminiferal repopulation of the Mediterranean after the Messinian (Late Miocene) event. *Palaeogeography, Palaeoclimatology, Palaeoecology*, 29: 189-214.

Chapter 7

Conclusions

Chapter 7

Conclusions

Conclusions

This PhD thesis aimed to study the paleoenvironmental conditions of the Mediterranean Basin, in particular the areas close to the Atlantic – Mediterranean connections, prior and after the Messinian Salinity Crisis (MSC). We were also interested in understanding whether there were some deposits related to the MSC in the Alboran Basin, where no evaporites have been found.

In the first place, we were able to demonstrate the impact and timing of the Messinian Salinity Crisis preconditioning phase both in the Western Mediterranean Basin and in the Atlantic Ocean studying cores and inland sections from regions proximal to the Strait of Gibraltar. To do so we performed high resolution micropaleontological and geochemical analyses on ODP Site 976 in the Alboran Basin and on Montemayor-1 core from the Guadalquivir Basin which allowed to create a precise age model for the two sites and to pinpoint the major changes occurring in the records. Furthermore, these observations were paired with micropaleontological analyses from Alboran Basin DSDP Site 121, industrial boreholes And-G1 and Alb-A1 and seismic lines which enabled to identify the Zanclean erosion and late Messinian deposits in the Alboran Basin.

Secondly, a causal mechanism was identified between the first restriction of the Mediterranean – Atlantic gateway/s and global-scale climate events.

Finally, it was possible to reconstruct the dynamics of the reestablishment of an efficient Mediterranean – Atlantic connection after the Zanclean reflooding by a detailed sedimentological and micropaleontological analyses of early Pliocene sediments from ODP Site 976 and Southern Spanish outcrops from Malaga, Nijar and Sorbas Basins.

1. Preconditioning of the MSC and related deposits

1.1 Mediterranean side: Alboran Basin

The planktic and benthic foraminifer analyses from Alboran Basin ODP Site 976 allowed the creation of an initial age model using bioevents as first order tie points. These included the FCO of *G. menardii* 5 group (7.36 Ma), the LCO of *G. menardii* 5 group (7.23 Ma), the FCO of *G. miotumida* group (7.24 Ma), the LO of *G. suterae* (7.17 Ma), the disappearance of *S. reticulata* (7.167 Ma), and S/D coiling change in *N. acostaensis*. A precise astronomical tuning

was further possible after the recognition of precessionally driven cyclical changes in the WOWPF, stable isotope and XRF records. Through this high-resolution age model, for the Tortonian and Messinian of the Alboran Basin we were able to precisely date environmental changes in this part of the Mediterranean so close to the Gibraltar arch gateway/s and the following observations were made.

- During the late Tortonian – early Messinian i.e., until 7.17 Ma, the WAB was characterized by deep open-marine sedimentation. High percentages of planktonic foraminifers typical of cold, nutrient-rich waters and benthic foraminifers typical of high oxygen levels and open marine conditions infer a deep-water well-ventilated environment, indicating efficient water exchange through the Gibraltar gateway/s. In particular, the absence of warm water planktic foraminifer genera *Globigerinoides* spp., encountered at other contemporaneous sites, could suggest that the eastward Atlantic inflow, moving along the southern Spanish coast may promote a circulation similar to that occurring today in the Alboran Basin. The resulting upwelling of cold nutrient rich waters could explain the thriving of cold-water foraminifer. These findings open the possibility, even though speculative, of the existence of a proto-Gibraltar strait as the main source of Atlantic inflow at that time.
- Starting from 7.17 Ma an increase in siliciclastic input compared to biogenic carbonate and a rise in the sedimentation rate are observed at Site 976 parallel to an evident amplification of cyclical changes both in the geochemical and micropaleontological records. We interpreted this event as the result of tectonic uplift in the Gibraltar Arc which resulted in increased river incision and consequent higher terrigenous input to the basin. The uplift is also probably responsible for the major restriction of the Betic and Rifian corridors at the beginning of the Messinian and represents the first step of restriction prior to the MSC. The reduced water exchange between the Mediterranean and Atlantic increased the sensitivity of the basin to climate forcing as seen by the amplified precession cyclicity. The restriction is reflected in the change in benthic foraminifer fauna, which became dominated by shallow infaunal taxa, tolerant to a wide range of conditions and suboptimal oxygen levels. These observations, paired with a significant drop in benthic $\delta^{13}\text{C}$ values suggests that the gateway restriction led to the decrease in bottom water oxygen levels and increase in its residence time.

-
- A detailed correlation with other Mediterranean records confirmed that the gateway restriction starting from 7.17 Ma recognized from the WAB records, contemporaneously affected different locations all over the basin, suggesting a Mediterranean-scale change in thermohaline circulation. From these data we conclude in the first place that the WAB and EAB were not separated by a sill but were both part of the Mediterranean realm. In second place, we were able to refine a Mediterranean circulation model for both before and after 7.17 Ma. The restriction of the gateways resulted in stratification of the WMB water column but while the bottom waters were depleted in oxygen, the intermediate waters were better ventilated. In the EMB, because of the presence of the Sicily sill, the impact of stratification was much higher and led to sapropel deposition, absent in the WMB.
 - The analyses of seismic profiles and borehole sediments from the WAB allowed the recognition of two Messinian units, one composed of plane parallel strata and one chaotic. The first has been related with turbidite deposition near the coast and more hemipelagic deposits in the central parts of the basin. The second, chaotic MTD unit retrieved in drilling cuttings of industrial wells And-G1 and Alb-A1, can be related to the MSC final stages triggered by a base-level change.
 - Through the astronomical tuning we were able to give an age to the first precession cycles of the Messinian below the major discontinuity observed in WAB seismic profiles. The irregular erosional surface (M reflector) is clearly visible at Site 976 where we estimated that at least 1.67 Ma and 455 m of the Messinian sedimentary record is missing.

1.2 Atlantic side: Guadalquivir Basin

A new high-resolution tuning of the lower interval of Montemayor-1 core located in the Guadalquivir Basin (6.37 Ma - 8 Ma) was produced by the combination of planktic foraminifer bioevents (LCO of *G. menardii* 4 group, FCO of *G. menardii* group 5, replacement of the *G. menardii* 5 group by the *G. miotumida* group and the *N. acostaensis* coiling change from sinistral to dextral) and astronomical tuning of the eccentricity driven cycles. Combining this new age model for the lower part of the record with previous age models and datasets for the middle (5.77 Ma- 6.37 Ma) and upper (5.33 Ma - 5.77 Ma) part of the Montemayor-1 core enabled to precisely date environmental changes happening in the Guadalquivir Basin from 8 to 5.33 Ma and relate them to Mediterranean and global events:

- From 7.15 – 7.17 Ma at Montemayor-1 site the bottom water residence time, temperature and salinity increase in concomitance with a shallowing of the basin inferred from the sedimentation rate and terrigenous supply rise. We associate this event with a reduction of the MOW as a consequence of the restriction of the last strand of the Betic corridor connecting the Mediterranean and the Atlantic, the GC.
- The restriction of the Betic corridor between 7.15 and 7.17 Ma is in line with the contemporaneous changes reported from the Alboran Basin and numerous other Mediterranean locations where a Mediterranean – Atlantic gateway restriction and reduced Mediterranean outflow are inferred at 7.17 Ma by the increased residence time and decreased oxygenation in the bottom part of the water column.
- The progressive increase in sedimentation rate (from 5 to 90 cm/kyr) visible from the Montemayor-1 data and the consequent restriction of the last strand of the Betic corridor can be related with the uplift of the Gibraltar Arc area that led to the progressive shallowing and infilling of the GB.
- The change in cyclicity that was seen in the upper part of the record by previous authors, where Northern Hemisphere insolation maxima is related with sediment enrichment in biogenic carbonate, while insolation minima are linked to an increase in terrigenous supply has been confirmed by our new data. Furthermore, the new planktic foraminifer data support the previously proposed mechanism, where the shallowing of the GB allowed for coarser sediment to reach Montemayor-1 site while the colder and arid climate present during Northern Hemisphere insolation minima had a negative effect on the vegetation cover resulting in more erosion and terrigenous input into the basin at the expense of the biogenic carbonate.

1.3 Global relevance of the Mediterranean and Atlantic MSC related events

The paleoenvironmental change that affected the Mediterranean and Atlantic margins at 7.17 Ma coincided with the LMCIS (7.6 to 6.8/7 Ma), a global event characterised by cooling and a shift to lighter $\delta^{13}\text{C}$. Consequently, in order to test to which extent, the global and local forcing affected these basins we confronted our isotope data with several sites from the global ocean.

- The comparison between Site 976 and ODP Site 1146 (South China Sea) isotope data showed how even if both basins register a simultaneous

$\delta^{13}\text{C}$ shift around 7.17 Ma, the phase relations of the isotope record with astronomical parameters (precession, obliquity) is different. Site 1146 reflects global phase relations connected to glacial stages, whereas the phase relations in the WAB depend on hydrological budget changes suggesting a much stronger local effect in the Mediterranean. This does not exclude the possibility that the gateway restriction effects on the Mediterranean could have been further amplified by the LMCIS.

- Analogously, the Monemayor-1 7.15 -7.17 Ma change could have been partly influenced by the LMCIS and global cooling, as may be inferred from a slight shift towards heavier benthic $\delta^{18}\text{O}$ and lighter benthic $\delta^{13}\text{C}$.

2. Zanclean reflooding of deep and marginal basins in the proximity of Gibraltar

The sedimentological, micropaleontological and stable isotope study of late Messinian – early Pliocene sections in the Spanish basins proximal to the strait of Gibraltar gave important information regarding the environmental conditions in the Mediterranean after the reestablishment of an efficient Mediterranean – Atlantic connection following the MSC.

- A dark layer, usually grey or black, identified at the MPB in deep and marginal basins all over the Mediterranean, and often enriched in organic matter, suggested that the early Pliocene was characterized by water column stratification, and reduced bottom water oxygen levels. Such conditions could have developed if the Atlantic inflow reaching the Mediterranean was more saline than the Mediterranean waters still under the influence of the Paratethys, causing them to sink and stratify the water column. Lower salinities of Mediterranean water are indicated by light benthic $\delta^{18}\text{O}$ values, much lighter than the Atlantic ones. The early Pliocene of Site 976 located in the Alboran Basin does not show a dark layer, probably because of its proximity with the Strait of Gibraltar and strong erosion produced by the inflowing Atlantic waters that could have eroded the basal Pliocene layers.
- The benthic foraminifer repopulation identified in the studied basins shows similarities with other events of more recent microfaunal recovery from hostile environments and repopulation following low-oxic episodes during sapropel deposition. The general repopulation trend shows a shift from stressed and unstable environments to

benthic associations indicating an amelioration of the circulation and bottom water ventilation. The first benthic faunas that appear are in line with reduced bottom water oxygen levels and stratified water column in agreement with the deposition of the dark layer.

- In all the studied marginal Spanish basins, the estimated palaeobathymetry for the early Pliocene was similar, ranging between 50 and 150 m and showed an increasing upward trend. These observations imply a progressive deepening of the Mediterranean margins as the Mediterranean – Atlantic connectivity gradually became more efficient. Furthermore, a comparison with palaeo-depths and repopulation sequences from other Mediterranean sites suggests that in the Mediterranean margins the reflooding may have been diachronous due to the effects of local tectonics and flexural responses to loading and unloading. At Site 976, the early Pliocene is characterised by a bathyal environment (> 1000 m).
- The high $\delta^{13}\text{C}$ levels from Site 976 testify that bottom water renewal in the deep basins was efficient immediately after the reflooding. The much lighter values found in Malaga Basin suggest that due to diachronous refill, shallow marginal basins needed more time to reach an efficient bottom water circulation.

Appendix

Appendix 1

List of acronyms

List of acronyms

Follows a list of the acronyms used in this thesis.

%P	Percentage Planktonic Foraminifers
Alb-A1	Alboran-A1
And-G1	Andalucia-A1
AUW	Atlantic Upwelling Water
BF/g	Benthic Foraminifer/gram
BFAR	Benthic foraminiferal accumulation rate
BFOI	Benthic Foraminifer Oxygen Index
CEWPF	Cold Eutrophic Water Planktic Foraminifers
DIC	Dissolved Inorganic Carbon
DSDP	Deep Sea Drilling Project
E/I	Epifaunal/Infaunal ratio
EAB	East Alboran Basin
EMB	East Mediterranean Basin
FCO	First Common Occurrence
GB	Guadalquivir Basin
GC	Guadalhorce Corridor
H index	Shannon diversity index
IODP	International Ocean Discovery Program
LCO	Last Common Occurrence
LIW	Levantine Intermediate Water
LM	Lago-Mare
LMCIS	Late Miocene Carbon Isotope Shift
LO	Last Occurrence
mbsf	metres below sea floor
mcd	metres composite depth
MOW	Mediterranean Outflow Water
MPB	Miocene - Pliocene Boundary
MSC	Messinian Salinity Crisis
MTD	Mass Transport Deposit
NADW	North Atlantic Deep Water
ODP	Ocean Drilling Project
OMZ	Oxygen Minimum Zone
ORL	Organic Rich Layer
PCA	Principal Component Analyses
S/D	Sinistral/Dextral
SCW	Southern Component Water
SST	Sea Surface Temperature
T.O.C.	Total Organic carbon
TWTT	Two-way Travel Time
WAB	West Alboran
WMB	West Mediterranean Basin
WMDW	West Mediterranean Deep Water
WOWPF	Worm Oligotrophic Water Planktic Foraminifera
WP	Working Package
XRF	X-Ray Fluorescence

Appendix 2

Article written in collaboration with
SALTGIANT project members.

F. Andretto, G. Aloisi, F. Raad, H. Heida, R. Flecker, K. Agiadi,
J. Lofi, S. Blondel, **F. Bulian**, A. Camerlenghi, A. Caruso,
R. Ebner, D. Garcia-Castellanos, V. Gaullier, L. Guibourdenche,
Z. Gvirtzman, T. M. Hoyle, P. T. Meijer, J. Moneron, F. J. Sierro,
G. Travan, A. Tzevahirtzian, I. Vasiliev, W. Krijgsman, Freshening
of the Mediterranean Salt Giant: controversies and certainties
around the terminal (Upper Gypsum and Lago-Mare) phases of the
Messinian Salinity Crisis, *Earth-Science Reviews*, Volume 216, 2021,
103577, ISSN 0012-8252.

DOI: <https://doi.org/10.1016/j.earscirev.2021.103577>



Contents lists available at ScienceDirect

Earth-Science Reviews

journal homepage: www.elsevier.com/locate/earscirev

Freshening of the Mediterranean Salt Giant: controversies and certainties around the terminal (Upper Gypsum and Lago-Mare) phases of the Messinian Salinity Crisis

F. Andreetto^{a,*}, G. Aloisi^b, F. Raad^c, H. Heida^d, R. Flecker^e, K. Agiadi^f, J. Lofi^c, S. Blondel^g, F. Bulian^h, A. Camerlenghi^g, A. Carusoⁱ, R. Ebner^j, D. Garcia-Castellanos^d, V. Gaullier^k, L. Guibourdenche^b, Z. Gvirtzman^{l,m}, T.M. Hoyle^{a,n}, P.T. Meijer^j, J. Moneron^{l,m}, F.J. Sierro^h, G. Travan^k, A. Tzevahirtzian^l, I. Vasiliev^o, W. Krijgsman^a

^a Paleomagnetic Laboratory "Fort Hoofdijk", Dept. of Earth Sciences, Utrecht University, Budapestlaan 17, 3584 CD Utrecht, The Netherlands

^b Université de Paris, Institut de physique du globe de Paris, CNRS, F-75005 Paris, France

^c Géosciences Montpellier, CNRS, Université de Montpellier, Montpellier, France

^d Geosciences Barcelona, GEO3BCN, CSIC, Solé i Sabarís s/n, Barcelona, Spain

^e BRIDGE, School of Geographical Sciences and Cabot Institute, University of Bristol, University Road, Bristol BS8 1SS, United Kingdom

^f Department of Palaeontology, University of Vienna, Althanstraße 14 (UZA ID), 1090 Vienna, Austria

^g Istituto Nazionale di Oceanografia e di Geofisica Sperimentale (OGS), Trieste, Italy

^h Department of Geology, University of Salamanca, Salamanca, Spain

ⁱ Dipartimento di Scienze della Terra e del Mare, Università degli studi di Palermo, via Archirafi 20-22, 90123 Palermo, Italy

^j Department of Earth Sciences, Utrecht University, Utrecht, The Netherlands

^k Univ. Lille, CNRS, Univ. Littoral Côte d'Opale, UMR 8187, LOG, Laboratoire d'Océanologie et de Géosciences, F 59000, Lille, France

^l Geological Survey of Israel, Jerusalem 95501, Israel

^m Institute of Earth Sciences, The Hebrew University of Jerusalem, Israel

ⁿ CASP, West Building, Madingley Rise, Madingley Road, Cambridge CB3 0UD, United Kingdom

^o Senckenberg Research Biodiversity and Climate Research Centre, Senckenberganlage 25, 60325 Frankfurt am Main, Germany

ARTICLE INFO

Keywords:

Messinian Salinity Crisis
Mediterranean stratigraphy
Connectivity proxies
Paleogeography
Paratethys
Lago-Mare

ABSTRACT

The late Miocene evolution of the Mediterranean Basin is characterized by major changes in connectivity, climate and tectonic activity resulting in unprecedented environmental and ecological disruptions. During the Messinian Salinity Crisis (MSC, 5.97-5.33 Ma) this culminated in most scenarios first in the precipitation of gypsum around the Mediterranean margins (Stage 1, 5.97-5.60 Ma) and subsequently > 2 km of halite on the basin floor, which formed the so-called Mediterranean Salt Giant (Stage 2, 5.60-5.55 Ma). The final MSC Stage 3, however, was characterized by a "low-salinity crisis", when a second calcium-sulfate unit (Upper Gypsum; substage 3.1, 5.55-5.42 Ma) showing (bio)geochemical evidence of substantial brine dilution and brackish biota-bearing terrigenous sediments (substage 3.2 or Lago-Mare phase, 5.42-5.33 Ma) deposited in a Mediterranean that received relatively large amounts of riverine and Paratethys-derived low-salinity waters. The transition from hypersaline evaporitic (halite) to brackish facies implies a major change in the Mediterranean's hydrological regime. However, even after nearly 50 years of research, causes and modalities are poorly understood and the original scientific debate between a largely isolated and (partly) desiccated Mediterranean or a fully connected and filled basin is still vibrant. Here we present a comprehensive overview that brings together (chrono)stratigraphic, sedimentological, paleontological, geochemical and seismic data from all over the Mediterranean. We summarize the paleo-environmental, paleohydrological and paleoconnectivity scenarios that arose from this cross-disciplinary dataset and we discuss arguments in favour of and against each scenario.

* Corresponding author.

E-mail address: f.andreetto@uu.nl (F. Andreetto).

<https://doi.org/10.1016/j.earscirev.2021.103577>

Received 1 November 2020; Received in revised form 4 February 2021; Accepted 25 February 2021

Available online 3 March 2021

0012-8252/© 2021 The Author(s). Published by Elsevier B.V. This is an open access article under the CC BY license (<http://creativecommons.org/licenses/by/4.0/>).

1. Introduction

At the end of the Miocene, orbital and tectonic drivers combined to alter the amount of water delivered to the Mediterranean Basin by the Atlantic Ocean from the west, the brackish Eastern Paratethys (i.e. Euxinic-Caspian Basin system) from the east and the major peri-Mediterranean freshwater drainage systems (e.g. African rivers and Rhône; Griffin, 2002; Gladstone et al., 2007; Van der Laan et al., 2006; Hilgen et al., 2007; Ryan, 2009; Flecker et al., 2015; Marzocchi et al., 2015, 2016, 2019; Simon et al., 2017; Krijgsman et al., 2018; Capella et al., 2020). The changes in extra and intrabasinal connectivity resulted in unprecedented paleoceanographic and paleohydrological budget changes that led to a relatively short-lived environmental and ecological crisis (approx. 660 kyr; 5.97-5.33 Ma), for which the term Messinian Salinity Crisis (MSC) was coined (Selli, 1954, 1960). Most conspicuous was the rapid accumulation of several kilometers of halite (i.e. ~ 1 million km^3) on the Mediterranean abyssal plains (e.g. Hsü, 1972; Ryan, 1973; Montadert et al., 1978; Haq et al., 2020). This happened within 50 kyr, from 5.60-5.55 Ma, according to Roveri et al. (2014a) and Manzi et al. (2018), or in >300 kyr, when starting at 5.97 Ma, as put forward by Meilijson et al. (2018, 2019).

During the ~ 200 kyr lapse (i.e. MSC Stage 3 following Roveri et al., 2014a; Fig. 1a) between the end of salt precipitation (5.55 Ma) and the restoration of the still enduring marine conditions (5.33 Ma), the Mediterranean underwent a sequence of paleohydrological and base-level changes that are the topic of intense and long-standing debates. The initial and still widely endorsed hypothesis was that the Mediterranean Sea, following the major drawdown event that led to halite deposition (i.e. Stage 2), maintained the isolated, deeply-desiccated geography containing a series of hypersaline (substage 3.1; 5.55-5.42 Ma) and

hyposaline (substage 3.2; 5.42-5.33 Ma) ponds which only received water from local streams and were colonized by Black Sea organisms carried by aquatic migratory birds (Fig. 1b; e.g. Ruggieri, 1967; Decima and Sprovieri, 1973; Decima and Wezel, 1971, 1973; Cita et al., 1978; Müller et al., 1990; Benson and Rakic-El Bied, 1991; Benson et al., 1991; Müller and Mueller, 1991; Butler et al., 1995; Orszag-Sperber et al., 2000; Rouchy et al., 2001; Kartveit et al., 2019; Madof et al., 2019; Camerlenghi et al., 2019; Caruso et al., 2020; Raad et al., 2021). As morphological and seismic reflection studies at the Strait of Gibraltar documented a ~ 400 km long erosional trough connecting the Gulf of Cadiz (Atlantic Ocean) to the Mediterranean Sea, this scenario of a lowered Mediterranean Sea was promptly linked to the termination of the MSC (McKenzie, 1999; Blanc, 2002; Garcia-Castellanos et al., 2009, 2020). This conclusion has recently been reinforced by the discovery of vast chaotic deposits sitting at the claimed Miocene/Pliocene transition in the area of the Malta Escarpment-Ionian Abyssal Plain (Micallef et al., 2018, 2019; Spatola et al., 2020).

In more recent years, the desiccated basin model was challenged by the observation of deposits that are uniform in terms of sedimentology and stratigraphic architecture (Roveri et al., 2008a), ostracod content (Gliozzi et al., 2007; Stoica et al., 2016) and geochemistry (McCulloch and De Deckker, 1989; Garcia-Veigas et al., 2018; Andreetto et al., 2021) throughout the Mediterranean marginal belt and of δD_n -alkanes and $\delta D_{\text{alkenones}}$ sharing similarities with the coeval Atlantic Ocean and Black Sea, respectively (Vasiliev et al., 2017). A model of a (relatively) full Mediterranean Sea developed (Fig. 1c), where the debate mainly concerns the provenance of the hydrological fluxes and the resultant hydrochemical composition of the water mass. In this scenario, the Mediterranean was first, during substage 3.1, transformed into a new gypsum-precipitating basin filled with marine and continent-derived

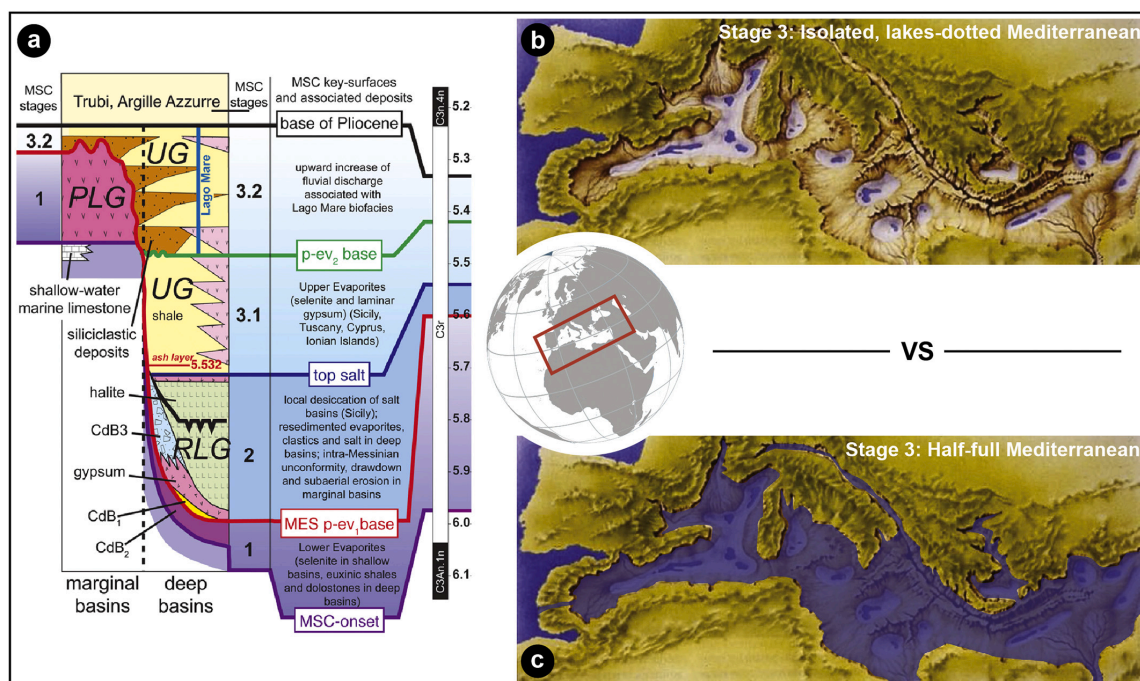


Fig. 1. (a) Consensus chronostratigraphic model for the MSC events (Roveri et al., 2014a). Stage 3, here of interest, spans between 5.55 Ma and 5.332 Ma, the astronomical ages of the base of the Upper Gypsum Unit (following Manzi et al., 2009) and Trubi Formation (Van Couvering et al., 2000) in the Sicilian Eraclea Minoa section, respectively. CdB: Calcare di Base; PLG: Primary Lower Gypsum; RLG: Resedimented Lower Gypsum; UG: Upper Gypsum. (b), (c) Map of the Mediterranean region showing the two extreme and mutually exclusive paleoenvironmental scenarios proposed to have featured the Mediterranean during Stage 3 (see discussion in Chapter 7; modified after Krijgsman et al., 2018).

waters (e.g. Manzi et al., 2009; Roveri et al., 2014c; Flecker et al., 2015; Vasiliev et al., 2017; García-Veigas et al., 2018; Grothe et al., 2020). Then, during substage 3.2, it became a brackish lake-sea comparable to the present-day Black Sea or Caspian Sea (Roveri et al., 2008a; Stoica et al., 2016; Andreetto et al., 2021), depending on whether a marine connection with the Atlantic was active (Manzi et al., 2009; Roveri et al., 2014b, 2014c; Flecker et al., 2015; Marzocchi et al., 2016; Vasiliev et al., 2017; García-Veigas et al., 2018) or not (e.g. McCulloch and De Deckker, 1989; Roveri et al., 2008a), and with a base-level fluctuating by hundreds of meters with precessional periodicity (Fortuin and Krijgsman, 2003; Ben Moshe et al., 2020; Andreetto et al., 2021). In the relatively full scenario, the revival of marine conditions is ascribed to either

connectivity changes (Marzocchi et al., 2016) or to a moderate sea-level rise (Andreetto et al., 2021). In contrast, Carnevale et al. (2006a, 2006b, 2008, 2018) and Grunert et al. (2016), based on the recovery of fish remains ascribed to marine species, proposed that fully marine conditions were in force in the Mediterranean already at the end of substage 3.1.

After nearly 50 years of research on both onshore and offshore localities (Fig. 2), the observations backing up the competing desiccated and full-basin Mediterranean models remain extremely difficult to reconcile. Uncertainties regarding the chronostratigraphic framework of Stage 3 deposits, the origin and migration of its characteristic biota, the meaning of the data derived from the applied geochemical techniques

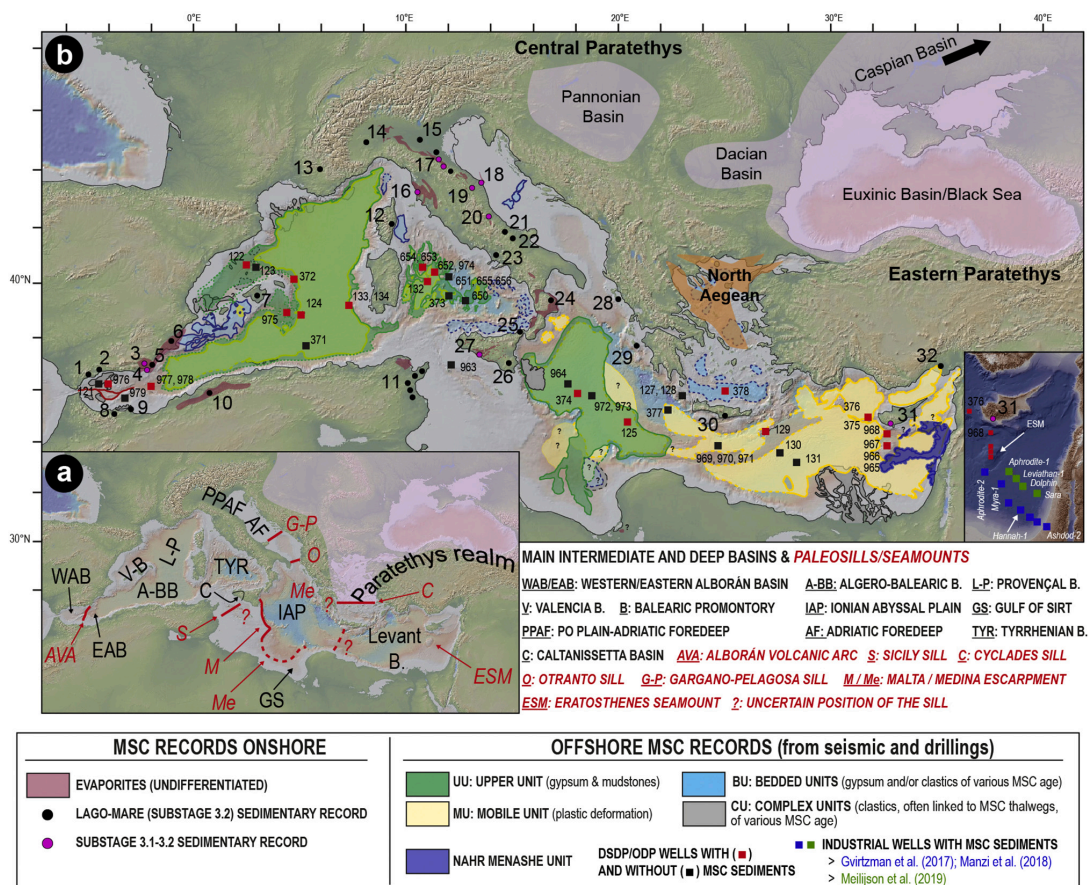


Fig. 2. Map of the Mediterranean Basin (modified from Lofi, 2018) showing: a) the location of the key intermediate and deep basins as well as physical thresholds that influenced the connectivity history of the Mediterranean; b) the onshore (i.e. basins and/or sections) and offshore (DSDP/ODP/Industrial drill sites) localities where deposits attributed to MSC Stage 3 have been studied. Mixed assemblages of Paratethyan-like ostracods and foraminifera are known from all mentioned onshore localities and some offshore locations (see text). The present-day spatial extent of the MSC seismic units, except for the Lower Unit, is also shown. The paleogeography of the (Eastern and Central) Paratethys and of the North Aegean domain is contoured after Van Baak et al. (2017) and Krijgsman et al. (2020a), respectively. W-E onshore localities: 1-6 Betic Cordillera (SE Spain): 1-Marbella and 2-Málaga basins (Guerra-Merchán et al., 2010); 3-Sorbas Basin (Roveri et al., 2009, 2019a); 4-Nijar Basin (Fortuin and Krijgsman, 2003); 5-Vera Basin (Fortuin et al., 1995); 6-Bajo Segura Basin (Soria et al., 2005, 2008a, 2008b); 7-Mallorca (Mas and Fornós, 2020); 8-Melilla Basin (Rouchy et al., 2003); 9-Boudinar Basin (Merzeraud et al., 2019); 10-Chelif Basin (Rouchy et al., 2007); 11-Sahel area (Frigui et al., 2016); 12-Aléria Basin and 13-Rhône Valley (Carbannel, 1978); 14-Piedmont Basin (Dela Pierre et al., 2011, 2016); 15-Po Plain (Ghielmi et al., 2010, 2013; Amadori et al., 2018); 16-Fine Basin (Cava Serredì section; Carnevale et al., 2006a, 2008). 17-21 Apennine system: Romagna sections (17, Roveri et al., 1998), Trave section (18, Iaccarino et al., 2008), Maccarone section (19, Bertini, 2006, Grossi et al., 2008; Sampalmieri et al., 2010; Pellen et al., 2017), Colle di Votta (20)-Fonte dei Pulcini (21)-Stingeti (22) sections (Cosentino et al., 2005, 2012, 2013, 2018), Mondragone 1 well (23, Cosentino et al., 2006), Crotone Basin (24, Roveri et al., 2008a); 25-27 Sicily: Villafranca Tirrena (25) and Licodia Eubea (26) sections (Sciuto et al., 2018), Caltanissetta Basin (27, Manzi et al., 2009); 28-Corfù (Pierre et al., 2006); 29-Zakinthos (Karakitsios et al., 2017b); 30-Crete (Cosentino et al., 2007); 31-Cyprus (Rouchy et al., 2001; Manzi et al., 2016a); 32-Adana Basin (Radeff et al., 2016).

and the relationship between the Mediterranean and its surrounding water bodies (i.e. Atlantic Ocean, Indian Ocean and Paratethys) all inhibit a clear understanding of the Mediterranean base-level and its hydrochemical structure.

In this paper we attempt to summarize all the existing, but heavily scattered, data resulting from ~50 years of cross-disciplinary studies with the aim of providing a comprehensive overview of the stratigraphic arrangement of Stage 3 onshore and offshore deposits, as well as of their sedimentological, paleontological, geochemical and seismic properties. Subsequently, we assemble the observations favoring both end-member scenarios of a relatively desiccated and relatively full Mediterranean. Finally, we focus on novel future analytical techniques and approaches that have the potential to constrain Mediterranean base-level during MSC Stage 3 as well as the changing hydrological fluxes and connectivity phases between the intra-Mediterranean basins and the neighboring Atlantic Ocean and Paratethyan domains as a mean of reconstructing the state of the art of the complex history of this enigmatic period of the Mediterranean history once and for all.

2. The terminal Stage 3 of the MSC

2.1. Historic overview of nomenclature and concepts

The final phase of the MSC (i.e. substage 3.2), also known as “Lago-Mare”, finds its sedimentary expression in cyclically-arranged terrigenous and evaporitic sediments hosting unique faunal assemblages of ostracods, mollusks and dinoflagellate cysts (dinocysts). They are related, at species level, to those inhabiting, during the Miocene, the brackish basins of the Paratethys realm (e.g. [Gložzi et al., 2007](#); [Stoica et al., 2016](#)). But what exactly is the “Lago-Mare”? This widely employed expression in the MSC literature encompasses a variety of meanings that make its application doubtful and misleading. The root of the wording “Lago-Mare” is to be found in the Russian scientific literature of the late 1800s. Nikolai [Andrusov \(1890\)](#) used the corresponding Russian term with a geographical and chronological connotation in reference to the series of central-eastern European basins that during the Miocene turned from marine settings to desalinated semi-isolated lakes with an endemic fresh-brackish water biota association (e.g. [Popov et al., 2006](#) and references therein). The original monograph of [Andrusov \(1890\)](#) was not widely available outside Russia, but his attendance of international conferences allowed his research to spread outside the Russian borders. From the publications of the French geologists [Suzette Gillet \(Gillet, 1932, 1933\)](#) and [Maurice Gignoux \(Gignoux, 1936a\)](#) we can state with relative certainty that the original meaning of the word “Lago-Mare” (here reported with the French counterpart “Lac-Mer”) had its provenance in the Russian literature:

“[...] An isolation of the basin, that became a brackish, isolated basin. Then, a uniform fauna populated this immense lac-mer which was divided [...] into Pannonian basin, [...] Dacique Basin, and Euxin and Caspian basin [...]” (Gillet, 1932).

“[...] During the Volhynien (Sarmatique inferior) there was a lac-mer of uniform fauna that extended through all the eastern Europe. [...] and the fauna of the eastern regions of that huge lac-mer was completely differentiated [sic] from the one in the western regions. [...]” (Gillet, 1933).

“[...] The Pontien fauna is not anymore a fauna characteristic of an internal saline sea, as in the Sarmantien, but is a fauna of a “desalinated lagoon”, a lac-mer, as the Russian geologists named it. [...]” (Gignoux, 1936b).

In the late 19th ([Capellini, 1880](#)) and 20th century ([Ogniben, 1955](#); [Ruggieri, 1962, 1967](#); [Decima, 1964](#)), late Messinian ostracod- and mollusk-bearing deposits in the Mediterranean were described at several Italian localities. Initially, the expressions “*Congerina* beds” ([Capellini, 1880](#)) and “*Melanopsis* beds” ([Ruggieri, 1962](#)) were used. Later on, [Ruggieri \(1967\)](#) pointed out the affinity of these faunal elements with

those of the Pontian of the Paratethys. Consequently, he speculated on a feasible Paratethys-like paleoenvironmental configuration for the Mediterranean in the latest Messinian and he coined the Italian translation (i.e. “Lago-Mare”) from the French “Lac-Mer” in reference to the shallow-water lakes claimed to be widely distributed across the Mediterranean. Progress in the 1970s in onshore and offshore exploration highlighted the temporally well-constrained distribution of the Paratethyan organisms in the Mediterranean ([Carbannel, 1978](#)). On this premise, [Hsü et al. \(1978a\)](#) proposed to use “Lago-Mare” to “designate the latest Messinian oligohaline environment, postdating evaporite deposition and predating Pliocene marine sedimentation [...] in order to distinguish it from “lac mer” which, strictly speaking, was a Paratethyan environment”. Notwithstanding the new definition, in various parts of the text they used “Lago-Mare” to refer to the Paratethyan lakes (pp. 1071-1072: “[...] The upper Messinian Mediterranean was flooded by a series of desert basins, some with salt lakes, prior to inundation by the Lago-Mare.”), thus giving rise to the confusion on how to use the term properly.

In the most recent stratigraphic overview of the MSC ([Fig. 1a](#); [Roveri et al., 2014a](#)), the terminal MSC stage is called Stage 3, which is in turn subdivided into substages 3.1 and 3.2 (also termed Lago-Mare). Beside such a chronostratigraphic definition, the term “Lago-Mare” has also been used for a typical biofacies of the late Messinian Mediterranean (e.g. [Fortuin et al., 1995](#); [Gložzi, 1999](#); [Gložzi and Grossi, 2008](#); [Sciuto et al., 2018](#)), for the pelitic beds encasing the Paratethyan-related fauna (i.e. a lithofacies; e.g. [Fortuin and Krijgsman, 2003](#); [Sciuto et al., 2018](#)), as the name of an informal lithostratigraphic unit (usually distinguished by its fossil content) sandwiched between the Sicilian Upper Gypsum and the Arenazzolo Fm. ([Fig. 4b](#); [Clauzon et al., 2005](#); [Londeix et al., 2007](#); [Popescu et al., 2009](#); [Bache et al., 2012](#)) and to denote multiple (3 to 4) spilling events of the Paratethys into the Mediterranean ([Clauzon et al., 2005, 2015](#); [Popescu et al., 2007, 2009, 2015](#); [Suc et al., 2011](#); [Bache et al., 2012](#); [Do Couto et al., 2014](#); [Frigui et al., 2016](#); [Mas and Fornós, 2020](#)).

This being a review, we use the widely employed definition of the model of [Roveri et al., 2014a](#)) ([Fig. 1a](#)) and regard the Lago-Mare as a “phase of massive biota migration from the Paratethys realm, cyclostratigraphically constrained between 5.42 Ma and 5.332 Ma ([Roveri et al., 2008a](#); [Grossi et al., 2011](#)), during which the Mediterranean sedimentary environments underwent an impressive freshening”. Nevertheless, we call for caution in the use of this definition of “Lago-Mare” in future studies, since 5.42 Ma as the (astronomical) age of the first entrance of Paratethyan organisms into the Mediterranean is likely to be incorrect (see subsection 5.1) and evidence of ‘impressive freshening’ are already present much earlier (e.g. at Eraclea Minoa; [Vasiliev et al., 2017](#); [García-Veigas et al., 2018](#)).

2.2. Development of a chronostratigraphic framework

Issues of the timing and duration of the MSC only began to be tackled in the 1990s, in parallel with discussion concerning the nature of its extreme paleoenvironments ([Schmalz, 1969](#); [Hsü et al., 1973a, 1973b, 1973c](#), [Hsü et al., 1978a, 1978b](#); [Nesteroff, 1973](#); [De Benedetti, 1982](#)). While published models ([Butler et al., 1995](#); [Clauzon et al., 1996](#); [Krijgsman et al., 1999a](#); [Rouchy and Caruso, 2006](#)) mostly converged on the (astronomical) age of the marine replenishment at the beginning of the Pliocene (5.332 Ma; [Van Couvering et al., 2000](#)), there were disagreements about the age of the onset of the MSC (synchronous vs diachronous) and of specific events within it (see discussion in [Roveri et al., 2014a](#)). Among these, the work of [Krijgsman et al. \(1999a\)](#) has obtained wide consensus. Their cyclostratigraphic tuning and correlation of continuous and bio-magnetostratigraphically constrained pre-evaporitic sections in Spain (Sorbas), Sicily (Giblicemi/Falconara) and Greece (Metochia) resulted in a synchronous age of 5.96±0.02 Ma for the MSC onset (later refined to 5.97 Ma by [Manzi et al., 2013](#)). The astronomical ages for the onset ([Krijgsman et al., 1999a](#)) and termination ([Van Couvering et al., 2000](#)) of the MSC are not contentious since

the characteristic sedimentary cyclicity and sediments' properties (e.g. color of the lithologies and biota content) of the pre- and post-MSC successions fit robustly with the insolation curve (see also Van der Laan et al., 2006 and Topper and Meijer, 2015).

The cyclic arrangement of the MSC sediments (Fig. 3a) led scientists to interpret that the same cyclostratigraphic approach could be used to gain precise dates for events within the MSC (e.g. Hilgen et al., 1995; Vai, 1997; Krijgsman et al., 1999b, 2001), bypassing the challenge posed by the unsuitability of the classic biomagnetostratigraphic tools for the MSC successions. Characteristic interference patterns of eccentricity and precession have been tentatively recognized in the Sicilian Eraclea Minoa section (see subsection 3.8; Van der Laan et al., 2006). However, clear orbital signals are typically poorly expressed in MSC records and, when they are present, like in Sicily, they are not (vertically) repeated with sufficient frequency to establish clear phase relations with the astronomical cyclicity. For this reason, the simple counting of cycles with no analysis of cyclostratigraphic pattern in proxy records has mostly been employed as a correlation method (Roveri et al., 2008a; Manzi et al., 2009; Manzi et al., 2016a; Cosentino et al., 2013).

The age of the base of Stage 3 is largely determined by correlating the sedimentary cycles of the Upper Gypsum unit (UG) at Eraclea Minoa (Sicily) with the astronomical curve La2004 (Laskar et al., 2004). The UG sedimentary cyclicity consists of alternating gypsum and mudstone beds of variable thickness (Figs. 5g-i; see subsection 3.8). Precessional variation of the Mediterranean freshwater budget tied tightly to the African monsoon and Atlantic storms are the drivers interpreted to lie behind the gypsum-mudstone cycles (e.g. Marzocchi et al., 2015, 2019; Simon et al., 2017). Variations of the freshwater discharge cause the pycnocline to shift vertically, resulting in brine concentration and gypsum precipitation during to the arid/dry phases of the precession cycles

(precession maxima-insolation minima) and brine dilution and mudstone deposition during the humid/wet phases (precession minima-insolation maxima) (Van der Laan et al., 2006; Manzi et al., 2009). Two different tuning options exist in literature (Van der Laan et al., 2006 versus Manzi et al., 2009; Fig. 3a):

1. Van der Laan et al. (2006) tentatively recognized sedimentary patterns that they correlated with the astronomical curves by using the same phase relationships between the sedimentary cycles and the astronomical cycles as are seen in Plio-Pleistocene sapropel-bearing marine successions of the Mediterranean (Hilgen, 1991). The four closely spaced gypsum beds III to VI were regarded as a cluster, i.e. the sedimentary expression of a 100 kyr eccentricity maximum (Hilgen, 1991; Strasser et al., 2006), whereas the preceding and following evaporite-free marly interval were attributed to a phase of low-amplitude precession oscillations caused by a 100 kyr eccentricity minimum (Fig. 3a). Tuning downward from the conformable Miocene/Pliocene boundary (Fig. 6d) and arguing that the precession peak at ~5.38 Ma, which has an extremely low amplitude, is not expressed in the sedimentary record, Van der Laan et al. (2006) correlated gypsums III to VI with the four successive precession/insolation peaks of the 100 kyr eccentricity maximum dated around 5.44 Ma and the overlying and underlying gypsum-free marly interval fell within 100 kyr eccentricity minimum cycles (Fig. 3a, right log). This tuning resulted in an astronomical age of ~5.51 Ma for the first gypsum bed in their log (i.e. gypsum II in the log of Manzi et al., 2009), and an approximate duration of 175 kyr for Stage 3 as whole.
2. An alternative tuning by Manzi et al., 2009; Fig. 3a, left log) argued that every precessional/insolation peak must have an expression in the rock record. Manzi et al. (2009) agreed with the solution of Van

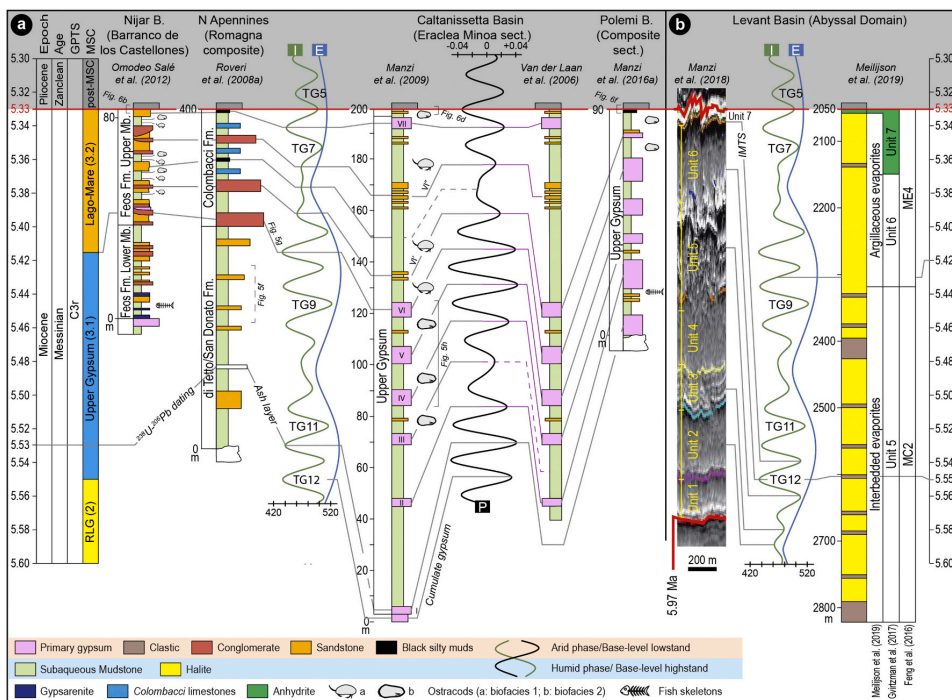


Fig. 3. (a), (b) Available astronomical tunings to astronomic curves of climatic precession (P), 100 kyr eccentricity (E) and 65°N insolation curve (I) of Laskar et al. (2004) of the lithological cyclicity of onshore Stage 3 sections (a) and of the seismic cycles and/or well logs (gamma ray and resistivity) of the MU in the Levant Basin (b). Tunings of onshore sections in (a) are carried out downward from the M/P boundary (conformable in all sections). Astronomically-tuned glacial (even numbers) and interglacial (odd numbers) stages (i.e. TG) as defined by Hodell et al. (1994) are also indicated.

der Laan et al. (2006) on the sedimentary inexpressiveness of the (barely visible) insolation minima peak at ~5.38 Ma. However, these authors considered the insolation minima peaks immediately above and below of too low amplitude to promote the conditions required for gypsum precipitation, but also too high not to have some sedimentary expression. They therefore identified sandstone horizons VI' and VI'' as the sedimentary response to these weak insolation/precession signals. The addition of two precessional cycles (i.e. a total of 9) resulted in an astronomical solution that was adjusted one precessional cycle lower than that of Van der Laan et al. (2006), translating into an age of 5.53 Ma for the base of the UG and a total duration of ~200 kyr for Stage 3. But the more conspicuous difference between the two astronomical solutions discussed lies in the timing at which gypsum precipitation occurred, restricted to the 100 kyr eccentricity maxima according to Van der Laan et al. (2006), extended to the 100 kyr eccentricity minima by Manzi et al. (2009).

An age of 5.53 Ma for the first gypsum bed was also obtained by the astronomical tuning of the Upper Gypsum in Cyprus (Manzi et al., 2016a), but there the tuning is performed just by following the recognition, from the base up, of 6 gypsum beds just like in Sicily and therefore arguing for a bed-to-bed correlation with the Sicilian gypsums I-VI. In the consensus model of Roveri et al. (2014a) the base of Stage 3 coincides with the base of the Sicilian UG, placed by Manzi et al. (2009) at 5.55 Ma (Fig. 1A). However, in the model of Manzi et al. (2009) this age is attributed to a cumulate gypsum horizon interpreted as laterally equivalent of the Halite (i.e. Stage 2), and therefore implying the kickoff of Stage 3 at 5.53 Ma (Fig. 3a).

The post-evaporitic successions of the Romagna (Cusercoli and Sapigno sections; Roveri et al., 1998) and Marche (e.g. Trave and Maccarone sections; Iaccarino et al., 2008; Cosentino et al., 2013) areas provided evidence that led to the splitting of Stage 3 into substage 3.1 and 3.2. In the resulting composite section (Roveri et al., 2008a), a shift in the sedimentary facies and stacking pattern is observed (see description in subsection 3.7). Correlation of the sedimentary cyclicity in Romagna was from the (conformable) base of the Pliocene downwards (or from an U-Pb-dated ash layer upward; Cosentino et al., 2013) and linked three fluvial conglomerates and two black mudstone layers of unknown sedimentological significance to the arid phases of the precession cycles (Fig. 3a; Roveri et al., 2008a). The greater thickness of the oldest conglomerate was possibly assumed to be evocative of an oscillation of the amplitude of the corresponding precession minima peak rather than the amplitude of the peaks responsible for the formation of the other facies. This approach resulted in an age of 5.42 Ma for the first conglomerate (i.e. the substage 3.1/3.2 transition; Fig. 5g) and an approximate duration of 90 kyr for substage 3.2 (the Lago-Mare phase). The same astronomical age is obtained by tuning the Upper Member of the Feos Formation in the Nijar Basin (Omodeo-Salé et al., 2012), where four pelite-conglomerate cycles plus one sandstone capped by the Miocene/Pliocene boundary mark the interval attributed to Stage 3.2 (Fortuin and Krijgsman, 2003).

Although the substage 3.1/3.2 transition is linked to a major Mediterranean-scale hydrological re-organization possibly coinciding with the migration of the Paratethyan biota (Roveri et al., 2008a; Grossi et al., 2011), the facies change used for its definition is hardly recognizable elsewhere (see Chapter 3). As such, other tools have been used to equip fragmentary and/or lithological cyclicity-lacking sections with an age model: the (highly controversial) ostracod biozonation (see subsection 5.1; e.g. Stoica et al., 2016; Karakitsios et al., 2017a; Cosentino et al., 2018; Caruso et al., 2020) and the astronomical tuning of magnetic susceptibility records (e.g. Fonte dei Pulcini section, Central Apennines; Cosentino et al., 2012).

Comparison of Atlantic oxygen isotope records (Van der Laan et al., 2005, 2006) and the chronostratigraphy of Roveri et al. (2014a) revealed that Stage 3 sedimentation started during a prominent global eustatic lowstand associated with oxygen isotope (glacial) stage TG12,

followed by a latest Messinian deglacial interval which comprised multiple obliquity- and possibly precession-forced global eustatic phases. As documented by Hodell et al. (2001) (later revised by Drury et al., 2018), Van der Laan et al. (2006) and Roveri et al. (2014a), the marine replenishment of the Mediterranean did not coincide with any major deglaciation, so non-eustatic causes of the Zanclean megaflood hypothesis are required.

3. Onshore domain: key sections, sedimentary expression and faunal content

3.1. The Alborán region

The westernmost outcrops of Stage 3 deposits in the Mediterranean are located in the Alborán region, close to the present-day Strait of Gibraltar (Fig. 2b). MSC deposits on the margins of this region are poorly developed, possibly because of a late Tortonian uplift that raised the margins above the Mediterranean water level (López-Garrido and Sanz de Galdeano, 1999). Near Malaga, however, two facies associations consisting of m-thick conglomerate-sandstone beds alternating with laminated pelites are documented in the Rio Mendelín section (informally referred to as “LM unit”; Guerra-Merchán et al., 2010) and attributed to (part of) the Lago-Mare phase (Fig. 4a) based on their paleontological content. These sediments are squeezed between the Paleozoic basement units, with an erosive contact and associated angular unconformity, and the Pliocene, from which they are separated by another erosional surface draped by conglomeratic accumulations (Fig. 6a). A well-preserved and diverse *in situ* Paratethyan-type ostracod and molluscan fauna (i.e. *Lymnocardinae* and *Dreissenidae*) typical of shallow waterbodies (up to 100 m deep; Grossi et al., 2008; Gliozi and Grossi, 2008) with low salinities (5-18‰) is reported from the pelitic units (Guerra-Merchán et al., 2010). The overlying Pliocene in the deeper depocenters starts with 30 m-thick littoral conglomerates with marine mollusks passing progressively upwards into deeper water facies, while fan deltas developed at the basin margins (López-Garrido and Sanz de Galdeano, 1999; Guerra-Merchán et al., 2010, 2014). Notably, the overall thickness of the Pliocene deposits reaches 600 m. The detailed regional studies by López-Garrido and Sanz de Galdeano (1999) and Guerra-Merchán et al. (2014) concluded that accommodation space was created during (Zanclean) sedimentation by local fault-driven subsidence, and that movement on these faults only reversed at the end of the Zanclean causing uplift.

An alternative scenario, based on the finding of (a few) specimens of the nannofossil *Ceratolithus acutus*, ascribed the LM unit of Guerra-Merchán et al. (2010) to the earliest Zanclean (Fig. 4b; Do Couto et al., 2014).

On the southern Alborán margin in Morocco, latest Messinian deposits are reported from the Boudinar and Melilla basins (Fig. 2b). Up to 100 m-thick chaotic deposits containing selenite gypsum fragments, azoic conglomerates, sandstones yielding planktic foraminifera and nannofossils and lacustrine limestones are capped by early Pliocene marine marls (Rouchy et al., 2003; Azdimousa et al., 2006; Cornée et al., 2016; Merzeraud et al., 2019). Due to their stratigraphic position, these continental to lacustrine deposits are interpreted as the local expression of the Lago-Mare phase (Cornée et al., 2016) or alternatively as Zanclean successions (Azdimousa et al., 2006).

3.2. Algeria

The Chelif Basin in Algeria (Fig. 2b) displays the typical marginal Messinian succession comprising Tortonian to lower Messinian blue marls, diatomite-bearing sediments (Tripoli unit), cyclically-arranged primary evaporites (13 couplets), ostracod-rich post-evaporitic deposits and Zanclean foraminiferal marls (Rouchy et al., 2007). The post-evaporitic sediments show a great lateral variability in both thickness (from few meters up to 125 m) and facies. They are mainly dominated by

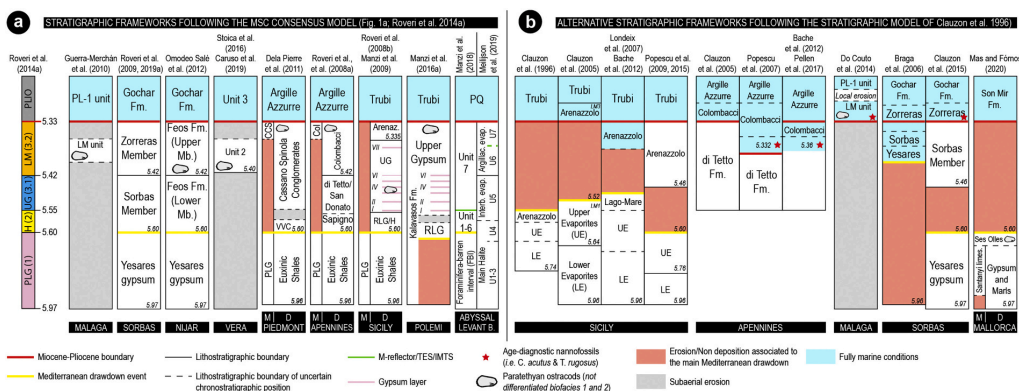


Fig. 4. Schematic overview of different chronostratigraphic models for some of the Messinian successions presented in Chapter 3. Note the large controversies in timing, duration and chronostratigraphic position of the main erosion phase between models in (a) and (b). Models in (a) follow the recently established MSC chronostratigraphic model of [Roveri et al. \(2014a\)](#), according to which the Mediterranean base-level dropped and halite deposited on sea floor during Stage 2 and the Upper Gypsum/Upper Evaporites-Lago-Mare sequence followed. Models in (b) were proposed following the alternative scenario of [Clauzon et al. \(1996, 2005\)](#), which envisaged two Lago-Mare episodes (LM1 and LM3) that occurred before and after the main Mediterranean drawdown event, during which LM2 was deposited in the deep desiccated basins ([Do Couto et al., 2014](#); [Popescu et al., 2015](#); see [Roveri et al., 2008c](#) and [Grothe et al., 2018](#) for further explanations). Note, in (b), the shifting of the position of the main erosional phase in Sicily through time as well as the time of the marine replenishment in the Apennines.

terrigeneous clastic lithologies, associated in the marginal areas with sandy carbonates and stromatolitic limestones. A mixed faunal assemblage of non-marine (Paratethyan-like ostracods) and marine (benthic and planktic foraminifera) organisms is present, showing an increase in ostracod species diversity from the bottom to the top ([Rouchy et al., 2007](#)).

3.3. Neogene basins of the Eastern Betics (Spain)

The external Neogene basins (Sorbas, Nijar, Vera and Bajo Segura) of the eastern Betic Cordillera (SE Spain; [Fig. 2b](#)) represent an important laboratory for understanding Messinian events. In particular, the Sorbas and Nijar basins preserve two allegedly continuous successions spanning the entire MSC (e.g. [Roveri et al., 2009](#); [Omodeo-Salé et al., 2012](#)). The two basins are similar in many respects. Their stratigraphic organization, for example, suggests they were connected for much of the late Miocene up until MSC Stage 1 ([Fortuin and Krijgsman, 2003](#)), which is represented by the gypsiferous Yesares Member (e.g. [Lu, 2006](#)). However, facies differences are prominent in the Stage 3 formations according to the chronostratigraphic frameworks of [Roveri et al. \(2009\)](#) for the Sorbas Basin and [Omodeo-Salé et al. \(2012\)](#) for the Nijar Basin ([Fig. 4a](#)). Lithostratigraphically, two members are discerned between the Yesares Member and the basal Zanclean: the Sorbas and Zorreras members in the Sorbas Basin ([Figs. 4a, 5a](#)) and the lower and upper members of the Feos Fm. in Nijar ([Figs. 3a, 4a](#); [Roep et al., 1998](#); [Krijgsman et al., 2001](#); [Fortuin and Krijgsman, 2003](#); [Braga et al., 2006](#); [Roveri et al., 2009, 2019a](#); [Omodeo-Salé et al., 2012](#)).

The Sorbas Member (see [Roep et al., 1998](#) and [Aufgebauer and McCann, 2010](#) for a more detailed sedimentological description) consists of three overlapping coarsening-upward depositional sequences made of offshore clays and marls passing upward into shelf muds and coastal sandstone bodies. Still unclear is the chemistry of the subaqueous environment during the formation of the Sorbas Member and the provenance of the water fluxes. These shallow-water deposits are conformably replaced upward by the Zorreras Member that comprises alternations of reddish siltstones and sandstones ([Fig. 5a](#)) organized in five (or eight) lithological cycles expressing continental environments ([Martín-Suárez et al., 2000](#); [Aufgebauer and McCann, 2010](#)). Up to four lenticular white limestone beds bearing brackish Paratethyan-like ostracods (*Cyprideis*, *Loxocorniculina djafari*) and freshwater species of

the family Limmocytheridae, bivalves and *Chara oogonia* ([Roep and Harten, 1979](#); [Aufgebauer and McCann, 2010](#)) are found interrupting the fluvialite sequence ([Fig. 5a](#)) and are linked to either episodic flooding by local rivers ([Braga et al., 2006](#); [Aufgebauer and McCann, 2010](#)) or episodic Mediterranean incursions ([Fortuin and Krijgsman, 2003](#); [Andreetto et al., 2021](#)). A correct interpretation of the paleo-depositional environment of these limestone beds is crucial for the discussion concerning the Mediterranean base-level position during the Lago-Mare phase. In fact, if the Sorbas Basin was relatively shallow during Zorreras deposition (50-100 m; [Roveri et al., 2019a, 2020](#)), repeated and sudden Mediterranean incursions would indicate that the Mediterranean Basin was relatively full and that its base level was oscillating, possibly with precessional periodicity ([Andreetto et al., 2021](#)). The contact between the Zorreras Mb. and the overlying near-shore Pliocene (<50 m depositional paleodepth; [Roveri et al., 2019a](#)) in the Sorbas Basin is conformable and expressed differently around the basin, ranging from a bivalves-rich bed overlain by a yellow, fossiliferous calcarenite floored by a gravelly lag deposit ([Mather et al., 2001](#)) to a grey marl horizon with marine foraminifera assemblages followed by a second shell-rich bed ([Roveri et al., 2019a](#)). Similar to the situation in Malaga, the rare identification of *Ceratolithus acutus* in sediments of the continental Zorreras Mb. led [Clauzon et al. \(2015\)](#) to put forward an alternative chronostratigraphic and paleoenvironmental interpretation for the Sorbas MSC succession, shifting the Zorreras Mb. into the Pliocene ([Fig. 4b](#)) and thus associating the presence of brackish Paratethyan-like ostracods with exchanges between the Mediterranean and Paratethys following the Mediterranean re-filling, at high sea level.

In the basin Nijar ([Fig. 2b](#)), the latest Messinian Feos Formation is bracketed at the base and top by an erosional surface along the basin margins and its correlative conformity in the deeper parts ([Fig. 3a](#); [Fortuin and Krijgsman, 2003](#); [Aguirre and Sánchez-Almazo, 2004](#); [Omodeo-Salé et al., 2012](#)). The Lower Feos Member consists of azoic, graded and locally slumped siliciclastic-carbonate beds alternating with gypsarenites and gypsilitites and including a laterally continuous Mn-rich bed ([Fortuin and Krijgsman, 2003](#); [Omodeo-Salé et al., 2012](#)). In the basin center (e.g. Barranco de los Castellones section; [Fig. 3a](#)) the Upper Feos member comprises four complete lithological cycles of m-thick conglomerate to sandstone beds alternating with laminated pelites ([Fig. 5b](#)), and one incomplete cycle, which only consists of a sandstone horizon conformably capped by the Pliocene Cuevas Fm. ([Fig. 6b](#);

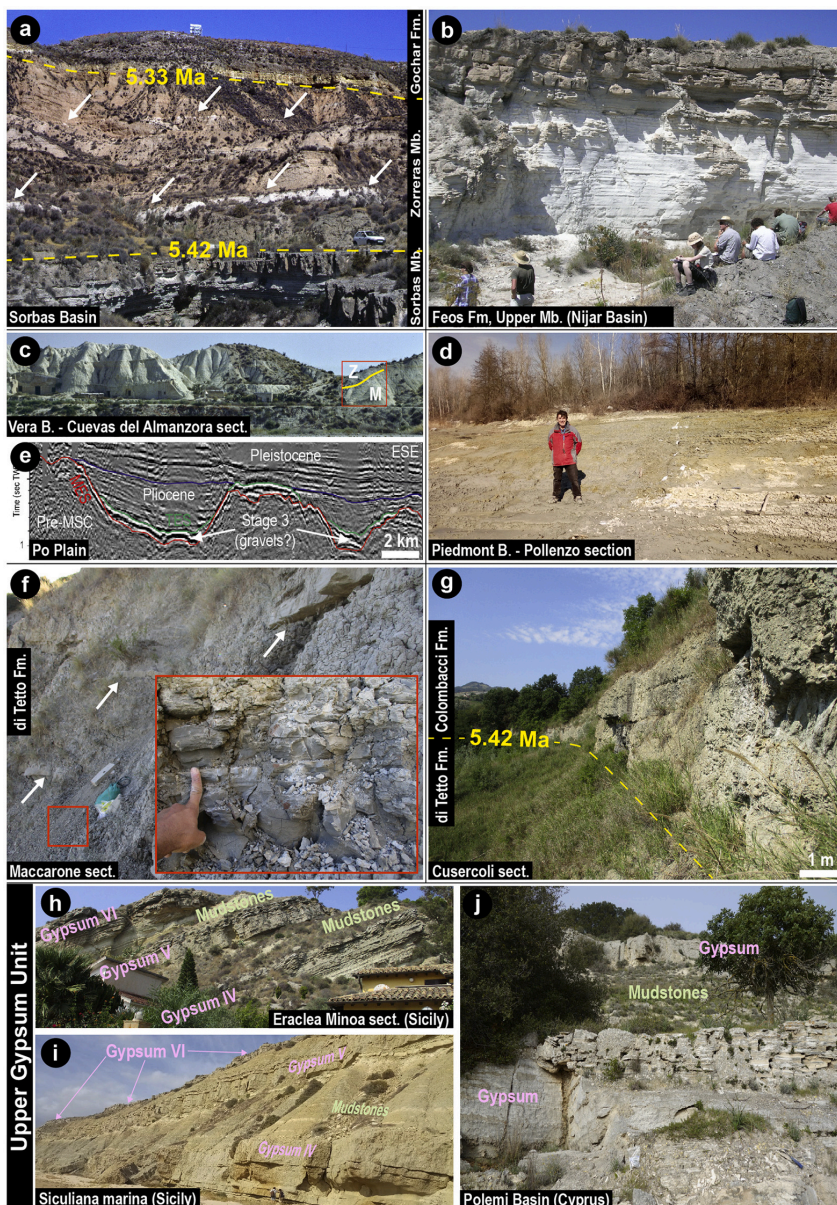


Fig. 5. Sedimentary expression of Stage 3 from selected onshore Mediterranean localities. (a) Photograph from the Sorbas Basin showing the red continental sediments of the Zorreras member with intercalated white limestones (white arrows; from Andreetto et al., 2021). The conformable resting of the Zorreras Mb. above the Sorbas Mb. and underneath the Gochar Fm. of Pliocene age is also appreciable. Car for scale. (b) One typical lithological (and precessional) cycle of the Upper Mb. of the Feos Fm. in the Nijar Basin, here constituted by an ostracod-bearing, white and laminated mudstone bed overlain by an azoic fluvial sandstone (courtesy of Anne Fortuin). (c) Panoramic view of the Cuevas del Almanzora section (from Andreetto et al., 2021). Red rectangle indicates the position of the section straddling the Messinian (M)/Zanclean (Z) transition and studied by Fortuin et al. (1995), Stoica et al. (2016), Caruso et al. (2020) and Andreetto et al. (2021). Buildings for scale. (d) The sub-unit a of the Piedmont Basin composed of azoic grey mudstones grading into yellowish, mammal-rich overbank deposits. (e) WNW-ESE seismic profile in the Po Plain showing incised valleys filled during Stage 3 by suggested clastic deposits and sealed by deep-water turbidites in the Zanclean (modified from Amadori et al., 2018). (f) Typical aspect of the di Tetto/San Donato Formation in the Northern Apennines composed by grey mudstones (detail in the inset) with interbedded sandstone bodies (white arrows). The picture is taken from the Maccarone section. (g) The di Tetto Fm.-Colombacci Fm. transition in the Cusercoli area (Eastern Romagna, Fig. 2b), defined by the facies change underlined by the appearance of a fluvial conglomerate. This lithostratigraphic boundary also corresponds to substage 3.1/3.2 boundary of Roveri et al. (2014a). (h), (i), (l) Lithological cycles of the Upper Gypsum Unit in Eraclea Minoa (h), Siculiana Marina (i) and Polemi (l) sections. Cycles are several m-thick and primarily composed by beds of primary gypsum alternating with mudstones bearing Paratethyan ostracods (at least in Eraclea Minoa).

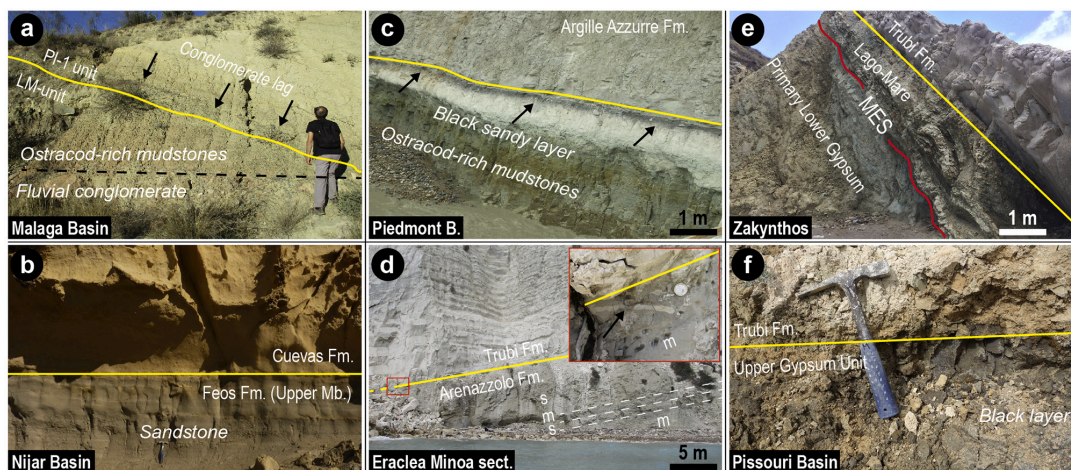


Fig. 6. Photographs of the Miocene/Pliocene boundary (yellow lines) from selected onshore Mediterranean localities. (a) Erosive M/P transition in the Mendelín section (Malaga Basin). Note the conglomeratic lag draping the erosional surface and sharply overlain by foraminifera-rich marls. (b) Conformable stratigraphic contact between the uppermost Messinian sandstone of the Feos Fm. and the Zanclean bioalcalarenites of the Cuevas Fm. in the Barranco de los Castellones section, Nijar Basin (hammer for scale; modified from Andreetto et al., 2021). (c) The Messinian/Zanclean boundary in the Pollenzo section (Piedmont Basin) marked by a characteristic black layer interbedded between Paratethyan ostracods-rich mudstones and marine foraminifera-rich marls (modified from Dela Pierre et al., 2016). (d) Uppermost segment of the Eraclea Minoa section (Caltanissetta Basin, Sicily) displaying the (non erosive) contact between the Pliocene Trubi Formation above and the sandy Arenazzolo Formation below. The inset is a close view of the transition, which occurs above a ~50 cm-thick burrowed mudstone horizon rich in Paratethyan ostracods and marine foraminifera. (e) Lago-Mare sediments in the Kalamaki section (Zakynthos) unconformable, through an erosional surface (i.e. the Messinian Erosional Surface, MES), over the PLG unit and also unconformable beneath the Trubi Fm. (modified from Karakitsios et al., 2017b). (f) Close view of the M/P boundary in the Pissouri Basin, where the foraminifera-rich Trubi marls lie above a black layer (paleosol according to Rouchy et al., 2001).

Fortuin and Krijgsman, 2003). A rich fauna of mixed brackish ostracods and marine foraminifera is found in all four pelitic beds (Bassetti et al., 2006). Its origin is questionable. These ostracods were regarded as endemic to the Mediterranean and inhabiting endorheic lakes by Bassetti et al. (2006). However, later they were shown to have been misidentified and were instead considered Paratethys-derived by Stoica et al. (2016; see subsection 5.1). Planktonic and deep-water benthic foraminifera are widely considered reworked by Fortuin and Krijgsman (2003), Bassetti et al. (2006) and Omodeo-Salé et al. (2012), in place by Aguirre and Sánchez-Almazo (2004).

In the Vera Basin (Fig. 2b), *in situ* gypsum deposits are missing because of widespread erosion or non-deposition and MSC deposits are only represented by ~12 m of laminated varicolored marly clays (Unit 2 Fig. 4a), which are best exposed in the Cuevas del Almanzora section (Fortuin et al., 1995; Fig. 5c). These clays contain a well-preserved and diversified *in situ* fauna of Paratethyan-like ostracod and shallow-water, benthic foraminifera mixed with physically reworked (mostly from the lower Messinian Abad marls) planktic and deep-water benthic foraminifera (Fortuin et al., 1995; Stoica et al., 2016; Caruso et al., 2020). The marly clays are assigned by Stoica et al. (2016) and Caruso et al. (2020) to (roughly) the whole late Messinian Lago-Mare phase (Fig. 4a) based on the ostracod biozonation of Grossi et al. (2011) and are considered to represent either sedimentation in an isolated lake subject to base-level and salinity fluctuations (Caruso et al., 2020) or deposition in a coastal lagoon that was connected to the water mass filling the open Mediterranean (Stoica et al., 2016; Andreetto et al., 2021). Similar to Malaga, these sediments are topped by an erosive surface draped by a conglomeratic accumulation which is overlain by the open marine fauna-rich sediments of the basal Zanclean (Fortuin et al., 1995; Caruso et al., 2020). This erosion feature likely indicates that the Miocene/Pliocene transition followed a base-level lowstand in the Vera Basin.

Stage 3 deposits (Garrucha Fm.) in the easternmost basin of the Betic Cordillera, the Bajo Segura Basin (Fig. 2b), are bounded below and above by two erosional surfaces related to lowered Mediterranean base-

levels and discontinuously present due to the widespread fluvial erosion that occurred at the Miocene/Pliocene boundary (Soria et al., 2005, 2008a, 2008b). The Garrucha Fm. shows a maximum thickness of 100 m in its type section (Soria et al., 2007, 2008b). It consists of 20–50 cm thick sandstone bodies interrupting a dominantly marly succession deposited in a subaqueous environment inhabited by *Cyprideis* sp. and euryhaline, shallow-water benthic foraminifera (*Ammonia beccarii*, *Elphidium granosum*, *Elphidium macellum*, *Haynesina germanica* and *Quinqueloculina laevigata*). Planktic foraminifera are also observed and for a long time were considered to be physically reworked (Soria et al., 2005, 2008b). However, some stratigraphic levels contain dwarf tests of long-ranging taxa such as *Globoturborotalita decoraperta*, *Globigerina bulloides*, and *Neogloboquadrina* spp. which recently have been interpreted as being *in-situ* mostly due to the absence of notable signs of reworking (Corbí and Soria, 2016). Among these dwarf taxa is *Neogloboquadrina acostaensis* (dextral; Corbí and Soria, 2016). Since this group is mainly dextral in the latest Messinian Atlantic successions (e.g. Siero et al., 1993; Bassetti et al., 2006), this may indicate that Atlantic inflow to the Mediterranean occurred during the late Messinian and the base level of the Mediterranean was high enough to reach the marginal Bajo Segura Basin. The Miocene/Pliocene boundary is, once again, marked by an erosional surface which outlines up to 200 m deep paleovalleys engraved down into the pre-MSC sediments and filled with conglomerates and sandstones of claimed coastal and shallow marine environments (Soria et al., 2005, 2008b; García-García et al., 2011; Corbí et al., 2016).

3.4. Mallorca

Mallorca, which constitutes an emerged segment of the Balearic Promontory (Fig. 2), does not expose the classical MSC evaporite sequence. Instead, two main MSC-related units are found above late Tortonian-Messinian reefal carbonates (Reef Complex Unit) and beneath the Pliocene: the Santanyí limestones and the Ses Olles Formation (Mas

and Fornós, 2020 and references therein). The Santanyí limestones are microbialites and oolite-dominated sediments in which a baleen whale neurocranium has been found (Mas et al., 2018a). This unit was interpreted either as a Terminal Carbonate Complex (TCC) laterally equivalent to the Primary Lower Gypsum (PLG) which has been drilled in the deeper parts of the bay of Palma (Mas and Fornós, 2020) or as time-equivalent to the Reef Complex Unit (e.g. Arenas and Pomar, 2010; Suárez-González et al., 2019). The Ses Olles Formation consists of marls, sandy-marls and marly-calcareous lacustrine deposits rich in in-situ freshwater *Chara* spp., brackish water Paratethyan-like mollusks and ostracods and littoral benthic foraminifera (*Elphidium* sp., *Ammonia* sp.).

The upper contact of the Ses Olles Formation with the Pliocene corresponds to an erosional ravinement surface draped by a progressive lag of coastal deposits usually containing coquinas and/or conglomerates (Mas, 2013, 2015; Mas and Fornós, 2020). The lower contact of the Ses Olles Formation with the Santanyí limestones is sporadically marked by a well-developed reddish paleosol (Mas, 2013, 2015; Mas and Fornós, 2020), which indicates that a (unquantified) period of subaerial exposure occurred before the emplacement of the Ses Olles Fm. However, in their more recent study, Mas and Fornós (2020) surprisingly conclude that the Ses Olles Formation has a conformable contact with the Santanyí limestones, ascribed to part of Stage 1. This led Mas and Fornós (2020) to conclude that the emplacement of the Ses Olles Fm. pre-dated the MSC peak and that the erosional surface marking the Miocene/Pliocene boundary is associated with a 270 kyr hiatus linked to the main MSC base-level drawdown (Fig. 4b). This conclusion is, however, in disagreement with the unconformity at the base of the Ses Olles Fm., which instead points to the deposition of the Ses Olles Fm. (and therefore to the arrival of the Paratethyan fauna in Mallorca) at some point during Stage 3 of Roveri et al. (2014a).

3.5. Piedmont Basin

The Piedmont Basin (NW Italy) contains the northernmost record of the MSC (Fig. 2b). The terminal MSC sediments (i.e. the Cassano Spinola Conglomerates Fm.) overlay pre-MSC units, the PLG deposits (Gessoso Solfifera Fm.) or reworked evaporites (Valle Versa chaotic complex, VVC) and underly the Zanclean marls of the Argille Azzurre Fm. (Dela Pierre et al., 2011).

The Cassano Spinola Conglomerates is splitted in two sub-units by Dela Pierre et al. (2016). Sub-unit a consists of azoic grey mudstones turning to yellowish silty mudstones (Fig. 5d) typified by in situ root traces, paleosols and mud cracks and including three/four intercalated lens-shaped, cross-bedded conglomeratic layers (Ghibaudo et al., 1985; Dela Pierre et al., 2011, 2016). Abundant land plant leaves and a diverse terrestrial vertebrate fauna are found in the yellowish siltstones, which have been interpreted as overbank deposits (Harzhauser et al., 2015; Colombo et al., 2017 and references therein). In this continental interval, a low-diversity fish fauna consisting of otoliths of marine and Paratethyan species is found (Grunert et al., 2016; Carnevale et al., 2018; Schwarzhaas et al., 2020). These otoliths were Sr-dated to the early-middle Miocene (Grunert et al., 2016). Nevertheless, they were concluded not to be physically reworked, but rather to have been transported by large marine predators, therefore implying a Piedmont Basin-(marine) Mediterranean connection was in force (Grunert et al., 2016; see subsection 5.6). Sub-unit b (i.e. Strati a Congeria sensu Sturani, 1973) is made of grey mudstones bearing a mixture of in-situ brackish water mollusks (Sturani, 1973; Esu, 2007) and ostracods (Trenkwalder et al., 2008) of Paratethyan affinity along with physically reworked foraminifera and calcareous nannofossils (Trenkwalder et al., 2008; Violanti et al., 2009). The transition to the Pliocene Argille Azzurre Fm. is sharp above a characteristic black and azoic sandy layer (Fig. 6c) rich in terrigenous and intrabasinal (i.e., glaucony and phosphates) grains and disarticulated valves of both brackish-water and continental bivalves, but barren of in-situ fossils (Trenkwalder et al., 2008). The occurrence, at its top and directly below the Argille Azzurre Fm., of

abundant *Thalassinoides* trace fossils filled with Pliocene sediments led Trenkwalder et al. (2008) and Dela Pierre et al. (2016) to interpret the top surface of this layer as an omission surface. This surface indicates a period of basin starvation (and therefore a hiatus) due to a sudden increase in water-depth, ascribed by Trenkwalder et al. (2008) to the Zanclean reflooding. This hiatus may have lasted for only part of the late Messinian (Violanti et al., 2009; Dela Pierre et al., 2016) or may have endured into the Pliocene (Trenkwalder et al., 2008).

3.6. Po Plain

To the east, the Messinian sediments in the Piedmont Basin disappear beneath the km-thick Plio-Quaternary succession of the Po Plain-Adriatic Foredeep (PPAF; Fig. 2a). By definition of Ghielmi et al. (2010) and Amadori et al. (2018), the PPAF includes two main elongated depocenters enclosed within the northern Apennines to the South and the Southern Alps to the North: the easternmost portion of the Po Plain and the whole present-day northern Adriatic Sea. Here, for simplicity, we include in the definition of PPAF also its westernmost depocenters of the Western Po Plain Foredeep.

The Messinian-Pleistocene sedimentary sequence, studied through the integration of seismic and borehole observations, is mostly represented by thick sequences of turbidite deposits in the foreland depocenter passing, towards the margins, to fluvial and deltaic systems related to the proximity of the marginal thrust-fold-belts (Cipollari et al., 1999; Ghielmi et al., 2010, 2013; Rossi et al., 2015a; Rossi, 2017). During MSC Stage 1, primary evaporites and dolomiticrites were deposited in some shallow-water settings, while evaporitic deposition was inhibited in the deep-water settings, where it was replaced by deposition of anoxic mudstones (Ghielmi et al., 2010). Instead, the post-evaporitic deposits consist of large thicknesses (up to 1 km) and volumes of coarse-grained clastics (LM1 and LM2 of Rossi and Rogledi, 1988; ME3 or Fusignano Fm. of Ghielmi et al., 2010; ME4 of Ghielmi et al., 2013; ME3b and possibly ME3a of Rossi et al., 2015a). Several authors (Ghielmi et al., 2010, 2013; Rossi et al., 2015a; Amadori et al., 2018; Cazzini et al., 2020) showed that these post-evaporitic sediments are the infilling of ca. N-S and NW-SE trending, V-shaped valleys (Fig. 5e). These valleys were carved at least as far as 50 km into the Alps, to a depth up to 1 km into the pre- and syn-evaporitic Messinian deposits and nicely shape the present-day river network of the southern Alps (Amadori et al., 2018).

Different mechanisms for the incision have been proposed, with major implications for the desiccated vs full Mediterranean controversy (Figs. 1b-c). Ghielmi et al. (2010, 2013), Rossi et al. (2015a), Amadori et al. (2018) and Cazzini et al. (2020) ascribed the valley incision along the PPAF northern margin to fluvial erosion, whose basinward shifting was triggered by the Stage 2 Mediterranean drawdown, estimated to have been around 800-900 m (Ghielmi et al., 2013; Amadori et al., 2018). In this case, Stage 3 deposition in the PPAF occurred in endorheic lakes fed by the Alpine rivers and kept isolated until the Zanclean, when the sudden sea-level rise following the Zanclean reflooding was enough to bypass morphological highs (e.g. Gargano-Pelagosa and/or Otranto paleosills) located in the southern Adriatic foredeep (Fig. 2a; see Pellen et al., 2017; Amadori et al., 2018; Manzi et al., 2020). Conversely, Winterberg et al. (2020) suggested that the over-deepened valleys on the southern slope of the Alps are related to Pleistocene glacial erosion. Although Winterberg et al. (2020) do not address the paleoenvironment during the Messinian, this interpretation does not rule out the possibility that (at least part of) Stage 3 sedimentation occurred in a PPAF connected to the Mediterranean water mass and that no catastrophic reflooding occurred at the Miocene/Pliocene boundary. The conclusion of a non-catastrophic refilling was also drawn by Pellen et al. (2017) on the basis of the onshore Adriatic record (see subsection 3.7).

3.7. Apennine system

The Messinian deposits resurface to the south of the PPAF sector and extensive sections are found in several basins on both the foreland domain (Adriatic side of the partially uplifted Apennine chain), subjected to compressional tectonics during the late Messinian, and the back-arc domain (Tyrrhenian side), contemporaneously affected by extension (Fig. 2b; Cipollari et al., 1999; Schildgen et al., 2014; Cosentino et al., 2018). Overall, the MSC record of the Apennines is subdivided into an evaporitic and post-evaporitic interval squeezed in between two marine units (Messinian Euxinic Shales Fm. at the base and Zanclean Argille Azzurre Fm. atop; Fig. 4a). Different vertical motions related to ongoing Apenninic tectonics resulted in the deposition of Stage 3 sediments with highly variable sedimentary expression and stratigraphic resolution from basin to basin. The post-evaporitic deposits are alternatively found resting unconformably, with an erosional contact associated to an angular unconformity, above the alternations of the Gessoso Solifera Fm./PLG, or conformably above evaporitic-free cycles lateral equivalent of the marginal PLG (Fig. 4a; e.g. Roveri et al., 1998, 2008a). This led to the conclusion that both shallow and deep-water successions are present in the Apennine foredeep system (Roveri et al., 2001).

The physical-stratigraphic model developed for the post-evaporitic interval in the Romagna area (i.e. Northern Apennines) and applied to the whole Apennine domain was subdivided into two allounits (named p-ev₁ and p-ev₂) based on a basin-wide shift in facies, overall stacking patterns and depositional trends (i.e. progradational and retrogradational, respectively; Roveri et al., 1998, 2001, 2005, 2008a; Manzi et al., 2005, 2007, 2020). Allounit p-ev₁ only accumulated in deep-water settings (e.g. Cusercoli, Sapiigno, Maccarone and Trave sections; Roveri et al., 1998; Iaccarino et al., 2008; Cosentino et al., 2013) during the subaerial exposure of the basin margins (e.g. Vena del Gesso Basin, Monticino quarry, Pellen et al., 2017). It starts with resedimented clastic evaporites (i.e. Sapiigno Fm.) followed by a coarsening- and shallowing-upward succession (i.e. di Tetto or San Donato Fm.) of mudstones with intercalated turbiditic sandstones (Fig. 5f) and a volcanoclastic marker bed dated initially by ⁴⁰Ar-³⁹Ar at ~5.5 Ma (Odin et al., 1997) and later by ²³⁸U-²⁰⁶Pb at 5.5320±0.0046/0.0074 Ma (Cosentino et al., 2013; Fig. 3a). Allounit p-ev₂ (i.e. Colombacci Fm.) occurs in the deeper depocenters in 4/5 sedimentary cycles consisting of three > 5 m-thick coarse-grained bodies (conglomerates and sandstones) and two black-colored mudstone beds alternating with fine-grained mudstones/clays with intercalated three micritic limestones (known in literature as *Colombacci* limestones; Figs. 3a, 5g; Bassetti et al., 2004). By contrast, an incomplete Colombacci Fm. deposited in the shallower thrust-top basins (e.g. Vena del Gesso Basin and Molise sections; Pellen et al., 2017; Cosentino et al., 2018). The p-ev₂ cycles have been interpreted as reflecting the alternation of wet (mudstones and *Colombacci* limestones in Eastern Romagna) and dry (coarse-grained facies and *Colombacci* limestones in the Maccarone section) phases controlled by Milankovitch-driven climatic factors (Fig. 3a; Roveri et al., 2008a; Cosentino et al., 2013) and, as such, they have been used for the astronomical tuning of the Colombacci Fm. to the Lago-Mare phase (Figs. 3a, 4a; see subsection 2.2). By contrast, Clauzon et al. (2005) and Popescu et al. (2007) moved the *Colombacci* Fm. into the Pliocene (Fig. 4b). However, this conclusion has been proven to rely on wrong stratigraphic and paleontological arguments (see Roveri et al., 2008c, Grothe et al., 2018 and subsection 5.5). Substage 3.2 records in the Apennines do not always contain the three prominent conglomeratic facies as in Romagna, but only laminated to massive clays with sandy intercalations equivalent to the ones typifying substage 3.1 records (e.g. Maccarone section; Sampalmieri et al., 2010; Cosentino et al., 2013; Fig. 5f). The absence of a lithological cyclicity that clearly mimics an orbital signal largely hampered the astronomical tuning of these clay-dominated sections, although an attempt has been made with the Maccarone section (Cosentino et al., 2013). The only exception is represented by the Fonte dei Pulcini section, which has been equipped with

an age framework by astronomical tuning of the magnetic susceptibility record (Cosentino et al., 2012). Despite the lack of outstanding lithological changes these sections are often provided with a lithostratigraphic subdivision using the same nomenclature as in the Romagna area. When applied, the di Tetto Fm.-Colombacci Fm. boundary is placed high in the sections, i.e. few tens of meters underneath the Miocene/Pliocene boundary, resulting in a much different thickness of the formations compared to the Romagna area.

Stage 3 sediments are poorly exposed on the Tyrrhenian Sea onshore side of Italy (Fig. 2b). The best known succession crops out in the Cava Serredi quarry in the Fine Basin (Tuscany; Bossio et al., 1978, 1993; Carnevale et al., 2006b, 2008). Here the MSC has a thickness of ~150 m, of which only the uppermost ~100 m are attributed, without clear arguments, to Stage 3 by Carnevale et al. (2006b). The lowermost ~40 m of the Stage 3 unit consists of mudstone with alternating sandstone bodies which have been attributed to Roveri et al. (1998)'s p-ev₁ allounit, while the uppermost ~60 m form the p-ev₂ allounit and include two prominent conglomerate bodies alternating with mudstones interbedded with sandstone horizons and black, organic-rich layers (Carnevale et al., 2006b). A few and more fragmented sections are also described on the Tyrrhenian Sea side of Italy by Cipollari et al. (1999).

The Miocene/Pliocene boundary is variably expressed through the Apennine system: unconformable above the ostracod-bearing clays and highlighted by erosional surfaces draped by conglomeratic accumulations (e.g. Stingeti section in Molise; Cosentino et al., 2018), conformable above 0.5-1 m-thick black mudstones similar to how it is observed in Piedmont and of equally unknown paleoenvironmental significance (e.g. Romagna area and Maccarone section; Roveri et al., 1998; Gennari et al., 2008) or conformable above the ostracod-rich mudstones (e.g. Maccarone and Fonte dei Pulcini sections; Cosentino et al., 2005, 2012, 2013; Sampalmieri et al., 2010).

All p-ev₁ deposits studied are almost devoid of in-situ biota, except for fish otoliths and three fish skeletons found in the upper substage 3.1 part of Cava Serredi (Carnevale et al., 2006b). The p-ev₂/Colombacci deposits, instead, host typical Paratethyan assemblages of brackish-water mollusks, ostracods, dinocysts and fish (Bassetti et al., 2003; Bertini, 2006; Popescu et al., 2007; Grossi et al., 2008; Iaccarino et al., 2008; Cosentino et al., 2012, 2018; Schwarzahns et al., 2020). A diverse array of marine fossils (benthic and planktic foraminifera, calcareous nannofossils, dinocysts and fish otoliths and skeletons) has also been reported from the horizons containing these Paratethyan taxa (Bertini, 2006; Carnevale et al., 2006a; Popescu et al., 2007; Pellen et al., 2017). While the autochthony of ostracods, when considered, is unquestioned, the allochthonous vs autochthonous character of the other mentioned fossils is disputed and still unclear (see Chapter 5).

3.8. Sicily

The MSC record is widely exposed on Sicily, mainly in the Caltanissetta Basin and in scattered locations on the Hyblean Plateau (i.e. Ragusa-Siracusa area) and the Messina area (Fig. 2b; Butler et al., 1995; Manzi et al., 2009; Sciuto et al., 2018). Like the Northern Apennines, it shows a complex distribution and variable stratigraphy that mirrors the structuring of Sicily into basins with different characters, geometries and depocenters which subsided at different times and rates (Butler et al., 1995; Catalano et al., 2013). This structural setting permitted the simultaneous deposition of shallow and intermediate-water sediments (Roveri et al., 2008b). Mostly found in the Caltanissetta Basin, these intermediate-water successions have for decades been considered the onshore counterpart of the offshore evaporitic trilogy seen in seismic data from the Western Mediterranean Basin (Decima and Wezel, 1973). More recently, Raad et al. (2021) attempted a similar onshore-offshore correlation but with the intermediate Central Mallorca Depression. The currently endorsed stratigraphic model (Fig. 4a), refined over the years by Decima and Wezel (1971, 1973), Decima et al. (1988), Butler et al. (1995), Garcia-Veigas et al. (1995), Rouchy and Caruso (2006),

Roveri et al. (2008b) and Manzi et al. (2009), envisages two ‘evaporitic cycles’. The ‘First cycle’, overlying both alluvial and deep-water sediments (Tripoli Fm., Licata Fm. and Terravecchia Fm.; see Maniscalco et al., 2019 and references therein), comprises the disputed Calcare di Base (Manzi et al., 2011, 2016b vs Caruso et al., 2015), PLG or Gessi di Cattolica Fm. (Decima and Wezel, 1973; Lugli et al., 2010) and the Halite Unit (Lugli et al., 1999). The ‘Second cycle’ comprises the Upper Gypsum (UG) or Gessi di Pasquasia Fm., which is only present in depocenters of the Caltanissetta Basin (see Manzi et al., 2009 for a detailed overview), sporadically overlain by the siliciclastic Arenazzolo Fm. (Decima and Wezel, 1973; Cita and Colombo, 1979). The whole succession is sealed by the Pliocene marine Trubi Fm. (Fig. 4a). The two evaporite cycles are separated by an erosional surface (MES) associated with an angular discordance broadly linked to the main Mediterranean drawdown event (e.g. Butler et al., 1995; Roveri et al., 2008b). Clauzon et al. (1996), however, placed the MES at the Arenazzolo Fm.-Trubi Fm. transition, implying that the entire evaporitic deposition in the Caltanissetta Basin pre-dated the offshore one, but they do not provide evidence of erosion at that level. In more recent publications from the same research group, the MES is shifted towards the base of the Arenazzolo Fm. (e.g. Bache et al., 2012), again without evidence of major erosion, and different ages are assigned (see Fig. 4b and Grothe et al., 2018 for details).

The Upper Gypsum successions are commonly incomplete in many of the Caltanissetta Basin sections (Pasquasia-Capodarso, Casteltermini, Alimena, Nicosia, Siciliana-Marina; Decima and Sprovieri, 1973; Rouchy and Caruso, 2006; Manzi et al., 2009; Fig. 5i). In the most complete section, Eraclea Minoa (Fig. 3a), the Upper Gypsum Unit consists of 6 (Van der Laan et al., 2006) to 7 (Manzi et al., 2009) primary gypsum beds with a repetitive internal organization of facies (see Schreiber, 1997 and Manzi et al., 2009 for facies description) interbedded with marls and lenticular terrigenous sandstone bodies, gypsarenites and gypsrudites (Fig. 5h). Two of the terrigenous sandstone bodies are highlighted by Manzi et al. (2009) in the thick (~60 m), *Cyprideis agrigentina*-rich (Grossi et al., 2015), marly interval dividing gypsum VI and VII for its alleged astronomical significance (Fig. 3a; see subsection 2.2). A mixed (physically reworked) marine (foraminifera and dinocysts) and (*in-situ*) brackish biota (ostracods and dinocysts) of Paratethyan origin characterizes the marly interbeds from at least gypsum III upwards (following the investigations carried on the Eraclea Minoa section; Bonaduce and Sgarrella, 1999; Rouchy and Caruso, 2006; Londeix et al., 2007; Grossi et al., 2015; Fig. 3a). Calcareous nannofossils have been found along with the above organisms in a more northerly location by Maniscalco et al. (2019) and considered reworked. Above the last gypsum, the ~6-7 m-thick Arenazzolo Fm. is found, represented by reddish arkosic cross-laminated and poorly consolidated sand (Bonaduce and Sgarrella, 1999; Roveri et al., 2008b) and interpreted as the expression of a shallow-water delta, albeit without a sedimentological investigation (e.g. Decima and Wezel, 1973; Cita and Colombo, 1979). The whole Stage 3 sequence is conformably overlain by the Zanclean marine Trubi Fm. in the basin center (e.g. at Eraclea Minoa and Capo Rossello; Fig. 6d; Broisma, 1975; Cita and Colombo, 1979; Van Couvering et al., 2000; Rouchy and Caruso, 2006; Manzi et al., 2009; Fig. 6d) and unconformably in the shallower, marginal areas (Manzi et al., 2009; Roveri et al., 2019b). Only Decima and Wezel (1973) and Raad et al. (2021) report the Miocene/Pliocene transition in the key, intermediate water-representative section of Eraclea Minoa as erosive. However, they do not provide evidence (e.g. photographic documentation) for the presence of an erosional unconformity and, moreover, Raad et al. (2021) erroneously refer to Cita and Colombo (1979), where no erosion is mentioned at the M/P boundary in Eraclea Minoa.

The bathymetric jump between the <100 m of water depth during the late Messinian and the >200 m at the base of the Trubi Fm. is often regarded as a key onshore evidence of the sudden and catastrophic Mediterranean-Atlantic re-connection at the Miocene/Pliocene boundary (e.g. Caruso et al., 2020). However, the real depth of the base of the

Trubi is all but obvious. In fact, variable estimates have been proposed based on the observed benthic foraminifera and/or psychrospheric ostracods at Capo Rossello and Eraclea Minoa: 200-500 m (Decima and Wezel, 1973), 600-800 m (Sgarrella et al., 1997, 1999; Barra et al., 1998), 1400-2400 m (Cita and Colombo, 1979).

3.9. Greece

Several MSC localities are reported from the Greek Ionian Islands (Corfu, Cephalonia and Zakynthos) and from Crete (Fig. 2b).

On the NW coast of Corfu (Aghios Stefanos section), the PLG unit is missing and only a 32 m-thick cyclically-arranged terrigenous succession is present comprising three m-thick conglomerate beds alternating with fine-grained deposits rich in unspecified species of brackish water ostracods (Pierre et al., 2006).

In the southern part of Zakynthos, an evaporitic succession composed of eight gypsum cycles (Kalamaki section) occurs above marine marly deposits (Karakitsios et al., 2017b). These gypsum beds were initially ascribed to the UG unit (Pierre et al., 2006) and later to the PLG (Karakitsios et al., 2017b). The gypsum unit is overlain by approximately ~13 m of siltstones and marls with scattered, cm-thick beds of sandstones, conglomerates and carbonates with nodular texture (Pierre et al., 2006; Karakitsios et al., 2017b). Although no ostracods are reported from this interval, due to its stratigraphic position the post-evaporitic unit is correlated to the Lago-Mare phase (Karakitsios et al., 2017b). Except for the rare presence of marine nannofossils (*Ceratolithus acutus* together with *Reticulofenestra zancleana*) just below the Miocene/Pliocene boundary, only reworked marine fauna has been reported from the post-evaporitic package (Karakitsios et al., 2017b). This dominantly terrigenous succession is unconformably overlain by the Zanclean Trubi Formation (Fig. 6e; Karakitsios et al., 2017b).

MSC deposits on Crete (e.g. Meulenkamp et al., 1979; Delrieu et al., 1993; Cosentino et al., 2007; Roveri et al., 2008a; Zachariasse et al., 2008, 2011) were deposited in Miocene extensional, fault-bound basins driven by tectonic subsidence that ceased in the late Pliocene and Pleistocene (Van Hinsbergen and Meulenkamp, 2006). Because of the strong tectonic and eustatic sea-level-related fragmentation of the stratigraphic record, reconstructing the late Miocene stratigraphy of Crete has not been straightforward (Zachariasse et al., 2008, 2011). Several primary and clastic gypsum facies are recognized, but their correlation with the MSC stratigraphy is disputed (see Cosentino et al., 2007; Roveri et al., 2008a, 2014a; Zachariasse et al., 2008). Coarse-grained, mammal-bearing terrigenous facies irregularly alternating with marls are in places found unconformably overlying the gypsum and separated from the Pliocene facies by an erosion surface (see Meulenkamp et al., 1979; Delrieu et al., 1993; Cosentino et al., 2007). In two localities on the Messarà Plain, Cosentino et al. (2007) described a highly diversified ostracod fauna with Paratethyan affinity in some early intervals.

Messinian evaporites and/or Lago-Mare deposits are also reported from the North Aegean region onshore in the Strymon Basin (Snel et al., 2006; Suc et al., 2015; Karakitsios et al., 2017a) and Dardanelles region (Melinte-Dobrinescu et al., 2009) and offshore (Prinos-Nestos Basin; Karakitsios et al., 2017a), but recent integrated studies suggested that the sections studied by the above listed authors are older than the MSC (see Krijgsman et al., 2020a, 2020b). In particular, Krijgsman et al. (2020a) proposed that for most, if not all, of the MSC the North Aegean was a brackish water, mostly Paratethyan-fed basin restricted by the Cyclades sill to the south (Fig. 2a) and forming a passageway for Paratethyan overspill waters towards the Mediterranean.

3.10. Cyprus

MSC deposits on Cyprus outcrop in the Pissouri, Psematismenos, Mesaoria and Polemi basins on the southerly fringe of the Troodos massif (Fig. 2b; Rouchy et al., 2001; Manzi et al., 2016a). According to

Rouchy et al. (2001) and Orszag-Sperber et al. (2009), sediments belonging to all MSC stages of Roveri et al. (2014a) are preserved in the Cypriot basins. By contrast, Robertson et al. (1995) and Manzi et al. (2016a) considered that PLG evaporites on Cyprus are only present as fragments reworked within a chaotic unit (the Lower Gypsum and Intermediate breccia units of Orszag-Sperber et al., 2009) and that the only *in situ* evaporites belong to the overlying Upper Gypsum Unit, which encompasses the whole of Stage 3 (Figs. 3a, 4a). A continuous, Eraclea Minoa-like section is not known in Cyprus (Manzi et al., 2016a). The best exposure of the lower 60 m of this unit is found in the Polemi Basin (Manzi et al., 2016a). It comprises up to six gypsum beds (the lower three of which are mainly selenitic, while the upper three are predominantly laminated; Fig. 3a). Gypsum beds range in thickness from 1 to 6 m and are separated by laminated marls (Fig. 5j) occasionally interbedded with conglomerates and sandstones (e.g. between the 5th and 6th gypsum layers; Rouchy, 1982; Rouchy et al., 2001; Manzi et al., 2016a). The sixth gypsum bed is reported by Rouchy et al. (2001) to be hollowed in the upper part with the cavities filled with overlying sediments. The similarity of the cyclicity and facies association of this Cyprus succession with the substage 3.1 interval of the Sicilian UG led Manzi et al. (2016a) to propose a bed-to-bed correlation and to recognize the substage 3.1/3.2 boundary at the top of the last gypsum bed (Fig. 3a). According to Orszag-Sperber et al. (2000) and Rouchy et al. (2001), this chronostratigraphic boundary coincides with a Mediterranean-scale sea-level drop, a conclusion that arises from the interpretation of the cavities in the uppermost gypsum as the product of karstic dissolution following a prolonged period of subaerial exposure.

The sedimentary sequence overlying the last gypsum bed and assigned by Manzi et al. (2016a) to the Lago-Mare phase lacks a clear and rhythmic sedimentary cyclicity. In the Pissouri Basin this interval (up to 25–30 m-thick) mostly consists of conglomerates, sandstones, limestones, paleosols (which appear as dm to m-thick dark marly horizons, in one case with pulmonated gastropods) and subordinated clay-marly horizons (Rouchy et al., 2001). By contrast, in the Polemi sections the clay-marly facies dominates this interval (Rouchy et al., 2001). *In situ* fresh-brackish water species of articulated mollusks (*Limnocardiidae*, *Melanopsis*), Paratethyan (*Loxocorniculina djafarovi*, *Euxynocythere praeaquana*) and Mediterranean (*Cyprideis agrigentina*) ostracods and foraminifera (*Ammonia beccarii*), *Characeae*, abundant fragments of the marine euryhaline fish *Clupeidae* and a fish skeleton of the euryhaline *Aphanius crassicaudus* are described from some of the substage 3.1 and 3.2 fine-grained facies and within the terrigenous laminae of some *balatino* gypsum (Orszag-Sperber et al., 2000; Rouchy et al., 2001; Orszag-Sperber, 2006; Manzi et al., 2016a). The upward change in diversity of the ostracod fauna seen elsewhere (e.g. Malaga, Nijar, Vera, Apennines and Eraclea Minoa) is not reported in Cyprus but this may be because no detailed study of ostracod assemblages in Stage 3 sediments has been published. The Miocene/Pliocene boundary, near Polemi village is described by Manzi et al. (2016a) as a sharp contact above a dark, organic-rich layer (Fig. 6f). It appears to be similar to the boundary reported from Piedmont (Fig. 6c; Trenkwalder et al., 2008; Dela Pierre et al., 2016) and Northern Apennines (Gennari et al., 2008; Grossi et al., 2008), if not for the presence, in Cyprus, of (possibly) *in situ* *Cyprideis agrigentina* (Manzi et al., 2016a). A layer with the same field appearance, thickness (~ 1 m) and stratigraphic position is reported in Pissouri by Rouchy et al. (2001), which they interpreted as a paleosol based on mottling, oxidized roots, carbonate concretions and plant fragments.

3.11. Southern Turkey

The tectonically active, during the Miocene, thrust-top basin of Adana in southern Turkey (Radeff et al., 2017) retains the most complete and better exposed easternmost successions of the MSC (Fig. 2b), whose deposits were attributed to the Handere Fm. (Cosentino et al., 2010; Radeff et al., 2016).

MSC Stage 3 finds expression in a >1 km thick continental unit unconformable, through an erosional surface, above the pre-evaporitic, Stage 1 anhydrite-shale alternations (Radeff et al., 2016) and resedimented gypsum-bearing Stage 2 deposits (Cosentino et al., 2010; Cipollari et al., 2013). This unit mainly consists of fluvial coarse- and fine-grained deposits representing channel fill and overbank deposits. Sporadically, some fine-grained intercalations are found containing a mixed brackish (ostracod) and marine (foraminifera and calcareous nannofossils) fauna. The ostracod fauna has affinity with the Paratethyan fauna but, unlike to many other Mediterranean onshore localities, is poorly diversified, with monospecific assemblages of *Cyprideis agrigentina* (Avadan section and T-191 borehole; Cipollari et al., 2013) or with *Cyprideis agrigentina* accompanied by rare to abundant specimens of *Loxoconcha muelleri*, *Euxinocythere (Maeotocythere) praeaquana*, and *Loxoconcha* sp. (Adana section; Faranda et al., 2013). Ostracods are often associated with *Ammonia beccarii* and rare *Elphidium* and *Cribrorhynchium*, which are the only foraminifera considered as autochthonous. Conversely, the entire nannoflora is interpreted as physically reworked (Cipollari et al., 2013; Faranda et al., 2013).

The Handere Fm. is followed by early Zanclean marine sediments (Avadan Fm.) deposited, according to the paleoecology of the benthic foraminifera species recognized, at bathymetries ranging from 200 to 500 m (Cipollari et al., 2013). The lithological nature of the Miocene/Pliocene boundary in the Adana Basin is not clear, but it occurs either above the continental or subaqueous, ostracod-bearing facies.

A similar stratigraphic sequence is present in the subsurface. Here, however, chaotic gypsum-bearing deposits are not found and two halite bodies ~20 and ~170 m-thick are present, separated and followed by fluvial gravels, sands and silts (Cipollari et al., 2013).

3.12. Summary of the onshore Stage 3 record

Most of the onshore Stage 3 records formed in shallow marginal Mediterranean basins, which underwent substantial uplift from the Messinian till nowadays and are assumed to have had their depocenter at ~200 to 50 m below the Atlantic level during the late Messinian (Roveri et al., 2014a, 2019a; Radeff et al., 2016, 2017). The Caltanissetta Basin (Sicily), some basins along the Apennines and (possibly) Cyprus represent, instead, possible onshore representative of intermediate basins. The nature and duration of these records is quite variable, and there are only six sections that may record an entire Stage 3 sequence (i.e. Sorbas, Nijar, Northern Apennines, Eraclea Minoa and Cyprus; Fig. 3a). Reasons for the fragmentary nature of the Stage 3 sedimentary record include different durations of subaerial exposure following the Stage 2 drawdown, local tectonics and associated syn-depositional erosion and deposition. One of the consequences of this is that any sedimentary cyclicity that resulted from orbital fluctuations is typically either less well developed or poorly preserved, making the chronology of Stage 3 rather uncertain or controversial in places.

Despite this variability, several fairly consistent characteristics are widely expressed. These are:

- 1) Stage 3 sedimentation follows a period of intensive tectonic and/or eustatic-driven erosion of the margins, as demonstrated by the frequent presence of erosional unconformities and/or chaotic Stage 2 deposits (RLG unit);
- 2) Stage 3 lithologies are mostly terrigenous (conglomerates, sandstones and mudstones) and deposited in a variety of continental (fan delta, fluvial channels and alluvial plains) and shallow water environments (endorheic lakes or water bodies connected with the Mediterranean water mass is the riddle). Carbonate intercalations are sometimes present (e.g. Sorbas Basin and *Colombacci* limestones in the Apennines). Stage 3 gypsum is only found in deeper-water intermediate basins of Caltanissetta in Sicily and Cyprus.
- 3) A diversified fossil assemblage with Paratethyan affiliation (ostracods, dinocysts, mollusks) is commonly found in the shallow-water

sediments of Lago-Mare successions. Only in the intermediate Caltanissetta Basin (Sicily) do these diversified Paratethyan forms (only ostracods) occur earlier, in the sediments from substage 3.1. Where these have been studied in detail, these assemblages typically show an increase in diversity with time (possibly every wet phase of the precession cycles). Some of these sediments also contain marine fossils and there is controversy over whether these are *in situ* and contemporaneous or reworked.

- 4) In outcrop, the Miocene/Pliocene boundary has four main sedimentary expressions: erosive and followed by a conglomeratic lag (e.g. Malaga, Vera, Mallorca; Fig. 6a); conformable above continental facies (e.g. Nijar Basin; Fig. 6b); conformable above ostracod-rich mudstones (e.g. Eraclea Minoa; Fig. 6d); sharp contact above a black layer of still largely unknown paleoenvironmental significance (Piedmont, Apennines and Cyprus; Fig. 6c, f).

For a better understanding of how Stage 3 developed across the Mediterranean these marginal records now need to be considered alongside the evidence from intermediate to deep offshore settings.

We note that alternative chronostratigraphic frameworks have been proposed for several onshore (Malaga, Sorbas, Mallorca, Apennines, Sicily) and offshore (Sites 134B, 976B, 978A) locations (see Fig. 4b for references), but we have omitted them as they are shown to rely on incorrect (bio)stratigraphic arguments (see Roveri et al., 2008c, Grothe et al., 2018 and subsection 5.5).

4. Offshore domain

The offshore Mediterranean is a complex array of variable-depth and morphologically complex subbasins framed by morphological highs or sills. Traditionally it is divided into two main domains (Fig. 2a), the Western and Eastern Mediterranean, with the intervening divide (or Sicily sill) situated in the Sicily channel at present with a maximum depth of 316 m. The Alborán Basin, the depressions on the Balearic Promontory, the Corsica, Valencia, Algero-Balearic, Liguro (or Sardo)-Provençal and Tyrrhenian basins belong to the "Western Mediterranean" (Fig. 2a). The Adriatic foredeep, the Ionian, Sirte, Aegean and Levant basins belong to the "Eastern Mediterranean" (Fig. 2a). Smaller-sized depressions, again surrounded by sills of variable depth, are identified and labelled within each of these subbasins.

Although the exact topography and hypsometry of the Messinian Mediterranean is difficult to reconstruct, this present-day geography is generally assumed to have been in place, with five main differences: (1) the Alborán Basin was split into a Western (WAB) and Eastern Alborán (EAB) by a volcanic arc (Booth-Rea et al., 2018); (2) the Tyrrhenian Basin was only partly opened (Lymer et al., 2018); (3) the precise depth and width of the ancient Sicily Sill are difficult to estimate, but may have been much deeper than today (~300 m; Meijer and Krijgsman, 2005; Jolivet et al., 2006). Paleodepth estimations for the Messinian configuration range from 380 m (Just et al., 2011) to 430 m (García-Castellanos et al., 2009); (4) one or two sills were present at the southern termination of the Adriatic foredeep (Pellen et al., 2017; Amadori et al., 2018; Manzi et al., 2020); (5) the North Aegean was partially isolated from the Mediterranean by the Cyclades Sill and with high Paratethyan affinity (Krijgsman et al., 2020a). Following the schematic classification of the Messinian sub-basins by Roveri et al. (2014a), all these subbasins are regarded as either intermediate (i.e. relatively deep-water, 200–1000 m) or deep (water depth > 1000 m).

Compared with the onshore domain, the offshore basins hold a far greater percentage of the total volume of MSC sediments (Ryan, 1973; Haq et al., 2020). The architecture, geometry and main lithologies of the MSC and younger deposits are well known thanks to the high density of seismic data and the fact that evaporites (halite particularly) are easily identified on seismic profiles due to their unusual seismic properties, especially compared to those of terrigenous and carbonate sediments (see Lofi et al., 2011a, 2011b; Lofi, 2018; Haq et al., 2020). However, the

detailed lithological, sedimentological, paleontological and geochemical nature and their chronostratigraphy are still poorly constrained offshore because these cannot be univocally defined on the basis of seismic data alone (Roveri et al., 2019b) and direct information about these deep MSC successions is limited to a small number of cores (16) drilled during the DSDP (Ryan et al., 1973; Hsü et al., 1978b) and ODP (Kastens et al., 1987; Comas et al., 1996; Emeis et al., 1996) drilling campaigns that penetrated exclusively the uppermost tens of meters of the deep MSC suite in very scattered localities (Fig. 2b). Only recently, access to industrial boreholes crossing the base of the halite in the deep Levant Basin has been granted, providing a rare glimpse of the deep MSC deposits in the easternmost part of the Mediterranean (Gvirtzman et al., 2017; Manzi et al., 2018; Meilijson et al., 2018, 2019).

The MSC is commonly described as tripartite ('Messinian trilogy') after Montadert et al., 1978) in the Western Mediterranean (Lower-Mobile-Upper units: LU-MU-UU, respectively). However, in the Ionian Basin is described as bipartite (MU-UU) by Camerlenghi et al. (2019) while according to Lofi et al. (2011a), Gvirtzman et al. (2013, 2017), Lofi (2018) and Camerlenghi et al. (2019), the Levant Basin consists of the MU and the UU is only present locally and possibly represented by evaporite-free terrigenous accumulations (Kartveit et al., 2019; Madof et al., 2019). The lack of many age constraints within the offshore MSC successions hampers unambiguous correlation with onshore sequences (Fig. 1a; Roveri et al., 2014a). Nevertheless, different authors have proposed onshore-offshore correlation of specific events (e.g. onset, Ochoa et al., 2015; and termination of the MSC, Biscaye et al., 1972, Iaccarino et al., 1999) and stratigraphic schemes (Decima and Wezel, 1971; Raad et al., 2021) based on and biostratigraphic evidence (Cosentino et al., 2006), ⁸⁷Sr/⁸⁶Sr isotope ratios (Roveri et al., 2014b; Gvirtzman et al., 2017; Manzi et al., 2018) and astronomical tuning of the deep seismic record (Ochoa et al., 2015, 2018; Manzi et al., 2018; Meilijson et al., 2018, 2019). Here we focus on the seismic and geological (core-derived) properties of the Upper Unit (and laterally grading/interfingering sediments when present), stratigraphically below the Plio-Quaternary deposits (PQ) suggesting that it belongs to (at least part of) Stage 3.

4.1. Western Alborán Basin and westernmost East Alborán Basin

The Alborán Basin has received particular attention because of its proximity to the Gibraltar Corridor (Estrada et al., 2011; Popescu et al., 2015 and references therein). Evaporites only occur on the eastern side of the EAB (which is treated in subsection 4.2; Fig. 2a). To the west of the volcanic archipelago (Booth-Rea et al., 2018, i.e. the WAB) and immediately to the east on the western side of the EAB only terrigenous sediments occur in the MSC interval (Booth-Rea et al., 2018; de la Peña et al., 2020). Sediments at the Miocene/Pliocene boundary appear in the seismic reflection data as parallel reflectors with increasing reflectivity (Comas et al., 1996, 1999; Booth-Rea et al., 2018). Locally, just below the M discontinuity, some of the reflectors suggest a chaotic seismic facies (Fig. 7a; Booth-Rea et al., 2018; Bulian et al., 2021). Miocene sediments with a maximum thickness of 100 m have been recovered from two out of nine holes drilled in the region (ODP 976B, 978A; Comas et al., 1996, 1999). These sediments mostly consist of claystones, siltstones and sandstones with *Chondrites* and *Zoophycos* ichnofacies at site 976B and include a conglomerate close to the Miocene/Pliocene boundary at Site 978A. The lack of age-diagnostic fossils hampers their correlation with the Geologic Time Scale (GTS). However, the presence,

¹ Lithostratigraphic and biostratigraphic information from DSDP and ODP cores are primarily extracted from the Scientific Shipboard Party documents, accessible from <https://www.marum.de/en/Research/Cores-at-BCR.html>. These documents are referenced in the text as follows: Ryan et al. (1973): DSDP 120-134; Hsü et al. (1978b): DSDP 371-378; Kastens et al. (1987): ODP 650-656; Comas et al. (1996): ODP 974-979; Emeis et al. (1996): ODP 963-973.

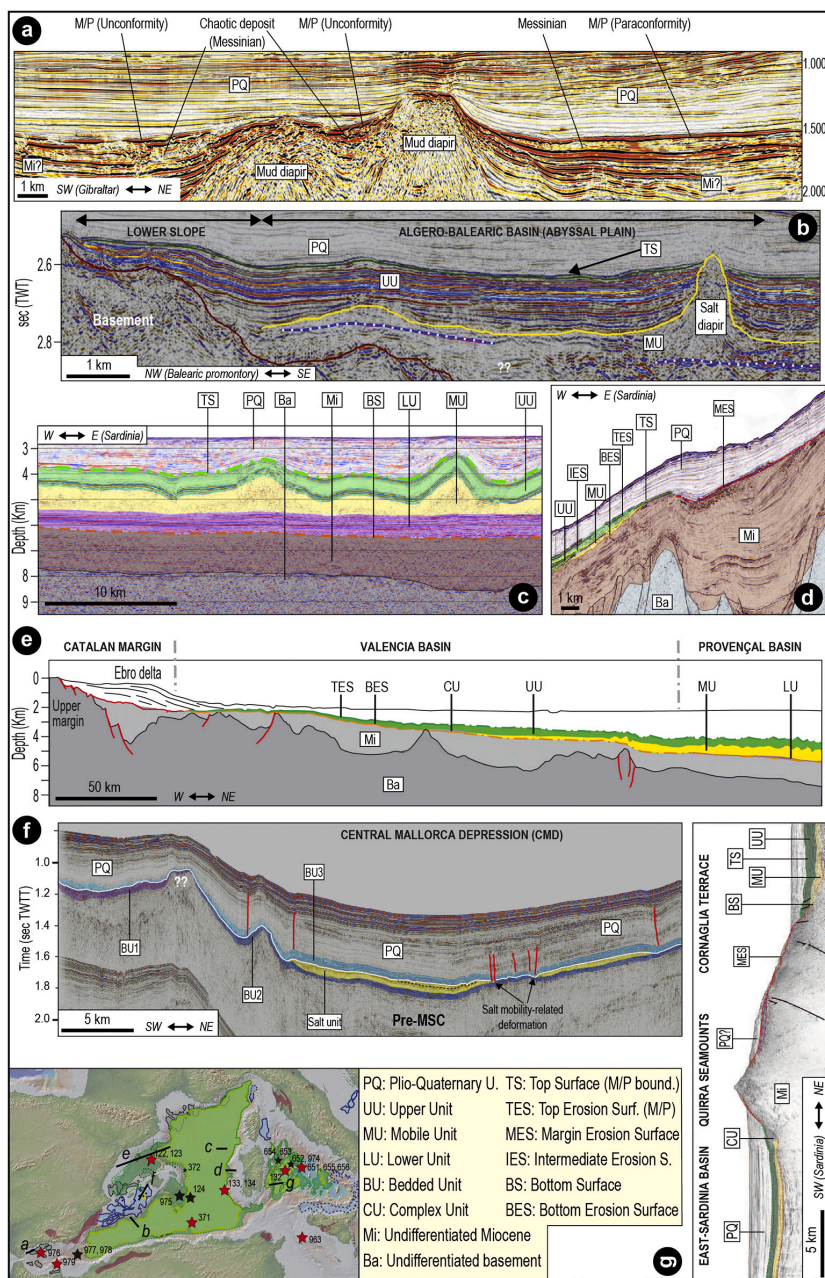


Fig. 7. Seismic profiles from intermediate-deep Western Mediterranean basins containing MSC markers/units. (a) Seismic reflection line CAB01-104 from the WAB (modified from Booth-Rea et al., 2018). The line shows the variable geometry of the inferred M/P boundary, erosive in proximity of mud diapirs, (para)conformable in tectonically undisturbed sectors. Chaotic reflectors are occasionally imaged below the inferred M/P boundary. (b) Seismic profile SF12-09 imaging the lower slope of the south Algero-Balearic margin and part of the Algero-Balearic abyssal plain (modified from Mocnik et al., 2014). Here a high reflecting and horizontally stratified UU covers a thin layer of MU evidenced by salt diapirism. Note the concordant deformation of the UU and MU. (c) Line MS-39 from the abyssal plain of the Liguro-Provençal Basin showing the Messinian trilogy and non-erosive bottom and top surfaces (BS and TS; Dal Cin et al., 2016). Halokinesis of MU gives rise to domes that deform the UU and PQ units. (d) Interpreted seismic profile from the lower-middle slope of the west Sardinian margin (modified from Dal Cin et al., 2016). Thin MU and UU are present on the lower slope, while on the middle slope (and upper slope here not shown) they converge in the margin erosion surface MES. (e) Line drawing of seismic line imaging from the Catalan margin (or Ebro Basin) to the abyss of the Liguro-Provençal basin (modified from Maillard et al., 2011b). Note the pinch out of the MU in the Valencia Basin and of the UU in the Ebro Basin, which is MSC free. (f) Interpreted seismic profile Simbad 15 crossing the depocenter of the CMD showing all the MSC units and erosional surfaces (modified from Raad et al., 2021). (g) Interpreted seismic profile MYS40 illustrating the MU-UU-PQ units in the East-Sardinia Basin and Cornaglia Terrace, separated by the MSC deposits-free Quirra Seamounts (modified from Lymer et al., 2018).

high in the Miocene section, of an oligotypic association of ostracods (*Candona* sp., *Loxoconcha muelleri*, and *Cyprideis* sp.) with different stages of growth (Site 978A; Iaccarino and Bossio, 1999) and Paratethyan dinocysts (including *Galeacysta etrusca*; see subsection 5.2; Popescu et al., 2015) indicates a latest Messinian (substage 3.2) age and brackish paleodepositional conditions. Foraminifera and nanofossils are also present, but all species recognized are of no help in narrowing down the paleoenvironmental interpretation because they are considered either definitely or likely to be reworked (Iaccarino and Bossio,

1999). By contrast, Popescu et al. (2015) interpreted some species of calcareous nanofossils (*Reticulofenestra pseudoumbilicus*, *Discoaster quinqueramus*, *Ceratolithus acutus*, *Triquetrorhabdulus rugosus*, *Amaurolithus primus*) and marine dinocysts as autochthonous.

The nature of the Miocene/Pliocene boundary is also uncertain. According to some authors, the “M” discontinuity is a high-amplitude reflector with evidence of erosion attributed to subaerial processes (Estrada et al., 2011; Urgeles et al., 2011) and locally (e.g. close to Site 121; Ryan et al., 1973) associated with an angular unconformity that

abruptly truncates the upper Miocene deposits and morphological highs (Comas et al., 1999; Estrada et al., 2011; Garcia-Castellanos et al., 2020). Although the M-reflector was drilled at Sites 976B, 977A and 978A, a lithological contact was only recovered at Site 976B coinciding with a major erosional surface between the early Messinian and the base of the Pliocene (Bulian et al., 2021). Only at Site 978A (and possibly 977A) was a few meters of what may be the contact interval recovered (Comas et al., 1996). This comprises a 25 m-thick cemented succession containing pebbles of volcanic and sedimentary rocks likely to derive from the Alborán substrate (46R, 620.9-630.67 mbsf, between the Pliocene-bearing core 45R and the Messinian-bearing core 47R; Comas et al., 1996). In contrast, Booth-Rea et al. (2018) concluded that the M-reflector is an unconformity only close to the mud diapirs and owes its erosive shape and angular discordance to the activity of these structures (Fig. 7a). In more undisturbed sectors these authors argue that the boundary is a paraconformity with no evidence of erosion (Fig. 7a). The lack of Messinian erosion in the shallow regions of the WAB margins has prompted the hypothesis that this area did not desiccate during the MSC (Booth-Rea et al., 2018; de la Peña et al., 2020). This contradicts much of the interpretation made of the DSDP and ODP cores of this interval in the Alborán Sea. The succession recovered by drilling from beneath the Pliocene comprises gravels that contain a mixed Miocene fauna. These sediments and their faunal content are thought to have been reworked from older sediments exposed as Alborán substrate with no evidence of an extensive wet Lago Mare interval immediately before the Zanclean (Comas et al., 1996).

Two W-E-aligned erosional channels straddling the Strait of Gibraltar and stretching for 390 km from the easternmost Gulf of Cádiz (Atlantic Ocean) into the Alborán Basin are clearly observed in seismic profiles (Garcia-Castellanos et al., 2009; Estrada et al., 2011). There is disagreement, however, concerning the timing and nature of their formation. These incisions are classically considered to occur at the very top of the MSC suite (when present) and to be the consequence of the Zanclean megaflood (Garcia-Castellanos et al., 2009, 2020; Estrada et al., 2011 among others). More recently, Krijgsman et al. (2018) highlighted that an accurate age determination for these channel incisions is lacking and that they might have been formed earlier during the MSC as a result of the Mediterranean-Atlantic gateway currents. Interpretation of E-W seismic profiles across the Alborán Basin combined with mammal records in Africa and Iberia led Booth-Rea et al. (2018) to suggest the existence of an emergent volcanic archipelago that temporarily connected southeastern Iberia with northern Africa, separating an open marine, Atlantic-influenced West Alborán Basin realm from a restricted, hydrologically complex Mediterranean realm to the east.

4.2. Eastern Alborán, Algero-Balearic and Liguro-Provençal basins

From the eastern margin of the EAB as far east as the Tyrrhenian coast of Italy, the Messinian (evaporites-bearing) trilogy LU-MU-UU is found and sealed by the PQ. The MU and UU are interpreted to fill the deepest depocenters (Algero-Balearic, Valencia and Liguro-Provençal basins; with minor interruptions due to seamounts) and the lower slope domain, where they comprise ~500 to ~800 m of UU and ~1000 m of MU/halite (Figs. 7b-d; Camerlenghi et al., 2009; Lofi et al., 2011a, 2011b; Geletti et al., 2014; Mocnik et al., 2014; Dal Cin et al., 2016; Lofi, 2018). Upslope, a thinner, possibly incomplete UU is locally described on the middle-upper continental slopes of Western Corsica (Guennoc et al., 2011) and Sardinia (Mocnik et al., 2014; Dal Cin et al., 2016) and the northern (Maillard et al., 2006) and southern (Maillard and Mauffret, 2013; Mocnik et al., 2014; Dal Cin et al., 2016) flanks of the Balearic Promontory, even though the structural settings of these locations are mostly dominated by erosion (Fig. 7d). MSC evaporites are absent on the continental shelves bordering the deep Algero-Balearic and Liguro-Provençal basins, where the PQ directly overlies the MES which, in turn, cuts through the middle Miocene deposits (Gorini et al., 2005; Lofi et al.,

2005). The only late Messinian sediments are present as Complex Units (Gulf of Lion, Bessis, 1986; Gorini et al., 2005; Lofi et al., 2005; Algerian Basin, Medaouri et al., 2014; Arab et al., 2016; Fig. 7e). CUs can have various origin (Lofi et al., 2011a, 2011b), but when identified at the outlet of drainage systems, they are commonly interpreted as Messinian clastics supplied by rivers (Lofi et al., 2005). In the Gulf of Lion, the MES is a high angle unconformity with substantial erosion along highly rugged relief thought to have been generated by fluvial incision (Lofi et al., 2005). In contrast, Roveri et al. (2014c) suggested that the drainage networks visible on the seismic could be of subaqueous origin.

When not involved in MU-related deformation processes, the UU appears as a highly reflective series of flat reflectors alternating with less reflective, but concordant, reflectors (Figs. 7b-c; Lofi et al., 2011a, 2011b) aggrading in the basin center and onlapping the margins (Fig. 7b; Camerlenghi et al., 2009; Lofi et al., 2011a, 2011b; Geletti et al., 2014; Mocnik et al., 2014; Dal Cin et al., 2016). The aggrading nature, shelf-ward thinning and the onlap terminations of the UU are interpreted as evidence of sedimentation in a lake with fluctuating base level (e.g. Lofi et al., 2005; Lofi et al., 2011a). In the abyssal plains (Figs. 2a, 7c), nine to ten cycles have been interpreted on high resolution seismic profiles as corresponding to gypsum-marl alternations (Geletti et al., 2014; Mocnik et al., 2014). At Sites 124 and 372, ~40-50 m of the UU have been drilled at the feet of the east Menorca continental rise and the northern Menorca slope, where 3-4 gypsum-marl cycles are recognized (Fig. 2b; Ryan et al., 1973; Hsü et al., 1978a). Primary gypsum facies are widely overprinted by post-depositional diagenetic processes, but the still recognizable laminated and clastic primary textures indicate precipitation at the water-air interface and emplacement by gravity flows, respectively (Lugli et al., 2015). The marl interbeds are made from stiff to firm dolomitic mud containing substantial quantities of detrital material intercalated with current-bedded sandstones and, at Site 124, with diatomites (Ryan et al., 1973). *Cyprideis* sp. specimens are reported from some mudstone interbeds at Site 372, while dwarf planktonic foraminifera are present just below the Miocene/Pliocene boundary at Site 124 (Ryan et al., 1973).

The Miocene/Pliocene boundary coincides with the top of the UU where present (labelled TES when erosional and TS when conformable; Lofi et al., 2011a, 2011b). In the abyssal plain-lower slope domain it appears to be undulating, although this geometry is related to the deformation of the underlying salt (Figs. 7b-c), and it actually corresponds to a sharp surface lacking signs of erosion (Lofi et al., 2011a, 2011b; Geletti et al., 2014; Mocnik et al., 2014). By contrast, the UU-PQ boundary commonly appears strongly erosional in the middle-upper slope and shelf domain, where it coincides with the MES (Fig. 7d; Lofi et al., 2005; Maillard et al., 2006; Geletti et al., 2014; Mocnik et al., 2014). Among the six DSDP-ODP Sites drilled in this region (Fig. 2b), only Hole 975B recovered the Miocene/Pliocene boundary (Iaccarino and Bossio, 1999; Marsaglia and Tribble, 1999). Here the Messinian is a few centimeters thick and consists of banded micritic silty clays with minor calcareous siltstones to sandstones typified by a diverse faunal assemblage consisting of dwarf planktonic foraminifera, *Ammonia tepida* tests and brackish Paratethyan ostracods (*Loxocorniculina djafari*, *Euxinocythere praeabaquana*, *Ammicythere idonea*, *Leptocythere limbata*, *Candona* sp., and *Cyprideis* sp.; Iaccarino and Bossio, 1999).

Halite is present at the bottom of Hole 134 drilled within the UU (Ryan et al., 1973; Sage et al., 2005; Lugli et al., 2015). High-resolution seismic profiles from both the Algero-Balearic and Ligurian-Provençal basins confirm the presence of a halite layer high in the UU sequence (Geletti et al., 2014; Mocnik et al., 2014). This layer is up to 50 m thick (Dal Cin et al., 2016) and is correlated with an erosional surface (called IES: Intermediate Erosional Surface by Lofi et al., 2011a, 2011b) associated with an angular unconformity which is better developed on the lower slope (Fig. 7d). Geletti et al. (2014) and Mocnik et al. (2014) interpreted this layer as autochthonous and indicative of at least one important sea level drop during UU deposition. However, this intra UU halite layer is always described from areas strongly affected by salt

diapirism (just like in the Ionian Abyssal Plain; see subsection 4.6.1) and is never found in adjacent, undisturbed areas (see Camerlenghi et al., 2009; Geletti et al., 2014; Mocnik et al., 2014; Dal Cin et al., 2016), two features that may suggest it has an allochthonous origin.

Site 134 shows evidence of a “desiccation crack” cutting through a sandy silt layer interbedded with unaffected laminated halite (Hsü et al., 1973c). Unfortunately, the core photograph of this crack has been published in two different orientations (Hsü et al., 1973a, 1973b), leading both Hardie and Lowenstein (2004) and Lugli et al. (2015) to question the evidence for subaerial desiccation. Because of these ambiguities, we suggest to dismiss this example from the book of evidence.

4.3. Valencia Basin

The Valencia Basin (VB; Fig. 2a) is an aborted rift formed during the late Oligocene-early Miocene opening of the back-arc Liguro-Provençal Basin (e.g. Jolivet et al., 2006). It is located between the Spanish Ebro Margin to the west and the Balearic Promontory to the east, while it grades into the Liguro-Provençal Basin to the E/NE (Fig. 7e; Maillard and Mauffret, 2006; Maillard et al., 2006).

Numerous exploratory boreholes exist on the western Ebro margin. These boreholes, tied to seismic data, confirm that MSC-related sediments on the northwestern shelf are missing (Fig. 7e; Urgeles et al., 2011; Pellen et al., 2019). The only MSC feature present is a prominent erosional surface (the MES) incising Serravallian-early Messinian sediments (Urgeles et al., 2011). By contrast, on the southwestern and southern part of the margin, well data show the presence of evaporitic sediments (e.g. Delta L and Golfo de Valencia D1 boreholes; Del Olmo, 2011; Del Olmo and Martín, 2016; Lozano, 2016). Del Olmo and Martín (2016) described these evaporites as primary selenites and ascribed them to MSC Stage 1 (their unit M7). Lozano (2016) described the same evaporitic deposits in the same boreholes as ‘white anhydrites’, leaving open the question as to whether the anhydrite is primary (sabhka’s) or secondary at the expense of a primary gypsum facies. On the eastern margin of the VB boreholes and seismic studies suggest there are no MSC units with only a prominent MES cutting pre-MSC sediments (Driussi et al., 2015; Raad et al., 2021). All authors conclude that the shelves of VB were exposed to subaerial erosion during and following the main drawdown.

MSC deposits are also absent along the slopes and, where present, consist of coarse- and fine-grained terrigenous facies filling valleys largely related to fluvial incision (Fig. 7e; Stampfli and Höcker, 1989).

A different situation features in the depocenter. Despite its present-day depth of > 2000 m, no MU is observed in the depocenter, as the salt pinches-out at the edge of the deeper Provençal Basin (Fig. 7e). Only the seismic properties of UU suggest that it is roughly continuous from the Provençal Basin into the VB (Fig. 7e; see subsection 4.2), although it thins from ~1000 m to < 500 m. The UU is characterized by aggrading and onlapping geometries towards the slopes, where it also thins out until it disappears along the middle-upper slope (Fig. 7e; Maillard et al., 2006; Cameselle and Urgeles, 2017). Maillard et al. (2006), Urgeles et al. (2011), Cameselle et al. (2014) and Cameselle and Urgeles (2017) all stated that the UU formed during an important Mediterranean-level lowstand (~1000 m). Several Complex Units (CU), with different origin, have been observed and described as belonging to the MSC (Cameselle and Urgeles, 2017).

DSDP Site 122, drilled at the mouth of a valley incision, recovered a few meters of sand-gravels made of well-rounded basalt, marine limestones, nodules of crystalline gypsum and mollusk fragments in a clay-silty matrix rich in deep-water benthonic foraminifera and early Pliocene nannofossils, all interpreted as erosional products of the VB seabed (Ryan et al., 1973). The uppermost Messinian in two industrial wells (Ibiza Marino and Cabriel boreholes; see Lozano, 2016) is represented by intercalations of clastic gypsum/anhydrite and marls (unit M8-P1 of Del Olmo and Martín, 2016). These are interpreted as turbidites sourced from the shelf and/or slope during a lowstand phase of the

Mediterranean base level (Del Olmo, 2011; Del Olmo and Martín, 2016; Cameselle and Urgeles, 2017).

In seismic profiles, the UU/PQ transition (M-reflector or TES) is locally both sharp and smooth (in more distal settings) and erosional (in more proximal settings; Fig. 7e). Maillard and Mauffret (2006) indicate that the smooth parts have been caused by increasing fresh water influx during the Lago-Mare phase, leading to dissolution of the evaporites, and the rough erosional segments are of subaerial origin. For Cameselle and Urgeles (2017), the top of the UU is a smooth and conformable downlap surface, representing the rapid inundation of the basin with only local minor erosional features.

4.4. Balearic Promontory

Sticking out from the surrounding deep-water locations, the Balearic Promontory (BP; Fig. 2a) is a continental high that has undergone tectonic extension since the late Serravallian (Roca and Guimera, 1992; Sabat et al., 2011). During the Messinian, it comprised in topographic lows/subbasins at different water depths and separated by structural highs/sills (Maillard et al., 2014; Driussi et al., 2015; Roveri et al., 2019b; Raad et al., 2021). The area has been the subject of multiple studies (Maillard et al., 2014; Driussi et al., 2015; Ochoa et al., 2015; Roveri et al., 2019b; Raad et al., 2021) and several controversies arose after the publication of Roveri et al. (2019b).

The first controversy concerns the Messinian paleodepth of the BP’s subbasins. According to Roveri et al. (2019b) the subbasins were shallow during the Messinian and acquired today’s paleodepths following a strong post-MSC subsidence; Maillard and Mauffret (2011), Maillard et al. (2014) and Raad et al. (2021), instead, consider the tectonic movements in the BP to have been minor since the late Miocene (Messinian) and the region to have been already structured as it is today during the MSC. Well-to-seismic ties in the shallower basins closer to the Spanish coast (i.e. Bajo Segura, San Pedro and Elche basins) comprise up to 14 Stage 1 primary gypsum-marl cycles similar to the onshore PLG unit (Lugli et al., 2010) truncated at the top by the MES (Soria et al., 2008a, 2008b; Ochoa et al., 2015). At first, Ochoa et al. (2015) concluded that all sediments overlying the MES are Pliocene in age. A later re-appraisal of the same downhole logging data and cuttings led Ochoa et al. (2018) to attribute the first ~13 m-thick micritic and evaporite-free sediments to the late Messinian (stage 2 or 3 of the MSC according to the authors). The MSC stratigraphy of the shallowest offshore basins of the BP closely resembles that described from cores and outcrops onshore Mallorca (see subsection 3.4; Roveri et al., 2019b).

High resolution seismic reflection data in the Central Mallorca Depression (CMD) highlighted up to 500 m of MSC deposits made of a Bedded Unit (BU) and a thin salt layer (Maillard et al., 2014; Driussi et al., 2015). This BU has never been drilled and, therefore, lacks lithological and chronostratigraphic constraints. Two contrasting chronostratigraphic and lithological interpretations are proposed: Roveri et al. (2019b) ascribed these sediments to Stage 2 and 3 and suggested that only reworked evaporites and halite are present. By contrast, following the seismostratigraphic description of Maillard et al. (2014), Ochoa et al. (2015) and Raad et al. (2021) inferred the presence of Stage 1 gypsum also in the CMD.

Raad et al. (2021) made a step forward by disclosing a possible tripartition of the BU unit (Fig. 7f). In their seismostratigraphic framework, Raad et al. (2021) noticed that the uppermost evaporite-bearing unit (called BU3), ~120 m-thick in the CMD, has geometric, stratigraphic and facies analogies with the astronomically-tuned UG unit of the Caltanissetta Basin (Fig. 3a) that endorse its attribution to Stage 3. Similar to the UU in the deepest basins (see subsection 4.2), BU3 consists of up to 9 low- and medium-amplitude reflectors that are interpreted as alternating terrigenous and gypsum beds (Maillard et al., 2014; Raad et al., 2021). Reflectors are parallel and continuous in the more distal areas, while they appear more chaotic in the more proximal sectors (Raad et al., 2021). The base of BU3 coincides with the erosional top of the salt,

interpreted as created by salt exposure, dissolution and locally salt gliding towards the depocenter (Fig. 7f; Raad et al., 2021). By contrast, the top of BU3, which corresponds to the Miocene/Pliocene boundary, is largely flat without signs of erosion (Fig. 7f; Maillard et al., 2014; Raad et al., 2021). An irregular geometry is sometimes visible, but is likely to be related to deformation of the underlying salt (Fig. 7f; Raad et al., 2021).

4.5. Tyrrhenian Basin

The Tyrrhenian Basin to the east of Sardinia is a back-arc basin that opened by continental rifting and oceanic spreading related to the eastward migration of the Apennine subduction system from middle Miocene to Pliocene times (Gaullier et al., 2014; Lymer et al., 2018; Loreto et al., 2020 and references therein). Three main domains are traditionally identified (Lymer et al., 2018 and references therein): 1) the East Sardinia Basin, with present-day water depths between 200–2000 m consisting of a system of seamounts and depressions that do not contain MSC sediments (Lymer et al., 2018); 2) the Cornaglia Terrace (2000–3000 m deep), a wide, flat area with dispersed structural highs; 3) the Tyrrhenian Basin s.s., with water depths varying from 3000–3600 m. Whether the Tyrrhenian Basin acquired the present-day topography and hypsometry before the MSC (Lymer et al., 2018) or at least part of it (e.g. Eastern Sardinia margin, where Site 654 is located, and Northern Tyrrhenian) was much shallower (possibly comparable to the Caltanissetta Basin; Roveri et al., 2014b) and underwent extension and subsidence during the Messinian-Pliocene (e.g. Kastens and Mascle, 1990; Loreto et al., 2020) is still unresolved.

The MSC units in seismic profiles from the Tyrrhenian Basin (Fig. 7g) are very similar to the ones described in the Algero-Balearic and Liguro-Provençal basins (Fig. 7b–c; Gaullier et al., 2014; Lymer et al., 2018). ODP Sites 652, 653 and 654 confirmed the seismic-inferred lithological nature of UU as consisting, of gypsum-mudstone alternations (8 are counted at Site 654; Kastens et al., 1987; Borsetti et al., 1990; Roveri et al., 2014b). Intercalations of ripple-cross-laminated, fine-grained, azoic sandstones occur within the mudstone intervals in places (Cita et al., 1990; Iaccarino and Bossio, 1999). In some mudstone samples, the ostracod *Cyprideis* sp. (Site 654) and *Candona* sp. (DSDP Hole 974B) and the foraminifera *Ammonia beccarii* and *Ammonia tepida* have been found, indicating a shallow-water (< 50 m) brackish environment (see subsections 5.1 and 5.4; Cita et al., 1990; Iaccarino and Bossio, 1999). $^{87}\text{Sr}/^{86}\text{Sr}$ isotope ratios of UU gypsum and planktic foraminifera of the overlying Pliocene (Unit 1 at Site 654) show values much lower (from 0.708627 to 0.708745) and roughly equivalent (from 0.708935 to 0.709112) to coeval ocean water (~0.709020–30; McArthur et al., 2012), respectively (Müller et al., 1990; Müller and Mueller, 1991). Similar $^{87}\text{Sr}/^{86}\text{Sr}$ values were obtained from the gypsum cored at Site 652 (0.708626–0.708773; Müller and Mueller, 1991).

The Miocene/Pliocene boundary at DSDP Site 132 is placed above a cross-bedded sand rich in quartz, mica, pyrite, rounded fragments of gypsum and specimens of *Ammonia beccarii* and *Elphidium macellus* (Ryan et al., 1973). In the adjacent ODP Site 653 a similar sandstone is found slightly below the biostratigraphically-defined Messinian/Pliocene boundary and ~70 cm of grey mudstones with foraminifera and nanofossils of undisclosed provenance are squeezed in between (Cita et al., 1990). These mudstones also contain rare dwarf planktic foraminifera (*Globorotalia acostaensis*, *Orbulina universa*, and *Globigerina bulbosa*; Cita et al., 1990).

Overall, the uppermost Messinian sediments of the Tyrrhenian Basin are interpreted as having been deposited in lakes with periodic episodes of increased salinity and dilution under the strong influence of high energy rivers and, perhaps occasionally, of the Atlantic (Cita et al., 1990; Müller et al., 1990; Müller and Mueller, 1991).

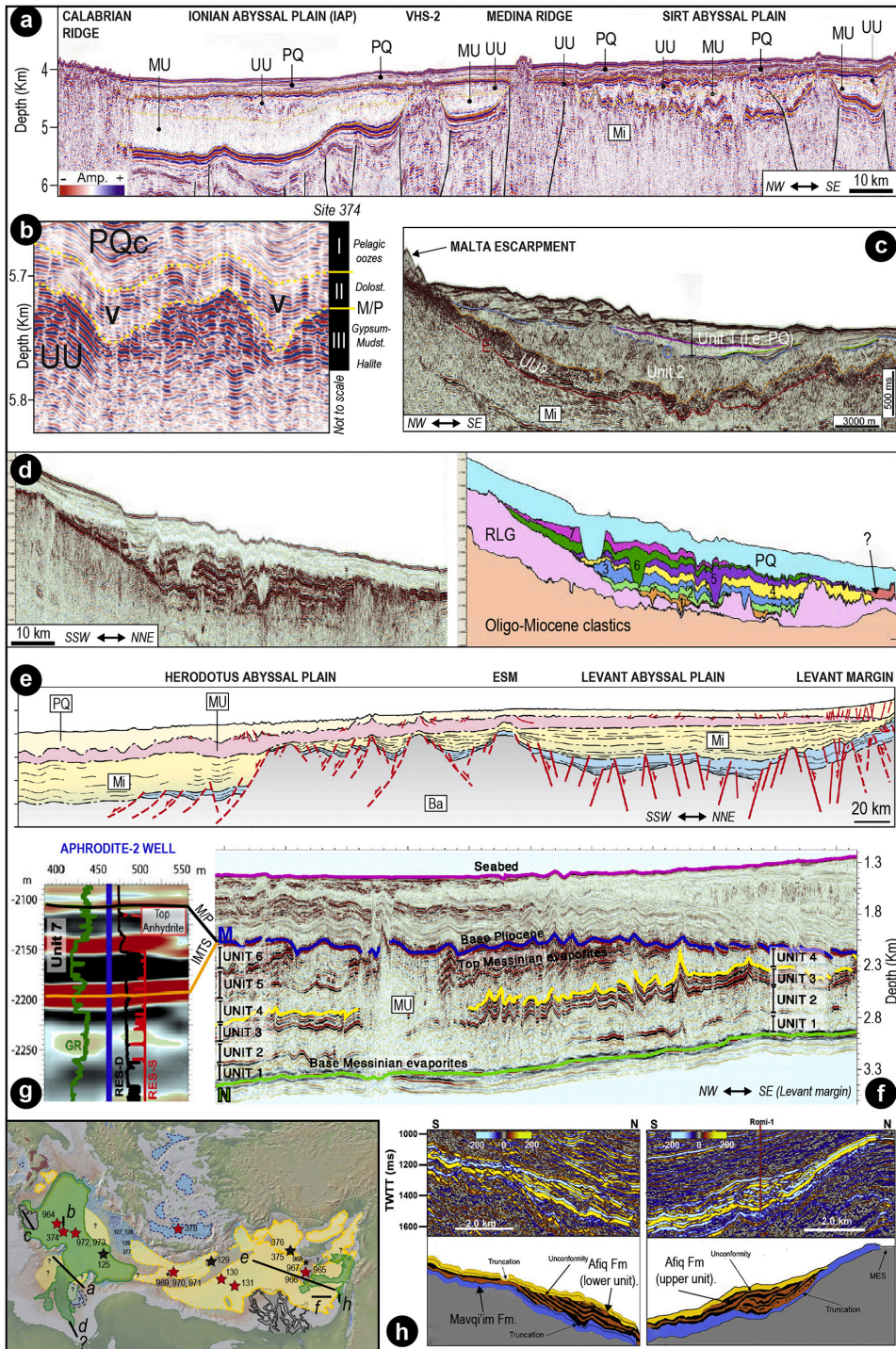
4.6. Ionian Basin

The deepest basin in the Mediterranean today is the Ionian Basin, with its lowest point at 5,267 meters. The so-called Ionian Abyssal Plain (IAP) is bounded on all sides by pre-MSC structural highs (Fig. 2a; Camerlenghi et al., 2019): the Malta Escarpment to the west; the Medina Escarpment to the south separating it from the Gulf of Sirt (Fig. 8a); the Gargano-Pelagosa and/or Otranto sill to the north dividing it from the Adriatic Foreland and, finally, an unnamed sill to the east, separating the IAP from the Levant Basin. Evidence from recent high-resolution seismic studies across the region have been used to support Stage 3 desiccation models (e.g. Hsü et al., 1978a, 1978b; Bowman, 2012; Micallef et al., 2018, 2019; Camerlenghi et al., 2019; Spatola et al., 2020).

4.6.1. Ionian Abyssal Plain

The typical “trilogy” of seismic units representing the MSC deposition in the Western Mediterranean is recognized also in the IAP by Gallais et al. (2018) and Mocnik et al. (2018). However, Camerlenghi et al. (2019) states the MSC sequence in the IAP is ~1,300 m-thick and composed of only two units (Fig. 8a). The lowermost 150–700 m-thick Mobile Unit (MU) is seismically transparent without discernible bedding and with diapiric structures, all features diagnostic of halite. By contrast, the 350–1,000 m-thick Upper Unit (UU) alternates highly reflective with acoustically transparent reflectors (Figs. 8a–b), similar to those described of the UU sequences of the Western Mediterranean (Figs. 7b–c). These are therefore assumed to represent gypsum-mudstone cycles (Camerlenghi et al., 2019). The uppermost 80 m of UU has been recovered from DSDP Site 374 (Hsü et al., 1978b), confirming the presence of gypsum (both primary cumulate and clastic; Lugli et al., 2015) alternating with mudstones (Unit III; Hsü et al., 1978b). These mudstones are largely barren of *in situ* fossils. However, the presence of some foraminifera and siliceous microfossils led Cita et al. (1978) and Hsü et al. (1978a) to suggest that sporadic marine incursions, possibly from the Indian Ocean, took place during Stage 3. Similar to Site 372, the basal part of Hole 374 intercepted one thin (~3.5 m) halite layer within the UU (Hsü et al., 1978b).

The UU and the overlying Zanclean (subunit PQc of Camerlenghi et al., 2019) reflectors are conformably folded throughout most of the abyssal plain, locally showing chaotic internal structure, irregular folding mimicking V-shaped incisions and truncations (Fig. 8b; Camerlenghi et al., 2019). These features are interpreted by Camerlenghi et al. (2019) as fluvial valleys carved in subaerially exposed evaporites by the Eso-Sahabi fluvial system, the closest fluvial drainage network to the area (see Micallef et al., 2018) that drained Libya in the late Miocene (Griffin, 2002) and has been traced across the Gulf of Sirt offshore (Sabato Ceraldi et al., 2010; Bowman, 2012). Several arguments counteract this interpretation: 1) the coherent, deformation, mostly of post-Messinian age, of both the UU and the lower Zanclean; 2) the absence of fluvial facies above the bottom of the “valleys”, which instead correspond to a mudstone interval that underwent post-depositional dolomitization (Unit II; see below; Fig. 8b); 3) the unlikelihood that the Eso-Sahabi fluvial system managed to bypass the Medina Ridge divide (Fig. 8a). Alternatively, the apparent incisions at the M/P boundary in the IAP may represent post-sedimentary folds resulting from post-Messinian tectonic and/or salt movements-driven deformation (e.g. Mocnik et al., 2018). At Site 374 the Miocene/Pliocene boundary has been recovered (Unit II), but its primary nature (likely a mudstone) is obscured by diagenesis (cementation by dolomite; Hsü et al., 1978b). A lithified dolostone at the (seismic) predicted depth of the M-Horizon is a characteristic of several sites. Sometimes this interval has been recovered (e.g. Sites 125 and 374; Ryan et al., 1973; Hsü et al., 1978b; Comas et al., 1996); at others the hard lithology is inferred by the torquing of the drill string (resistance to turning) accompanied by bouncing of the drill bit at the (e.g. Sites 122, 124, 125, 132, 133 and 134; Ryan et al., 1973). Dolomitization was (Hsü et al., 1973a, 1973b; Ryan et al., 1973) and still is (e.g. Ryan, 2009) largely considered a



(caption on next page)

Fig. 8. Seismic profiles from intermediate-deep Eastern Mediterranean basins containing MSC markers/units (see Fig. 7 for abbreviations). (a) High-resolution seismic line MS27 imaging the PQ and the uppermost MSC's UU and MU in the Ionian Abyssal Plain and Gulf of Sirt (modified from Camerlenghi et al., 2019). Note how the MSC units are thinner, more difficult to distinguish and more deformed in the Sirt Abyssal Plain than in the IAP. PQ, UU and MU all overlap the structural highs of the Medina Ridge and VHS-2 sill. (b) High-resolution imaging of the lower part of the Plio-Quaternary (PQc unit) and upper part of the Messinian (UU) in the IAP (Camerlenghi et al., 2019). The MSC-PQ boundary is a highly irregular surface, describing apparent V-shaped incisions (symbol V) of controversial origin (see subsection 4.6.1 for insights). Note the coherent deformation of PQc with the underlying MSC sequence and the absence of fluvial facies within the incisions (Unit II is made of lower Pliocene dolomitic marls recovered in Site 374 drilled nearby the seismic line; see text). (c) Multichannel seismic reflection profile MEM-07-203 running approximately parallel to the Malta Escarpment and showing the relationship between Unit 2 of Micallef et al. (2018) with the overlying and underlying Zanclean and Messinian sediments, respectively (modified from Spatola et al., 2020). (d) Uninterpreted (left) and interpreted (right) seismic profiles showing the cyclic and channelized nature of the uppermost Messinian observed in the offshore Sirt Basin (modified from Bowman, 2012). (e) Interpreted 2D regional WNW–ESE seismic profile crossing the continental shelf and offshore Levant Basin and the Herodotus Abyssal Plain (Jagger et al., 2020). Note the lateral continuity of the Messinian MU. (f) Seismic profile from the Levant Basin showing the 6 sub-units distinguished inside the MU as well as its lower (N-reflector) and upper (M-reflector) boundaries (modified from Gvirtzman et al., 2013). (g) High-resolution seismic reflection image with wireline logs from Aphrodite-2 well illustrating that M-reflector previously considered as top evaporitic sequence and M/P boundary here consists of a ~100-m-thick unit (i.e. Unit 7 of Gvirtzman et al., 2017) in which different layers are distinguished (modified from Gvirtzman et al., 2017). (h) Interpreted and uninterpreted seismic profiles imaging the Mavqi'im and Afq formations described in the canyons on the Levant continental margin (modified from Ben Moshe et al., 2020).

"diagnostic feature of tidal (sabkha) sediments" (Friedman, 1973, pp. 705). Its occurrence at locations with present-day water depth exceeding 2000 m was therefore considered strong evidence that the Mediterranean floor was subaerially exposed prior to the Zanclean marine replenishment (e.g. Ryan et al., 1973). It is, however, now widely accepted that dolomite precipitation is not exclusive of sabkha environments, but rather is a common process also in bottom sediments under a relatively deep water column (see Dela Pierre et al., 2012, 2014 and references therein). In the specific case of the offshore Mediterranean's M/P boundary on the Ionian Abyssal Plain, already in the '70s dolomitization was thought to have occurred after burial (Hsü et al., 1978b), a conclusion recently reinforced by McKenzie et al. (2017).

4.6.2. Malta Escarpment

At the foot of the Malta Escarpment, Micallef et al. (2018, 2019) and Spatola et al. (2020) amalgamated the MU and UU into one seismic unit, Unit 3, which is separated from the Plio-Quaternary marine sediments (Unit 1) by Unit 2, a chaotic transparent seismic package (Fig. 8c). Unit 2 has a maximum thickness of 760–860 m, a volume of 1430–1620 km³ and a wedge-shaped geometry that thins eastwards, disappearing before reaching the IAP (Micallef et al., 2018). Micallef et al. (2018) and Spatola et al. (2020) proposed a lithological/sedimentological interpretation of this chaotic body, suggesting it is composed of well-sorted sediments of the Pelagian Platform to the west of the Malta Escarpment, with coarser material at the mouth grading into more distal finer sediments. This chaotic body has recently been attributed to the Zanclean megaflood during its passage from the western to the eastern Mediterranean via a gateway located in south-eastern Sicily (Micallef et al., 2018, 2019; Spatola et al., 2020). Given the rapidity of the reflooding (≤ 2 years, Garcia-Castellanos et al., 2009, 2020), this interpretation implies rapid mass deposition. Other interpretations of this Unit 2 include being the result of extensive marine mass movement (Polonia et al., 2011), being folded UU (Butler et al., 2015) or being a complex unit built during lower sea level phases (Lofi et al., 2011a, 2011b).

4.6.3. Gulf of Sirt

The Gulf of Sirt (or Sirt embayment; Figs. 2a, 8a), the offshore extension of the Sirt Basin onshore Libya (Griffin, 2002 and references therein), is cross-cut by high-density seismic and well datasets as a result of oil potential of the region (Fiduk, 2009). However, only few studies have tackled the MSC (e.g. Hallett, 2002; Fiduk, 2009; Bowman, 2012).

In the Sirt embayment the MSC unit(s) is unevenly distributed in sub-basins controlled by a pre-existing topography, there is little distinction between the MU and UU, the overall thickness of the MSC unit(s) is lower and the degree of deformation is higher than in the adjacent IAP (Fig. 8a; Camerlenghi et al., 2019). The presence of halite in the Sirt embayment is debated, but most authors think it is absent (see Fiduk, 2009; Sabato Ceraldi et al., 2010; Lofi, 2018; Jagger et al., 2020; Fig. 2b). Bowman (2012) distinguishes seven seismic units within the

MSC-related sequence (Fig. 8d). On the basis of high-resolution 3D and 2D data, each seismic unit has been interpreted consisting of clastics filling erosional channels cutting up to 100 m deep and wide (Fig. 8d) and evaporites (gypsum and anhydrite) alternating with precessional cyclicity (Bowman, 2012). The presence of anhydrite in the topmost part of the sequence is confirmed by the B1 NC 35A well (Hallett, 2002). Sabato Ceraldi et al. (2010) and Bowman (2012) envisaged a three-step evolution of each unit: 1) evaporitic deposition during precession maxima in a dried out Sirt embayment; 2) erosion of the valleys during the arid-wet transition fed by the Eso-Sahabi paleofluvial system; 3) filling of the valleys with the fluvial sediments during the wet phase. Based on this chronostratigraphic interpretation, the evaporite cycles should be time equivalent to most of Stage 3, with the upper four seismic units reflecting the Lago-Mare phase (Fig. 1a).

4.7. Levant Basin

4.7.1. Abyssal plain

Old seismic data in the Levant Basin show an up to 2 km-thick, high velocity, acoustically transparent sequence bounded by the N-reflector at the base and the M-reflector at the top (Figs. 8e-f; Ryan, 1978; Netzeband et al., 2006). This sequence thickens and extends for tens of kilometers towards WNW and thins eastward along the continental margin (Fig. 8e), where the N and M-reflectors converge forming the condensed MSC section of the Mavqi'im and Afq formations (described in subsection 4.7.2; Gvirtzman et al., 2017; Manzi et al., 2018). High resolution 2D and 3D industrial seismic and well data from the southern Levant Basin revealed that this transparent sequence is largely made of pure halite with internal stratification picked out by diatomite, clay- and clastic-rich layers that allowed the division of the sequence into six sub-units, basinward-tilted and truncated at the top by the flat TES (Fig. 8f; Gvirtzman et al., 2013, 2015, 2017; Feng et al., 2016, 2017; Manzi et al., 2018; Meilijson et al., 2018, 2019). Clastic beds ~3 to 20 m-thick are abundant in the highly reflective and chaotic Unit 5 (i.e. Interbedded evaporites of Meilijson et al., 2019; MC2 unit of Feng et al., 2016; Figs. 3b, 4a), where they are interbedded with evaporites (probably halite with minor occurrences of anhydrite) varying in thickness from ~6 to 30 m (Manzi et al., 2018; Meilijson et al., 2019). Paleontological analyses of cuttings probably belonging to one of the clastic beds revealed the presence of a few mollusk fragments, ostracods, echinoid spines and a relatively rich assemblage of benthic and planktic foraminifera which Meilijson et al. (2019) concluded to be reworked. Based on seismic and well-log data, clastic intercalations (probably of clays, silts and sands) within a halite-dominated sequence are thought to persist in the overlying Unit 6, although they diminish in thickness and frequency (Gvirtzman et al., 2013; Feng et al., 2016; Meilijson et al., 2019). The expression of the end of the MSC is highly controversial. Until recently, the M-reflector of Ryan (1978) (later renamed as the Top Erosion Surface, TES; Lofi et al., 2011a, 2011b) bounding Unit 6 at the top was

considered to be the Miocene/Pliocene boundary (Fig. 8f; Ryan, 1978; Gvirtzman et al., 2013; Feng et al., 2016). Instead, Gvirtzman et al. (2017) showed that in higher resolution seismic data the M-reflector/ TES is a bundle of reflectors forming a distinct layer (Unit 7) overlying a truncation surface (i.e. Unit 6/7 boundary) that they re-labelled intra-Messinian truncation surface (IMTS; Fig. 8g) and ascribed to subaqueous dissolution rather than subaerial incision (e.g. Bertoni and Cartwright, 2007; Lofi et al., 2011a, 2011b; Kartveit et al., 2019; Madof et al., 2019). This conclusion was recently corroborated by the independent study of Kirkham et al. (2020). Analysis of gamma-ray and resistivity logs in three deep basin wells (Aphrodite-2, Myra-1, Sara-1; Fig. 2b) and correlation with the Or-South-1 well (located between the deep basin and the shelf) showed that Unit 7 maintains a constant thickness of ~100 m-thick and consists of clastic-rich anhydrite of undisclosed provenance. Meilijson et al. (2019)'s lithological interpretation of industrial boreholes slightly farther to the NE (Fig. 2b) give Unit 7 a significantly smaller thickness (5 m; Fig. 3b). Independent studies offshore Lebanon and Syria (Kartveit et al., 2019; Madof et al., 2019) describe a unit (Nahr Menashe complex) interpreted as a thicker (up to 300 m; Madof et al., 2019), but lateral equivalent of Gvirtzman et al. (2017)'s Unit 7. Based on its channelized morphology identified upslope near the Lebanese coast, Kartveit et al. (2019) and Madof et al. (2019) interpreted the Nahr Menashe Unit and the IMTS underneath as fluvial in origin, deposited/formed on a subaerially exposed floor of the Levant Basin. Six (Madof et al., 2019) to eight (Madof and Connell, 2018) lobes were identified and are proposed to have stacked with precessional frequency. The Nahr Menashe sequence has been correlated by the same authors with the Abu Madi Fm. located within the Messinian canyons offshore Egypt (Abdel Aal et al., 2000; Loncke et al., 2006; Abdel-Fattah, 2014), the Handere Formation offshore Turkey (Radeff et al., 2017) and with the Eosahabi deposits offshore Libya (Bowman, 2012). This interpretation implies a low base-level during the final stage of the MSC.

Manzi et al. (2018) and Meilijson et al. (2018, 2019) attempted astronomical dating of the abyssal MSC succession of the Levant Basin by integrating biostratigraphy on the pre-MU succession, reflector counting within the MU (only Meilijson et al., 2019) and well-log data (Fig. 3b). They achieved two contrasting results that gave rise to an outstanding controversy (Figs. 3b, 4a). Manzi et al. (2018) proposed that Stage 1 in the deep Levant is represented by a foraminifera-barren, evaporite-free shales interval labelled FBI (foraminifer barren interval) observed in the deep Aphrodite-2 well and in the more proximal Myra-1 well. In this interpretation Unit 7 comprises the whole of Stage 3 (with the IMTS corresponding to the Stage 2/3 transition) and all halite deposition took place in ~50 kyr estimated during Stage 2 of the MSC (Fig. 1a; Roveri et al., 2014a). By contrast, the FBI is not present in the Dolphin well targeted by Meilijson et al. (2019), which is located in an intermediate position between the Aphrodite-2 and Myra-1 wells studied by Manzi et al., 2018; Fig. 2b). Instead, in the Dolphin well a relatively open-marine, foraminifera-rich sequence extends below the (conformable) base of the MU, placed in correspondence to a ~2 to 5.5 m-thick anhydrite/shale (Unit 0; Manzi et al., 2018 and Meilijson et al., 2018, respectively). Astronomical tuning of the ~33 cycles counted in the MU in the Dolphin well, which are assumed to be precessional, results in the Main Halite body (i.e. Unit 0-4 of Gvirtzman et al., 2013 and Manzi et al., 2018) spanning MSC Stage 1 and 2, the Interbedded Evaporites/Unit 5 covering substage 3.1 and the Argillaceous Evaporites/Unit 6-7 to encompass the Lago-Mare phase (Figs. 3b, 4a). In this interpretation from Meilijson et al. (2019), halite deposition in the Levant Basin started in Stage 1 and persisted throughout the entire MSC, including Stage 3, during which more allocthonous material was delivered to the basin (Fig. 3b). Madof and Connell (2018) and Madof et al. (2019) also attempted an astronomical tuning of the Nahr Menashe Unit, concluding that it spans throughout substage 3.2 and part of substage 3.1. Feng et al. (2016) claim, however, that the impressive thickness of clastics found in the Levantine MU is more indicative of distinct short-term events (shorter than the precession cycle) associated with transport of

extraordinary power and magnitude.

Late Messinian sediments have also been recovered at several DSDP (129, 375, 376; Ryan et al., 1973; Hsü et al., 1978b) and ODP Sites (965, 967, 968; Emeis et al., 1996), but the assignment of the retrieved sediments to seismostratigraphic units is problematic. Nevertheless, they provide several key nuggets of precious information about the Stage 3 paleoenvironment:

- Sites 965 and 966, located roughly on the crest of the Eratosthenes Seamount, just south of Cyprus (Fig. 2b), recovered soil structures above the evaporites indicating exposure above sea level (Robertson, 1998a, 1998b; Maillard et al., 2011a; Reiche et al., 2016).
- ODP Sites 967 and 968, located at the base of the northern and southern slope of Eratosthenes Seamount (Fig. 2b), respectively, revealed the presence, within the MSC interval, of calcareous turbidites with Cyprus-derived clasts and clays containing *Ammonia tepida*, *Cyprideis pannonica* and *pulmonate gastropods* (Blanc-Valleron et al., 1998; Robertson, 1998a,b; Reiche et al., 2016).
- Abundant *Cyprideis pannonica* specimens were also recovered from DSDP Sites 375 and 376 drilled on the crest of the Florence Rise, west of Cyprus (Fig. 2b; Hsü et al., 1978b).
- Abundant, well-preserved *Ammonia* tests and *Cyprideis* specimens are also known from Site 129A (Fig. 2b), occurring with dwarf planktonic foraminifera (Ryan et al., 1973).

All the evidence listed above suggest that a base-level fall leading to subaerial exposure occurred at some point(s) during Stage 3 in the Eastern Mediterranean (Ryan, 2009). However, it must be kept in mind that both the Florence Rise and Eratosthenes Seamount are likely to have been much more elevated during the Messinian than they are today because of Pliocene-Quaternary subsidence related to the Cyprus subduction zone (Robertson, 1998a, 1998b; Maillard et al., 2011a; Reiche et al., 2016).

Sites 375 and 376 display several discrete layers of primary and clastic gypsum interbedded in the *Cyprideis*-rich mudstones (McCulloch and De Deckker, 1989; Lugli et al., 2015). This succession shares several similarities with sites drilled in the Western Mediterranean (e.g. ODP 654A) and Ionian Basin (DSDP 374), where they have been correlated with the seismic Upper Unit (see subsections 4.5 and 4.6). This may suggest that a Western Mediterranean-like gypsum-bearing UU was also locally deposited in the easternmost abyss of the Mediterranean (see Güneş et al., 2018).

4.7.2. Levant continental margin

Evaporitic and non-evaporitic deposits are buried beneath PQ deposits (Yafo Formation) along the Levant continental margin, where they are mostly preserved within canyons carved underwater in pre-Messinian time (Druckman et al., 1995; Lugli et al., 2013). Within the Afq canyon, Druckman et al. (1995) distinguished three formations in the Messinian sequence: the evaporitic Mavqi'im Formation, 115 m-thick and mostly composed of anhydrite in places interbedded with micritic limestones; the Be'eri Formation, comprising gypsum; the Afq Formation, varying in thickness from 30 to 90 m and consisting of conglomerates, sandstones and marls interpreted as representing fluvial and lacustrine-marsh environments (Druckman et al., 1995). The Afq Fm. is only present in the deepest portions of the canyon where it overlies the Mavqi'im Fm. By contrast, the Be'eri gypsum is only found along the canyon shoulders covered by the Pliocene, at elevations > 600 m with respect to the Mavqi'im Fm. Based on Sr values, Druckman et al. (1995) attributed the Mavqi'im Fm. to MSC Stage 1, the Be'eri Fm. to substage 3.1 and the Afq Fm. to the Lago-Mare phase. These authors also suggested that gypsum precipitation occurred under subaqueous conditions, with the water level ~600 m (i.e. the difference in altitude between the Mavqi'im and Be'eri fms.) higher during the deposition of the Be'eri Fm. Two base-level falls of approximately the same magnitude are thought to have occurred between the evaporitic phases and after

Mavqi'im deposition. A lowstand phase was therefore in force during Afiq deposition (Druckman et al., 1995).

However, combining stratigraphic, sedimentological and geochemical (Sr isotopes) considerations, Lugli et al. (2013) revealed the clastic nature of both the Mavqi'im and Be'eri evaporites and suggested the persistent drowning of the canyon(s), filled with turbidites (Lugli et al., 2013). Due to the presence of clastic evaporites, Gvirtzman et al. (2017) suggested that the Mavqi'im Formation is a condensed section encompassing MSC Stage 2 and early Stage 3, while the evaporite-free Afiq Formation represents the Lago-Mare phase.

Ben Moshe et al. (2020) ascribed (at least part of) the Afiq Fm. to the whole of Stage 3 as a wedge-shape clastic complex lying on top of the Mavqi'im Fm. and with the basal surface corresponding to the relative conformity of the MES developed landward, at the expense of the Mavqi'im Fm (Fig. 8h). Ben Moshe et al. (2020) distinguished a lower sub-unit composed of clastic gypsum and with fore-stepping and down-stepping internal geometry typical of progradational wedges, and an upper sub-unit containing anhydrite fragments and marls with Lago-Mare fauna (e.g. *Cyprideis torosa*; Rosenfeld, 1977) and with seismic characteristics typical of a transgressive systems tract. Incisions are reported throughout the Afiq Fm. at different depths, while erosional surfaces bound both sub-units (Ben Moshe et al., 2020). In particular, the surface capping the upper subunit and correlated to the M horizon or TES basinward (see subsection 4.7.1) shows dendritic drainage patterns of gullies and channels (Ben Moshe et al., 2020).

Ben Moshe et al. (2020) identify the variation of base level specifically during Stage 3 by analyzing the morphology of truncation surfaces bounding the Afiq Formation on the continental margin of the Levant Basin. This suggests high amplitude fluctuations of base-level in the order of one hundred meters, with development of subaerial erosion surfaces and the deposition of clastics and incision by fluvial drainage systems that occurred during the lowstand phases, while aggradational units (of unknown lithological nature) accumulated during the high-stand phases. According to their analysis, base level dropped down to a maximum 535 m during Afiq deposition (i.e. below the maximum 430 m estimated paleodepth of the Sicily Sill; Garcia-Castellanos et al., 2009), implying hydrological disconnection between the Eastern and Western basins at various times during Stage 3. A regression to 615-885 m is proposed to have occurred at the top of the Afiq Fm., pre-dating the abrupt refilling at the base of the Zanclean (e.g. Micallef et al., 2018, 2019; Garcia-Castellanos et al., 2020; Spatola et al., 2020).

4.8. Summary of the offshore Stage 3 record

Knowledge of the Stage 3 sequence offshore is mainly based on the integration of seismic interpretations and analysis of material recovered from fragmentary and unevenly distributed DSDP/ODP/industrial cores.

- MSC sediments are absent on the eroded continental shelves bordering the deep basins, except in the Messinian thalwegs and at their mouth. Here the PQ lies directly above the MES which, in turn, cuts through the pre-MSC deposits (Fig. 7e). A similar stratigraphic arrangement is found along the middle-upper slopes (Fig. 7d), although the presence of a thin, possibly incomplete UU in morphological depressions is sometimes postulated. Seamounts also lack MSC Stage 3 sediments and are strongly incised by the MES (Fig. 7g).
- The thick UU is widespread and roughly present everywhere in the abyssal plains from west of the Alborán volcanic arc to the eastern edge of the Ionian Basin (Fig. 2b). In the abyssal plains its seismic facies appears homogeneous, comprising parallel and relatively continuous high amplitude reflections (Figs. 7b-c). The UU pinches out towards the foot of continental slopes and seamounts (Figs. 7b, d-g), where it can be irregularly bedded or relatively well bedded (Lofi et al., 2011a, 2011b).

The uppermost part of the Bedded Units (defined in depressions physically disconnected from the abyssal plains and, therefore, from the UU; e.g. CMD and Corsica Basin; Maillard et al., 2014; Thinon et al., 2016; Raad et al., 2021) shows seismic features comparable to those of the UU.

- Drill Sites revealed that the reflections of relatively high amplitude in seismic profiles correspond to gypsum and mudstone alternations with sporadic intercalations of massive to cross-bedded sandstones. Some mudstone interbeds contain low-diversity assemblages of benthic organisms (ostracods, foraminifera and diatoms) indicative of shallow to neritic environments. Except for dwarfed forms of planktonic foraminifera and the monospecific nannofossil assemblages described by Castradori (1998), the rest of planktonic foraminifera and nannofossils are largely regarded as reworked.
- The deep Levant Basin contains a ~1.8-2.0 km-thick MU (Figs. 8e-f), consisting of 6 to 7 seismic units depending on the resolution of the seismic employed. In high resolution seismic data, the lateral equivalent of part of the UU is identified as a ~100-m-thick, clastic-rich, anhydrite layer (Unit 7 of Gvirtzman 1207) offshore Israel, thickening to 300 m offshore Lebanon (Nahr Menashe complex, Madof et al., 2019). The Levant Basin still has major controversies concerning the timing of halite deposition (~50 kyr vs ~550 kyr; Manzi et al., 2018 vs Meilijson et al., 2019), the origin of the clastic accumulations overlying the halite (fluvial vs subaqueous) and the presence or absence of gypsum-mudstone cycles.
- Apart from the halite flow-related deformation, the Miocene/Pliocene boundary (i.e. UU/PQ transition) is conformable in intermediate (e.g. Balearic Promontory) and deep (WAB, EAB, Algero-Balearic, Liguro-Provençal, Tyrrhenian, Ionian and Levant) depocenters, while it shows signs of erosion on the shelf domain and along the upper-middle continental slopes and seamounts. Clear arguments of floor exposure at the M/P boundary are absent in all drill sites but 978A.

5. The paleontological perspective

Paleontological data have been used to define and identify Stage 3 sediments, but have also been a source of profound contention over the interpretation of its paleoenvironmental and paleohydrological nature. Biotic groups impacted by the evolution of the gateways linking the Mediterranean with the Atlantic, Indian Ocean and Paratethys include marine species (e.g. foraminifera, calcareous nannofossils, fish) and brackish water-species (ostracods, fish, mollusks and dinocysts endemic or with affinity to species of the Paratethys region) that were unable to migrate when these corridors were closed, and terrestrial species (e.g. mammals) that, conversely, got across the gateway during periods of exposure (see Colombero et al., 2017; Booth-Rea et al., 2018; Mas et al., 2018b). Analysis of these faunal datasets provides key insights into likely gateway dimensions and the timing of their opening, restriction and closure (e.g. Palcu et al., 2017). Furthermore, they are a key constraint on the water sources likely to have been affecting the Mediterranean during MSC Stage 3.

5.1. Ostracods

Ostracods are by far the most prolific faunal group during Stage 3. Brackish species are known from both land sections and deep-sea cores across the whole Mediterranean (see Fig. 2b for sites and references; Fig. 9a). Two characteristic biofacies are commonly distinguished: Biofacies 1 (Bonaduce and Sgarrella, 1999) or *Cyprideis* assemblage (Iaccarino and Bossio, 1999) consists of a monospecific population of *Cyprideis* species or of an oligotypic population dominated by *Cyprideis* species alongside rare specimens of *Tyrrhenocythere ruggierii*, *Loxococoncha kochi*, *Loxococoncha muelleri* and *Caspiocypris alta*; Biofacies 2 (Bonaduce

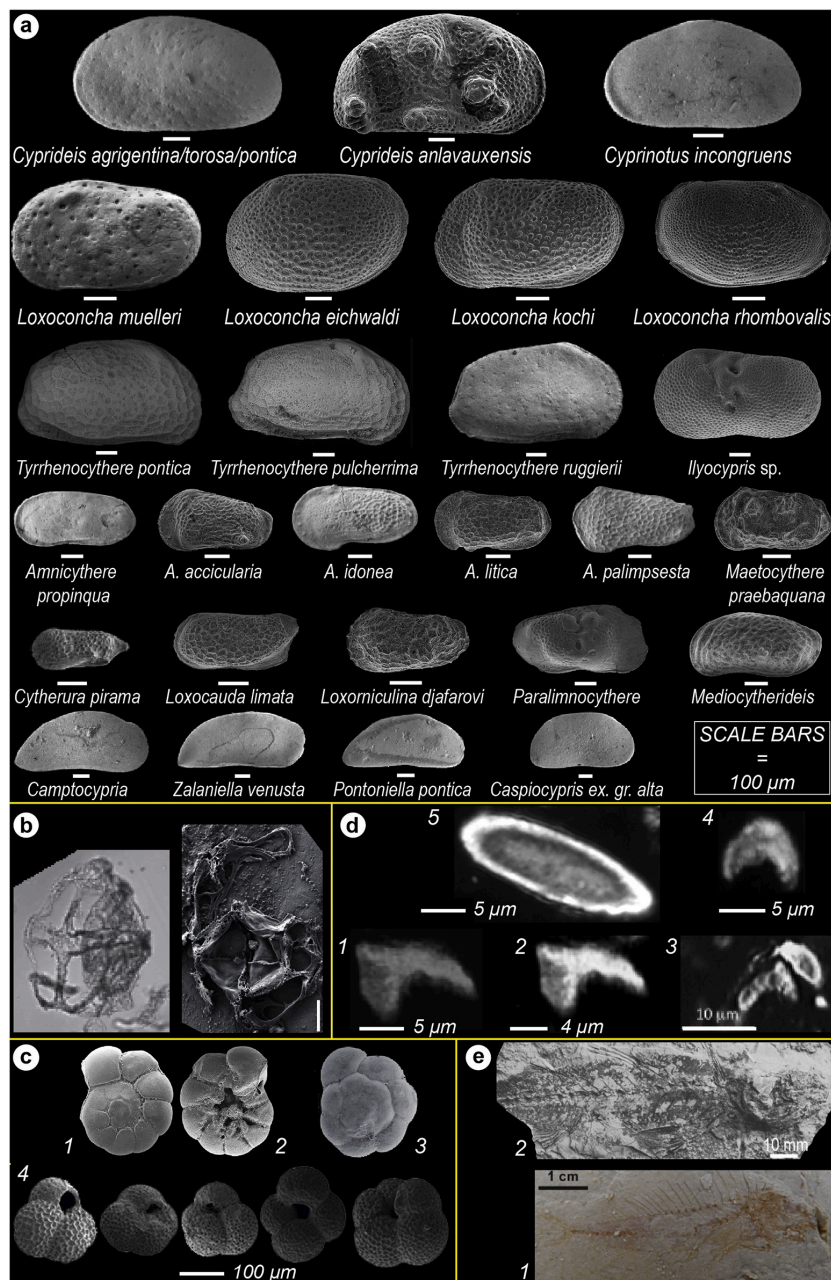


Fig. 9. Photomicrographs of the key micro- and macrofossils featuring Stage 3 sediments. (a) Scanning electron microscope (SEM) photographs of the more common Paratethyan ostracod species in substage 3.1 and 3.2 sediments (compiled from Stoica et al., 2016, Cosentino et al., 2018 and Sciuto et al., 2018). (b) Photomicrographs of the Paratethyan dinoflagellate cyst *Galeacysta etrusca* under the optical microscope (left) and SEM (right) (modified from Do Couto et al., 2014 and Grothe et al., 2018). Scale=20 μm . (c) SEM microphotographs of the euryhaline, shallow-water benthic foraminifera *Ammonia beccarii* (1-spiral side, 2-umbilical side) and *Ammonia tepida* (3-spiral side; Carnevale et al., 2019) and of the dwarf fauna of planktonic foraminifera from the Bajo Segura Basin (4; Corb  and Soria, 2016). (d) Photographs in polarized light (crossed nicols) of some specimens of *Ceratolithus acutus* (1-3) described in the Lago-Mare unit of Malaga (1-Do Couto et al., 2014), the Zorreras Mb. of Sorbas (2-Clauzon et al., 2015) and the Colombacci Fm. of the Northern Apennines (3-Popescu et al., 2017) and of destroyed (4) and intact (5) ascidian spicules of *Micrascidiscus* sp. (Golovina et al., 2019). Note that *C. acutus* specimens closely resemble ascidian spicules of *Micrascidiscus* sp., which may lead to misinterpretation of the *C. acutus* (see Golovina et al., 2019), and that pictures 1 and 2 are identical, despite they are attributed to samples taken from two different localities. (e) Articulated skeletons of marine fish from substage 3.1 mudstone horizons in Cyprus (1-*Aphanius crassicaudus*; Manzi et al., 2016a) and substage 3.2 deposits in Cava Serredi (2-*Mugil cf. cephalus*; Carnevale et al., 2018).

and Sgarrella, 1999) or *Loxocorniculina djafarovi* assemblage (Iaccarino and Bossio, 1999) has a higher species diversity characterized by the abundant occurrence of truly Paratethyan species belonging to the genera *Amnicythere*, *Loxoconcha*, *Loxocauda*, *Cytheromorpha*, *Cyprinotus* and *Tyrrhenocythere* (see species names in Fig. 9a). The number of species reported in the onshore sections is variable, ranging from a dozen (e.g. Caruso et al., 2020) to more than sixty (e.g. Gliozzi et al., 2007; Grossi et al., 2008). This variability is not explained, but it may result from the

application of different taxonomic concepts that resulted in the recognition of more or fewer species (Stoica et al., 2016) or from local environmental conditions that differed from basin to basin and resulted in different patterns of colonization.

Compared to the onshore domain, the ostracod fauna offshore is impoverished. Monospecific assemblages of *Cyprideis* sp. (Sites 372, 129A, 376, 654A, 967, 968; Ryan et al., 1973; Cita et al., 1990) or oligospecific assemblages dominated by *Cyprideis* and rare specimens of

Candona sp. (Hole 974B, Iaccarino and Bossio, 1999) and *L. muelleri* (Hole 978, Iaccarino and Bossio, 1999) are the more widely reported. Interestingly, these assemblages are always associated with *Ammonia* sp. tests and, in some cases, with other species of shallow-water, euryhaline benthic foraminifera (see subsection 5.4). Only in Hole 975, close to the M/P boundary is a more heterotypic ostracod assemblage found (*Euxinocythere praeabaquana*, *Amnicocythere idonea*, *Leptocythere limbata*, *Loxocorniculina djafarovi*, *Candona* sp., and *Cyprideis* sp.; Iaccarino and Bossio, 1999) and lacking of euryhaline benthic foraminifera. The likely cause of the widespread barrenness of ostracods in most of the offshore samples is perhaps because environmental conditions in the deep basins (depth and/or salinity) where not suitable to permit population by this benthic fauna (see below for the ecological requirements; e.g. Hsü et al., 1978b in reference to Site 374). Finally, one must bear in mind that studying these organisms require much more material (some hundreds of grams) than the quantity of core sediments usually processed (i.e. ~10 cm³; Iaccarino and Bossio, 1999).

The paleoecology (salinity and depth ranges) of Stage 3 ostracods has been based on both observations of few species that still live in the Caspian and Black seas today and have affinities with the Stage 3 species and on the interpretation of sedimentological, geochemical and mineralogical data of the surrounding sediments (see Gliozzi and Grossi, 2008 and Grossi et al., 2008 for insights). Biofacies 1 is thought to represent very shallow water environments (i.e. <15 m) with salinity fluctuating between mesohaline and hypersaline when the euryhaline *Cyprideis* is dominant. Instead, more stable oligo-mesohaline water is inferred when the other species are more abundant in Biofacies 1. The variegated Biofacies 2, on the other hand, is thought to represent somewhat deeper environments (up to 100 m) and less salty conditions (oligo-low mesohaline; Gliozzi and Grossi, 2008; Grossi et al., 2008; Caruso et al., 2020).

Some authors consider the time when the Paratethyan ostracods arrived in the Mediterranean to be well constrained (e.g. Roveri et al., 2008a; Grossi et al., 2011; Cosentino et al., 2018) by the scarce occurrence of the first Paratethyan immigrant *Loxocorniculina muelleri* 20 cm below the ash layer in the Colla di Votta section, which has a ²³⁸U-²⁰⁶Pb age of 5.5320±0.0074 Ma (Cosentino et al., 2013), and in the chaotic deposits of the Adana Basin, ascribed to Stage 2 (Paranda et al., 2013). Instead, the first appearance of *Loxocorniculina djafarovi* has been considered to coincide with the biofacies 1-2 shift and to have occurred Mediterranean-wide synchronously at 5.40 Ma (Roveri et al., 2008a; Grossi et al., 2011; Cosentino et al., 2013). Roveri et al. (2008a) also showed Biofacies 2 diversity as increasing linearly through the Lago-Mare phase, reaching its maximum diversity just beneath the Miocene/Pliocene boundary and before disappearing in the Pliocene. Following the claimed synchronicity of the FO of both *Loxocorniculina muelleri* and *Loxocorniculina djafarovi*, Roveri et al. (2008a) and Grossi et al. (2011) recognized one biozone in each biofacies: the *Loxocorniculina muelleri* Biozone, spanning from 5.59 to 5.40 Ma, and the *Loxocorniculina djafarovi* Biozone, whose boundaries correspond respectively to the first (5.40 Ma) and last occurrence (5.33 Ma) of *L. djafarovi* in the Mediterranean. This biozonation, erected by Grossi et al. (2011), is often used for dating incomplete successions (e.g. Vera Basin; Stoica et al., 2016; Caruso et al., 2020). However, the first appearance of a diversified ostracod assemblage (including *Loxocorniculina djafarovi*) occurred in already cycle 3 of the Sicilian Upper Gypsum at Eraclea Minoa (Fig. 3a; Grossi et al., 2015), which has an astronomical age of 5.45 Ma (Van der Laan et al., 2006) or 5.47 Ma (Manzi et al., 2009). Furthermore, the sudden appearance of Biofacies 2 and its linear, upward increase in diversity have not been recognized in localities like Nijar and Malaga, where biofacies 1 and 2 are found stacked in more than one lithological (possibly precession-controlled) cycle in the Lago-Mare succession (Bassetti et al., 2006; Guerra-Merchán et al., 2010). These findings argue that the appearance of Paratethyan ostracods in the Mediterranean may not have been synchronous, therefore casting serious doubts upon the biostratigraphic relevance of the Mediterranean ostracods.

Except for *Cyprideis* specimens, where species attribution is debated

(see discussion in Stoica et al., 2016), the affinity of all other ostracod species observed in Mediterranean Stage 3 sediments (Fig. 9a) with those of the Eastern Paratethys basins (i.e. Dacian, Euxinic and Caspian) has been demonstrated in several publications (e.g. Ruggieri, 1967; Gliozzi et al., 2007; Stoica et al., 2016; Sciuto et al., 2018). Only Bassetti et al. (2003, 2006) have questioned the Paratethyan affinity by suggesting that species from the Northern Apennines and Nijar Basin have ambiguous affinities with Paratethyan fauna as described in the mainly Russian literature from the '60-'70s. However, these differences between the late Messinian Mediterranean and Paratethyan ostracods resulted from misidentifications and/or a different use of species nomenclature (Stoica et al., 2016). Recently acquired knowledge of the Pontian assemblages of the Dacian, Euxinic and Caspian basins now permit to trace the provenance of Mediterranean Stage 3 ostracod species from the entire Black Sea region (Stoica et al., 2016) and, for a few species, from the Dacian (Stoica et al., 2013; Lazarev et al., 2020), Caspian (Van Baak et al., 2016) and North Aegean (see references in Krijgsman et al., 2020a) basins.

The means by which the ostracods travelled from the Paratethys to and across the Mediterranean during Stage 3 is as crucial for reconstructing the Stage 3 paleoenvironment as it is poorly addressed in onshore studies or overlooked in seismic and computational studies. Two migratory mechanisms have been suggested:

1) the aerial dispersion of ostracods through the migration of aquatic birds (Benson, 1978; Caruso et al., 2020); this hypothesis was proposed because, in a Mediterranean concluded to have been desiccated, it was the only possible migration mechanism.

2) direct aqueous migration by the ostracods themselves (which are planktonic in the larval stage) through the establishment of similar paleoenvironmental conditions; by this mechanism, the dispersion of Paratethyan ostracod fauna from right across the Mediterranean requires E-W intraconnection and a Mediterranean water-level high enough to reach the marginal basins (Gliozzi et al., 2007; Stoica et al., 2016; Sciuto et al., 2018; Sciuto and Baldanza, 2020).

Finally, Carnevale et al. (2006a, 2006b, 2008, 2018) recognized the Paratethyan affinity of the Mediterranean Stage 3 species but, in view of their occurrence with *in-situ* species of marine fish, they suggested that Stage 3 ostracods descended from a Paratethyan stock that migrated into the Mediterranean well before the MSC and survived the extreme salinity conditions of Stage 1 and 2 in marginal, fresher water refugia. In this scenario the brackish water ostracod assemblages found in Stage 3 have no paleoecological significance for Stage 3 paleoenvironment (Carnevale et al., 2006a, 2006b, 2008, 2018). However, there are two, unflagged problems with this hypothesis: 1) the Mediterranean-Central Paratethys connection through the Trans-Tethyan gateway in Slovenia already closed in the early Tortonian (Kováč et al., 2007; Sant et al., 2017; Palcu et al., 2017); 2) No Paratethyan ostracod species have been found in the Mediterranean before the MSC (see Gliozzi et al., 2007).

5.2. Dinoflagellate cysts

Dinoflagellate cysts (dinocysts) are the fossil remains of unicellular protists that live in the upper water column of many water bodies (e.g. Zonneveld et al., 2013; Mudie et al., 2017). They can be used as paleoenvironmental indicators and for biostratigraphy, providing the ages of speciation and extinction events, as well as supplying evidence of age diagnostic dispersals of characteristic taxa/assemblages. Influxes of these microorganisms into a basin may occur as the result of interconnection with another basin and dinocysts can therefore be useful indicators of the open gateways between adjacent basins and the resultant changes in conditions (e.g. Grothe et al., 2018). In the case of the MSC, presence of *in situ* marine and/or Paratethys dinocyst assemblages in a marginal basin are likely to indicate the presence of Atlantic and/or Eastern Paratethys water (respectively) in the Mediterranean and (relatively) high water level conditions (e.g. Pellen et al., 2017).

Palynological studies on the late Messinian Mediterranean dinocysts

record are rather scarce, confined to a limited number of outcrops (Malaga Basin, Do Couto et al., 2014; Northern Apennines, Bertini, 2006; Popescu et al., 2007; Iaccarino et al., 2008; Cosentino et al., 2012; Pellen et al., 2017; Caltanissetta Basin, Londeix et al., 2007) and deep wells (976B, 977A, 978A and 134B, Popescu et al., 2015). These studies describe substage 3.1 as being barren of dinocysts. By contrast, substage 3.2 dinocyst assemblages are diverse particularly a few meters/tens of meters below the Miocene/Pliocene boundary and show recurrent vertical variation in abundance between brackish, Paratethyan-type taxa and marine stenohaline and euryhaline species. Taxa with Paratethyan affinities are largely considered to be autochthonous by all aforementioned authors. The extent to which reworking may have affected the marine assemblages is more controversial and debated between none (in Malaga and in the Apennines; Popescu et al., 2007; Do Couto et al., 2014; Pellen et al., 2017), partial (in the uppermost part of the Sicilian Upper Gypsum; Londeix et al., 2007) and total (in the Apennines; e.g. Bertini, 2006; Iaccarino et al., 2008; Cosentino et al., 2012). Given the extent of the implications (i.e. re-establishment of a Mediterranean-Atlantic flow or connection earlier than the Zanclean; e.g. Pellen et al., 2017), this is an issue that will require further clarification.

A key dinocyst influencing our understanding of the late Miocene Lago-Mare phase is *Galeacysta etrusca* (Fig. 9b; see Bertini and Corradini, 1998; Popescu et al., 2009 and Grothe et al., 2018 for more insights). This species was originally described from sediments in the Mediterranean (Corradini and Biffi, 1988), but has since been discovered in much older deposits in Paratethys (Magyar et al., 1999a, 1999b). The earliest recorded occurrence of *Galeacysta etrusca* is in sediments from the Pannonian Basin dated at ~8 Ma (Magyar et al., 1999a, 1999b). It subsequently dispersed throughout Paratethys at ~6 Ma and was present in the Black Sea throughout the MSC interval (Grothe et al., 2014, 2018). Despite a Mediterranean-Eastern Paratethys connection that is thought to have been established at ~6.1 Ma (Krijgsman et al., 2010; Van Baak et al., 2016; Grothe et al., 2020), *G. etrusca* is not found in the Mediterranean during MSC Stages 1, 2 and 3.1 (5.97-5.42 Ma; Bertini, 2006; Londeix et al., 2007; Magyar et al., 2007; Iaccarino et al., 2008; Gennari et al., 2013) and is only reported in the uppermost part of the Lago-Mare phase, very close to the transition to the Pliocene (e.g. Bertini, 2006; Londeix et al., 2007; Popescu et al., 2007; Iaccarino et al., 2008; Cosentino et al., 2012; Pellen et al., 2017). This implies that *Galeacysta etrusca* may have migrated from Paratethys into the Mediterranean after 5.42 Ma or that environmental conditions in the Mediterranean and in its marginal basins were only suitable for this species (and more generally the whole dinocysts Paratethyan contingent) to proliferate in the uppermost Messinian. Several authors report multiple occurrences of *Galeacysta etrusca* within the Zanclean (e.g. Clauzon et al., 2005; Londeix et al., 2007; Popescu et al., 2007, 2015; Do Couto et al., 2014; Clauzon et al., 2015), but these interpretations are based on the use of an alternative stratigraphic model for the MSC sections (Fig. 4b; see Grothe et al., 2018 for details).

5.3. Diatoms

Among the fresh-brackish organisms found in Stage 3 sediments are also species of diatoms. To date (and to our knowledge), there are no onshore studies that have ever looked for these organisms. By contrast, two samples from DSDP Site 124 in the Algero-Balearic Basin (Fig. 2b) revealed the presence of littoral planktonic forms accompanied by brackish water, and even freshwater, euryhaline, benthonic, and epiphytic species in considerable numbers (Hajós, 1973). Diatoms of undisclosed paleoecological significance are also reported from the ~60 cm-thick mudstone bed between an anhydrite and halite bed found in the last core of Site 134 (Ryan et al., 1973). According to Hajós (1973) and Ryan (2009), the diatoms found in these drill cores attest to an extremely low salinity and a base level in the Balearic and Valencia basins below wave action. Further study of these indicative species and a wider distribution is required to apply this interpretation more

generally.

5.4. Foraminifera

A reasonably diverse benthic and planktic foraminiferal assemblage containing no age-diagnostic taxa have been found co-occurring with the brackish Paratethyan fauna in both the onshore and offshore record throughout the Mediterranean (Fig. 2b for localities and references).

The benthic foraminifera assemblage is dominated by euryhaline representatives of the genus *Ammonia*, which today dwell in marginal marine (lagoons, estuaries, fjords and deltas) and lacustrine environments at depths < 50 m and tolerate salinities of up to 50‰ (Milker and Schmiedl, 2012; Consorti et al., 2020). *Ammonia tepida* and *Ammonia beccari* (Fig. 9c) are by far the most abundant species in both onshore (see Fig. 2b for localities and references) and offshore (e.g. Site 968A, Blanc-Valleron et al., 1998; Sites 375, 376, 965-968, Orszag-Sperber, 2006) localities, where they co-occur with ostracods belonging to Biofacies 1. Other commonly occurring benthic euryhaline taxa are *Elphidium* sp., *Criboelphidium excavatum*, *Haynesina* sp., *Nonion* sp., *Quinqueloculina* sp., *Discorbis* sp. and *Trichohyalus* sp., *Brizalina dentelata*, *Bulimina echinate* and *Bolivina* spp. (Ryan et al., 1973; Hsü et al., 1978a, 1978b; Rouchy et al., 2001, 2003, 2007; Iaccarino et al., 2008; Caruso et al., 2020). These species are frequently mixed with poorly preserved and older in age bathyal species (e.g. Caruso et al., 2020).

Planktic foraminifera are represented both by species whose last occurrence pre-dates the MSC (e.g. *Praeorbulina* spp., *Paragloborotalia partimlabiata*, *P. siakensis*, *Neogloboquadra atlantica praeatlantica*, *Globigerinoides subquadratus*, *Globorotalia saheliana*, *Globorotalia conomiozea*, *Acarina* sp., *Hedbergella* sp.) and by taxa with extended biostratigraphic ranges (e.g. *Sphaeroidinellopsis seminulina*, *Turborotalia quinqueloba*, *Globorotalia miotumida*, *Globoturborotalita decoraperta*, *Neogloboquadra acostaensis*, *Neogloboquadra* spp., *Orbulina universa*, *Globigerinoides trilobus*, *Globigerinoides obliquus*, *Globorotalia scitula*, *Globigerina bulloides*, *G. Mediterranea* and *G. humerosa*; see Fig. 2b for references).

The mixing of foraminifera species with different ecological and salinity requirements and the widespread agreement that the brackish Paratethyan fauna are autochthonous (see subsection 5.1) has always complicated the interpretation of the origin of the foraminiferal assemblages. Among the benthic species, *Ammonia* taxa and the other benthic euryhaline taxa are generally considered autochthonous because they are typically well-preserved and their ecological and salinity requirements could be compatible with those of the Paratethyan ostracods.

The habitat of these benthic foraminifera today in environments both influenced by and disconnected from the open ocean indicates that the Stage 3 sediments in which they occur were deposited in a shallow-water environment subject to salinity fluctuations (Caruso et al., 2020 and references therein), but they do not provide insights into the water provenance. By contrast, the poor preservation, older age and low diversity of the bathyal taxa strongly suggest that these species are reworked (Bassetti et al., 2006; Iaccarino et al., 2008; Caruso et al., 2020). Their mode of life is also incompatible with the shallower water elements of the faunal assemblage. The planktic species which went extinct before the MSC are also undoubtedly reworked (Iaccarino et al., 2008; Caruso et al., 2020). It is more challenging to discriminate between *in situ* and reworked specimens of the long range Neogene taxa. Most of them are considered to be reworked because of their scarcity, their occurrence with *in situ* brackish organisms and their poor preservation (e.g. Iaccarino et al., 2008; Caruso et al., 2020). A more complex controversy surrounds the long-range dwarf specimens (Fig. 9c) occurring in onshore substage 3.1 (di Tetto Fm. in the Trave section; Iaccarino et al., 2008) and Lago-Mare sediments (Upper Mb. of the Nijar Feos Fm., Fortuin and Krijgsman, 2003; Aguirre and Sánchez-Almazo, 2004; Bassetti et al., 2006; Sorbas Basin, Roveri et al., 2019a; Bajo Segura Basin, Corbí and Soria, 2016; Colombacci Fm. in Northern Apennines localities, Casati et al., 1976; Colalongo et al., 1976; Rio and Negri, 1988;

Popescu et al., 2007; Cyprus, Rouchy et al., 2001) and in some offshore localities (e.g. Sites 124, 125, 129A, 132, 134, 372, 376, 653, 974B, 975, 978; Cita, 1973; Cita et al., 1978; Kastens et al., 1987; Cita et al., 1990; Iaccarino and Bossio, 1999). This fauna is variably interpreted as:

1) reworked and size-sorted during transport, therefore lacking any paleoenvironmental significance (e.g. Kastens et al., 1987; Iaccarino and Bossio, 1999; Fortuin and Krijgsman, 2003; Bassetti et al., 2006);

2) *in situ* and indicating normal marine conditions (Aguirre and Sánchez-Almazo, 2004; Braga et al., 2006) or temporary Atlantic incursions (Rouchy et al., 2001);

3) *in situ* and indicative of high-stress environments (Keller and Abramovich, 2009), such as restricted and/or diluted marine environments (Corbó and Soria, 2016; Corbó et al., 2016, 2020). However, the paleoecological significance of dwarfism in foraminifer tests is not well understood and, given its potential implications for the Lago-Mare environment, it needs to be explored in greater detail.

5.5. Calcareous nannofossils and the *C. acutus conundrum*

Calcareous nannofossils are the fossil remains of coccolithophores, single-celled marine algae which dwell in the eutrophic and photic zone of the ocean (e.g. Ziveri et al., 2004). The potential recognition of marine calcareous nannofossils in marginal Stage 3 deposits would therefore have implications for the Mediterranean base-level and the hydrological riddle of MSC Stage 3. However, like foraminifera and dinocysts, the *in situ* versus reworking issue also impacts the nannoflora.

MSC Stage 3 is crossed by three important nannofossil bio-events astronomically calibrated in the ocean record: the top of *Discoaster quinqueramus* at 5.537 Ma, the base of *Ceratolithus acutus* at 5.36 Ma and the top of *Triquetrorhabdulus rugosus* at 5.231 Ma (Backman et al., 2012; Agnini et al., 2017). Most of the (few) studies that addressed the nannoflora component of Stage 3 deposits did not report taxa belonging to the biozones defined by these bio-events, but only taxa of Cenozoic and Cretaceous age, clearly physically reworked (e.g. Sites 132, 134, 653, 654A, 967A, 969B, Ryan et al., 1973; Hsü et al., 1978b; Müller et al., 1990; Castradori, 1998; Piedmont Basin, Trenkwalder et al., 2008; Violanti et al., 2009; Trave, Fonte dei Pulcini and Stinget sections and Mondragone well in the Apennines, Cosentino et al., 2006, 2012, 2018; Iaccarino et al., 2008). An exception is the nannoflora observed in the uppermost Messinian sediments at Sites 978A, 975B and 967A (Levant Basin; Fig. 2b). Here, among the plethora of reworked and long-ranging Neogene taxa, Castradori (1998) reported the anomalous abundance of *Sphenolithus* spp (mostly *Sphenolithus gr abies/moriformis*). Although the assemblage points to the absence of a primary marine signature, the unlikely possibility that reworking and/or sorting lies behind the observed peak of *Sphenolithus* spp. led Castradori (1998) to conclude that at least one incursion of marine water occurred during the (uppermost) Lago-Mare.

By contrast, some authors (i.e. Popescu et al., 2007, 2015; Do Couto et al., 2014; Clauzon et al., 2015; Pellen et al., 2017) described the nannofossil assemblage the Lago-Mare LM Unit in Malaga, the Zorreras Member in Sorbas, the uppermost di Tetto/Colombacci Fm. in some Apenninic localities and offshore in the Alborán Basin as having good preservation and showing no erratic fluctuations, all characteristics that led to their interpretation as autochthonous and to the conclusion that these sediments were deposited in a Mediterranean already replenished of Atlantic water (Fig. 4b). In addition, these authors reported the low abundance, but continuous presence of the biostratigraphic markers for the Zanlean *Triquetrorhabdulus rugosus* and *Ceratolithus acutus* (Fig. 9d) below the formally defined Miocene/Pliocene boundary (Van Couvering et al., 2000) in several onshore and offshore Mediterranean (as well as Paratethyan) localities (see Popescu et al., 2017 for details and a complete list of finding locations).

Such findings (especially that of *C. acutus*) are in sharp disagreement with most of the existing literature and have resulted in an important debate amongst the MSC community (e.g. Popescu et al., 2007, 2008 vs

Roveri et al., 2008c and Stoica et al., 2016 vs Popescu et al., 2017), not only for their paleoenvironmental implications (i.e. presence of Atlantic water in the Mediterranean), but also for the chronostratigraphic repercussions (Fig. 4b). The chronostratigraphic value of *C. acutus* lies in its short temporal distribution straddling the M/P boundary (astrochronologically calibrated at 5.332 Ma; Van Couvering et al., 2000; Lourens et al., 2004). However, the corresponding biozone is established in oceanic areas (Zone CNPL1: 5.36-5.05 Ma; Backman et al., 2012; Agnini et al., 2017) and is considered not applicable to the Mediterranean region during the MSC due to the harsh physicochemical conditions that are unsuitable for marine biota (Di Stefano and Sturiale, 2010). The interpretation of these nannofossil assemblages in the westernmost areas of the Mediterranean has been countered with several observations: (1) the observation of these age-diagnostic taxa is often not replicated by other studies (e.g. Roveri et al., 2008a; Van Baak et al., 2015; Krijgsman et al., 2020b); (2) *Ceratolithus acutus* is very rare also in fully marine open-ocean sediments (e.g. Di Stefano and Sturiale, 2010); (3) despite being rare in the late Messinian Mediterranean, this species has never been documented together with other long-range taxa, generally predominant in the assemblage, in Stage 3 deposits (see discussion in Krijgsman et al., 2020b). Recently, Golovina et al. (2019) showed that the morphology and size of *C. acutus* overlaps with the shape and dimensions of destroyed ascidian spicules (i.e. calcareous elements produced by benthic tunicates; Fig. 9d), providing an explanation for erroneous identification of *C. acutus* in the Black Sea Basin (Golovina et al., 2019) and perhaps in the western Mediterranean Lago-Mare sediments as well.

5.6. Fish

Fossil fish remains provide information about salinity and depth and have been used to contradict the brackish nature of the Lago-Mare deposits by Carnevale et al. (2006a, 2006b, 2008, 2018) and Grunert et al. (2016). Euryhaline fish species inhabit marine to brackish environments and dominate settings with strong salinity variations while stenohaline fish have specific salinity requirements (marine, brackish, or freshwater) and cannot survive under different conditions. Demersal fish (i.e. those living in or immediately above the sea floor) have specific depth requirements, whereas pelagic fish occupy the water column within a wide range of depth variable from species to species. Fossil fish remains are found either as articulated or disarticulated skeletal parts, including teeth and otoliths, which are identified to the species level. Articulated fish skeletons typically indicate autochthonous deposition because of the difficulty in reworking and transporting intact skeletons. Otoliths and fish teeth are much more likely to be transported.

Otoliths and rare articulated skeletons (Fig. 9e) of marine and Paratethyan species have been reported from Stage 3 deposits, but commonly huge volumes of sediment are required to find even quite small numbers of these fossils (e.g. 20 tons from Moncucco, 6 tons from Cava Serredi, 700 kg from Capanne di Bronzo; Schwarzshans et al., 2020), much more than what is expected for normal marine deposits (i.e. < 30 kg; Agiadi et al., 2017; Karakitsios et al., 2017b).

Substage 3.1 sediments contain articulated skeletons (Fig. 9e) of the marine fish species *Lampanyctus licatae* and *Mauroliscus muelleri*, and the shallow water, euryhaline species *Aphanius crassicaudus* in the Lower Feos Member in the Nijar Basin (de la Chapelle and Gaudant, 1987) and the marls of the first UG cycle in the Polemi Basin (Manzi et al., 2016a; Fig. 3a). Cava Serredi (Tuscany), Verduno and Moncucco (Piedmont) are the only other localities in which fish remains (only otoliths) in (claimed) substage 3.1 sediments are known (Carnevale et al., 2006a, 2008, 2018; Grunert et al., 2016).

The more diverse and abundant ichthyofaunal record occurs in substage 3.2 in a few marginal sections on the Italian peninsula (Ciabot Cagna in the Piedmont Basin; Cava Serredi and Podere Torricella in Tuscany; Capanne di Bronzo, La Vicenne and Ca' Ciuccio in thrust-top basins of the Northern and Central Apennines). The Lago-Mare fish

remains mainly comprise otoliths of both euryhaline and stenohaline taxa indicative of marine, brackish, and freshwater habitats (Carnevale et al., 2018). Three articulated skeletons of the euryhaline marine taxa *Mugil cf. cephalus* (Fig. 9e), the marine Indo-Pacific species *Spratelloides gracilis* and of *Gobius* sp. have been identified at Cava Serredi in a horizon < 1 m below the Miocene/Pliocene boundary (Carnevale et al., 2006b). The dominant stenohaline families in these assemblages are Gobiidae, a family of demersal fish occupying shallow-water marine, brackish and freshwater environments, and Myctophidae, which are marine mesopelagic fish that live below 200 m depth during the day, but feed at night in surface waters. A recent review of the Tortonian-Zanclean Gobiidae of the Mediterranean (Schwarzahns et al., 2020) showed that the otoliths of this family, described by Carnevale et al. (2006a, 2008, 2018) and Grunert et al. (2016) as belonging to marine Atlantic species, instead belong to brackish and freshwater species of Paratethyan affinity inhabiting sheltered prodelta environments. In fact, no normal marine demersal taxa were recognized in these assemblages by Schwarzahns et al. (2020). As for the Myctophidae, the vast majority of the taxa belonging to this family were recovered in Moncucco and Verduno from alluvial plain silty mudstones along with terrestrial mammals (Dela Pierre et al., 2011; Colombo et al., 2017 and references therein), pointing to a physically reworked origin. When $^{87}\text{Sr}/^{86}\text{Sr}$ isotope ratios are measured (Carnevale et al., 2008; Grunert et al., 2016), the resulting Sr-based age of the otoliths is > 7 Ma, therefore further arguing against their in-situ origin. Since the good preservation of the otoliths suggests they did not suffer physical reworking (Carnevale et al., 2006a, 2006b, 2008, 2018; Grunert et al., 2016), predators foraging in open marine settings and migrating to marginal environments are proposed as a way out of the enigma (Carnevale et al., 2008, 2018; Grunert et al., 2016; Colombo et al., 2017). However, Carnevale et al. (2006a) also rule out that so well preserved otoliths may have suffered post-mortem transport and action of the digestive acids in the stomach of predators. Rare findings of Myctophidae from Ciabot Cagna (3 species), Cava Serredi (1 species), Capanne di Bronzo (1 species) and Podere Torricella (6 species) (Carnevale et al., 2018) are all from sections where the host sediments have not been studied in sufficient detail to be clear about the *in situ* or reworked nature of the fossil assemblage. This lack of sedimentological uncertainty also extends to the stratigraphic position of many samples, because a stratigraphic log is provided for only a few sections (i.e. Ca' Ciuccio, Cava Serredi and Moncucco; Carnevale et al., 2006a, 2006b). What this stratigraphic information suggests is that euryhaline fish taxa are widespread throughout substage 3.2, whereas strictly Myctophidae, which are an oceanic, marine stenohaline species, only occur very close to the base of the Pliocene, plausibly corresponding to the uppermost lithological cycle in substage 3.2 (~5.35–5.33 Ma; Carnevale et al., 2018).

5.7. Summary of the Stage 3 paleontological record

The aquatic fossil record of MSC Stage 3 indicates that substage 3.1 in onshore sections is mostly barren, while diverse assemblages characterize substage 3.2 deposits. By contrast, the deep record as a whole contains relatively few, low diversity assemblages. This might be as a consequence either of the limited sample locations recovered from the offshore areas (see Fig. 2b) or because the environmental conditions in the intermediate-deep basins were less favorable for sustaining the life forms typical of the onshore domain. Nevertheless, the assemblages that are found in both marginal and deep locations comprise mixed brackish and marine species.

Brackish species are mostly represented by ostracods and dinocysts (and mollusks here not addressed because poorly studied; see Esu, 2007 and Guerra-Merchán et al., 2010). Prominent is the affinity of these late Messinian Mediterranean brackish species with the same species that were simultaneously dwelling in the Eastern Paratethyan basins (Dacian, Euxinic and Caspian) and in the North Aegean. Since these organisms were not present in the Mediterranean at any time before the

MSC, they are considered, with a broad consensus, as *in situ*. This conclusion is further corroborated by the mixing of adult and juvenile forms in the ostracod assemblages and by the good preservation of the specimens, which do not show typical evidence of physical reworking like abrasion, dissolution, or fragmentation. Still problematic is the time of their arrival in the Mediterranean and their likelihood as biostratigraphic tool. From our review it seems more likely that truly Paratethyan species of ostracods entered the Mediterranean already during substage 3.1, when they colonized intermediate-deep settings, while they entered the marginal basins at different times during substage 3.2. As for dinocysts, characteristic is their occurrence only in the uppermost Messinian. However, it must be noted that samples from the substage 3.1 interval are rarely processed for dinocysts, especially in age model-equipped sections (Fig. 3a). The route followed by the Paratethyan immigrants is equally contested and important for paleoenvironmental and paleohydrological interpretations. In view of a desiccated Mediterranean, their migration can only have taken place passively by means of aquatic migratory birds. Conversely, the homogeneity of the ostracod assemblages throughout the Mediterranean marginal basins is more indicative of the presence of a water body fed by Eastern Paratethys and connecting all Mediterranean subbasins, therefore implying relatively high water-level conditions (at least at times when ostracod-bearing sediments deposited; see Andreetto et al., 2021).

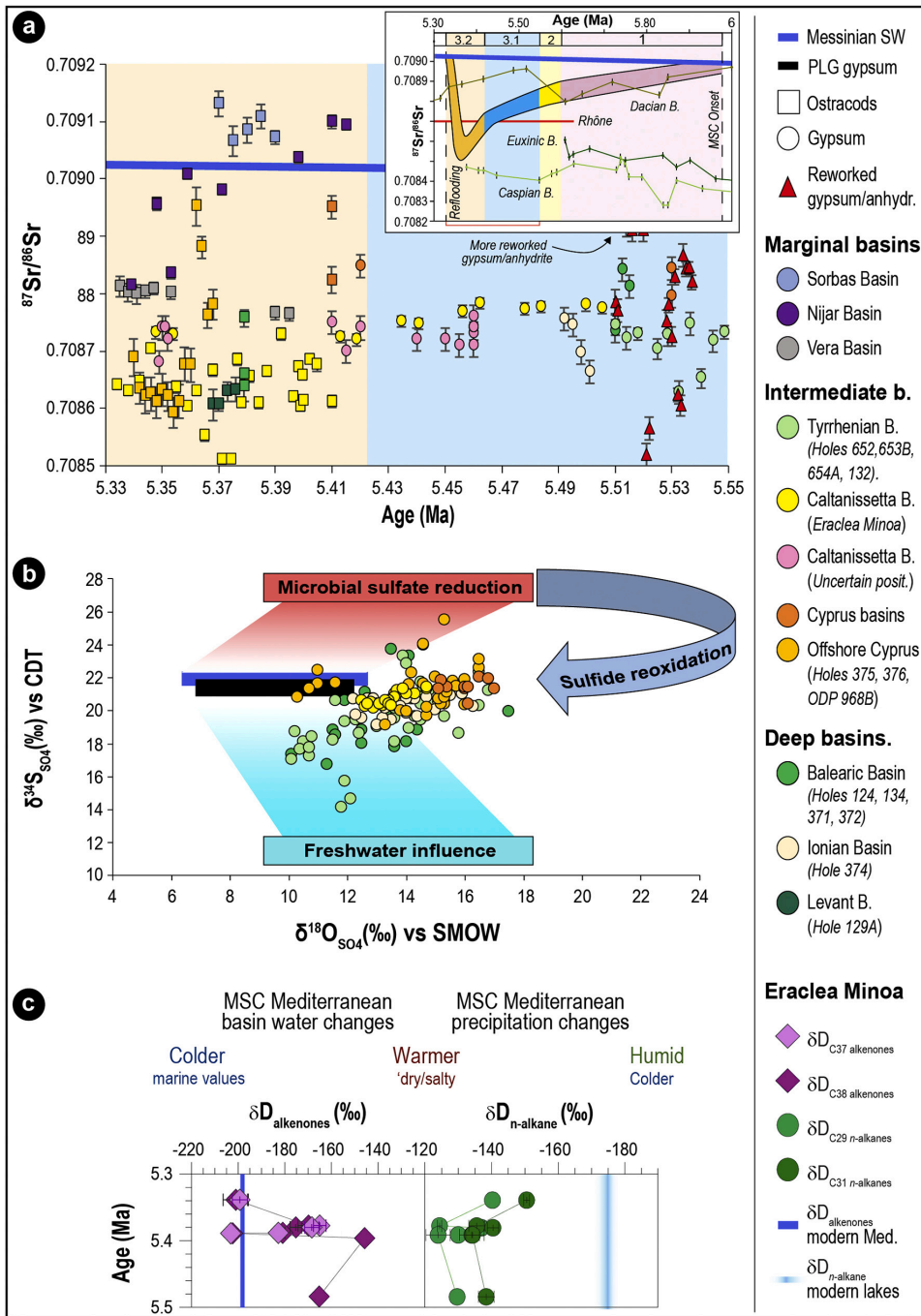
Marine assemblages are composed by foraminifera, nannofossils, dinocysts and calcareous nannofossils. Their reworked or *in situ* nature is in many cases contested but critical for paleoenvironmental interpretation. The picture that emerges from our review is that an open marine signature is questionable in the foraminifera, nannofossils, dinocyst and fish records, as well as in other biotic groups (e.g. corals, echinoids and mammals) here not tackled (and for which we refer the reader to Dominici et al., 2018 and Carnevale et al., 2019). All marine representatives of the above mentioned categories were reintroduced into the Mediterranean only at the beginning of the Pliocene and at the expense of the Paratethys species that, instead, disappeared. Collectively, these observations lead us to conclude that the marine model as conceived by Carnevale et al. (2006a, 2006b, 2008, 2018) and Grunert et al. (2016) has no foundation and therefore will not be further discussed.

6. The geochemical perspective

Variations in the water sources draining into the Mediterranean are expected to be reflected also in (geo)chemical properties of the paleo-depositional environments. Important information about the nature of the connectivity framework of the Mediterranean can be gained by interpreting geochemical signals that respond to the presence or absence of an exchange with a chemically-unique water body. Four main geochemical proxies have been applied so far to MSC Stage 3 sedimentary and paleontological records. These includes both radiogenic (Sr isotope ratios) and stable isotopes (sulfate and oxygen) measured on fossils and minerals and hydrogen isotopes on molecular biomarkers. This section summarizes the dataset available for geochemical proxies (Fig. 10; Supplementary material 1) and its interpretation(s) for MSC Stage 3.

6.1. Strontium isotope ratios ($^{87}\text{Sr}/^{86}\text{Sr}$)

The available strontium isotope data for Stage 3 (Fig. 10a; Supplementary material 1) derive from measurements on both Ca-bearing fossils (ostracod valves, mollusk shells, fish otoliths; Fig. 9a) and minerals (calcite and gypsum), where Sr^{2+} dissolved in an aqueous solution substitutes Ca atoms due to their similar ionic radius (e.g. Hajj et al., 2017). Here we screen the available dataset and discuss only results that (1) reflect the original primary isotopic signal, i.e. the isotopic signal of the fluid at time of shell calcification or mineral precipitation, and (2) for which timing of mineral precipitation can be constrained. This screening excludes bulk carbonate samples (e.g. *Colombacci* limestones;



(caption on next page)

Fig. 10. Isotopic record of MSC Stage 3 for the Mediterranean Basin. (a) Compilation of MSC Stage 3 $^{87}\text{Sr}/^{86}\text{Sr}$ isotope data sourced from ostracod valves and gypsum crystals (see Supplementary material 1 and subsection 6.1 for references). Data are plotted with the global $^{87}\text{Sr}/^{86}\text{Sr}$ seawater curve (McArthur et al., 2012). Error bars indicate analytical error, which is so small in some cases that no error bars are visible at this scale. To not complicate the figure, horizontal error bars have not been added for the sections/cores provided of a chronostratigraphic framework and for which age uncertainties are present (i.e. all but Nijar and Vera basins, Eraclea Minoa and onshore Cyprus; see Fig. 3). Note that none of the $^{87}\text{Sr}/^{86}\text{Sr}$ isotope ratios but one from Nijar plot on the ocean curve. In the inset is shown the Mediterranean Sr record for the entire MSC as well as the time-equivalent Eastern Paratethys record (modified after Andreetto et al., 2021). (b) Plot of $\delta^{34}\text{S}_{\text{SO}_4}$ and $\delta^{18}\text{O}_{\text{SO}_4}$ in Stage 3 gypsum and anhydrite beds from onshore and offshore localities (see Supplementary material 1 and subsection 6.2 for references). No measures are available from the marginal basins, where gypsum did not deposit during Stage 3. The dark blue and black rectangles represent the sulfate isotopic composition of the Global Messinian ocean and Stage 1 (PLG) evaporites, respectively. The light blue area represents the sulfate isotopic composition of mixtures of Messinian marine waters with non-marine sources. The red area represents the isotopic composition of the residual sulfate ion in a basin where marine Messinian sulfate is consumed by microbial sulfate reduction to produce H_2S . The arrow represents the isotope trajectory of dissolved sulfate resulting from the mixing of residual ^{34}S -enriched sulfate produced by MSR and ^{34}S -depleted sulfate produced by H_2S oxidation. All the published $\delta^{34}\text{S}_{\text{SO}_4}$ and $\delta^{18}\text{O}_{\text{SO}_4}$ values are provided corrected with the fractionation factors $\delta^{34}\text{S} = +1.65\text{‰}$ and $\delta^{18}\text{O} = +3.5\text{‰}$ to smooth the isotopic fractionation effects experienced by dissolved sulfate and to reason on values reproducing the isotopic composition at the time of gypsum precipitation. (c) δD isotopes of C_{29} and C_{31n} -alkanes and C_{37} and C_{38} long chain alkenones recorded in the Stage 3 gypsums and marls of the Eraclea Minoa section (modified from Vasiliev et al., 2017). Blue lines indicate the values recorded in the present day lacustrine settings for the n -alkanes (Sachse et al., 2006) and in the alkenones from the Mediterranean in the recent times (Van der Meer et al., 2007). Error bars indicate standard errors of the mean.

Bassetti et al., 2004), which contain carbonate compounds of various and/or unknown provenance, measurements from mollusk shells and ooliths (e.g. Carnevale et al., 2008; Grunert et al., 2016; Roveri et al., 2019a), because they are made of mineral phases easily altered during diagenesis (e.g. aragonite; Marcano et al., 2015), and data coming from reworked material (e.g. all reworked gypsum or transported foraminifera). $^{87}\text{Sr}/^{86}\text{Sr}$ isotope ratios have also been measured by Müller and Mueller (1991) and Roveri et al. (2014b) on the halite beds recovered at Sites 134, 374 and 376 (Ryan et al., 1973; Hsü et al., 1978b). Although they provide interesting interpretative aspects, we do not consider these Sr measurements because the position of Sr in the crystal lattice of halite is unknown and the removal of all contaminants, that is not a straightforward procedure (see Meilijson et al., 2019), is not clear it was achieved by Müller and Mueller (1991) and Roveri et al. (2014b). As a matter of fact, there is no consistency between data generated from roughly the same interval in Core 134 by Müller and Mueller (1991) (0.708968) and Roveri et al. (2014b) (0.708800-0.708896). Added to this is the uncertainty over the provenance of halite in Sites 134 and 374 (see subsections 4.2 and 4.6.1), which violates both criteria mentioned above.

The general trend of the Mediterranean $^{87}\text{Sr}/^{86}\text{Sr}$ isotope ratio during the MSC deviates from the ocean curve towards the less radiogenic values of the major peri-Mediterranean rivers and Paratethys and returns abruptly to oceanic values at the Miocene/Pliocene boundary (Fig. 10a inset). This trend is regarded to reflect the progressive restriction of Mediterranean-Atlantic exchange and the relative increase in the proportion of non-marine source waters (Topper et al., 2011; Roveri et al., 2014a). At first glance it seems that each MSC Stage was characterized by a well-defined range of Sr ratios (Fig. 10a inset), an observation that led Roveri et al. (2014b) to attribute a chronostratigraphic value to MSC $^{87}\text{Sr}/^{86}\text{Sr}$ ratios. A closer look, however, shows that MSC substages are anything but homogeneous with respect to $^{87}\text{Sr}/^{86}\text{Sr}$ ratios. At least in the marginal basins, local lithological differences in the catchments (each lithology carries a unique $^{87}\text{Sr}/^{86}\text{Sr}$ fingerprint; see subsection 8.1.1) explain the different Sr isotopic compositions from basin to basin (see Schildgen et al., 2014; Modestou et al., 2017; Andreetto et al., 2021), therefore arguing against the use of $^{87}\text{Sr}/^{86}\text{Sr}$ ratios for chronostratigraphic purposes in the MSC record.

Most of the data characterizing substage 3.1 (Fig. 10a) are from the Eraclea Minoa gypsum (Fig. 5h). These data define a narrow range of Sr isotope ratios between 0.708747 and 0.708793 (García-Veigas et al., 2018). Similar values were reported from both Eraclea Minoa and the nearby Sculiana Marina section (0.708710-0.708760; Keogh and Butler, 1999; Fig. 5i). The dominance of Sicily samples gives the appearance of a consistent Sr isotope signal for gypsum beds. However, data points from elsewhere (Cyprus, Manzi et al., 2016a; DSDPs 122, 371 and 372 in the Algero-Balearic Basin, ODPs 652, 653 and 654 in the Tyrrhenian Basin, DSDP 374 in the Ionian Basin; Müller et al., 1990; Müller and

Mueller, 1991; Roveri et al., 2014b) display a wider range (from ~ 0.7087 to 0.708847; Fig. 10a) that may indicate a different hydrological regime for each basin (e.g. Müller et al., 1990; Müller and Mueller, 1991; Ryan, 2009). The one published Sr isotope value for ostracods found within one of the marl interbeds at Eraclea Minoa also has a lower value outside the typical Sicily gypsum range (Grossi et al., 2015). This suggests that a different hydrological regime may also have characterised precession minima stages of the precessional cycle.

The Sr isotope dataset for the Lago-Mare phase includes the lowest values measured on MSC sediments (between gypsum VI and VII at Eraclea Minoa; Fig. 3a; Grossi et al., 2015) and the widest range of ratios spanning from 0.7085 to 0.7091, which is above coeval oceanic values (Fig. 10a). Again, the conspicuously high Sr isotope values in substage 3.2 come from two areas, the marginal basins of southern Spain (Andreetto et al., 2021 and references therein; Figs. 5a-c) and the intermediate Polemi Basin on Cyprus (McCulloch and De Deckker, 1989). The lower values are drawn from right across the intermediate-deep Mediterranean (Algero-Balearic, Sicily, Levant; Fig. 2a) and are therefore more likely to represent a Mediterranean-wide Sr isotope signal.

New Sr isotope data from Eastern Paratethys (i.e. Dacian and Caspian basins; Fig. 2b) are now available for the interval corresponding to MSC Stage 3 (inset Fig. 10a). The $^{87}\text{Sr}/^{86}\text{Sr}$ ratios of the Dacian Basin (0.708865-0.708982; Vasiliev et al., 2010; Grothe, 2016) are slightly lower than coeval ocean water (0.709020), but much higher than coeval Mediterranean values. However, the Dacian Basin is regarded as highly restricted from the Mediterranean throughout the MSC (Vasiliev et al., 2010). By contrast, the Caspian has very low values (0.708402 to 0.708473, Grothe et al., 2020) which are thought to reflect both the very low Sr isotope ratio of the Volga river (0.708020; Vasiliev et al., 2010 and references therein) and some input from the Mediterranean (Grothe et al., 2020).

6.2. Sulfate isotopes

Sulfur isotopic investigations have been carried out only on sulfate minerals (gypsum and more rarely anhydrite) of the MSC Stage 3 deposits with samples drawn from both onshore intermediate sequences (Caltanissetta Basin and Cypriot basins) and deep basinal records (Sites 122, 124, 125A, 132, 134, 372, 374, 375, 376, 652, 653, 654, 968, 969, 970; Fig. 10b; Fontes et al., 1973; Pierre, 1974, 1982; Pierre and Fontes, 1978; Ricchiuto and McKenzie, 1978; Pierre and Rouchy, 1990; Blanc-Valleron et al., 1998). Because the incorporation of dissolved sulfate into gypsum produces a nearly constant fractionation of $\delta^{18}\text{O}$ (+3.5‰) and $\delta^{34}\text{S}$ (+1.65‰) at earth surface temperatures (Thode and Monster, 1965; Lloyd, 1968; Warren, 2016), $\delta^{18}\text{O}$ and $\delta^{34}\text{S}$ isotopic values measured in gypsum should be corrected with the above mentioned fractionation factors in order to reconstruct the sulfate isotopic composition of the

basin waters at the time of gypsum formation.

The deep Mediterranean samples exhibit a wide range of $\delta^{34}\text{S}_{\text{SO}_4}$, but the majority of samples display $\delta^{34}\text{S}_{\text{SO}_4}$ values between 18 and 22‰, strongly indicative of a marine origin of the sulfate forming the gypsum (Fig. 10b; Fontes et al., 1973; Pierre, 1974, 1982; Pierre and Fontes, 1978; Pierre and Rouchy, 1990; Blanc-Valleron et al., 1998). The $\delta^{34}\text{S}_{\text{SO}_4}$ values lower than marine sulfate in the dataset are generally considered to represent a greater influence of continental sulfate input to the basin (Fig. 10b; Pierre, 1974; Pierre and Fontes, 1978; Pierre and Rouchy, 1990). By contrast, the data display $\delta^{18}\text{O}_{\text{SO}_4}$ isotopic values that deviate substantially from marine $\delta^{18}\text{O}_{\text{SO}_4}$ values towards higher values (Fig. 10). This is consistent with the influence of sulfate produced by reoxidation of reduced sulfur compounds generated by microbial sulfate reduction (MSR; Kaplan and Rittenberg, 1964; Brunner and Bernasconi, 2005; Sim et al., 2011; Leavitt et al., 2013). The microbial use of SO_2^{18}O leads to an equilibration of $\delta^{18}\text{O}_{\text{SO}_4}$ with ambient water oxygen, whereas the $\delta^{34}\text{S}_{\text{SO}_4}$ returns towards its initial value as a higher fraction of sulfide produced by MSR is re-oxidated. This mechanism has been suggested for Sites in the Algero-Balearic, Tyrrhenian and Ionian basins and offshore Cyprus (Pierre, 1974; Pierre and Fontes, 1978; Pierre and Rouchy, 1990). Although some authors have suggested that partial equilibration of sulfate oxygen toward $\delta^{18}\text{O}_{\text{H}_2\text{O}}$ values of the basin enriched in heavy oxygen isotopes by evaporation have led to an increase in $\delta^{18}\text{O}_{\text{SO}_4}$ values without significant changes in $\delta^{34}\text{S}_{\text{SO}_4}$ (Fontes et al., 1973; Pierre, 1974; Ricciuto and McKenzie, 1978), this hypothesis seems highly unlikely as the abiotic equilibration between sulfate and water oxygen take about 20 Myr at normal marine pH (Lloyd, 1968; Longinelli and Craig, 1967; Turchyn et al., 2006). Moreover, the microbial sulfate reduction process is supported by the presence of pyrite at Sites 132, 654A and 968 (Pierre, 1982; Pierre and Rouchy, 1990; Blanc-Valleron et al., 1998) and the existence of filaments of possible microbial origin at Site 654A (Pierre and Rouchy, 1990).

The sulfate isotopic values reported by Longinelli (1979) and Pierre (1982) from the Upper Gypsum of Eraclea Minoa (Caltanissetta Basin, Sicily) are considerably more scattered than those from a recent study by García-Veigas et al., 2018; Fig. 10b). Such discrepancies are probably a consequence of different sample selection: García-Veigas et al. (2018) analyzed only pristine whitish selenite and balatino samples, while Longinelli (1979) and Pierre (1982) analyzed all types of gypsum-bearing samples such as “gypsiferous marl” and gypsum laminae intercalated in carbonate or diatomaceous intervals. These less pristine samples probably contain high quantities of ^{34}S -depleted solid sulfides or diagenetic gypsum formed by oxidation of sulfides (see Liu et al., 2017 for more details on this process) and are therefore unlikely to be representative of the primary gypsum facies. Once these data are excluded, the Eraclea Minoa sulfate values ($\delta^{18}\text{O}_{\text{SO}_4}$ from 12.4 to 14.6‰ and $\delta^{34}\text{S}_{\text{SO}_4}$ from 21.0 to 22.3‰) suggest a marine origin of the sulfate and stable redox conditions during gypsum deposition (Fig 9.b; García-Veigas et al., 2018). Interestingly, the Eraclea Minoa sulfate values are in compliance with the isotopic values ($\delta^{18}\text{O}_{\text{SO}_4}$ = 15.2 to 16.8‰; $\delta^{34}\text{S}_{\text{SO}_4}$ = 20.4 to 21.9‰) measured by Pierre (1982) in the Polemi Basin (Cyprus).

6.3. Hydrogen isotopes on molecular biomarkers

From the point of view of the application of organic geochemistry proxies, the Miocene Mediterranean Basin received little attention so far, with biomarker-based proxies that have been mostly applied to (a limited number of) pre-MSC sequences (Tzanova et al., 2015; Herbert et al., 2016; Mayer et al., 2017; Naticchio et al., 2017, 2019; Vasiliev et al., 2019) and pre-Stage 3 sedimentary records (Lower Evaporites on Sicily, Andersen et al., 2001; Vena del Gesso Basin, Sinninghe Damsté et al., 1995 and Vasiliev et al., 2017; Levant Basin, Meilijson et al., 2019). To date, only one study analyzed Stage 3 samples (Vasiliev et al., 2017). This study used compound specific hydrogen isotope (δD) analyses, measured on both terrestrial (long chain C_{29} and C_{31n} -alkanes;

Sachse et al., 2006) and aquatic (alkenes; Englebrecht and Sachs, 2005) biomarkers from the gypsum beds of the Upper Gypsum at Eraclea Minoa to reconstruct the hydrological cycle during gypsum precipitation.

Both $\delta\text{D}_{\text{C}_{29n}\text{-alkane}}$ and $\delta\text{D}_{\text{alkenes}}$ results (Fig. 10c) suggested that conditions in Sicily were significantly dryer than today, with highly enriched values of $\delta\text{D}_{\text{C}_{29n}\text{-alkanes}}$ (up to -125‰). The $\delta\text{D}_{\text{alkenes}}$ varied between values suggesting evaporative conditions (-125‰) and values typical for present-day $\delta\text{D}_{\text{alkenes}}$ in the Mediterranean (-203‰) (Vasiliev et al., 2017).

No time-equivalent biomarker data from the open ocean settings are currently available. Instead, Vasiliev et al. (2017) compared their Mediterranean data with data from the Black Sea (DSDP 42B Hole 380 and Taman peninsula; Vasiliev et al., 2013, 2015). The Upper Gypsum $\delta\text{D}_{n\text{-alkanes}}$ were more enriched when compared to their time equivalent deposits of the DSDP 42B 380 borehole of the Black Sea (-180‰). This probably reflects the more intracontinental position of the Black Sea which commonly translates into more depleted values for $\delta\text{D}_{\text{precipitation}}$ used by the vegetation, resulting in more depleted $\delta\text{D}_{\text{C}_{29n}\text{-alkanes}}$. However, there is a 30 to 40‰ enrichment relative to present in the $\delta\text{D}_{n\text{-alkanes}}$ (i.e. $\delta\text{D}_{\text{precipitation}}$) in both Mediterranean and Paratethys domains, indicating concurrent changes in both areas during the latest phase of the MSC.

Both the Mediterranean and Paratethyan samples contain $\delta\text{D}_{\text{alkenes}}$ with low values ($\sim -200\text{‰}$) (Fig. 10c) leading Vasiliev et al. (2017) to suggest that either the surface water from the Upper Gypsum was derived from the Black Sea, or that the Mediterranean and Paratethys were exchanging surface water during gypsum precipitation. Similarity between the relative contribution of the C_{37} , C_{38} and C_{39} alkenes at Eraclea Minoa and one of the Black Sea samples may suggest common alkenone producers for the two areas, again supporting the idea of a Mediterranean-Paratethys connection during Stage 3 (Vasiliev et al., 2017).

A final speculative insight from this biomarker dataset is that the relative contribution of alkenones found in the Upper Gypsum of Eraclea Minoa is strikingly similar to present-day open marine samples, even though *Emiliania huxleyi*, the principal ocean alkenone producer today, did not exist in the late Miocene. Vasiliev et al. (2017) suggested that this could imply the existence of a connection to the open ocean during Upper Gypsum deposition in Sicily (i.e. throughout Stage 3; Fig. 3a).

6.4. Oxygen isotopes

Oxygen stable isotope data ($\delta^{18}\text{O}$) are available from bulk samples (Rouchy et al., 2001, 2003, 2007; Pierre et al., 2006; Cosentino et al., 2012), gypsum (Pierre and Fontes, 1978; Ricciuto and McKenzie, 1978; Lugli et al., 2007), mollusk shells (Carnevale et al., 2008; Grunert et al., 2016) and ostracod valves (Cosentino et al., 2012; Grossi et al., 2015).

For all the sub-basins for which there is latest Messinian data (e.g. Sites 974 and 975; Eraclea Minoa section, Sicily; Aghios Stefanos section, Corfu; Kalamaki section, Zakynthos; Pissouri Basin, Cyprus; Rouchy et al., 2001, Pierre et al., 2006), each has its own range of oxygen isotopic compositions and its own degree of variability. Values from above the Miocene/Pliocene boundary regain seawater values of 0.3 to 1 ‰ (e.g. Pierre et al., 2006).

In marginal marine settings and lakes, the controls over $\delta^{18}\text{O}$ are poorly constrained as oxygen does not respond simply to the freshwater flux, but to a combination of variables such as temperature, rainfall and evaporation (e.g. Placzek et al., 2011). Freshwater input may contribute to the signal, resulting in $\delta^{18}\text{O}$ more negative than seawater (0.3‰ to 0.8‰ SMOW; Dettman et al., 2004), but under prevailing evaporating conditions it is likely that the $\delta^{18}\text{O}$ will be primarily influenced by evaporation, leading to $\delta^{18}\text{O}$ more positive than seawater (e.g. Dettman et al., 2004), making any data very difficult to interpret. Furthermore, the lack of a unique $\delta^{18}\text{O}$ signature for each water source makes oxygen isotopes a difficult tracer proxy to use.

6.5. Summary of the Stage 3 geochemical dataset

The variety of paleoenvironmental and connectivity proxies applied to MSC Stage 3 record provide valuable insights into the hydrological conditions during Stage 3. The more outstanding results from all discussed proxies are that:

- 1) Paleodepositional subaqueous environments where gypsum was precipitating and ostracods and biomarker-producers were thriving were strongly dominated by non-oceanic inputs;
- 2) An indisputable marine signal is absent and only regained above the M/P boundary.

Sulfate and oxygen isotopes are currently difficult to use for water provenance reconstruction because the non-marine sources (local and major rivers and Eastern Paratethys) that are likely to be of influence lack distinctive isotopic signatures and, especially for oxygen, respond to a combination of controls (e.g. temperature, rainfall, evaporation) with local variability. $\delta^{34}\text{S}_{\text{SO}_4}$ are claimed by several authors to be an evidence of the presence of an Atlantic inflow ($\delta^{34}\text{S}_{\text{SO}_4}=22\%$; Turczyn and Schrag, 2004) in a Mediterranean strongly affected by non-marine waters (Manzi et al., 2009, 2016a; García-Veigas et al., 2018 among others). However, the same values can be obtained by means of the recycling of PLG deposits ($\sim 23\%$; Lu et al., 2001; Lugli et al., 2010; García-Veigas et al., 2018).

Similarities between the $\delta\text{D}_{\text{alkenones}}$ of the Upper Gypsum at Eraclea Minoa and coeval Black Sea sediments and $\delta\text{D}_{n\text{-alkanes}}$ similar to present-day marine settings, suggest that Eastern Paratethys and the Atlantic were simultaneously contributing to the Mediterranean hydrological budget. $^{87}\text{Sr}/^{86}\text{Sr}$ isotope ratios are a useful water-mass tracer because each water body carries a unique Sr isotope fingerprint (see subsection 8.1.1). Our plotting of Stage 3 $^{87}\text{Sr}/^{86}\text{Sr}$ isotope values (Fig. 10a) highlights the large geographical variability of the values and the sharp division between Sr isotope ratios measured in marginal basins versus those in intermediate-deep water locations. This is only noticeable in substage 3.2, since no (or not enough) material suitable for Sr analysis is present in substage 3.1 deposits from the marginal basins. Some authors see this variability as an indication of isolated subbasins with unique hydrological conditions driven by their catchment rivers (e.g. Müller et al., 1990; Müller and Mueller, 1991; Ryan, 2009). If some degree of connection was present, it involved only neighbouring basins (e.g. Tyrhenian subbasins; Müller et al., 1990; Müller and Mueller, 1991). A recent comparison of the Sr isotope record of the Spanish marginal basins of Sorbas, Nijar and Vera with the Sr isotope ratios likely to have typified the local riverine sources demonstrated that a local sources-mixed signal expected from an endorheic lake in that location is absent. In this instance mixing of intrabasinal water sources with a non-marine Mediterranean water mass is used to explain the measured values (Andreotto et al., 2021). If this explanation is more widely applicable, then it may result in a re-interpretation of the spread of Sr isotope data from the latest Messinian interval.

To conclude, geochemical proxies have great potential to test the different scenarios, but data are currently too numerically and geographically limited to be robust.

7. Paleoenvironmental scenarios for freshening the salt giant: desiccated versus full Mediterranean

The riddle of the Mediterranean environmental and hydrological conditions during Stage 3 is a highly debated topic and it is key to understanding the means by which open marine conditions were restored at the base of the Zanclean and on the potential impact that the Atlantic-Mediterranean re-connection had on the Atlantic and global climate (Flecker et al., 2015; Capella et al., 2019). In this chapter, the paleoenvironmental scenarios, in terms of base-level position (desiccated or full Mediterranean) and hydrological configuration (connections to the

Atlantic and/or Paratethys), proposed for the Mediterranean during Stage 3 are described, as well as the different timings of the reflooding (instantaneous, gradual, step-like increments). The low-salinity Stage 3 followed the hypersaline Stage 2 and the transition between the two likely influences the plausibility of the various paleoenvironmental scenarios proposed for the terminal stage. We therefore first summarize the current understanding of the configuration of the Mediterranean during Stage 2 and the enduring controversies (see Roveri et al., 2014a for a more extensive review).

7.1. Stage 2 (5.59-5.55 Ma): formation of the Mediterranean salt giant

Numerical modelling based on hydrological budget calculations shows that in order to reach salinity levels compatible with halite saturation and to accumulate the substantial thicknesses of halite observed in the seismic profiles (Ryan, 1973; Haq et al., 2020), the Atlantic-Mediterranean gateway needs to have permitted inflow from the Atlantic, but may have completely blocked outflow (Blanc, 2002; Krijgsman and Meijer, 2008). Numerical models also showed that without Atlantic inflow into the Mediterranean Sea its base level is forced to drop on time scales in the order of a few thousand years by virtue of the basin's negative hydrological budget, where more water is lost to the atmosphere by evaporation than is received from rainfall and river runoff (e.g. Meijer and Krijgsman, 2005; Krijgsman and Meijer, 2008; Simon et al., 2017). The idea of a drawdown is supported by several arguments: (1) the widespread presence, from the margins to the slopes, of the Messinian Erosional Surface cutting through Stage 1 and pre-MSC deposits and canyon incisions following today's drainage networks (e.g. Chumakov, 1973; Clauzon, 1982; Lofi et al., 2005, 2011a, 2011b; Loget et al., 2006; Maillard et al., 2006, 2020; Estrada et al., 2011; Just et al., 2011; Urgeles et al., 2011; Amadori et al., 2018; Lymer et al., 2018; Cazzini et al., 2020; Figs. 5e, 7e); (2) their morphology interpreted as subaerial in origin; (3) the clastic fans at the outlet of the valleys onlapped by Stage 3 deposits and interpreted as fluvial accumulations (e.g. Lofi et al., 2005; Maillard et al., 2006; Pellen et al., 2019). A number of studies have tried to quantify the magnitude of the sea-level fall by compensating for the isostatic vertical motion since the Messinian to obtain the original depth of the erosional features and Messinian deposits. However, this depends on the assumptions about when the drawdown occurred relative to the halite precipitation: before (e.g. Cartwright and Jackson, 2008; Bache et al., 2009, 2012), during (e.g. Ryan, 2008, 2009) or after (e.g. Ryan, 1978; Bertoni and Cartwright, 2007; Lofi et al., 2011a, 2011b). How shallow the Mediterranean became during Stage 2 is also a matter of disagreement. Estimates in the Western Mediterranean vary from a maximum drawdown of 2500 m (Ryan, 1976) to 1000-1500 m (Bache et al., 2012) in the Gulf of Lion, 800-1200 m in the Balearic promontory (Mas et al., 2018b) and 400 m in the Ebro delta region (Frey-Martinez et al., 2004). A later backstripping analysis of this delta yielded a drawdown of ~ 1300 m (Urgeles et al., 2011). East of the Sicily sill, backstripping studies estimated base-level drops of 1800-2000 m in the Ionian basin (Micallef et al., 2018, 2019; Camerlenghi et al., 2019; Spatola et al., 2020), 800-900 m in the Adriatic foredeep and Po plain (Ghielmi et al., 2013; Amadori et al., 2018), 800-1300 m (Ben-Gal et al., 2005), 600 (Druckman et al., 1995) and 800 m (Cartwright and Jackson, 2008) in the Levant Basin.

None of these quantifications could unequivocally constrain the timing of the drawdown within the MSC sequence, but numerical modeling studies show that, if the blocking of the outflow was controlled by a tectonic uplift counteracted by inflow erosion across the Strait of Gibraltar, then the expected drawdown of the Mediterranean Sea should be moderate (< 400 m; and possibly harmonic) due to an equilibrium between incision and uplift before the complete blocking of inflow and larger (up to complete desiccation) only after tectonic uplift overcame incision rates (García-Castellanos and Villaseñor, 2011). The same model suggests that the initiation of halite precipitation might overlap in time with the late primary gypsum deposition, right before the full

disconnection from the Atlantic Ocean.

The interpretation of the deep evaporites and their associated seismic markers (erosional surfaces and deep engravings along the shelf-slope systems) is not straightforward. Recently, it was suggested that the deep evaporitic facies and the seismic morphological features could have been produced without a significant drop of the Mediterranean base-level, therefore promoting the persistence of a relatively deep-water Mediterranean basin even during halite deposition (Lugli et al., 2013, 2015; Roveri et al., 2014b). For example, Roveri et al. (2014c) proposed that downslope flows of dense, hypersaline waters sourced from evaporation in shallower water areas could have generated both the observed shelf-slope erosion and have created a deep brine, super-saturated in the ions necessary for precipitating halite. These subaqueous hyperpycnal flows are consistent with the observed clastic evaporites that filled the Levant margin canyons (Lugli et al., 2013) and, more generally, with the widespread presence of Complex Units at the outlet of the MES drainage systems (see Lofi et al., 2005, 2011a, 2011b; Lofi, 2018). These sediments are dominated by reworked PLG that would have been exposed by a sea-level fall as little as 200 m (Lugli et al., 2010). However, the hypersaline environment that is presumed to be established by these hyperpycnal flows during the deposition of the RLG is in contrast with the occurrence of the Paratethyan ostracod *L. muelleri* within the clastic evaporites (RLG) in several marginal sections (e.g. Adana Basin, Faranda et al., 2013; Radeff et al., 2016, 2017).

Whatever the state of Mediterranean base-level during Stage 2, the more commonly used chronostratigraphic model for the MSC (Fig. 1a; Roveri et al., 2014a) states that massive halite precipitation ceased at 5.55 Ma and was superseded by an environment that, with precession periodicity (Fig. 3a), cycled between gypsum precipitation and conditions that saw fresh-brackish organisms thriving. The question is whether these conditions cycled homogeneously in several isolated lakes or in basins largely connected to the same Atlantic and Eastern Paratethys-influenced water mass (Fig. 11).

7.2. Stage 3 (5.55-5.33 Ma): resumption of (upper) gypsum precipitation and Paratethys fauna invasion

7.2.1. An isolated Mediterranean dotted by sabkhas and lakes

The first and long-lasting paleoenvironmental interpretation of the evaporite-bearing UG/UU units and (possibly) time-equivalent evaporite-free units (e.g. LM Unit in Malaga, Sorbas and Zorras Mb. in Sorbas, Feos Fm. in Nijar, Cassano Spinola Conglomerates in Piedmont, San Donato/Colombacci fms. in the Apennines, Handere Fm. in Turkey) envisaged their sedimentation in a Mediterranean mostly isolated from the Paratethys (which may have added water only to some basins in the Eastern Mediterranean) and totally isolated from the Atlantic where, in each subbasin, continental settings (e.g. alluvial plains, river channels, alluvial fans, playa lakes, sabkhas) alternated/interfingered with shallow, endorheic lakes (Figs. 11a, c; e.g. Ruggieri, 1962, 1967; Decima and Sprovieri, 1973; Decima and Wezel, 1973; Friedman, 1973; Hsü et al., 1973a, 1973b, 1973c; Hsü et al., 1978a, 1978b; Ryan et al., 1973; Sellii, 1973; Sturani, 1973; Sissingh, 1976; Benson, 1978; Bossio et al., 1978; Cita et al., 1978, 1990; Ricchiuto and McKenzie, 1978; Ryan, 1978, 2008, 2009; Cita and Colombo, 1979; Orszag-Sperber and Rouchy, 1979; Ghibaudo et al., 1985; Müller et al., 1990; Benson and Rakic-El Bied, 1991; Benson et al., 1991; Müller and Mueller, 1991; Orszag-Sperber et al., 2000; Rouchy et al., 2001, 2003, 2007; Blanc, 2002; Lofi et al., 2005, Lofi et al., 2011b; Bassetti et al., 2006; Rouchy and Caruso, 2006; Bertoni and Cartwright, 2007; Cameselle and Urgeles, 2017; Amadori et al., 2018; Camerlenghi et al., 2019; Kartveit et al., 2019; Madof et al., 2019; Ben Moshe et al., 2020; Caruso et al., 2020; Cazzini et al., 2020; Raad et al., 2021). The full disconnection is also supported by observations that support an abrupt Zanclean reflooding (e.g. Blanc, 2002; Micallef et al., 2018, 2019; Garcia-Castellanos et al., 2020; Spatola et al., 2020), since a rapid outburst flood requires a large sea level difference prior to the flood that can only be developed in a scenario of a full Mediterranean-Atlantic disconnection (Garcia-Castellanos et al., 2009; Garcia-Castellanos and Villaseñor, 2011). Although rarely explicitly stated, all these studies must assume that:

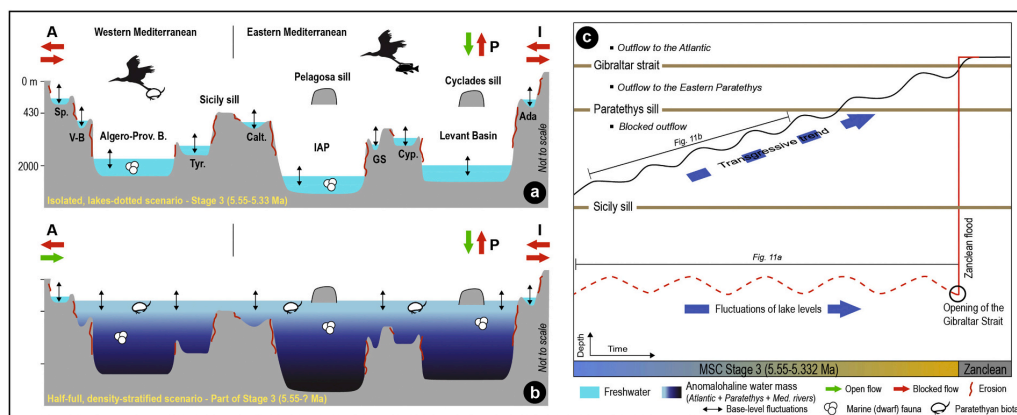


Fig. 11. (a), (b) Schematic W-E profiles across the Mediterranean Basin showing the contrasting paleoenvironmental, paleohydrological and paleoconnectivity interpretations proposed for Stage 3. When a water flow is present (green arrow) from and/or to an extra-Mediterranean water mass (i.e., A: Atlantic Ocean; I: Indian Ocean; P: Eastern Paratethys), the direction of the arrow gives the direction of flow. For simplicity, water added by the major and local rivers is not shown, but it adds to the hydrological budget at any time in each scenario. Note the main difference between the isolated (a) and density-stratified (b) scenario lies in the connectivity framework (Atlantic connection closed and negligible influence from the Paratethys in the isolated scenario; influence from both Atlantic and Paratethys in the density-stratified scenario), which affects the position of the base level of the Mediterranean water mass and its hydrochemistry (see extensive discussion in subsection 7.2). Abbreviations: Sp.: SE Spain; V-B: Valencia Basin; Tyr: Tyrrhenian Basin; Calt: Caltanissetta Basin; IAP: Ionian Abyssal Plain; GS: Gulf of Sirt; Cyp: Cyprus; Ada: Adana Basin. See Fig. 2 for the geographic position of each basin. (c) Schematic plot showing the evolution of the Mediterranean base-level during Stage 3 according to both the isolated (red line) and half-full (black line) scenarios. The critical sills for controlling intra- and extra-Mediterranean connectivity are also shown.

- 1) all Paratethyan biota (and possibly other organisms of undisclosed provenance like diatoms) migrated passively via aquatic migratory birds across the entire Mediterranean (Fig. 11a; Benson, 1978; Benson and Rakic-El Bied, 1991; Caruso et al., 2020);
- 2) chemical and physical conditions (brackish water and water depth not exceeding 100 m; e.g. Hajós, 1973; Gliozzi and Grossi, 2008) that allowed alternated conditions suitable for gypsum to precipitate and Paratethyan biota and euryhaline benthic foraminifera to thrive were related to changes in the local freshwater budget;
- 3) The marine isotopic signals in UU/UG gypsum (Fig. 10) are entirely the reflection of the lithologies that are leached by continental waters in surficial and/or underground drainage areas (e.g. Ryan, 2009; Raad et al., 2021);
- 4) Stage 3 gypsum precipitated in extremely shallow-water (playa lakes) to completely dried environments (sabkhas) and the excessive sulfate necessary is completely derived from “clastic reworking, dissolution, re-precipitation and diagenesis of materials belonging to the PLG and halite of the previous MSC Stage 2” (Ryan, 2009).

Observations supporting a Mediterranean isolated throughout Stage 3 and only at the mercy of local freshwater inputs (Fig. 11a) are: (1) the lack of evidence for in situ marine fauna and flora in UU (e.g. Ryan et al., 1973; Hsü et al., 1978a; Cita et al., 1990; Ryan, 2009; Lofi et al., 2011a); (2) the shallow-water mode of life and highly likely in-situ nature of ostracods and euryhaline, shallow-water benthic foraminifera observed in DSDP/ODP wells from intermediate and deep basins (e.g. Cita et al., 1978; Iaccarino and Bossio, 1999; Figs. 9a-c); (3) the bathymetric contrast (up to several hundred meters) between the late Messinian paleoenvironments and the marine Zanclean on top (e.g. Cita and Colombo, 1979; Bonaduce and Sgarrella, 1999; Caruso et al., 2020); (4) the presence of paleosols in Cyprus (Orszag-Sperber et al., 2000; Rouchy et al., 2001) and on the crest of the Eratosthenes seamount (Robertson, 1998a, 1998b); (5) the erosional features preserved both offshore on the continental shelves and lower-middle slope domain and interpreted in most seismic stratigraphic studies as the result of subaerial exposure (e.g. Lofi et al., 2005; Lofi et al., 2011b; Lymer et al., 2018; Ben Moshe et al., 2020); (6) the pinching out of the UU/BU units towards evaporite-free pre-Messinian structural highs (Figs. 7b-g; Figs. 8a, e; Ryan, 2009; Lymer et al., 2018; Camerlenghi et al., 2019; Raad et al., 2021); (7) the more abundant terrigenous clasts and reworked calcareous fossils in Stage 3 samples compared to the overlying, deep-water Pliocene (Ryan et al., 1973; Hsü et al., 1978b; Ryan, 2009); (8) the erosional nature of the M-reflector/TES/IMTS in the Levant Basin (Figs. 8e-g), by some linked to subaerial exposure of the Levant seafloor (e.g. Bertoni and Cartwright, 2007; Lofi et al., 2011a, 2011b; Maillard et al., 2011a) before the emplacement of deposits interpreted as fluvial from seismic observations (Bowman, 2012; Radeff et al., 2017; Leila et al., 2018; Kartveit et al., 2019; Madof et al., 2019). Furthermore, (9) isolated hydrological circuits with unique chemical composition are regarded by Camerlenghi et al. (2019) as the most plausible explanation for the W-E change in the MSC sedimentary expression in the deep basins, represented by the trilogy LU-MU-UU in the Algero-Balearic and Liguro-Provençal basins, missing the LU in the Tyrrhenian and (possibly) Ionian basins, by terrigenous deposits with hiatuses in the WAB and Adriatic foredeep and by halite, anhydrite and clastics in the Levant Basin (Interbedded and Argillaceous evaporites of Meilijson et al., 2019; Fig. 3b).

The main problems with the isolated scenario lasting throughout Stage 3 are: (1) it does not provide an explanation neither for the homogeneity of Paratethyan ostracod assemblages in the marginal basins (e.g. Gliozzi et al., 2007; Stoica et al., 2016), an aspect difficult to explain when fauna migration takes place passively via either birds or wind, nor for the biomarkers (Vasiliev et al., 2017), which cannot be transported effectively by aquatic birds; (2) it does not explain the mismatch between $^{87}\text{Sr}/^{86}\text{Sr}$ isotope ratios measured on marginal ostracods and Sr values expected from endorheic lakes fed with local

freshwaters (e.g. Andreetto et al., 2021); (3) it misses to substantiate, with geochemical arguments, the precipitation of gypsum in lakes, a process that is everything but straightforward (see Warren, 2016 for insights); (4) except for the salt-bearing basins, the source(s) of solutes which makes freshwater-fed endorheic lakes brackish and causes similar physico-chemical conditions to exist in each lake is also difficult to explain in the context of a Mediterranean only at the mercy of local rivers.

7.2.2. The half-full, density-stratified Mediterranean scenarios

An alternative concept to the isolated scenario envisages the Mediterranean connected with the Atlantic and/or the Eastern Paratethys and relatively full of water connecting the different subbasins (Fig. 11b). To our knowledge, this scenario was first developed by McCulloch and De Deckker (1989) on the basis of the similar $^{87}\text{Sr}/^{86}\text{Sr}$ ratios from marginal (Spain and Cyprus) and deep (Levantine and Algero-Balearic) basins. This intuition was a significant departure from the far more in vogue desiccated scenario (see conclusion of Hsü et al., 1973b), and for this was long overlooked. Sr isotope ratios lower than contemporary ocean water led McCulloch and De Deckker (1989) to conclude that a brackish water mass created by the mixing of water from the peri-Mediterranean rivers (e.g. Nile, Rhône and African rivers that no longer flow today, etc.; see Griffin, 2002 and Gladstone et al., 2007) with water of the Eastern Paratethys filled the Mediterranean, resembling the Caspian Sea today. This conclusion is consistent with the impoverished (or absent) marine fauna and flora of Stage 3 sediments and the enhanced assemblage of fresh-brackish water biota (see subsection 5.7; Figs. 9a-c), but is problematic as a viable origin for Stage 3 gypsum to precipitate at depth. Furthermore, climate models for the late Miocene fail to fill the Mediterranean Basin with fluvial and Paratethys waters alone (Gladstone et al., 2007; Marzocchi et al., 2016, 2019; Simon et al., 2017). A marine contribution is therefore required to fill the Mediterranean (Marzocchi et al., 2016). In the event, the contribution is most likely to have derived from the Atlantic via the Gibraltar Corridor (Flecker et al., 2015; Booth-Rea et al., 2018; Krijgsman et al., 2018) either through a karst system (Krijgsman et al., 2018) or an emerged volcanic archipelago in the Alborán Basin (Booth-Rea et al., 2018). In fact, although an Indian Ocean contribution was proposed (Cita et al., 1978; Hsü et al., 1978a) and the possibility discussed (Ryan, 2009; Vai, 2016), palinspastic reconstructions concluded that the Neo-Tethys Mediterranean-Indian Ocean connection via southern Turkey and Iran already closed before the Tortonian (Rögl, 1998; Popov et al., 2004; Gargani et al., 2008; Bialik et al., 2019; Gülyüz et al., 2020), while a seaway via the Red Sea and Gulf of Aden, although not completely ruled out (e.g. Schütz, 1994; Bosworth et al., 2005; Gargani et al., 2008; Ryan, 2009), is highly contested (e.g. Meulenkamp and Sissingh, 2003; Segev et al., 2017).

In light of this, Roveri et al. (2014c), Gvirtzman et al. (2017), Vasiliev et al. (2017), García-Veigas et al. (2018) and Grothe et al. (2020) suggested that the Mediterranean was likely density-stratified during this interval as a result of the simultaneous influx of isotopically-different marine and non-marine (major Mediterranean rivers and Eastern Paratethys) water sources (Fig. 11b). This connectivity framework resulted in a brackish layer carrying low-salinity (mostly Paratethyan) biota (Gliozzi et al., 2007; Stoica et al., 2016; Grothe et al., 2018, 2020; Figs. 9a-b) to lay on top of a more saline layer formed by Atlantic-derived seawater from which UU/UG gypsum (Figs. 5h-j, 7b-g, 8a-d), that facies analyses demonstrated to result from subaqueous deposition (Hardie and Lowenstein, 2004; Lugli et al., 2015), precipitated at intermediate and greater depths (e.g. García-Veigas et al., 2018). A dense, anoxic deep-water mass, possibly inherited from Stage 2, is envisaged at the bottom of the Mediterranean by Marzocchi et al. (2016) and García-Veigas et al. (2018), albeit without conclusive arguments, and by Gvirtzman et al. (2017) following the observation that the tilted halite body of the Levant Basin was simultaneously eroded landward and preserved basinward (Fig. 8f).

This scenario accounts for the erosive/non-depositional features

(Figs. 5e, 6a, e) and continental/lacustrine facies (Figs. 5a-b, d-g) widespread around the margins and shelves and suggestive of a Mediterranean base-level somewhat lower than the Atlantic level suggesting a one-way inflow from both the Atlantic and the Eastern Paratethys after Stage 2 (e.g. Marzocchi et al., 2016; Figs. 11b, c), a connectivity configuration that effectively translates in a half-full Mediterranean (e.g. Krijgsman and Meijer, 2008). Refilling as a result of persistent Atlantic inflow, in part perhaps because of the latest Messinian deglaciation (see subsection 2.2; Van der Laan et al., 2006; Hilgen et al., 2007), would have resulted in the establishment of two-way exchange first with the Paratethys at some point during the Lago-Mare phase and later, i.e. slightly before or at the Messinian/Zanclean boundary, with the Atlantic Ocean (Fig. 11c; Marzocchi et al., 2016). The moment the Mediterranean base-level reached the sill with the adjacent water body (Paratethys and Atlantic) and a two-way exchange was initiated, the density contrast will have prompted an enhanced inflow into the Mediterranean (Marzocchi et al., 2016). The overall transgressive trend leading to the Zanclean marine replenishment was accompanied by base-level fluctuations in the order of 400 ± 100 m every precessional cycle (Fig. 11c; Fortuin and Krijgsman, 2003; Ben Moshe et al., 2020; Andreetto et al., 2021). These fluctuations are ascribed to switch in the Mediterranean freshwater budget driven by the African summer monsoon and Atlantic winter storms (e.g. Marzocchi et al., 2015, 2019; Simon et al., 2017). Since higher freshwater discharge rates occur at precession minima times and their Stage 3 sedimentary expression is considered to be the mudstone intervals (Fig. 3a; Manzi et al., 2009), mudstone interbeds (both onshore and offshore; e.g. Figs. 5h-j) represent the highest stand episodes (e.g. Manzi et al., 2009; Roveri et al., 2008a; Omodeo-Salé et al., 2012; Fig. 3), while continental facies onshore (e.g. conglomerates in the Apennines; Fig. 5g) and offshore (clastic beds in the Levant Basin) and gypsum beds (Algero-Balearic, Liguro-Provençal, CMD, Tyrrhenian, Caltanissetta, Ionian, Sirte and Polemi-Pissouri basins; Figs. 5h-j) represent the lowstand (e.g. Roveri et al., 2008a; Manzi et al., 2009; Meilijson et al., 2019; Fig. 3). If Atlantic was the major source of sulfate for Stage 3 gypsum (e.g. García-Veigas et al., 2018) and an intervening, relatively shallow (Sicily) sill was establishing Western and Eastern Mediterranean division during the MSC (e.g. García-Castellanos et al., 2009, 2020; Micallef et al., 2018), the presence of Stage 3 gypsum to the east of the Sicily sill (Fig. 2b) implies that the Mediterranean base level never dropped below the (maximum estimated) paleodepth of the sill (i.e. ~ 430 m; García-Castellanos et al., 2009) during Stage 3 and Western and Eastern Mediterranean remained connected also during the arid (lowstand) phases of the precession cycles.

A Mediterranean step-wise refilled and at times filled with water up to the marginal belt agrees with: (1) Paratethyan biota being present only in intermediate-deeper settings during substage 3.1, but more widespread including marginal settings during substage 3.2; (2) the W-E homogeneity of Paratethyan ostracod assemblages around the Mediterranean marginal belt (Gliozzi et al., 2007; Stoica et al., 2016; Sciuto et al., 2018; Sciuto and Baldanza, 2020; Fig. 9a); (3) the presence, in marginal basins, of Paratethyan fish (Bannikov et al., 2018; Schwarzhans et al., 2020), dinocysts (e.g. Pellen et al., 2017; Fig. 9b) and biomarkers (Vasiliev et al., 2017; Fig. 10c); (4) the occurrence of a monospecific assemblage of abundant *Sphenolithus* spp. just below the M/P boundary at ODP Sites 978, 975 and 967 (Castradori, 1998); (5) the requirement of water from the Mediterranean to explain the Sr isotope ratios of ostracods that inhabited marginal subaqueous environments (Andreetto et al., 2021); (6) the Atlantic-like sulfate values (although variably diluted and affected by microbial processes; Fig. 10b) of the UU/UG gypsum beds (García-Veigas et al., 2018); (7) the presence of long chain alkenones in the Sicilian UG beds similar to those observed in present-day marine settings (Fig. 10c; Vasiliev et al., 2017).

Major problems also exist with the half-full stratified scenario: (1) it does not provide a proper mechanism for gypsum precipitation at several hundreds, or thousands, meters water depth; (2) it fails to explain how unquestionable shallow-water (< 50 m) benthic organisms

such as *Ammonia tepida* and *Cyprideis* sp. could survive at hundreds of meters of depth and beyond; (3) it does not provide an explanation for the high abundance of coarse-grained detritus at intermediate and deep-water locations, especially when compared to deep-water Pliocene samples, as well as for the broad absence of MSC deposits in the shelf domain; (4) a persistent Atlantic inflow without outflow seems to be a configuration that cannot be maintained stable for ~ 200 kyr. Indeed, models coupling the inflow of marine waters with the erosion of the gateway channel concluded that, if the Mediterranean level was lowered by at least several hundred meters below present sea level, any small overtopping of water from the Atlantic would inevitably trigger a fast refill of the basin that, if responsible for the erosion trough the Alborán Basin, should have involved an unprecedented water discharge and be completed within a few years or less (García-Castellanos et al., 2020 and references therein). The scenario arising from Meilijson et al., 2019, Figs. 3b, 4a) is also problematic for a high base-level Mediterranean. In order to simultaneously reach precipitation of gypsum and halite in different basins sharing the same water, the water has to be of high salinity and stratified. Simon and Meijer (2017) demonstrated that this can be achieved with slow overturning circulation, but it is currently unclear how realistic this process is.

7.3. Demise of the MSC (5.33 Ma): the Zanclean marine replenishment

The conspicuous and abrupt transition to normal marine sediments in the Mediterranean is globally and historically important because it is the origin of the stratigraphic position of the Miocene/Pliocene boundary (Van Couvering et al., 2000). From an ocean perspective, it is not an ideal stratigraphic location being difficult to locate from biozone data even in the adjacent Atlantic (Hodell et al., 2001; Krijgsman et al., 2004; Van den Berg et al., 2015). However, from a Mediterranean perspective it provides a clear and unambiguous end to the MSC and the restoration of normal marine conditions. All evidence show that the onset of the Zanclean marine replenishment followed a period of relative lowstand that exposed all the Mediterranean margins (see subsection 3.12; Figs. 6a-b, f) and kept intermediate and deep basins underwater (see subsection 4.8). Yet again, the key dispute concerns the exact depth of the Mediterranean base level preceding the Miocene/Pliocene transition.

Building on the isolated Mediterranean scenario, base level immediately before the early Zanclean was more than thousand kilometers below eustatic sea level (Fig. 10e; e.g. Hsü et al., 1973a; Blanc, 2002; Loget et al., 2006; García-Castellanos et al., 2009; Pérez-Asensio et al., 2012; García-Alix et al., 2016; Amadori et al., 2018; Micallef et al., 2018, 2019; Camerlenghi et al., 2019; Kartveit et al., 2019; Madof et al., 2019; Ben Moshe et al., 2020; Caruso et al., 2020; Cazzini et al., 2020; Mas and Fornós, 2020; Spatola et al., 2020). Hydrodynamic erosional models allowed a reinterpretation of the erosional features across the strait of Gibraltar (Campillo et al., 1992; Blanc, 2002) suggesting that a sudden breach of the Mediterranean-Atlantic divide at Gibraltar resulted in a vast cascade of Atlantic water that refilled the entire Mediterranean in less than 2 years (i.e. rates of ten meters per day) spilling first into the Western Mediterranean (see the extensive review in García-Castellanos et al., 2020) and then, after reaching the level of the Sicily sill, pouring into the Eastern Mediterranean (Micallef et al., 2018, 2019; Ben Moshe et al., 2020; Spatola et al., 2020). This concept of catastrophic refilling has led to terms such as “Zanclean flood” or “deluge”. Evidence supporting the catastrophic flood mechanism mostly comes from the seismic reflection dataset and includes: 1) the presence of >250 m deep and 390-km-long incisions on both sides of the Gibraltar Strait (García-Castellanos et al., 2020); 2) the detection of (allegedly) Pliocene-aged chaotic sedimentary bodies stretching for kilometers in the Alborán Basin (García-Castellanos et al., 2020 and references therein) and Ionian Basin at the foot of the Malta Escarpment (Micallef et al., 2018, 2019; Spatola et al., 2020; Fig. 8c). A further argument is the bathymetric jump of several hundred meters between the late Messinian and the early

Pliocene sediments (e.g. Caruso et al., 2020; Fig. 6d).

Instantaneous sea level rise is not the only possible refilling model. Bache et al. (2012) suggested the reflooding occurred in two steps at ~5.60 Ma, accompanied by a moderate (≤ 500 m) rise, followed by a rapid rise of 600–900 m at around 5.46 Ma tracking the deposition of the deep basin evaporites and resulting from the collapse of the Gibraltar divide. There is also the reconnection model that follows from a Stage 3 Mediterranean that is already relatively full and with the base level possibly oscillating of 400 ± 100 m with precessional frequency (Fig. 10h; Fortuin and Krijgsman, 2003; Ben Moshe et al., 2020; Andreetto et al., 2021). In this case, only a sea level rise of a few hundred meters is required to restore the Mediterranean to the Atlantic level (Fig. 10h), which was hypothesized to have occurred in the last precessional cycle of the Messinian (Marzocchi et al., 2016; Fig. 3a).

In detail, the re-establishment of a fully marine faunal diversity and oceanic geochemistry (e.g. $^{87}\text{Sr}/^{86}\text{Sr}$ ratios and $\delta^{18}\text{O}$) occurred more gradually over one or more precessional cycles in the earliest Zanclean (e.g. Iaccarino et al., 1999; Pierre et al., 1998, 2006; Cipollari et al., 2013; Roveri et al., 2019a; Bulian et al., 2021). This suggests that stressed ecological conditions at first only suitable for opportunistic organisms to survive (e.g. Bulian et al., 2021) developed (or persisted) in the Mediterranean as marine replenishment occurred (e.g. Rouchy et al., 2003). One possible mechanism for achieving this may be the physico-chemical turnover in the water column triggered by the re-established two-way exchange with the Atlantic which, for reasons that are largely unknown, took time (at least one precession cycle; Pierre et al., 2006) to displace surficial Paratethyan water and restore normal marine conditions (Marzocchi et al., 2016).

8. Methods and proxies to better reconstruct base level and connectivity changes

Chronological uncertainty and spatial variability limit the use of both sedimentological and paleontological information to achieve a comprehensive and coherent basin-wide interpretation of the conditions and drivers of Stage 3 environments and water levels. Alternative methods are therefore required to clarify connectivity relationships and constrain base-level conditions. This section explores the principles and potential of geochemical, backstripping and numerical modelling techniques that could be used to further test existing hypotheses and enhance understanding of the complex environmental conditions experienced by the Mediterranean during the latest Messinian.

8.1. Geochemical proxies

Radiogenic strontium isotopes. Radiogenic strontium isotope ratio ($^{87}\text{Sr}/^{86}\text{Sr}$) is a widely applied geochemical tool in provenance studies, including the reconstruction of the hydrological circuit and connectivity of basins with little or null oceanic entries. Its potential to detect the provenance of the hydrological fluxes derives from the unique $^{87}\text{Sr}/^{86}\text{Sr}$ ratio that typifies each water source and from the negligible effects of isotopic fractionation during the liquid-solid transition (see Hajj et al., 2017).

Mineral phases precipitating in endorheic lakes uptake Sr with $^{87}\text{Sr}/^{86}\text{Sr}$ ratio that reflects the mixing of all feeding surficial and underground streams and whose $^{87}\text{Sr}/^{86}\text{Sr}$ fingerprint hinges on the composition and age of watershed bedrock (see Peucker-Ehrenbrink and Fiske, 2019; Andreetto et al., 2021 and references therein). When river water mixes with seawater such as in the oceans, semi-enclosed basins or estuaries, mineral phases uptake Sr with oceanic $^{87}\text{Sr}/^{86}\text{Sr}$ ratios because the high oceanic Sr concentration (~7.8 mg/l today; Veizer, 1989) masks the impact of the ~100 times lower concentrated continental Sr-sources (~0.0780 mg/l; Palmer and Edmond, 1992). This is valid as long as a certain ratio of continental-marine water mixing is fulfilled, beyond which $^{87}\text{Sr}/^{86}\text{Sr}$ ratios deviate towards the $^{87}\text{Sr}/^{86}\text{Sr}$ ratios of the non-marine source(s) (Ingram and Sloan, 1992). For the

Mediterranean to attain non-marine $^{87}\text{Sr}/^{86}\text{Sr}$ ratios (like during the MSC), Topper et al. (2014) calculated a mixing of at least 1:4 (Atlantic: freshwater) to be required.

If Mediterranean subbasins hosted endorheic lakes (Figs. 10c, e), the $^{87}\text{Sr}/^{86}\text{Sr}$ isotope ratios measured on ostracod valves or gypsum crystals of each lake are expected to generate a scattered distribution by virtue of the different geology in the hinterland of each basin. By contrast, some degree of connection between different basins and the Mediterranean water mass (Figs. 10d, f) is expected to result in more homogeneous $^{87}\text{Sr}/^{86}\text{Sr}$ ratios because, although isotopically-different, local rivers mix with a water mass that has the same $^{87}\text{Sr}/^{86}\text{Sr}$ value and (much higher) Sr concentration for each basin (Andreetto et al., 2021). In this scenario, differences in the $^{87}\text{Sr}/^{86}\text{Sr}$ ratios between basins are likely the reflection of the different $^{87}\text{Sr}/^{86}\text{Sr}$ ratio of the local input in each basin (Andreetto et al., 2021). The application of numerical models assists to identify and quantify the different water sources feeding the basin(s) in question and (e.g. Placzek et al., 2011; Topper et al., 2011, 2014; Doebbert et al., 2014; Rossi et al., 2015b; Modestou et al., 2017; Grothe et al., 2020; Andreetto et al., 2021).

Sulfate isotopes. When sulfate-bearing minerals precipitate in a basin they uptake dissolved S and O with $\delta^{34}\text{S}_{\text{SO}_4}$ and $\delta^{18}\text{O}_{\text{SO}_4}$ isotopic composition that, once corrected for the fractionation effects during liquid-solid transition (see subsection 6.2), can be assimilated to that of the mother brine. The higher concentrated source of sulfate is seawater (with present-day $\delta^{34}\text{S}_{\text{SO}_4}=21.15\pm 0.15\text{‰}$ and $\delta^{18}\text{O}_{\text{SO}_4}=8.67\pm 0.21\text{‰}$, Johnston et al., 2014; with Messinian values of $\sim 22\pm 0.2\text{‰}$ for the $\delta^{34}\text{S}_{\text{SO}_4}$ and $\sim 9\pm 2\text{‰}$ for the $\delta^{18}\text{O}_{\text{SO}_4}$; Turchyn and Schrag, 2004; Markovic et al., 2016; Masterson et al., 2016). Significantly higher inputs from the ~1000 times less concentrated riverine freshwater (both surficial and underground) with respect to the ocean water (more than 1:5 according to Lu et al., 2001) can modify the marine $\delta^{34}\text{S}_{\text{SO}_4}$ and $\delta^{18}\text{O}_{\text{SO}_4}$ isotopic composition of the mother brine (Utrilla et al., 1992; Lu et al., 2001) and have it deviated from that of the ocean (Lu et al., 2001). This deviation is normally towards lower values, because river-derived dissolved sulfate is generally depleted in heavy isotopes ^{34}S and ^{18}O compared to oceanic sulfate because these isotopes mainly come from the oxidation of ^{34}S -depleted pyrite (FeS_2) on the continents and to a lesser extent from the dissolution of older sulfate-bearing minerals (Claypool et al., 1980; Turchyn and Schrag, 2004; Burke et al., 2018). However, when marine sulfate is preferentially leached in the catchment, ^{34}S of the freshwater-dissolved sulfate and $[\text{SO}_4^{2-}]$ likely increase, therefore reducing the continental-marine mixing ratio necessary to deviate the resulting sulfate isotopic signature away from marine values. Unfortunately, the sulfate isotopic composition is not provided for a number of major Mediterranean rivers (Burke et al., 2018) nor for the Eastern Paratethys and it is hardly assessed with the catchment-forming lithologies (Liu et al., 2017; Burke et al., 2018), making sulfate isotopes still an unsuitable tracer of non-marine water provenance in Mediterranean subbasins.

Deviation of $\delta^{34}\text{S}_{\text{SO}_4}$ and $\delta^{18}\text{O}_{\text{SO}_4}$ from the marine average can also be the result of isotopic fractionation during microbial sulfate reduction (MSR; Fritz et al., 1989; Berner, 1999). MSR produces ^{34}S -depleted hydrogen sulfide (~0 to 70% lighter than initial sulfate; Brunner and Bernasconi, 2005; Sim et al., 2011; Leavitt et al., 2013) and induces the enrichment in ^{34}S and ^{18}O of the residual sulfate pool (Kaplan and Rittenberg, 1964; Thode and Monster, 1965; Turchyn et al., 2006; Wortmann et al., 2007). Therefore, if isotopically light H_2S produced by MSR leaves the system as a sulfide mineral (most likely pyrite), the resulting dissolved sulfate would have $\delta^{34}\text{S}_{\text{SO}_4}$ and $\delta^{18}\text{O}_{\text{SO}_4}$ isotopic signatures higher than the oceanic one (Brunner et al., 2005). However, if the MSR-produced H_2S is re-oxidized back to sulfate through abiotic or microbial sulfide oxidation, isotopically light sulfate will be brought back to the ^{34}S -enriched sulfate pool, producing little or no enrichment in ^{34}S observed in the resulting sulfate (Gomes and Johnston, 2017 and references therein; Pellerin et al., 2019). Slight deviations from marine $\delta^{18}\text{O}_{\text{SO}_4}$ and $\delta^{34}\text{S}_{\text{SO}_4}$ values of sulfate reflect both biological sulfur

cycling and/or freshwater riverine inputs (e.g. Utrilla et al., 1992; Lu et al., 2001; Turchyn et al., 2009) (Fig. 10b). Untangling the relative importance of these processes is key to understanding the Mediterranean sulfur isotope record and gleaned paleoenvironmental insights into Stage 3.

Hydrogen isotopes. Organic geochemistry biomarker-based tools can be used as independent proxies for reconstructing sea surface temperatures, relative changes in the basin hydrology and, indirectly, salinity. Basin water properties are reflected in a variety of life forms. Different types of organisms produce specific organic compounds that serve as molecular biomarkers. These large biomolecules record the changes in the hydrogen isotopic composition of the water used by different groups of biomarker producers (i.e. different organisms). The principle behind the method is to measure δD on biomarkers produced in Mediterranean Sea waters (e.g. alkenones, produced by a few species of haptophyte coccolithophores algae) during the MSC and compare the results with the δD signals retrieved from biomarkers produced in the open ocean ideally at the same time intervals. The influence of precipitation on the changes in hydrological budget can be monitored by measuring the δD of long chain *n*-alkanes (Sachse et al., 2006), biomarkers predominantly produced by higher terrestrial plants that rely on precipitation for plant growth, therefore reflecting the changes in the δD of the precipitation. The extreme base level drop(s) suggested for the Mediterranean during the MSC would, in principle, indicate a negative precipitation (P) + runoff (R) – evaporation (E) ratio. Such a negative water budget ($E > P + R$) results in waters increasingly enriched in δD whereas, a positive water balance ($E < P + R$) results instead in a negative shift of δD values. The analysis of compound specific δD of alkenones, long and short chain *n*-alkanes can be used to constrain $E/(P+E)$ relationships.

8.2. Backstripping analyses

Backstripping uses paleobathymetry, sea level and sediment thickness to quantify the tectonic and isostatic components of subsidence. If tectonic subsidence or uplift history are known relative to the current position and depth of paleoshoreline markers, an inverse approach allows base level to be estimated. A number of approaches have been applied to the MSC, using erosional surfaces (e.g. Amadori et al., 2018), terraces (Micallef et al., 2018) or fluvial network characteristics (Urgeles et al., 2011) as paleoshoreline indicators. The relief on erosional features has also been used to estimate minimum base-level variation (Frey-Martinez et al., 2004).

Apart from the quantitative constraints on base level that backstripping provides, consideration of the regional implications of isostatic subsidence and the gravitational impact of redistributing water masses (such as in the cascading model of Roveri et al., 2014c; Fig. 10b) and evaporite precipitation is important in gateway regions like Gibraltar, which due to their shallow and restricted nature are exceptionally sensitive to vertical motions. Here, both flexural effects and gravitational effects on local sea level on the Atlantic side of the strait has the potential to influence Mediterranean-Atlantic connectivity driving paleoenvironmental changes in the basin itself (Coulson et al., 2019).

8.3. Modelling

Numerical models can be used complementary to lab- and field-based studies, or to find answers to open questions by testing the physical plausibility of hypotheses and their compatibility with the available sedimentological/stratigraphic/paleontological/geochemical data, which have to constrain model results and not adjust to it. For example, whether gypsum beds in marginal/intermediate basins can precipitate at the same time as the halite in deep basins is an intriguing question that circulates in the MSC literature (e.g. Van Couvering et al., 1976), but whether this is physically and geochemically possible is yet to be answered. In a first model analysis, Simon and Meijer (2017) found that the required stratification can indeed be achieved for specific

conditions including a slow overturning circulation. A different approach is needed to determine whether such slow circulation is to be expected or if other scenarios should be considered. A thermo-haline stratification that enables coeval precipitation of two evaporites for a considerable time span might also influence the degree of heterogeneity of other parameters, such as strontium concentration. Previous models showed the influence of the Atlantic Ocean and major rivers (Topper et al., 2014) and of evaporation (Flecker et al., 2002) on the Sr value of a basin with restricted oceanic inflow and assuming a homogeneous distribution of strontium throughout the water column (Flecker et al., 2002; Topper et al., 2011, 2014; Modestou et al., 2017), but it is uncertain if this holds true in conditions of water stratification. New insights into this behavior would have consequences for the way the strontium dataset (Fig. 10a) must be interpreted. Another loose end where the model approach can provide insight relates to the question whether a high water level could have been reached without an inflow from the Atlantic. Climate simulations conducted by Gladstone et al. (2007), Simon et al. (2017) and Marzocchi et al. (2019) indicate that this is not possible with today's bathymetry. A quantitative analysis exploring the Mediterranean water level reached in different situations (i.e. with or without an Atlantic or Paratethys in and outflow) and with information on the Mediterranean hypsometry that may be provided by isostatic restoration of the seafloor topography (flexural backstripping) could help understanding how the Messinian Salinity Crisis ended.

9. Certainties, open problems and future directions

Our understanding of the nature of MSC Stage 3 has evolved considerably over the last fifty years. However, there are still such disparate models for the paleoenvironmental conditions and basin connectivity that led to Stage 3 deposition and that express the challenges that the study of this interval presents: it is a relatively short interval and its sedimentary expression varies spatially. It is no surprise that the main point of contention lies in reconciling the observations from seismic profiles and well data, which are largely interpreted as favoring the desiccated scenario, with the sedimentological, paleontological and geochemical data from the marginal basins record, largely discontinuous and unaddressed from seismic-based and computational-based studies and mainly supporting the full-Mediterranean hypothesis.

To a large extent this mismatch is the result of the lack of intersection of the two datasets. Some Stage 3 onshore localities are meticulously studied from the stratigraphic, sedimentological, paleontological and geochemical point of view, showing remarkably consistent and homogenous trends and patterns (as previously highlighted by Roveri et al., 2008a). However, changes at precessional and subprecessional scale are difficult to trace from one exposure to another and are well below the level of seismic resolution, making onshore-offshore correlation at this scale impossible. Even correlation between onshore sections is problematic since most of the stratigraphic sections are incomplete, with erosion surfaces at the bottom and/or top (i.e. the Miocene/Pliocene boundary), and this lack of stratigraphic continuity frustrates attempts to constrain ages by cyclostratigraphy. A future focus on strengthening the available chronostratigraphic framework (Fig. 3) and making it inclusive of the fragmented outcrops is required to better understand the paleoenvironmental and paleohydrological changes suffered by the Mediterranean marginal belt through time. The successful drilling of the three IODP proposals currently in the scheduling pool (see Camerlenghi and Aloisi, 2020), all of which propose to recover Stage 3 sediments, will also provide transformative information enabling far better offshore-onshore correlation and interpretation of currently enigmatic seismic data. In the meantime, re-evaluation of existing DSDP and ODP material, particularly through the application of more novel geochemical techniques and, where possible, access to material collected during industrial drilling would be helpful for understanding the deep Mediterranean Basin during this interval.

Extensive paleontological studies have established that Stage 3

contains *in situ* biota assemblages of Paratethyan provenance implying brackish water conditions. More problematic is the differentiation of *in situ* and reworked marine microfauna and flora and the paleoecological significance of dwarfism in marine calcareous microfossils/algae. These have important repercussions for the Mediterranean connectivity and base-level reconstruction.

The geochemical dataset for Stage 3, particularly strontium isotopes and hydrogen isotopes on biomarkers, is both demonstrably valuable in providing key constraints on connectivity and environmental conditions, and frustratingly inadequate in terms of data distribution. It has great potential as a constraint on quantitative sensitivity analysis of the different hydrochemistry scenarios that follow from the endmember Stage 3 hypotheses, but substantially more data is required.

An approach which combines geological, geochemical, geophysical and paleontological data with numerical modelling (e.g. climate simulations, backstripping analyses and paleoclimatographic models) will provide a more accurate reconstruction of Mediterranean paleogeography and the processes that occurred during the final phase of the Messinian Salinity Crisis.

Data availability

The compilation of strontium, sulfate and hydrogen isotope data plotted in figure 9, as well as some of the available, and here not (graphically) shown, oxygen isotope values is accessible in separate excel spreadsheets (Supplementary material 1).

Declaration of Competing Interest

The authors whose names are listed immediately below certify that they have NO affiliations with or involvement in any organization or entity with any financial interest (such as honoraria; educational grants; participation in speakers' bureaus; membership, employment, consultancies, stock ownership, or other equity interest; and expert testimony or patent/licensing arrangements), or non-financial interest (such as personal or professional relationships, affiliations, knowledge or beliefs) in the subject matter or materials discussed in this manuscript.

Acknowledgments

We thank the entire SALTGIANT community for many profitable workshops that inspired the development of this manuscript. This research was supported by the project SALTGIANT-Understanding the Mediterranean Salt Giant, a European project which has received funding from the European Union's Horizon 2020 research and innovation program, under the Marie Skłodowska-Curie [grant agreement No 765256]. We greatly thank the two reviewers Domenico Cosentino and William Ryan and the editor Alessandra Negri for the fruitful comments provided that led to a substantial improvement of the manuscript.

Appendix A. Supplementary data

Supplementary data to this article can be found online at <https://doi.org/10.1016/j.earscirev.2021.103577>.

References

- Abdel Aal, A., El Barkooky, A., Gerrits, M., Meyer, H., Schwander, M., Zaki, H., 2000. Tectonic evolution of the eastern Mediterranean Basin and its significance for hydrocarbon prospectivity in the ultradeepwater of the Nile Delta. *Lead. Edge* 19, 1086–1102. <https://doi.org/10.1190/1.1438485>.
- Abdel-Fattah, M.I., 2014. Petrophysical characteristics of the messinian abu madi formation in the baltim east and north fields, offshore Nile delta, Egypt. *J. Pet. Geol.* 37 (2), 183–195.
- Agiadi, K., Antonarakou, A., Kontakiotis, G., Kafousia, N., Moissette, P., Cornée, J.-J., Manoutsoglou, E., Karakitsios, V., 2017. Connectivity controls on the late Miocene eastern Mediterranean fish fauna. *Int. J. Earth Sci.* 106, 1147–1159. <https://doi.org/10.1007/s00531-016-1355-7>.
- Agini, C., Monechi, S., Raffi, I., 2017. Calcareous nannofossil biostratigraphy: historical background and allocation in Cenozoic chronostratigraphy. *Lethaia* 50 (3), 447–463.
- Aguirre, J., Sánchez-Almazo, I.M., 2004. The Messinian post-evaporitic deposits of the Gafares area (Almería-Níjar basin, SE Spain). A new view of the “Lago-Mare” facies. *Sediment. Geol.* 168, 71–95.
- Amadori, C., Garcia-Castellanos, D., Toscani, G., Sternai, P., Fantoni, R., Ghielmi, M., Di Giulio, A., 2018. Restored topography of the Po Plain-Northern Adriatic region during the Messinian base level drop-implications for the physiography and compartmentalization of the paleo-Mediterranean basin. *Basin Res.* 30 (6), 1247–1263. <https://doi.org/10.1111/bre.12302>.
- Andersen, N., Paul, H.A., Bernasconi, S.M., McKenzie, J.A., Behrens, A., Schaeffer, P., Albrecht, P., 2001. Large and rapid climate variability during the Messinian salinity crisis: evidence from deuterium concentrations of individual biomarkers. *Geology* 29, 799–802.
- Andreotto, F., Matsubara, K., Beets, C.J., Fortuin, A.R., Flecker, R., Krijgsman, W., 2021. High Mediterranean water-level during the Lago-Mare phase of the Messinian Salinity Crisis: insights from the Sr isotope records of Spanish marginal basins (SE Spain). *Paleogeogr. Paleoclimatol. Paleoevol.* 562.
- Andrusov, D., 1890. Les Dreissenidae fossiles et actuelles d'Eurasie. *Geol. Min.* 25, 1–683 (in Russian).
- Arab, M., Rabineau, M., Déverchère, J., Bracene, R., Belhai, D., Roure, F., Marok, A., Bouyahiaoui, B., Granjeon, D., Andriessen, P., Sage, F., 2016. Tectonostratigraphic evolution of the eastern Algerian margin and basin from seismic data and onshore-offshore correlation. *Mar. Pet. Geol.* 77, 1355–1375. <https://doi.org/10.1016/j.marpetgeo.2016.08.021>.
- Arenas, C., Pomar, L., 2010. Microbial deposits in upper Miocene carbonates, Mallorca, Spain. *Paleogeogr. Paleoclimatol. Paleoevol.* 297 (2), 465–485.
- Aufgebauer, A., McCann, T., 2010. Messinian to Pliocene transition in the deep part of the Sorbas Basin, SE Spain—a new description of the depositional environment during the Messinian Salinity Crisis. *Neues Jahrbuch für Geologie und Paläontologie-Abhandlungen* 259 (2), 177–195.
- Azdimoua, A., Poupeau, G., Rezqi, H., Asebry, L., Bourgeois, J., Ait Brahim, L., 2006. Géodynamique des bordures méridionales de la mer d'Alboran; alication de la stratigraphie séquentielle dans le bassin neogene de Boudinar Rif oriental. *Maroc. Bull. Inst. Sci. Rabat* 28, 9–18.
- Bache, F., Olivet, J.-L., Gorini, C., Rabineau, M., Baztan, J., Aslanian, D., Suc, J.-P., 2009. Messinian erosional and salinity crisis: view from the Provence basin (Gulf of Lions, western Mediterranean). *Earth Planet. Sci. Lett.* 286, 139–157.
- Bache, F., Popescu, S.-M., Rabineau, M., Gorini, C., Suc, J.-P., Clauzon, G., Olivet, J.-L., Rubino, J.-L., Melinte-Dobrescu, M.C., Estrada, F., Londeix, L., Armijo, R., Meyer, B., Jolivet, L., Jouannic, G., Leroux, E., Aslanian, D., Reiz, A.T.D., Mocochain, L., Dumurdzanov, N., Zagorchev, I., Lesić, V., Tomić, D., Namik Çağatay, M., Brun, J.-P., Sokoutis, D., Csato, I.T., Ucaruk, G., Çakır, Z., 2012. A two-step process for the reflooding of the Mediterranean after the Messinian Salinity Crisis. *Basin Res.* 24, 125–153. <https://doi.org/10.1111/j.1365-2117.2011.00521.x>.
- Backman, J., Raffi, I., Rio, D., Fornaciari, E., Pálke, H., 2012. Biozonation and biochronology of Miocene through Pleistocene calcareous nannofossils from low and middle latitudes. *Newsl. Stratigr.* 45, 221–244.
- Bannikov, A.F., Schwarzzhans, W., Carnevale, G., 2018. Neogene Paratethyan croakers (Teleostei, Sciaenidae). *Riv. Ital. Paleontol. Stratigr.* 124, 535–571.
- Barra, D., Bonaduce, G., Sgarrella, E., 1998. Paleoenvironmental bottom water conditions in the early Zanclean of the Capo Rossello area (Agrigento, Sicily). *Boll. Soc. Paleontol. Ital.* 37, 61–88.
- Bassetti, M.A., Miculan, P., Lucchi, F.R., 2003. Ostracod faunas and brackish-water environments of the late Messinian Sapigno section (northern Apennines, Italy). *Paleogeogr. Paleoclimatol. Paleoevol.* 198 (3–4), 335–352.
- Bassetti, M.A., Manzi, V., Lugli, S., Roveri, M., Longinelli, A., Lucchi, F.R., Barbieri, M., 2004. Paleoenvironmental significance of Messinian post-evaporitic lacustrine carbonates in the northern Apennines, Italy. *Sediment. Geol.* 172 (1–2), 1–18.
- Bassetti, M.A., Miculan, P., Sierro, F.J., 2006. Evolution of depositional environments after the end of Messinian Salinity Crisis in Nijar basin (SE Betic Cordillera). *Sediment. Geol.* 188–189, 279–295.
- Ben Moshe, L., Ben-Avraham, Z., Enzel, Y., Schattner, U., 2020. Estimating drawdown magnitudes of the Mediterranean Sea in the Levant basin during the Lago Mare stage of the Messinian Salinity Crisis. *Mar. Geol.* 106215 <https://doi.org/10.1016/j.margeo.2020.106215>.
- Ben-Gal, Y., Ben-Avraham, Z., Buchbinder, B., Kendall, C.G.S.C., 2005. Post-Messinian evolution of the Southeastern Levant Basin based on two-dimensional stratigraphic simulation. *Mar. Geol.* 221 (1–4), 359–379.
- Benson, R.H., 1978. The paleoecology of the ostracods of DSDP Leg 42A. In: Hsu, K., Montadert, L. (Eds.), *Initial Reports of the Deep-Sea Drilling Project*, 42. U.S. Government Printing Office, Washington, pp. 777–787.
- Benson, R.H., Rakić-El Bied, K., 1991. The Messinian paratratotype at Cuevas de Almazora, Vera Basin, SE Spain: refutation of the deep-basin, shallow-water hypothesis? *Micropaleontology* 37 (3), 289–302.
- Benson, R.H., Rakić-El Bied, K., Bonaduce, G., 1991. An important current reversal (influx) in the Rifian Corridor (Morocco) at the Tortonian-Messinian boundary: the end of Tethys Ocean. *Paleoceanography* 6 (1), 165–192.
- Berner, R.A., 1999. Atmospheric oxygen over Phanerozoic time. *Proc. Natl. Acad. Sci.* 96, 10955.
- Bertini, A., 2006. The Northern Apennines palynological record as a contribute for the reconstruction of the Messinian paleoenvironments. *Sediment. Geol.* 188, 235–258.

- Bertini, A., Corradini, D., 1998. Biostratigraphic and paleoecological significance of *Galeacysta erusca* in the "Lago-Mare" facies from the Mediterranean area (Neogene). *Dino NTNU Vitensk. Mus. Rep. Bot. ser. 6*, 15–16. Abstract.
- Bertoni, C., Cartwright, J., 2007. Major erosion at the end of the Messinian Salinity Crisis: evidence from the Levant Basin, Eastern Mediterranean. *Basin Res.* 19, 1–18.
- Bessis, F., 1986. Some remarks on the study of subsidence of sedimentary basins. Application to the Gulf of Lions margin (Western Mediterranean). *Mar. Pet. Geol.* 3, 37–63.
- Bialik, O.M., Frank, M., Betzler, C., Zammit, R., Waldmann, N.D., 2019. Two-step closure of the Miocene Indian Ocean Gateway to the Mediterranean. *Sci. Rep.* 9 (1), 1–10. <https://doi.org/10.1038/s41598-019-45308-7>.
- Biscaye, P.E., Ryan, W.B.F., Wezel, F.C., 1972. Age and nature of the Pan-Mediterranean subbottom reflector M. *The Mediterranean Sea* 83–90.
- Blanc, P.L., 2002. The opening of the Plio-Quaternary Gibraltar Strait: assessing the size of a cataclysm. *Geodin. Acta* 15, 303–317.
- Blanc-Valleron, M.-M., Rouchy, J.-M., Pierre, C., Badaut-Trauth, D., Schuler, M., 1998. Evidence of Messinian nonmarine deposition at site 968 (Cyprus lower slope). In: *Proceedings of the Ocean Drilling Program, Scientific Results*. ODP Sci. Results 160, Texas, USA, pp. 43–445.
- Bonaduce, G., Sgarrella, F., 1999. Paleocological interpretation of the latest Messinian sediments from southern Sicily (Italy). *Sci. Geol. Ital. Mem.* 54, 83–91.
- Booth-Rea, G., Ranero, R., Grevenmeyer, I.C., 2018. The Alboran volcanic-arc modulated the Messinian faunal exchange and salinity crisis. *Sci. Rep.* 8 <https://doi.org/10.1038/s41598-018-31307-7>.
- Borsetti, A.M., Curzi, P.V., Landuzzi, V., Mutti, M., Ricci Lucchi, F., Sartori, R., Tomadini, L., Zuffa, G.G., 1990. Messinian and pre-Messinian sediments from ODP Leg 107 Sites 652 and 654 in the Tyrrhenian Sea: sedimentologic and petrographic study and possible comparisons with Italian sequences. In: Kastens, K.A., Mascle, J., et al. (Eds.), *Proceedings of the Ocean Drilling Program, Scientific Results*, 107, pp. 169–186.
- Bossio, A., Esteban, M., Giannelli, L., Longinelli, A., Mazzanti, R., Mazzei, R., Ricci Lucchi, F., Salvatore, G., 1978. Some aspects of the upper Miocene in Tuscany. In: *Messinian Seminar*, vol. 4. Pacini, Pisa, 88 pp.
- Bossio, A., Costantini, A., Lazzarotto, A., Liotta, D., Mazzanti, R., 1993. Rassegna delle conoscenze sulla stratigrafia del Neoaototono toscano. *Mem. Soc. Geol. Ital.* 49, 17–98.
- Bosworth, W., Huchon, P., Mc Clay, K., 2005. The Red Sea and Gulf of Aden Basins. *J. Afr. Earth Sci.* 43, 334–378.
- Bowman, S.A., 2012. A comprehensive review of the MSC facies and their origins in the offshore Sirt Basin, Libya. *Pet. Geosci.* 18, 457–469. <https://doi.org/10.1144/petgeo2011-070>.
- Braga, J.C., Martín, J.M., Riding, R., Aguirre, J., Sanchez-Almazo, I.M., Dinares-Turell, J., 2006. Testing models for the Messinian salinity crisis: the Messinian record in Almería, SE Spain. *Sediment. Geol.* 188–189, 131–154. <https://doi.org/10.1016/j.sedgeo.2006.03.002>.
- Brolsma, M.J., 1975. Lithostratigraphy and Foraminiferal assemblages of the Miocene/Pliocene transitional strata at Capo Rossello and Eraclea Minoa (Sicily, Italy): *Kon. Ned. Akad. Wetensch. Amsterdam Proc* 78, 1–40.
- Brunner, B., Bernasconi, S.M., 2005. A revised isotope fractionation model for dissimilatory sulfate reduction in sulfate reducing bacteria. *Geochim. Cosmochim. Acta* 69, 4759–4771.
- Brunner, B., Bernasconi, S.M., Kleikemper, J., Schroth, M.H., 2005. A model for oxygen and sulfur isotope fractionation in sulfate during bacterial sulfate reduction processes. *Geochim. Cosmochim. Acta* 69, 4773–4785.
- Bulian, F., Sierro, F.J., Santiago, L., Jiménez-Espejo, F.J., Bassetti, M.A., 2021. Messinian West Alboran Sea record in the proximity 1 of Gibraltar: early signs of Atlantic-Mediterranean gateway restriction. *Mar. Geol.* 434.
- Burke, A., Present, T.M., Paris, G., Rae, E.C.M., Sandilands, B.H., Gaillardet, J., Peucker-Ehrenbrink, B., Fischer, W.W., McClelland, J.W., Spencer, R.G.M., Voss, B.M., Adkins, J.F., 2018. Sulfur isotopes in rivers: Insights into global weathering budgets, pyrite oxidation, and the modern sulfur cycle. *Earth Planet. Sci. Lett.* 496, 168–177.
- Butler, R.W.H., Likhoshin, W.H., Grasso, M., Pedley, H.M., Ramberti, L., 1995. Tectonics and sequence stratigraphy in Messinian Basins, Sicily: constraints on the initiation and termination of the Mediterranean salinity crisis. *Geol. Soc. Am. Bull.* 107, 425–439.
- Butler, R.W.H., Maniscalco, R., Sturiale, G., Grasso, M., 2015. Stratigraphic variations control deformation patterns in evaporite basins: Messinian examples, onshore and offshore Sicily (Italy). *J. Geol. Soc.* 172, 113–124.
- Camerlenghi, A., Aloisi, V., 2020. Uncovering the Mediterranean Salt Giant (MEDSALT)-Scientific Networking as Incubator of Cross-disciplinary Research in Earth Sciences. *Eur. Rev.* 28 (1), 40–61. <https://doi.org/10.1017/S1062798719000255>.
- Camerlenghi, A., Accetella, D., Costa, S., Lastras, G., Acosta, J., Canals, M., Wardell, N., 2009. Morphogenesis of the SW Balearic continental slope and adjacent abyssal plain, Western Mediterranean Sea. *Int. J. Earth Sci.* 98, 735–750.
- Camerlenghi, A., Del Ben, A., Hübscher, C., Forlin, E., Geletti, R., Brancatelli, G., Micallef, A., Sautle, M., Facchin, L., 2019. Seismic markers of the Messinian salinity crisis in the deep Ionian Basin. *Basin Res.* [bre.12392](https://doi.org/10.1111/bre.12392).
- Camelle, A.L., Urgeles, R., 2017. Large-scale margin collapse during Messinian early sea-level drawdown: the SW Valencia trough, NW Mediterranean. *Basin Res.* 29, 576–595. <https://doi.org/10.1111/bre.12170>.
- Camelle, A.L., Urgeles, R., De Mol, B., Camerlenghi, A., Canning, J.C., 2014. Late Miocene sedimentary architecture of the Ebro Continental Margin (Western Mediterranean): implications for the Messinian Salinity Crisis. *Int. J. Earth Sci.* 103 (2), 423–440.
- Campillo, A.C., Maldonado, A., Mauffret, A., 1992. Stratigraphic and Tectonic evolution of the Western Alboran Sea late Miocene to recent. *Geo-Mar. Lett.* 12, 165–172.
- Capella, W., Flecker, R., Hernández-Molina, F.J., Simon, D., Meijer, P.T., Rogerson, M., Sierro, F.J., Krijgsman, W., 2019. Mediterranean isolation preconditioning the Earth System for late Miocene climate cooling. *Sci. Rep.* 9 (1), 1–8. <https://doi.org/10.1038/s41598-019-40208-2>.
- Capella, W., Spakman, W., van Hinsbergen, D.J., Chertova, M.V., Krijgsman, W., 2020. Mantle resistance against Gibraltar slab dragging as a key cause of the Messinian Salinity Crisis. *Terra Nova* 32 (2), 141–150. <https://doi.org/10.1111/ter.12444>.
- Capellini, G., 1880. Gli strati a Congerie o la formazione gessosa sofferla nella provincia di Pisa e nei dintorni di Livorno. *Mem. R. Accad. Lincei., Cl. Sci. Fis. Mat. Nat.* 5, 1–64.
- Carbonnel, G., 1978. La zone à Loxoconcha djaffarovi Schneider (ostracodes, Miocène supérieur) ou le Messinien de la vallée du Rhône. *Rev. Micropaleontol.* 21 (3), 106–118.
- Carnevale, G., Landini, W., Sarti, G., 2006a. Mare versus Lago-mare: marine fishes and the Mediterranean environment at the end of the Messinian Salinity Crisis. *J. Geol. Soc.* 163 (1), 75–80. <https://doi.org/10.1144/0016-764904-158>.
- Carnevale, G., Caputo, D., Landini, W., 2006b. Late Miocene fish otoliths from the Colombacci Formation (Northern Apennines, Italy): implications for the Messinian 'Lago-mare' event. *Geol. J.* 41 (5), 537–555. <https://doi.org/10.1002/gj.1055>.
- Carnevale, G., Longinelli, A., Caputo, D., Barbieri, M., Landini, W., 2008. Did the Mediterranean marine reflooding precede the Miocene/Pliocene boundary? Paleontological and geochemical evidence from upper Messinian sequences of Tuscany, Italy. *Paleogeogr. Paleoclimatol. Paleoecol.* 257, 81–105. <https://doi.org/10.1016/j.paleo.2007.09.005>.
- Carnevale, G., Dela Pierre, F., Natalicchio, M., Landini, W., 2018. Fossil marine fishes and the "Lago Mare" event: Has the Mediterranean ever transformed into a brackish lake? *Newsl. Stratigr.* 51, 57–72. <https://doi.org/10.1127/nos/2016/0343>.
- Carnevale, G., Gennari, R., Lozar, F., Natalicchio, M., Pellegrino, L., Dela Pierre, F., 2019. Living in a deep desiccated Mediterranean Sea: An overview of the Italian fossil record of the Messinian salinity crisis. *Boll. Soc. Paleontol. Ital.* 58, 109–140. <https://doi.org/10.4435/BSPL.2019.04>.
- Cartwright, J.A., Jackson, M.P.A., 2008. Initiation of gravitational collapse of an evaporitic basin margin: the Messinian saline giant, Levant Basin, eastern Mediterranean. *Geol. Soc. Am. Bull.* 120, 399–413.
- Caruso, A., Pierre, C., Blanc-Valleron, M.M., Rouchy, J.M., 2015. Carbonate deposition and diagenesis in evaporitic environments: the evaporative and sulphur-bearing limestones during the settlement of the Messinian Salinity Crisis in Sicily and Calabria. *Palaeogeogr. Palaeoclimatol. Palaeoeol.* 429, 136–162. <https://doi.org/10.1016/j.paleo.2015.03.035>.
- Caruso, A., Blanc-Valleron, M.M., Da Prato, S., Pierre, C., Rouchy, J.M., 2020. The late Messinian "Lago-Mare" event and the Zanclean Reflooding in the Mediterranean Sea: new insights from the Cuevas del Almanzora section (Vera Basin, South-Eastern Spain). *Earth Sci. Rev.* 200, 102993 <https://doi.org/10.1016/j.earscirev.2019.102993>.
- Casati, P., Bertozzi, P., Cita, M.B., Longinelli, A., Damiani, V., 1976. Stratigraphy and paleoenvironment of the Messinian "Colombacci" Formation in the periadriatic trough. A pilot study. *Memorie della Società Geologica Italiana* 16, 173–195.
- Castradori, D., 1998. Calcareous nanofossils in the basal Zanclean of the Eastern Mediterranean Sea: remarks on paleoceanography and sapropel formation. In: Robertson, A.H.F., Emeis, K.C., Richter, C., Camerlenghi, A. (Eds.), *Proceedings of the Ocean Drilling Program*. US Government Printing Office, Washington, pp. 113–123. *Scientific Results* 160.
- Catalano, R., Valenti, V., Albanese, C., Accaino, F., Sulli, A., Tinivella, U., Morticelli, M. G., Zanolla, C., Giustiniani, M., 2013. Sicily's fold-thrust belt and slab roll-back: the SI. RI. PRO. seismic crustal transect. *J. Geol. Soc.* 170 (3), 451–464.
- Cazzini, F.F., Amadori, C., Bosino, A., Fantoni, R., 2020. New seismic evidence of the Messinian paleomorphology beneath Lake Maggiore area (Italy). *Ital. J. Geosci.* 139 (2), 195–211. <https://doi.org/10.3301/IJG.2019.26>.
- Chumakov, I.S., 1973. Pliocene and Pleistocene deposits of the Nile valley in Nubia and upper Egypt. In: Ryan, W.B.F., Hsu, K.J., et al. (Eds.), *Initial Reports of the Deep Sea Drilling Project*, 13. US Govern. Print. Office, Washington, DC, pp. 1242–1243.
- Cipollari, P., Cosentino, D., Gliozzi, E., 1999. Extension- and compression-related basins in central Italy during the Messinian Lago-Mare event. *Tectonophysics* 315 (1–4), 163–185.
- Cipollari, P., Cosentino, D., Radeff, G., Schildgen, T.F., Faranda, C., Grossi, F., Gliozzi, E., Smedile, A., Gennari, R., Darbas, G., Dudas, F.O., Gürbüz, K., Nazik, A., Echter, H., 2013. Easternmost Mediterranean evidence of the Zanclean flooding event and subsequent surface uplift Adana Basin, southern Turkey. *Geol. Soc. Lond., Spec. Publ.* 372 (1), 473–494. <https://doi.org/10.1144/SP372.5>.
- Cita, M.B., 1973. Inventory of biostratigraphical findings and problems. *Init. Rep. Deep-Sea Drilling Project*. 13 (2), 1045–1065.
- Cita, M.B., Colombo, L., 1979. Sedimentation in the latest Messinian at Capo Rossello (Sicily). *Sedimentology* 26, 497–522.
- Cita, M.B., Wright, R.C., Ryan, W.B.F., Longinelli, A., 1978. Messinian paleoenvironments. In: Hsu, K.J., Montadert, L., et al. (Eds.), *Initial Reports of the Deep Sea Drilling Project*, 42. U.S. Government Printing Office, Washington D.C., pp. 1003–1035.
- Cita, M.B., Santambrogio, S., Melillo, B., Rogate, F., 1990. Messinian Paleoenvironments: New Evidence from the Tyrrhenian Sea (ODP LEG 107). In: *Proceedings of the Ocean Drilling Program, Scientific Results*, 107, pp. 211–227.
- Clauzon, G., 1982. Le canyon messinien du Rhône: Une preuve décisive du "desiccated deep basin model" (Hsu, Cita et Ryan, 1973). *Bull. Soc. Geol. Fr.* 24, 231–246.

- Clauzon, G., Suc, J.-P., Gautier, F., Berger, A., Loutre, M.F., 1996. Alternate interpretation of the Messinian salinity crisis, controversy resolved? *Geology* **24**, 363–366.
- Clauzon, G., Suc, J.P., Popescu, S.M., Marunteanu, M., Rubino, J.L., Marinescu, F., Melinte, M.C., 2005. Influence of Mediterranean sea-level changes on the Dacic Basin (Eastern Paratethys) during the late Neogene: the Mediterranean Lago Mare facies deciphered. *Basin Res.* **17** (3), 437–462. <https://doi.org/10.1111/j.1365-2117.2005.00269.x>.
- Clauzon, G., Suc, J.-P., Do Couto, D., Jouanin, G., Melinte-Dobrinescu, M.C., Jolivet, L., Quillévéré, F., Lebret, N., Mocoehain, L., Popescu, S.-M., Martinell, J., Doménech, R., Rubino, J.-L., Gumiaux, C., Warny, S., Bellas, S.M., Gorini, C., Bache, F., Rabineau, M., Estrada, F., 2015. New insights on the Sorbas Basin (SE Spain): the onshore reference of the Messinian salinity crisis. *Mar. Pet. Geol.* **66**, 71–100. <https://doi.org/10.1016/j.marpetgeo.2015.02.016>.
- Claypool, G.E., Holsen, W.T., Kaplan, I.R., Sakai, H., Zak, I., 1980. The age curves of sulfur and oxygen isotopes in marine sulfate and their mutual interpretation. *Chem. Geol.* **28**, 199–260.
- Colalongo, M.L., Cremonini, G., Farabegoli, E., Sartori, R., Tampieri, R., Tomadin, L., 1976. Paleoenvironmental study of the “Colombacci” Formation in Romagna (Italy): the cella section. *Mem. Soc. Geol. Ital.* **16**, 197–216.
- Colombero, S., Alba, D.M., D’Amico, C., Delfino, M., Esu, D., Giuntelli, P., Harzhauser, M., Mazza, P.P.A., Mosca, M., Neubauer, T.A., Pavia, G., Pavia, M., Villa, A., Carnevale, G., 2017. Late Messinian mollusks and vertebrates from Moncucco Torinese, north-western Italy. Paleoeological and paleoclimatological implications. *Paleoantol. Electron.* **1–66**, 20.1.10A.
- Comas, M.C., Zahn, R., Klaus, A., et al., 1996. Proceedings of the Ocean Drilling Program, Initial Reports, v. 161: College Station, Texas, Ocean Drilling Program.
- Comas, M.C., Platt, J.P., Soto, J.I., Watts, A.B., 1999. 44. The origin and tectonic history of the Alboran Basin: Insights from leg 161 results: Proceedings of the Ocean Drilling Program. *Sci. Res.* **161**, 555–580.
- Consorti, L., Sabbatino, M., Parente, M., 2020. Insights on the paleoecology of Ammonia (Foraminifera, Rotalioidea) from Miocene carbonates of central and southern Apennines (Italy). *Paleogeogr. Paleoclimatol. Paleocool.* **110105** <https://doi.org/10.1016/j.paleo.2020.110105>.
- Corbí, H., Soria, J.M., 2016. Late Miocene-early Pliocene planktonic foraminifer event-stratigraphy of the Bajo Segura basin: a complete record of the western Mediterranean. *Mar. Pet. Geol.* **77**, 1010–1027. <https://doi.org/10.1016/j.marpetgeo.2016.08.004>.
- Corbí, H., Soria, J.M., Lancis, C., Giannetti, A., Tent-Manclús, J.E., Dinarès-Turell, J., 2016. Sedimentological and paleoenvironmental scenario before, during, and after the Messinian Salinity Crisis: The San Miguel de Salinas composite section (western Mediterranean). *Mar. Geol.* **379**, 246–266. <https://doi.org/10.1016/j.margeo.2016.05.017>.
- Corbí, H., Soria, J.M., Giannetti, A., Yébenes, A., 2020. The step-by-step restriction of the Mediterranean (start, amplification, and consolidation phases) preceding the Messinian Salinity Crisis (climax phase) in the Bajo Segura basin. *Geo-Mar. Lett.* **1–21**. <https://doi.org/10.1007/s00367-020-00647-7>.
- Cornée, J.J., Munch, P., Achali, M., Merzadour, G., Azdimoua, A., Quillevere, F., Melinte-Dobrinescu, M., Chaix, C., Ben Moussa, A., Lofi, J., Seranne, A., Moissette, P., 2016. The Messinian erosional surface and early Pliocene reflowing in the Alboran Sea: new insights from the Bouadinar basin. *Morocco. Sediment. Geol.* **333**, 115–129. <https://doi.org/10.1016/j.sedgeo.2015.12.014>.
- Corradini, D., Biffi, U., 1988. Etude des dinokistes à la limite Messien-Pliocène dans la coupe Cava Serredi, Tos cane, Italie. *Bulletin des Centres de Recherche Exploration-Production Elf-Aquitaine* **12** (1), 221–236.
- Cosentino, D., Cipollari, P., Mastro, S.L., Giampaolo, C., 2005. High-frequency cyclicity in the latest Messinian Adriatic foreland basin: insight into paleoclimate and paleoenvironments of the Mediterranean Lago-Mare episode. *Sediment. Geol.* **178** (1–2), 31–53. <https://doi.org/10.1016/j.sedgeo.2005.03.010>.
- Cosentino, D., Federici, I., Cipollari, P., Gliozzi, E., 2006. Environments and tectonic instability in central Italy (Garigliano Basin) during the late Messinian Lago-Mare episode: new data from the onshore Mondragone I well. *Sediment. Geol.* **188**, 297–317. <https://doi.org/10.1016/j.sedgeo.2006.03.010>.
- Cosentino, D., Gliozzi, E., Pionzi, G., 2007. The late Messinian Lago-Mare episode in the Mediterranean Basin: preliminary report on the occurrence of Paratethyan ostracod fauna from central Crete (Greece). *Geobios* **40** (3), 339–349. <https://doi.org/10.1016/j.geobios.2007.01.001>.
- Cosentino, D., Darbaş, G., Gürbüz, K., 2010. The Messinian salinity crisis in the marginal basins of the peri-Mediterranean orogenic systems: examples from the central Apennines (Italy) and the Adana Basin (Turkey). *EGUGA* **24**62.
- Cosentino, D., Bertini, A., Cipollari, P., Florindo, F., Gliozzi, E., Grossi, F., Lo Mastro, S., Sprovieri, M., 2012. Orbital forced paleoenvironmental and paleoclimate changes in the late postevaporitic Messinian of the central Mediterranean Basin. *USA Bull.* **124** (3–4), 499–516. <https://doi.org/10.1130/B30462.1>.
- Cosentino, D., Buchwaldt, R., Sampalmeri, G., Iadanza, A., Cipollari, P., Schildgen, T.F., Hinnov, L.A., Ramezani, J., Bowring, S.A., 2013. Refining the Mediterranean “Messinian gap” with high-precision U-Pb zircon geochronology, central and northern Italy. *Geology* **41**, 323–326. <https://doi.org/10.1130/G33820.1>.
- Cosentino, D., Bracone, V., D’Amico, C., Cipollari, P., Esu, D., Faranda, C., Frezza, V., Gliozzi, E., Grossi, F., Gupperieri, P., Iadanza, A., Kotsakis, D., Soulié-Marsche, I., 2018. The record of the Messinian salinity crisis in mobile belts: insights from the Molise allocthonous units (southern Apennines, Italy). *Paleogeogr. Paleoclimatol. Paleocool.* **503**, 112–130. <https://doi.org/10.1016/j.paleo.2018.04.028>.
- Coulson, S., Pico, T., Austerermann, J., Powell, E., Moucha, R., Mitrovica, J.X., 2019. The role of isostatic adjustment and gravitational effects on the dynamics of the Messinian salinity crisis. *Earth Planet. Sci. Lett.* **525**, 115760.
- Dal Cin, M., Del Ben, A., Moenik, A., Accaino, F., Geletti, R., Wardell, N., Zgur, F., Camerlenghi, A., 2016. Seismic imaging of late Miocene (Messinian) evaporites from western Mediterranean back-arc basins. *Pet. Geosci.* **22**, 297–308. <https://doi.org/10.1144/ptegoe2015-096>.
- De Benedetti, A., 1982. The problem of the origin of the salt deposits in the Mediterranean and of their relations to other salt occurrences in the Neogene formations of the contiguous regions. *Mar. Geol.* **49**, 91–114.
- de la Chapelle, G., Gaudant, J., 1987. Découverte de deux nouveaux gisements de poissons fossiles messiniens dans le bassin de Nijar-Carboneras (Andalousie Orientale): Signification paleoecologique et implications paleogeographiques.
- de la Peña, L.G., Ranero, C.R., Gràcia, E., Booth-Rea, G., 2020. The evolution of the westernmost Mediterranean basins. *Earth Sci. Rev.* **103445**.
- Decima, A., 1964. Ostracodi del Gen. Cyprideis JONES del Neogene e del Quaternario italiani. *Paleont. Italica*, **57**, p. 81.
- Decima, A., Sprovieri, R., 1973. Comments on late Messinian microfaunas in several sections from Sicily. In: Drooger, C.W. (Ed.), *Messinian Events in the Mediterranean*. North-Holland Pub. Co, Amsterdam, pp. 229–234.
- Decima, A., Wezel, F.C., 1971. Osservazioni sulle evaporiti Messiniane della Sicilia centro-meridionale. *Rivista Mineraria Siciliana* **130**–134, 172–187.
- Decima, A., Wezel, F.C., 1973. Late Miocene evaporites of the Central Sicilian Basin. In: Ryan, W.B.F., Hsu, K.J. (Eds.), *Initial Reports of the Deep Sea Drilling Project*, vol. 13. U.S. Gov. Print. Off, Washington, DC, pp. 1234–1240.
- Decima, A., Schreiber, B.C., McKenzie, J.A., 1988. The origin of “evaporative” limestones: an example from the Messinian of Sicily (Italy). *J. Sediment. Petrol.* **58**–2, 256–272.
- Del Olmo, W.M., 2011. The Messinian in the Gulf of Valencia and Alboran Sea (Spain): paleogeography and paleoceanography implications. *Rev. Soc. Geol. Esp.* **24**, 1–22.
- Del Olmo, W.M., Martín, D., 2016. The Messinian record of Spanish onshore and offshore data (Atlantic Ocean and Western Mediterranean Sea). *Pet. Geosci.* **22** (4), 291–296.
- Dela Pierre, F., Bernardi, E., Cavagna, S., Clari, P., Gennari, R., Irace, A., Lozar, F., Lugli, S., Manzi, V., Natalicchio, M., Roveri, M., Violanti, D., 2011. The record of the Messinian salinity crisis in the Tertiary Piedmont Basin (NW Italy): The Alba section revisited. *Paleogeogr. Paleoclimatol. Paleocool.* **310**, 238–255. <https://doi.org/10.1016/j.paleo.2011.07.017>.
- Dela Pierre, F., Clari, P., Bernardi, E., Natalicchio, M., Costa, M., Cavagna, S., Lozar, F., Lugli, S., Manzi, V., Roveri, M., Violanti, D., 2012. Messinian carbonate-rich beds of the Tertiary Piedmont Basin (NW Italy): microbially-mediated products straddling the onset of the salinity crisis. *Paleogeogr. Paleoclimatol. Paleocool.* **34**, 78–93. <https://doi.org/10.1016/j.paleo.2012.05.022>.
- Dela Pierre, F., Clari, P., Natalicchio, M., Ferrando, S., Giustetto, R., Lozar, F., Lugli, S., Manzi, V., Roveri, M., Violanti, D., 2014. Flocculent layers and bacterial mats in the mudstone interbeds of the Primary Lower Gypsum unit (Tertiary Piedmont Basin, NW Italy): archives of paleoenvironmental changes during the Messinian salinity crisis. *Mar. Geol.* **335**, 71–87. <https://doi.org/10.1016/j.margeo.2014.05.010>.
- Dela Pierre, F., Natalicchio, M., Lozar, F., Bonetto, S., Carnevale, G., Cavagna, S., Clari, P., Colombero, S., Violanti, D., 2016. The northernmost record of the Messinian salinity crisis (Piedmont Basin, NW Italy). *Geol. F. Trips* **8**, 1–58. <https://doi.org/10.33011/GFT.2016.03>.
- Delrieu, B., Rouchy, J.M., Foucault, A., 1993. La surface d’érosion finmessinienne en Crète centrale (Grèce) et sur le pourtour méditerranéen: Rapports avec la crise de salinité méditerranéenne. *Comptes rendus de l’Académie des sciences. Série 2, Mécanique, Physique, Chimie, Sciences de l’univers, Sciences de la Terre* **316**, no. 4, pp. 527–533.
- Detttam, D.L., Flessa, K.W., Roopnarine, P.D., Schöne, B.R., Goodwin, D.H., 2004. The use of oxygen isotope variation in shells of estuarine mollusks as a quantitative record of seasonal and annual Colorado River discharge. *Geochim. Cosmochim. Acta* **68** (6), 1253–1263.
- Di Stefano, A., Sturiale, G., 2010. Refinements of calcareous nanofossil biostratigraphy at the Miocene/Pliocene Boundary in the Mediterranean region. *Geobios* **43** (1), 5–20.
- Do Couto, D., Popescu, S.-M., Suc, J.-P., Melinte-Dobrinescu, M.C., Barhoun, N., Gorini, C., Jolivet, L., Poort, J., Jouanin, G., Auxietre, J.-L., 2014. Lago Mare and the Messinian salinity crisis: evidences from the Alboran Sea (S. Spain). *Mar. Pet. Geol.* **52**, 57–76. <https://doi.org/10.1016/j.marpetgeo.2014.01.018>.
- Doebbert, A.C., Johnson, C.M., Carroll, A.R., Beard, B.L., Pietras, J.T., Carson, M.R., Norsted, B., Throckmorton, L.A., 2014. Controls on Sr isotopic variation in lacustrine systems: Eocene green river formation, Wyoming. *Chem. Geol.* **380**, 172–189. <https://doi.org/10.1016/j.chemgeo.2014.04.008>.
- Dominici, S., Danise, S., Benvenuti, M., 2018. Pliocene stratigraphic paleobiology in Tuscany and the fossil record of marine megafauna. *Earth Sci. Rev.* **176**, 277–310.
- Drusoni, O., Maillard, A., Ochoa, D., Lofi, J., Chanier, F., Gaullier, V., Briais, A., Sage, F., Siero, F., Garcia, M., 2015. Messinian Salinity Crisis deposits widespread over the Balearic Promontory: insights from new high-resolution seismic data. *Mar. Pet. Geol.* **66**, 41–54. <https://doi.org/10.1016/j.marpetgeo.2014.09.008>.
- Druckman, Y., Buchbinder, B., Martiniotti, G.M., Tov, R.S., Aharon, P., 1995. The buried Afik Canyon (eastern Mediterranean, Israel): a case study of a Tertiary submarine canyon exposed in Late Messinian times. *Mar. Geol.* **123** (3–4), 167–185.
- Drury, A.J., Westerhold, T., Hodell, D., Röhl, U., 2018. Reinforcing the North Atlantic backbone: revision and extension of the composite splice at ODP Site 982. *Clim. Past* **14** (3), 321–338.
- Emeis, K.-C., Robertson, A.H.F., Richter, C., et al., 1996. *Proc. ODP, Initial Reports*, 160: College Station, TX (Ocean Drilling Program).
- Englebrecht, A.G., Sachs, J.P., 2005. Determination of sediment provenance at drift sites using hydrogen isotopes and unsaturation ratios in alkenones. *Geochim. Cosmochim. Acta* **69**, 4253–4265.

- Estrada, F., Ercilla, G., Gorini, C., Alonso, B., Vazquez, J.T., García-Castellanos, D., Juan, C., Maldonado, A., Ammar, A., Elabbasi, M., 2011. Impact of pulsed Atlantic water inflow into the Alboran Basin at the time of the Zanclean flooding. *GeoMar. Lett.* 31, 361–376.
- Esu, D., 2007. Latest Messinian “Lago-Mare” Lymnocaridinae from Italy: close relations with the Pontian fauna from the Dacic Basin. *Geobios* 40 (3), 291–302. <https://doi.org/10.1016/j.geobios.2006.10.003>.
- Faranda, C., Gliozzi, E., Cipollari, P., Grossi, F., Darbaş, G., Gürbüz, K., Cosentino, D., 2013. Messinian paleoenvironmental changes in the easternmost Mediterranean Basin: Adana Basin, southern Turkey. *Turk. J. Earth Sci.* 22 (5), 839–863. <https://doi.org/10.3906/yer-1205-11>.
- Feng, Y.E., Yankelzon, A., Steinberg, J., Reshef, M., 2016. Lithology and characteristics of the Messinian evaporite sequence of the deep Levant Basin, Eastern Mediterranean. *Mar. Geol.* 376, 118–131. <https://doi.org/10.1016/j.margeo.2016.04.004>.
- Feng, Y.E., Steinberg, J., Reshef, M., 2017. Intra-salt deformation: implications for the evolution of the Messinian evaporites in the Levant basin, eastern Mediterranean. *Mar. Pet. Geol.* 88, 251–267.
- Fiduk, J.C., 2009. Evaporites, petroleum exploration, and the Cenozoic evolution of the Libyan shelf margin, central North Africa. *Mar. Pet. Geol.* 26 (8), 1513–1527.
- Flecker, R., de Villiers, S., Ellam, R.M., 2002. Modelling the effect of evaporation on the salinity-⁸⁷Sr/⁸⁶Sr relationship in modern and ancient marginal-marine systems: the Mediterranean Messinian Salinity Crisis. *Earth Planet. Sci. Lett.* 203, 221–233.
- Flecker, R., Krijgsman, W., Capella, W., de Castro Martins, C., Dmitrieva, E., Maysner, J.P., Marzocchi, A., Modestu, S., Ochoa, D., Simon, D., Tulbure, M., van den Berg, B., van der Schee, M., de Lange, G., Ellam, R., Govers, R., Gutjahr, M., Hilgen, F., Kouwenhoven, T., Lofi, J., Meijer, P., Sierro, F.J., Bachtiri, N., Barhoun, N., Alami, A.C., Chacon, B., Flores, J.A., Gregory, J., Howard, J., Lunt, D., Ochoa, M., Pancost, R., Vincent, S., Youfi, M.Z., 2015. Evolution of the late Miocene Mediterranean-Atlantic gateways and their impact on regional and global environmental change. *Earth Sci. Rev.* 150, 365–392. <https://doi.org/10.1016/j.earscirev.2015.08.007>.
- Fontes, J.-C., Letolle, R., Nesteroff, D., Ryan, W.B.F., 1973. Oxygen, Carbon, Sulfur and Hydrogen stable isotopes in carbonate and sulfate mineral phases of Neogene evaporites, sediments and in interstitial waters. Texas A.M University, O.D.P.C.S., TX, United States (Ed.). In: *Initial Reports of the Deep Sea Drilling Project, Covering Leg 13 of the Cruises of the Drilling Vessel Glomar Challenger* Lisbon, Portugal to Lisbon, Portugal, August-October 1970., United States, pp. 788–796.
- Fortuin, A.R., Krijgsman, W., 2003. The Messinian of the Nijar basin (SE Spain): sedimentation, depositional environments and paleogeographic evolution. *Sediment. Geol.* 160, 213–242.
- Fortuin, A.R., Kelling, J.M.D., Roep, T.B., 1995. The enigmatic Messinian -Pliocene section of Cuevas del Almanzora (Vera Basin, SE Spain) revisited-erosional features and strontium isotope ages. *Sediment. Geol.* 97, 177–201.
- Frey-Martinez, J.F., Cartwright, J.A., Burgess, P.M., Bravo, J.V., 2004. 3D seismic interpretation of the Messinian Unconformity in the Valencia Basin, Spain. *Geol. Soc. Lond. Mem.* 29 (1), 91–100.
- Friedman, G.M., 1973. Petrographic data and comments on the depositional environment of the Miocene sulfates and dolomites at Sites 124, 132, and 134, western Mediterranean Sea. In: Ryan, W.B.F., Hsü, K.J., et al. (Eds.), *Initial Reports of the Deep Sea Drilling Project 13*. U. S. Government Printing Office, Washington, pp. 695–708.
- Frignì, M., Youssef, M.B., Ouaja, M., 2016. Evidence of “Lago-Mare” episode around the Messinian-Pliocene boundary in eastern Tunisia (central Mediterranean). *J. Afr. Earth Sci.* 123, 57–74. <https://doi.org/10.1016/j.jafrearthsci.2016.07.007>.
- Fritz, P., Basharmal, G.M., Drimmie, R.J., Ibsen, J.J., Qureshi, R.M., 1989. Oxygen isotope exchange between sulphate and water during bacterial reduction of sulphate. *Chem. Geol.* 79, 99–105.
- Gallais, F., Gutscher, M.A., Graindorge, D., Klaeschen, D., 2018. 12.B&E-Ionian Basin. In: *J. Lofi (Ed.), Seismic Atlas of the Messinian salinity crisis markers in the Mediterranean sea*. Volume 2. - Mémoires de la Société géologique de France, n.s., 2018, t. 181, and Commission for the Geological Map of the World, pp. 41–44.
- García-Alix, A., Minwer-Barakat, R., Martín Suárez, E., Freudenthal, M., Aguirre, J., Kaya, F., 2016. Updating the Europe-Africa small mammal exchange during the late Messinian. *J. Biogeogr.* 43 (7), 1336–1348.
- García-Castellanos, D., Villaseñor, A., 2011. Messinian salinity crisis regulated by competing tectonics and erosion at the Gibraltar arc. *Nature* 480, 359–363. <https://doi.org/10.1038/nature10651>.
- García-Castellanos, D., Estrada, F., Jiménez-Munt, I., Gorini, C., Fernández, M., Vergés, J., De Vicente, R., 2009. Catastrophic flood of the Mediterranean after the Messinian salinity crisis. *Nature* 462, 10. <https://doi.org/10.1038/nature08555>.
- García-Castellanos, D., Micallef, A., Estrada, F., Camerlenghi, A., Ercilla, G., Periañez, R., Abril, J.M., 2020. The Zanclean mega-flood of the Mediterranean—Searching for independent evidence. *Earth Sci. Rev.* 201, 103061. <https://doi.org/10.1016/j.earscirev.2019.103061>.
- García-García, F., Corbi, H., Sorja, J.M., Viseras, C., 2011. Architecture analysis of a river flood-dominated delta during an overall sea-level rise (Early Pliocene, SE Spain). *Sediment. Geol.* 237, 102–113.
- García-Veigas, J., Ortí, F., Rosell, L., Ayora, C., Rouchy, J.M., Lugli, S., 1995. The Messinian salt of the Mediterranean: geochemical study of the salt from the Central Sicily Basin and comparison with the Lorca Basin (Spain). *Bull. Soc. Géol. Fr* 166, 699–710.
- García-Veigas, J., Cendón, D.I., Gibert, L., Lowenstein, T.K., Artiaga, D., 2018. Geochemical indicators in Western Mediterranean Messinian evaporites: Implications for the salinity crisis. *Mar. Geol.* 403, 197–214. <https://doi.org/10.1016/j.margeo.2018.06.005>.
- Gargani, J., Moretti, I., Letouzey, J., 2008. Evaporite accumulation during the Messinian Salinity Crisis: the Suez rift case. *Geophys. Res. Lett.* 35 (2) <https://doi.org/10.1029/2007GL032494>.
- Gaullier, V., Chanier, F., Lymer, G., Vendeville, B., Maillard, A., Thion, I., Lofi, J., Sage, F., Loncke, L., 2014. Salt tectonics and crustal tectonics along the Eastern Sardinian margin, Western Tyrrhenian: new insights from the «METYSS 1» cruise. *Tectonophysics*. <https://doi.org/10.1016/j.tecto.2013.12.015>.
- Geletti, R., Zgur, F., Del Ben, A., Buriola, F., Fais, S., Fedi, M., Forte, E., Mocknik, A., Paoletti, V., Pipan, M., Ramella, R., Romeo, R., Romi, A., 2014. The Messinian Salinity Crisis: new seismic evidence in the West-Sardinian Margin and Eastern Sardo-Provençal basin (West Mediterranean Sea). *Mar. Geol.* 351, 76–90. <https://doi.org/10.1016/j.margeo.2014.03.019>.
- Gennari, R., Iaccarino, S.M., Di Stefano, A., Sturiale, G., Cipollari, P., Manzi, V., Roveri, M., Cosentino, D., 2008. The Messinian–Zanclean boundary in the Northern Apennine. *Stratigraphy* 5, 307–322.
- Gennari, R., Manzi, V., Angeletti, L., Bertini, A., Biffi, U., Ceregato, A., Rosso, A., 2013. A shallow water record of the onset of the Messinian salinity crisis in the Adriatic foredeep (Legnagnone section, Northern Apennines). *Paleogeogr. Paleoclimatol. Paleogeogr.* 386, 145–164.
- Ghibaud, G., Clari, P., Perello, M., 1985. Litostratigrafia, sedimentologia ed evoluzione tettonico-sedimentaria dei depositi miocenici del margine sud-orientale del bacino terziario ligure-piemontese (Vallù Borbera, Scrvia e Lemme). In memoria di Carlo Sturani. *Boll. Soc. Geol. Ital.* 104 (3), 349–397.
- Ghielmi, M., Minervini, M., Nini, C., Rogledi, S., Rossi, M., Vignolo, A., 2010. Sedimentary and tectonic evolution in the eastern Po-Plain and northern Adriatic Sea area from Messinian to Middle Pleistocene (Italy). *Rendiconti Lincei* 21 (1), 131–166. <https://doi.org/10.1007/s12210-010-0101-5>.
- Ghielmi, M., Minervini, M., Nini, C., Rogledi, S., Rossi, M., 2013. Late Miocene-Middle Pleistocene sequences in the Po Plain-Northern Adriatic Sea (Italy): the stratigraphic record of modification phases affecting a complex foreland basin. *Marine and Petroleum Geology, Special Issue: The Geology of the Pre-Adriatic Basin and of the Adriatic Sea* 42, 50–81. <https://doi.org/10.1016/j.margeo.2012.11.007>.
- Gignoux, M., 1936a. *Géologie stratigraphique*, 2^e édition. Masson, Paris.
- Gignoux, M., 1936b. *Géologie stratigraphique*, 2^e édition. Masson, Paris.
- Gillet, S., 1932. Essai de classification du Miocene supérieur et du Pliocene inférieur de Roumanie. La Transylvanie et le Banat. *Comptes Rendus Hebdomadaires des séances de l'Académie des sciences*. Séance 27 Décembre, 1932. Académie des Sciences, Paris.
- Gillet, S., 1933. Essai de classification du Miocene supérieur et du Pliocene inférieur de Roumanie. Le bassin dacique. *Comptes Rendus Hebdomadaires des séances de l'Académie des sciences*. 01/1933. Académie des Sciences, Paris.
- Gladstone, R., Flecker, R., Valdes, P., Lunt, D., Markwick, P., 2007. The Mediterranean hydrologic budget from a Late Miocene global climate simulation. *Paleogeogr. Paleoclimatol. Paleoeoc.* 251 (2), 254–267. <https://doi.org/10.1016/j.paleo.2007.03.050>.
- Gliozzi, E., 1999. A late Messinian brackish water ostracod fauna of Paratethyan aspect from Le Vicenne Basin (Abruzzi, central Apennines, Italy). *Paleogeogr. Paleoclimatol. Paleoeoc.* 151 (1–3), 191–208.
- Gliozzi, E., Grossi, F., 2008. Late Messinian lago-mare ostracod paleoecology: a correspondence analysis approach. *Paleogeogr. Paleoclimatol. Paleoeoc.* 264 (3–4), 288–295. <https://doi.org/10.1016/j.paleo.2007.03.055>.
- Gliozzi, E., Ceci, M.E., Grossi, F., Ligiós, S., 2007. Paratethyan ostracod immigrants in Italy during the Late Miocene. *Geobios* 40 (3), 325–337. <https://doi.org/10.1016/j.geobios.2006.10.004>.
- Golovina, L.A., Radionova, E.P., van Baak, C.G., Krijgsman, W., Palcu, D.V., 2019. A Late Maotian age (6.7–6.3 Ma) for the enigmatic “Pebby Breccia” unit in DSDP Hole 380A of the Black Sea. *Paleogeogr. Paleoclimatol. Paleoeoc.* 533, 109269. <https://doi.org/10.1016/j.paleo.2019.109269>.
- Gomes, M.L., Johnston, D.T., 2017. Oxygen and sulfur isotopes in sulfate in modern euxinic systems with implications for evaluating the extent of euxinia in ancient oceans. *Geochim. Cosmochim. Acta* 205, 331–359.
- Gorini, C., Lofi, J., Duval, C., Dos Reis, A.T., Guennoc, P., Lestrat, P., Mauffret, A., 2005. The Late Messinian salinity crisis and Late Miocene Tectonism: interaction and consequence on the physiography and post-rift evolution of the gulf of Lions margin. *Mar. Pet. Geol.* 22, 695–712.
- Griffin, D.L., 2002. Aridity and humidity: two aspects of the late Miocene climate of North Africa and the Mediterranean. *Paleogeogr. Paleoclimatol. Paleoeoc.* 182 (1–2), 65–91.
- Grossi, F., Cosentino, D., Gliozzi, E., 2008. Late Messinian Lago-Mare ostracods and paleoenvironments of the central and eastern Mediterranean Basin. *Boll. Soc. Paleontol. Ital.* 47 (2), 131–146.
- Grossi, F., Gliozzi, E., Cosentino, D., 2011. Paratethyan ostracod immigrants mark the biostatigraphy of the Messinian Salinity Crisis. *Joannae Geologie und Palaeontologie* 11, 66–68.
- Grossi, F., Gliozzi, E., Anadón, P., Castorina, F., Voltaggio, M., 2015. Is *Cyprideis agrentina* Decima a good paleosalinometer for the Messinian Salinity Crisis? Morphometrical and geochemical analyses from the Eraclea Minoa section (Sicily). *Paleogeogr. Paleoclimatol. Paleoeoc.* 419, 75–89. <https://doi.org/10.1016/j.paleo.2014.09.024>.
- Grothe, A., 2016. *The Messinian Salinity Crisis: a Paratethyan perspective* (Doctoral dissertation, University Utrecht).
- Grothe, A., Sangiorgi, F., Mulders, Y.R., Vasiliev, I., Reichart, G.-J., Brinkhuis, H., Stoica, M., Krijgsman, W., 2014. Black Sea desiccation during the Messinian Salinity Crisis: fact or fiction? *Geology* 42 (7), 563–566. <https://doi.org/10.1130/G35503.1>.

- Grothe, A., Sangiorgi, F., Brinkhuis, H., Stoica, M., Krijgsman, W., 2018. Migration of the dinoflagellate *Galaeacysta etrusca* and its implications for the Messinian Salinity Crisis. *Newsl. Stratigr.* 51 (1), 73–91. <https://doi.org/10.1127/nos/2016/0340>.
- Grothe, A., Andreotto, F., Reichart, G.J., Wolthers, M., Van Baak, C.G., Vasiliev, I., Stoica, M., Sangiorgi, F., Middelburg, J.J., Davies, G.R., Krijgsman, W., 2020. Paratethys pacing of the Messinian Salinity Crisis: low salinity waters contributing to gypsum precipitation? *Earth Planet. Sci. Lett.* 532, 116029 <https://doi.org/10.1016/j.epsl.2019.116029>.
- Grunert, P., Harzhauser, M., Rosenthal, V., Carnevale, G., 2016. Estuarine Lago Mare fauna from the Tertiary Piedmont Basin indicates episodic Atlantic/Mediterranean exchange during the final stage of the Mediterranean Salinity Crisis. *Paleogeogr. Paleoclimatol. Paleocool.* 457, 70–79. <https://doi.org/10.1016/j.paleo.2016.06.005>.
- Guennoc, P., Réhault, J.P., Thionon, I., 2011. West-Corsica Margin: MSC basal units. In: Lofi, J., et al. (Eds.), *Mémoires de la Société géologique de France and World Geological Map Commission ed.*, pp. 1–72.
- Guerra-Merchán, A., Serrano, F., Garcés, M., Gofas, S., Esu, D., Gliozzi, E., Grossi, F., 2010. Messinian Lago-Mare deposits near the Strait of Gibraltar (Malaga basin, S Spain). *Paleogeogr. Paleoclimatol. Paleocool.* 285 (3–4), 264–276. <https://doi.org/10.1016/j.paleo.2009.11.019>.
- Guerra-Merchán, A., Serrano, F., Hlila, R., El Kadiri, K., de Galdeano, C.S., Garcés, M., 2014. Tectono-sedimentary evolution of the peripheral basins of the Alboran Sea in the arc of Gibraltar during the latest Messinian-Pliocene. *J. Geodyn.* 77, 158–170. <https://doi.org/10.1016/j.jog.2013.12.003>.
- Gülüz, E., Durak, H., Özkaptan, M., Krijgsman, W., 2020. Paleomagnetic constraints on the early Miocene closure of the southern Neo-Tethys (Van region; East Anatolia): Inferences for the timing of Eurasia-Arabia collision. *Glob. Planet. Chang.* 185, 103089. <https://doi.org/10.1016/j.gloplacha.2019.103089>.
- Güneş, P., Aksu, A.E., Hall, J., 2018. Internal seismic stratigraphy of the Messinian evaporites across the northern sector of the eastern Mediterranean Sea. *Mar. Pet. Geol.* 91, 297–320. <https://doi.org/10.1016/j.marpetgeo.2018.01.016>.
- Gvirtzman, Z., Reshef, M., Buch-Leviatan, O., Ben-Avraham, Z., 2013. Intense salt deformation in the Levant Basin in the middle of the Messinian salinity crisis. *Earth Planet. Sci. Lett.* 379, 108–119.
- Gvirtzman, Z., Reshef, M., Buch-Leviatan, O., Groves-Gidney, G., Karcz, Z., Makovsky, Y., Ben-Avraham, Z., 2015. Bathymetry of the Levant basin: interaction of salt-tectonics and surficial mass movements. *Mar. Geol.* 360, 25–39. <https://doi.org/10.1016/j.margeo.2014.12.001>.
- Gvirtzman, Z., Manzi, V., Calvo, R., Gavrieli, I., Gennari, R., Lugli, S., Reghizzi, M., Roveri, M., 2017. Intra-Messinian truncation surface in the Levant Basin explained by subaqueous dissolution. *Geology* 45 (10), 915–918. <https://doi.org/10.1130/G39113.1>.
- Hajj, F., Poszwa, A., Bouchez, J., Guérol, F., 2017. Radiogenic and “stable” strontium isotopes in provenance studies: a review and first results on archaeological wood from shipwrecks. *J. Archaeol. Sci.* 86, 24–49. <https://doi.org/10.1016/j.jas.2017.09.005>.
- Hajós, M., 1973. 34.5. The Mediterranean diatoms. In: *Proceedings of the Ocean Drilling Program: Initial report. Part A*, 944.
- Hallett, D., 2002. *Petroleum Geology of Libya*. Elsevier Inc., New York, 503 pp.
- Haq, B., Gorini, C., Baur, J., Moneron, J., Rubino, J.L., 2020. Deep Mediterranean’s Messinian evaporite giant: how much salt? *Glob. Planet. Chang.* 184, 103052 <https://doi.org/10.1016/j.gloplacha.2019.103052>.
- Hardie, L.A., Lowenstein, T.K., 2004. Did the Mediterranean Sea dry out during the Miocene? A reassessment of the evaporite evidence from DSDP Legs 13 and 42A cores. *J. Sediment. Res.* 74, 453–461.
- Harzhauser, M., Neubauer, T.A., Georgopoulou, E., Esu, D., D’Amico, C., Pavia, G., Giuntelli, P., Carnevale, G., 2015. Late Messinian continental and Lago-Mare gastropods from the Tertiary Piedmont Basin. *NW Italy. Boll. Soc. Paleontol. Ital.* 54, 1–53. <https://doi.org/10.4435/BSP12015.1>.
- Herbert, T.D., Lawrence, K.T., Tzanova, A., Peterson, L.C., Caballero-Gill, R., Kelly, C.S., 2016. Late Miocene global cooling and the rise of modern ecosystems. *Nat. Geosci.* 9, 843–847. <https://doi.org/10.1038/ngeo2813>.
- Hilgen, F.J., 1991. Astronomical calibration of Gauss to Matuyama sapropels in the Mediterranean and implication for the geomagnetic polarity time scale. *Earth Planet. Sci. Lett.* 104 (2–4), 226–244.
- Hilgen, F.J., Krijgsman, W., Langereis, C.G., Lourens, L.J., Santarelli, A., Zachariasse, W. J., 1995. Extending the astronomical (polarity) time scale into the Miocene. *Earth Planet. Sci. Lett.* 136, 495–510.
- Hilgen, F., Kuiper, K., Krijgsman, W., Snel, E., van der Laan, E., 2007. Astronomical tuning as the basis for high resolution chronostratigraphy: the intricate history of the Messinian Salinity Crisis. *Stratigraphy* 4 (2–3), 231–238.
- Hodell, D.A., Benson, R.H., Kent, D.V., Boersma, A., Rakec-Id Bied, K., 1994. Magnetostratigraphic, biostratigraphic, and stable isotope stratigraphy of an Upper Miocene drill core from the Salé Briqueuete (northwest Morocco): a high-resolution chronology for the Messinian stage. *Paleoceanography* 9, 835–855.
- Hodell, D.A., Curtis, J.H., Sierro, F.J., Raymo, M.E., 2001. Correlation of late Miocene to early Pliocene sequences between the Mediterranean and North Atlantic. *Paleoceanography* 16, 164–178.
- Hsü, K.J., 1972. Origin of Saline Giants: a critical review after the discovery of the Mediterranean evaporite. *Earth-Sci. Rev.* 8, 371–396.
- Hsü, K.J., Ryan, W.B.F., Cita, M., 1973a. Late Miocene desiccation of the Mediterranean. *Nature* 242, 240.
- Hsü, K.J., Cita, M.B., Ryan, W.B.F., 1973b. The origin of the Mediterranean evaporites. In: Ryan, W.B.F., Hsü, K.J., et al. (Eds.), *Initial Reports of the Deep Sea Drilling Project*, 13. U. S. Government Printing Office, Washington, pp. 1203–1231.
- Hsü, K.J., Montadert, L., Bernoulli, D., Cita, M.B., Erikson, A., Garrison, R.G., Kidd, R.B., Mélières, F., Müller, C., Wright, R., 1978a. History of the Mediterranean salinity crisis. In: Hsü, K.J., Montadert, L., et al. (Eds.), *Initial Reports of the Deep Sea Drilling Project*. U.S. Government Printing Office, Washington, DC.
- Hsü, K.J., Montadert, L., Bernoulli, D., Bizon, G., Cita, M., Erikson, A., Fabricius, F., Garrison, R.E., Kidd, R.B., Mélières, F., Müller, C., Wright, R.C., 1978b. Initial reports of the deep sea drilling project: DSDP volume XLII Part 1.
- Iaccarino, S., Bossio, A., 1999. Paleoenvironment of uppermost Messinian sequences in the western Mediterranean (Sites 974, 975, and 978). In: *Proceedings of the Ocean Drilling Program, Scientific Results* (Vol. 161, 529–541). College Station, TX: Ocean Drilling Program.
- Iaccarino, S.M., Cita, M.B., Gaboardi, S., Gruppini, G.M., 1999. 15. High-Resolution Biostratigraphy at the Miocene/Pliocene boundary in Holes 974b and 975b, Western Mediterranean. In: *Proceedings of the Ocean Drilling Program: Scientific Results*, Vol. 161, p. 197.
- Hsü, K.J., Ryan, W.B.F., Schreiber, B.C., 1973c. Petrography of a halite sample from Hole 134-Balearic Abyssal Plain. In: Ryan, W.B.F., Hsü, K.J., et al. (Eds.), *Initial Reports of the Deep Sea Drilling Project*, 13. U. S. Government Printing Office, Washington, pp. 708–711.
- Iaccarino, S.M., Bertini, A., Di Stefano, A., Ferraro, L., Gennari, R., Grossi, F., Lirer, F., Manzi, V., Menichetti, E., Ricci Lucchi, M., Taviani, M., Sturiale, G., Angeletti, L., 2008. The Trave section (Monte dei Corvi, Ancona, central Italy): an integrated paleontological study of the Messinian deposits. *Stratigraphy* 5 (3–4), 281–306.
- Ingram, B.L., Sloan, D., 1992. Strontium isotopic composition of estuarine sediments as paleosalinity-paleoclimate indicator. *Science* 255, 68–72.
- Jagger, L.J., Bevan, T.G., McClay, K.R., 2020. Tectono-stratigraphic evolution of the SE Mediterranean passive margin, offshore Egypt and Libya. *Geol. Soc. Lond., Spec. Publ.* 476 (1), 365–401.
- Johnston, D.T., Gill, B.C., Masterson, A., Beirne, E., Casciotti, K.L., Kna, A.N., Berelson, W., 2014. Placing an upper limit on cryptic marine sulphur cycling. *Nature* 513, 530–533.
- Jolivet, L., Augier, R., Robin, C., Suc, J.-P., Rouchy, J.-M., 2006. Lithospheric-scale geodynamic context of the Messinian Salinity Crisis. *Sediment. Geol.* 188–189, 9–33. <https://doi.org/10.1016/j.sedgeo.2006.02.004>.
- Just, J., Hübscher, C., Betzler, C., Lüdmann, T., Reichert, K., 2011. Erosion of continental margins in the Western Mediterranean due to sea-level stagnancy during the Messinian Salinity Crisis. *Geo-Mar. Lett.* 31 (1), 51–64.
- Kaplan, I.R., Rittenberg, S.C., 1964. Microbiological fractionation of sulphur isotopes. *Microbiology* 34, 195–212.
- Karakitsios, V., Cornée, J., Tsourou, T., Moissette, P., Kontakiotis, G., Agiadi, K., Manoutsoglou, E., Triantaphyllou, M., Koskeridou, E., 2017a. Messinian salinity crisis record under strong freshwater input in marginal, intermediate, and deep environments: the case of the North Aegean. *Paleogr. Paleoclimatol. Paleocool.* 485, 316–335. <https://doi.org/10.1016/j.palaeo.2017.06.020>.
- Karakitsios, V., Roveri, M., Lugli, S., Manzi, V., Gennari, R., Antonarakou, A., Triantaphyllou, M., Agiadi, K., Kontakiotis, G., Kafousia, N., de Rafelis, M., 2017b. A record of the Messinian salinity crisis in the eastern Ionian tectonically active domain (Greece, eastern Mediterranean). *Basin Res.* 29, 203–233. <https://doi.org/10.1111/br.12173>.
- Kartveit, K.H., Ulsund, H.B., Johansen, S.E., 2019. Evidence of sea level drawdown at the end of the Messinian salinity crisis and seismic investigation of the Nahr Menashe unit in the northern Levant Basin, offshore Lebanon. *Basin Res.* 31 (5), 827–840. <https://doi.org/10.1111/br.12347>.
- Kastens, K.A., Mascle, J., 1990. The geological evolution of the Tyrrhenian Sea: An introduction to the scientific results of ODP Leg 107. In: *Proceedings of the Ocean Drilling Program, Scientific Results* (Vol. 107, No. 3), p. 26. College Station, TX (Ocean Drilling Program).
- Kastens, K.A., Mascle, J., Auroux, C., et al., 1987. *Proc. ODP, Init. Repts.*, 107. College Station, TX (Ocean Drilling Program). <https://doi.org/10.2973/odp.proc.ir.107.1987>.
- Keller, G., Abramovich, S., 2009. Lilliput effect in late Maastrichtian planktic foraminifera: response to environmental stress? *Paleogeography. Paleoclimatol. Paleocool.* 284, 47–62.
- Keogh, S.M., Butler, R.W.H., 1999. The Mediterranean water body in the late Messinian: interpreting the record from marginal basins on Sicily. *J. Geol. Soc.* 156 (4), 837–846.
- Kirkham, C., Bertoni, C., Cartwright, J., Lensky, N.G., Sirota, I., Rodriguez, K., Hodgson, N., 2020. The demise of a ‘salt giant’ driven by uplift and thermal dissolution. *Earth Planet. Sci. Lett.* 531, 115933 <https://doi.org/10.1016/j.epsl.2019.115933>.
- Kováč, M., Andreyeva-grigorovich, A., Bajraktarević, Z., Brzobohatý, R., Filipescu, S., Fodor, L., Harzhauser, M., Nagy-marosy, A., Oszczyppik, N., Pavelić, D., Rögl, F., Saffić, B., Sliva, U., Studenćka, B., 2007. Badenian evolution of the Central Paratethys Sea: paleogeography, climate and eustatic sea-level changes. *Geol. Carpathica* 58, 579–606.
- Krijgsman, W., Meijer, P.T., 2008. Depositional environments of the Mediterranean “Lower Evaporites” of the Messinian salinity crisis: constraints from quantitative analyses. *Mar. Geol.* 253 (3–4), 73–81. <https://doi.org/10.1016/j.margeo.2008.04.010>.
- Krijgsman, W., Hilgen, F.J., Raffi, I., Sierro, F.J., Wilson, D.S., 1999a. Chronology, causes, and progression of the Messinian salinity crisis. *Nature* 400, 652–655.
- Krijgsman, W., Hilgen, F.J., Marabini, S., Vai, G.B., 1999b. New paleomagnetic and cyclostratigraphic age constraints on the Messinian of the Northern Apennines (Vena del Gesso Basin, Italy). *Mem. Soc. Geol. Ital.* 54, 25–33.
- Krijgsman, W., Fortuin, A.R., Hilgen, F.J., Sierro, F.J., 2001. Astrochronology for the Messinian Sorbas basin (SE Spain) and orbital (precessional) forcing for evaporite cyclicity. *Sediment. Geol.* 140, 43–60.

- Krijgsman, W., Gaborardi, S., Hilgen, F.J., Iaccarino, S., Kaemel, E.D., Laan, E.V.D., 2004. Revised astrochronology for the Ain el Beida section (Atlantic Morocco): no glacio-eustatic control for the onset of the Messinian Salinity Crisis. *Stratigraphy* 1, 87–101.
- Krijgsman, W., Stoica, M., Vasiliev, I., Popov, V.V., 2010. Rise and fall of the Paratethys Sea during the Messinian Salinity Crisis. *Earth Planet. Sci. Lett.* 290 (1–2), 183–191. <https://doi.org/10.1016/j.epsl.2009.12.020>.
- Krijgsman, W., Capella, W., Simon, D., Hilgen, F.J., Kouwenhoven, T.J., Meijer, P.Th., Sierro, F.J., Tulbure, M.A., van den Berg, B.C.J., van der Schee, M., Flecker, R., 2018. The Gibraltar Corridor: watergate of the Messinian Salinity Crisis. *Mar. Geol.* 403, 238–246. <https://doi.org/10.1016/j.margeo.2018.06.008>.
- Krijgsman, W., Palcu, D., Andreetto, F., Stoica, M., Mandic, O., 2020a. Changing seas in the late Miocene Northern Aegean: a Paratethyan arcoach to Mediterranean basin evolution. *Earth Sci. Rev.* 103386 <https://doi.org/10.1016/j.earscirev.2020.103386>.
- Krijgsman, W., Stoica, M., Hoyle, T.M., Jorissen, E.L., Lazarev, S., Rausch, L., Bista, D., Alçiçek, M.C., Ilgar, A., van den Hoek Ostende, L.W., Mayda, S., Raffi, I., Flecker, R., Mandic, O., Neubauer, T.A., Wesselingh, F.P., 2020b. The myth of the Messinian Dardanelles: Late Miocene stratigraphy and paleogeography of the ancient Aegean-Black Sea gateway. *Paleogeogr. Paleoclimatol. Paleocool.* 110033 <https://doi.org/10.1016/j.paleo.2020.110033>.
- Van der Laan, E., Gaborardi, S., Hilgen, F.J., Lourens, L.J., 2005. Regional climate and glacial control on high-resolution oxygen isotope records from Ain El Beida (latest Miocene, NW Morocco): a cyclostratigraphic analysis in the depth and time domain. *Paleoceanography* 20. <https://doi.org/10.1029/2003PA000995>. PA1001.
- Van der Laan, E., Snel, E., de Kaemel, E., Hilgen, F.J., Krijgsman, W., 2006. No major deglaciation across the Miocene-Pliocene boundary: integrated stratigraphy and astronomical tuning of the Loulja sections (Bou Regreg area, NW Morocco). *Paleoceanography* 21. <https://doi.org/10.1029/2005PA001193>. PA3011.
- Laskar, J.J., Robutel, P., Joutel, F., Gastineau, M., Correia, A.C.M., Levrard, B., 2004. A long term numerical solution for the insolation quantities of the Earth. *Astron. Astrophys.* 428, 261–285.
- Lazarev, S., de Leeuw, A., Stoica, M., Mandic, O., van Baak, C.G.C., Vasiliev, I., Krijgsman, W., 2020. From Khersonian drying to Pontian “flooding”: Late Miocene stratigraphy and paleoenvironmental evolution of the Dacian Basin (Eastern Paratethys). *Glob. Planet. Chang.* 103224 <https://doi.org/10.1016/j.gloplacha.2020.103224>.
- Leavitt, W.D., Halevy, L., Bradley, A.S., Johnston, D.T., 2013. Influence of sulfate reduction rates on the Phanerozoic sulfur isotope record. *Proc. Natl. Acad. Sci.* 110, 11244.
- Leila, M., Moscarriello, A., Segvić, B., 2018. Depositional facies controls on the diagenesis and reservoir quality of the Messinian Qawasim and Abu Madf formations, onshore Nile Delta, Egypt. *Geol. J.* 54 (3), 1797–1813.
- Liu, J., Li, S., Zhong, J., Zhu, X., Guo, Q., Lang, Y., Han, X., 2017. Sulfate sources constrained by sulfur and oxygen isotopic compositions in the upper reaches of the Xijiang River, China. *Acta Geochimica* 36, 611–618.
- Lloyd, R.M., 1968. Oxygen isotope behavior in the Sulfate-Water System. *J. Geophys. Res.* 1896–1977 (73), 6099–6110.
- Lofi, J., 2018. Seismic Atlas of the Messinian salinity crisis markers in the Mediterranean sea. Volume 2 - Mémoires de la Société géologique de France, n.s., 2018, t. 181, and Commission for the Geological Map of the World, 72 p. + DVD. <https://doi.org/10.10682/2018M ESSINV2>.
- Lofi, J., Gorini, C., Berne, S., Clauzon, G., Dos Reis, A.T., Ryan, W.B.F., Steckler, M.S., 2005. Erosional processes and paleo-environmental changes in the Western Gulf of Lions (SW France) during the Messinian Salinity Crisis. *Mar. Geol.* 217, 1–30. <https://doi.org/10.1016/j.margeo.2005.02.014>.
- Lofi, J., Sage, F., Déverchère, J., Loncke, L., Maillard, A., Gaullier, V., Thonin, I., Gillet, H., Guennoc, P., Gorini, C., 2011a. Refining our knowledge of the Messinian salinity crisis records in the offshore domain through multi-site seismic analysis. *Bulletin de la Société géologique de France* 182 (2), 163–180.
- Lofi, J., Déverchère, J., Gaullier, V., Gillet, H., Gorini, C., Guennoc, P., Loncke, L., Maillard, A., Sage, F., Thonin, I., 2011b. Seismic atlas of the “Messinian Salinity Crisis” markers in the Mediterranean and Black seas. Commission for the Geological Map of the World and Mémoires de la Société Géologique de France. *Nouv. Ser.* 72.
- Loget, N., Davy, P., Van Den Driessche, J., 2006. Mesoscale fluvial erosion parameters deduced from modelling the Mediterranean sea-level drop during the Messinian (late Miocene). *J. Geophys. Res.* 111, F03005.
- Loncke, L., Gaullier, V., Masclé, J., Vendeville, B., Camerla, L., 2006. The Nile deep-sea fan: An example of interacting sedimentation, salt tectonics, and inherited subsalt paleotopographic features. *Mar. Pet. Geol.* 23, 297–315. <https://doi.org/10.1016/j.marpetgeo.2006.01.001>.
- Loxideix, L., Benzakour, M., Suc, J.P., Turon, J.L., 2007. Messinian paleoenvironments and hydrology in Sicily (Italy): the dinoflagellate cyst record. *Geobios* 40 (3), 233–250. <https://doi.org/10.1016/j.geobios.2006.12.001>.
- Longinelli, A., 1979. Isotope geochemistry of some Messinian evaporates: paleoenvironmental implications. *Paleogeogr. Paleoclimatol. Paleocool.* 29, 95–123.
- Longinelli, A., Craig, H., 1967. Oxygen-18 variations in sulfate ions in sea water and saline lakes. *Science* 156 (3771), 56–59.
- López-Garrido, A.C., Sanz de Galdeano, C., 1999. Neogene sedimentation and tectonic-eustatic control of the Malaga basin, South Spain. *J. Pet. Geol.* 22 (1), 81–96.
- Loretto, M.F., Zitellini, N., Ranero, C.R., Palmiotto, C., Prada, M., 2020. Extensional tectonics during the Tyrrhenian back-arc basin formation and a new morpho-tectonic map. *Basin Res.* 33 (1), 138–158.
- Lourens, L., Hilgen, F., Shackleton, N.J., Laskar, J., Wilson, D., 2004. The Neogene period. In: Gradstein, F.M., Ogg, J.G., Smith, A.G. (Eds.), *A Geologic Time Scale* 2004. Cambridge Univ. Press, Cambridge, pp. 409–440.
- Lozano, D.O., 2016. Astrobiocronological Constraints on Margin to deep basin correlations across the Balearic Promontory and the Valencia basin (Doctoral dissertation, Universidad de Salamanca).
- Lu, F.H., 2006. Lithofacies and water-body record of Messinian evaporites in Nijar Basin, SE Spain. *Sediment. Geol.* 188, 115–130.
- Lu, F.H., Meyers, W.J., Schoonen, M.A., 2001. S and O (SO4) isotopes, simultaneous modeling, and environmental significance of the Nijar Messinian gypsum, Spain. *Geochim. Cosmochim. Acta* 65, 3081–3092.
- Lugli, S., Schreiber, B.C., Triberti, B., 1999. Giant polygons in the Realmonte mine (Agrigento, Sicily): evidence for the desiccation of a Messinian halite basin. *J. Sediment. Res.* 69, 764–771.
- Lugli, S., Bassetti, M.A., Manzi, V., Barbieri, M., Longinelli, A., Roveri, M., 2007. The Messinian “Vena del Gesso” evaporites revisited: characterization of isotopic composition and organic matter. In: Schreiber, B.C., Lugli, S., Babel, M. (Eds.), *Evaporites through Space and Time*. Special Publications, 285. Geological Society, London, pp. 143–154.
- Lugli, S., Manzi, V., Roveri, M., Schreiber, B.C., 2010. The Primary Lower Gypsum in the Mediterranean: a newfacies interpretation for the first stage of the Messinian salinity crisis. *Paleogeogr. Paleoclimatol. Paleocool.* 297, 83–99. <https://doi.org/10.1016/j.paleo.2010.07.017>.
- Lugli, S., Gennari, R., Gvirtzman, Z., Manzi, V., Roveri, M., Schreiber, B.C., 2013. Evidence of clastic evaporites in the canyons of the Levant Basin (Israel): implications for the Messinian Salinity Crisis. *J. Sediment. Res.* 83, 942–954. <https://doi.org/10.2110/jsr.2013.72>.
- Lugli, S., Manzi, V., Roveri, M., Schreiber, B.C., 2015. The deep record of the Messinian salinity crisis: evidence of a non-desiccated Mediterranean Sea. *Paleogeogr. Paleoclimatol. Paleocool.* 433, 201–218. <https://doi.org/10.1016/j.paleo.2015.05.017>.
- Lymer, G., Lofi, J., Gaullier, V., Maillard, A., Thonin, I., Sage, F., Chanier, F., Vendeville, B.C., 2018. The Western Tyrrhenian Sea revisited: New evidence for a rifted basin during the Messinian Salinity Crisis. *Mar. Geol.* 398, 1–21. <https://doi.org/10.1016/j.margeo.2017.12.009>.
- Madof, A.S., Connell, S.D., 2018. Northern Levant Basin. In: Lofi, et al. (Eds.), *Atlas of the Messinian Salinity Crisis markers in the Mediterranean and Black Seas/Mémoires de la Société géologique de France* 179. World Geological Map Commission, pp. 60–62.
- Madof, A.S., Bertoni, C., Lofi, J., 2019. Discovery of vast fluvial deposits provides evidence for drawdown during the late Miocene Messinian salinity crisis. *Geology* 47 (2), 171–174. <https://doi.org/10.1130/G45873.1>.
- Magyar, I., Geary, D.H., Lantos, M., Müller, P., Sütö-Szentai, M., 1999a. Integrated biostratigraphic, magnetostratigraphic and chronostratigraphic correlations of the Late Miocene Lake Pannon deposits. *Acta Geol. Hung.* 42 (1), 5–31.
- Magyar, I., Geary, D.H., Müller, P., 1999b. Paleogeographic evolution of the late miocene Lake Pannon in Central Europe. *Paleogeogr. Paleoclimatol. Paleocool.* 147 (3–4), 151–167.
- Maillard, A., Mauffret, A., 2006. Relationship between erosion surfaces and Late Miocene Salinity Crisis deposits in the Valencia Basin (northwestern Mediterranean): evidence for an early sea-level fall. *Terra Nova* 18 (5), 321–329. <https://doi.org/10.1111/j.1365-3121.2006.00696.x>.
- Maillard, A., Mauffret, A., 2011. Valencia through. In: Lofi, et al. (Eds.), *Atlas of the Messinian Salinity Crisis markers in the Mediterranean and Black Seas/Mémoires de la Société géologique de France* 179. World Geological Map Commission (72 pp.).
- Maillard, A., Mauffret, A., 2013. Structure and present-day compression in the offshore area between Alicante and Ibiza Island (Eastern Iberian Margin). *Tectonophysics* 591, 116–130.
- Maillard, A., Gorini, C., Mauffret, A., Sage, F., Lofi, J., Gaullier, V., 2006. Offshore evidence of polyphase erosion in the Valencia Basin (Northwestern Mediterranean): scenario for the Messinian Salinity Crisis. *Sediment. Geol.* 188–189, 69–91.
- Maillard, A., Hübscher, C., Benkhelil, J., Tahchi, E., 2011a. Deformed Messinian markers in the Cyprus Arc: tectonic and/or Messinian Salinity Crisis indicators? *Basin Res.* 23, 146–170.
- Maillard, A., Lofi, J., Déverchère, J., Gaullier, V., Loncke, L., Sage, F., Thonin, I., Guennoc, P., Gillet, H., Gorini, C., 2011b. Synthesis. In: Lofi, J., Déverchère, J., et al. (Eds.), *Seismic Atlas of the Messinian Salinity Crisis Markers in the Offshore Mediterranean Domain*. – CCGM & Mém. Soc. géol. Fr., n.s., 179, 72 p.
- Maillard, A., Driussi, O., Lofi, J., Briais, A., Chanier, F., Hübscher, C., Gaullier, V., 2014. Record of the Messinian Salinity Crisis in the SW Mallorca area (Balearic Promontory, Spain). *Mar. Geol.* 357, 304–320. <https://doi.org/10.1016/j.margeo.2014.10.001>.
- Maillard, A., Gaullier, V., Lézin, C., Chanier, F., Odonne, F., Lofi, J., 2020. New onshore/offshore evidence of the Messinian Erosion Surface from key areas: The Ibiza-Balearic Promontory and the Orosei-Eastern Sardinian margin. Découverte de la surface d'érosion messinienne onshore/offshore dans deux lieux clés: le Promontoire Baléares (Ibiza) et la marge est-sarde (Orosei). *Bulletin de la Société Géologique de France* 191 (1), <https://doi.org/10.1051/bsgf/2020007>.
- Maniscalco, R., Casciano, C.I., Distefano, S., Grossi, F., Di Stefano, A., 2019. Facies analysis in the Second Cycle Messinian evaporites predating the early Pliocene re-flooding: the Balza Soletta section (Corvillo Basin, central Sicily). *Ital. J. Geosci.* 138 (3), 301–316. <https://doi.org/10.3301/IJG.2019.06>.
- Manzi, V., Lugli, S., Ricci Lucchi, F., Roveri, M., 2005. Deep-water clastic evaporites deposition in the Messinian Adriatic foredeep (northern Apennines, Italy): did the Mediterranean ever dry out? *Sedimentology* 52, 875–902.
- Manzi, V., Roveri, M., Gennari, R., Bertini, A., Biffi, U., Giunta, S., Iaccarino, S.M., Lanci, L., Lugli, S., Negri, A., Riva, A., Rossi, M.E., Taviani, M., 2007. The deep-water counterpart of the messinian lower evaporites in the apennine foredeep: the fananello section (northern Apennines, Italy). *Paleogeogr. Paleoclimatol. Paleocool.* 251, 470–499.

- Manzi, V., Lugli, S., Roveri, M., Schreiber, B.C., 2009. A new facies model for the Upper Gypsum of Sicily (Italy): chronological and paleoenvironmental constraints for the Messinian salinity crisis in the Mediterranean. *Sedimentology* 56. <https://doi.org/10.1111/j.1365-3091.2009.01063.x>, 1937–1960.
- Manzi, V., Lugli, S., Roveri, M., Schreiber, B.C., Gennari, R., 2011. The Messinian CdB (Sicily, Italy) revisited. *Geol. Soc. Am. Bull.* 123, 347–370. <https://doi.org/10.1130/B30262.1>.
- Manzi, V., Gennari, R., Hilgen, F., Krijgsman, W., Lugli, S., Roveri, M., Sierro, F.J., 2013. Age refinement of the Messinian salinity crisis onset in the Mediterranean. *Terra Nova* 25 (4), 315–322.
- Manzi, V., Lugli, S., Roveri, M., Dela, Pierre F., Gennari, R., Lozar, F., Natalicchio, M., Schreiber, B.C., Taviani, M., Turco, E., 2016a. The Messinian salinity crisis in Cyprus: A further step towards a new stratigraphic framework for Eastern Mediterranean. *Basin Res.* 28, 207–236. <https://doi.org/10.1111/bre.12107>.
- Manzi, V., Gennari, R., Lugli, S., Minelli, N., Reghizzi, M., Roveri, M., Schreiber, B.C., 2016b. Comment on “Carbonate deposition and diagenesis in evaporitic environments: the evaporative and sulphur-bearing limestones during the settlement of the Messinian Salinity Crisis in Sicily and Calabria” by Caruso et al., 2015. *Palaeo3*, 429, 136E162. *Palaeogeogr. Palaeoclimatol. Palaeoecol.* 459, 585–596.
- Manzi, V., Gennari, R., Lugli, S., Persico, D., Reghizzi, M., Roveri, M., Schreiber, B.C., Calvo, R., Gavrieli, I., Gvirtzman, Z., 2018. The onset of the Messinian salinity crisis in the deep Eastern Mediterranean basin. *Terra Nova* 30 (3), 189–198. <https://doi.org/10.1111/ter.12325>.
- Manzi, V., Argnani, A., Corcagnani, A., Lugli, S., Roveri, M., 2020. The Messinian salinity crisis in the Adriatic foredeep: evolution of the largest evaporitic marginal basin in the Mediterranean. *Mar. Pet. Geol.* 115, 104288 <https://doi.org/10.1016/j.marpetgeo.2020.104288>.
- Marcano, M.C., Frank, T.D., Mukasa, S.B., Lohmann, K.C., Taviani, M., 2015. Diagenetic incorporation of Sr into aragonitic bivalve shells: Implications for chronostratigraphic and paleoenvironmental interpretations. *Depositional Record* 1 (1), 38–52. <https://doi.org/10.1016/j.marpetgeo.2020.104288>.
- Markovic, S., Paytan, A., Li, H., Wortmann, U.G., 2016. A revised seawater sulfate oxygen isotope record for the last 4Myr. *Geochim. Cosmochim. Acta* 175, 239–251.
- Marsaglia, K.M., Tribble, J.S., 1999. Petrography and mineralogy of the uppermost Messinian section and the Pliocene/Miocene boundary at Site 975, Western Mediterranean Sea. In: *Proc. ODP, Sci. Results, Vol. 161*, pp. 3–20. Ocean Drilling Program College Station, TX.
- Martín-Suárez, E., Freudenthal, M., Krijgsman, W., Fortuin, R., 2000. On the age of the continental deposits of the Zorerras Member (Sorbas Basin, SE Spain). *Geobios* 33, 505–512.
- Marzocchi, A., Lunt, D.J., Flecker, R., Bradshaw, C.D., Farnsworth, A., Hilgen, F.J., 2015. Orbital control on late Miocene climate and the North African monsoon: insight from an ensemble of sub-precessional simulations. *Clim. Past* 11 (10), 1271–1295. <https://doi.org/10.5194/cpd-11-2181-2015>.
- Marzocchi, A., Flecker, R., Van Baak, C.G.C., Lunt, D.J., Krijgsman, W., 2016. Mediterranean outflow pump: an alternative mechanism for the Lago-mare and the end of the Messinian Salinity Crisis. *Geology* 44, 523–526. <https://doi.org/10.1130/G37646.1>.
- Marzocchi, A., Flecker, R., Lunt, D.J., Krijgsman, W., Hilgen, F.J., 2019. Precessional drivers of late Miocene Mediterranean sedimentary sequences: African summer monsoon and Atlantic winter storm tracks. *Paleoceanogr. Paleoclimatol.* 34 (12), 1980–1994. <https://doi.org/10.1029/2019PA003721>.
- Mas, G., 2013. Definició i caracterització de la Formació ses Olles (Lago mare, messinià terminal) a l'illa de Mallorca (illes balears, mediterrània Occidental). *Bolletí de la Societat d'Història Natural de Balears* 56, 209–231.
- Mas, G., 2015. El registre estratigràfic del Messinià a terminal i del Pliocè a l'illa de Mallorca. Relacions amb la crisi de salinitat de la mediterrània. PhD Thesis. Universitat de les Illes Balears. <http://www.tdx.cat/handle/10803/375904>.
- Mas, G., Fornós, J.J., 2020. The messinian salinity crisis in Mallorca: New insights for a western mediterranean stratigraphic scenario. *Mar. Pet. Geol.* 104656 <https://doi.org/10.1016/j.marpetgeo.2020.104656>.
- Mas, G., Bisconti, M., Torres-Roig, E., Juárez, J., Sacarès, J., 2018a. The last whale of the Messinian. First record of a mysticete cetacean from the Mediterranean Messinian Salinity Crisis. In: 1st Paleontological Virtual Congress. Book of Abstracts—Paleontology in the Virtual Era, Vol. 97.
- Mas, G., Maillard, A., Alcover, J.A., Fornós, J.J., Bover, P., Torres-Roig, E., 2018b. Terrestrial colonization of the Balearic Islands: New evidence for the Mediterranean sea-level drawdown during the Messinian Salinity Crisis. *Geology* 46 (6), 527–530. <https://doi.org/10.1130/G40260.1>.
- Masterson, A.L., Wing, B.A., Paytan, A., Farquhar, J., Johnston, D.T., 2016. The minor sulfur isotope composition of Cretaceous and Cenozoic seawater sulfate. *Paleoceanography* 31, 779–788.
- Mather, A., Martín, J.M., Harvey, A.M., Braga, J.C., 2001. A Field Guide to the Neogene Sedimentary Basins of the Almería Province, South-East Spain., 186–189. Blackwell Science, Oxford.
- Mayer, J.P., Flecker, R., Marzocchi, A., Kouwenhoven, T.J., Lunt, D.J., Pancost, R.D., 2017. Precession driven changes in terrestrial organic matter input to the Eastern Mediterranean leading up to the Messinian Salinity Crisis. *Earth Planet. Sci. Lett.* 462, 199–211. <https://doi.org/10.1016/j.epsl.2017.01.029>.
- McArthur, J.M., Howarth, R.J., Shields, G.A., 2012. Strontium isotope stratigraphy. In: *Gradstein, F.M., Ogg, J.G., Schmitz, M.D., Ogg, G.M. (Eds.), The Geological Time Scale 2012*. Elsevier B.V., Oxford, pp. 127–144.
- McCulloch, M.T., De Deckker, P., 1989. Sr isotope constraints on the Mediterranean environment at the end of the Messinian salinity crisis. *Nature* 342, 62–65.
- McKenzie, J.A., 1999. From desert to deluge in the Mediterranean. *Nature* 400, 613–614.
- McKenzie, J.A., Evans, N., Hodell, D., Aloisi, G., Vasconcelos, C., 2017. Subsurface dolomite formation during post-depositional flow of sulphate-bearing fluids from underlying salt giants: Early Pliocene example at DSDP Leg 42A, Site 374, Ionian Abyssal Plain. *EGU6* 10166.
- Medaoui, M., Déverchère, J., Grandjeon, D., Bracene, R., Badji, R., Ouabadi, A., Yelles, K., Bendib, F., 2014. The transition from Alboran to Algerian basins (Western Mediterranean Sea): chronostratigraphy, deep crustal structure and tectonic evolution at the rear of a narrow slab rollback system. *J. Geodyn.* 77, 186–205. <https://doi.org/10.1016/j.jog.2014.01.003>.
- Meijer, P.T., Krijgsman, W., 2005. A quantitative analysis of the desiccation and re-filling of the Mediterranean during the Messinian Salinity Crisis. *Earth Planet. Sci. Lett.* 240 (2), 510–520.
- Meilijon, A., Steinberg, J., Hilgen, F., Bialik, O.M., Waldmann, N.D., Makovsky, Y., 2018. Deep-basin evidence resolves a 50-year-old debate and demonstrates synchronous onset of Messinian evaporite deposition in a non-desiccated Mediterranean. *Geology* 46 (3), 243–246. <https://doi.org/10.1130/G39868.1>.
- Meilijon, A., Hilgen, F., Sepúlveda, J., Steinberg, J., Fairbank, V., Flecker, R., Waldmann, N.D., Spaulding, S.A., Bialik, O.M., Boudinot, F.G., Illner, P., Makovsky, Y., 2019. Chronology with a pinch of salt: integrated stratigraphy of Messinian evaporites in the deep Eastern Mediterranean reveals long-lasting halite deposition during Atlantic connectivity. *Earth-Sci. Res.* 194, 374–398. <https://doi.org/10.1016/j.earscirev.2019.05.011>.
- Melinete-Dobriescu, M.C., Suc, J.-P., Clauzon, G., Popescu, S.-M., Armijo, R., Meyer, B., Bilekin, D., Çağatay, M.N., Ucakarsu, G., Jouannic, G., Fauquette, S., Çakir, Z., 2009. The Messinian salinity crisis in the Dardanelles region: Chronostratigraphic constraints. *Paleogeogr. Palaeoclimatol. Palaeoecol.* 278, 24–39. <https://doi.org/10.1016/j.paleo.2009.04.009>.
- Merzeraud, G., Achalhi, M., Cornee, J.J., Münch, P., Azdimoua, A., Moussa, A.B., 2019. Sedimentology and sequence stratigraphy of the late-Messinian-Early Pliocene continental to marine deposits of the Boudinar basin (North Morocco). *J. Afr. Earth Sci.* 150, 205–223. <https://doi.org/10.1016/j.jafrearsci.2018.11.002>.
- Meulenkamp, J.E., Sissingh, W., 2003. Tertiary paleogeography and tectonostratigraphic evolution of the Northern and Southern Peri-Tethys platforms and the intermediate domains of the African-Eurasian convergent plate boundary zone. *Paleogeogr. Palaeoclimatol. Palaeoecol.* 196 (1–2), 209–228.
- Meulenkamp, J.E., Dermitzakis, M., Georgiades-Dikeoulia, E., Jonkers, H.A., Boger, A., 1979. Field Guide to the Neogene of Crete. Publication of the Department of Geology and Paleontology, University of Athens, A. 32, pp. 1–32.
- Micallef, A., Camerlenghi, A., Garcia-Castellanos, D., Cunaro Otero, D., Gutscher, M.-A., Barreca, G., Spatola, D., Facchin, L., Geletti, R., Krastel, S., Gross, F., Urlaub, M., Sulli, A., Baslone, L., Baslone, G., 2018. Evidence of the Zanclean megaflood in the eastern Mediterranean Basin. *Sci. Rep.* 8, 1–8. <https://doi.org/10.1038/s41598-018-19446-3>.
- Micallef, A., Camerlenghi, A., Georgiopolou, A., Garcia-Castellanos, D., Gutscher, M.-A., Lo Iacono, C., Huvenne, V.A.L., Mountjoy, J.J., Paul, C.K., Le Bas, T., Spatola, D., Facchin, L., Accettella, D., 2019. Geomorphologic evolution of the Malta Escarpment and implications for the Messinian evaporative drawdown in the eastern Mediterranean Sea. *Geomorphology* 327, 264–283. <https://doi.org/10.1016/j.geomorph.2018.11.012>.
- Milker, Y., Schmiedl, G., 2012. A taxonomic guide to modern benthic shelf foraminifera of the western Mediterranean Sea. *Paleoentol. Electron.* 15 (2), 1–134. <https://doi.org/10.26879/271>.
- Mocnik, A., Camerlenghi, A., Del Ben, A., Geletti, R., Wardell, N., Zgur, F., 2014. The Messinian Salinity Crisis in the West-Mediterranean Basins: comparison between two rifted margins. In: *Proceedings of the 33rd NGTGS Conference, Bologna, Vol. 1*, pp. 156–163.
- Mocnik, A., Del Ben, A., Camerlenghi, A., Geletti, R., Sautle, M., 2018. 12. Ionian Basin. In: *J. Lofi (Ed.), Seismic Atlas of the Messinian salinity crisis markers in the Mediterranean sea. Volume 2. - Mémoires de la Société géologique de France, n.s., 2018, t. 181, and Commission for the Geological Map of the World*, pp. 41–44.
- Modestou, S., Simon, D., Gutjahr, M., Marzocchi, A., Kouwenhoven, T.J., Ellam, R.M., Flecker, R., 2017. Precessional variability of $^{87}\text{Sr}/^{86}\text{Sr}$ in the late miocene sorbas basin: An interdisciplinary study of drivers of interbasin exchange. *Paleoceanography* 32 (6), 531–552.
- Montadert, L., Letouzey, J., Maufré, A., 1978. Messinian event: seismic evidence. In: *Hsu, K.J., Montadert, L. et al. (Eds.), Initial Reports of the Deep Sea Drilling Project, 1*. US Government Printing Office, Washington, DC, pp. 1037–1050.
- Mudie, P.J., Marret, F., Mertens, K.N., Shumilovskikh, L., Leroy, S.A., 2017. Atlas of modern dinoflagellate cyst distributions in the Black Sea Corridor: from Aegean to Aral Seas, including Marmara, Black, Azov and Caspian Seas. *Mar. Micropaleontol.* 134, 1–152.
- Müller, D.W., Mueller, P.A., 1991. Origin and age of the Mediterranean Messinian evaporites: implications from Sr isotopes. *Earth Planet. Sci. Lett.* 107 (1), 1–12.
- Müller, D.W., Mueller, P.A., McKenzie, J.A., 1990. Strontium isotopic ratios as fluid tracers in Messinian evaporites of the Tyrrhenian Sea (western Mediterranean Sea). In: *Proceedings of the Ocean Drilling Program, Scientific Results (Vol. 107, 603–614)*. College Station, Tex.: Ocean Drill. Program.
- Natalicchio, M., Birgel, D., Peckmann, J., Lozar, F., Carnevale, G., Liu, X., Hinrichs, K.-U., Dela Pierre, F., 2017. An archaean biomarker record of paleoenvironmental change across the onset of the Messinian salinity crisis in the absence of evaporites (Piedmont Basin, Italy). *Org. Geochem.* 113, 242–253.
- Natalicchio, M., Dela Pierre, F., Birgel, D., Brunsack, H., Carnevale, G., Gennari, R., Gier, S., Lozar, F., Pellegrino, L., Sabino, M., Schnetger, B., Peckmann, J., 2019. Paleoenvironmental change in a precession-paced succession across the onset of the Messinian salinity crisis: insight from element geochemistry and molecular fossils.

- Paleogeogr. Paleoclimatol. Paleoecol. 518, 45–61. <https://doi.org/10.1016/j.paleo.2019.01.009>.
- Nesteroff, W.D., 1973. Un modèle pour les évaporites messinienne en Méditerranée, bassins peu profonds avec dépôt d'évaporites lagunaires. In: Drooger, C.W. (Ed.), *Messinian Events in the Mediterranean*. North-Holland Publ. Co., Amsterdam, pp. 68–81.
- Netzeband, G., Hübscher, C., Gajewski, G., 2006. The structural evolution of the Messinian evaporites in the Levantine Basin. *Mar. Geol.* 230, 249–273.
- Ochoa, D., Sierro, F.J., Lofi, J., Maillard, A., Flores, J.A., Suárez, M., 2015. Synchronous onset of the Messinian evaporite precipitation: First Mediterranean offshore evidence. *Earth Planet. Sci. Lett.* 427, 112–124. <https://doi.org/10.1016/j.epsl.2015.06.059>.
- Ochoa, D., Sierro, F.J., Hilgen, F.J., Cortina, A., Lofi, J., Kouwenhoven, T., Flores, J.A., 2018. Origin and implications of orbital-induced sedimentary cyclicity in Pliocene well-logs of the Western Mediterranean. *Mar. Geol.* 403, 150–164. <https://doi.org/10.1016/j.margeo.2018.05.009>.
- Odin, G.S., Vai, G.B., Cosca, M., Tateo, F., Hunziker, J.C., 1997. Integrated stratigraphy of the Maccarone section. In: Montanari, A., Odin, G.S., Coccioni, R. (Eds.), *Miocene Stratigraphy: An Integrated Approach: Developments in Paleontology and Stratigraphy*, 15. Elsevier Science B.V., Amsterdam, Netherlands, pp. 531–545.
- Ognibeni, L., 1955. Le argille scagliose del Crotonese. *Memorie e Note dell'Istituto di Geologia Alicantina di Napoli* 6, 1–72.
- Omodeo-Salé, S., Gennari, R., Lugli, S., Manzi, V., Roveri, M., 2012. Tectonic and climatic control on the Late Messinian sedimentary evolution of the Nijar Basin (Betic Cordillera, Southern Spain). *Basin Res.* 24, 314–337. <https://doi.org/10.1111/j.1365-2117.2011.00527.x>.
- Orszag-Sperber, F., 2006. Changing perspectives in the concept of “Lago-Mare” in Mediterranean Late Miocene evolution. *Sediment. Geol.* 188, 259–277. <https://doi.org/10.1016/j.sedgeo.2006.03.008>.
- Orszag-Sperber, F., Rouchy, J.M., 1979. Le Miocène terminal et le Pliocène inférieur au sud de Chypre, livret-guide, 5e séminaire sur le Messinien. Chypre, 60 p.
- Orszag-Sperber, F., Rouchy, J.M., Blanc-Valleron, M.M., 2000. La transition Messinien-Pliocène en Méditerranée orientale (Chypre): la période du Lago-Mare et sa signification. *Comptes Rendus de l'Académie des Sciences-Séries IIA-Earth and Planet. Sci.* 331 (7), 483–490.
- Orszag-Sperber, F., Caruso, A., Blanc-Valleron, M.M., Merle, D., Rouchy, J.M., 2009. The onset of the Messinian salinity crisis: insights from Cyprus sections. *Sediment. Geol.* 217 (1–4), 52–64. <https://doi.org/10.1016/j.sedgeo.2009.03.006>.
- Palcu, D.V., Golovina, L.A., Vernyhorova, Y.V., Popov, S.V., Krijgsman, W., 2017. Middle Miocene paleoenvironmental crises in Central Eurasia caused by changes in marine gateway configuration. *Glob. Planet. Chang.* 158, 57–71. <https://doi.org/10.1016/j.gloplacha.2017.09.013>.
- Palmer, M.R., Edmond, J.M., 1992. Controls over the strontium isotope composition of river water. *Geochim. Cosmochim. Acta* 56 (5), 2099–2111.
- Pellen, R., Popescu, S.-M., Suc, J.-P., Melinte-Dobrincescu, M.C., Rubino, J.-L., Rabineau, M., Marabini, S., Loget, N., Casero, P., Cavazza, W., Head, M.J., Aslanian, D., 2017. The Apennine foredeep (Italy) during the latest Messinian: Lago Mare reflects competing brackish and marine conditions based on calcareous nannofossils and dinoflagellate cysts. *Geobios* 50, 237–257. <https://doi.org/10.1016/j.geobios.2017.04.004>.
- Pellen, R., Aslanian, D., Rabineau, M., Suc, J.P., Gorini, C., Leroux, E., Blanpied, C., Silenziario, C., Popescu, S.M., Rubino, J.L., 2019. The Messinian Ebro River incision. *Glob. Planet. Chang.* 181, 102988 <https://doi.org/10.1016/j.gloplacha.2019.102988>.
- Pellerin, A., Antler, G., Holm, S.A., Findlay, A.J., Crookford, P.W., Turchyn, A.V., Jørgensen, B.B., Finster, K., 2019. Large sulfur isotope fractionation by bacterial sulfide oxidation. *Sci. Adv.* 5 eaaw1480-eaaw1480.
- Pérez-Asensio, J.N., Aguirre, J., Schmiedl, G., Civis, J., 2012. Impact of restriction of the Atlantic-Mediterranean gateway on the Mediterranean Outflow Water and eastern Atlantic circulation during the Messinian. *Paleoceanography* 27 (3). <https://doi.org/10.1029/2012PA002309>.
- Peucker-Ehrenbrink, B., Fiske, G.J., 2019. A continental perspective of the seawater 87Sr/86Sr record: A review. *Chem. Geol.* 510, 140–165. <https://doi.org/10.1016/j.chemgeo.2019.01.017>.
- Pierre, C., 1974. Contribution – l'étude sédimentologique et isotopique des évaporites messiniennes de la Méditerranée; implications géodynamiques. Thesis, University of Paris.
- Pierre, C., 1982. Teneurs en isotopes stables (18O, 2H, 13C, 34S) et conditions de genèse des évaporites marines : Alicantina à quelques milieux actuels et au Messinien de la Méditerranée, Ecole Normale Supérieure. Université Paris Sud Orsay, p. 262.
- Pierre, C., Fontes, J.-C., 1978. Isotope Composition of Messinian sediments from the Mediterranean Sea as indicators of paleoenvironments and diagenesis. In: Texas A M University, O.D.P.C.S., TX, United States (Ed.), Initial reports of the Deep Sea Drilling, covering Leg 42 of the cruises of the drilling vessel Glomar Challenger Malaga Spain to Istanbul Turkey. April-May 1975. University of California. Scrips Institution of Oceanography, National Science Foundation, National Ocean Sediment Coring Program, pp. 635–650.
- Pierre, C., Rouchy, J.M., 1990. Stable isotope composition of carbonates in the Tyrrhenian Sea, Sulemont to Pierre, C., Rouchy, JM (1990): Sedimentary and diagenetic evolution of Messinian evaporites in the Tyrrhenian Sea (ODP Leg 107, Sites 652, 653, and 654): petrographic, mineralogical, and stable isotope records. In: Kastens, K.A., Mascle, J., et al. (Eds.), Proceedings of the Ocean Drilling Program, Scientific Results, College Station, TX (Ocean Drilling Program), 107, pp. 187–210. <https://doi.org/10.2973/odp.proc.sr.107.131.1990>. PANGAEA.
- Pierre, C., Rouchy, J.M., Blanc-Valleron, M.-M., 1998. Sedimentological and stable isotope changes at the Messinian-Pliocene boundary in the eastern Mediterranean. In: Robertson, A.H.F., Emeis, K.-C., Richter, C., Camerlenghi, A. (Eds.), Proc. O.D.P., Sci. Res., vol. 160. Ocean Drilling Program, College Station, TX, pp. 3–8.
- Pierre, C., Caruso, A., Blanc-Valleron, M.M., Rouchy, J.M., Orszag-Sperber, F., 2006. Reconstruction of the paleoenvironmental changes around the Miocene-Pliocene boundary along a West-East transect across the Mediterranean. *Sediment. Geol.* 188, 319–340. <https://doi.org/10.1016/j.sedgeo.2006.03.011>.
- Placzek, C.J., Quade, J., Patchett, P.J., 2011. Isotopic tracers of paleohydrologic change in large lakes of the Bolivian Altiplano. *Quat. Res.* 75 (1), 231–244. <https://doi.org/10.1016/j.yqres.2010.08.004>.
- Polonia, A., Torelli, L., Mussoni, P., Gasperini, L., Artoni, A., Klaeschen, D., 2011. The Calabria Arc subduction complex in the Ionian Sea: Regional architecture, active deformation, and seismic hazard. *Tectonics* 30 (5).
- Popescu, S.M., Melinte, M.-C., Suc, J.-P., Clauzon, G., Quillévère, F., Sütö-Szentai, M., 2007. Earliest Zanclean age for the Colombacci and uppermost Di Tetto formations of the “latest Messinian” northern Apennines: New paleoenvironmental data from the Maccarone section (Marche Province, Italy). *Geobios* 40 (3), 359–373. <https://doi.org/10.1016/j.geobios.2006.11.005>.
- Popescu, S.-M., Melinte, M.-C., Suc, J.-P., Clauzon, G., Quillévère, F., Sütö-Szentai, M., 2008. Marine reflooding of the Mediterranean after the Messinian Salinity Crisis predates the Zanclean GSSP. Reply to the “Comment on ‘Earliest Zanclean age for the Colombacci and uppermost Di Tetto formations of the “latest Messinian” northern Apennines: new paleoenvironmental data from the Maccarone section (Marche Province, Italy)’” by Popescu et al. (2007). *Geobios* 40 (359–373) authored by Roveri et al. *Geobios* 41, 657–660.
- Popescu, S.M., Dalesme, F., Jouannic, G., Escarguel, G., Head, M.J., Melinte-Dobrincescu, M.C., Sütö-Szentai, M., Bakrac, K., Clauzon, G., Suc, J.P., 2009. Galeacysta etrusca complex: dinoflagellate cyst marker of Paratethyan influxes to the Mediterranean Sea before and after the peak of the Messinian Salinity Crisis. *Palynology* 33 (2), 105–134.
- Popescu, S.-M., Dalibard, M., Suc, J.-P., Barhoun, N., Melinte-Dobrincescu, M.C., Bassetti, M.A., Deaconu, F., Head, M.J., Gorini, C., Do Couto, D., Rubino, J.-L., Auxietre, J.-L., Floodpage, J., 2015. Lago Mare episodes around the Messinian-Zanclean boundary in the deep southwestern Mediterranean. *Mar. Pet. Geol.* 66, 55–70. <https://doi.org/10.1016/j.marpetgeo.2015.04.002>.
- Popescu, S.M., Melinte-Dobrincescu, M.C., Suc, J.P., Do Couto, D., 2017. Ceratolithus acutus (= C. armatus), calcareous nannofossil marker of the marine reflooding that terminated the Messinian salinity crisis: Comment on “Paratethyan ostracods in the Spanish Lago-Mare: More evidence for interbasinal exchange at high Mediterranean sea level” by Paleoogeogr., Paleoclimatol., Paleoecol. 441, 854–870. *Paleogeogr. Paleoclimatol. Paleoecol.* 485, 986–989. <https://doi.org/10.1016/j.paleo.2016.07.011>.
- Popov, S.V., Rögl, F., Rozanov, A.Y., Steininger, F.F., Shcherba, I.G., Kovac, M., 2004. Lithological-paleogeographic maps of Paratethys-10 maps late Eocene to pliocene.
- Popov, S.V., Shcherba, I.G., Ilyina, L.B., Nevevskaya, L.A., Paramonova, N.P., Khondkarian, S.O., Magyar, I., 2006. Late Miocene to Pliocene paleogeography of the Paratethys and its relation to the Mediterranean. *Paleoecol. Paleoclimatol. Paleoecol.* 238 (1–4), 91–106.
- Raad, F., Lofi, J., Maillard, A., Tzavahirtzian, A., Caruso, A., 2021. The Messinian Salinity Crisis deposits in the Balearic Promontory: an undeformed analog of the MSC Sicilian basins? *Mar. Pet. Geol.* 104777 <https://doi.org/10.1016/j.marpetgeo.2020.104777>.
- Radeff, G., Cosentino, D., Cipollari, P., Schildgen, T.F., Iadanza, A., Strecker, M.R., Darbas, G., Gurbuz, K., 2016. Stratigraphic architecture of the upper Messinian deposits of the Adana Basin (southern Turkey): implications for the Messinian salinity crisis and the Taurus petroleum system. *Ital. J. Geosci.* 135, 408–424.
- Radeff, G., Schildgen, T.F., Cosentino, D., Strecker, M.R., Cipollari, P., Darbas, G., Gürbüz, K., 2017. Sedimentary evidence for late Messinian uplift of the SE margin of the Central Anatolian Plateau: Adana Basin, southern Turkey. *Basin Res.* 29, 488–514. <https://doi.org/10.1111/bre.12159>.
- Reiche, S., Hübscher, C., Ehrhardt, A., 2016. The impact of salt on the late Messinian to recent tectonostratigraphic evolution of the Cyprus subduction zone. *Basin Res.* 28 (5), 569–597. <https://doi.org/10.1111/bre.12122>.
- Ricchiuto, T.E., McKenzie, J.A., 1978. Stable Isotopic investigation of Messinian sulfate samples from DSDP. LEG 42. Eastern Mediterranean Sea. In: Texas A M University, O.D.P.C.S., TX, United States (Ed.), Initial reports of the Deep Sea Drilling covering Leg 42 of the cruises of the drilling vessel Glomar Challenger. Malaga, Spain to Istanbul, Turkey. April-May 1975. University of California. Scrips Institution of Oceanography, National Science Foundation, National Ocean Sediment Coring Program, pp. 657–660.
- Rio, D., Negri, A., 1988. Calcareous nannofossils (Monticchio Quarry, Faenza). In: De Giuli, C., Vai, G.B. (Eds.), Fossil Vertebrates in the Lamone Valley, Romagna Apennines. Field Trip Guidebook of the International Workshop “Continental faunas at the Miocene/Pliocene boundary”, Faenza, pp. 55–57.
- Robertson, A.H.F., 1998a. Late Miocene paleoenvironments and tectonic settings of the southern margin of Cyprus and the Eratosthenes Seamount. In: Robertson, A.H.F., Emeis, K.C., Richter, C., Camerlenghi, A. (Eds.), Proc. ODP, Sci. Res., vol. 160 Ocean Drilling Program, College Station, TX, pp. 453–463.
- Robertson, A.H., 1998b. Tectonic significance of the Eratosthenes Seamount: a continental fragment in the process of collision with a subduction zone in the eastern Mediterranean (Ocean Drilling Program Leg 160). *Tectonophysics* 298 (1–3), 63–82.
- Robertson, A.H.F., Eaton, S., Follows, E.J., Payne, A.S., 1995. Depositional processes and basin analysis of Messinian evaporites in Cyprus. *Terra Nova* 7, 233–253.
- Roca, E., Guimera, J., 1992. The Neogene structure of the eastern Iberian margin: structural constraints on the crustal evolution of the Valencia trough (western Mediterranean). *Tectonophysics* 203, 203–218.

- Roep, Th.B., Van Harten, D., 1979. Sedimentological and ostracodological observations on Messinian post-evaporite deposits in some southeastern Spanish basins. *Annales Géologiques des Pays Helléniques* 3, 1037–1044.
- Roep, T.B., Dabrio, C.J., Fortuin, A.R., Polo, M.D., 1998. Late highstand patterns of shifting and steing coastal barriers and washover-fans (Late Messinian, Sorbas Basina, SE Spain). *Sediment. Geol.* 116, 27–56.
- Rögl, F., 1998. Paleogeographic considerations for Mediterranean and Paratethys seaways (Oligocene to Miocene). *Ann. Naturhist. Mus. Wien* 9 9 A, 279310.
- Rosenfeld, A., 1977. The fine pores of *Cyprideis torosa* (Jones, 1850) from the Messinian Mavqî'im Formation in the coastal plain and continental shelf of Israel as an indicator of paleoenvironment. *Isr. J. Earth Sci.* 26, 89993.
- Rossi, M., 2017. Outcrop and seismic expression of stratigraphic patterns driven by accommodation and sediment sily tularounds: Implications on the meaning and variability of unconformities in syn-orogenic basins. *Mar. Pet. Geol.* 87, 112–127. <https://doi.org/10.1016/j.marpetgeo.2017.03.032>.
- Rossi, M., Rogledi, S., 1988. Relative sea-level changes, local tectonic setting and basin margin sedimentation in the interference zone between two orogenic belts: seismic stratigraphic examples from Padan foreland basin, northern Italy. In: *Fan Deltas: Sedimentology and Tectonic Settings*, pp. 368–384.
- Rossi, M., Minervini, M., Ghielmi, M., Rogledi, S., 2015a. Messinian and Pliocene erosional surfaces in the Po Plain-Adriatic Basin: Insights from allostratigraphy and sequence stratigraphy in assessing play concepts related to accommodation and gateway turnarounds in tectonically active margins. *Marine Petroleum Geol.* The Messinian events and hydrocarbon exploration in the Mediterranean 66, 192–216. <https://doi.org/10.1016/j.marpetgeo.2014.12.012>.
- Rossi, C., Vilas, L., Arias, C., 2015b. The Messinian marine to nonmarine gypsums of Jumilla (Northern Betic Cordillera, SE Spain): Isotopic and Sr concentration constraints on the origin of parent brines. *Sediment. Geol.* 328, 96–114. <https://doi.org/10.1016/j.sedgeo.2015.08.007>.
- Rouchy, J.M., 1982. La crise évaporitique messinienne de Méditerranée: nouvelles propositions pour une interprétation génétique. Thesis, Mem. p. 280. Mus. Natn. Hist. Nat, Paris.
- Rouchy, J.M., Caruso, A., 2006. The Messinian salinity crisis in the Mediterranean basin: a reassessment of the data and an integrated scenario. *Sediment. Geol.* 188, 35–67. <https://doi.org/10.1016/j.sedgeo.2006.02.005>.
- Rouchy, J.M., Orszag-Sperber, F., Blanc-Valleron, M.M., Pierre, C., Rivière, M., Combourieu-Nebout, N., Panayides, I., 2001. Paleoenvironmental changes at the Messinian-Pliocene boundary in the eastern Mediterranean (southern Cyprus basins): significance of the Messinian Lago-Mare. *Sediment. Geol.* 145 (1–2), 93–117.
- Rouchy, J.M., Pierre, C., Et-Touhami, M., Kerzazi, K., Caruso, A., Blanc-Valleron, M.M., 2003. Late Messinian to Early Pliocene paleoenvironmental changes in the Mellilla Basin (NE Morocco) and their relation to Mediterranean evolution. *Sediment. Geol.* 163 (1–2), 1–27.
- Rouchy, J.M., Caruso, A., Pierre, C., Blanc-Valleron, M.M., Bassetti, M.A., 2007. The end of the Messinian salinity crisis: evidences from the Chelif Basin (Algeria). *Paleogeogr. Paleoclimatol. Paleocool.* 254 (3–4), 386–417. <https://doi.org/10.1016/j.paleo.2007.06.015>.
- Roveri, M., Manzi, V., Bassetti, M.A., Merini, M., Ricci Lucchi, F., 1998. Stratigraphy of the Messinian post-evaporitic stage in eastern-Romagna (northern Apennines, Italy). *G. Geol.* 60, 119–142.
- Roveri, M., Bassetti, M.A., Ricci Lucchi, F., 2001. The Mediterranean Messinian salinity crisis: an Apennines foredeep perspective. *Sediment. Geol.* 140, 201–214.
- Roveri, M., Boscolo Gallo, A., Rossi, M., Gennari, R., Iaccarino, S.M., Lugli, S., Manzi, V., Negri, A., Rizzini, F., Taviani, M., 2005. The Adriatic foreland record of Messinian events (central Adriatic sea, Italy). *Geotecta* 4 (139), 158.
- Roveri, M., Bertini, A., Cosentino, D., Di Stefano, A., Gennari, R., Gliozzi, E., Grossi, F., Iaccarino, S.M., Lugli, S., Manzi, V., Taviani, M., 2008a. A high-resolution stratigraphic framework for the latest Messinian events in the Mediterranean area. *Stratigraphy* 5 (3–4), 323–342.
- Roveri, M., Lugli, S., Manzi, V., Schreiber, B.C., 2008b. The Messinian Sicilian stratigraphy revisited: new insights for the Messinian salinity crisis. *Terra Nova* 20 (6), 483–488. <https://doi.org/10.1111/j.1365-3121.2008.00842.x>.
- Roveri, M., Bertini, A., Cipollari, P., Cosentino, D., Di Stefano, A., Florindo, F., Gennari, R., Gliozzi, E., Grossi, F., Iaccarino, S., Lugli, S., Manzi, V., 2008c. Comment on “Earliest Zanclean age for the Colombacci and uppermost Di Tetto formations of the “latest Messinian” northern Apennines: new paleoenvironmental data from the Maccarone section (Marche Province, Italy)” by Popescu et al. (2007) *Geobios* 40 (359–373). *Geobios* 41, 669–675.
- Roveri, M., Gennari, R., Lugli, S., Manzi, V., 2009. The Terminal Carbonate Complex: the record of sea-level changes during the Messinian salinity crisis. *GeoActa* 8 (63), 63–77.
- Roveri, M., Flecker, R., Krijgsman, W., Lofi, J., Lugli, S., Manzi, V., Sierro, F.J., Bertini, A., Camerlenghi, A., De Lange, G., Govers, R., Hilgen, F.J., Hübscher, C., Meijer, P.Th., Stoica, M., 2014a. The Messinian salinity crisis: past and future of a great challenge for marine sciences. *Mar. Geol.* 349, 113–125. <https://doi.org/10.1016/j.margeo.2014.02.002>.
- Roveri, M., Lugli, S., Manzi, V., Gennari, R., Schreiber, B.C., 2014b. High resolution strontium isotope stratigraphy of the Messinian deep Mediterranean basins: implications for marginal to central basins correlation. *Mar. Geol.* 349, 113–125. <https://doi.org/10.1016/j.margeo.2014.01.002>.
- Roveri, M., Manzi, V., Bergamasco, A., Falciieri, F., Gennari, R., Lugli, S., 2014c. Dense shelf water cascading and Messinian canyons: a new scenario for the Mediterranean salinity crisis. *Am. J. Sci.* 314, 751–784. <https://doi.org/10.2475/05.2014.031>.
- Roveri, M., Gennari, R., Persico, D., Rossi, F.P., Lugli, S., Manzi, V., Reghizzi, M., Taviani, M., 2019a. A new chronostratigraphic and paleoenvironmental framework for the end of the Messinian salinity crisis in the Sorbas Basin (Betic Cordillera, southern Spain). *Geol. J.* 54 (3), 1617–1637. <https://doi.org/10.1002/gj.3256>.
- Roveri, M., Gennari, R., Ligli, M., Lugli, S., Manzi, V., Reghizzi, M., 2019b. The synthetic seismic expression of the Messinian salinity crisis from onshore records: implications for shallow-to deep-water correlations. *Basin Res.* 31 (6), 1121–1152. <https://doi.org/10.1111/bre.12361>.
- Roveri, M., Lugli, S., Manzi, V., Reghizzi, M., Rossi, F.P., 2020. Stratigraphic relationships between shallow-water carbonates and primary gypsum: insights from the Messinian succession of the Sorbas Basin (Betic Cordillera, Southern Spain). *Sediment. Geol.* 105678 <https://doi.org/10.1016/j.sedgeo.2020.105678>.
- Ruggieri, G., 1962. La serie marine pliocenica e quaternaria della Val Marecchia: *Atti Accad. Sci. Lett. Arti Palermo* 19, 1–169.
- Ruggieri, G., 1967. The Miocene and later evolution of the Mediterranean sea. Adams and Ager (Eds.). In: *Aspects of Tethyan Biogeography*: Syst. Ass. Publ. 7, p. 238.
- Ryan, W.B.F., 1973. Geodynamic implications of the Messinian crisis of salinity. In: Drooger, C.W. (Ed.), *Messinian Events in the Mediterranean*. North-Holland Publ. Co., Amsterdam, Netherlands, pp. 26–38.
- Ryan, W.B.F., 1976. Quantitative evaluation of the depth of the western Mediterranean before, during and after the late Miocene salinity crisis. *Sedimentology* 23, 791–813.
- Ryan, W.B.F., 1978. Messinian badlands on the southeastern margin of the Mediterranean Sea. *Mar. Geol.* 27, 349–363.
- Ryan, W.B.F., 2008. Modeling the magnitude and timing of evaporative drawdown during the Messinian salinity crisis. *Stratigraphy* 5, 227–243.
- Ryan, W.B.F., 2009. Decoding the Mediterranean salinity crisis. *Sedimentology* 56 (1), 95–136.
- Ryan, W.B.F., Hsü, K.J., Cita, M.B., Dumitrica, P., Lort, P., Maync, W., Nesteroff, W.D., Pautot, P., Stradner, H., Wezel, F.C., 1973. In: Ryan, W.B.F., Hsü, K.J. (Eds.), *Initial Reports of the Deep Sea Drilling Project*, Vol. 13. U.S. Government Printing Office, Washington, DC, p. 1447.
- Sabat, F., Gelabert, B., Rodriguez-Perea, A., Giménez, J., 2011. Geological structure and evolution of Mallorca: implications for the origin of the Western Mediterranean. *Tectonophysics* 510, 217–238.
- Sabato Ceraldi, T., Kamel, M., Mason, T., Poole, A., Hossack, J., Slack, J., Fraser, A., 2010. Messinian seismic facies in offshore Sirt Basin Libya and implications for sub-Messinian seismic imaging. In: Paper presented at TOG 2008-Technology of Oil and Gas, Forum and Exhibition, 21–23 October, Tripoli.
- Sachse, D., Radke, J., Gleixner, G., 2006. δD values of individual n-alkanes from terrestrial plants along a climatic gradient - implications for the sedimentary biomarker record. *Org. Geochem.* 37, 469–483.
- Sage, F., Von Gronefeld, G., Déverchère, J., Gaullier, V., Maillard, A., Gorini, C., 2005. A record of the Messinian salinity crisis on the western Sardinia margin, northwestern Mediterranean. *Mar. Pet. Geol.* 22, 757–773.
- Sampalmieri, G., Iadanza, A., Cipollari, P., Cosentino, D., Lo Mastro, S., 2010. Paleoenvironments of the Mediterranean Basin at the Messinian hypersaline/hyposaline transition: evidence from natural radioactivity and microfossils of post-evaporitic successions of the Adriatic sub-basin. *Terra Nova* 22 (4), 239–250. <https://doi.org/10.1111/j.1365-3121.2010.00939.x>.
- Sant, K., Palcu, V., Mandic, D., Krijgsman, O., 2017. Changing seas in the Early-Middle Miocene of Central Europe: a Mediterranean approach to Paratethyan stratigraphy. *Terra Nova* 29 (5), 273–281.
- Schildgen, T.F., Cosentino, D., Frijia, G., Castorina, F., Dudas, F.Ö., Iadanza, A., Sampalmieri, G., Cipollari, P., Caruso, A., Bowring, S.A., Strecker, M.R., 2014. Sea level and climate forcing of the Sr isotope composition of Late Miocene Mediterranean marine basins. *Geochem. Geophys. Geosyst.* 15, 2964–2983. <https://doi.org/10.1002/2014GC005332>.
- Schmalz, R.F., 1969. Deep-water evaporite deposition, a genetic model. *Am. Assoc. Pet. Geol. Bull.* 53, 798–823.
- Schreiber, B.C., 1997. Field trip to Ercles Mino: Upper Messinian. “Neogene Mediterranean Paleocoenography”, Excursion Guide Book Palermo-Caltanissetta-Agrigento-Erice (Sicily), 24–27 September 1997, pp. 72–80.
- Schütz, K.L., 1994. Structure and stratigraphy of the Gulf of Suez, Egypt, in Interior Rift Basins, edited by S. M. Landon. AAPG Mem. 59, 57–96.
- Schwarzans, W., Agiadi, K., Carnevale, G., 2020. Late Miocene-Early Pliocene evolution of Mediterranean gorges and their environmental and biogeographic significance. *Riv. Ital. Paleontol. Stratigr.* 126 (3).
- Sciuto, F., Baldanza, A., 2020. Full restoration of marine conditions after the late Messinian Mediterranean Lago-Mare phase in Licodia Eubea and Villafranca Tirrena areas (east Sicily). *Carnets de géologie*.
- Sciuto, F., Baldanza, A., Temani, R., Privitera, G., 2018. New reports of Paratethyan ostracods affinity from the Mediterranean Basin (Sicily, Italy). *Paleontologia Electronica* 21 (1), 1. <https://doi.org/10.26879/800>.
- Segev, A., Avni, Y., Shahar, J., Wald, R., 2017. Late Oligocene and Miocene different seaways to the Red Sea-Gulf of Suez rift and the Gulf of Aqaba-Dead Sea basins. *Earth Sci. Rev.* 171, 196–219. <https://doi.org/10.1016/j.earscirev.2017.05.004>.
- Selli, R., 1954. Il Bacino del Metauro. *Giorn. Geol.* 24, 1–294.
- Selli, R., 1960. Il Messiniano Mayer-Eymar 1867. Proposta di un neostratotipo. *Giornale di Geologia* 28, 1–33.
- Selli, R., 1973. An outline of the Italian Messinian. In: Drooger, C.W. (Ed.), *Messinian Events in the Mediterranean*, pp. 150–171. Amsterdam (Kon. Nedl. Akad. Wetensch.).
- Sgarrella, F., Sprovieri, R., Di Stefano, E., Caruso, A., 1997. Paleocoenographic conditions at the base of the Pliocene in the Southern Mediterranean Basin. *Riv. Ital. Paleontol. Stratigr.* 103, 207–220.
- Sgarrella, F., Sprovieri, R., Di Stefano, E., Caruso, A., Sprovieri, M., Bonaduce, G., 1999. The Capo Rossello Bore-Hole (Agrigento, Sicily): cyclostratigraphic and

- paleoceanographic reconstructions from quantitative analyses of the Zanclean foraminiferal assemblages. *Riv. Ital. Paleontol. Stratigr.* 105, 303–322.
- Sierro, F.J., Flores, J.A., Civis, J., Gonza, J.A., France, G., 1993. Late Miocene globorotaliid event-stratigraphy and biogeography in the NE-Atlantic and Mediterranean. *Mar. Micropaleontol.* 21 (1–3), 143–167.
- Sim, M.S., Bosak, T., Ono, S., 2011. Large sulfur isotope fractionation does not require disproportionation. *Science* 333, 74–77.
- Simon, D., Meijer, P.T., 2017. Salinity stratification of the Mediterranean Sea during the Messinian crisis: A first model analysis. *Earth Planet. Sci. Lett.* 479, 366–376.
- Simon, D., Marzocchi, A., Flecker, R., Lunt, D.J., Hilgen, F.J., Meijer, P.T., 2017. Quantifying the Mediterranean freshwater budget throughout the late Miocene: New implications for sapropel formation and the Messinian Salinity Crisis. *Earth Planet. Sci. Lett.* 472, 25–37.
- Sinninghe Damsté, J.S., Frewin, N.L., Kenig, F., De Leeuw, J.W., 1995. Molecular indicators for palaeoenvironmental changes in a Messinian evaporitic sequence (Vena del Gesso, Italy). I: Variations in extractable organic matter of ten cyclically deposited marl beds. *Org. Geochem.* 23, 471–483.
- Sissingh, W., 1976. Aspects of late Cenozoic evolution of the South Aegean ostracode fauna. *Paleogeogr., Paleoclimatol., Paleoecol.* 20, 131–146.
- Snel, E., Mănuțeanu, M., Meulenkamp, J.E., 2006. Calcareous nannofossil biostratigraphy and magnetostratigraphy of the upper Miocene and lower Pliocene of the Northern Aegean (Orphanic Gulf-Strimon Basin areas), Greece. *Paleogeogr. Paleoclimatol., Paleoecol.* 238 (1–4), 125–150. <https://doi.org/10.1016/j.paleo.2006.03.022>.
- Soria, J.M., Caracuel, J.E., Yébenes, A., Fernández, J., Viseras, C., 2005. The stratigraphic record of the Messinian salinity crisis in the northern margin of the Bajo Segura basin (SE Spain). *Sediment. Geol.* 179 (3), 225–247. <https://doi.org/10.1016/j.sedgeo.2005.05.011>.
- Soria, J.M., Caracuel, J.E., Corbí, H., Dinarés-Turell, J., Lancis, C., Tent-Manclús, J.E., Yébenes, A., 2007. Estratigrafía y biomagnetostratigrafía del Messiniense en la sección del Garruchal (Cuenca del Bajo Segura). Implicaciones para la Crisis de Salinidad del Mediterráneo. *Geogaceta* 41, 215–218.
- Soria, J.M., Caracuel, J.E., Corbí, H., Dinarés-Turell, J., Lancis, C., Tent-Manclús, J.E., Yébenes, A., 2008a. The Bajo Segura basin (SE Spain): implications for the Messinian Salinity Crisis in the Mediterranean margins. *Stratigraphy* 5, 259–265.
- Soria, J.M., Caracuel, J.E., Corbí, H., Dinarés-Turell, J., Lancis, C., Tent-Manclús, J.E., Viseras, C., Yébenes, A., 2008b. The Messinian-Early Pliocene stratigraphic record in the southern Bajo Segura basin (Betic Cordillera, Spain). Implications for the Mediterranean salinity crisis. *Sediment. Geol.* 203, 267–288.
- Spatola, D., del Moral-Erencia, J.D., Micallef, A., Camerlenghi, A., Garcia-Castellanos, D., Gupta, S., Bohorquez, P., Gutscher, M.A., Bertoni, C., 2020. A single-stage megafoof at the termination of the Messinian salinity crisis: geophysical and modelling evidence from the eastern Mediterranean Basin. *Mar. Geol.* 106337 <https://doi.org/10.1016/j.margeo.2020.106337>.
- Stampfli, J., Höcker, C.F.W., 1989. Messinian paleorelief from a 3D seismic survey in the Tarrasco concession area (Spanish Mediterranean Sea). *Geology in Minjbow* 68, 201–210.
- Stoica, M., Lazăr, I., Krijgsman, W., Vasiliev, I., Jipa, D., Floroiu, A., 2013. Paleoenvironmental evolution of the East Carpathian foredeep during the late Miocene-early Pliocene (Dacian Basin; Romania). *Glob. Planet. Chang.* 103, 135–148. <https://doi.org/10.1016/j.gloplacha.2012.04.004>.
- Stoica, M., Krijgsman, W., Fortuin, A., Gloiziz, E., 2016. Paratethyan ostracods in the Spanish Lago-Mare: More evidence for intra-basinal exchange at high Mediterranean sea level. *Paleogeogr. Paleoclimatol., Paleoecol.* 441, 854–870. <https://doi.org/10.1016/j.paleo.2015.10.034>.
- Strasser, A., Hilgen, F.J., Heckel, P.H., 2006. Cyclostratigraphy-concepts, definitions, and applications. *Newsl. Stratigr.* 42 (2), 75–114.
- Sturani, C., 1973. A fossil eel (*Anguilla* sp.) from the Messinian of Alba (Tertiary Piedmont Basin). Paleoenvironmental and paleogeographic implications. In: Messinian Events in the Mediterranean. K. Nederl. Akad. Wetensch, Amsterdam, pp. 243–255.
- Suárez-González, P., Arenas, C., Benito, M.I., Pomar, L., 2019. Interplay between biotic and environmental conditions in prealt Messinian microbialites of the western Mediterranean (Upper Miocene, Mallorca, Spain). *Paleogeogr. Paleoclimatol., Paleoecol.* 533, 109–242.
- Suc, J.-P., Do Couto, D., Melinte-Dobrescu, M.C., Macaleț, R., Quilléveré, F., Clauzon, G., Csato, I., Rubino, J.-L., Popescu, S.-M., 2011. The Messinian salinity crisis in the Dacic Basin (SW Romania) and early Zanclean Mediterranean-Paratethys high sea-level connection. *Paleoecol.* 310, 256–272. <https://doi.org/10.1016/j.paleo.2011.07.018>.
- Suc, J.-P., Popescu, S.-M., Do Couto, D., Clauzon, G., Rubino, J.-L., Melinte-Dobrescu, M.C., Quilléveré, F., Brun, J.-P., Dumurdzanov, N., Zagorchev, I., Lesić, V., Tomić, D., Sokoutis, D., Meyer, B., Macaleț, R., Rifelj, H., 2015. Marine gateway vs. fluvial stream within the Balkans from 6 to 5 Ma. *Mar. Pet. Geol.* 66 (1), 231–245. <https://doi.org/10.1016/j.marpetgeo.2015.01.013>.
- Thinon, I., Guennoc, P., Serrano, O., Maillard, A., Lasseur, E., Réhault, J.P., 2016. Seismic markers of the Messinian Salinity Crisis in an intermediate-depth basin: data for understanding the Neogene evolution of the Corsica Basin (Northern Tyrrhenian Sea). *Mar. Pet. Geol.* 77, 1274–1296. November 2016. <https://doi.org/10.1016/j.marpetgeo.2016.02.017>.
- Thode, H.G., Monster, J., 1965. Sulfur-Isotope Geochemistry of Petroleum, Evaporites, and Ancient Seas. In: Young, A., Galley, J.E. (Eds.), *Fluids in Subsurface Environments*. American Association of Petroleum Geologists, p. 0.
- Topper, R.P.M., Meijer, P.T., 2015. The precessional phase lag of Messinian gypsum deposition in Mediterranean marginal basins. *Paleogeogr. Paleoclimatol., Paleoecol.* 417, 6–16.
- Topper, R.P.M., Flecker, R., Meijer, P.T., Wortel, M.J.R., 2011. A box model of the Late Miocene Mediterranean Sea: implications from combined 87Sr/86Sr and salinity data. *Paleoceanography* 26. <https://doi.org/10.1029/2010PA002063>. PA3223.
- Topper, R.P.M., Lugli, S., Manzi, V., Roveri, M., Meijer, P.T., 2014. Precessional control of Sr ratios in marginal basins during the Messinian salinity crisis? *Geochim. Geophys. Geosyst.* 15–5, 1926–1944. <https://doi.org/10.1002/2013GC005192>.
- Trenkwalder, S., Violanti, D., D'Attri, A., Lozar, F., Dela Pierre, F., Irace, A., 2008. The Miocene/Pliocene boundary in the Early Pliocene micropaleontological record: new data from the Tertiary Piedmont Basin (Moncucco quarry, Torino Hill, northwestern Italy). *Boll. Soc. Paleontol. Ital.* 47, 87–103.
- Turchyn, A.V., Schrag, D.P., 2004. Oxygen Isotope Constraints on the Sulfur Cycle over the Past 10 Million Years. *Science* 303, 2004.
- Turchyn, A.V., Sivan, O., Schrag, D.P., 2006. Oxygen isotopic composition of sulfate in deep sea pore fluid: evidence for rapid sulfur cycling. *Geobiology* 4, 191–201.
- Turchyn, A.V., Schrag, D.P., Coccioni, R., Montanari, A., 2009. Stable isotope analysis of the Cretaceous sulfur cycle. *Earth Planet. Sci. Lett.* 285, 115–123.
- Tzanova, A., Herbert, T.D., Peterson, L., 2015. Cooling Mediterranean Sea surface temperatures during the Late Miocene provide a climate context for evolutionary transitions in Africa and Eurasia. *Earth Planet. Sci. Lett.* 419, 71–80. <https://doi.org/10.1016/j.epsl.2015.03.016>.
- Urgeles, R., Camerlenghi, A., Garcia-Castellanos, D., De Mol, B., Garces, M., Verges, J., Haslam, I., Hardman, M., 2011. New constraints on the Messinian sealevel drawdown from 3D seismic data of the Ebro margin, western Mediterranean. *Basin Res.* 23, 123–145. <https://doi.org/10.1111/j.1365-2117.2010.00477.x>.
- Utrilla, R., Pierre, C., Orti, F., Pueyo, J.J., 1992. Oxygen and sulphur isotope compositions as indicators of the origin of Mesozoic and Cenozoic evaporites from Spain. *Chem. Geol.* 102, 229–244.
- Vai, G.B., 1997. Chapter E3 Cyclostratigraphic estimate of the messinian stage duration. In: Montanari, A., Odin, G.S., Coccioni, R. (Eds.), *Miocene Stratigraphy: An Integrated Approach*. Dev. Paleontol. Stratigr. 15, 463–476.
- Vai, G.B., 2016. Over half a century of Messinian salinity crisis. *Bol. Geol. Min.* 127 (2), 625–641.
- Van Baak, C.G.C., Radionova, E.P., Golovina, L.A., Raffi, I., Kuiper, K.F., Vasiliev, I., Krijgsman, W., 2015. Messinian events in the Black Sea. *Terra Nova* 27, 433–441. <https://doi.org/10.1111/ter.12177>.
- Van Baak, C.G., Stoica, M., Grothe, A., Aliyeva, E., Krijgsman, W., 2016. Mediterranean-Paratethys connectivity during the Messinian salinity crisis: The Pontian of Azerbaijan. *Glob. Planet. Chang.* 141, 63–81. <https://doi.org/10.1016/j.gloplacha.2016.04.005>.
- Van Baak, C.G., Krijgsman, W., Magyar, I., Sztanó, O., Golovina, L.A., Grothe, A., Hoyle, T.M., Mandić, O., Patina, I.S., Popov, S.V., Radionova, E.P., Stoica, M., Vasiliev, I., 2017. Paratethys response to the Messinian salinity crisis. *Earth Sci. Rev.* 172, 193–223. <https://doi.org/10.1016/j.earscirev.2017.07.015>.
- Van Couvering, J.A., Berggren, W.A., Drake, R.E., Aguirre, E., Curtis, G.H., 1976. The terminal Miocene event. *Mar. Micropaleontol.* 1, 263–286.
- Van Couvering, J.A., Castradori, D., Cita, M.B., Hilgen, F.J., Rio, D., 2000. The base of the Zanclean Stage and of the Pliocene Series. *Episodes* 23, 179–187.
- Van den Berg, B.C.J., Sierro, F.J., Hilgen, F.J., Flecker, R., Larrasoana, J.C., Krijgsman, W., Flores, J.A., Mata, M.P., Martín, E.B., Civis, J., González-Delgado, J.A., 2015. Astronomical tuning for the upper Messinian Spanish Atlantic margin: disentangling basin evolution, climate cyclicity and MOW. *Glob. Planet. Chang.* 135, 89–103.
- Van der Meer, M.T.J., Baas, M., Rijpstra, I.C., Marino, G., Rohling, E.J., Sinninghe Damsté, J.S., Schouten, S., 2007. Hydrogen isotopic compositions of long-chain alkenones record freshwater flooding of the Eastern Mediterranean at the onset of sapropel deposition. *Earth Planet. Sci. Lett.* 262, 594–600.
- Van Hinsbergen, D.J., Meulenkamp, J.E., 2006. Neogene supradetachment basin development on Crete (Greece) during exhumation of the South Aegean core complex. *Basin Res.* 18 (1), 103–124.
- Vasiliev, I., Reichart, G.-J., Davies, G.R., Krijgsman, W., Stoica, M., 2010. Strontium isotope ratios of the Eastern Paratethys during the Miocene/Pliocene transition; Implications for interbasinal connectivity. *Earth Planet. Sci. Lett.* 292, 123–131. <https://doi.org/10.1016/j.epsl.2010.01.027>.
- Vasiliev, I., Reichart, G.-J., Krijgsman, W., 2013. Impact of the Messinian Salinity Crisis on Black Sea hydrology - insights from hydrogen isotopes on molecular biomarkers. *Earth Planet. Sci. Lett.* 362, 272–282. <https://doi.org/10.1016/j.epsl.2012.11.038>.
- Vasiliev, I., Reichart, G.-J., Grothe, A., Sinninghe Damsté, J.S., Krijgsman, W., Sangiorgi, F., Weijers, J.W.H., van Roij, L., 2015. Recurrent phases of drought in the upper Miocene of the Black Sea region. *Paleogeogr. Paleoclimatol., Paleoecol.* 423, 18–31.
- Vasiliev, I., Mezger, E.M., Lugli, S., Reichart, G.J., Manzi, V., Roveri, M., 2017. How dry was the Mediterranean during the Messinian salinity crisis? *Paleogeogr. Paleoclimatol., Paleoecol.* 471, 120–133. <https://doi.org/10.1016/j.paleo.2017.01.032>.
- Vasiliev, I., Karakitsios, V., Bouloubassi, I., Agiadi, K., Kontakiotis, G., Antonarakou, A., Triantaphyllou, M., Gogou, A., Kafousia, N., de Rafélis, M., Zarkogiannis, S., Kaczmarski, F., Parinos, C., Pasadakis, N., 2019. Large sea surface temperature, salinity, and productivity preservation changes preceding the onset of the Messinian Salinity Crisis in the eastern Mediterranean Sea. *Paleoceanogr. Paleoclimatol.* 34, 182–202. <https://doi.org/10.1029/2018PA003438>.
- Veizer, J., 1989. Strontium isotopes in seawater through time. *Annu. Rev. Earth Planet. Sci.* 17 (1), 141–167.
- Violanti, D., Trenkwalder, S., Lozar, F., Gallo, L.M., 2009. Micropaleontological analyses of the Nazrole core: biostratigraphy and paleoenvironment of the late Messinian and early Zanclean of Piedmont (Northwestern Italy). *Boll. Soc. Paleontol. Ital.* 48, 167–181.

- Warren, J.K., 2016. *Evaporites: A geological compendium*. Springer.
- Winterberg, S., Picotti, V., Willett, S.D., 2020. Messinian or Pleistocene valley incision within the Southern Alps. *Swiss J. Geosci.* 113 (1), 1–14. <https://doi.org/10.1186/s00015-020-00361-7>.
- Wortmann, U.G., Chernyavsky, B., Bernasconi, S.M., Brunner, B., Böttcher, M.E., Swart, P.K., 2007. Oxygen isotope biogeochemistry of pore water sulfate in the deep biosphere: Dominance of isotope exchange reactions with ambient water during microbial sulfate reduction (ODP Site 1130). *Geochim. Cosmochim. Acta* 71, 4221–4232.
- Zachariasse, W.J., van Hinsbergen, D.J.J., Fortuin, A.R., 2008. Mass wasting and uplift on Crete and Karpathos (Greece) during the Early Pliocene related to beginning of South Aegean left-lateral, strike slip tectonics. *Geol. Soc. Am. Bull.* 120, 976–993.
- Zachariasse, W.J., van Hinsbergen, D.J.J., Fortuin, A.R., 2011. Formation and fragmentation of a late Miocene supradetachment basin in central Crete: implications for exhumation mechanisms of high-pressure rocks in the Aegean forearc. *Basin Res.* 23 (6), 678–701. <https://doi.org/10.1111/j.1365-2117.2011.00507.x>.
- Ziveri, P., Baumann, K.H., Bockel, B., Bollmann, J., Young, J., 2004. Present day coccolithophore-biogeography in the Atlantic Ocean. In: *Coccolithophores: From Molecular Processes to Global Impact*. Springer Verlag, pp. 403–428.
- Zonneveld, K.A., Marret, F., Versteegh, G.J., Bogus, K., Bonnet, S., Bouimtarhan, I., Crouch, I.E., Esper, O., 2013. Atlas of modern dinoflagellate cyst distribution based on 2405 data points. *Rev. Paleobot. Palynol.* 191, 1–197.

Appendix 3

Abstract, Introduction and
Conclusions in Spanish

Resumen

Durante el Mioceno tardío, los procesos tectónicos llevaron al cierre de las conexiones Mediterráneo - Atlánticas, aislando progresivamente la cuenca del Mediterráneo del océano global. Este cambio en la configuración de los canales interoceánicos modificó radicalmente los patrones de circulación, el tiempo de residencia y la salinidad de las aguas del Mediterráneo, dando lugar al extraordinario cambio paleoambiental conocido como la crisis de la salinidad del Messiniense. Este evento duró entre 5.97 y 5.33 Ma (millones de años), dando lugar al depósito de enormes acumulaciones de evaporitas tanto en las cuencas mediterráneas marginales como en las profundas. Ahora, más de 50 años después de que el *Glomar challenger* se aventurara en las aguas del Mediterráneo y se descubrieran las evaporitas en cuencas profundas, el debate sobre las condiciones y el momento del depósito del gigante de la sal del Mediterráneo sigue en curso, ya que muchas teorías sobre la dinámica y la cronología del cierre y reapertura de los canales interoceánicos del arco de Gibraltar están a la espera de ser validadas.

En esta óptica, el estudio de sondeos marinos y afloramientos en las proximidades del actual estrecho de Gibraltar es fundamental para comprender mejor la evolución de los canales interoceánicos entre el Mediterráneo y el Atlántico. En esta tesis realizamos un análisis detallado de foraminíferos bénticos y planctónicos, así como análisis geoquímicos (rayos-X e isótopos estables) y sedimentológicos de varios testigos sedimentarios (ODP 976, DSDP 121) y pozos industriales (Andalucía-G1, Alborán-A1) de la cuenca de Alborán, afloramientos de algunas cuencas del sur de España incluyendo Níjar, Sorbas y Málaga y un sondeo de la cuenca del Guadalquivir (Montemayor-1). Los resultados obtenidos, junto con la interpretación de los perfiles sísmicos adquiridos en la cuenca de Alborán, dieron lugar a nuevos conocimientos y resultados para una mejor comprensión de la evolución del Mioceno tardío al Plioceno temprano de los canales interoceánicos Mediterráneo-Atlántico y los efectos de la restricción en los entornos mediterráneos antes y después de la crisis de salinidad del Messiniense. Los principales resultados de esta tesis se enumeran y describen a continuación.

- Una estratigrafía de foraminíferos planctónicos de alta resolución realizada en los sondeos 976 y Montemayor-1 en combinación con la calibración de los ciclos geoquímicos con las curvas astronómica de referencia hizo posible la creación de un marco cronoestratigráfico fiable. Disponer de un marco cronoestratigráfico firme permitió precisar el momento en el que el levantamiento de los corredores del arco de Gibraltar empezó a afectar a la cuenca del Mediterráneo y al corredor Bético.
- El primer signo de la restricción de los canales interoceánicos Mediterráneo-Atlántico es visible en la cuenca mediterránea desde hace 7.17 Ma, cuando la tectónica activa en el arco de Gibraltar comenzó a levantar los corredores Bético y Rifeño. En el sondeo ODP 976, el levantamiento es visible por el aumento en la entrada de material terrígeno a la cuenca de Alborán y el incremento de las tasas de sedimentación, relacionado con una mayor erosión fluvial. Por otro lado, el cambio de foraminíferos bénticos de ambiente marino abierto, con

alto contenido de oxígeno, a taxones infaunales poco profundos, tolerantes a una amplia gama de condiciones y niveles de oxígeno subóptimos, junto con una caída significativa en los valores bentónicos de $\delta^{13}\text{C}$, sugieren que la restricción de entrada condujo a la disminución en los niveles de oxígeno en el agua del fondo y al aumento de su tiempo de residencia mucho antes del inicio de la crisis de salinidad del Messiniense.

- Una correlación entre los datos del sondeo ODP 976 y otros registros del Mediterráneo confirmó que la restricción de las conexiones interoceánicas hace 7.17 Ma afectó, al mismo tiempo, a diferentes lugares en todo el Mediterráneo, lo que permite inferir la existencia de un cambio a escala mediterránea en la circulación termohalina. A partir de estos datos concluimos que la cuenca oeste de Alborán y la cuenca este de Alborán no estaban separadas por un umbral en ese momento, sino que ambas formaban parte del ámbito mediterráneo. Además, fue posible crear un modelo de circulación mediterránea refinado para antes y después del evento de 7.17 Ma.
- La restricción de los canales interoceánicos Atlántico - Mediterráneo visible en el registro mediterráneo desde 7.17 Ma, es evidente también a partir de los datos geoquímicos del sondeo Montemayor-1 en la cuenca del Guadalquivir. Dado que los datos geoquímicos de Montemayor-1 revelan que después de 7.15-7.17 Ma la cuenca estaba bañada por una sola masa de agua, probablemente atlántica, creemos que la conexión entre el Mediterráneo y el Atlántico, a través del corredor Bético, estaba restringida en ese momento. En consecuencia, sugerimos que la restricción del último corredor Bético, la cuenca del Guadalhorce, pudo ocurrir entre 7.15 y 7.17 Ma y provocar los cambios mencionados anteriormente en el paleoambiente mediterráneo.
- Debido a que la restricción de los canales interoceánicos fue contemporánea con el Cambio Global del Isótopo de Carbono del Mioceno Tardío (LMCIS), la comparación entre registros mediterráneos y globales fue importante discernir entre los efectos globales y locales. Dado el sincronismo del cambio en el registro de $\delta^{13}\text{C}$ global y local del Mediterráneo, un proceso global sin duda afectó a esa cuenca. Sin embargo, las relaciones de fase opuesta de las señales globales y locales de $\delta^{13}\text{C}$ con los parámetros orbitales, junto con un cambio de mayor magnitud, identificado en nuestro registro isotópico de la cuenca oeste de Alboran, sugiere que la huella local fue mas marcada que la global. Un efecto similar se puede ver en el registro de Montemayor-1, donde además de los cambios relacionados con el levantamiento del arco de Gibraltar, la señal global no se puede excluir.
- Finalmente, a través del desarrollo de esta tesis, se muestra cómo la capa oscura frecuentemente enriquecida en materia orgánica, presente en el límite Mioceno - Plioceno en varias cuencas mediterráneas marginales y profundas, sugiere que la inundación del Zancleanse creó una estratificación de la columna de agua, reduciendo los niveles de oxígeno del agua profunda. Tal estratificación podría ser el resultado del hundimiento de una masa de agua atlántica, más salina, que ingresa a una cuenca mediterránea, menos salina, y aún bajo la influencia del

Paratethys. La secuencia de repoblación de foraminíferos bentónicos identificada en la base del Plioceno muestra similitudes con eventos más recientes de repoblación de ambientes hostiles o posteriores a episodios de bajo oxígeno durante el depósito de sapropeles. Sin embargo, los valores atlánticos del $\delta^{13}\text{C}$ bentónico registrados en la cuenca de Alborán sugieren que la renovación y circulación del agua del fondo fueron eficientes durante el Zancliense temprano, evitando la reducción de $\delta^{13}\text{C}$ en el fondo marino observada después de 7.17 Ma. Además, las ligeras discrepancias en las secuencias de repoblación de foraminíferos bentónicos de las cuencas marginales en el límite Mioceno - Plioceno, y los valores mucho más ligeros de $\delta^{13}\text{C}$ bentónico en la cuenca de Málaga pueden sugerir una inundación diacrónica de las cuencas marginales menos profundas.

Introducción

Desde el comienzo de la tectónica de placas hace 2 Ga (Stern, 2007), la deriva continental ha estado moviendo masas de tierra creando y destruyendo mares, abriendo y cerrando vías marítimas que influyen en la circulación oceánica y en el clima. En el Eoceno, la apertura del paso de Drake entre América del Sur y la Antártida y del corredor de Tasmania entre la Antártida y Australia marcó el inicio de la Corriente Circumpolar Antártica que indujo un aumento de la productividad y el consiguiente secuestro de CO₂ atmosférico, contribuyendo al enfriamiento global y glaciación antártica (Scher and Martin, 2006; Scher et al., 2015). A partir de 4.6 Ma, la formación del Istmo de Panamá afectó profundamente la circulación oceánica profunda, considerándose la causa principal del establecimiento de la circulación termohalina del Atlántico norte, mientras que en el Plioceno contribuyó a la intensificación de la glaciación del Hemisferio Norte (Haug and Tiedemann, 1998). Por lo tanto, para comprender los mecanismos causales detrás del cambio climático local y global es necesario, en muchos casos, el estudio de la evolución de la distribución de masas de tierra y agua. Teniendo esto en cuenta, la tesis doctoral aquí presentada tiene como objetivo investigar los cambios en la conexión entre el Atlántico y el Mediterráneo, mediante el análisis de sondeos marino y afloramientos en tierra en las áreas próximas al Estrecho de Gibraltar.

En la actualidad, el Mediterráneo está conectado con el Océano Atlántico a través del estrecho de Gibraltar, un canal de tan solo 13 km de ancho. Este último, a finales del Tortonense (11.63 a 7.25 Ma), muy probablemente no existió, y el intercambio de agua entre el Mediterráneo y el Atlántico se producía a través de los corredores Bético y Rifeño ubicados respectivamente, al Sur de España y Norte de África (Roveri and Manzi, 2006; Flecker et al., 2015). Los corredores, junto con la cuenca de Alborán, se sitúan sobre la zona de convergencia y colisión entre las placas africana y europea (Booth-Rea et al., 2007; Do Couto et al., 2016; Spakman et al., 2018). En el Oligoceno (30-25 Ma), la convergencia entre estas placas se ralentizó, iniciando un retroceso de la fosa hacia el este-oeste y un *slab rollback* que resultó en una extensión del retro-arco (Rosenbaum et al., 2002; Heit et al., 2017) acompañada de una migración hacia el oeste del dominio de Alborán (Jolivet and Faccenna, 2000; Booth-Rea et al., 2007; Soto et al., 2010; Gómez de la Peña et al., 2020). Justo después del límite Tortonense – Messiniense (7.24 Ma; Hilgen et al., 1995), la migración hacia el oeste del dominio de Alborán se detuvo y el *slab rollback* se desaceleró (Spakman et al., 2018), iniciando un *slab tear* a partir del margen oriental de la actual costa sur española que se propagó hacia el oeste, llegando al Atlántico (Govers, 2009; Garcia-Castellanos and Villaseñor, 2011; Mancilla et al., 2015). Como consecuencia, un movimiento topográfico dinámico levantó el sistema Bético (Garcia-Castellanos and Villaseñor, 2011; Van den Berg et al., 2018; Capella et al., 2020) restringiendo el corredor Bético (Krijgsman et al., 1999; Martín et al., 2014; Flecker et al., 2015; Capella et al., 2018). La edad del cierre de la última conexión a través de las Béticas (Corredor del Guadalhorce) aún es objeto de debate, variando entre el Tortonense superior (~7.6 Ma; Van der Schee et al., 2018) y el Messiniense medio (6.18 Ma; Martín et al., 2001; Pérez-Asensio et al., 2012; Martín et al., 2014; Pérez-Asensio et al., 2014). Un levantamiento similar se produjo en la costa opuesta de Alborán, donde los corredores rifeños se vieron restringidos por la progresiva indentación hacia el sur del margen marroquí,

produciendo el espesamiento de la corteza (Fadil et al., 2006) que culminó con el cierre completo de su sector sur entre 7.1 -6.9 Ma. Los sectores norte, por su parte, permanecieron cerrados desde 7.35 hasta 7.25 Ma (Tulbure et al., 2017; Capella et al., 2018). En el registro sedimentológico del Mar Mediterráneo, el primer signo de restricción de los canales interoceánicos se identificó hace 7.17 Ma (Kouwenhoven et al., 1999; Seidenkrantz et al., 2000). A partir de este momento, los registros de aguas profundas en el Mediterráneo oriental muestran un cambio faunístico, donde especies de foraminíferos típicas de ambientes óxicos y marinos abiertos son remplazados por especies de foraminíferos bentónicos característicos de ambientes subóxicos y sometidos a mayor grado de estrés ambiental (Seidenkrantz et al., 2000; Blanc-Valleron et al., 2002; Kouwenhoven et al., 2003; Kouwenhoven et al., 2006; Di Stefano et al., 2015). Al mismo tiempo depósitos de materiales ricos en materia orgánica o sapropeles se vuelve mucho más frecuente (Santarelli et al., 1998; Seidenkrantz et al., 2000; Hüsing et al., 2009). El proceso de restricción alcanzó su punto máximo en la edad de 5.971 Ma, lo que resultó en el depósito masivo de materiales evaporíticos de varios kilómetros de espesor en diferentes cuencas mediterráneas, un evento conocido como la crisis de salinidad Messiniense (Selli, 1964; Hsü et al., 1973; Selli, 1973).

En este trabajo nos centramos, en primer lugar, en las fases iniciales de la restricción de los canales interoceánicos Mediterráneo - Atlántico del Mioceno tardío. Además de establecer una cronología firme y comprender los primeros efectos que la restricción tuvo sobre la cuenca occidental de Alborán (sondeo ODP 976), tratamos de entender la relación de este evento local con los cambios climáticos globales. En segundo lugar, se investiga el mismo evento en el margen sur español (sondeo Montemayor-1), actual cuenca del Guadalquivir y corredor marino en el Mioceno tardío. Finalmente, se intenta comprender la dinámica del restablecimiento a principios del Plioceno de dicha conexión marina y cuáles fueron las consecuencias sobre la fauna marina, tanto en las cuencas profundas (cuenca oeste de Alborán), como en las marginales (cuencas de Málaga, Sorbas, Níjar). Estos objetivos generales se resumen a través de un conjunto de objetivos específicos, descritos a continuación en forma de preguntas de investigación:

1. ¿Cuáles son las evidencias de restricción de las conexiones interoceánicas Atlántico - Mediterráneas en las áreas mediterráneas más próximas al arco de Gibraltar (cuenca oeste de Alborán)?
 - a. ¿Cuándo se produjo la primera restricción de las conexiones Atlántico - Mediterráneas?
 - b. ¿Cuáles fueron las causas de tal restricción?
 - c. ¿Hay alguna facies relacionada con la crisis de salinidad del Messiniense que se pueda encontrar en la Cuenca de Alborán?
 - d. ¿Es posible estimar el hiato producido por la inundación Zancliense?

Estas preguntas han sido tratadas en el Capítulo 3, a partir del análisis en detalle del contenido micropaleontológico y geoquímico del sondeo ODP 976 de la cuenca oeste de Alborán, el sondeo DSDP 121 y los pozos industriales And-G1 y Alb-A1. Además, se utilizaron secciones sísmicas disponibles de la misma zona para evaluar los hiatos y el aspecto de las diferentes facies del Messiniense.

2. ¿Cómo afectó el primer evento de restricción Mediterráneo - Atlántico a los ambientes marinos del Mediterráneo?
 - a. ¿Dónde estaban ubicados los canales interoceánicos Atlántico - Mediterráneos?
 - b. ¿Cuál fue el mecanismo causal entre los cambios paleogeográficos en el Mediterráneo y los cambios climáticos globales?

Estas preguntas se contestan en el Capítulo 4, donde se evalúan los cambios en los entornos marinos mediterráneos y los patrones de circulación a través de un estudio de la distribución de foraminíferos béntonicos y las curvas de isótopos estables del sondeo ODP 976.

3. ¿El aislamiento del Mediterráneo fue desencadenado por la restricción de un canal interoceánico situado en el corredor bético?
 - a. ¿Los primeros signos de restricción de los canales interoceánicos Mediterráneo-Atlánticos se produjeron por la desconexión definitiva del corredor del Guadalhorce?
 - b. En caso afirmativo, ¿cuándo se cerró definitivamente el corredor del Guadalhorce?
 - c. ¿Cuáles fueron las consecuencias del cierre del corredor en la cuenca del Guadalquivir?

Las respuestas a estas cuestiones se desarrollan en el Capítulo 5, donde se precisa el momento del cierre del corredor del Guadalhorce a través de datos geoquímicos y distribución de foraminíferos planctónicos del sondeo Montemayor-1.

4. ¿Cómo afectó la inundación Zancliense del Mediterráneo sus entornos y la fauna marinos?
 - a. ¿Qué especies de foraminíferos béntonicos prosperaron después del restablecimiento de una conexión eficiente Mediterráneo - Atlántica?
 - b. ¿Cuál fue la respuesta sedimentológica a las inundaciones en cuencas profundas y marginales?
 - c. ¿Fue la inundación sincrónica en todo el Mediterráneo?
 - d. ¿Cuál fue la profundidad de las cuencas profundas y marginales del Mediterráneo en el límite Mioceno - Plioceno?

Estas últimas cuestiones se desarrollan en el Capítulo 6 a través de un análisis de foraminíferos béntonicos y isótopos estables de afloramientos del Plioceno temprano de las cuencas de Sorbas, Nijar y Málaga (Sur de España).

Conclusiones

Esta tesis doctoral tuvo como objetivo estudiar las condiciones palaeoambientales de la cuenca Mediterránea, en particular de las áreas cercanas a las conexiones Atlántico – Mediterráneo, antes y después de la crisis de salinidad del Messiniense. También nos interesaba conocer la posible existencia de depósitos relacionados con ese evento en la cuenca de Alborán, en la que no se habían encontrado evaporitas hasta el momento.

En primer lugar, pudimos demostrar el impacto y el comienzo de la fase de acondicionamiento de la crisis de salinidad del Messiniense, tanto en la cuenca del Mediterráneo Occidental, como en el Océano Atlántico, a partir del estudio de sondeos y afloramientos de las regiones próximas al Estrecho de Gibraltar. Para ello, realizamos análisis micropaleontológicos y geoquímicos de alta resolución en el sondeo ODP 976, en la Cuenca de Alborán y en el sondeo Montemayor-1, de la Cuenca del Guadalquivir, lo que permitió crear un modelo de edad preciso para los dos sondeos y señalar los principales cambios que ocurren en el registro. Además, estas observaciones, combinadas con los análisis micropaleontológicos llevados a cabo en el sondeo DSDP 121, los pozos industriales And-G1 y Alb-A1 y las líneas sísmicas de la Cuenca de Alborán, fue posible identificar la erosión del Zancliense y los depósitos del Messiniense tardío en la cuenca de Alborán.

En segundo lugar, se identificó un mecanismo casual entre la primera restricción de las conexiones Mediterráneo – Atlánticas y los eventos climáticos de escala global.

Finalmente, fue posible reconstruir la dinámica del restablecimiento de una conexión eficiente entre el Mediterráneo y el Atlántico después de la inundación Zancliense, mediante un análisis sedimentológico y micropaleontológico detallado sobre los sedimentos del Plioceno temprano del sondeo ODP 976 y de los afloramientos del sur de España, localizados en las cuencas de Málaga, Níjar y Sorbas.

1. Acondicionamiento del MSC y depósitos relacionados

1.1. Borde Mediterraneo: la cuenca de Alborán

Los análisis de foraminíferos benthónicos y planctónicos del sondeo ODP 976 de la Cuenca de Alborán permitieron la creación de un modelo de edad inicial, utilizando bioeventos como puntos de enlace de primer orden. Éstos, incluyeron la primera aparición común del grupo *G. menardii* 5 (7.36 Ma), la última aparición común del grupo *G. menardii* 5 (7.23 Ma), la primera aparición común del grupo *G. miotumida* (7.24 Ma), la última aparición de *G. suterae* (7.17 Ma), la desaparición de *S. reticulata* (7.167 Ma), y cambio de enrollamiento de sinistrorso a destrorso en *N. acostaensis*. El reconocimiento de cambios cíclicos impulsados por precesión en los registros de foraminíferos planctónicos cálidos, isótopos estables y rayos-X permitió llevar a cabo un *tuning* astronómico preciso de los sedimentos. A través de este modelo de edad de alta resolución para el Tortoniense y el Messiniense de la cuenca de Alborán, pudimos datar con precisión los cambios ambientales en esta parte del Mediterráneo cercana a los

corredores del arco de Gibraltar. Finalmente, fue posible realizar las siguientes observaciones.

- Durante el Tortoniense tardío – Messiniense temprano, es decir, hasta 7.17 Ma, la cuenca oeste de Albarán se caracteriza por una ambiente profundo y sedimentación marina profunda. Los altos porcentajes de foraminíferos planctónicos típicos de aguas frías ricas en nutrientes y foraminíferos bentónicos típicos de altos niveles de oxígeno y condiciones marinas abiertas obtenidos permiten inferir un ambiente de aguas profundas bien ventilado, lo que indica un intercambio de agua eficiente a través de el/los estrecho/s de Gibraltar. En particular, la ausencia de foraminíferos planctónicos de aguas cálidas del género *Globigerinoides* spp., encontrados en otros sitios contemporáneos, podría sugerir que el flujo de entrada del Atlántico, moviéndose a lo largo de la costa sur de España, pudo promover una circulación similar a la que ocurre hoy en día en la Cuenca de Alborán. El *upwelling* resultante de aguas frías ricas en nutrientes podría explicar la proliferación de foraminíferos de agua fría. Estas observaciones abren la posibilidad, aunque especulativa, de la existencia de un proto-estrecho de Gibraltar como principal fuente de entrada de aguas Atlánticas en ese momento en el Mediterráneo.
- Una correlación detallada con otros registros mediterráneos confirmó que la restricción de los estrechos Betico y Rifeño, a partir de 7.17 Ma, identificado mediante evidencias en los sedimentos de la cuenca oeste de Albarán, afectó simultáneamente a diferentes lugares de la cuenca, lo que sugiere la existencia de un cambio a escala Mediterránea en la circulación termohalina. De estos datos concluimos, en primer lugar, que las cuencas este y oeste de Albarán no estaban separados por un umbral, sino que ambos formaban parte del ámbito mediterráneo. En segundo lugar, pudimos refinar un modelo de circulación mediterránea antes y después de 7.17 Ma. La restricción de las conexiones Mediterráneo – Atlánticas resultó en la estratificación de la columna de agua de la cuenca oeste del Mediterráneo, pero mientras en las aguas de fondo el oxígeno era reducido, las aguas intermedias estaban mejor ventiladas. En la cuenca este del Mediterráneo, debido a la presencia del umbral de Sicilia, el impacto de la estratificación fue mucho mayor y condujo al depósito de sapropeles, ausentes en el oeste del Mediterráneo.
- Los análisis de perfiles sísmicos y sedimentos de sondeos localizados en la cuenca oeste de Alborán permitieron reconocer dos unidades Messinienses, una compuesta por estratos planos paralelos y otra caótica. La primera unidad se ha relacionado con depósitos de turbiditas cerca de la costa y depósitos hemipelágicos en las partes centrales de la cuenca. La segunda unidad caótica de transporte en masa (MTD), recuperada en los recortes de perforación de los pozos industriales And-G1 y Alb-A1, puede relacionarse con las etapas finales de la crisis de salinidad del Messiniense, desencadenadas por un cambio de nivel de base.
- A través del *tuning* astronómico pudimos dar una edad a los primeros ciclos de precesión del Messiniense por debajo de la evidente discontinuidad erosiva

observada en los perfiles sísmicos de la cuenca oeste de Alboran. La superficie de erosión irregular (reflector M) es claramente visible en el sondeo 976, donde estimamos la ausencia de, como mínimo, 1.67 Ma y 455 m del registro sedimentario del Messiniense.

1.2. Borde Atlántico: la cuenca de Guadalquivir

Un modelo de edad de alta resolución del intervalo inferior (6.37 Ma - 8 Ma) del sondeo de Montemayor-1, ubicado en la Cuenca del Guadalquivir, fue producido por la combinación de bioeventos de foraminíferos planctónicos (última aparición común del grupo *G. menardii* 4, primera aparición común del grupo *G. menardii* 5, reemplazo del grupo *G. menardii* 5 por el grupo *G. miotumida* y el cambio de enrollamiento de *N. acostaensis* de sinistrorso a dextrorso) y del *tuning* astronómico de los ciclos de excentricidad reconocidos. La combinación de este nuevo modelo de edad para la parte inferior del registro con modelos de edad y datos anteriores para la parte media (5.7 Ma-6.37 Ma) y superior (5.33 Ma-5.77 Ma) del sondeo de Montemayor-1, permitió datar con precisión los cambios ambientales que ocurrieron en la Cuenca del Guadalquivir desde 8 a 5.33 Ma y su relación con eventos Mediterráneos y globales:

- Desde 7.15 - 7.17 Ma en el sondeo Montemayor-1, el tiempo de residencia, la temperatura y la salinidad del agua del fondo aumentan en concomitancia con una somerización de la cuenca, inferida por la mayor tasa de sedimentación y el aumento de los aportes de material terrígeno. Asociamos este evento a una reducción de la salida de agua Mediterránea, como consecuencia de la restricción del último tramo del corredor Bético que conecta el Mediterráneo y el Atlántico, el Guadalhorce.
- La restricción del corredor Bético entre 7.15 y 7.17 Ma es coherente con los cambios contemporáneos reportados en la cuenca de Alborán y muchas otras localidades Mediterráneas. Allí, en 7.17 Ma el aumento del tiempo de residencia y disminución de la oxigenación de las aguas profundas sugieren una restricción de las conexiones Mediterráneo - Atlánticas y una reducción del flujo de salida de las aguas Mediterráneas.
- El aumento progresivo de la tasa de sedimentación (de 5 a 90 cm/kyr) visible a partir de los datos de Montemayor-1 y la consiguiente restricción del último tramo del corredor Bético, pueden estar relacionados con el levantamiento de la zona del arco de Gibraltar que condujo a la progresiva somerización y relleno de la cuenca de Guadalquivir.
- El cambio en la ciclicidad que se vio en la parte superior del registro por autores anteriores, donde los máximos de insolación del Hemisferio Norte están relacionados con el enriquecimiento de sedimentos en carbonato biogénico, mientras que los mínimos de insolación están relacionados con un aumento en los aportes terrígenos, ha sido confirmado por nuestros nuevos datos. Además, los nuevos datos de foraminíferos planctónicos corroboran el mecanismo propuesto anteriormente, en el que la somerización de la cuenca de Guadalquivir permitió que los sedimentos más gruesos llegaran hasta el sondeo

Montemayor-1, mientras que el clima más frío y árido, presente durante los mínimos de insolación del Hemisferio Norte, tuvo un efecto negativo en la cubierta vegetal, resultando en una mayor erosión y aportes terrígenos a la cuenca a expensas del carbonato biogénico.

1.3 Relevancia global de los eventos relacionados con el MSC del Mediterráneo y el Atlántico

El cambio paleoambiental que afectó a los márgenes del Mediterráneo y Atlántico en 7.17 Ma coincidió con el Cambio del Isótopo de Carbono del Mioceno Tardío (7.6 a 6.8/7 Ma), un evento global caracterizado por un enfriamiento y un cambio hacia valores más ligeros de $\delta^{13}\text{C}$. En consecuencia, para probar en qué medida eventos globales y locales afectaron a estas cuencas, confrontamos nuestros datos isotópicos con varios sondeos ubicados en el Océano Global.

- La comparación entre los datos isotópicos del sondeo 976 y 1146 (Mar de China Meridional) mostró cómo, incluso si ambas cuencas registran un cambio simultáneo de $\delta^{13}\text{C}$ alrededor de 7.17 Ma, las relaciones de fase del registro isotópico con parámetros astronómicos (precesión, oblicuidad) son diferentes. El sondeo 1146 refleja relaciones de fase globales conectadas a etapas glaciales, mientras que las relaciones de fase en la cuenca oeste de Alborán dependen de cambios en el balance hídrico que sugieren un efecto local mucho más fuerte en el Mediterráneo. Esto no excluye la posibilidad de que los efectos de restricción de los estrechos Mediterraneo – Atlánticos pudiesen verse amplificadas por el Cambio del Isótopo de Carbono del Mioceno Tardío en el Mediterráneo.
- Análogamente, el cambio evidente en los registros geoquímicos y micropaleontológicos del sondeo Montemayor-1 a partir de 7.15 -7.17 Ma podría haber sido influenciado, en parte, por el Cambio del Isótopo de Carbono del Mioceno Tardío y el enfriamiento global, como puede deducirse de un ligero cambio hacia un $\delta^{18}\text{O}$ bentónico más pesado y un $\delta^{13}\text{C}$ bentónico más ligero.

2. Inundación Zancliense de cuencas profundas y marginales en las proximidades de Gibraltar

El estudio sedimentológico, micropaleontológico y de isótopos estables de afloramientos del Messiniense tardío – Plioceno temprano en cuencas españolas próximas al estrecho de Gibraltar proporcionó información importante sobre las condiciones ambientales en el Mediterráneo tras el restablecimiento de una conexión eficiente Mediterráneo-Atlántico después de la crisis de salinidad del Messiniense.

- Una capa oscura, generalmente gris o negra, identificada en el límite Mioceno – Plioceno en cuencas profundas y marginales de todo el Mediterráneo, y a menudo enriquecida en materia orgánica, sugirió que el Plioceno temprano se caracterizó por la estratificación de la columna de agua y la reducción de los niveles de oxígeno de las aguas profundas. Tales condiciones podrían haberse desarrollado si la afluencia atlántica que llega al Mediterráneo fuera más salina

que las aguas Mediterráneas, aún bajo la influencia del Paratethys, lo que provocó el hundimiento y estratificación la columna de agua. Los niveles de salinidad más bajas de las aguas del Mediterráneo están indicados por valores ligeros de $\delta^{18}\text{O}$ bentónico, mucho más ligeros que los del Atlántico. El Plioceno temprano del sondeo 976 situado en la cuenca de Alborán no muestra una capa oscura, probablemente por su proximidad con el estrecho de Gibraltar y la fuerte erosión producida por las aguas del Atlántico que podrían haber erosionado las capas basales del Plioceno.

- La repoblación de foraminíferos bentónicos identificada en las cuencas estudiadas muestra similitudes con otros eventos más recientes de recuperación microfaunística de ambientes hostiles y repoblaciones después de episodios de bajo oxígeno, durante los episodios de depósito de un sapropel. La tendencia general de repoblación muestra un cambio desde ambientes estresados e inestables hacia asociaciones bentónicas que indican una circulación mas eficaz y una mejora en la ventilación en el fondo. Las primeras faunas bentónicas que aparecen son coherentes con niveles reducidos de oxígeno en el agua profunda y una columna de agua estratificada, como sugiere el depósito de la capa oscura.
- En todas las cuencas marginales españolas estudiadas, la paleobatimetría estimada para el Plioceno inferior fue similar, oscilando entre 50 y 150 m con una tendencia creciente. Estas observaciones implican una progresiva profundización de los márgenes Mediterráneos a medida que la conectividad Mediterráneo - Atlántica se hacía cada vez más eficiente. Además, una comparación con paleo-profundidades y secuencias de repoblación en otras zonas del Mediterráneo sugiere que, en los márgenes mediterráneos, la reinundación puede haber sido diacrónica debido a los efectos de la tectónica local y las respuestas de flexión a la carga y descarga. En el sondeo 976, el Plioceno temprano se caracteriza por un ambiente batial (> 1000 m).
- Los altos niveles de $\delta^{13}\text{C}$ del sondeo 976 testifican que la renovación del agua del fondo en las cuencas profundas fue eficiente inmediatamente después de la nueva inundación. Los valores mucho más ligeros encontrados en la cuenca de Málaga sugieren que, debido al relleno diacrónico, las cuencas marginales poco profundas necesitaron más tiempo para alcanzar una circulación de agua de fondo eficiente.

Referencias

- Blanc-Valleron, M.-M., Pierre, C., Caulet, J., Caruso, A., Rouchy, J.-M., Cespuglio, G., Sprovieri, R., Pestrea, S. and Di Stefano, E., 2002. Sedimentary, stable isotope and micropaleontological records of paleoceanographic change in the Messinian Tripoli Formation (Sicily, Italy). *Palaeogeography, Palaeoclimatology, Palaeoecology*, 185(3-4): 255-286.

- Booth-Rea, G., Ranero, C. R., Martínez-Martínez, J. M. and Grevemeyer, I., 2007. Crustal types and Tertiary tectonic evolution of the Alborán sea, western Mediterranean. *Geochemistry, Geophysics, Geosystems*, 8(10).
- Capella, W., Barhoun, N., Flecker, R., Hilgen, F., Kouwenhoven, T., Matenco, L., Sierro, F. J., Tulbure, M., Yousfi, M. Z. and Krijgsman, W., 2018. Palaeogeographic evolution of the late Miocene Rifian Corridor (Morocco): reconstructions from surface and subsurface data. *Earth-Science Reviews*, 180: 37-59.
- Capella, W., Spakman, W., van Hinsbergen, D. J., Chertova, M. V. and Krijgsman, W., 2020. Mantle resistance against Gibraltar slab dragging as a key cause of the Messinian Salinity Crisis. *Terra Nova*, 32(2): 141-150.
- Di Stefano, A., Baldassini, N. and Alberico, I., 2015. Surface-water conditions in the Mediterranean Basin during earliest Pliocene as revealed by calcareous nannofossil assemblages: Comparison between western and eastern sectors. *Palaeogeography, Palaeoclimatology, Palaeoecology*, 440: 283-296.
- Do Couto, D., Gorini, C., Jolivet, L., Le Bret, N., Augier, R., Gumiaux, C., d'Acremont, E., Ammar, A., Jabour, H. and Auxietre, J.-L., 2016. Tectonic and stratigraphic evolution of the Western Alboran Sea Basin in the last 25 Myrs. *Tectonophysics*, 677: 280-311.
- Fadil, A., Vernant, P., McClusky, S., Reilinger, R., Gomez, F., Ben Sari, D., Mourabit, T., Feigl, K. and Barazangi, M., 2006. Active tectonics of the western Mediterranean: Geodetic evidence for rollback of a delaminated subcontinental lithospheric slab beneath the Rif Mountains, Morocco. *Geology*, 34(7): 529-532.
- Flecker, R., Krijgsman, W., Capella, W., De Castro Martins, C., Dmitrieva, E., Mayser, J. P., Marzocchi, A., Modestou, S., Ochoa, D., Simon, D., Tulbure, M., Van Den Berg, B., Van Der Schee, M., De Lange, G., Ellam, R., Govers, R., Gutjahr, M., Hilgen, F., Kouwenhoven, T., Lofi, J., Meijer, P., Sierro, F. J., Bachiri, N., Barhoun, N., Alami, A. C., Chacon, B., Flores, J. A., Gregory, J., Howard, J., Lunt, D., Ochoa, M., Pancost, R., Vincent, S. and Yousfi, M. Z., 2015. Evolution of the Late Miocene Mediterranean–Atlantic gateways and their impact on regional and global environmental change. *Earth-Science Reviews*, 150: 365-392.
- García-Castellanos, D. and Villaseñor, A., 2011. Messinian salinity crisis regulated by competing tectonics and erosion at the Gibraltar arc. *Nature*, 480(7377): 359.
- Gómez de la Peña, L., Ranero, C. R., Gràcia, E. and Booth-Rea, G., 2020. The evolution of the westernmost Mediterranean basins. *Earth-Science Reviews*: 103445.
- Govers, R., 2009. Choking the Mediterranean to dehydration: the Messinian salinity crisis. *Geology*, 37(2): 167-170.
- Haug, G. H. and Tiedemann, R., 1998. Effect of the formation of the Isthmus of Panama on Atlantic Ocean thermohaline circulation. *Nature*, 393(6686): 673-676.
- Heit, B., Mancilla, F. d. L., Yuan, X., Morales, J., Stich, D., Martín, R. and Molina-Aguilera, A., 2017. Tearing of the mantle lithosphere along the intermediate-depth seismicity zone beneath the Gibraltar Arc: The onset of lithospheric delamination. *Geophysical Research Letters*, 44(9): 4027-4035.

-
- Hilgen, F., Krijgsman, W., Langereis, C., Lourens, L., Santarelli, A. and Zachariasse, W., 1995. Extending the astronomical (polarity) time scale into the Miocene. *Earth and Planetary Science Letters*, 136: 495-510.
- Hsü, K. J., Ryan, W. B. F. and Cita, M. B., 1973. Late miocene desiccation of the mediterranean. *Nature*, 242(5395): 240-244.
- Hüsing, S., Kuiper, K., Link, W., Hilgen, F. J. and Krijgsman, W., 2009. The upper Tortonian–lower Messinian at Monte dei Corvi (Northern Apennines, Italy): completing a Mediterranean reference section for the Tortonian stage. *Earth and Planetary Science Letters*, 282(1-4): 140-157.
- Jolivet, L. and Faccenna, C., 2000. Mediterranean extension and the Africa-Eurasia collision. *Tectonics*, 19(6): 1095-1106.
- Kouwenhoven, T., Seidenkrantz, M.-S. and Van der Zwaan, G., 1999. Deep-water changes: the near-synchronous disappearance of a group of benthic foraminifera from the Late Miocene Mediterranean. *Palaeogeography, Palaeoclimatology, Palaeoecology*, 152(3-4): 259-281.
- Kouwenhoven, T., Morigi, C., Negri, A., Giunta, S., Krijgsman, W. and Rouchy, J.-M., 2006. Paleoenvironmental evolution of the eastern Mediterranean during the Messinian: Constraints from integrated microfossil data of the Pissouri Basin (Cyprus). *Marine Micropaleontology*, 60(1): 17-44.
- Kouwenhoven, T. J., Hilgen, F. J. and Van Der Zwaan, G. J., 2003. Late Tortonian–early Messinian stepwise disruption of the Mediterranean–Atlantic connections: constraints from benthic foraminiferal and geochemical data. *Palaeogeography, Palaeoclimatology, Palaeoecology*, 198(3-4): 303-319.
- Krijgsman, W., Langereis, C., Zachariasse, W., Boccaletti, M., Moratti, G., Gelati, R., Iaccarino, S., Papani, G. and Villa, G., 1999. Late Neogene evolution of the Taza-Guercif Basin (Rifian Corridor, Morocco) and implications for the Messinian salinity crisis. *Marine Geology*, 153(1-4): 147-160.
- Mancilla, F. d. L., Booth-Rea, G., Stich, D., Pérez-Peña, J. V., Morales, J., Azañón, J. M., Martín, R. and Giaconia, F., 2015. Slab rupture and delamination under the Betics and Rif constrained from receiver functions. *Tectonophysics*, 663: 225-237.
- Martín, J. M., Braga, J. C. and Betzler, C., 2001. The Messinian Guadalhorce corridor: the last northern, Atlantic–Mediterranean gateway. *Terra Nova*, 13(6): 418-424.
- Martín, J. M., Puga-Bernabéu, A., Aguirre, J. and Braga, J. C., 2014. Miocene Atlantic-Mediterranean seaways in the Betic Cordillera (Southern Spain). *Revista de la sociedad geológica de España*, 27(1): 175-186.
- Pérez-Asensio, J. N., Aguirre, J., Schmiedl, G. and Civis, J., 2014. Messinian productivity changes in the northeastern Atlantic and their relationship to the closure of the Atlantic–Mediterranean gateway: implications for Neogene palaeoclimate and palaeoceanography. *Journal of the Geological Society*, 171(3): 389-400.
- Pérez-Asensio, J. N., Aguirre, J., Schmiedl, G. and Civis, J., 2012. Impact of restriction of the Atlantic-Mediterranean gateway on the Mediterranean Outflow Water and eastern Atlantic circulation during the Messinian. *Paleoceanography*, 27(3).

- Rosenbaum, G., Lister, G. S. and Duboz, C., 2002. Reconstruction of the tectonic evolution of the western Mediterranean since the Oligocene. *Journal of the Virtual Explorer*, 8: 107-130.
- Roveri, M. and Manzi, V., 2006. The Messinian salinity crisis: Looking for a new paradigm? *Palaeogeography, Palaeoclimatology, Palaeoecology*, 238(1-4): 386-398.
- Santarelli, A., Brinkhuis, H., Hilgen, F., Lourens, L., Versteegh, G. and Visscher, H., 1998. Orbital signatures in a Late Miocene dinoflagellate record from Crete (Greece). *Marine Micropaleontology*, 33(3-4): 273-297.
- Scher, H. D. and Martin, E. E., 2006. Timing and climatic consequences of the opening of Drake Passage. *science*, 312(5772): 428-430.
- Scher, H. D., Whittaker, J. M., Williams, S. E., Latimer, J. C., Kordesch, W. E. and Delaney, M. L., 2015. Onset of Antarctic Circumpolar Current 30 million years ago as Tasmanian Gateway aligned with westerlies. *Nature*, 523(7562): 580-583.
- Seidenkrantz, M.-S., Kouwenhoven, T., Jorissen, F., Shackleton, N. and Van der Zwaan, G., 2000. Benthic foraminifera as indicators of changing Mediterranean-Atlantic water exchange in the late Miocene. *Marine geology*, 163(1-4): 387-407.
- Selli, R., 1964. The Mayer-Eymar Messinian 1867. Proposal for a neostratotype. *Proc. 21st IGC Copenhagen 1960*, 28: 311-333.
- Selli, R., 1973. An outline of the Italian Messinian. *Messinian events in the Mediterranean*, 7: 150-171.
- Soto, J. I., Fernandez-Ibanez, F., Talukder, A. R. and Martinez-Garcia, P., 2010. Miocene shale tectonics in the northern Alboran Sea (western Mediterranean).
- Spakman, W., Chertova, M. V., van den Berg, A. and van Hinsbergen, D. J., 2018. Puzzling features of western Mediterranean tectonics explained by slab dragging. *Nature Geoscience*, 11(3): 211.
- Stern, R., 2007. When and how did plate tectonics begin? Theoretical and empirical considerations. *Chinese Science Bulletin*, 52(5): 578-591.
- Tulbure, M., Capella, W., Barhoun, N., Flores, J., Hilgen, F., Krijgsman, W., Kouwenhoven, T., Sierro, F. J. and Yousfi, M. Z., 2017. Age refinement and basin evolution of the North Rifian Corridor (Morocco): No evidence for a marine connection during the Messinian Salinity Crisis. *Palaeogeography, Palaeoclimatology, Palaeoecology*, 485: 416-432.
- Van den Berg, B. C. J., Sierro, F. J., Hilgen, F. J., Flecker, R., Larrasoña, J. C., Krijgsman, W., Flores, J. A. and Mata, M. P., 2018. Imprint of Messinian Salinity Crisis events on the Spanish Atlantic margin. *Newsletters on Stratigraphy*, 51(1): 93-115.
- Van der Schee, M., Van den Berg, B. C., Capella, W., Simon, D., Sierro, F. J. and Krijgsman, W., 2018. New age constraints on the western Betic intramontane basins: A late Tortonian closure of the Guadalhorce Corridor? *Terra Nova*, 30(5): 325-332.

Acknowledgments

Acknowledgements

Acknowledgments

Four years have passed since the SALTGIANT interview in Paris and since then I have lived so many adventures and learned countless things, about geology but mostly about myself. During these years of living in Spain I was very lucky to meet a lot of new people, make a great deal of new colleagues and friends that supported me throughout this entire process that hopefully will allow me to add a Dr. before my name. With the following lines I want to thank my mentors, old and new friends and my family for their scientific and emotional contribution that made possible the realization of this PhD dissertation.

In the first place, it is only fair to thank my PhD supervisor, Francisco J. Sierro, better known as Paco, for his invaluable supervision, support, and tutelage during the course of my PhD degree. My gratitude extends to Tanja Kouwenhoven, who thought me so many things and was always willing to help me when I was stuck. Thank you for acting like a second unofficial supervisor and for your support and constructive criticism which was essential in shaping my final dissertation. I also thank Santiago Ledesma and Francisco Jimenez-Espejo for their mentorship and words of encouragement.

I would like to thank my friends, lab mates, colleagues and research team from the Group of Oceanic Geoscience (GGO) at Salamanca University for a cherished time spent together in the lab, and in social settings. Jose Ignacio, Abel, Lines, Blanca, Montse, Andres, Alba, Lucia, Javi and Thibault thank you. My appreciation goes in particular to my fellow PhD students which support was essential to overstep all the obstacles that came across my way. Alba, I would not have made it without our Friday night Gin&Tonic appointments, they were essential for maintaining my sanity.

From the bottom of my heart I would like to express my deepest appreciation to all the members of the SALTGIANT project, both fellow ESRs and supervisor. Our stimulating and sometimes heated discussions about the Messinian Salinity Crisis played a fundamental role into understanding this complex topic and undoubtedly contributed to my thesis. Moreover, I will always specially cherish all the conversations, beers, and good food that I shared with my ESR colleagues during our numerous trips all around the Mediterranean. Bea, Gaia, Ronja, Laetitia, Jimmy, Hanneke, Siem, Simon, Fede, Fadl, Mariam, Athina, Maria and Michael thank you for sharing this experience with me.

In seguito, devo ringraziare in particolar modo le mie Abruzzesi preferite. Ringrazio Elena, Miri e soprattutto Giulia per il supporto ricevuto in questi anni che anche se veniva da lontano è stato fondamentale per me. Ringrazio poi Alessandra, diventata parte della mia famiglia in questi ultimi anni, per essere stata con me in tante avventure, da Brema a Trieste, alla Croazia e Spagna. Ti ringrazio perché hai sempre creduto in me e nelle mie capacità.

Nisam na vas zaboravila, bez brige. Hvala mojim Hrvaticama Evi, Eni, Karmen i Oretti koje su kroz ove posljednje godine bile uz mene i vjerovala u moje sposobnosti. Hvala vam na svemu.

Furthermore, I thank my first Spanish friend, Dani that with his energy, jokes and infinite places to take me out always made my days better. Thank you for being a good friend and for all the cubos de cervesa! I am sure there will be many more.

Finalmente, un ringraziamento tutto speciale va ai miei genitori, che mi hanno accompagnato incondizionatamente sia psicologicamente che fisicamente durante questo percorso e che mi hanno seguito sempre in tutte le mie tappe che mi hanno portato fin qui. Il merito di aver concluso anche questo capitolo lo condivido con loro.

Como ultimo, pero seguramente la persona que mas de cerca ha vivido las consecuencias de este doctorado, agradezco a Diego que me ha aguantado desde el principio de esa aventura cuando el Messiniense y el español eran un misterio todavía. Gracias por tu apoyo.

Curriculum vitae

Curriculum vitae

M.Sc. FRANCESCA BULIAN

CONTACT INFORMATION

fra.bulian@usal.es

francesca.bulian@gmail.com

PERSONAL INFORMATION

Date of birth: 10 January 1994, Rijeka, Croatia.

EDUCATION

PhD in geology and micropaleontology (October 2018 – ongoing until February 2022)

University of Salamanca (Spain)

Project: SALTGIANT (Understanding the Mediterranean Salt Giant)

Dissertation title: Late Miocene-Early Pliocene offshore onshore sedimentary records in the vicinity of Gibraltar

Supervisor: Francisco J. Sierro, University of Salamanca

Master's Degree in Geology and Land Management (October 2015 – December 2017)

University of Bologna (Italy)

Magna Cum Laude

Project: WASA (The Wadden Sea as an archive of landscape evolution, climate change and settlement history: Exploration – analyses – predictive modelling)

Thesis title: Multi-proxy analyses of a marine sediment core of the Wadden Sea (Eastfrisia), Germany

Supervisors: Bernd Zolitschka (GEOPOLAR), Bremen University

Veronica Rossi, University of Bologna

Bachelor's Degree in Geological Sciences (September 2012 – July 2015)

University of Bologna (Italy)

Thesis title: Geochemical and Environmental Analysis of Water and Sediments of the Veovača Lake (Vareš, Bosnia and Herzegovina)

Supervisor: Enrico Dinelli, University of Bologna

High school degree (September 2008 - May 2012)

Mathematical scientific high school “Scuola Media Superiore Italiana-SMSI”, Rijeka (Croatia)

GRANTS AND FELLOWSHIPS

2020 Utrecht University (the Netherlands): visiting PhD student (14th March – 14th June 2020)

Benthic foraminifera recognition

Supervisors: Wout Krijgsman and Tanja Kouwenhoven

2019 Naturgy Madrid (Spain): visiting PhD student (1st October – 5th December 2019)

Interpretation of seismic 2D-3D profiles in Kingdome suite software

Supervisor: Santiago Ledesma

2018 Marie Skłodowska-Curie grant at Salamanca University (Spain): Horizon 2020, grant agreement n° 765256: PhD student position (October 2018 – ongoing until February 2022)

Supervisor: Francisco J. Sierro

2017 Erasmus grant at Bremen University (Germany): research for MS dissertation (March 2017 – October 2017)

Supervisor: Bernd Zolitschka

2016 National Research Council, Institute for Atmospheric Sciences and Climate in Bologna (Italy): internship (November 2016 – February 2017)

Recovery of meteorological data for the study of climate change on time scales over a hundred years

Supervisor: Michele Brunetti

2014 National Research Council-Institute of Marine Sciences in Bologna (Italy): internship (September 2014 – December 2014)

Acquisition of magnetic measurements such as NRM, ARM, IRM and magnetic susceptibility

Supervisor: Luigi Vigliotti

FIELD EXPERIENCE

- 2021** - PhD project **field work and sampling** in Sorbas Basin (Spain)
- 2019** - PhD project **field work** in Sorbas Basin (Spain)
- PhD project **field work** in Sicily (Italy)
- 2018** - PhD project **field work and sampling** in Malaga Basin (Spain)
- PhD project **field work and sampling** in the Cadiz and Manilva area (Spain)
- 2017** - Undergraduate **field work and coring** at lake Zwischenahner Meer (Germany)
- Undergraduate **field work and coring** in the Wadden Sea (Wilhelmshafen, Germany)
- 2015** - **Oceanographic Cruise** in the Tyrrhenian Sea (1-15th September 2015) GeoHazaris (National Research Council-Institute of Marine Sciences, Bologna, Italy): monitoring scientific instruments for seismic data acquisition
- Undergraduate **field work and sampling** at lake Veovača (Vareš, Bosnia and Herzegovina)
- 2014** - Undergraduate **field work and geological mapping** in the Dolomites (Italy)

WORKSHOPS, SHORT COURSES, AND SUMMER SCHOOLS

- 2021** 3rd SaltGiant field course: **Dead Sea hypersaline environments** (21st – 25th November, Dead Sea Israel)
- 2nd SaltGiant field course: **Drilling training school** (25th – 31st October 2021, Sorbas, Spain)
- SaltGiant Short Course **Pre-history and history of salt use** (4th – 8th October 2021, 19 hours, Museum of Republika Srpska, Banja Luka/Tuzla, Bosnia and Herzegovina)
- Magellan Plus Workshop **BlackGate: Black Sea – Mediterranean Gateway Exchange** (22nd – 24th September 2021, Senckenberg Biodiversity and Climate Research Centre, Frankfurt, Germany)
- SaltGiant Short Course **Social Sciences** (14th – 17th June 2021, 28 hours, Sorbonne University, Paris, France)

- 2019** - SaltGiant Short Course **Modern and Ancient oceans** (25th – 29th November 2019, 40 hours, University of Salamanca, Spain)
- SaltGiant Short Course **Numerical Modelling in the Earth Sciences** (7th – 10th October 2019, 32 hours, Utrecht University, the Netherlands)
- USSP – **Urbino Summer School in Paleoclimatology** (10th – 26th July 2019, 80 hours, University of Urbino, Italy)
- SaltGiant Short Course **Seismic Data Acquisition, Processing, Interpretation** (17th – 19th June 2019, 25.5 hours, University of Trieste, Italy)
- 1st SaltGiant Field Course: **Introduction to MSC (Messinian Salinity Crises) Geology** (29th April – 3rd May 2019, 40 hours, Sicily, Italy)
- MEDSALT Training School: **The Messinian Salinity Crisis from a Fieldwork Perspective** (22nd – 27th April 2019, 40 hours, Sorbas, Spain)
- ECORD Training Course: **Virtual Shipboard Work Experience** (25th – 29th March 2019, MARUM – Center for Marine Environmental Sciences and the IODP Bremen Core Repository, 40 hours, University of Bremen, Germany)

PROFESSIONAL DEVELOPMENT

- 2021** - **Field work assistant** during master student field trip in Sorbas basin, 32 hours
- **Assistant professor** during practical work on microscope with master students (basic sediments, planktonic and benthonic foraminifer recognition), 8 hours
- 2019** - **Trainer** during the SaltGiant Short Course Modern and Ancient oceans (25th – 29th November 2019, 3 hours, University of Salamanca, Spain)

SOFT SKILLS TRAINING

- 2021** Managing Research: SISSA Medialab short course (9th – 13th April 2021, virtual meeting)
- 2019** Communicating Research, Journalism and Controversial Issues: SISSA Medialab short course (20th – 21st June 2019, Palermo, Italy)

2018 Communicating Research and Scientific Writing: SISSA Medialab short course (28th – 29th November 2018, Palermo, Italy)

CONFERENCE PRESENTATIONS

Oral presentations

5. **Bulian F.**, Sierro F. J., Jiménez-Espejo, F. J.: *Tectonically driven gateway restriction effects on the sedimentary record of a semi enclosed basin: The Mediterranean case study*. 35th meeting of Sedimentology (21th – 25th June, 2021, virtual meeting).
4. **Bulian F.**, Kouwenhoven T. J., Sierro F. J., Krijgsman, W.: *Geochemical and micropaleontological evidence of the Messinian Salinity Crisis preconditioning phase in the West Alboran Basin*. EGU General assembly 2021 (19th – 30th April 2021, virtual meeting).
3. **Bulian F.**, Sierro F. J., Kouwenhoven T. J., Jiménez-Espejo, F. J., Krijgsman W.: *Primi effetti di connessione ristretta Mediterraneo-Atlantica sul record sedimentario profondo del Mare di Alboran Occidentale*. Quarto Convegno dei geologi marini italiani 2021 (4th – 8th February 2021, virtual meeting).
2. **Bulian F.**, Sierro F. J.: *Revision of the Alboran sea Tortonian-Pliocene record: possible new insights on Mediterranean-Atlantic connectivity during the Messinian Salinity Crises*. EGU General assembly 2020 (4th – 8th May 2020, virtual meeting).
1. **Bulian F.**, Sierro F. J.: *Revised chronology of Alboran Sea (southwestern Mediterranean) cores and boreholes from Upper Miocene to Lower Pliocene*. RCMNS INTERIM COLLOQUIUM 2019 Continental-marine interaction during the Neogene in the Mediterranean area (9th – 12th September 2019, Granada, Spain).

Poster presentations

2. **Bulian F.**, Sierro F. J., Kouwenhoven T. J., Ledesma S.: *The Messinian Salinity Crisis in the West Alboran Basin: Tortonian to Pliocene foraminifer and stable isotope record from ODP Site 976*. AAPG Europe Region GTW: Evaporite processes and systems – integrating perspectives (18th – 20th October 2021, virtual meeting).
1. **Bulian F.**, Sierro F. J.: *The MSC in the Alboran basin: from its preconditioning to the Zanclean re-flooding*. Final MEDSALT Symposium (25th – 27th, February 2020, Piran, Slovenia).

PEER-REVIEWED PUBLICATIONS

4. **Bulian** F., Kouwenhoven T. J., Jiménez-Espejo F. J., Krijgsman W., Andersen N., and Sierro F. J., *in press.*: Impact of the Mediterranean-Atlantic connectivity and the late Miocene carbon shift on deep-sea communities in the Westernmost Mediterranean. *Palaeogeography, Palaeoclimatology, Palaeoecology* (Q1).
3. Andreetto, F., Aloisi, G., Raad, F., Heida, H., Flecker, R., Agiadi, K., Lofi, J., Blondel, S., **Bulian**, F., Camerlenghi, A. and Caruso, A., 2021. Freshening of the Mediterranean Salt Giant: Controversies and certainties around the terminal (Upper Gypsum and Lago-Mare) phases of the Messinian Salinity Crisis. *Earth-Science Reviews*, p.103577. <https://doi.org/10.1016/j.earscirev.2021.103577> (Q1)
2. **Bulian**, F., Sierro, F.J., Ledesma, S., Jiménez-Espejo, F.J. and Bassetti, M.A., 2021. Messinian West Alboran Sea record in the proximity of Gibraltar: Early signs of Atlantic-Mediterranean gateway restriction. *Marine Geology*, 434, p.106430. <https://doi.org/10.1016/j.margeo.2021.106430> (Q1)
1. **Bulian**, F., Enters, D., Schlütz, F., Scheder, J., Blume, K., Zolitschka, B. and Bittmann, F., 2019. Multi-proxy reconstruction of Holocene paleoenvironments from a sediment core retrieved from the Wadden Sea near Norderney, East Frisia, Germany. *Estuarine, Coastal and Shelf Science*, p.106251. <https://doi.org/10.1016/j.ecss.2019.106251> (Q1)

PAPERS IN PREPARATION

4. **Bulian** F., Sierro F. J., Jiménez-Espejo F. J., Andersen N., *in prep.*: The timing of closure of the last Betic corridor strand inferred from new geochemical and planktic foraminifer data from Montemayor-1 core (Guadalquivir Basin)
3. Agiadi K., Hohmann N., Gliozzi E., Thivaiou D., Taviani M., Bosellini F., Bianucci G., Collareta A., Londeix L., Faranda C., **Bulian** F., Koskeridou E., Lozar F., Mancini A-M., Dominici S., Moissette P., Bajo Campos I., Borghi E., Iliopoulos G., Antonarakou A., Kontakiotis G., Besiou E., Zarkogiannis S., Harzhauser M., Sierro f. j., Vasiliev I., Camerlenghi A., García-Castellanos D., *in prep.*: The impact of the Messinian Salinity Crisis on the taxonomic composition of the Mediterranean marine biota.
2. Ebner R., **Bulian** F., Meijer P., Sierro F. J., and Kouwenhoven T. J., *in prep.*: From open marine to restricted conditions: A transient model approach to the 7.17 Ma Mediterranean event.
1. **Bulian** F., Sierro F. J., Kouwenhoven T. J., Andersen N., and Krijgsman W., *in prep.*: Westernmost Mediterranean Sea Early Pliocene environments and

Mediterranean – Atlantic connectivity deduced from benthic foraminifers and stable isotope data.

SERVICE

Peer reviewer: *Sedimentary Geology*

OUTREACH

- 2020** - European Researchers' Night: Activities with the general public
- International Day of Women and Girls in Science: Speed dating with scientists
- 2018** **Bulian F.**, 2018. Influenza culturale del clima: come i cambiamenti climatici degli ultimi 8.000 anni condizionarono la vita umana. *La Battana*, 208, 9-42, EDIT (Croatia)
- 2014** GEODAY at University of Bologna (Italy): Activities with the wider public
- 2013** GEODAY at University of Bologna (Italy): Children's activities and geological games

Blog: <https://thesaltgiantfellowship.wordpress.com/> (contributor)

LANGUAGES

Croatian, Italian, English, Spanish: fluent speaking and writing
German: basic level

